

Bangor University

DOCTOR OF PHILOSOPHY

Identification and analysis of DNA repair pathways that contribute to the survival of cells after nucleoside analogue treatment in *Schizosacharomyces pombe*

Gasasira Uwamahoro, Marie-Fabrice

Award date:
2013

Awarding institution:
Bangor University

[Link to publication](#)

General rights

Copyright and moral rights for the publications made accessible in the public portal are retained by the authors and/or other copyright owners and it is a condition of accessing publications that users recognise and abide by the legal requirements associated with these rights.

- Users may download and print one copy of any publication from the public portal for the purpose of private study or research.
- You may not further distribute the material or use it for any profit-making activity or commercial gain
- You may freely distribute the URL identifying the publication in the public portal ?

Take down policy

If you believe that this document breaches copyright please contact us providing details, and we will remove access to the work immediately and investigate your claim.

BANGOR UNIVERSITY
SCHOOL OF BIOLOGICAL SCIENCES

**Identification and analysis of DNA repair pathways that
contribute to the survival of cells after nucleoside
analogue treatment in *Schizosacharomyces pombe***

Ph.D. thesis 2013

Gasasira Uwamahoro Marie-Fabrice

Abstract

Nucleoside analogues (NA) are a group of anti-cancer drugs that are widely used in cancer therapy. It is therefore important to understand the cellular responses to these drugs in order to improve therapy. In this PhD project, I have used the amenable model, *Schizosaccharomyces pombe* to study DNA repair mechanisms that are involved in cell survival to two of the most widely used anti-cancer nucleoside analogues, Gemcitabine (GemC) and Cytarabine (AraC). Screening of a genome wide gene deletion library and analysis of specific DNA repair mutants strongly suggested a role of DNA repair mechanisms in survival of cells to GemC and AraC treatment. Identified gene products that may play a role in the survival to the two drugs include the multifunctional MRN (Mrn11-Rad50-Nbs1)-Ctp1^{CtIP} complex, nucleotide excision repair (NER) recognition factors Rhp41-Rhp42^{XPC} and Rhp14^{XPA} and 5' incision nuclease Swi10^{ERCC1}, and base excision repair (BER) abasic site endonuclease Apn2^{APE1} and the glycosylase Nth1^{NTH1}. However, while most members of the NER pathway were required for survival, the 3' incision nuclease Rad13^{XPG} mutant was not sensitive to GemC and AraC indicating that the nuclease is not involved in survival to NA treatment and suggesting an unorthodox role of the NER in the repair of DNA lesions induced by NAs. Post-replication repair (PRR) DNA polymerase Rev3^{REV3} and mismatch repair (MMR) exonuclease Exo1^{EXO1} mutants were also not sensitive to GemC and AraC, suggesting that the gene products are not involved in cell survival. Interestingly, mutants in the PRR PCNA ubiquitinating factor Rhp18^{RAD18} and the BER nuclease Rad2^{FEN-1} showed a slight resistance in comparison to WT. This resistance was significantly increased when the BER uracil glycosylase Ung1^{UNG1} and the MMR proteins Mlh1^{MLH1}, Msh2^{MSH2} and Msh6^{MSH6} were absent suggesting that the presence of the gene products might enhance drug activity. In addition to the role of DNA repair mechanisms, analysis of the genome wide deletion library suggested a role of several genome maintenance mechanisms in the response to GemC. These include the DNA damage and DNA replication checkpoints, telomere maintenance and chromatin remodelling. Results in this thesis suggest that the genetic background of patients plays a pivotal role in the response to NA therapies as for examples patients with mutations in the MMR repair pathway may be more resistant rendering the therapy less effective.

Acknowledgements

I would like to dedicate this thesis to my father, Ephrem Gasasira, for his support and unconditional love and to my young sister, Assumpta Gasasira for her invaluable presence throughout this time.

My sincere thanks to Bangor University and to the North West Cancer Research Fund who have funded this project.

I express my wholeheartedly felt thanks to my supervisor, Dr Edgar Hartsuiker for his precious presence throughout this challenging time. For his kindness and cheerfulness that made my time in his laboratory most enjoyable. All the work herein described could not be achieved without his support, patience and daily input.

Sincere thanks to my internal examiner, Dr Thomas Caspari for his direct involvement and advice. I thank him for our innumerable discussions and for sharing his inestimable knowledge on yeast research in general and the checkpoint machinery in particular. I also thank him for providing me with the checkpoint mutant strains used in this project.

I express my deeply felt thank you to the chairmen of the project, Professor David Shepherd for his time and advice during the first part of this project and Professor Deri Tomos for his kind input during the last months of the project.

I also express my thank you to Dr Nick Rhind and Dr Adam Watson for their kind supply of plasmids and strains used in this project.

My sincere thanks also go to all members of the Hartsuiker laboratory at the NWCRFI- Bangor University for their kindness, cheerfulness and daily support. I sincerely thank Dr Andrea Keszthelyi for her direct involvement and for kindly sharing data that were used in this project. I also thank her for her genuine presence and generosity and for patiently proofreading my thesis. Un grand merci to Dr Isabelle Colson for our endless discussions on the library analysis. I also profoundly thank her for her kind input and revision of the thesis. I also express a deeply felt thank you to Dr Rolf Kraehenuehl and Dr Oliver Fleck for kindly providing me with strains that were used in this project, and for sharing their invaluable knowledge on

the yeast research. I also sincerely thank Dr Ellen Vernon, Dr Alessa Jaendling, Karim Garrido and Tamara Jordan for their daily presence and support.

I would also like to express my thank you to other members of the D2 laboratory at Bangor University, especially to Boyin Liu for his precious assistance with use of the fluorescent microscopy and to Natalia Harrison for her kind presence and invaluable technical assistance.

Lastly, I sincerely thank my sisters Alice and Clarisse Gasasira and my brother Basile Gasasira, for their endless support. Without their daily presence and encouragement I could not have achieved this project. I also express a deeply felt thank you to all my friends who stood by me during this challenging time.

Abbreviations

53BP1	p53 binding protein
4-NQO	4-nitroquinoline 1-oxide
6-4 PPs	6-4 photoproducts
9_1_1	Rad9- Rad1- Hus1
ABC	ATP-binding cassettes
ACS	ARS consensus sequence
adh	Alcohol dehydrogenase
ADP	adenosine diphosphate
ambic	ammonium bicarbonate
AMP	adenosine monophosphate
AP site	abasic (purine/pyrimidine) site
APE1	AP endonucleases
AraC	arabinosylcytosine, cytarabine
AraC-DP	cytarabine diphosphate
AraC-MP	cytarabine monophosphate
AraC-TP	cytarabine triphosphate
ARS	autonomously replicating sequences
ATM	ataxia telangiectesia mutated
ATP	adenosine tri-phosphate
ATR	ATM and Rad3 related
ATRIP	ATR interacting protein
BER	Base-excision repair
BIR	break induced replication
BRCA	breast cancer susceptibility gene
BRCT	BRCA C Terminus
Cdc	cell division cycle
CDK	cyclin dependent kinases
CEM	Human T cell lymphoblast-like cell line
CNDAC	2'-C-cyano-2'-deoxy-1- β -D-arabino-pentofuranosylcytosine
CNT	concentrative transporter
CPDs	cyclobutane pyrimidine dimers
CPT	camptothecin
CS	Cockayne syndrome
CTP	cytidine triphosphate
DAPI	4',6-diamidino-2-phenylindol
dCK	deoxycytidine kinase
DDT	DNA damage tolerance
dFdC	2', 2'-difluorodeoxycytidine
dFdCDP	2', 2'-difluorodeoxycytidine diphosphate
dFdCMP	2', 2'-difluorodeoxycytidine monophosphate
dFdCTP	2', 2'-difluorodeoxycytidine triphosphate

dGK	deoxyguanosine kinase
DHFR	Dihydrofolate reductase
dHJ	double Holliday Junction
dmdNK	Drosophila melanogaster deoxynucleotide kinase
DMSO	Dimethyl Sulfoxide
DNA	Deoxyribonucleic acid
DNA-PKcs	DNA-dependent protein kinase
dNK	deoxynucleotides kinase
dNs	deoxynucleosides
dNTPs	deoxynucleoside triphosphate
DSB	Double strand break
DSBR	double strand break repair
dTMP	deoxythymidine monophosphate
dTTP	deoxythymidine triphosphate
dUMP	deoxyuridine-5'-monophosphate
EDTA	Ethylenediamine tetraacetic acid
ELN	Extra low nitrogen
EMM	Edinburg minimal media
ENT	equilibrative transporter
Exo1	Exonuclease1
FA	Fanconi Anaemia
FHA	Forkhead associated
FRT	FLP recognition site
G418	Geneticin
GemC	Gemcitabine
GFP	green fluorescent protein
GG-NER	Global genome NER
GINS	Go-Ichi-Ni-San
GMP	Guanosine monophosphate
HA	human hemagglutinin
HCl	Hydrochloric acid
hENT1	human equilibrative transporter1
HJ	Holliday Junction
HNPPC	Nonpolyposis Colon Cancer
HPLC	high-pressure liquid chromatography
HR	homologous recombination
hsdCK	human deoxycytidine kinase
HTLF	Helicase Like Transcription Factor
HU	hydroxyurea
ICLs	interstrand/intrastrand crosslinks
IDLs	insertion/deletion loops
IMP	inosine-5'-monophosphate
KCl	potassium chloride
KH ₂ PO ₄	Monopotassium phosphate

LB	L-Broth (Lysogeny-Broth)
LiAc	Lithium Acetate
MCM	minichromosome maintenance
MDC1	Mediator of DNA damage checkpoint protein 1
methylene-TFH	methylene tetrahydrofolate
MgCl ₂	Magnesium chloride
MLH1	MutL homologue
MMEJ	microhomology-mediated end joining
MMR	Mismatch repair
MMS	Methyl Methanesulfonate
MPG	Methylpurine DNA glycosylase
MRN	Mre11-Rad50-Nbs1
MSH	MutS homologues
NA	nucleoside analogue
Na ₂ EDTA	disodium ethylenediaminetetraacetate
Na ₂ HPO ₄	sodium phosphate
NaAc	sodium acetate
NaCl	sodium chloride
NaOH	sodium hydroxide
NAT	Nourseothricin
Nbs	Nijmegen Breakage Syndrome
NDP	nucleoside diphosphate
NER	Nucleotide-excision repair
NHEJ	non homologous end joining
OGG1	8-oxoG DNA glycosylase
OMP	orotidine-5'-monophosphate
ORC	origin recognition complex
ORF	open reading frame
PARP	poly(AD-ribose) polymerase
PBS	phosphate-buffered saline
PCNA	proliferating cell nuclear antigen
PCNA	proliferating cell nuclear antigen
PEG	polyethylene glycol
PMS2	post-meiotic segregation
PNK	polynucleotide kinase
pol	polymerase
pre-RC	pre-replicative complex
PRPP	5-phosphorybosylpyrophosphate
PRR	post replicative repair
RFC	replication factor C
RNA	ribonucleic acid
RNApolII	RNA polymerase II
RNR	ribonucleotide reductase
ROS	reactive oxygen species

RPA	replication protein A
<i>S. cerevisiae</i>	<i>Saccharomyces cerevisiae</i>
<i>S. pombe</i>	<i>Schizosaccharomyces pombe</i>
SAX	strong anion exchange
SCAN	Spinocerebellar Ataxia with Axonal Neuropathy
SDS	sodium dodecyl sulfate
SDSA	synthesis dependent strand annealing
SHPRH	SNF2 Histone Linker PHD Ring Helicase
SSA	single strand annealing
SSB	single strand break
ssDNA	single stranded DNA
TAE	Tris-Acetate-EDTA
TBE	Tris-Borate-EDTA
TBZ	Thiabendazole
TCA	Trichloro acetic acid
TCR	transcription-coupled repair
TDD	Trichiodystrophy
TDG	Thymine/Uracil glycosylase
Tdp1	tyrosyl DNA phosphodiesterase,
TE	Tris-EDTA
TK	thymidine kinase
TLS	Translesion synthesis
Top1/2	topoisomerase1/2
TopBP1	topoisomerase II binding protein
TS	Thymidylate synthase
UDP	uridine diphosphate
UMP	uridine-5'-monophosphate
UNG1	Uracil DNA glycosylase
UTP	uridine triphosphate
UV	ultraviolet
UVER	UV-damaged DNA endonuclease-dependent excision repair
XP	xeroderma pigmentosum
YE/YEA	yeast extract/agar
YNB/YNBA	Yeast nitrogen base/agar
53BP1	p53 binding protein
4-NQO	4-nitroquinoline 1-oxide
6-4 PPs	6-4 photoproducts
9_1_1	Rad9- Rad1- Hus1
ABC	ATP-binding cassettes
ACS	ARS consensus sequence
Adh	Alcohol dehydrogenase
ADP	adenosine diphosphate
ambic	ammonium bicarbonate

AMP	adenosine monophosphate
AP site	abasic (purine/pyrimidine) site
APE1	AP endonucleases
AraC	arabinosylcytosine, cytarabine
AraC-DP	cytarabine diphosphate
AraC-MP	cytarabine monophosphate
AraC-TP	cytarabine triphosphate
ARS	autonomously replicating sequences
ATM	<i>ataxia telangiectesia</i> mutated
ATP	adenosine tri-phosphate
ATR	ATM and Rad3 related
ATRIP	ATR interacting protein
BER	Base-excision repair
BIR	break induced replication
BRCA	breast cancer susceptibility gene
BRCT	BRCA C Terminus
Cdc	cell division cycle
CDK	cyclin dependent kinases
CNDAC	2'-C-cyano-2'-deoxy-1-β-D-arabino-pentofuranosylcytosine
CNT	concentrative transporter
CPDs	cyclobutane pyrimidine dimers
CPT	camptothecin
CS	Cockayne syndrome
CTP	cytidine triphosphate
DAPI	4',6-diamidino-2-phenylindol
dCK	deoxycytidine kinase
DDT	DNA damage tolerance
dFdC	2', 2'-difluorodeoxycytidine
dFdCDP	2', 2'-difluorodeoxycytidine diphosphate
dFdCMP	2', 2'-difluorodeoxycytidine monophosphate
dFdCTP	2', 2'-difluorodeoxycytidine triphosphate
dGK	deoxyguanosine kinase
DHFR	Dihydrofolate reductase
dHJ	double Holliday Junction
<i>dmdNK</i>	<i>Drosophila melanogaster</i> deoxynucleotide kinase
DMSO	Dimethyl Sulfoxide
DNA	Deoxyribonucleic acid
DNA-PKcs	DNA-dependent protein kinase
dNK	deoxynucleotides kinase
dNs	deoxynucleosides
dNTPs	deoxynucleoside triphosphate
DSB	Double strand break
DSBR	double strand break repair

dTMP	deoxythymidine monophosphate
dTTP	deoxythymidine triphosphate
dUMP	deoxyuridine-5'-monophosphate
EDTA	Ethylenediamine tetraacetic acid
ELN	Extra low nitrogen
EMM	Edinburg minimal media
ENT	equilibrative transporter
Exo1	Exonuclease1
FA	Fanconi Anaemia
FHA	<u>Forkhead associated</u>
FRT	FLP recognition site
G418	Geneticin
GemC	Gemcitabine
GFP	green fluorescent protein
GG-NER	Global genome NER
GINS	<u>Go-Ichi-Ni-San</u>
GMP	Guanosine monophosphate
HA	human hemagglutinin
HCl	Hydrochloric acid
hENT1	human equilibrative transporter1
HJ	Holliday Junction
HNPPC	Nonpolyposis Colon Cancer
HPLC	high-pressure liquid chromatography
HR	homologous recombination
<i>hscCK</i>	human deoxycytidine kinase
HTLF	Helicase Like Transcription Factor
HU	hydroxyurea
ICLs	interstrand/intrastrand crosslinks
IDLs	insertion/deletion loops
IMP	inosine-5'-monophosphate
KCl	potassium chloride
KH ₂ PO ₄	Monopotassium phosphate
LB	L-Broth (Lysogeny-Broth)
LiAc	Lithium Acetate
MCM	minichromosome maintenance
MDC1	Mediator of DNA damage checkpoint protein 1
methylene-TFH	methylene tetrahydrofolate
MgCl ₂	Magnesium chloride
MLH1	<u>MutL</u> homologue
MMEJ	microhomology-mediated end joining
MMR	Mismatch repair
MMS	Methyl Methanesulfonate
MPG	Methylpurine DNA glycosylase
MRN	Mre11-Rad50-Nbs1

MSH	<u>MutS</u> homologues
NA	nucleoside analogue
Na ₂ EDTA	disodium ethylenediaminetetraacetate
Na ₂ HPO ₄	sodium phosphate
NaAc	sodium acetate
NaCl	sodium chloride
NaOH	sodium hydroxide
NAT	Nourseothricin
Nbs	Nijmegen Breakage Syndrome
NDP	nucleoside diphosphate
NER	Nucleotide-excision repair
NHEJ	non homologous end joining
OGG1	8-oxoG DNA glycosylase
OMP	orotidine-5'-monophosphate
ORC	origin recognition complex
ORF	open reading frame
PARP	poly(AD-ribose) polymerase
PBS	phosphate-buffered saline
PCNA	proliferating cell nuclear antigen
PCNA	proliferating cell nuclear antigen
PEG	polyethylene glycol
PMS2	<u>post-meiotic</u> <u>segregation</u>
PNK	polynucleotide kinase
pol	polymerase
pre-RC	pre-replicative complex
PRPP	5-phosphorybosylpyrophosphate
PRR	post replicative repair
RFC	replication factor C
RNA	ribonucleic acid
RNApolII	RNA polymerase II
RNR	ribonucleotide reductase
ROS	reactive oxygen species
RPA	replication protein A
<i>S. cerevisiae</i>	<i>Saccharomyces cerevisiae</i>
<i>S. pombe</i>	<i>Schizosaccharomyces pombe</i>
SAX	strong anion exchange
SCAN	Spinocerebellar Ataxia with Axonal Neuropathy
SDS	sodium dodecyl sulfate
SDSA	synthesis dependent strand annealing
SHPRH	SNF2 Histone Linker PHD Ring Helicase
SSA	single strand annealing
SSB	single strand break
ssDNA	single stranded DNA
TAE	Tris-Acetate-EDTA

TBE	Tris-Borate-EDTA
TBZ	Thiabendazole
TCA	Trichloro acetic acid
TCR	transcription-coupled repair
TDD	Trichiodystrophy
TDG	Thymine/Uracil glycosylase
Tdp1	tyrosyl DNA phosphodiesterase,
TE	Tris-EDTA
TK	thymidine kinase
TLS	Translesion synthesis
Top1/2	topoisomerase1/2
TopBP1	topoisomerase II binding protein
TS	Thymidylate synthase
UDP	uridine diphosphate
UMP	uridine-5'-monophosphate
UNG1	Uracil DNA glycosylase
UTP	uridine triphosphate
UV	ultraviolet
	UV-damaged DNA endonuclease-dependent excision
UVER	repair
XP	xeroderma pigmentosum
YE/YEA	yeast extract/agar
YNB/YNBA	Yeast nitrogen base/agar

Table of Contents

1	INTRODUCTION	1
1.1	GENOME INSTABILITY AND CANCER.....	1
1.1.1	<i>Cancer as a genetic disease</i>	1
1.1.2	<i>The cell cycle and DNA replication</i>	2
1.1.2.1	The cell cycle.....	2
1.1.2.2	DNA replication.....	3
1.1.3	<i>DNA damage checkpoint and repair pathways</i>	7
1.1.3.1	DNA damage	9
1.1.3.2	DNA damage checkpoints	10
1.1.3.3	DNA repair pathways	14
1.1.3.3.1	Excision repair pathways.....	16
1.1.3.3.2	DNA Strand Break Repair	25
1.1.3.4	Post replication repair (PRR).....	35
1.1.3.5	DNA repair genes and cancer prone syndromes.....	38
1.2	DNA DAMAGING AGENTS IN CANCER THERAPY	39
1.2.1	<i>Topoisomerase poisons</i>	40
1.2.1.1	Topoisomerases.....	40
1.2.1.2	Examples of topoisomerases poisons	41
1.2.1.3	Survival of cancer cells to topoisomerase poisons	44
1.2.2	<i>Nucleoside analogues (NAs)</i>	46
1.2.2.1	Biosynthesis of physiological nucleosides.....	46
1.2.2.2	Mechanism of action of nucleoside analogues.....	52
1.2.2.3	Cellular response to NAs.....	60
1.3	THE PROJECT.....	61
1.3.1	<i>S. pombe as a model organism</i>	62
1.3.2	<i>Scope of the project</i>	65
2	MATERIALS AND METHODS	66
2.1	MATERIALS.....	66
2.1.1	<i>List of strains</i>	66
2.1.2	<i>List of primers</i>	69
2.1.3	<i>Plasmids</i>	75
2.1.4	<i>Media</i>	76
2.1.5	<i>General Buffers</i>	76
2.1.6	<i>Various</i>	76
2.2	METHODS.....	77
2.2.1	<i>Yeast methods</i>	77
2.2.1.1	<i>S. pombe</i> crosses.....	77
2.2.1.2	<i>S. pombe</i> spot tests.....	78
2.2.1.3	<i>S. pombe</i> transformation	78
2.2.1.4	DNA extraction from yeast cells.....	80
2.2.1.5	DAPI staining and microscope observation	81
2.2.1.6	Western Blot.....	81
2.2.1.7	HPLC measurement of free intracellular GemC-TP and dNTPs levels (Kumar <i>et al.</i> , 2010)	83
2.2.2	<i>Molecular biology</i>	87
2.2.2.1	PCR, restriction digest, agarose gel electrophoresis, DNA measurement and ligation.....	87
2.2.2.2	Small scale plasmid purification (boiling lysis miniprep).....	88
2.2.2.3	Site directed mutagenesis (Agilent Technologies QuickChange Site-directed Mutagenesis kit Revision B.01).....	89

3	SETTING UP A SYSTEM TO STUDY NUCLEOSIDE ANALOGUES IN <i>S. POMBE</i>	90
3.1	KINASES	90
3.1.1	<i>Kinase constructs</i>	91
3.1.2	<i>Sensitivity of strains with kinases to NAs</i>	95
3.2	INTEGRATION OF THE <i>hENT1</i> TRANSPORTER	99
3.2.1	<i>Test sensitivity of strains with hENT1 transporter</i>	99
3.2.2	<i>Test presence of transporter in <i>S. pombe</i> cells</i>	101
3.2.3	<i>Construct a stable hENT1/kinase strain</i>	103
3.2.3.1	<i>Clone hENT1 into pFA6a-natMX6</i>	105
3.2.3.2	<i>Integrate hENT1 into <i>S. pombe</i></i>	109
3.2.4	<i>Test sensitivity of reverse mutated hENT1/kinase strains to GemC and AraC</i>	112
3.3	FURTHER CHARACTERISATION OF THE SYSTEM	117
3.3.1	<i>YE rich medium affects growth of cells with the transporter and kinase</i>	117
3.3.2	<i>Cells with kinase and transporter are more sensitive to gemcitabine in EMM than in YEL</i>	122
3.3.3	<i>DNA damage checkpoint is activated by YE media</i>	129
3.4	DISCUSSION	132
4	BIONEER (V2) GENOME WIDE DELETION LIBRARY SCREEN	136
4.1	LIBRARY SCREEN: ANALYSIS	136
4.1.1	<i>Screen of the library</i>	136
4.1.2	<i>Integration of hsdCK kinase and hENT1 transporter into the library</i>	139
4.1.3	<i>Visual screening</i>	141
4.2	SUB LIBRARY ANALYSIS: OPTIMIZATION OF ANALYSIS METHOD	164
4.2.1	<i>Method 1: ranking by areas under growth curves</i>	168
4.2.2	<i>Method 2: ranking by growth rate (R value)</i>	176
4.2.3	<i>Method 3: ranking mutants by final growth (K value)</i>	182
4.3	SUB LIBRARY ANALYSIS: RANKING MUTANTS	184
4.4	GENE ONTOLOGY (GO) ANALYSIS	207
4.5	DISCUSSION	213
4.5.1	<i>Specific mutants from the library screen</i>	213
4.5.2	<i>Analysis of sequence orphan genes</i>	218
4.5.3	<i>Conclusion</i>	220
5	REPAIR OF NA-INDUCED DNA DAMAGE	221
5.1	MRN-CTIP ^{CTP1} COMPLEX MUTANTS ARE HIGHLY SENSITIVE TO GEMC AND ARAC	222
5.2	NER AND BER MUTANTS ARE SENSITIVE TO GEMC AND ARAC TREATMENT BUT MMR AND PRR MUTANTS ARE RESISTANT TO THE DRUGS	229
5.2.1	<i>rhp14, rhp41/rhp42 and swi10 defective mutants are highly sensitive to GemC and AraC but rad13Δ mutants are resistant to both drugs</i>	230
5.2.2	<i>nth1 and apn2 mutants are highly sensitive to GemC and AraC</i>	232
5.2.3	<i>Mismatch repair (MMR) defective mutants are more resistant to GemC and AraC compared to WT cells</i>	234
5.2.4	<i>Post replication repair (PRR) mutants are not sensitive to GemC and AraC</i>	237
5.3	SENSITIVITY OF DOUBLE MUTANTS TO GEMC	239
5.3.1	<i>The MRN complex genetically interacts with nth1 and acts in parallel with apn2 and rhp14 in response to GemC</i>	239
5.3.2	<i>NER epistasis analyses</i>	243
5.4	DISCUSSION	245

6	THE FLP NICK SYSTEM: A TOOL TO STUDY DNA BOUND PROTEIN COMPLEXES.....	260
6.1	STRATEGY TO CONSTRUCT “FLP NICK” STRAINS	261
6.1.1	Integrate FLP-H305L_HA into <i>S. pombe</i>	263
6.1.1.1	Cloning HA tagged FLP-H305L into pAW8ENdel cre-lox plasmids	263
6.1.1.2	Transform FLP H305L_HA into <i>S. pombe</i>	273
6.1.1.3	Integrate 3HA-KAN into “FLP strains”	276
6.1.1.4	Expressing FLP proteins	278
6.1.2	Integrate FRT sequence into <i>S. pombe</i>	280
6.1.2.1	Cloning the FRT sequence into pFA6a-natMX6.....	282
6.1.2.2	Transform FRT sequence into <i>S. pombe</i>	284
6.2	ANALYSIS OF “FLP NICK” STRAINS.....	286
6.3	DISCUSSION.....	290
7	GENERAL DISCUSSION	294
7.1	GEMC MIGHT INDUCE ARRESTED REPLICATION FORK	295
7.2	MRE11 REMOVES GEMC FROM THE DNA TO ALLOW REPAIR	296
7.3	NER AND BER EXCISION REPAIR GENES PLAY A ROLE IN SENSITIVITY TO GEMC AND ARAC.....	300
7.4	MMR AND PRR DEFECTIVE MUTANTS ARE RESISTANT TO TREATMENT WITH GEMC AND ARAC.....	305
7.5	CONCLUSION	307
	REFERENCES.....	308
	APPENDICES.....	333
I.	ALIGNMENT OF BACK MUTATED HENT1 AFTER INTEGRATION INTO <i>S. POMBE</i>	333
II.	LIST OF LIBRARY MUTANTS THAT WERE SENSITIVE IN ALL THREE INDEPENDENT SCREENS	338
III.	LIST OF LIBRARY MUTANTS THAT DID NOT GROW IN ALL THREE INDEPENDENT SCREENS	341
IV.	OVER-REPRESENTED BIOLOGICAL PROCESSES IN THE SUB LIBRARY (456 SENSITIVE MUTANTS) AT SIGNIFICANCE LEVEL OF 0.05%.....	344

List of figures

Figure 1-1 Schematic representation of the replication process	6
Figure 1-2 Simplified representation of the DNA damage checkpoint response following replication fork arrest	13
Figure 1-3 Simplified chart showing main DNA lesions and repair pathways.	15
Figure 1-4 Schematic representation of the two subpathways of base excision repair.	18
Figure 1-5 Schematic representation of the nucleotide excision repair pathway.	21
Figure 1-6 Schematic representation of the mismatch repair pathway	24
Figure 1-7A Overview of the double strand break repair by the Non Homologous End Joining pathway.	27
Figure 1-7B Repair of DSBs by Homologous Recombination.	31
Figure 1-7C. MRN complex structure.	34
Figure 1-8 DNA damage tolerance.	37
Figure 1-9 Schematic representation of cell death induced by CPT.	43
Figure 1-10A Chemical structure of nucleotides.	47
Figure 1-10B Overview of de novo synthesis of deoxynucleotides.	50
Figure 1-11A Simplified overview of NA induced cell death.	54
Figure 1-11B Structures of deoxycytidine and its analogues AraC and GemC.	54
Figure 1-12 Illustration of <i>S. pombe</i> cell cycle.	64
Figure 3-1 Strategy to integrate kinases into <i>S. pombe</i>.	92
Figure 3-2 Integration of kinases into <i>S.pombe</i> genome	94
Figure 3-3 Cells with kinases are sensitive to GemC and AraC.	96
Figure 3-4 Cells with kinases show reduced growth in presence of GemC.	98
Figure 3-5 Cells with hENT1 show same sensitivity to GemC and araC as cells without transporter.	100
Figure 3-6 Confirmation of presence of hENT1 in <i>S. pombe</i> strains by PCR.	102
Figure 3-7 Outline of the strategy used to construct a stable kinase/transporter <i>S. pombe</i> strain	104
Figure 3-8 Cloning mhENT1 into pFA6a-natMX6 vector.	107
Figure 3-8 (D) Sequence and reverse mutated hENT1	108
Figure 3-9A Integrate hENT1 into <i>S. pombe</i> genome	110
Figure 3-9B. PCR to check integration of hENT1	111
Figure 3-10A. Strains with WT hENT1/ kinase are highly sensitive to GemC and AraC	113
Figure 3-10B. Cells with the new transporter are sensitive to low concentrations of GemC and AraC.	114
Figure 3-11 Cells with kinases and transporter, hsdCK, MG70 (B) and dmdNK, MG81 (A) are highly sensitive to GemC	116
Figure 3-12A. Cells with transporter and kinases show reduced growth in rich YEL media	119
Figure 3-12B. Cells with transporter and kinases are elongated in rich media.	120
Figure 3-12C. dNTP levels are increased in cells with the transporter in YEL.	121
Figure 3-13 hsdCK cells are more sensitive to GemC in EMM media than in YEL media.	123
Figure 3-14 Intracellular GemC-TP levels are higher in EMM than in YEL and dNTPs pools decrease in presence of the drug.	125
Figure 3-15A. dNs rescued effect of GemC in EMM.	127
Figure 3-15B. GemC-TP levels are decreased by addition of dNs in EMM (1) and dNTPs levels increase in the presence of dNs (2).	128
Figure 3-16 rad3ts checkpoint defective mutants were affected by YEL.	131
Figure 4-1A Pre-screen of the library	138
Figure 4-1B. Example of library screen plates.	138

Figure 4-2 Integration of transporter and kinase into the Bioneer deletion library by crosses.	140
Figure 4-3A. Selection of GemC concentrations for the sub library analysis by analysing distribution of treated mutants.	166
Figure 4-3B. Illustration of the three methods used to quantify mutants` growth	167
Figure 4-4A. Growth curves of selected library mutants	169
Figure 4-4B. Using Microsoft Excel to apply the trapezoid rule to determine the area under the curve.	170
Figure 4-4C Ranking of mutants by the total area under curves at 150nM of GemC.	171
Figure 4-4D. Sensitivity of mutants at 250nM.	172
Figure 4-4E. Ranking at 250nM is biased by slow growth phenotype.	173
Figure 4-4F. Ranking mutants by relative growth defect	175
Figure 4-5 Determining R values for the different mutants.	178
Figure 4-5	179
Figure 4-5	180
Figure 4-6 A screenshot of a biological network as generated by Cytoscape.	212
Figure 4-7A. Actin like protein arp8 is sensitive to GemC and AraC.	217
Figure 4-7B. swi3 is sensitive to GemC and AraC.	217
Figure 5-1 rad50Δ and mre11-D65N mutants without transporter were more sensitive to GemC than the WT	223
Figure 5-2A. MRN mutants with hsdCK/hENT1 were sensitive to GemC and AraC.	225
Figure 5-2B. MRN mutants with dmdNK/hENT1 were sensitive to GemC and AraC.	226
Figure 5-3 top1 deletion does not increase resistance of rad50Δ mutant to GemC in cells with hsdCK/hENT1	228
Figure 5-4 NER mutants with hsdCK/hENT1 are sensitive to GemC and AraC.	231
Figure 5-5 Sensitivity of BER mutants with hsdCK/hENT1 to GemC and AraC	233
Figure 5-6 MMR mutants with hsdCK/hENT1 are resistant to GemC and not to AraC.	236
Figure 5-7 PRR mutants with hsdCK/hENT1 are resistant to GemC and AraC	238
Figure 5-8A. Different sensitivity of mre11-D65N double mutants with hsdCK/hENT1 to GemC.	241
Figure 5-8B. Different sensitivity of rad50 double mutants with hsdCK/hENT1 to GemC.	242
Figure 5-9 Sensitivity of NER double mutants with hsdCK/hENT1 to GemC	244
Figure 5-10 Possible repair mechanisms that may respond to GemC and AraC (NA) induced DNA damage as suggested by analysis of DNA repair mutants.	259
Figure 6-1 General strategy used to construct “FLP-nick” strains.	262
Figure 6-2 Construction of pAW8NdeI_FLP H305L_HA plasmids.	264
Figure 6-3 Mutating NdeI site into the FLP H305L gene by site directed mutagenesis.	266
Figure 6-4A. Cloning of H305L gene into cre lox pAW8ENdeI_OSS_cgfp plasmid.	269
Figure 6-4B. Cloning of H305L gene into cre lox pAW8ENdeI_CyGFP plasmids.	270
Figure 6-5 Replacing CyEGFP tag by HA tag in pAW8ENdeI_FLP H305L_CyEGFP plasmids.	272
Figure 6-6A. Integration of FLP H305L_HA into S. pombe	274
Figure 6-6B. PCR checking integration of FLP H305L_HA into S. pombe	275
Figure 6-7 Integration of the 3HA tag into “FLP” strains.	277
Figure 6-8 Detection of FLP expression by western blot	279
Figure 6-9 General strategy used to integrate FRT target into S. pombe.	281
Figure 6-10 Cloning of the FRT sequence into pFA6a-natMX6.	283
Figure 6-11 Integrate FRT sequence into the S. pombe genome.	285
Figure 6-12 FLP-nick MRN defective strains are resistant to FLP induction with uracil during continuous exposure.	287
Figure 6-13 FLP-nick MRN defective strains show a reduced growth after 30 minutes incubation with uracil	289

Figure 7-1 Incorporated GemC levels are higher in mre11-D65N mutants than WT _____ 299

Figure 7-2 Schematic representation of possible repair of GemC-induced damage by NER and BER.
_____ 304

Figure 7-3 Schematic representation of possible enhancement of drug toxicity by MMR. _____ 306

List of tables

<i>Table 1-1 List of human DNA checkpoint and repair proteins and their yeast homologues.</i>	8
<i>Table 2-1 List of strains.</i>	68
<i>Table 2-2 List of primers used for PCRs.</i>	74
<i>Table 2-3 List of primers used for sequencing.</i>	75
<i>Table 2-4 List of used plasmids.</i>	75
<i>Table 4-1 Library mutants scored as “sensitive” in at least one of three independent screens and analysed under sub library.</i>	142
<i>Table 4-2 Ranking mutants by growth rate values</i>	181
<i>Table 4-3 Ranking mutants by endpoint.</i>	183
<i>Table 4-4. List of mutants ranked by sensitivity to 50nM of GemC.</i>	186
<i>Table 4-5 List of over-represented biological processes GOs in the highly sensitive mutants of the sub library.</i>	208
<i>Table 4-6 List of sequence orphan genes that were sensitive to GemC.</i>	219
<i>Table 5-1 Representation of phenotype growth of different mutants.</i>	255
<i>Table 5-2 Summary sensitivity of MRN mutants.</i>	256
<i>Table 5-3 Summary sensitivity of different repair mutants</i>	257
<i>Table 5-4 Summary sensitivity of different double mutants</i>	258

1 INTRODUCTION

1.1 Genome instability and cancer

1.1.1 Cancer as a genetic disease

Worldwide cancer incidence in 2008 was estimated to be over 12 million new cases, with cancer related mortality estimated to be over 7 million (data from GLOBOCAN, 2008). In the UK, 157,275 people died from cancer in 2010 (data available from cancer research UK). Most frequent cancers included breast, prostate and lung cancers. Understanding the mechanisms underlying the development of cancer is a key step in the battle against the disease, and countless efforts have been put in research to resolve the mystery behind the disorder.

More than a century ago, German physiologist Johannes Mueller suggested that cancer results from abnormal cellular growth (Haggard, 1938). This breakthrough suggestion constituted the basis for cancer research aiming to understand differences between cancer and normal cells, and research has shown that cancer is formed of a mass of cells resulting from uncontrolled proliferation. Six “hallmarks of cancer” have been proposed (Hanahan and Weinberg, 2000) that lead to cancer development. These are self-sufficiency in growth signals, insensitivity to growth-inhibitory signals, evasion of programmed cell death, limitless replicative potential, sustained angiogenesis, and tissue invasion. A common enabling feature of the six hallmarks is **genomic instability**, which was proposed as the corner stone of cancer development (Negrini *et al.*, 2010, Hanahan and Weinberg, 2011). Whether in cancers resulting from inherited mutations or sporadic cancers, genomic instability is at the basis of the loss of control of regulation and uncontrolled cell growth leading to the development of cancer. Genomic instability arises from increased mutation rates caused by loss of function of genes involved in preserving the genome integrity. The “two hit-hypothesis” proposed by Knudson (1971) suggested that at least two mutations are required for cancer to develop. Mutations can affect a series of genes, and defects in genes which play a role in DNA repair and checkpoint response have been identified to play a role in cancer predisposition (Eyfjord and Bodvarsdottir, 2005; Negrini *et al.*, 2010). Amongst identified tumour suppressors (genes that protect cells from developing into cancer) are the breast cancer susceptibility genes BRCA1 and BRCA2 which, if mutated, increase predisposition to breast cancer development and play a role in double strand break repair. Another well studied

tumour suppressor is the TP53 gene (which encodes the apoptosis inducer protein p53). Cells with non functional p53 escape apoptosis and are predisposed to cancer (Negrini *et al.* 2010).

Genomic instability can result in a range of genetic alterations and can be divided into two major groups: gross chromosomal rearrangements (that can be detected by microscopy) and small DNA mutations (substitutions, deletions and insertions) which can be detected by sequencing. Chromosomal rearrangement is associated amongst others with failure in the mitotic spindle checkpoint, preventing cells to achieve accurate chromosome segregation, but can also result from telomere fusion resulting from inaccurate repair of double strand breaks near telomere regions (Muraki *et al.*, 2012). Mutations within DNA sequences are mainly associated with replication errors and incorrect or failing DNA repair (Aguilera and Gomez-Gonzales, 2008).

1.1.2 The cell cycle and DNA replication

1.1.2.1 The cell cycle

The cell cycle is essential for all living organisms, required for their reproduction and development. It is divided into four phases, Mitosis (M), Synthesis (S) and two gap phases (G1 and G2). Non dividing cells, such as nerve cells, are kept in a quiescent phase known as G0. G1 and G2 represent separation of phases at which cells prepare to enter M and S phases. During G1, the phase following Mitosis, cells start to synthesise proteins through transcription and translation (Houtgraaf *et al.*, 2006), G1 ends with the beginning of S phase. G2 follows S phase and cells continue to grow in preparation for M phase. S phase represents the crucial step of the cell cycle where DNA is duplicated into two identical copies through a process known as **DNA replication**, during which each strand of DNA serves as a template to synthesize a new strand. Mitosis is the phase of the cell cycle, during which chromosomes are segregated equally to two cells, before restarting the cell cycle.

Progression of the cell cycle is tightly regulated by mechanisms collectively referred to as “**checkpoints**”. The role of the DNA damage checkpoints is to coordinate events during the cell cycle by ensuring that no damage is left unrepaired before progression to the next phase of the cycle. DNA replication and the DNA damage checkpoint machinery that controls replication accuracy will be discussed in next paragraphs.

1.1.2.2 DNA replication

DNA replication requires multiple proteins that are highly conserved and tightly regulated to coordinate the process. Replication starts by the recognition of the replication origin, after which the DNA is unwound to allow formation and passage of the replicative complex. Each strand of the DNA is copied and one strand of DNA gives rise to two identical copies.

A. Initiation

Replication is initiated at specific sequences known as origins of replication. A well characterised origin of replication is the *S. cerevisiae* autonomously replicating sequence (ARS). ARS contain a consensus sequence (ARS consensus sequence, ACS) which serves as the binding site of subsequent replication proteins. ACS is highly conserved and plays an important role in replication initiation and a single mutation in the ACS region can lead to loss of ARS function (Newlon, 1996). The *S. cerevisiae* ACS was identified as a ~15 bp A-T rich sequence [5'-(A/T)TTTAT(A/G)TTT(A/T)-3']. In other eukaryotes however, ARS consensus are not well characterised. In humans, one well studied origin of replication is the Dihydrofolate reductase (DHFR) locus, located at the 3' end of the DHFR coding gene (Zhu *et al.*, 2005). Three main DHFR replication sites (ori- β , ori- β' and ori- γ) were identified and are located within 11-kb, in the Hamster, (Kobayashi *et al.*, 1998) and 55-kb, in humans, (Zhu *et al.*, 2005) in the spacer region between DHFR and the following coding sequence.

The highly conserved origin recognition complex (ORC, *Figure 1-1*), composed of 6 subunits (orc1-orc6), is also essential for the initiation of DNA replication, as it recognises the origin sequence and acts as a platform to recruit other proteins that form the pre-replicative complex (pre-RC). ORC proteins display ATPase activities, but only the ATP binding activity of orc1 is required for the binding of the complex to the origin sequence (Sclafani and Holzen, 2007). Other than ORC proteins, the pre-RC is composed of proteins of the minichromosome maintenance (MCM) complex (Mcm2-7) and cell division cycle proteins Cdc6 and Cdt1, required for the assembly of the pre-RC (Mendez and Stillman, 2003). Cdc6 also possesses ATPase activity, interacts with ORC and increases the binding specificity of the complex by inhibiting non-specific DNA binding. Cdt1 interacts with Cdc6 and facilitates the loading of the MCM complex (Zhu *et al.*, 2005; Nasheuer *et al.*, 2006). The MCM

complex exerts the helicase activity required to start replication by unwinding the double helix DNA and allowing loading of replicative proteins. Studies in various models (Nasheuer *et al.*, 2006) suggest that Mcm4, Mcm6 and Mcm7 exert the helicase activity whereas Mcm2, Mcm3 and Mcm5 possess a regulatory function.

The pre-RC is activated by phosphorylation of Cdc6 by cyclin dependent kinases (CDKs) and phosphorylation of the MCM complex by the Dbf4 dependent kinase Cdc7 (also called DDK). Phosphorylation is followed by loading of other proteins required for the formation of the replication initiation complex. These include Mcm10, Cdc45 and the GINS (Go-Ichi-Ni-San, named after Japanese numbers 5-1-2-3) complex. Mcm10 interacts with all subunits of the MCM complex and is required for the recruitment of both Cdc45 and replication protein A (RPA). In addition, Mcm10 interacts with polymerase α and stimulates the polymerase α /primase complex in yeast (Zhu *et al.*, 2005; Nasheuer *et al.*, 2006). Cdc45 interacts with Orc2 but also with pre-RC, Mcm2 and elongation proteins (which are involved in synthesis and elongation of the newly synthesised DNA strand), RPA and polymerases α and ϵ which suggests that Cdc45 plays a role as a “communicator” between initiation and elongation of the replication fork (Mendez and Stillman, 2003; Zhu *et al.*, 2005; Nasheuer *et al.*, 2006). GINS is composed of Sld5 (Synthetic Lethal with Dpb11, yeast orthologue of the human TopBP1, Nasheuer *et al.*, 2006), and the proteins Psf1 (Partner with Sld5), Psf2 and Psf3. GINS associates with replication origins in a Cdc45-dependent manner and is required for the initiation of replication. The complex also forms a ring like structure, which suggests that it acts as a clamp for other replication factors (Zhu *et al.*, 2005).

Following loading of initiation proteins, DNA double helices are unwound to allow replication proteins to process. The unwinding of DNA is a prerequisite for replication and is carried out by proteins known as replicative helicases. Helicases break hydrogen bonds between two entwined single DNA strands, a reaction that requires ATP hydrolysis (van Brabant *et al.*, 2000; Li and Araki, 2013). Several helicases might act in a eukaryotic cell to unwind DNA for replication. The MCM 4-6-7 complex exhibits a weak helicase activity *in vitro* (Nasheuer *et al.*, 2006) however this activity is enhanced in presence of Cdc45 and GINS (Li and Araki, 2013). The MCM helicase is located on the template strand at the 5' end and moves to 3' end (Nasheuer *et al.*, 2006, Li and Araki, 2013). Other replicative helicases

include the yeast Dna2 helicase and mouse helicase B. Mutants defective in either helicase could not carry out replication (Waga and Stillman, 1998).

B. DNA synthesis

DNA synthesis starts with the loading of the polymerase α /primase (pol α /primase) complex, also known as “primosome assembly” (Waga and Stillman, 1998). The RNA polymerase primase initiates replication by synthesising a short RNA primer of around 10 nucleotides, which is then extended by pol α to a length of ~40 nucleotides, forming a RNA-DNA primer that serves as a template for other polymerases (Waga and Stillman, 1998; Nasheuer *et al.*, 2006). RPA interacts with pol α /primase and stimulates its activity (Waga and Stillman, 1998). In addition, RPA facilitates the loading of replication factor C (RFC) and proliferating cell nuclear antigen (PCNA), which are required for the extension of the synthesised DNA. RFC is required for the loading of PCNA, which forms a ring-like structure around the DNA. PCNA is loaded at the junction between the primer and the template and acts as a platform for polymerase δ and polymerase ϵ , but also stimulates pol α and δ activities (Waga and Stillman, 1998). PCNA also shows binding activity to FEN-1 and DNA ligase 1, required for processing (FEN-1) and sealing (ligase 1) of synthesised DNA. Polymerases δ and ϵ are loaded in replacement of pol α /primase, which dissociates after primer synthesis, and extend the nascent DNA strands. DNA extension of one strand (5'-3') gives a long unique fragment referred to as “leading strand” whereas the other strand (3'-5') is synthesised through a fragmented strand, known as “lagging strand”, formed of Okazaki fragments, which are a result of the polar specificity of polymerases (5'-3' synthesis). Okazaki fragments are short DNA sequences (120-300bp), (Nasheuer *et al.*, 2006) and are processed by FEN-1 exo/endonuclease, which removes the RNA primer attached to the fragments and allows DNA ligase 1 to seal the gap by linking the 3'-hydroxyl and 5'-phosphate ends. Other than FEN-1, Dna2 helicase, which also possesses a nuclease activity, also processes Okazaki fragments by removing long flaps that are not removed by FEN-1 nuclease activity (Nasheuer *et al.* 2006). Possible replication errors (insertion, deletion or substitution) are corrected by the proofreading activity of Pol δ polymerase (Nasheuer *et al.*, 2006).

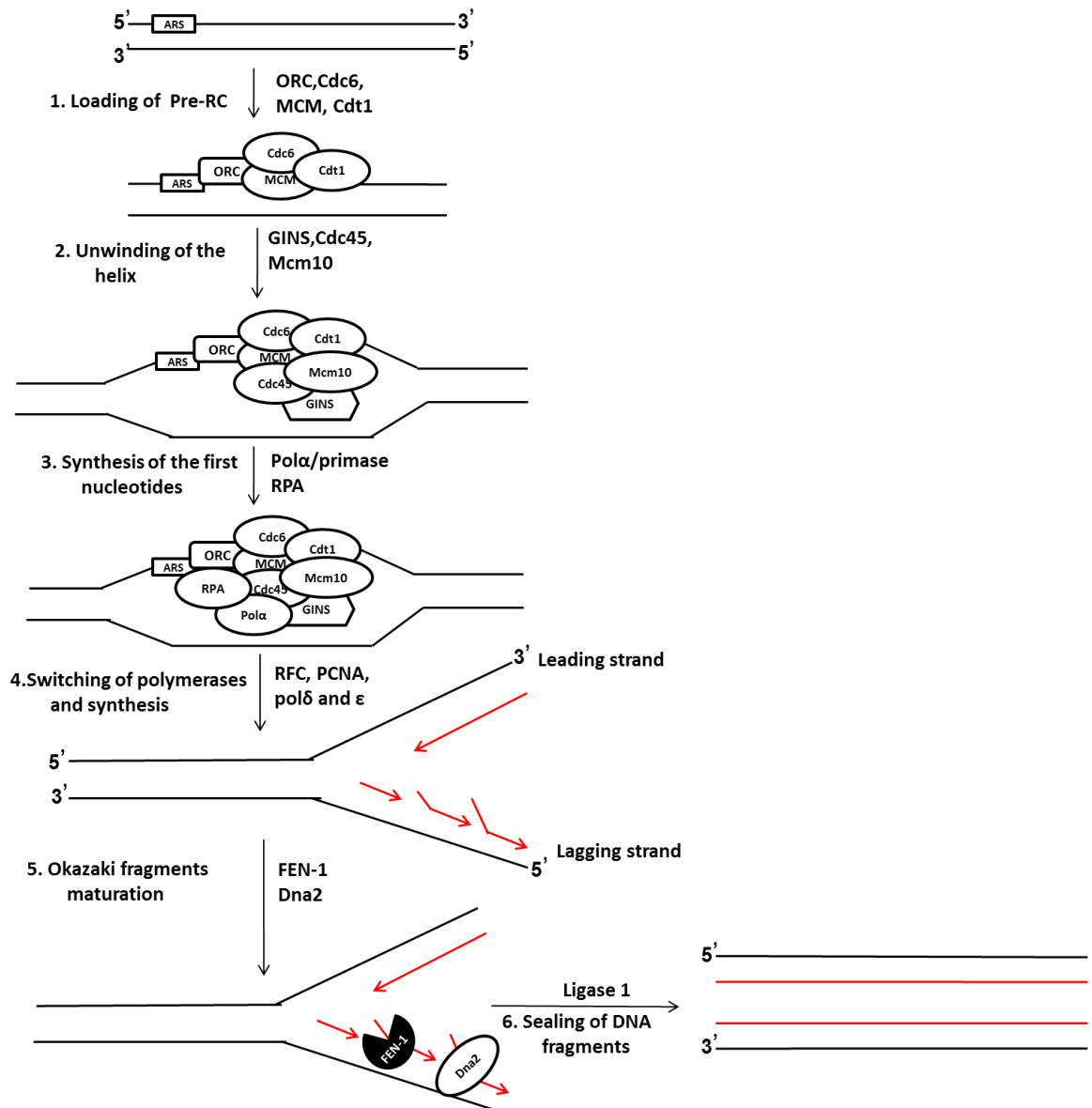


Figure 1-1 Schematic representation of the replication process. Several proteins and protein complexes work together to ensure that the process is accurately carried out. The origin of replication sequence is recognised by the ORC multiprotein complex, which binds the DNA and recruits other proteins. Cdc6 and Cdt1 act as a platform for the loading of the MCM complex, which exerts its helicase activity to unwind the double helix and to allow the replisome to move along the DNA. Cdc45 and GINS are loaded and activate MCM helicases while Mcm10 regulates the helicases (Sclafani and Holzen, 2007). RPA is then loaded and facilitates the recruitment of PCNA but also stimulates pol α /primase activity, which synthesises a RNA-DNA primer, a key step in replication initiation. The PCNA clamp is loaded and associates with polymerases pol δ and pol ϵ , which proceed to the synthesis of the DNA, and the strands are sealed by ligase 1. Okazaki fragments (small red arrows) are processed by FEN-1 and Dna2 to allow ligase 1 to close the nick between the fragments.

1.1.3 DNA damage checkpoint and repair pathways

Due to high homology between yeast (*S. pombe* and *S. cerevisiae*) and human genes, studies often describe homologues between the different organisms. *Table 1-1* shows conversion of different human DNA checkpoint and repair genes and their yeast homologues.

Table 1-1 List of human DNA checkpoint and repair proteins and their yeast homologues. Source: Friedberg, 2006; Lambert and Carr, 2005

human	<i>S. pombe</i>	<i>S. cerevisiae</i>	Function
_	apn1	APN1	AP endonuclease
APE1	apn2	APN2	AP endonuclease
ATM	tel1	TEL1	checkpoint
ATR	rad3	MEC1	checkpoint
ATRIP	rad26	DDC2	checkpoint
BRCA1	crb2	RAD9	Checkpoint and HR
BRCA2	_	_	HR
CHK1	chk1 (Rad27)	CHK1	kinase (checkpoint)
CHK2	cds1	RAD53	kinase (checkpoint)
CSA	_	RAD28	damage recognition in TC-NER
CSB	rhp26	RAD26	damage recognition in TC-NER
CtIP	ctp1	SAE2	MRN complex collaborator
ERCC1-XPF	swi10-rad16	RAD10-RAD1	5' incision in NER
EXO1	exo1	EXO1	exonuclease
FEN1	rad2	RAD27	nuclease
HR23A	rhp23	RAD23	binds distorted DNA in NER
HUS1	hus1	MEC3	DNA damage sensor (9-1-1 complex)
Ku70/Ku80	pku70/pku80	YKU70/YKU80	DNA end binding in NHEJ
LIG1	cdc17	CDC9	ligase, DNA joining
LIG3	_	_	DNA ligase
MLH1-PMS2	mlh1	PMS1	dimer, active in MMR
MRE11	mre11 (rad32)	MRE11	exo and endo nuclease (MRN complex)
MSH2	msh2/Swi8	MSH2	mismatch and loop recognition
MPG (MAG)	mag1	MAG	DNA glycosylase
MSH3	msh3/Swi4	MSH3	loop recognition
MSH6	msh6	MSH6	mismatch recognition
NBS1	nbs1	XRS2	MRN complex
NTH1	nth1	NTG1,NTG2	Glycosylase in removal of damaged pyrimidine
OGG1	_	OGG1	Glycosylase in removal of 8-oxoG
PARP1	_	_	Poly (ADP-ribose) polymerase
PCNA	pcn1	POL30	clamp, protein loading platform
POLk	_	_	PRR polymerase
POLI/POL η	eso1	_	RAD30
RAD1	rad1	RAD17	DNA damage sensor (9-1-1 complex)
RAD17	rad17	RAD24	DNA damage sensor
RAD18	rhp18	RAD18	PCNA ubiquitination in PRR
RAD50	rad50	RAD50	MRN complex
RAD51	rhp51	RAD51	formation of filament in HR
RAD52	rad22	RAD52	accessory protein for HR
RAD9	rad9	DDC1	DNA damage sensor (9-1-1 complex)
REV1	rev1	REV1	PRR polymerase
REV3	rev3	REV3	pol ζ subunit (PRR)
REV7	rev7	REV7	pol ζ subunit (PRR)
RFC	rfc1	CDC44	Replication factor
RPA	ssb	RFA	binds ssDNA
TDG	thp1	_	Glycosylase in removal of T andU
TDP1	tdp1	TDP1	exonuclease in removal of Top1-DNA complexes
TopBP1	rad4/cut5	DBP1	Checkpoint binds to Rad9
UNG1	ung1	UNG1	Glycosylase in removal of Uracil
XPA	rhp14	RAD14	Binds DNA in NER
XPB	rrcc3sp	RAD25	helicase TFIIH subunit, active in NER
XPC	rhp41/rhp42	RAD4	binds distorted DNA in NER
XPD	rad5	RAD3	helicase TFIIH subunit, active in NER
XPG	rad13	RAD2	3' incision in NER
XRCC1	_	_	Accessory factor for LIG3

1.1.3.1 DNA damage

Although some mutations are inherited, the majority of cancer-inducing mutations result from various damage to the genome. These mutations might affect genes involved in cellular growth regulation and lead to uncontrolled growth and tumour development (Schar, 2001). Exogenous damage can be the result of ionising radiation, ultraviolet light, and DNA damaging chemicals, whereas endogenous damage arises from metabolic intermediates such as reactive oxygen species and products of lipid peroxidation (Hoeijmakers, 2001; Houtgraaf *et al.*, 2006). Moreover, spontaneous errors can occur following physiological processes such as DNA replication (Schofield and Hsieh, 2003). Damage to the DNA includes lesions that affect individual bases as well as damage to the DNA backbone.

Base damage is mainly caused by endogenous processes such as hydrolysis, oxidation, alkylation, and deamination of bases, but can also arise as a result of exposure to ionising radiation, UV and chemicals (Huffman *et al.*, 2005; Houtgraaf *et al.*, 2006).

Depurination (removal of the base from the sugar) of purine nucleotides by hydrolysis results in the formation of abasic sites, which, if unrepaired, can lead to mutations during replication whereas deamination of bases such as the formation of uracil from cytidine can lead to changes in the coding sequence (Scharer, 2003). Other forms of base damage include O⁶-methylguanine, thymine glycol and 8-oxoguanine resulting from the action of reactive oxygen species (ROS) and ionising radiation, which mainly exert their cytotoxic effects by blocking replication and transcription (Scharer, 2003; Sancar *et al.*, 2004).

Additionally, lesions referred to as bulky adducts interfere with base pairing and cause distortion of the DNA double helix, disrupting transcription and replication. Bulky adducts are mainly caused by UV light and include pyrimidine dimers (T-T and T-C) (Hoeijmakers, 2001; Scharer, 2003).

DNA mismatches include base mispairs (e.g. A/C or G/T) and insertion/deletion loops (IDLs) that are mistakenly introduced by polymerases during replication or arise following formation of heteroduplex DNA during homologous recombination (Schofield and Hsieh, 2003).

Other DNA lesions that impede cellular functions are breaks that affect one or both strands of the DNA.

Single strand breaks are divided into two groups: direct breaks, which arise from attacks to the DNA, for example attack of deoxyribose by free radicals, and indirect breaks, which result from intermediate steps in other cellular mechanisms, for example breaks caused by excision repair pathways (Caldecott, 2003).

Double strand breaks (DSBs) constitute the most harmful lesion to DNA, as a single DSB can lead to cell death (Pardo *et al.*, 2009). They arise mainly from ionizing radiation, but can also result from attack of chemicals such as anti-cancer drugs (e.g: etoposide). Additionally, DSBs can arise after a collision of the replication fork with a single strand break leading to a one sided DSB (Khanna and Jackson, 2001) and they are also intermediates in physiological processes. For example, DSBs are produced by endonucleases during mating-type switching in *S.cerevisiae*, for homologous recombination and chromosome segregation during meiosis in eukaryotes, and in V(D)J (Variable Diverse Joining) recombination, for production of immunoglobulins (Pardo *et al.*, 2009). Failure to repair a DSB can lead to chromosome rearrangement and chromosome loss.

DNA crosslinks (ICLs) include DNA interstrand crosslinks, which occur between two bases of opposite strands of DNA, and DNA intra crosslinks that occur on the same DNA strand. ICLs are mainly caused by crosslinking agents such as nitrogen mustards (Noll *et al.*, 2006) and are highly toxic as they block DNA replication and transcription (Scharer, 2003).

1.1.3.2 DNA damage checkpoints

DNA damage checkpoint proteins detect damage into the DNA and delay cell cycle progression until the mistake is corrected or apoptosis is induced. Proteins of the DNA damage checkpoint machinery can be classified into three major components: sensors, which recognise the damage, transducers, which ensure correct interaction between different proteins, and effectors, that activate subsequent mechanisms. In addition, proteins classified as “mediators” act in combination with transducers. These proteins act in coordination to interrupt cycle progression at G1/S, intra-S or G2/M phases. At the core of the checkpoint are *ataxia telangiectesia* mutated (ATM, Tel1 in *S. pombe*) and ATM and Rad3 related (ATR, Rad3 in *S. pombe*), two kinases that are classified as “checkpoint transducers” and act by phosphorylating several proteins. ATM^{Tel1} responds mainly to DSBs, whereas ATR^{Rad3} is involved in response to single stranded DNA (ssDNA) at stalled replication forks (Eyfjord and

Bodvarsdottir, 2005). ATM is the gene that is mutated in *ataxia telangiectasia (A-T)*, a human condition characterised by neurodegeneration, immunodeficiency and cancer predisposition. Mutations in ATR are associated with an A-T like condition known as Seckel syndrome (Sancar *et al.*, 2004; Eyfjord and Bodvarsdottir, 2005).

The checkpoint pathway involves many proteins that interact with each other. In regards to this project, which examines cellular response to nucleoside analogue (NA), mainly incorporated during DNA replication (explained in paragraph 1.2.2), I will give a general overview of the intra-S checkpoint pathway which is activated following slowed or arrested replication.

ATR/Chk1 checkpoint

One kind of damage following replication fork stalling is the formation of ssDNA, which results from the action of MCM helicases that continue to unwind the DNA (Branzei and Foiani, 2005), and which constitutes a signal for the checkpoint. The first sensor of ssDNA is the RPA protein, which coats the single stranded DNA to form a complex that initiates the subsequent checkpoint response (*Figure 1-2*). In human, RPA-coated ssDNA recruits ATR via ATR interacting protein (ATRIP) which recognises the RPA-bound ssDNA. ATR-ATRIP associates with the 9-1-1 (Rad9- Rad1- Hus1) complex and its loader Rad17 (Branzei and Foiani, 2005; Stracker *et al.*, 2009). The 9-1-1 complex then acts in a clamp-like manner encircling the DNA and recruits topoisomerase II binding protein (TopBP1). The resulting protein complex activates ATR (Reinhardt and Yaffe, 2009). Along with “mediator” proteins (for example the breast cancer gene BRCA1 and p53 binding protein 53BP1), activated ATR mediates subsequent reactions by phosphorylating the checkpoint effector kinase Chk1, which in turn phosphorylates Cdc25A of the Cdc25 phosphatase family (Cdc25A, B and C) and marks the Cdc25A for degradation (Stracker *et al.*, 2009; Reinhardt and Yaffe 2009). Inactivation of Cdc25 leads to cell cycle arrest whereas unphosphorylated Cdc25 promotes progression of the cycle (Houtgraaf *et al.*, 2006). In *S. pombe*, however the checkpoint during replication is carried out by Cds1 kinase (human Chk2) (Lindsay *et al.*, 1998) while *S. pombe* Chk1 acts in G2 phase (Walworth and Bernards, 1996).

ATM/Chk2 checkpoint

In response to double strand breaks that might form for example when replication forks encounter a single stranded DNA or a nick, (Pardo *et al.*, 2009), ATM is recruited to the site by the MRN (Mre11-Rad50-Nbs1) complex, a sensor for DSBs (Lambert and Carr, 2005; Williams *et al.*, 2010) (*Figure 1-2*). Some evidence of the role of the MRN complex in recognising DSBs (reviewed by Jiri and Jiri, 2007) includes the rapid assembly of Nbs1 at DSB, the requirement of Nbs1 for the recruitment of ATM and the specific recruitment of the MRN complex to DSBs and not to other type of DNA lesion. ATM is activated by phosphorylation or acetylation (Reinhardt and Yaffe, 2009) and activated ATM phosphorylates histone H2Ax close to the lesion, which in turn recruits the MDC1 mediator. MDC1 is also phosphorylated by ATM and recruits an E3 ubiquitin ligase RNF8 and, together with Ubc13, mediates histone H2Ax ubiquitination, a step followed by recruitment of BRCA and 53BP1. ATM then phosphorylates the effector kinase Chk2, which, similarly to Chk1, acts on Cdc25A to inhibit cycle progression (Reinhardt and Yaffe, 2009).

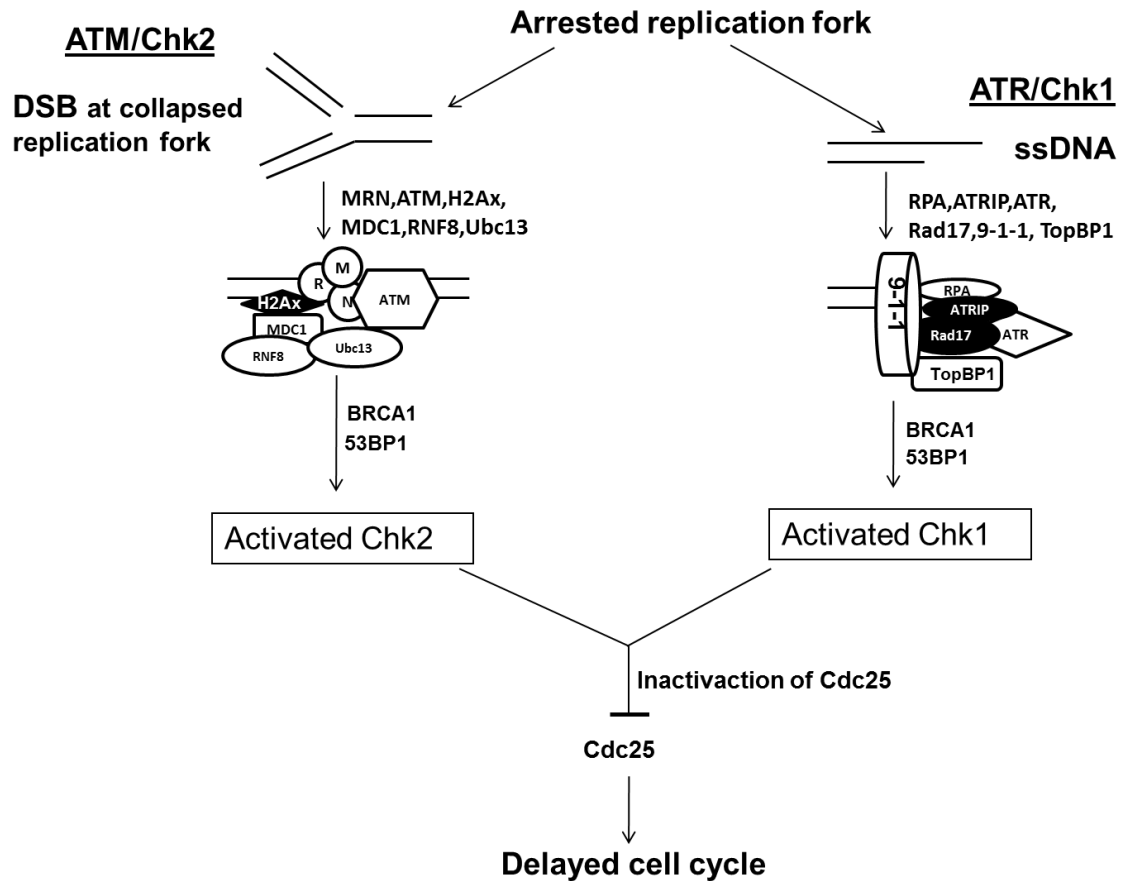


Figure 1-2 Simplified representation of the DNA damage checkpoint response following replication fork arrest. Coordinated proteins act together to halt cell cycle progression and allow repair of the replication damage and restart of the replication fork, or trigger programmed cell death. Two parallel pathways can be activated in the S-phase checkpoint depending on the damage. DSBs are recognised by the MRN complex, which recruits the ATM kinase, which, with the help of mediator proteins, phosphorylates Chk2, a step that leads to inactivation of Cdc25 and cell cycle arrest. ssDNA is coated by RPA protein and recognised by Rad17 and the 9-1-1 complex. ATR is recruited and leads to activation of Chk1, which, similarly to Chk2, inactivates Cdc25.

1.1.3.3 DNA repair pathways

To deal with errors that may lead to genomic instability, organisms have evolved a complex network of mechanisms that aim to protect the genome. These mechanisms, known as DNA repair pathways, play a major role by preventing errors to be passed on to daughter cells following cell division. However, in regard to cancer, repair mechanisms play two roles. Failure in one or more repair proteins may lead to the development of cancer or cancer prone syndromes (detailed in paragraph 1.1.3.5), whereas their high repair efficiency plays a role in resistance to DNA damaging cancer drugs (paragraphs 1.2.1.3 and 1.2.2.3). As cancer cells are often defective in DNA repair genes, it is important to understand repair mechanisms in order to improve cancer therapy.

The human genome is constantly threatened by internal and external hazards causing a variety of damage to the genome. Repair mechanisms are divided into pathways depending on the type of the lesion (illustrated in Figure 1-3). The main DNA repair pathways in mammalian cells are: (1) Nucleotide-excision repair (NER), for the repair of bulky adducts (mainly caused by UV light) and intrastrand crosslinks; (2) Base-excision repair (BER), which mainly deals with lesions that affect single bases; (3) Mismatch repair (MMR), for the repair of mismatches and insertion/deletions occurring during replication, and (4) Double strand break repair (homologous recombination, HR and non homologous end joining, NHEJ) that repairs DNA double strand breaks (Fleck, 2004; Houtgraaf *et al.*, 2006).

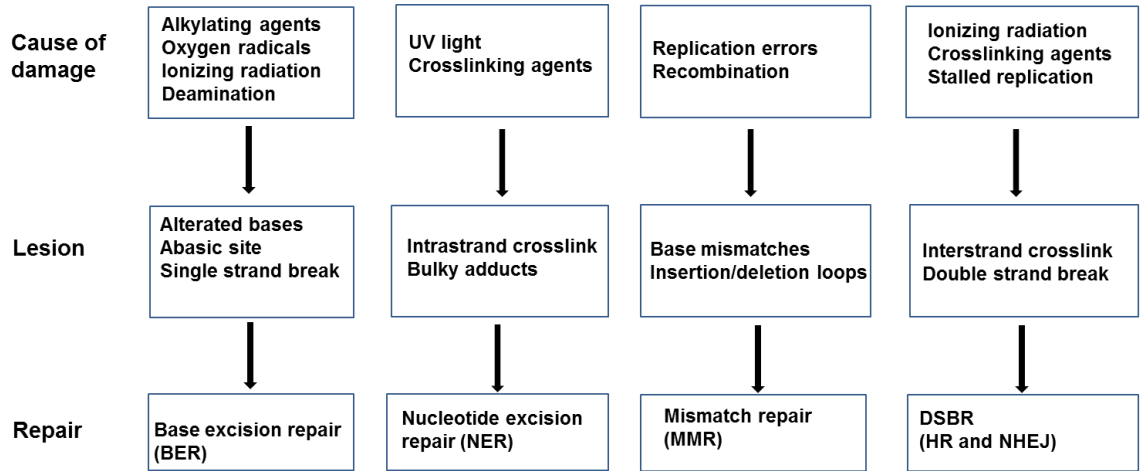


Figure 1-3 Simplified chart showing main DNA lesions and repair pathways. DNA damage resulting from various attacks and physiological errors are repaired by distinct mechanisms depending on the nature of the lesion (Fleck, 2004; Houtgraaf *et al*, 2006).

1.1.3.3.1 Excision repair pathways

Excision repair pathways include BER, NER and MMR. The principle of these repair mechanisms is based on a “cut – and – patch” mechanism in which the damaged sequence is removed and new DNA is synthesised and ligated to fill in the gap.

A. Base excision repair (BER)

Base lesions constitute the most common error that occurs in the genome, therefore BER is one of the most important guardians of the genome and plays a major role in preventing mutations. The BER pathway is divided into two sub-pathways depending on the number of bases that are removed during the repair process: the short patch pathway removes a single base, whereas the long patch pathway removes 2-10 bases (Sancar *et al.*, 2004). The pathway choice is determined by the type of glycosylases that remove the damaged base. Monofunctional glycosylases (only possessing the glycosylase activity) initiate both short and long patch pathways whereas, bifunctional glycosylases (possessing both glycosylase and lyase activities) mainly act in the short patch pathway (Krokan *et al.*, 2000). Glycosylic activity is involved in removal of the damaged base from the sugar while the lyase activity processes the abasic site (Krokan *et al.*, 2000).

At the initiation step (*Figure 1-4*), glycosylases recognise and remove the damaged base by cleaving the bond between the base and the sugar, leaving an abasic site (AP site) in the genome. Several glycosylases have been identified in human, which differ by their substrate specificity. Monofunctional glycosylases include Uracil DNA glycosylases (UDG), UNG1 (mitochondrial) and UNG2 (nuclear), (Krokan *et al.*, 2000) and Thymine/Uracil glycosylase (TDG) which recognise uracil-related damage and Methylpurine DNA glycosylase (MPG), which recognises alkylated purines. Bifunctional glycosylases include 8-oxoG DNA glycosylase (OGG1) which deals with oxydised purines and NTH1 which removes oxydised pyrimidines (Krokan *et al.*, 2000; Memisoglu and Samson, 2000; Scharer, 2003). An *S. pombe nth1Δ* mutant is sensitive to the alkylating agent methyl methanesulphonate (MMS) which methylates bases, suggesting a role of the gene in BER (Osman *et al.*, 2003).

The resulting AP site is processed by either the endonuclease activity of AP endonucleases (APE1) or the lyase activity carried out by some of the bifunctional glycosylases like Nth1 (Osman *et al.*, 2003; Boiteux and Guillet, 2004). APE1

cleaves the phosphodiester bond at 5' of the AP site and releases the abasic sugar-phosphate (review, Kanamitsu and Ikeda, 2010). In *S. pombe*, two genes, *apn1* and *apn2*, are thought to encode proteins which exert the APE1 activity (Fleck, 2004). The role of *S. pombe apn2* in BER was confirmed by the observation that *apn2*Δ mutants were highly sensitive to MMS when compared to WT (Alseth *et al.*, 2004). On the other hand *apn1* deleted mutants showed a similar survival in response to MMS as WT cells (Osman *et al.*, 2003) suggesting that the gene does not play a major role in BER (or that *apn1*'s role is redundant) in *S. pombe*.

In higher eukaryotes, after the incision step, poly(AD-ribose) polymerase (PARP) and polynucleotide kinase (PNK) protect and clean the ends in preparation for DNA synthesis (Hoeijmakers, 2001).

In the short patch BER pathway, the gap is filled by polβ and ligation is carried out by the XRCC1-ligase 3 complex (Hoeijmakers, 2001), while in the long patch BER pathway, the synthesis is carried out by polβ and polδ/ε, which are loaded by the proliferating cell nuclear antigen, PCNA. In the long patch, Polδ/ε synthesises DNA after removal of a flap of 2-8 nucleotides (Krokan *et al.*, 2000; Kelley *et al.*, 2003) by FEN-1 endonuclease. DNA ligase 1 then seals the gap (Scharer, 2003). In *S. pombe*, the FEN1-activity is carried out by the homologous Rad2 nuclease. Deletion of *rad2* leads to high sensitivity of cells to MMS confirming the role of *rad2* in BER (Kunz and Fleck, 2001). In addition, Rad2 exerts a 5' →3' exonuclease activity to remove damaged base in UV-damaged DNA endonuclease dependent excision (UVER), a NER-independent repair pathway of UV induced DNA damage in *S. pombe* (Fleck, 2004).

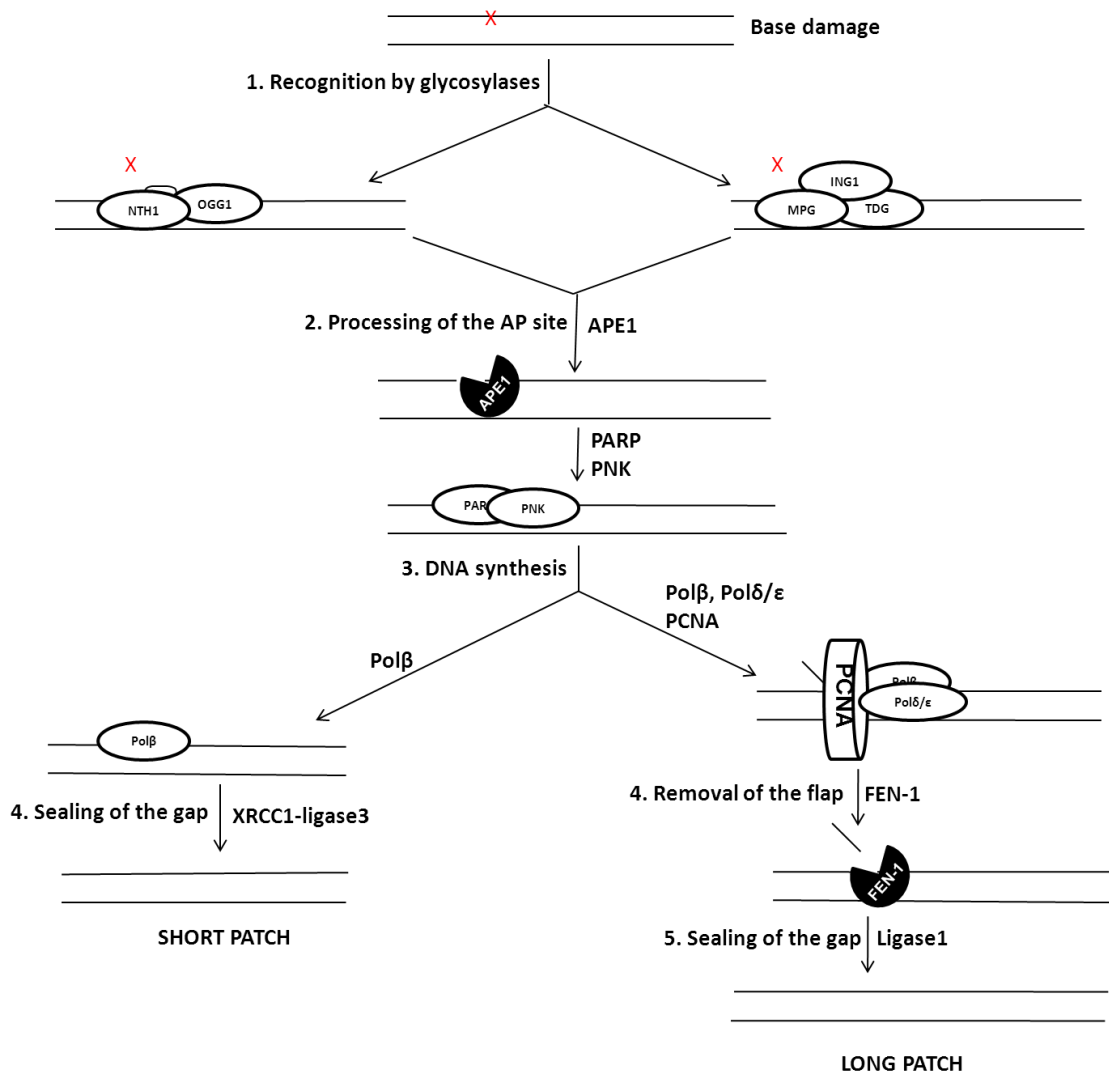


Figure 1-4 Schematic representation of the two subpathways of base excision repair. Damaged bases are removed by glycosylases, leaving an abasic site, which is processed by APE1 nuclease in presence of PARP and PNK. In short patch repair, Pol β synthesises a new strand that is sealed by ligase ligase3 in complex with XRCC1. In the long patch sub-pathway, DNA synthesis is carried out by Pol β and pol δ/ϵ loaded by PCNA. FEN-1 endonuclease removes the DNA flap and ligase 1 seals the gap.

B. Nucleotide excision repair (NER)

The NER pathway acts to repair bulky adducts that are mainly caused by UV light and lead to distortion of the DNA helix (Hoeijmakers, 2001; Fleck, 2004). These lesions include cyclobutane pyrimidine dimers (CPDs) and 6-4 photoproducts (6-4 PPs). Several proteins are involved in human NER and the cooperative binding of the proteins and the kinetic proofreading activities enhance the specificity of the mechanism (Sancar *et al.*, 2004).

Two sub-pathways (*Figure 1-5*) which differ in the initiation step, act in NER. Global genome NER (GG-NER) deals with lesions that can occur anywhere in the genome, while transcription-coupled repair (TCR) deals with damage affecting transcription.

In TCR, NER is initiated by the blockage of RNA polymerase II (RNA polII) followed by the binding to DNA of two TCR specific proteins, CSA and CSB, which remove RNA polII to make the lesion available for repair.

GG-NER is initiated by the specific protein complex XPC-hHR23B, which scans the genome for lesions, then binds the damage to recruit subsequent NER proteins (Hoeijmakers, 2001; Houtgraaf *et al.*, 2006). XPC is believed to be the initiator of GG-NER that recognises the lesion (Naegeli and Sugasawa, 2011). Studies of the *S. cerevisiae* XPC homologue Rad4 have shown that the protein localises at the 3' of the lesion (Fuss and Tainer, 2011; Naegeli and Sugasawa, 2011). In *S. pombe* the activity of XPC in detection of UV induced damage is accomplished by two XPC homologues Rhp41 and Rhp42. When treated with UV, an *rhp41 rhp42* double mutant showed high sensitivity (similar to other NER mutants) compared to *rhp41* and *rhp42* single mutants suggesting that the two homologues have redundant roles in NER dependent UV damage repair (Marti *et al.*, 2003). TFIIH and its helicase subunits, XPB and XPD, are recruited and proceed to the initial unwinding of the DNA. Replication protein A (RPA) and the NER protein XPA are then recruited. XPA facilitates the assembly of subsequent proteins, whereas RPA stabilises the proteins complex (de Laat *et al.*, 1999). It has been shown in mammalian cells that XPA is required for lesion recognition as well as for the formation of the pre-incision complex (Shuck *et al.*, 2008). Similarly, the *S. pombe* XPA homologue, Rhp14, has been demonstrated to play an important role in NER as *rhp14*Δ mutants showed high sensitivity to UV treatment and purified *rhp14* protein showed DNA binding activity, emphasising its role in the recognition of DNA lesions (Hohl *et al.*, 2001). The damaged strand is then incised at both ends of the damage. The 3' incision is carried

out by XPG endonuclease and the 5' DNA end is incised by ERCC1-XPF. The incision releases a 25-32 nucleotides fragment and leaves a gap which is filled by Pol δ/ϵ and ligated by ligase 1 (de Laat *et al.*, 1999; Scharer, 2003; Sancar *et al.*, 2004). In *S. pombe*, the incision is carried out by XPF/ERCC1 homologue Rad16/Swi10 and XPG homologue, Rad13. The homology of Swi10 to the human ERCC1 was shown by a rescue of *swi10* deficiency by ERCC1 expression in fission yeast (Rodel *et al.*, 1997).

Additionally to the core NER proteins mentioned above, other proteins have been shown to play a role in NER repair, these include the damaged-DNA binding protein DDB which may act as an accessory factor (Scharer, 2003; Fleck, 2004).

Moreover, an additional NER independent UV damage repair pathway has been identified in *S. pombe*. Termed UV-damaged DNA endonuclease-dependent excision repair (UVER), the pathway depends on a *S. pombe* specific gene, *uve1* and acts in a redundant way with NER to repair UV induced damage. Indeed, UVER was identified following observations that, *S. pombe* NER defective cells are less sensitive to UV than *S. cerevisiae* and that the mutants can still repair UV induced lesions (Fleck, 2004).

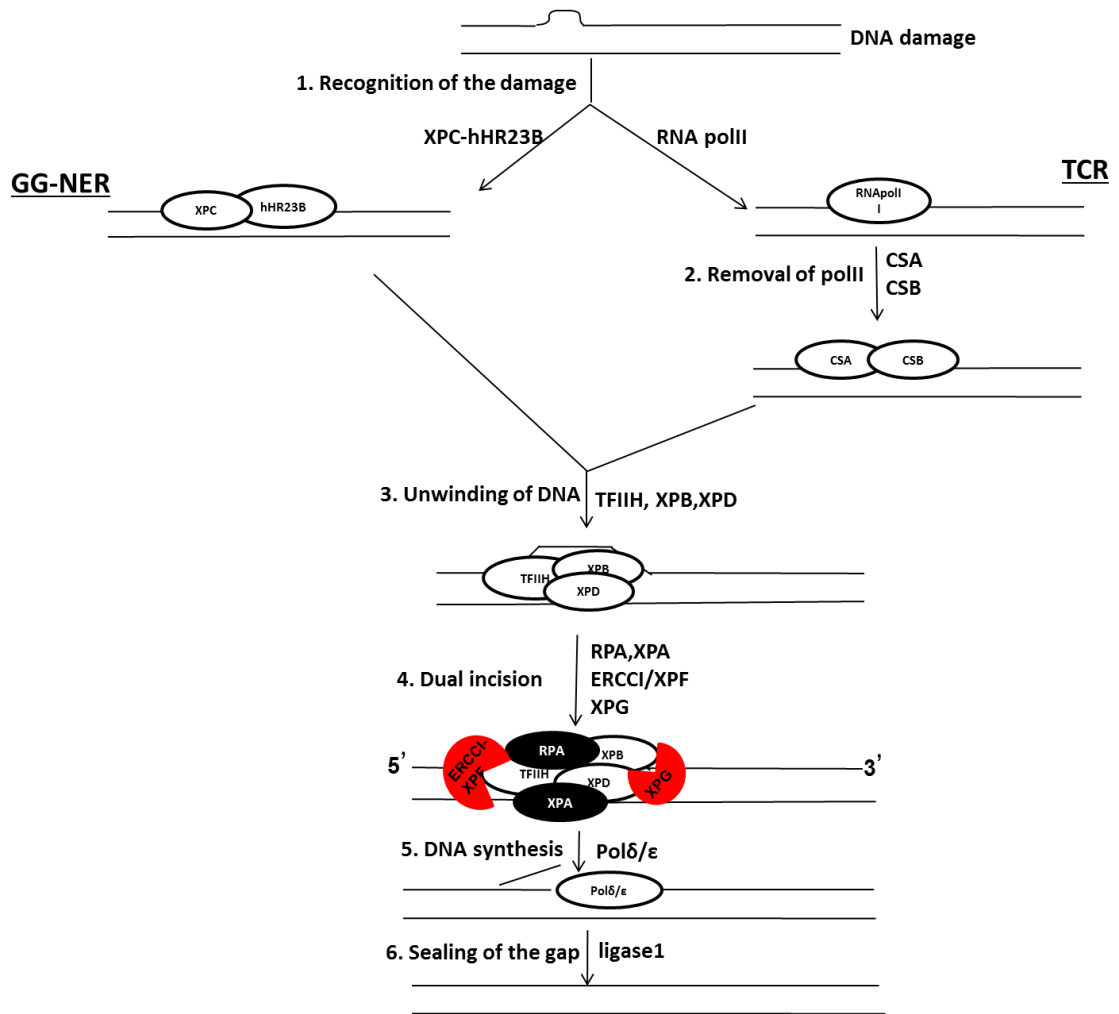


Figure 1-5 Schematic representation of the nucleotide excision repair pathway. In Global Genome repair (GG-NER), the genome is scanned for the damage by the XPC-hHR23B complex, which binds the damaged site and recruits subsequent repair proteins. In Transcription Coupled Repair (TCR), the response is triggered by the blockage of RNA polymerase II, which acts as a signal for recruitment of TCR specific proteins CSA and CSB, which in turn act by removing RNA polII, making the lesion accessible for repair. TFIIH and its helicase subunits XPB and XPD partially unwind DNA at the site of lesion and allow loading of RPA, which stabilises the protein complex, and XPA, which assembles subsequent proteins. Dual incision (5' incision by ERCC1/XPF and 3' incision by XPG) is then carried out on the damaged strand. The gap is filled by polymerases δ and ϵ and sealed by ligase 1.

C. Mismatch Repair (MMR)

MMR repairs DNA base mismatches and insertion/deletion loops (IDLs) that occur mainly during DNA replication, but can also result from strand exchange during homologous recombination (Schofield and Hsieh, 2003). Although DNA replication is highly accurate and the proofreading activity of polymerases contributes to the small error rate of the process, nucleotides are still introduced that result in mismatched base pairs. *In vitro* studies suggest that the error rate of replication polymerases is about 1 in 10^8 (Loeb and Loeb, 2000). MMR acts by recognising and removing the erroneous nucleotides and contributes to the accuracy of DNA replication and integrity of the genome.

Repair is initiated by recognition of the error by the *E. coli* MutS homologues, the MSH proteins. MSH2 forms a heterodimer with MSH6 for the recognition of single base mispairs and with MSH3 for the recognition of IDLs (Figure 1-6). In *S. pombe*, Msh homologues Msh2 (also known as Swi8) and Msh6 recognise single mismatches whereas the complex of Msh2 and Msh3 (or Swi4) recognises IDLs.

The prime challenge of the MMR is to recognise which base is incorrect. In *E. coli*, strand discrimination between the template and the newly synthesised strand (most likely to contain the mis-incorporated base) is facilitated by methylation of specific DNA sequences. Because MMR occurs after replication but before the methylation process, it uses the methylated parental strand for discrimination (Scharer, 2003). The methylation, however, is not used in eukaryotic cells where it is thought that strand discrimination is made possible by nicks or gaps that occur in the newly synthesised strand (Fleck, 2004).

The bacterial MutL homologue, MLH1-PMS2 (post-meiotic segregation protein) heterodimer is then recruited to coordinate interactions between the recognition complex and other proteins. The PCNA clamp is loaded on the site of the lesion and leads to the formation of a loop with the mismatch on its top. PCNA is thought to increase specificity and efficiency of MMR by increasing the specificity of MSH proteins for the mismatch (Schofield and Hsieh, 2003). Prior to synthesis of a new strand, the mismatch is removed by the endonuclease FEN-1 (Hoeijmakers, 2001) and exonuclease 1 (Exo1, Schofield and Hsieh, 2003). The role of *S. pombe* Exo1 in MMR was shown by its interaction with mismatch recognition protein Msh2 (Tishkoff *et al.*, 1997) and in *S. cerevisiae*, *exo1* defective mutants exhibited mildly increased mutation rates (Schofield and Hsieh, 2003) suggesting the role of this

nuclease in MMR. In addition, *exo1* defective mice mutants were defective in MMR (Wei *et al.*, 2003). RPA stabilises the DNA ends, DNA polymerase Pol α fills the gap and DNA ligase 1 seals the DNA (Peltomaki, 2003; Scharer, 2003, Schofield and Hsieh 2003; Stojic *et al.*, 2004; Seifert and Reichrath, 2006; Houtgraaf *et al.*, 2006).

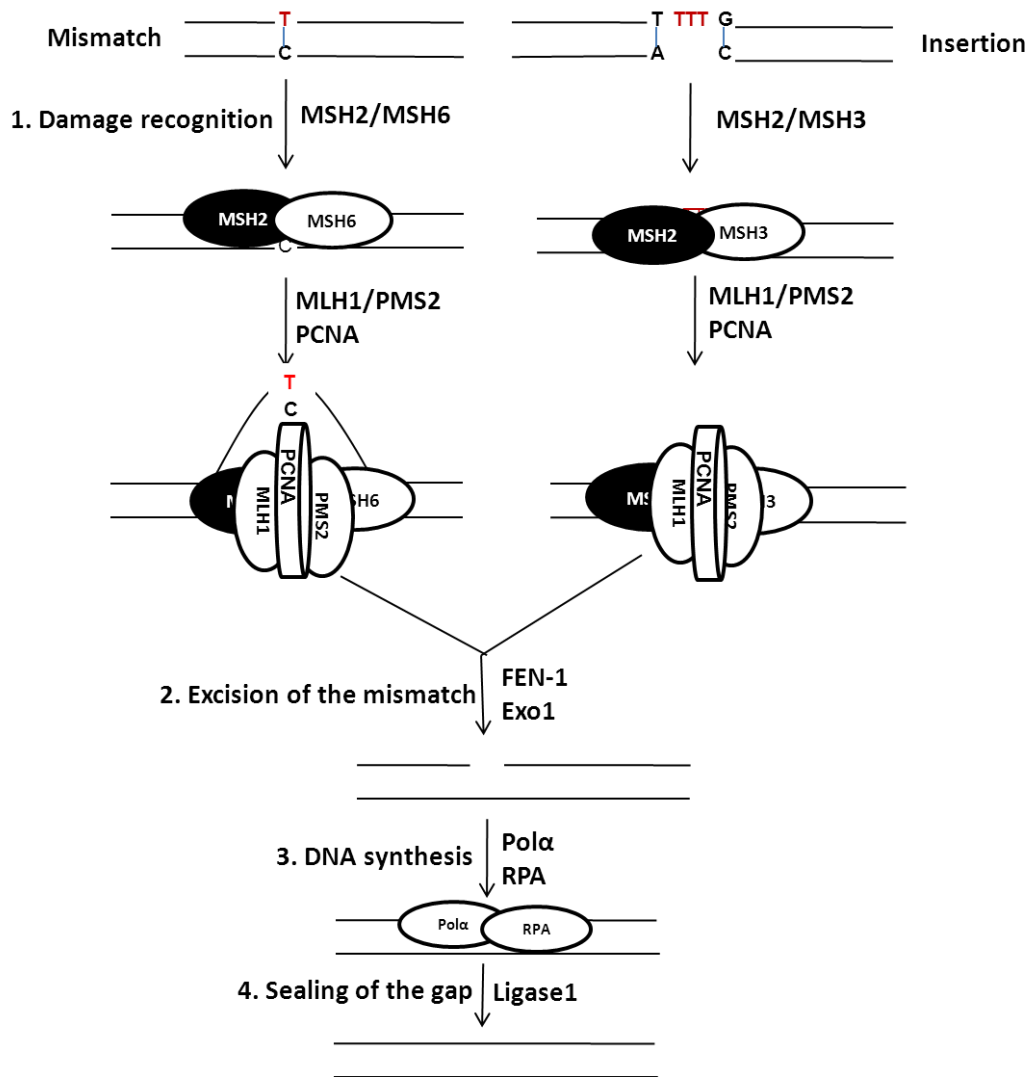


Figure 1-6 Schematic representation of the mismatch repair pathway. Recognition heterodimers (MSH2/MSH6 for single mismatch and MSH2/MSH3 for IDLs) recognise the mismatches and recruit MLH1/PMS2, which coordinates the interactions between the recognition proteins and other repair proteins. A loop with the mismatch on the top is formed following loading of PCNA. The mismatch is then degraded by nucleases leaving a gap which is filled by pol α and sealed by ligase 1.

1.1.3.3.2 DNA Strand Break Repair

Single strand breaks, which are often intermediates of physiological processes such as excision repair, are repaired by BER as described above. DSBs constitute the most harmful damage to the DNA and one DSB can lead to cell death if not repaired (Pardo *et al.*, 2009). It is therefore crucial that these lesions are rapidly repaired to prevent genomic instabilities and cell death. Two main pathways have evolved to protect the genome against DSBs: **homologous recombination** (HR) pathways require an intact DNA strand as template to copy the missing information and repair the break, while **non homologous end joining** (NHEJ) joins the broken ends without requirement for a template. In addition, three other mechanisms have been linked to repair of DSBs. These are microhomology-mediated end joining (MMEJ), break induced replication (BIR) and single strand annealing (SSA). MMEJ joins broken ends in an error-prone manner by aligning short (5-25bp) homologous sequences with the broken ends before joining (McVey and Lee, 2008). BIR acts to repair double strand break when only one end of the break can be used for the repair. The DSB end invades homologous sequence and induces a replication of the chromosome template (Pardo *et al.*, 2009). SSA repairs DSBs where no homologous template has been found, and DNA resection of long stretched of homology generated long single stranded DSBs. These single stranded ends are annealed together and the break is repaired (Pardo *et al.*, 2009). In this paragraph, I will discuss the two main repair mechanisms NHEJ and HR.

A. Non Homologous End Joining (NHEJ)

The NHEJ repair pathway is the simpler of the two DSBR pathways, as it joins broken DNA ends without the requirement of extended sequence homology. Additional to its role in DSBR, NHEJ is also involved in physiological processes such as V (D) J recombination and telomere maintenance (Karran, 2000; Pfeiffer *et al.*, 2000; Scharer, 2003; Pardo *et al.*, 2009). Additionally, the mechanism is thought to be involved in repair of DSBs resulting from the action of Top2 poisons (Malik *et al.*, 2006) which cause formation of DSBs by blocking the enzyme on the DNA (detailed in paragraph 1.2.1.2). Indeed, cells defective in NHEJ repair system show hypersensitivity to etoposide, an anticancer drug that targets Top2 (Malik *et al.*, 2006).

Due to the fact that NHEJ does not use a template for the repair of breaks, it is less accurate than HR, as it might lead to loss or insertion of nucleotides. In addition, because ligation of non compatible DNA ends is not efficient, NHEJ might need nucleases to process the DSB ends (Hoeijmakers, 2001; Pardo *et al.*, 2009), and DNA polymerases to fill the gap before ligation (Pardo *et al.*, 2009).

In the NHEJ repair pathway (*Figure 1-7A*), the lesion is recognised by the Ku70/Ku80 heterodimer, which binds to both ends of a DSB in a ring like structure (Wyman and Kanaar, 2006) and recruits the catalytic subunit of the DNA-dependent protein kinase (DNA-PKcs) to the site of lesion. The precise role of the DNA-PKcs in NHEJ is not clear in humans (Wyman and Kanaar 2006) and DNA-PKcs has not been yet identified in *S. pombe* (Manolis *et al.*, 2001). The Ku/DNA-PKcs complex protects broken ends from nucleases and recruits the ligase 4-XRCC4 heterodimer, which seals the ends together. XRCC4 is believed to be required for the stability of ligase 4 and it stimulates its activity (Karran, 2000; Sancar *et al.*, 2004; Wyman and Kanaar, 2006). In addition, it has been shown that nucleases are needed for processing of the damaged ends. *S. cerevisiae* Exo1 nuclease and Tdp1 phosphodiesterase have been shown to have a role in improving the efficiency of NHEJ (Bahmed *et al.*, 2010; Bahmed *et al.*, 2011). A controversial role of the MRN (Mre11, Rad50, Nbs1) complex in NHEJ is still under investigation (Lamarche *et al.*, 2010). Analysis of HeLa cells (Huang and Dynan, 2002) has shown that the MRN complex is required to restore efficient end joining in presence of other NHEJ components, suggesting that the protein complex is required by the pathway in mammalian cells. Similarly, studies in *S. cerevisiae* have suggested that MRX (Mre11, Rad50, Xrs2^{Nbs1}) stimulates Dnl4-Lif1 (ligase 4-XRCC4 equivalent) in DNA end joining (Symington, 2002). In *S. pombe*, however, Manolis *et al.* (2001) have shown that components of the MRN complex (Rad50 and Mre11) are not required for NHEJ repair while Reis *et al* (2012) have suggested that *S. pombe* MRN complex is required for NHEJ.

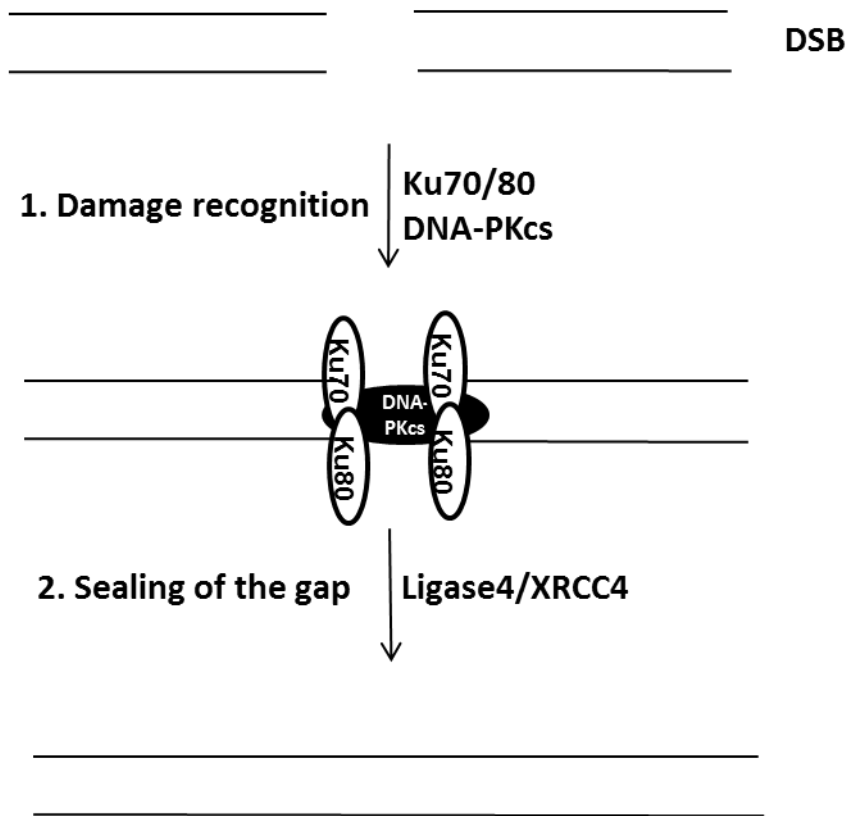


Figure 1-7A Overview of the double strand break repair by the Non Homologous End Joining pathway. Broken ends are recognised by the Ku70/80 complex, which recruits DNA-PKcs. The complex Ku-DNA-PKcs protects the ends which are then rejoined by the ligase 4.

B. Homologous recombination (HR)

Homologous recombination, a process conserved in all organisms, is a mechanism by which a molecule of DNA serves as a template for the synthesis of another DNA strand. HR refers to the exchange occurring between two DNA sequences with perfect or nearly perfect homology, whereas non-homologous recombination refers to exchange between two DNA molecules with little or no homology (Symington, 2002). Other than its role in repair, the mechanism is also important in meiotic recombination.

Homologous recombination is mostly carried out by proteins encoded by genes of the RAD52 epistasis group that have initially been identified in *S. cerevisiae*. These genes include *mre11*, *rad50*, *nbs1*, *rad51/52/54/55/57/59* and *rdh54* (Symington, 2002). HR repairs the DNA with very high accuracy, as the presence of homologous sequence prevents loss of genetic information.

Three steps characterize HR (*Figure 1-7B*): (a) processing of DNA strands at broken ends to create single strand overhang, (b) strand invasion and exchange, and (c) resolution of recombination intermediates.

The processing of DNA ends is carried out by nucleases which digest the 5' DNA end leaving a 3' single strand tail that searches for homology and invades the template sequence. The involvement of the MRN complex in the first step of HR has been confirmed by several studies in eukaryotes (Symington, 2002, Pardo *et al.*, 2009). However, the Mre11 exonuclease of the MRN complex exerts a 3'-5' activity, while the nucleolytic degradation required for DSBs resection is a 5'-3' activity, suggesting that the exonuclease activity of the protein is not required for the processing step of HR. This was supported by observations that Mre11 nuclease deficient mutants are not defective in HR (Scharer, 2003). The requirement of end processing is, however, a crucial step of the process and other protein candidates have been suggested that contribute to the degradation of the 5' end. *S. cerevisiae*, Sae2 (human CtIP, *S. pombe* Ctp1) has been shown to contribute to DSB ends resection (Clerici *et al.*, 2005) and this role has been confirmed both in mammalian cells (Sartori *et al.*, 2007) and *S. pombe* (Limbo *et al.*, 2007). In addition, *Xenopus laevis* (Liao *et al.*, 2008) and *S. cerevisiae* (Zhu *et al.*, 2008) DNA2 helicases have also shown a role in processing 5'→3' DNA strand ends. The role of DNA2 helicase in DNA end resection was also shown in human (Nimonkar *et al.*, 2011, Peng *et al.*, 2012). Another exonuclease, Exo1, has been proposed as a candidate for the

processing step in HR (Li and Heyer, 2008; Pardo *et al.*, 2009). Indeed, studies in *S. cerevisiae* have shown that *exo1* deleted mutants showed a reduced resection activity that was synergistic to the absence of *mre11*, suggesting that Exo1 nuclease activity requires the presence of Mre11 nuclease (Llorente and Symington, 2004). Similarly, resection activity of human Exo1 was also stimulated by the MRN complex (Nimonkar *et al.*, 2011). Additionally, analysis of *S. pombe* proteins have shown that Mre11 nuclease activity and Ctp1 are essential for removal of both MRN and Ku complexes from the DNA (Langerak *et al.*, 2011), which in turn allows DNA processing by Exo1 nuclease and initiation of HR.

The core reaction of HR is the **search for homology and strand invasion**. This step is carried out by the 3' end tail coated by Rad51 recombinase, the central protein of the strand invasion process (Scharer, 2003). Prior to binding of Rad51, ssDNA is bound by RPA, which has affinity for ssDNA (Li and Heyer, 2008).

The RPA-ssDNA complex is subsequently bound by BRCA2 in mammalian cells, (Pardo *et al.*, 2009) or Rad52 in *S. cerevisiae*, (Symington, 2002; Pardo *et al.*, 2009), which facilitates the loading of Rad51 by removing RPA, and by Rad54, which mediates the homology search by Rad51 and the pairing to the homologous sequence. The complex then forms a filament which scans the genome searching for homologous sequences (Pardo *et al.*, 2009).

In mammals, Rad51 has 5 paralogs (Rad51B, Rad51C, Rad51D, Xrcc2 and Xrcc3) (Li and Heyer 2008; Pardo *et al.*, 2009) the precise role of each of these proteins in HR, however is not clear.

The Rad51 filament invades the homologous sequence and anneals to the complementary strand, forming a hybrid or heteroduplex DNA and the displacement loop (D-loop, *Figure 1-7B*). The 3' end of the invading filament then acts as a primer for the synthesis of the template DNA, which allows recovery of the lost sequence.

In HR, the D-loop is **processed** by two pathways: synthesis dependent strand annealing (SDSA) or double strand break repair (DSBR).

In SDSA (*Figure 1-7B*), DNA strands are annealed in a process that always leads to a non-crossover product and involves a series of mechanistic steps. After invasion of the 3' ends, the invading strand is extended, removed from the template and returned to the broken DNA to allow annealing (Paques and Haber, 1999). In yeast, several proteins are thought to be involved in SDSA, these include Rad52 and Rad1-10 endonucleases (Li and Heyer, 2008; Pardo *et al.*, 2009).

In DSBR, an intermediate cross-like structure known as a double Holliday Junction (dHJ) is formed by the returning invading strand (*Figure 1-7B*). Resolution of the dHJ is carried out by resolvases, which cut symmetrically to the junction sites and leave DNA nicks that are then ligated (Svendsen and Harper, 2010), leading to the formation of a crossover or a noncrossover product depending on the site at which the resolvases cut (Pardo *et al.*, 2009). In human, resolvase activity is carried out by GEN1 (*S. cerevisiae* Yen1, Ip *et al.*, 2008).

A double HJ can also be dissolved by other pathways. The dissolution of dHJ is carried out by a combined action of the human BLM (gene mutated in Bloom's syndrome) helicase (*S. pombe* Rqh1, *S. cerevisiae*, Sgs1) and topoisomerase III (TopIII), and leads to a non crossover product. The BLM gene encodes a helicase of the RecQ helicases family, which are homologous to the *E. coli* helicase RecQ. Other than Bloom syndrome, deficiency in WRN and RTS, RecQ helicases is associated with Werner's syndrome and Rothmund-Thomson syndromes respectively, characterised by genomic instability and predisposition to cancer development (Nakayama, 2002). The helicase promotes branch migration of the HJ (Karow *et al.*, 2000) by unwinding the DNA, giving a loop-like structure resolved by the incision of one strand by TopIII (Krogh and Symington, 2004; Pardo *et al.*, 2009; Svendsen and Harper, 2010).

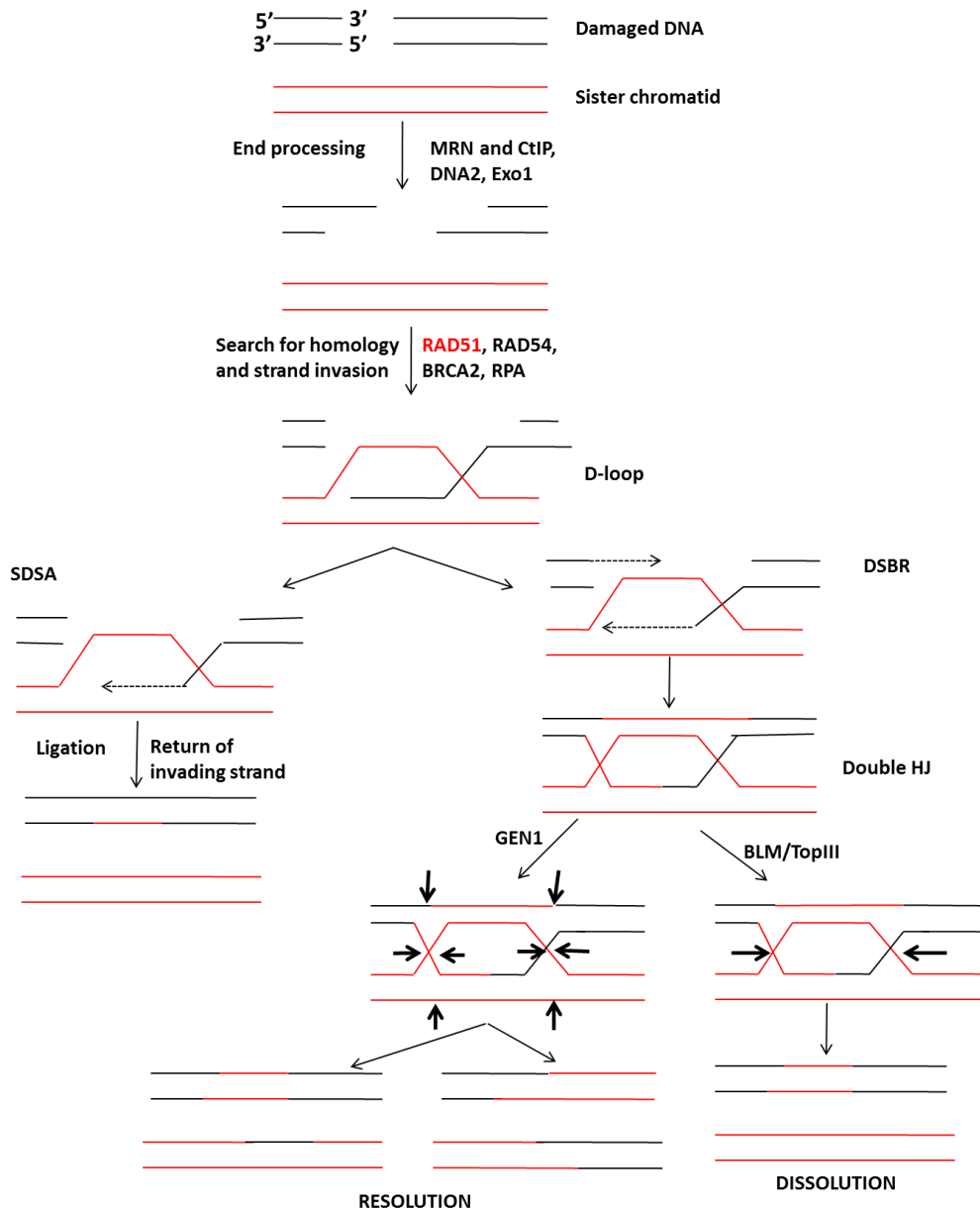


Figure 1-7B Repair of DSBs by Homologous Recombination. The 5' ends of the break are processed by nucleases after which the Rad51 coated 3' end searches for homology and invades a sister chromatid (or homologous chromosome) with homologous sequence to form the D-loop. The D-loop structure can be resolved by either of two pathways, synthesis dependent strand annealing (SDSA) or double strand break repair (DSBR) involving a double Holliday Junction (dHJ). In SDSA, newly synthesised DNA is ligated after return of the invading strand and the process leads to a non crossover product. The HJ is either dissolved, giving a non crossover product, or resolved, leading to a crossover and a non crossover products.

C. The MRN-CtIP complex

The MRN (Mre11, Rad50 and NBS1), (*S. cerevisiae* MRX, Mre11, Rad50, Xrs2), complex is a highly conserved protein complex that plays a key role in repair of DSBs, but has also a role in other cellular processes such as DNA damage signalling, meiosis, and telomere maintenance (Lamarche *et al.*, 2010). The ability of the MRN complex to sense DSB makes it one of the most important protein complexes of living organisms, and several disorders have been associated with mutations in one or more MRN proteins. These include the cancer susceptible syndromes Nijmegen Breakage Syndrome (NBS), developed following mutations in *nbs1*, and ataxia telangiectasia-like disorder (ATLD) caused by mutations in *mre11*. Analysis of yeast MRN mutant suggested that the protein complex is involved in early stages of meiotic recombination. The function of the complex in meiotic recombination is attributed to its ability to remove the meiotic recombination initiator Spo11 (*S. pombe* Rec12) from DSB ends, which in turn initiates DNA ends resection required for recombination. Indeed, it has been shown in both *S. cerevisiae* (Symington, 2002) and *S. pombe* (Hartsuiker *et al.*, 2009a) that MRN deficient mutants are unable to remove Spo11^{Rec12} from the DNA. The removal of Spo11 is associated with the ability of the complex to process DNA ends through its nuclease Mre11, and its associated protein CtIP (Hartsuiker *et al.*, 2009a). The role of the MRN complex in telomere maintenance is evidenced by the presence of shortened telomeres in MRN-defective mutants (Paques and Haber, 1999). The complex also controls DSB checkpoint and damage signalling via its interaction with the checkpoint core kinases ATM and ATR (Williams *et al.*, 2010), and it has been shown that in *S. pombe*, Mre11 nuclease and CtIP^{Ctp1} (a sub-component of the MRN complex) regulate activation of the checkpoint effector kinase Chk1 by ATR^{Rad3} (Limbo *et al.*, 2011).

The MRN complex is composed of three proteins, Mre11 nuclease, Rad50 and NBS1 (Xrs2 in *S. cerevisiae*) which assemble as a hexamer formed of two units of each member (Figure 1-7C). The central protein of the complex is the Mre11 nuclease, which is bound to two Rad50 ATP-binding cassettes (ABC) domains, via their Mre11 binding sites and, to Nbs1 by its flexible “adapter”. Rad50 coiled coil and zinc hook domains complete the structure.

Rad50 is a ~150kDa protein containing two ABC domains that are juxtaposed to the Mre11 binding site at one end, and a zinc hook in the middle (zn hook), which allows dimerization and bridging of DNA by the complex (Williams *et al.*, 2010, Lamarche

et al., 2010). The two subunits are joined by a coiled coil domain referred to as the “flexible arms” of the complex, which allows interactions between distant DNA ends. The “DNA bridging” ability of rad50 is essential for the function of the MRN complex (Williams *et al.*, 2010).

Mre11 is a 83kDa highly conserved protein (Symington,2002), which exerts single-strand endonuclease as well as a double strand 3’-5’ exonuclease activities, but lacks 5’-3’ exonuclease activity. Mre11 is composed of a phosphodiesterase domain within which an Nbs1 binding site is located, and two DNA binding domains between which a Rad50 binding site is located. Mre11 is the core protein of the MRN complex and it has been shown that in absence of Mre11, Rad50 and Nbs1^{Xrs2} can’t interact in *S. cerevisiae* (Symington, 2002). Mre11 activities have been shown to be crucial in the processing of DSBs induced by DNA damaging agents, as well as DSBs with modified ends such as trapped top1 (Hartsuiker *et al.*, 2009b; Pardo *et al.*, 2009).

Nbs1 is a 95kDa protein formed of an FHA (Forkhead associated) domain and two BRCT (BRCA C Terminus) domains on its N terminus, and ATM and Mre11 binding sites on its C terminus. The binding properties of the FHA/BRCT domains allow the complex to recruit other proteins such as CtIP and ATM (Symington, 2002; Williams *et al.*, 2010).

CtIP, Ctp1 in *S. pombe* and Sae2 in *S. cerevisiae*, interacts with the MRN complex and collaborates with the complex in DSB repair (Limbo *et al.*, 2007). The precise mechanism by which the protein acts is, however, still under investigation. *In vitro* studies have suggested a role of *S. cerevisiae* Sae2 (CtIP homologues) in 5’-3’ exonuclease activity (Nicolette *et al.*, 2010) but this activity is not confirmed in other eukaryotes. Because, Mre11 lacks the 5’-3’ processing activity which is required for initiation of recombination, it is speculated that CtIP may carry out the essential 5’-3’ resection. Additional to its role in DSB repair, *S. pombe* Ctp1 has also been shown to play a role in meiotic HR (measured by a decrease in spore viability in *ctp1* deleted mutants, (Limbo *et al.*, 2007) and *ctp1* deleted mutants are defective in removal of DNA bound Rec12^{Sp011} (Hartsuiker *et al.*, 2009a) and top2 (Hartsuiker *et al.*, 2009b) from DNA, showing a role of the protein in resection of modified DNA ends.

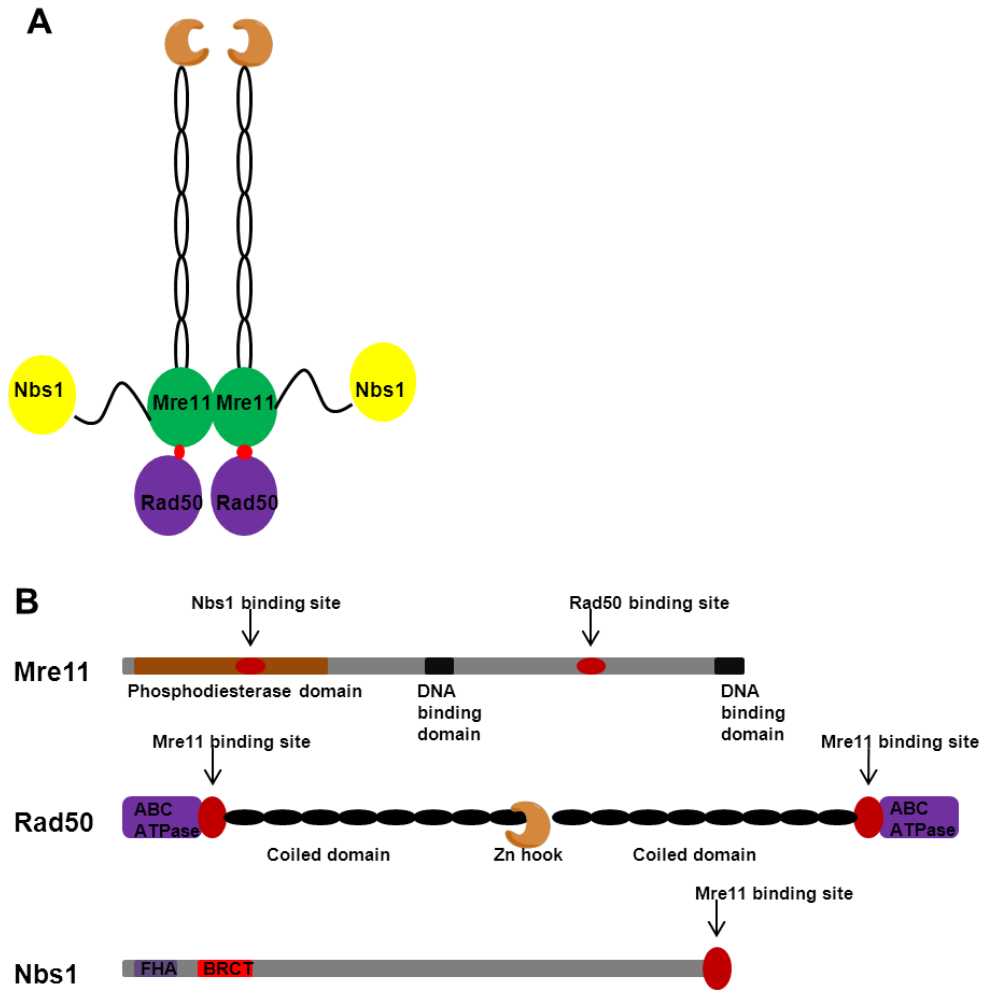


Figure 1-7C. MRN complex structure. (1) The complex is assembled as a hexamer composed of two units of each member. (2) Detailed domains of each component of the complex.

1.1.3.4 Post replication repair (PRR)

Post replication repair (PRR), also referred to as DNA damage tolerance (DDT), refer to a group of mechanisms that allow the replication fork to bypass an error (without repairing it) in the DNA and contribute to the survival of a cell with DNA damage. The processes might constitute a threat to the genome as mutations are not corrected, which can lead to genomic instability, but they are also advantageous in that they allow cell to replicate and survive an otherwise lethal damage. PRR is activated by ubiquitination of PCNA which triggers a switch between replication and PRR processes. Indeed, while PCNA acts to coordinate proteins during normal replication, it also serves as a start point of the PRR following replication fork stalling. When the replication fork encounters an obstacle, PCNA is ubiquitinated at Lys164 which in turn allows switch between replication and PRR (Chang and Cimprich, 2009)

Two pathways act in PRR: error prone Translesion synthesis (TLS) and error free template switching (Chang and Cimprich, 2009). The two mechanisms differ in their ability to “correct” the error, and the choice of the pathway is determined by postranslational modifications of PCNA (Chang and Cimprich, 2009; Waters *et al.*, 2009). In *S. cerevisiae*, monoubiquitination of PCNA by the Rad18/Rad6 complex leads to error prone TLS, while further polyubiquitination by Rad5 favours the error free template switch (Lee and Myung, 2008). In human, Rad5 has two orthologs, HTLF (Helicase Like Transcription Factor) and SHPRH (SNF2 Histone Linker PHD Ring Helicase) (Chang and Cimprich, 2009).

TLS is carried out by error prone TLS polymerases, which differ from replicative polymerases by the lack of proofreading activity, allowing completion of replication without requirement of high accuracy. TLS starts by the insertion of a nucleotide opposite the damaged site. The inserted nucleotide is then extended and the replication can be accomplished without repair of the lesion. The process (*Figure 1-8*) involves a polymerase switch step where the replicative polymerase is replaced by a TLS polymerase to allow bypassing the lesion, and a switch back from TLS to replicative polymerase to allow continuation of replication (Waters *et al.*, 2009). Eukaryotic TLS polymerases include REV1, pol ζ (composed of Rev3 and Rev7 subunits), pol κ , pol η and pol ι (Waters *et al.*, 2009). Analysis of human pol ζ suggested that the polymerase is unable to insert the first nucleotide and acts in combination with pol ι (Johnson *et al.*, 2000). In this model, pol ι places the first

nucleotide opposite a lesion (T-T dimer), which is then extended by pol ζ . In vitro analysis of *S. cerevisiae* pol ζ also showed that the enzyme is unable to insert a nucleotide opposite a T-T dimer but that it efficiently extends the DNA where a nucleotide was inserted (Johnson *et al.*, 2012). In addition, in vitro observation that pol ζ associates with two subunits of replication polymerase pol δ (pol31 and pol32), supports the “polymerases switching model” for TLS in *S. cerevisiae* (Johnson *et al.*, 2012), as the two processes interact with each other.

The template switching by-pass of the DNA damage is less understood and is thought to involve modifications in the structure of the replication fork, allowing the non-damaged strand to act as a replication template (Chang and Cimprich, 2009). In this model (*Figure 1-8*) an intermediate structure known as chicken foot is formed and the DNA is synthesised, leading to the formation of a Holliday junction-like structure, which is then resolved (Li and Heyer, 2008; Chang and Cimprich, 2009). The resolution of the chicken foot is not clearly elucidated and it has been suggested that it might involve the same proteins as homologous recombination. In vitro analysis of human HR proteins Rad54, Rad51 and the BLM helicase suggested that they are also required in the template switch model to by-pass DNA damage during replication (Bugreev *et al.*, 2011), probably by unwinding the DNA and initiating strand invasion.

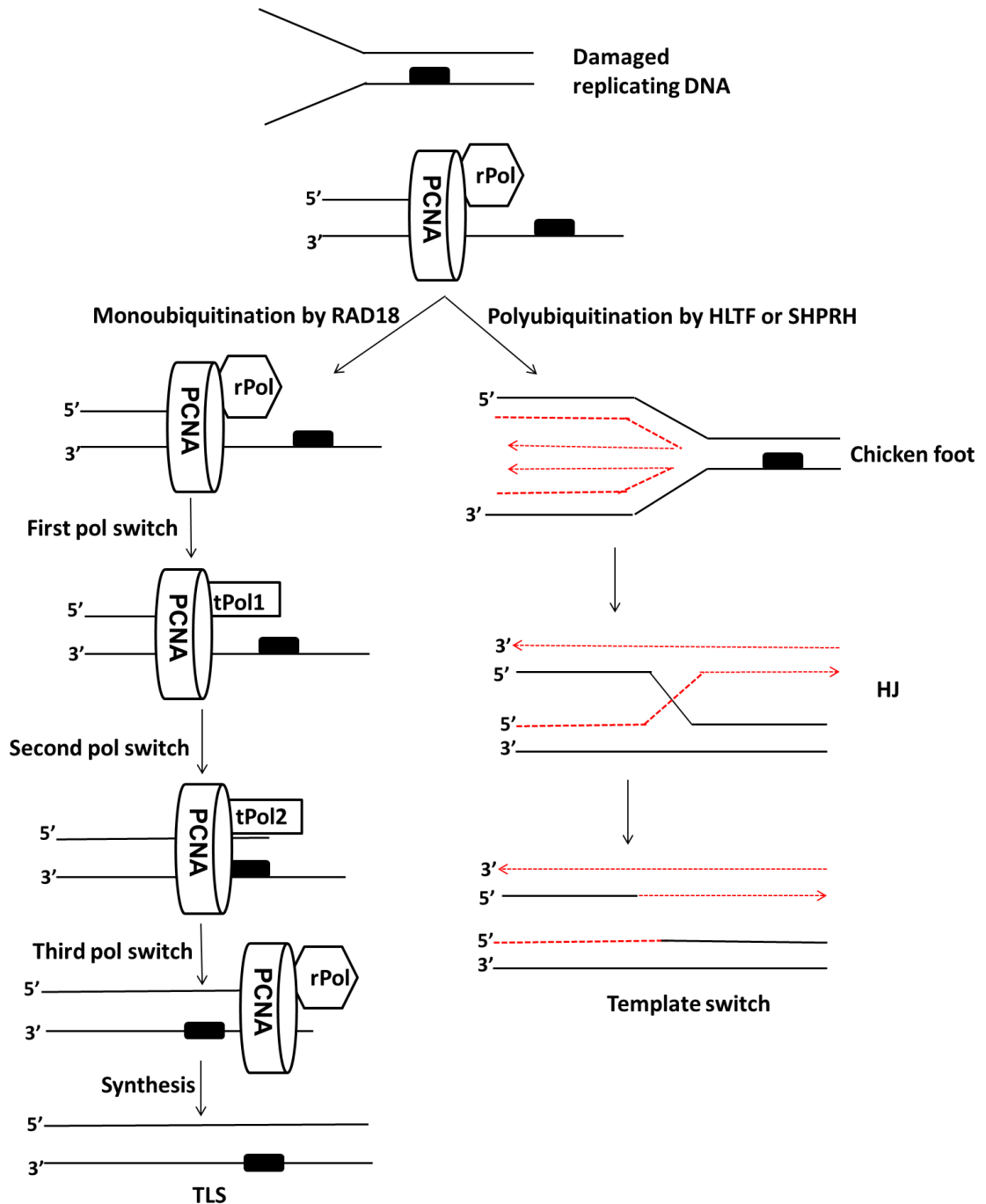


Figure 1-8 DNA damage tolerance. Two pathways act in damage tolerance to restart replication. TLS involves a series of switches between replicative polymerases (rPol) and translesion polymerases (tPol). tPol1 (e.g. polI) initiates TLS by placing a first nucleotide opposite the lesion, tPol2 (e.g. pol ζ) extends the DNA and once the lesion is bypassed, replicative polymerases finish DNA synthesis. Loading of polymerases is facilitated by the PCNA. In the template switch model, an intermediate structure is formed that is resolved into two intact copies.

1.1.3.5 DNA repair genes and cancer prone syndromes

Failing to accurately repair DNA damage can be fatal to cells and lead to genomic instability and cancer development. Widely studied cases include the role of BRCA2 (involved in HR) deficiency in breast cancer development. Several cancer-prone syndromes have been associated with inherited defects in other DNA repair pathways, emphasising the core role of these mechanisms in repressing carcinogenesis.

No severe human condition has yet been identified as a result of defective BER (Hoeijmakers, 2001; Scharer, 2003), but mutations affecting activity of APE1 nuclease, pol β polymerase and XRCC1 (of the XRCC1-ligase 3 complex) in mice led to embryonic lethality (Hoeijmakers, 2001; Scharer, 2003; Houtgraaf *et al.*, 2006), showing the importance of the BER. In human, mutations in UNG glycosylase are associated with the development of the immune deficiency disorder Hyper IGM, characterised by higher levels of IgM antibodies, and mutations in LIG1 were identified in patients with lymphoma, growth retardation, sun sensitivity and immunodeficiency (Maynard *et al.*, 2009).

Defects in NER are responsible for xeroderma pigmentosum (XP), a photosensitive syndrome which enhances risks of developing skin cancer (Sancar *et al.*, 2004, Kleijer *et al.*, 2008). Moreover, NER has been linked to at least two other syndromes: Cockayne syndrome (CS) and Trichiodystrophy (TDD) (Moses, 2001; Hoeijmakers, 2001). Unlike XP, however, CS and TDD don't lead to cancer development (Kleijer *et al.*, 2008). XP patients display a total defect in GGR and a partial defect in TCR and mutations affect XPA-XPG genes. CS and TDD patients only have a defect in TCR, and CS patients show mutations in CSA and CSB genes (Hoeijmakers, 2001; Scharer, 2003).

Defects in MMR, MLH1 and MSH2 genes have been linked to the development of Hereditary Nonpolyposis Colon Cancer (HNPCC), a syndrome that enhances the risk of colon cancer development (Hoeijmakers, 2001; Peltomaki, 2003).

Mutations in TDP1, a protein involved in the repair of SSBs resulting from removal of Top1, have been linked to a neurodegenerative disease, Spinocerebellar Ataxia with Axonal Neuropathy (SCAN1) (Caldecott, 2003), and mutations in the checkpoint kinase ATM are associated with ataxia telangiectasia, a neurodegenerative syndrome characterised by sensitivity to X-rays (Hoeijmakers, 2001). Specific mutations in MRE11 lead to the development of ataxia

telangiectasia-like disorder, and a defect in NBS1 is responsible for the development of Nijmegen Breakage Syndrome (NBS), a human disorder characterised by immunodeficiency, growth retardation and predisposition to cancer (Hoeijmakers, 2001). Another well studied cancer susceptibility syndrome is the Fanconi Anaemia (FA) syndrome, which is caused by a defect in several genes referred to as “FA genes” which play a role in DNA damage checkpoint and DNA repair (Moraes *et al.*, 2012).

Additional to inherited mutations, sporadic mutations in DNA repair can also lead to cancer development. Sporadic mutations in the BER gene *XRCC1* for example have been associated with lung and sporadic breast cancer (Moraes *et al.*, 2012). Amongst other mutations identified in sporadic cancers are, the CSB (TC-NER protein) involved in breast, colon and pancreatic cancers, MRE11 (HR) involved in breast cancer, DNA-PKcs (NHEJ) involved in lung cancer (Negrini *et al.*, 2010) and MMR involved in colorectal tumours (Martin *et al.*, 2010).

1.2 DNA damaging agents in cancer therapy

The use of DNA as a target in cancer therapy goes back to the beginning of the twentieth century with the discovery of DNA alkylating agents (Hurley, 2002). The principle of DNA damaging treatments lies in the ability to induce damage into the DNA and prevent cancer cells to grow and proliferate. Because cancer cells possess mutations into “DNA guardians” (e.g. mutations in DNA repair genes) they are most likely to be affected by the drugs, which in turn lead to their death. On the contrary, healthy cells are able to repair drug induced DNA damage and can survive the treatment. DNA damaging agents can hence target cancer cells with minimal effect on normal cells.

DNA targeting agents include DNA-DNA crosslinkers, UV and X-ray irradiation, DNA intercalators, and molecules that lead to the formation of DNA breaks (Hurley, 2002). The latter group comprises molecules such as topoisomerase poisons, which act by blocking topoisomerase on the DNA. In addition, nucleoside analogues are part of a group of DNA-targeting molecules which kill proliferating cancer cells by inhibiting DNA synthesis (discussed in paragraph 1.2.2). Molecules that target the nucleic acid are often referred to as “DNA-directed” drugs.

1.2.1 Topoisomerase poisons.

1.2.1.1 Topoisomerases

Topoisomerases are a family of ubiquitous enzymes that are conserved from bacteria to eukaryotes, and are very important for the function of a cell. They act in many cellular processes such as replication, recombination and transcription by changing the topology of the supercoiled DNA (and resolving DNA catenanes) in a cleavage and religation reaction (Liu, 1989; Baker *et al.*, 2009).

Topoisomerases have been classified into two types: Type I (eg. Top1 and Top3) cuts one strand of the DNA and uncoils the DNA by swivelling the other strand around the broken strand and Type II (eg. Top2) cleaves both DNA strands (Baker *et al.*, 2009).

In mammalian cells, six topoisomerase genes are expressed, two TOP1 (nuclear TOP1 and mitochondrial TOP1), two TOP2 (TOP2 α and β) and two TOP3 (TOP3 α and β) (Pommier, 2009).

The catalytic mechanism of action is characterised by a four step cycle for both groups of enzymes. In the **first step**, the enzymes bind to the substrate DNA, Top1 has a preference for supercoiled regions whereas Top2 shows preference for supercoiled regions and also binds to specific nucleic acid sequences (Pommier *et al.*, 1998; Pommier, 2009). The **second step** is the cleavage and formation of a covalent complex with the cleaved DNA. Top1 forms a complex at the 3'-end of the broken DNA while top2 is attached to the 5'-end (Pommier, 2009). Cutting of DNA by topoisomerases is carried out through the action of a tyrosyl residue of the enzymes (Wang, 1998), which attacks the phosphodiester bond of the DNA and leads to DNA breakage. The enzymes are then linked to the DNA by a phosphotyrosine bond (Wang, 1998). The transient DNA-topoisomerase complexes are referred to as "cleavable complexes". The **third step** consists in uncoiling the double stranded DNA (or resolving DNA catenanes) and in the **fourth step**, the DNA is ligated. To allow ligation, topoisomerases are removed from the DNA. The removal step is rapidly carried out as the conversion of the transient cleavable complex into a stabilized DNA-protein complex can harm the cell, notably by interfering with replication and transcription (Li and Liu, 2001). The ability of DNA-topoisomerase complexes to induce DNA damage has been used to treat cancer by using anticancer drugs known as topoisomerase poisons. The drugs act by increasing

the half-life of DNA-topoisomerase complexes, leading to the formation of a DNA bound protein, which, if not removed, causes permanent strand breaks which can be lethal for the cell, for example by blocking the progress of the replication fork.

1.2.1.2 Examples of topoisomerases poisons

Chemicals that affect cellular activities of topoisomerases can be divided into two categories: compounds that decrease the overall activity of the enzymes, also called catalytic inhibitors, and compounds that increase levels of enzyme-DNA cleavable complexes, also referred to as topoisomerase poisons. Commonly used topoisomerase poisons include camptothecin (CPT) derivatives (e.g. Irinotecan and topotecan), which block Top1, and etoposide derivatives, which block Top2 (Pommier, 2004; Baldwin and Osheroff, 2005).

A. Camptothecin (CPT) and mechanisms of action

Initially isolated from a Chinese tree, *Camptotheca acuminata* (Hsiang *et al.*, 1989), camptothecin (CPT) derivatives have rapidly become essential compounds in cancer treatment. CPT derivatives are used to treat a broad range of cancers, including ovarian and colo-rectal cancers (Pommier, 2009). The cellular target of CPT is Top1, indicated by the observation that *top1Δ* yeast cells show resistance to the drug and the fact that CPT resistant human cells showed a point mutation in Top1 (Pommier, 2009).

CPT acts by stabilizing the cleavable Top1-DNA complex (*Figure 1-9*). It is located at the interface between Top1 and DNA on the 3'-phosphoryl end of the broken strand (Li and Liu 2001) and inhibits the religation step. It has been shown that CPT binds neither the enzyme nor the DNA but it binds the complex (Liu *et al.*, 2000; Pommier, 2009). The toxicity of CPT lies in the ability of the CPT-top1 complex to induce DNA strand breaks, for example DSBs which might occur as a result of a collision between a replication fork and the complex (*Figure 1-9*). It has been shown that CPT toxicity is enhanced in S-phase (Liu *et al.*, 2000), emphasizing the role of the stalled replication fork in the toxicity of the drug. During S-phase, when the replication fork encounters a CPT-induced single strand break, it stops and generates a DSB, which is lethal for the cell (Pfeiffer *et al.*, 2000). Non replicating cells, however, can also be affected by the drug. This cytotoxicity is partly explained by the collision of the cleavable Top1-DNA-CPT complex with the RNA polymerase

which leads to transcription arrest and formation of a single strand break with CPT-top1 on one end (Liu *et al.*, 2000).

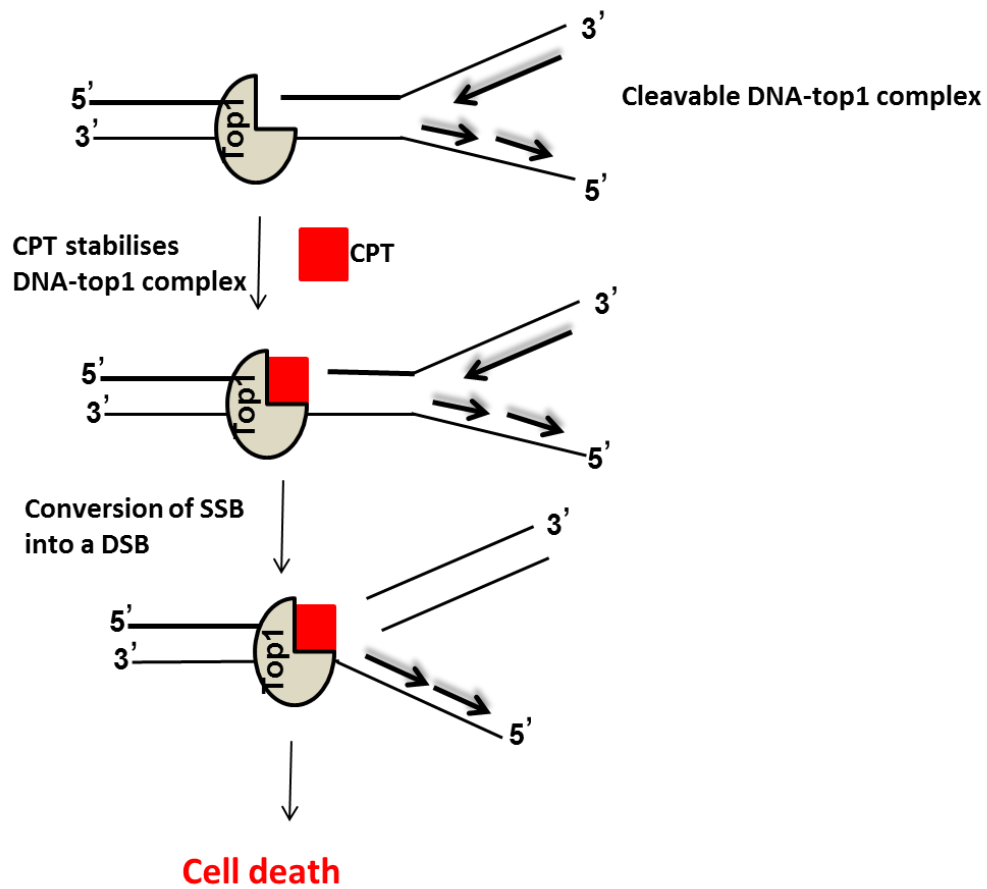


Figure 1-9 Schematic representation of cell death induced by CPT. Top1 acts ahead of the replication fork to unwind the double helix and allow passage of the replisome. After cleavage of DNA, top1 is reversibly fixed to protect broken ends. In the presence of CPT, the half-life of the DNA-top1 complex is increased and when replication fork encounters the complex, it is stopped, resulting in replication arrest and formation of a one-sided DSB, which triggers cell cycle delay and apoptosis.

B. Etoposide

Etoposide is a synthetic derivative of Podophyllotoxin, a natural toxin isolated from *Podophyllum peltatum* (Deweese and Osheroff, 2009). Etoposide and its derivatives are one of the most frequently used anticancer drugs, used in treatment of leukaemia, breast, and lung cancers.

As for Top1, breaks generated by Top2 are usually short lived and are essential (Burden and Osheroff, 1998). Etoposide acts at the top2-DNA interface and stabilises the top2-DNA complex (Deweese and Osheroff, 2009), which results in inhibition of ligation of DNA and formation of DSBs, which if unrepaired lead to cell cycle delay and cell death.

1.2.1.3 Survival of cancer cells to topoisomerase poisons

Two approaches are taken to identify genes that are involved in resistance of cells to drugs: analysis of specific mutants and genome-wide screens. Several studies analysing DNA repair mutants in yeast have shown that cells defective in DNA repair mechanisms are hypersensitive to topoisomerase poisons (reviewed in Rogojina *et al.*, 2007) suggesting a role of the pathways in repair of topoisomerase poisons induced DNA damage. In addition to repair-related response, it has also been shown that mutations affecting levels of topoisomerases confer resistance to the drugs. Indeed, cells expressing low levels of the enzymes showed resistance to top1 (Pommier, 2009) and top2 (Nitiss, 2009) poisons. Moreover, genome-wide screens are used to identify gene deletions that increase sensitivity to topoisomerase poisons in yeast (Deshpande *et al.*, 2009; Pan *et al.*, 2012). In this section, I will focus on the role of DNA damage repair, in particular the role of the MRN complex in repair of topoisomerase poisons-induced DSBs.

Cells that resist to topoisomerase poisons treatment must first remove the trapped enzymes from the DNA to allow repair. The first candidate identified for removal of topoisomerase1-drug complexes is Tdp1, *tyrosyl DNA phosphodiesterase*, yeast as *tdp1* Δ mutants are hypersensitive to topoisomerase1 poisons, suggesting involvement of the enzyme in repair of top1 complexes (Pouliot *et al.*, 1999). However, it has been reported that the enzyme has a poor activity for top1 in vitro (Deb ethune *et al.*, 2002) and *TDPI* deleted *S. cerevisiae* mutants showed only slight sensitivity to CPT in comparison to *MRE11* defective mutants (Pouliot *et al.*, 2001), suggesting the

existence of an alternative Tdp1-independent pathway in repair of CPT-induced strand breaks.

The study of *S. pombe* mutants has established a role of the MRN complex in sensitivity to topoisomerase poisons, and analysis of Mre11 and Ctp1 (*S. cerevisiae* Sae2) mutants has shown that the proteins are involved in the removal of topoisomerase covalent complexes from the DNA. As it has been observed that Mre11 and Ctp1 play a role in removal of the meiotic recombination initiator Rec12 from the DNA (Hartsuiker *et al.*, 2009a) and, because Rec12 induced DSBs show similarities to topoisomerase induced breaks, Hartsuiker *et al.* (2009b) have investigated the role of *S. pombe mre11* (*mre11^{rad32}-D65N* mutants which lack exo and endonuclease activities) and *ctp1* (*ctp1* deleted mutants) in removing topoisomerases from the DNA. Results showed that *ctp1*Δ mutants were defective in Top2 removal but were proficient for Top1 removal. *ctp1*Δ mutants showed a high sensitivity to CPT and TOP-53, and the levels of covalently linked Top2 were increased in TOP-53 treated cells but levels of covalently linked Top1 were decreased in CPT treated cells. These results suggested that Ctp1 plays a role in removal of Top2 but not Top1 (Hartsuiker *et al.*, 2009b). On the other hand, *mre11-D65N* mutants showed increased levels of covalently linked Top1 and Top2 when compared to WT cells. In addition, *mre11-D65N* mutants were hypersensitive to both CPT and the etoposide derivative, TOP-53 but showed a very mild sensitivity to other DNA damaging agents (γ -irradiation and Methyl Methanesulfonate, MMS). These results suggested that Mre11 is involved in the removal of Top1 and Top2 (Hartsuiker *et al.*, 2009b). In addition to the role of *mre11* and *ctp1*, a *rad50S* separation of function mutant was analysed (Hartsuiker *et al.*, 2009b) to further assess the role of the MRN complex in survival to CPT and TOP-53. *rad50S* is a temperature sensitive point mutant (*rad50-K81I*) which is defective in meiosis but proficient in mitotic DNA repair. Analysis of *S. pombe rad50S* has shown that the mutant induces meiotic breaks but that the breaks were not repaired (Young *et al.*, 2002). Failure of the *rad50S* mutants to proceed to meiotic recombination was attributed to the inability of the mutant to remove Rec12 from the DNA (Hartsuiker *et al.*, 2009a). In that regards, *rad50S* mutants were analysed to assess their role in removal of topoisomerase-drug complexes. Results showed that, in comparison to *rad50*Δ mutants (defective in repair function) which were hypersensitive to all DNA damaging agents (CPT, TOP-53, MMS and γ -irradiation), *rad50S* mutants were

highly sensitive to CPT and TOP-53 (at the restrictive temperature, 34°C) but only slightly sensitive to MMS and γ -irradiation (Hartsuiker *et al.*, 2009a). Together, these results suggest that the MRN complex responds to topoisomerase poisons-induced DNA damage and contributes to the resistance of cells by removing the enzyme from the DNA. However, the exact mechanisms by which MRN-CtIP^{Ctp1} acts to remove the drug-topoisomerase complexes are not fully understood.

1.2.2 Nucleoside analogues (NAs)

NAs are molecules that are structurally similar to physiological nucleosides. They are used by the cell and disrupt cellular function. NAs have been successfully used as anticancer drugs but also in treatment of viral infection. In this introduction, I will focus on mechanisms of action of NAs and their use in cancer therapy.

1.2.2.1 Biosynthesis of physiological nucleosides

To understand mechanisms underlying NA toxicity, I will first give an overview of physiological nucleosides, how they are synthesised in cells and their roles in synthesis of nucleic acids.

Phosphorylated nucleosides (also named nucleotides) are the building blocks of nucleic acids and are vital for all living organisms. They are composed of a pentose sugar (ribose for the formation of RNA or deoxyribose for formation of DNA), a nitrogen base (purines or pyrimidines) and one or more phosphate groups (*Figure 1-10A*). Nucleic acids consist of nucleotides which are bound to each other through phosphodiester bonds between individual nucleotides. In nucleic acids, a purine base is bound to a pyrimidine base. The DNA is formed of double helixes which are linked together by hydrogen bonds between bases.

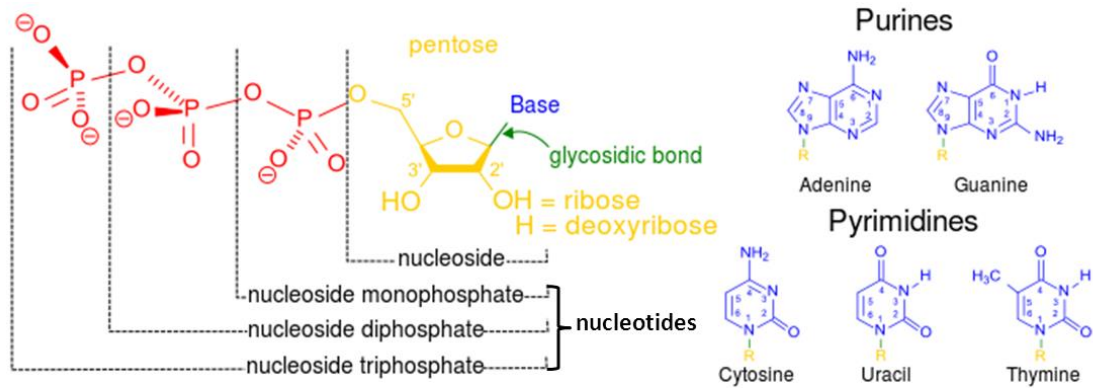


Image from <http://en.wikipedia.org/wiki/Nucleoside>

Figure 1-10A Chemical structure of nucleotides. A nucleoside is formed of a sugar and a base (either a purine or a pyrimidine) linked together by a glycosidic bond. Phosphorylated nucleosides are also referred to as nucleotides. “R” on the bases indicates the binding site of the sugar.

Two pathways are involved in the synthesis of nucleotides: (1) the ***de novo* pathway** synthesises ribonucleotides from small molecules such as amino acids, ribose-5'-phosphate and CO₂ into ribonucleoside monophosphate, which is further phosphorylated by kinases to form ribonucleoside triphosphate (or ribonucleotide) (Van Rompay *et al.*, 2003). The *de novo* synthesis of deoxyribonucleotide involves a reduction of ribonucleotide into the deoxy form by replacing the 2'-OH group of ribose by a hydrogen molecule (Stryer, 1988; Van Rompay *et al.*, 2003). This reaction is catalysed by an enzyme called ribonucleotide reductase (RNR) (Huang and Graves, 2003). (2) The **salvage pathway** recycles products of DNA degradation (free bases and nucleosides) and converts them into nucleotides via diverse reactions.

A. *de novo* Deoxy/ribonucleotides synthesis.

de novo synthesis (Figure 1-10B) starts with 5-phosphorybosylpyrophosphate (PRPP), the nucleotide precursor. Purine ribonucleotides (adenosine and guanosine) are synthesised in a complex pathway, which starts by the conversion of PRPP into inosine-5'-monophosphate (IMP), the primary purine product. The pathway requires a 10 step succession of condensations involving several enzymes such as PRPP amidotransferase, which catalyses the rate limiting first reaction (Kornberg and Baker, 1992; Rudolf, 1994).

IMP is converted into adenylylate or adenosine monophosphate (AMP) by the actions of adenylosuccinate synthase and adenylosuccinate lyase. AMP is then phosphorylated into adenosine diphosphate (ADP) and adenosine tri-phosphate or adenine (ATP) by adenylylate and nucleoside diphosphate (NDP) kinases respectively.

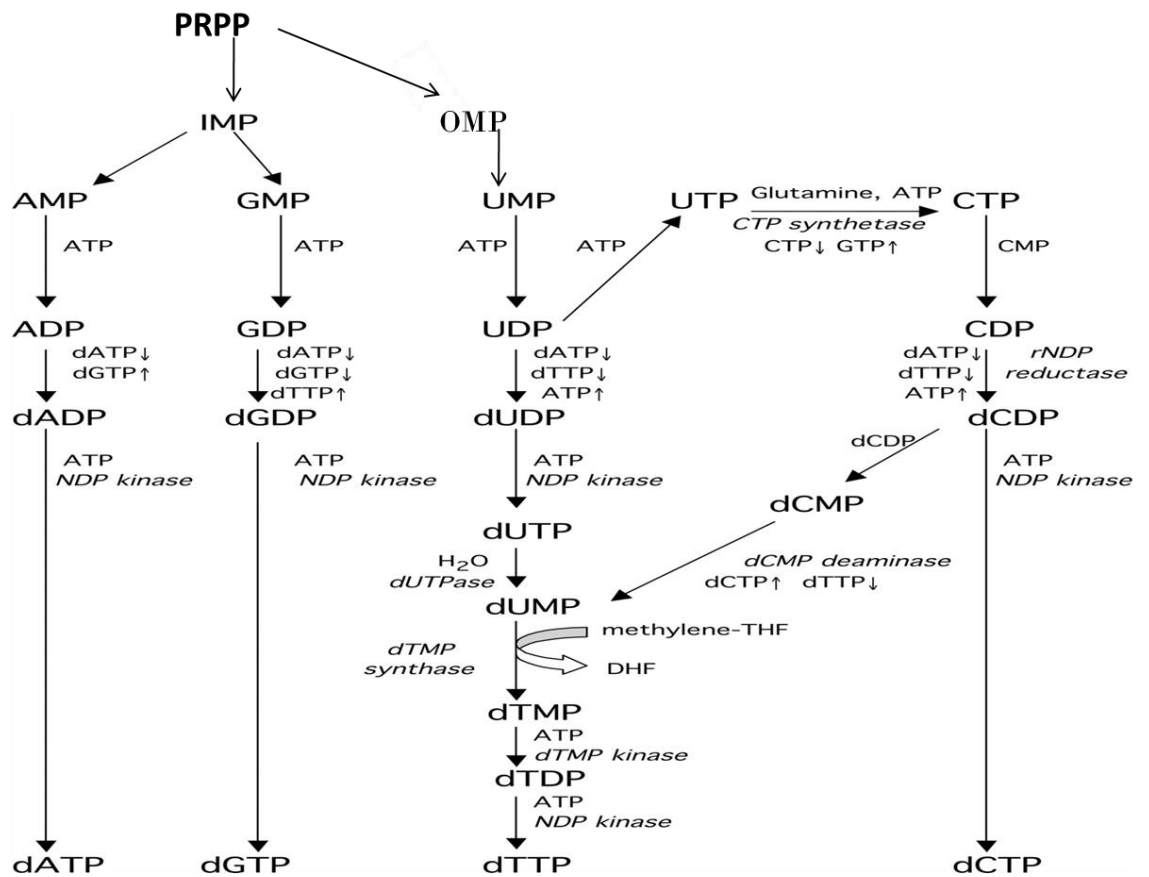
Guanosine monophosphate (GMP) results from the actions of IMP dehydrogenase which transforms IMP into xanthylate and GMP synthase (or xanthylate aminase), which transforms xanthylate into GMP. Guanylate kinase phosphorylates GMP into GDP (guanosine di-phosphate) and NDP kinase phosphorylates GDP into GTP (guanosine tri-phosphate or guanosine).

Pyrimidine ribonucleotides (uridine and cytidine), are synthesised by the conversion of PRPP into orotidine-5'-monophosphate (OMP or orotate) by a 5 step reaction. OMP is converted into uridine-5'-monophosphate (UMP or uridylylate) under action of OMP decarboxylase.

UMP is then phosphorylated into uridine diphosphate (UDP) by uridylate kinase and into uridine triphosphate (UTP) by NDP kinase. The reaction of UTP with glutamine is catalysed by CTP synthetase and gives cytidine triphosphate (CTP).

The reduction of ribonucleotides to deoxyribonucleotides is carried out by RNR, which catalyses the process of replacing the 2'-hydroxyl group of ribose by a hydrogen atom in the deoxyribose. RNR is the central enzyme of the *de novo* synthesis of deoxynucleotides and is tightly regulated to maintain balanced dNTP pools. Mammalian RNR is composed of two subunits: the accessory large subunit R1 and the catalytic small subunit R2 (Mathews, 2006; Rampazzo *et al.*, 2010). The activity of RNR is cell cycle dependent with higher activity at the G1/S interphase, and is regulated through R2 subunit which shows expression levels fluctuations during cell cycle, while R1 levels remain constant (Mathews, 2006). The activity of the enzyme is both allosterically regulated and genetically controlled at the transcription level (Elledge *et al.*, 1992; Mathews, 2006). Mutations in allosteric control sites results in unbalanced dNTP pools (Mathews, 2006), while DNA damage induce expression of a p53 dependent R2 subunit termed p53R2 (Tanaka *et al.*, 2000). In addition, *in vitro* analysis of mouse RNR suggested a role of dNTP concentration in regulation of the enzyme activity (Chimpoy and Mathews, 2001). Due to its high importance, RNR has become an important target for cancer drugs, which aim to kill cancer cells by decreasing dNTP pools and inhibit DNA synthesis (e.g.: clofarabine, which is used in treatment of acute leukemia).

Thymidine (deoxythymidine triphosphate, dTTP), which is specific to DNA, is synthesised by methylation of deoxyuridine-5'-monophosphate (dUMP) to deoxythymidine monophosphate (dTMP) by dTMP synthase (Thymidylate synthase, TS) which catalyses the transfer of a methylene group from methylene tetrahydrofolate (methylene-TFH) (Stryer, 1988; Papamichael, 2000). dTMP is then phosphorylated into dTDP and dTTP by NDP kinases. dUMP results either from the action of dCMP deaminase on dCMP or from dUTPase on dUTP. Methylation of dUMP is carried out by thymidylate synthase (TS or dTMP synthase).



Modified from C.K. Mathews, The FASEB Journal, vol.20 July 2006

Figure 1-10B Overview of de novo synthesis of deoxynucleotides. A succession of reactions involving several enzymes and intermediate products converts PRPP, the nucleotides precursor, into ribonucleosides and deoxyribonucleotides triphosphates (dNTPs).

B. Salvage deoxy/ribonucleotides synthesis

Salvage dNTP synthesis pathways “recycle” products from nucleic acid degradation and convert them into nucleotides. Due to the hydrophilic nature of nucleosides which prevent them from diffusing through the cellular membrane, transporters are needed to import nucleosides into the cell and allow their conversion into nucleotides (Van Rompay *et al.*, 2003). Because of the negative charge from the phosphate groups, nucleoside transporters only accept non-phosphorylated nucleosides as substrates (Galmarini *et al.*, 2001; Van Rompay *et al.*, 2003).

The main salvage pathways include: (1) conversion of bases into ribonucleotides catalysed by phosphoribosyl transferase, (2) conversion of bases into nucleosides catalysed by nucleoside phosphorylase, (3) conversion of bases into deoxynucleosides catalysed by nucleoside transglycosylase and (4) conversion of nucleosides into nucleotides catalysed by nucleoside kinases (Kornberg and Baker 1992). Two classes of transporters have been identified in human cells. (1) The equilibrative transporters (ENTs), encoded by the SLC29 gene family, are sodium independent and allow transport of nucleosides depending on the intracellular concentrations of nucleosides (Pastor-Anglada *et al.*, 2004, Jordheim *et al.*, 2005). Four members of this family have been identified (ENT1-4), which shares a broad affinity for purine and pyrimidine nucleosides and are ubiquitously distributed in tissues (Podgorska *et al.*, 2005). (2) The concentrative transporters (CNTs), encoded by the SLC28 gene family, import nucleosides against a concentration gradient provided by transmembrane sodium concentration (Galmarini *et al.*, 2001; Huang and Graves, 2003). Three members (CNT1-3) have been identified. CNT transporters have a more localised distribution, CNT1 is localised in kidney, liver and brain amongst others; CNT2 is localised in kidney, liver, brain, pancreas and heart for example, while CNT3 is found in pancreas, lung, liver and placenta (Podgorska *et al.*, 2005). CNTs have greater affinity for pyrimidine nucleosides (Galmarini *et al.*, 2001). Although transport of nucleosides into cells is an important step, as mutations into transporters affect intracellular deoxynucleoside pools, the rate limiting step of the nucleoside salvage pathway is the phosphorylation of nucleosides into the phosphate form, which, traps phosphorylated nucleotides inside the cell due to their negative charge (Arnér and Eriksson, 1995).

Phosphorylation is carried out by kinases and four deoxynucleotides kinases (dNKs) have been identified in human cells. These include thymidine kinase 1 (TK1),

thymidine kinase 2 (TK2), deoxycytidine kinase (dCK), and deoxyguanosine kinase (dGK) (Galmarini *et al.*, 2001; Van Rompay *et al.*, 2003).

Although the name of the kinase is based on the preferred substrate of the enzyme, they may phosphorylate other nucleosides. TK2 for example proceeds to phosphorylation of deoxythymidine, deoxyuridine, but also deoxycytidine, whereas dCK phosphorylates deoxycytidine, deoxyadenosine and deoxyguanosine. dCK has also been reported to phosphorylate most of the clinically important anticancer NAs (Van Rompay *et al.*, 2003; Jordheim *et al.*, 2005).

1.2.2.2 Mechanism of action of nucleoside analogues

NAs exert their toxicity by being incorporated into nucleic acids during their synthesis or by inhibiting enzymes involved in dNTP synthesis, which, in turn leads to depletion of dNTP pools and inhibition of DNA synthesis (Kaye, 1998; Galmarini *et al.*, 2002).

Purine analogues include cladribine and fludarabine which have been used for malignant disorders of the blood (Galmarini *et al.*, 2002). Pyrimidine analogues include arabinosylcytosine (AraC), which has activity in acute myelogenous leukemia, and Gemcitabine (GemC), used in solid tumours such as pancreatic and bladder cancers. Although NAs have different pharmacology and metabolism, their general target is to inhibit DNA synthesis. After import through specific transporters, the pro drugs are activated by phosphorylation and are incorporated into the DNA and/or inhibit key enzymes of the nucleic acid synthesis (Figure 1-11A). As for physiological nucleosides, the rate limiting step of NAs activity is their phosphorylation by the deoxycytidine kinase (Jordheim and Dumontet, 2007).

To illustrate action of NAs on DNA synthesis, two of the most widely used anticancer NAs, AraC and GemC, used in this project, will be discussed as examples. Used in a wide range of cancer treatments, AraC and GemC are analogues of deoxycytidine containing a modification on the second carbon of the sugar moiety. Although the drugs are similar in structure, their pharmacodynamic effects are different. Compared to AraC, GemC has been reported to be more cytotoxic. In fact Gemcitabine is thought to be more lipophilic, which facilitates transport through the cellular membrane and also has greater affinity for deoxycytidine kinase (Heinemann *et al.*, 1988) than Ara-C. The greater cytotoxicity of GemC can also be attributed to the “masked chain termination” process, explained by the observation that a natural

nucleoside is added after GemC incorporation into replicating DNA. The added nucleotide “masks” the drug and protects from repair excision (Galmarini *et al.*, 2002). In addition, GemC is also incorporated into RNA and GemC-DP inhibits RNR, effects that are not observed with AraC. Gemcitabine is mainly incorporated into replicating DNA while AraC is also incorporated during DNA repair (Galmarini *et al.*, 2002; Pourquier *et al.*, 2002, Van Rompay *et al.*, 2003), however for both analogues the incorporation is higher in replicating cells (Iwasaki *et al.*, 1997).

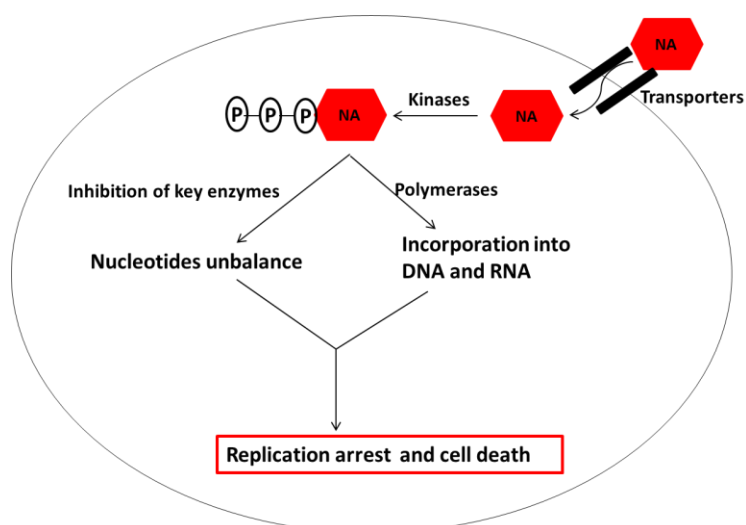


Figure 1-11A Simplified overview of NA induced cell death. NA pro drugs are imported into cells via specific transporters. They are then transformed into their phosphorylated form by kinases. The active forms exert their activity either by being incorporated into nucleic acids or inhibiting key enzymes of the nucleotide synthesis. Both actions lead to replication arrest and cell death.

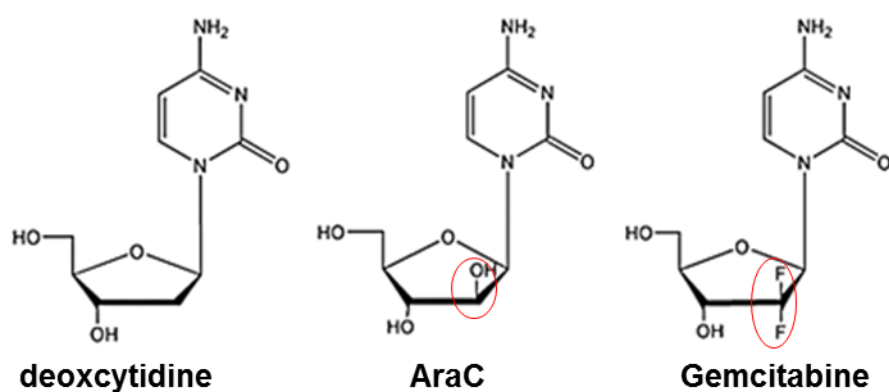


Figure 1-11B Structures of deoxycytidine and its analogues AraC and GemC. AraC differs from deoxycytidine by the presence of a hydroxyl (OH) group at the second C of the sugar and Gemcitabine differs by the addition of two fluorine (F) atoms at the second C of the sugar.

A. AraC

Also named 1- β -D-arabinofuranosylcytosine, cytosine arabinoside or cytarabine, AraC was the first NA with modifications in the sugar moiety to be used in cancer treatment (Ewald *et al.*, 2008a). AraC differs from its physiological analogue, deoxycytidine, by addition of an extra hydroxyl group on the second carbon of the sugar (Figure 1-11B). This structure resembles to that of ribocytidine (present in RNA), but with the OH group located on the opposite side.

Used in treatment of acute leukaemia and lymphomas, it has been reported as one of the most active agents leading to a complete remission in about 30% of the patients (Galmarini *et al.*, 2002). The penetration of AraC into cells depends on plasma concentrations. However, with a standard dose (SD, 100-200mg/m² corresponding to a plasma concentration of 0.5-1 μ M), the uptake of AraC is dependent on the expression of the transporter (Galmarini *et al.*, 2001, Galmarini *et al.*, 2002).

AraC is imported into cells by both ENT and CNT transporters (Van Rompay *et al.*, 2003) and phosphorylated into monophosphate (AraC-MP), diphosphate (AraC-DP) and triphosphate (AraC-TP) active forms by deoxycytidine kinase, dCK and pyrimidine nucleoside kinases respectively (Galmarini *et al.*, 2001; Van Rompay *et al.*, 2003).

AraC-TP exerts its cytotoxicity by either inhibiting DNA polymerase or being incorporated into DNA in competition with dCTP. AraC-TP incorporation leads to stalling of replication forks as it is a poor substrate for extension by polymerases (Galmarini *et al.*, 2001; Sampath *et al.*, 2003; Ewald *et al.*, 2008a).

The cytotoxicity of AraC is limited due to low affinity for dCK, deamination and rapid cellular elimination of AraC-TP (Galmarini *et al.*, 2002).

Additionally to DNA synthesis-related cytotoxicity, it has been shown in human leukemia cell lines that incorporation of AraC contributes to cell death by increasing topoisomerase I cleavage complexes (Pourquier *et al.*, 2000). This increase was mainly attributed to inhibition of the religation step.

B. Gemcitabine (GemC)

Gemcitabine (2', 2'-difluorodeoxycytidine or dFdC) differs from deoxycytidine in that it possesses two fluor atoms on the second carbon of the sugar (Figure 1-11B). The drug is used in treatment of a large panel of solid tumours including lung, pancreatic, breast and bladder cancers.

Similarly to other NAs, GemC is imported into cells by nucleosides transporters and phosphorylated into the active triphosphate form by kinases. The triphosphate form is mainly incorporated into DNA but it is also incorporated into RNA (Ruiz van Haperen *et al.*, 1993). Additionally to inhibition of replication by incorporation into DNA, GemC also exerts its toxicity by inhibiting RNR (inhibited by GemC-DP), CTP synthetase (inhibited by GemC-TP) and thymidylate synthase (inhibited by GemC-UMP), key enzymes of nucleotide synthesis (Mini *et al.*, 2006). The mechanisms of action and regulation of GemC are illustrated in Figure 1-11C.

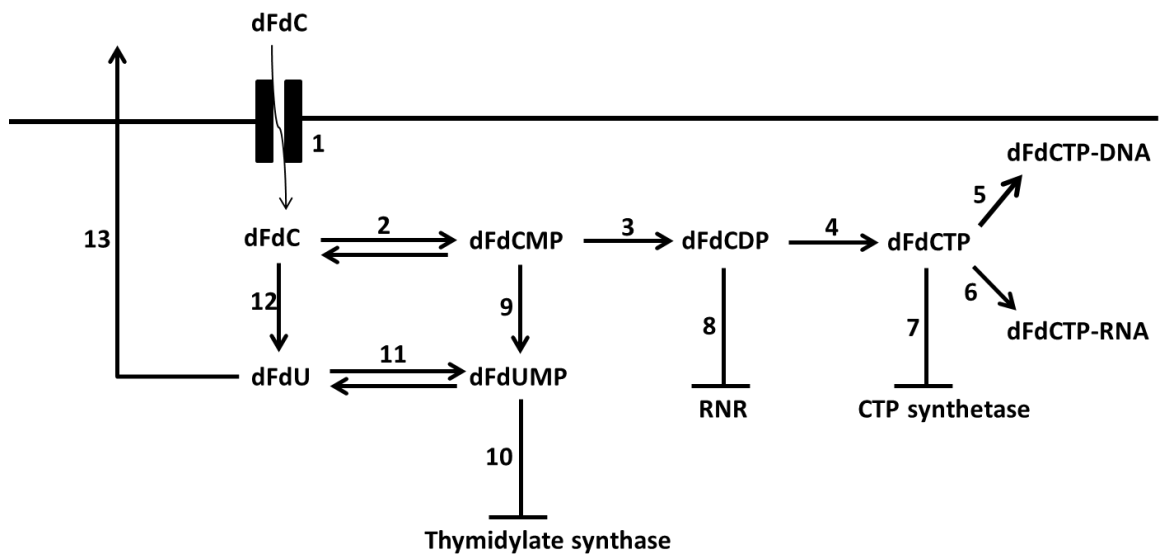


Figure 1-11C Metabolism and mechanisms of action of GemC (dFdC). The dFdC pro drug is imported into cells via nucleotide transporters (1) and phosphorylated into its monophosphate form, dFdCMP by deoxycytidine kinase (2), dephosphorylation of dFdCMP into dFdC by 5' nucleotidase can also occur at this step. dFdCMP is subsequently phosphorylated into dFdCDP (3) and dFdCTP (4) by mono and diphosphate kinases respectively. dFdCTP is then incorporated into DNA (5) and RNA (6). Either form of phosphorylated dFdC acts on key enzymes of nucleotide synthesis, dFdCTP inhibits CTP synthetase (7) while dFdCDP inhibits RNR (8) and dFdUMP, resulting from the action of deoxycytidine monophosphate deaminase on dFdCMP (9) and phosphorylation of dFdU (11), inhibits thymidylate synthase (10). Deamination of dFdC (12) leads to formation of dFdU. Numbers in the figure are randomly attributed and don't reflect the order of occurrence in the cell. The figure was copied from Mini *et al.* (2006).

As for AraC, gemcitabine is imported into cells by both ENT and CNT transporters, mainly hENT1/2 and hCNT1-3 (Mini *et al.*, 2006). Drug uptake by transporters is highly correlated with cytotoxicity and cells deficient in hENT1 showed a high increase in drug resistance (Mini *et al.*, 2006; Oguri *et al.*, 2007). In hENT1 proficient cells however, the rate limiting step of the drug activity is the phosphorylation of dFdC into the monophosphate form dFdCMP by the deoxycytidine kinase. Inhibition of dCK activity and expression led to resistance while overexpression of the kinase increased sensitivity of cells to the drug (Van Rompay *et al.*, 2003). Further phosphorylation is carried out by pyrimidine kinases, which convert dFdCMP into dFdCDP (diphosphate) and dFdCTP (triphosphate) (Galmarini *et al.*, 2001).

Activated dFdCTP is mainly incorporated into replicating DNA by polymerases and leads to chain termination, but the drug has also been reported to be incorporated into RNA, which inhibits its synthesis (Galmarini *et al.*, 2001). The incorporation of GemC into RNA and its role is, however, controversial. Ruiz van Haperen *et al* (1993) have shown that the drug is incorporated into RNA and that this incorporation inhibits RNA synthesis in the CEM (Human T cell lymphoblast-like) cell line after 24 hours incubation while another study with the same cell line (Huang *et al.*, 1991) suggested that GemC was not incorporated into RNA and that GemC does not inhibit RNA synthesis after 4 hours incubation. Because the studies measured incorporation into RNA at different time points [4h for Huang *et al* and 24h for Ruiz van Haperen *et al* (results for cesium precipitation)], there is a possibility that the differences are due to accumulation of the drug after a long time exposure. Indeed it was observed in both studies that RNA synthesis was not inhibited after 4h incubation with GemC, it is therefore possible that measurements of RNA incorporation at a same timepoint would have shown similar levels of the drug in both studies. However using a different nucleic acid separation method (acid precipitation/ enzymic separation instead of cesium gradient centrifugation used by Huang *et al.*, 1991), Ruiz van Haperen *et al* (1993) showed that GemC was incorporated into RNA of CEM cells after 4 hours incubation. Moreover, Ruiz van Haperen *et al* also observed RNA incorporation of GemC in two other cell lines (murine colon carcinoma cell line, Colon 26-10 and human ovarian carcinoma cell line A2780). To my knowledge these are the only reported studies that have evaluated incorporation of GemC into RNA

and due to conflictual results, the possible incorporation of GemC into RNA is still to be proven.

In addition, *in vitro* studies have shown that, once GemC-TP is incorporated into DNA, a natural nucleotide is added, which masks the drug and might prevent repair mechanisms from detecting the abnormality into the newly synthesised DNA (Galmarini *et al.*, 2001; Galmarini *et al.*, 2002). This phenomenon is known as “masked DNA chain termination” and contributes to the drug toxicity. The high toxicity of GemC is also attributed to the capacity of the drug to inhibit key enzymes of nucleotide synthesis. This action not only contributes to DNA synthesis arrest by decreasing nucleotide pools but it also improves drug activity by increasing incorporation into DNA as it reduces the concentration of competing nucleotides. This process is known as “self-potential” of the drug. The most important action that leads to self-potential is the inhibition of ribonucleotide reductase, RNR by GemC-DP. Overexpression of RNR led to an increase in GemC resistance in cancer cells, emphasising the role of the enzyme in inhibition of drug activity (Mini *et al.*, 2006). In addition, measurement of intracellular dNTP pools has shown a similar decrease in Gemcitabine-treated cells compared to cells treated with hydroxyurea (0.1 μ M of GemC and 5mM of HU were used), a RNR inhibitor (Heinemann *et al.*, 1990). GemC-TP also inhibits CTP-synthetase, an enzyme that converts UTP into CTP, and dFdUMP inhibits Thymidylate synthase, which acts by converting dUMP into dTMP (Mini *et al.*, 2006). dFdUMP results from the conversion of dFdCMP by deoxycytidine monophosphate deaminase. In addition to the basic GemC toxicity, it has been shown that dFdU (difluorodeoxyuridine), resulting from deamination of dFdC by deoxycytidine deaminase and dephosphorylation of dFdUMP, also contributes to dFdC toxicity by being incorporated into DNA and RNA (Velkamp *et al.*, 2008).

Moreover, similarly to AraC, it has also been shown that GemC induces the top1-mediated DNA-protein cleavage complex (Pourquier *et al.*, 2002), which enhances the drug activity in a leukemia cell line. A human ovarian cancer cell line resistant to Gemcitabine also showed a decreased top1 expression (Bergman *et al.*, 2000) emphasising the possible role of the enzyme in Gemcitabine toxicity.

1.2.2.3 Cellular response to NAs

Following incorporation into DNA, GemC and AraC cause cell death by arresting the replication fork which leads to chain termination or induces nicks into DNA (Ewald *et al.*, 2008a).

One possible cellular response to NA treatment is the induction of apoptosis or programmed cell death, which is activated by the damage and leads to cell death. Apoptosis is activated by checkpoint mechanisms which sense damage caused by NAs. A study by Feng *et al* (2000) has shown a direct correlation between NA toxicity and p53 expression. Deletion of the apoptosis inducing protein led to resistance of cells to NAs, Ara-C, GemC, and fludarabine treatment whereas expression of p53 vector in p53 null cells enhanced drug sensitivity.

Cells can also survive NA treatment, an effect that can arise from failure of the drugs to induce arrested replication fork, DNA damage or apoptosis. Three main mechanisms characterise this type of resistance: (1) mutations in transporters, kinases and enzymes involved in NAs degradation affect NAs toxicity by limiting intracellular levels of active NAs, (2) failure to inhibit target enzymes such as polymerases and RNR and (3) dysfunctions in checkpoint mechanisms that results in failure to activate apoptosis (Galmarini *et al.*, 2002; Jordheim *et al.*, 2005). The role of the checkpoint in response to NAs treatment was shown by the increased sensitivity of cells in the absence of ATM and ATR, two core proteins of the checkpoint machinery (Ewald *et al.*, 2008a).

In addition, DNA repair mechanisms can also contribute to cellular resistance to the drugs. The possible role of the DNA repair response to NA-induced damage was supported by several studies. Interaction of DNA-PK, a NHEJ protein, with p53 in response to GemC treatment (Achanta *et al.*, 2001) suggested a response of the protein to the NA while increased sensitivity of Mre11 and Rad50 (but not Nbs1) deficient cells to GemC (Ewald *et al.*, 2008b) suggested a role of the DSBR proteins in response to the drug. Deletion of NER proteins CSB, XPB, XPF and ERCC1 also led to increased sensitivity to CNDAC (2'-C-cyano-2'-deoxy-1- β -D-arabino-pentofuranosylcytosine), a NA which leads to formation of SSB after incorporation into the DNA. Following incorporation of CNDAC into DNA, addition of a natural nucleotide by polymerases leads to cleavage of CNDAC phosphodiester bond, which in turn creates a nick into the DNA (Wang *et al.*, 2008). Hypersensitivity of NER

defective mutants to CNDAC, thus suggested a role of the NER pathway in response to the drug (Ewald *et al.*, 2008a; Wang *et al.* 2008).

DNA repair mechanisms are highly important cellular processes, which protect the genome against internal and external attacks and contribute to genome integrity and cellular resistance to cancer development. The studies mentioned above, however, imply that the mechanisms may also play an important role in DNA damaging anticancer drugs survival and interfere with treatment success. Understanding the response of repair mechanisms to DNA damaging agents is hence a key step in improving therapy. Moreover, because cancer cells are often defective in DNA repair genes, it is likely that this contributes to the high sensitivity of cancer cells to NA treatment in comparison to healthy cells which can efficiently repair drug induced damage.

1.3 The project

NAs kill proliferating cancer cells by inhibiting replication, which leads to cell death. NAs have been widely used in treatment of solid cancers (e.g: breast, lung, pancreatic and bladder cancers) and malignancies (Galmarini *et al.*, 2002). The use of AraC in treatment of acute leukaemia, for example, has led to a complete remission in up to 30% cases (doses of 100–200 mg/m² administered intravenously each day on days 1–7, Galmarini *et al.*, 2002). If combined with an anthracycline, complete remission in AraC-treated patients can reach up to 75% (Galmarini *et al.*, 2002), showing the importance of the drug in cancer treatment. The use of NAs in cancer treatment however is limited by the fact that cancer cells have shown resistance the drugs (Galmarini *et al.*, 2002; Jordheim *et al.*, 2005) and a better understanding of these resistance mechanisms constitutes a crucial step in improving NAs therapy as it can contribute to identification of novel molecular targets. In addition, identification of DNA repair genes that are involved in response to NA can help “targeting” patients with specific mutants. In fact it is now an attractive approach in cancer therapy which aims to use DNA damaging agents in treatment of cancer cells with specific defect in DNA repair (Moraes *et al.*, 2012). Some studies have suggested a possible role of DNA repair proteins in survival to NA treatment (Achanta *et al.*, 2001; Ewald *et al.*, 2008a; Ewald *et al.*, 2008b). In this project, we sought to identify and analyse the role of genes involved in response to NA treatment

using the fission yeast, *Schizosaccharomyces pombe* (*S. pombe*) as a model organism.

1.3.1 *S. pombe* as a model organism

Fission yeast is easily physically and genetically manipulated and hence a powerful tool in genetic studies (Forsburg, 2001). Two yeast species have been extensively used as model organisms, the budding yeast *Saccharomyces cerevisiae* and the fission yeast *Schizosaccharomyces pombe*.

S. pombe was first isolated in African beer which gave it its name, “pombe” meaning “beer” in Swahili. Unlike budding yeast where the daughter cell is generated after formation of a “bud” on the parental cell, fission yeast divides by elongation of the parental cell, after which a septum separates the two cells once the daughter cell is mature. The cell cycle of fission yeast is illustrated in *Figure 1-12*.

S. pombe has been widely used in molecular genetic studies of several cellular mechanisms including cell cycle, checkpoint and DNA repair (Lehmann, 1996). The attribution of the 2001 Nobel Prize in physiology or medicine to one of the eminent *S. pombe* researchers, Sir Paul Nurse, for his work on the cell cycle, as well as the release of the fully sequenced *S. pombe* genome the same year, have strengthened interest in fission yeast research. Importantly, several *S. pombe* genes were shown to have homologues in higher eukaryotes, stressing the evolutionary conservation between the yeast and human genomes. Amongst identified *S. pombe* genes, fifty share homology with human disease genes and half of those are cancer-related (Wood *et al*, 2002), which emphasises the importance of yeast in cancer research.

A mature *S. pombe* cell is a rod-shaped cell of 2-3 μm in diameter and 7-14 μm in length. *S. pombe* has a relatively small genome of around 4,824 predicted genes distributed over three chromosomes and possesses a low redundancy with only a few genes located twice on the genome (Yanagida, 2002), making this yeast an ideal model for genetic analysis. Because many genes are conserved, findings in the fission yeast can often be extended to higher eukaryotes and humans in particular, which present a valuable tool in studying human diseases.

S. pombe also presents multiple practical advantages, with a short doubling time (2.5-4 hours for WT), results are quickly obtained in comparison to higher eukaryotes. Additionally, because it is easy to manipulate, insertion and deletion of genes is relatively straightforward and the progeny containing genes of interest are quickly

obtained by crosses. This ability to easily inactivate genes has been used to carry out genome-wide screens aiming to identify the role of novel genes and a *S. pombe* genome-wide deletion library containing over 3000 deletions of non-essential genes is available for purchase (Bioneer).

In most laboratories, yeast strains are kept as haploid cells and diploid cells can be easily generated for specific purposes.

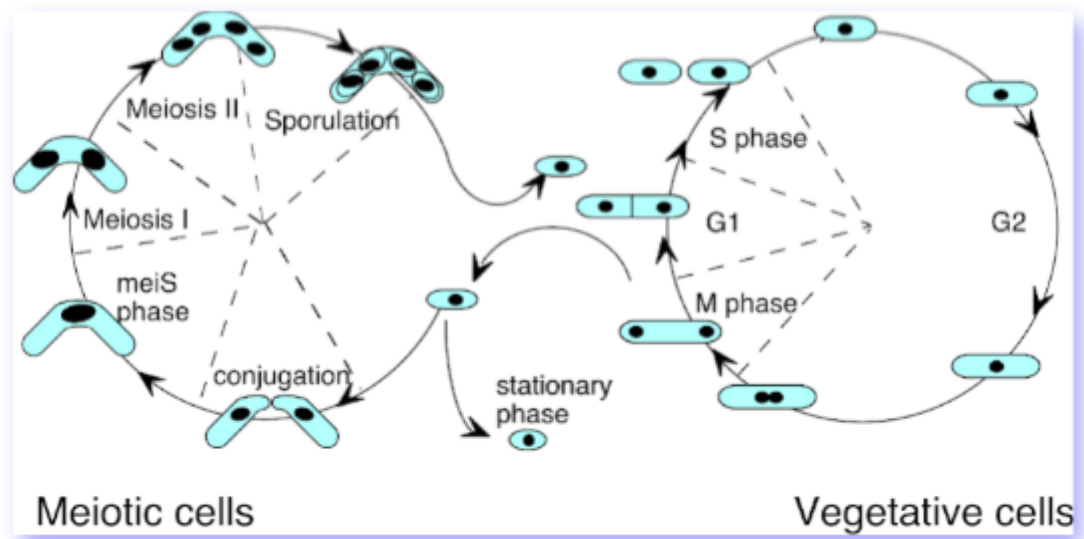


Figure 1-12 Illustration of *S. pombe* cell cycle. Four phases characterise the cell cycle in vegetative cells similarly to mammalian cells. Unlike mammalian cells however, where G1 phase is predominant, *S. pombe* dividing cells spend most time in G2. Meiosis is characterised by the formation of spores which result in the formation of single cells. The image was taken from <http://www-bcf.usc.edu/~forsburg/main4.html>.

1.3.2 Scope of the project

The aim of this project is to identify and analyse genes that play a role in survival to NA treatment. As mentioned in paragraph 1.2.1.3, DNA repair mechanisms play an essential role in resistance to cancer drugs and several groups have identified a role of the MRN complex in resistance to topoisomerase poisons. This role is attributed to the ability of the complex to remove DNA-bound topoisomerases and allow subsequent repair (Hartsuiker *et al.*, 2009b). Because NAs are incorporated into the DNA, we hypothesised that, for cells to survive the treatment, NAs must be removed and that this might require a similar removal mechanism as topoisomerase removal. I assessed the role of the MRN complex in removal and resistance to NA treatment and carried out a screen of a *S. pombe* genome-wide deletion library to identify novel genes that might be responsible for NA resistance. In addition, I analysed specific DNA repair mutants and their potential role in survival to NA treatment. Two DNA-directed and widely used anticancer nucleoside analogues, GemC and AraC were used for this project.

As a complementary project, we also sought to set up a system that would allow further investigation of the removal of topoisomerases-drug complexes from the DNA. Although it is now established that the Mre11 nuclease plays a key role in this removal, the exact mechanism by which the proteins are removed remains unclear. The system referred to as “FLP-nick system” uses a step arrest mutant of the FLP recombinase (FLP H305L) (Parsons *et al.*, 1988) to create a permanent DNA bound protein. The system has successfully been established in *S. cerevisiae* (Nielsen *et al.*, 2009), and mainly takes advantage of the ability of the FLP enzyme to recognise a specific site, the FLP recognition site (FRT), which can be arbitrary inserted into the genome and allows study of specific regions.

2 Materials and Methods

2.1 Materials

2.1.1 List of strains

MG stock number	Genotype	Origin
MG006	<i>h+ura4::adh-hsdCK leu1+-adh-hENT1</i>	EH966
MG018	<i>h-</i>	EH429
MG019	<i>h+</i>	EH722
MG020	<i>Smt0-0 ura4-D18</i>	EH68
MG021	<i>h+ (leu1-32)Ura4::adh-dmdNK</i>	EH844
MG022	<i>h+ (leu1-32)Ura4::adh-hsdCK</i>	EH845
MG028	<i>h+ (leu1-32)Ura4::adh-dmdNK mre11-D65N</i>	EH1089
MG042	<i>h-leu1-32 ura4-D18 ade6M210 his7-366 leu1::[leu+-adh:hENT his7+-adh:hsv-tk]</i>	EH865
MG043	<i>h+ leu1+-adh:hENT1</i>	EH968
MG044	<i>h- leu1+-adh:hENT1</i>	EH969
MG052*	<i>h-urg1::loxP-hph-loxM3 ade6-704 leu1-32</i>	AW430
MG070	<i>h+ura4::adh-hsdCK-NAT^R-adh-hENT1</i>	This study
MG071	<i>h+ ura4:adh-hENT1</i>	This study
MG080	<i>h-smt0 mat1M-cyh^S rpl42-cyh^R</i>	EH1099
MG081	<i>h+ura4::adh-dmdNK-NAT^R-adh-hENT1</i>	This study
MG083	<i>h+ura4::adh-dmdNK-NAT^R-adh-hENT1 ura4-aim</i>	This study
MG085	<i>h+ura4::adh-hsdCK-NAT^R-adh-hENT1 ura4-aim</i>	This study
MG086	<i>h- urg1::loxP-FLP-loxM3-3HA:kan^R ade6-704 leu1-32</i>	This study
MG090	<i>h- urg1::loxP-FLP1SS-loxM3-3HA:kan^R ade6-704 leu1-32</i>	This study
MG091	<i>h- urg1::loxP-FLP2SS-loxM3-3HA:kan^R ade6-704 leu1-32</i>	This study
MG102	<i>h-smt0 mat1M-cyh^S rpl42-cyh^R ura4::adh-hsdCK-NAT^R-adh-hENT1 ura4-aim</i>	This study
MG104	<i>h+ura4::adh-dmdNK-leu1+ adh::hENT1 leu1-32</i>	EH970
MG107	<i>h+ura4::adh-hsdCK-NAT^R-adh-hENT1 ura4-aim swi10::kan^R</i>	This study
MG111	<i>h+ura4::adh-hsdCK-NAT^R-adh-hENT1 ura4-aim rad13::hphMX4^R</i>	This study
MG115	<i>h+ura4::adh-hsdCK-NAT^R-adh-hENT1 rhp18::ura4</i>	This study
MG117	<i>h+ura4::adh-dmdNK-NAT^R-adh-hENT1 ura4-aim rad50::kan^R</i>	This study
MG119	<i>h+ura4::adh-hsdCK-NAT^R-adh-hENT1 ura4-aim rad50::kan^R</i>	This study
MG121	<i>h+ura4::adh-dmdNK-NAT^R-adh-hENT1 ura4-aim mre11-D65N</i>	This study

MG stock number	Genotype	Origin
MG130	<i>h-urg1::loxp-hph-loxM3 ade6-704 FRTrev NAT^R</i>	This study
MG131	<i>h-ura4::adh-hsdCK-NAT^R-adh-hENT1 ura4-aim ctp1::kan^R</i>	This study
MG132	<i>h-urg1::loxp-hph-loxM3 ade6-704 FRTfw NAT^R</i>	This study
MG133	<i>h-urg1::loxp-FLP-3HA kan^R ade6-704 leu1-32 FRTrev NAT^R</i>	This study
MG135	<i>h-urg1::loxp-FLP1SS-3HA kan^R ade6-704 leu1-32 FRTrev NAT^R</i>	This study
MG148	<i>h-urg1::loxp-FLP-3HA kan^R leu1-32 FRTfw NAT^R</i>	This study
MG151	<i>h-urg1::loxp-FLP1SS-3HA kan^R leu1-32 FRTfw NAT^R</i>	This study
MG159	<i>h-urg1::loxp-FLP-3HA kan^R FRTrev NAT^R mre11-D65N</i>	This study
MG160	<i>h-urg1::loxp-FLP1SS-3HA kan^R FRTrev NAT^R mre11-D65N</i>	This study
MG164	<i>h-ura4::adh-dmdNK-NAT^R-adh-hENT1 ura4-aim ctp1::kan^R</i>	This study
MG165	<i>h-urg1::loxpFLP-3HA kan^R FRTfw NAT^R mre11-D65N</i>	This study
MG166	<i>h-urg1::loxpFLP1SS-3HA kan^R FRTfw NAT^R mre11-D65N</i>	This study
MG175	<i>h-smt0 ura4::adh-dmdNK mre11-D65N</i>	EH1111
MG176	<i>h+ ura4::adh-dmdNK rad50::kan^R</i>	EH1112
MG177	<i>h-smt0 ura4::adh-hsdCK mre11-D65N</i>	EH1113
MG178	<i>h-smt0 ura4::adh-hsdCK rad50::kan^R</i>	EH1114
MG182	<i>h-smt0 ura4::adh-hsdCK -NAT^R-adh-hENT1 mre11-D65N</i>	EH1118
MG269	<i>h+ura4::adh-hsdCK-NAT^R-adh-hENT1 rev3:hphMX4^R ura4-aim</i>	This study
MG270	<i>h+ura4::adh-hsdCK-NAT^R-adh-hENT1 mlh1::kan^R ura4-aim</i>	This study
MG273	<i>h+ura4::adh-hsdCK-NAT^R-adh-hENT1 exo1::ura4</i>	This study
MG274	<i>h+ura4::adh-hsdCK-NAT^R-adh-hENT1 nth1::ura4</i>	This study
MG276	<i>h-ura4::adh-hsdCK-NAT^R-adh-hENT1 rhp14::kan^R ura4-aim</i>	This study
MG278	<i>h+urg1::loxpFLP-3HA kan^R FRTfw NAT^R Rad50::LEU2 leu1-32</i>	This study
MG279	<i>h+urg1::loxpFLP1SS-3HA kan^R FRTfw NAT^R Rad50::LEU2 leu1-32</i>	This study
MG281	<i>h-ura4::adh-hsdCK-NAT^R-adh-hENT1top1::LEU2 ura4-aim leu1-32</i>	This study
MG293	<i>h+ura4::adh-dmdNK-NAT^R-adh-hENT1nbs1::kan^R ura4-aim</i>	This study
MG295	<i>h-ura4::adh-hsdCK-NAT^R-adh-hENT1nbs1::kan^R ura4-aim</i>	This study
MG297	<i>h-ura4::adh-hsdCK-NAT^R-adh-hENT1 ura4-aim mre11-D65N</i>	AK038
MG300	<i>h+ura4::adh-hsdCK-NAT^R-adh-hENT1rad2::LEU2leu1-32 ura4-aim</i>	This study
MG303	<i>h+ura4::adh-hsdCK-NAT^R-adh-hENT1msh2::his3his3-D1 ura4-aim</i>	This study
MG309	<i>h+ura4::adh-hsdCK-NAT^R-adh-hENT1 ung1::kan^R ura4-aim</i>	This study
MG312	<i>h+ura4::adh-hsdCK-NAT^R-adh-hENT1rad13::hphrhp14::kan^R ura4-aim</i>	This study
MG319	<i>h+ura4::adh-hsdCK-NAT^R-adh-hENT1 apn2::kan^R ura4-aim</i>	This study
MG328	<i>h-ura4::adh-hsdCK-NAT^R-adh-hENT1 pms1::kan^R ura4-aim</i>	This study

MG stock number	Genotype	Origin
MG349	<i>h+ura4::adh-hsdCK-NAT^R-adh-hENT1 top1::LEU2 rad50::kan^R ura4-aim leu1-32</i>	This study
MG350	<i>h-ura4::adh-hsdCK-NAT^R-adh-hENT1 top1::LEU2 rad50::kan^R ura4-aim leu1-32</i>	This study
MG355	<i>h+ura4::adh-hsdCK-NAT^R-adh-hENT1 mre11-D65N nth1::ura4</i>	This study
MG356	<i>h-ura4::adh-hsdCK-NAT^R-adh-hENT1 mre11-D65N nth1::ura4</i>	This study
MG357	<i>h+ura4::adh-hsdCK-NAT^R-adh-hENT1 rad50::KAN nth1::ura4</i>	This study
MG362	<i>h+ura4::adh-hsdCK-NAT^R-adh-hENT1 rad13::hph^R swi10::kan^R ura4-aim</i>	This study
MG363	<i>h+ura4::adh-hsdCK-NAT^R-adh-hENT1 rad3ts</i>	This study
	<i>h+ura4::adh-hsdCK-NAT^R-adh-hENT1 ura4-aim apn2::kan^R mre11-D65N</i>	AK069
	<i>h-ura4::adh-hsdCK-NAT^R-adh-hENT1 rhp14::ura4 mre11-D65N</i>	AK091
	<i>h+ura4::adh-hsdCK-NAT^R-adh-hENT1 rhp14::ura4 rad50::KAN^R</i>	AK093
	<i>h+ura4::adh-hsdCK-NAT^R-adh-hENT1 apn2::kan^R rad50::LEU2</i>	AK104
	<i>h+ura4::adh-hsdCK-NAT^R-adh-hENT1 msh6::ARG ura4-aim</i>	AK119
	<i>h-smt0 ura4-D18 rad50::kan^R</i>	EH65
	<i>h-smt0 ura4-D18 mre11-D65N</i>	EH805
	<i>h-smt0 leu1-32 ura4::adh-dmdNK mre11-D65N</i>	EH1088
	<i>h-smt0 leu1-32 ura4::adh-dmdNK rad50::kan^R</i>	EH1090
	<i>h-smt0 ura4::adh-dmdNK</i>	EH1092

Table 2-1 List of strains. “EH” strains were obtained from the lab strain collection of Dr Edgar Hartsuiker. “AK” strains were kindly provided by Dr Andrea Keszthelyi (NWCRFI-Bangor University), *rad3ts* checkpoint mutant (*h- rad3ts ura4-D18*) was a gift from Dr Thomas Caspari (Bangor University), MMR mutants (*mlh1*, OL937 and *msh2*, OL1348) and NER mutant (*rhp41 rhp42*, TM2) were a gift from Dr Oliver Fleck (NWCRFI-Bangor University). NER mutant (*rhp14*, R022), BER mutant (*nth1*, R0176) and PRR mutant (*rev3*, R016) were kindly provided by Dr Rolf Kraehenbuehl (NWCRFI-Bangor University). The mentioned mutants were crossed to *hsdCK/hENT1* strains to integrate both genes, and the resulting strains were used for the analysis. Cre-lox base strain, AW430, was a kind gift from Dr Adam Watson (Genome Damage and Stability Centre-University of Sussex).

2.1.2 List of primers

Number	Name	Sequence	Use
P001	Flp-NdeI_quik_F	5`CGCACTAGTTTCTCGGTACTATGCTTATGATCCA ATATCAAAGG-3`	Forward primer for FLP NdeI site directed mutagenesis
P002	Flp-NdeI_quik_R	5`CCTTTGATATTGGATCATAAGCATAGTACCGAGA AACTAGTGCG-3`	Reverse primer for FLP NdeI site directed mutagenesis
P005	FLP-NdeI-F	5`GCGCGCCATATGCCACAATTTGGTATATTATG-3`	Forward primer PCR FLP from pFV17DH305L plasmid
P006	FLP-SacI-R	5`GCGCGGAGCTCTTATATGCGTCTATTTATGTAG G-3`	Reverse primer PCR FLP from pFV17DH305L plasmid
P011	ENT1-FW	5`GCGCGCCTCCCGTGGAATTTTTTC-3`	Forward primer to check presence of hENT1 in hENT1- strains
P012	ENT1-REV	5`GCGCGCAGCTGGCTTCACTTTCT-3`	Reverse primer to check presence of hENT1 in hENT1- strains
P013	FRT-SalI-F	5`GCGCGCGTCGACGAAGTTCCTATACTTTCTAGAG AATAGGAACTTCCGAATAGGAACTTCGTCGACGC GCGC-3`	Forward FRT oligonucleotide
P014	FRT-SalI-R	5`GCGCGCGTCGACGAAGTTCCTATTCGGAAGTTC TATTCTCTAGAAAGTATAGGAACTTCGTCGACGCG CGC-3`	Reverse FRT oligonucleotide
P015	FW-adh	5`GCGCGCTTAATTAAGCATGCCCTACAACA ACTA AG-3`	Forward primer to isolate adh/hENT1- from EH969 genomic DNA

Number	Name	Sequence	Use
P016	Rev-ENT1	5'GCGCGCGGCGCGCCCTCTAGATCACACAATTGC CCGGAACAG-3'	Reverse primer to isolate adh/hENT1- from EH969 genomic DNA
P019	HA-F_BglII NdeI mutated	5'GCGCGCAGATCTTACCCATACGATGTTCTGACT ATGCGGGCTATCCGTATGACGTCCCGGACTATGCA GGATCCTATCCATACGACGTTCCAGATTACGCTTA AAGATCTGCGCGC-3'	Forward HA tag oligonucleotide
P020	HA-R_BglII NdeI mutated	5'GCGCGCAGATCTTTAAGCGTAATCTGGAACGTC GTATGGATAGGATCCTGCATAGTCCGGGACGTCAT ACGGATAGCCCGCATAGTCAGGAACATCGTATGG GTAAGATCTGCGCGC-3'	Reverse HA tag oligonucleotide
P021	hENTmut1F	5'CTCAGTGCCATCTTCAACAATGTCATGACCCTAT GTGCCATGTGC-3'	Forward to reverse the two first mutations of hENT1-
P022	hENTmut1R	5'GCACATGGCACATAGGGTCATGACATTGTTGAA GATGGCACTGAG-3'	Reverse to reverse the two first mutations of hENT1-
P023	hENTmut2F	5'GGGGAGCAGGAGACCAAGTTGGACCTCATTAGC AAAGGAGAGG-3'	Forward to reverse the third mutation of hENT1-
P024	hENTmut2R	5'CCTCTCCTTTGCTAATGAGGTCCA ACTTGGTCTC CTGCTCCCC-3'	Reverse to reverse the third mutation of hENT1-
P025	hENTmut3F	5'GTGAAGCCAGCTGAGGCAGAGACCGCAGGAGCC ATCATGGCC-3'	Forward to reverse the fourth mutation of hENT1-
P026	hENTmut3R	5'GGCCATGATGGCTCCTGCGGTCTCTGCCTCAGCT GGCTTCAC-3'	Reverse to reverse the fourth mutation of hENT1-

Number	Name	Sequence	Use
P027	hENTmut4F	5`CGCTATTGCCAGTGGCTCGGAACTATCAGAAAG TGCCTTCGGC-3`	Forward to reverse the fifth mutation of hENT1-
P028	hENTmut4R	5`GCCGAAGGCACTTTCTGATAGTTCCGAGCCACTG GCAATAGCG-3`	Reverse to reverse the fifth mutation of hENT1-
P029	Ura4-FW	5`TACTCTTTGGTAAAATTTTATGTAGCGACTAAAA TATTA ACTATTATAGATAAACACCTTGGGAATAAAA AAGTAATTTGCTATAGTAATTTATTAACATTGGA TGGCGGCGTTAGTATC-3`	Forward primer to PCR adhhENT1 from pFA6a- NatMX6
P030	Ura4-Rev	5`ACATCTTTCATTGGCTTTGTACATAGTTATCATT ACAAGTCTAAAAAAATTCACTCTTTTCTTATTCAA TGTCAATCCAAGAGAAAAGATTGTGGTAATGGCA TGCCCTACAACA ACTAAG-3`	Reverse primer to PCR adhhENT1 from pFA6a- NatMX6
P031	5`hENTcheck-fw	5`GCCTTGTTTGCGTTTGTTTCTTAGGCG-3`	Forward 5' check integration of hENT into <i>S.</i> <i>pombe</i> without kinase
P032	5`hENTcheck-rev	5`GTTTTCAAGAACTTGTCATTTGATATG-3`	Reverse 5' check integration of hENT into <i>S.</i> <i>pombe</i>
P033	3`hENTcheck-fw	5`GAAAAGAAAAGGAATGATAAGAGAAGG-3`	Forward 3' check integration of hENT into <i>S.</i> <i>pombe</i>
P034	3`hENTcheck-rev	5`GTTCCAACACCAATGTTTATAACCAAG-3`	Reverse 3' check integration of hENT into <i>S.</i> <i>pombe</i>
P036	5`FLP check-rev	5`GCAGGAATCAATTTCTTTAATGAGGC-3`	Reverse primer for PCR to check FLP integration at 5` end

Number	Name	Sequence	Use
P037	3`FLP check-fw	5`CATTGAAGGATGAGACTAATCCAATTG-3`	Forward primer for PCR to check FLP integration at 3` end
P038	3`FLP check-rev	5`CTTCTACAAATCCCAAATGTTGACATG-3`	Reverse primer for PCR to check FLP and 3-HA integration at 3` end
P040	3`URA4 check-FW	5`CTGAAGAAGTGATTGTAAACTGCGGTAG-3`	Forward primer for PCR to check FRT integration at 5` end
P041	5`hENTcheck-fw-NK	5`GCGCGCCAGCAAGCGCCAGAGGGTCGCC-3`	Forward 5' check integration of hENT into <i>S.pombe</i> with dmdNK kinase
P042	5`hENTcheck-fw-CK	5`GCGCGCGGTCAAAGAGTTTTTGTACT-3`	Forward 5' check integration of hENT into <i>S. pombe</i> with hsdCK kinase
P043	5`FLP check-fw-urg1	5`CGGTCTAAGAAGGCGCAACGATG-3`	Forward primer for PCR to check FLP integration at 5` end
P044	HAintFW	5`GGGTAGTGCTGAAGGAAGCATACGATACCCCGCATGGAATGGGATAATATCACAGGAGGTACTAGACTACCTTTCATCCTACATAAATAGACGCATACGGATCCCCGGTTAATTAA-3`	Forward primer for PCR 3-HA from pFA6a-3HA-kanMX6 plasmid
P045	HAintREV	5`AAAGTTTCGAGAATTTATACAATGAAGGTAATTAAACACATGTATGTGAAATTTAAAATAAACATGGTCCTTCTGTGACGTCTAAAACAGATGGGCAAGCGAATTCGAGCTCGTTTTAAAC-3`	Reverse primer for PCR 3-HA from pFA6a-3HA-kanMX6 plasmid

Number	Name	Sequence	Use
P046	HA5`check-fw	5`GCGCGCAATGTTGTGGGAAATTGGAGCG-3`	Forward primer for PCR to check 3-HA integration at 5` end
P047	HA5`check-rev	5`GCGCGCGATAGGATCCTGCATAGTCCG-3`	Reverse primer for PCR to check 3-HA integration at 5` end
P048	HA3`check-fw	5`GCGCGCACTCATGGTGATTTCTCACTTG-3`	Forward primer for PCR to check 3-HA integration at 3` end
P049	5`hphcheck-rev	5`GCGCGCGACGAGGCAAGCTAAACAGATCT-3`	Reverse PCR primer for negative control of FLP integration at 5` end
P050	3`hphcheck-fw	5`GCGCGCTAACGCCGCCATCCAGTTTAAAC-3`	Forward PCR primer for negative control of FLP integration at 3` end
P053	FRTintURA4REV	5`TAACATTGCCAGTAAGTAAGAATTGATCCTATTG TTAGCAACTTTGGCTTGTGTTTCATACTGACAATG CATCTTAGTGTTTTTTATTCTTCTCATGTCATGGAT GGCGGCGTTAGTATC-3`	Reverse primer for FRT integration into "FLP" strains
P056	FRTcheck5`REV	5`GCGGTGATGTGAGAACTGTATCCTAGCA-3`	Reverse primer for PCR to check FRT integration at 5` end
P057	FRTcheck3`FW	5`CTCGCGACGGAGTTCGCCGGCGAGC-3`	Forward primer for PCR to check FRT integration at 3` end
P058	FRTcheck3`REV	5`GCGATTCTTCTCATGTCATGGATGGCGG-3`	Reverse primer for PCR to check FRT integration at 3` end

Number	Name	Sequence	Use
P059	FRTintURA4FW	5'CTTTTCTCGGAGTATAATACACAATATCGGTGC AAATAGGTTTTAAAATTGCTCCAATCACATGTTCT TAAGAAAAAACGTCAAAGAAATCTAAGTGAAG CTTCGTACGCTGCAGG-3'	Forward primer for FRT integration into "FLP" strains

Table 2-2 List of primers used for PCRs. Primers were ordered from Eurofins MWG and were re-suspended in H₂O to a stock concentration of 100μM.

Number	Name	Sequence	Use
Seq001	Nde-FW	TGAAGGGCCTAACGGAGITGACTAATGTTG	sequence NdeI mutation into the FLP
Seq002	FW seq FLP	GTTTAAAGGCTAATTTTGTGAAAC	Forward sequence to check FLP clone into pAW8ENR plasmids and FLP integration into <i>S.pombe</i>
Seq003	Rev seq FLP	CCGCATAACTTCGATATAATAAC	Reverse sequence to check FLP clone into pAW8ENR plasmids and FLP integration into <i>S.pombe</i>
Seq004	HA-FW	AAAGGTTTCATTACTTTGCTGCC	sequence HA tag pAW8ENR plasmids
Seq005	FW seq FRT/FW seq Adh	GGACATATTGTCGTTAGAACG	Sequence hENT1 and FRT into pFA6a-NatMX6
Seq006	FRT int seq	GAAAAAGTCGATGCCTTGTTGCGTTTG	Sequence FRT into <i>S.pombe</i>
Seq007	FW seq Adh	GGACATATTGTCGTTAGAACG	hENT1 forward sequence
Seq008	INT Seq hENT	GGAATTTTTTCATGACGGCC	hENT1 internal sequence
Seq009	Rev Seq hENT	GATGTATGGCTAAATGTACG	hENT1 reverse sequence
Seq010	Nde-FW	TGAAGGGCCTAACGGAGITGACTAATGTTG	sequence NdeI mutation into the FLP

Table 2-3 List of primers used for sequencing. Primers were ordered from Eurofins MWG.

2.1.3 Plasmids

Stock number	plasmid	Source
MG19	pFA6a-NatMX6	(Hentges, Van Driessche et al. 2005)
MG43	pFA6a-3HA-kanMX6	(Bahler, Wu et al. 1998)
MG01	pFV17D	(Nielsen, Bentsen et al. 2009)
MG02	pFV17D H305L	(Nielsen, Bentsen et al. 2009)
MG05	pFV17D H305L-NdeImut	this study
MG06	pAW8E (euroscarf)	(Watson, Werler et al. 2011) and personal communication
MG29	pAW8ENdeI_0SS_CyEGFP	(Watson, Werler et al. 2011) and personal communication
MG30	pAW8ENdeI_1SS_CyEGFP	(Watson, Werler et al. 2011) and personal communication
MG31	pAW8ENdeI_2SS_CyEGFP	(Watson, Werler et al. 2011) and personal communication
MG35	pAW8ENdeI_0SS_FLP H305L_HA	This study (Note: contains STOP codon after the FLP gene)
MG36	pAW8ENdeI_1SS_FLP H305L_HA	This study (Note: contains STOP codon after the FLP gene)
MG37	pAW8ENdeI_2SS_FLP H305L_HA	This study (Note: contains STOP codon after the FLP gene)
MG32	pFS181-hENT1	(Sivakumar, Porter-Goff et al. 2004) Note: mutated hENT1
MG38	pFA6a-NatMX6_hENT1	This study (Note: backmutated hENT1)

Table 2-4 List of used plasmids.

2.1.4 Media

LB (L-Broth): tryptone 10g/l, yeast extract 5g/l, sodium chloride 5g/l, and agar 12g/l for LB agar.

YE and YEA (yeast extract (agar)): yeast extract 5 g/l, glucose 30 g/l, arginine 0.1 g/l, adenine 0.1 g/l, leucine 0.1 g/l, uracil 0.1 g/l, histidine 0.1 g/l and agar 25 g/l (for YEA)

YNB/YNBA (Yeast nitrogen base agar): for 1 l : YNB 1.9 g, ammonium sulphate 5 g, glucose 20 g and agar (25 g/l)

ELN (Extra low nitrogen): EMM powder 27.3 g/l, ammonium chloride 0.05 g/l, uracil 0.1 g/l, leucine 0.1 g/l, histidine 0.1 g/l, arginine 0.1 g/l, adenine 0.2 g/l, agar (25 g/l)

SOC: 2 % Bacto tryptone, 0.5 % yeast extract, 10mM NaCl, 2.5mM KCl, 10mM MgCl₂, 10mM MgSO₄, 20mM glucose)

EMM (Edinburg minimal media): EMM powder 27.3 g/l supplemented either by ammonium chloride 5 g/l or glutamate 3.75 g/l and agar (25 g/l).

Media components were purchased from FORMEDIUM™

2.1.5 General Buffers

Preparations for specific buffers are given in section where appropriate.

EDTA (Ethylenediamine tetraacetic acid), 0.5M (pH 8.0): 186.1 g Na₂EDTA.2H₂O, 10M NaOH to adjust pH and H₂O to 1 l.

PBS (phosphate-buffered saline) buffer, 10x: for 1l, add 80 g NaCl, 2 g KCl, 5 g Na₂HPO₄.7H₂O, 2 g KH₂PO₄ and H₂O to 1l

TAE (Tris-Acetate-EDTA) buffer for gel purification, 50x: 242g Tris base, 57.1 ml glacial acetic acid, 37.2 g Na₂EDTA.2H₂O and H₂O to 1l

TBE (Tris-Borate-EDTA) buffer for routine electrophoresis, 10x: 108 g Tris base, 55 g boric acid, 40 ml 0.5M EDTA (20mM) and H₂O to 1l

TE (Tris-EDTA) buffer for DNA re-suspension, 1x: 10mM Tris-HCl pH 7.5, 1mM EDTA

Bromo phenol blue loading buffer, 10x: 5 ml TBE 10x, 4 g sucrose, 25 mg bromophenol blue and H₂O to 10 ml.

2.1.6 Various

Antibiotics: Nourseothricin (NAT, Werner Bioagents), Geneticin (G418, Melford), Hygromycin (Melford), Ampicillin (Melford), Cycloheximide (Melford).

DNA damaging agents: CPT (Acros Organics), Gemcitabine (GemC, Sigma), Cytarabine (AraC, Sigma), Methyl methanesulfonate (MMS, Acros Organics) and UV (CL-1000 ultraviolet crosslinker, UVP)

Enzymes: Restriction enzymes (purchased from NEB, New England Biolabs) and specific DNA polymerases, used for PCRs are mentioned in the relevant results sections. With the exception of *AscI*, *BglIII* and *PacI* which had a concentration of 10,000U/ml, restriction enzymes were at a stock concentration of 20,000U/ml.

T4 ligase was purchased from NEB, RNase A was purchased from Fisher and Proteinase K was purchased from Melford.

2.2 Methods

2.2.1 Yeast methods

2.2.1.1 *S. pombe* crosses

The ability of yeast to exchange genes during meiosis was used to construct new strains with genes of interest. When *S. pombe* cells are starved for nitrogen, they conjugate and form spores. Success of the cross is assessed by observing asci (group of four spores) in a microscope. To cross, mix strains (a loop full of each) with different mating types in a drop of water on ELN media (containing limiting amount of nitrogen to induce starvation) and incubate 2-4 days at 25°C.

Random spore analysis was used to select new recombinants resulting from crosses:

- Re-suspend a loop full of the crossed material in a solution containing 1/1000 diluted snail gut enzyme (β -Glucuronidase, Sigma), which kills parental vegetative cells, and incubate overnight at room temperature.
- Plate 500 spores on appropriate non selective media and incubate at 30°C until formation of colonies.
- Streak single colonies on non selective media and incubate for two days (or more depending on the media)
- Replica plate on selective media and incubate for at least two days at 30°C.

To cross the *S. pombe* genome wide deletion library: the library (Bioneer library V2) was thawed from -80°C for about 30 minutes in a cold room and cells were transferred into 96 well plates containing 50 μ l of minimal EMM media, supplemented with amino acids (leucine, adenine and uracil 0.1g/l), using a 96 pin replicator. Cells were then

incubated for 5 days at 30°C and crossed to MG102 (MG102 strain was pre grown in EMM media to reach cell density of $5 \cdot 10^6$ cells/ml). 50µl of MG102 culture were added to the library and mixed well using a multi well plate vortex. Cells were then transferred to ELN plates using a 48 pin replicator, and incubated for 5 days at 25°C.

Yeast mating type was determined using iodine which stains spore walls dark: cross strains resulting from the crosses to a known h^+ or h^- strain on ELN medium are incubated at 25°C for 2 days and exposed to iodine vapour for at least 5 minutes.

Freeze strains: To store strains, re-suspend a loop full of cells in 50 % glycerol in YEL and freeze at -80°C

2.2.1.2 *S. pombe* spot tests

Spot tests are used to assess survival of a strain following a chronic exposure to a toxic agent. Cells are grown to 10^7 cells/ml and diluted (10 fold) five times. 10µl of each dilution is plated on media containing the drugs to be tested, dried and incubated at the appropriate temperature.

2.2.1.3 *S. pombe* transformation

Gene integration and/or replacement into *S. pombe* genome were carried out by transformation using a Lithium Acetate (LiAc) *S. pombe* transformation protocol (Bahler *et al.*, 1998).

Prior to transformation, DNA was purified using phenol chloroform extraction:

- Mix 1 volume of phenol chloroform with the DNA and centrifuge at maximum speed, room temperature for 5 minutes
- Collect DNA from supernatant and precipitate with 1/10 volume of 3M NaAc (Sodium acetate) and 1 volume of isopropanol
- Centrifuge at maximum speed, room temperature for 15 minutes and wash the pellet with ethanol 70% (add 1ml of ethanol, spin at maximum speed for 1 minute and discard the supernatant)
- Air dry the pellet and re-suspended in TE buffer

For the transformation:

- Inoculate one colony in 10 ml YE and incubate overnight at 30°C
- Count cells with haemocytometer, dilute the culture and grow cells to 1×10^7 /ml. To calculate the number of cells N to be inoculated at time point 0 (N_0) use the

formula $N_t = 2^G \times N_0$, N_t stands for number of cells at the desired time, N_0 for initial number of cells, G for number of generations (generation time for wild type in rich media *S. pombe* = 2,5 hours).

- Spin 10 ml of the cell suspension at 3000 rpm for 5 minutes at room temperature
- Wash in 1 ml of 0.1M LiAc-TE (Lithium Acetate): re-suspend cells in LiAc-TE solution and spin at maximum speed for 30 seconds at room temperature (LiAc-TE preparation: 0.1M LiAc in TE 1x)
- Re-suspend cells in 100 µl of LiAc-TE
- Add 2µl of 10mg/ml carrier DNA (sonicated salmon sperm, Stratagene) and 10µl of DNA
- Mix and incubate 10 minutes at room temperature
- Add 260 µl of 40% PEG (polyethylene glycol, 4000) /LiAc-TE (40 g of PEG in 100 ml of LiAc-TE) to precipitate the DNA
- Incubate 1 hour at 30°C
- Add 43 µl of DMSO (Dimethyl Sulfoxide) to facilitate DNA transport through the cell walls
- Heat shock 5 minutes at 42°C
- Spin at maximum speed for 1 minute at room temperature and wash the pellet in 1 ml of water (re-suspend in 1 ml of water and spin at maximum speed for 1 minute)
- Re-suspend the pellet in 500 µl of water and plate on non selective media (250 µl/plate), incubate overnight at 30°C
- Replica plate the resulting lawn on selective medium and incubate at 30°C until formation of single colonies

Colony PCR to check gene integration

Re-suspend cells from one colony in 25 µl of H₂O, boil for 5 minutes and add a mix containing 5 µl of taq buffer, 3 µl of MgCl₂, 10 µl of dNTPs, 0.5 µl of each primer 10µM, 5 µl of H₂O and 1 µl of *Taq* DNA polymerase (NEB). PCR conditions: 2 minutes 94°C; 40 cycles of 1 minute 94°C, 1 minute 45°C, 2 minutes 65°C; and 10 minutes 65°C

General PCR conditions to check gene integration from genomic DNA

PCR reaction: 5 µl of Buffer 10x, 3 µl of MgCl₂ 25mM, 5 µl of dNTPs 2mM each, 1 µl of each primer 10µM, 100 ng of DNA, 0.5 µl of *Taq* DNA polymerase and H₂O to 50 µl.

PCR conditions: 2 minutes at 95°C, 30 cycles of (denaturation: 30 seconds at 95°C, annealing and elongation: depends on the product and primers and will be specified in the appropriate result sections) each, final extension 5 minutes at 72°C.

2.2.1.4 DNA extraction from yeast cells

Genomic DNA to use as PCR template was extracted from *S. pombe* genome using the following protocol:

- Grow cells to $1 \cdot 10^7$ cells/ml in 10 ml
- Spin down 10 ml of cells at 3000x g for 5 minutes at room temperature
- Wash in 1 ml of TE in a screw cap tube
- Re-suspend in 250 µl of TE and add 1 volume of phenol chloroform to extract proteins
- Add 2 eppendorf lids of glass beads to lyse cell walls
- Ribolyse: 3x 30 seconds at 6.5 (Ribolyser: Precellys24, Bertin Technologies)
- Spin at maximum speed at room temperature for 5 minutes
- Collect nucleic acids in the upper phase into a new tube
- Add 2 µl of RNase 50 µg/ml to digest RNA and incubate at 37°C for 30 minutes
- Add 2 µl of sodium dodecyl sulfate (SDS) 10 % and 2 µl of proteinaseK 5mg/ml to remove the remaining proteins and incubate an hour at 55°C
- Extract proteins two times with 1 volume of phenol chloroform using eppendorf tubes
- Precipitate DNA with 1:10 volume of 3M NaAc (sodium acetate) and 2 volumes of ethanol 96 %
- Vortex and centrifuge 15 minutes at maximum speed at room temperature
- Wash with 1 ml of ethanol 70%
- Remove the supernatant and air dry the pellet
- Re-suspend the pellet in 100 µl of TE

2.2.1.5 DAPI staining and microscope observation

DAPI (4',6-diamidino-2-phenylindol) staining was used to visualise cell nuclei using the following protocol:

- Spin down $5 \cdot 10^6$ cells and re-suspend in 50 μ l of water
- To fix cells, add 200 μ l of methanol to the cell suspension.
- Wash the mixture in 1x PBS buffer
- Re-suspend cells in 1 ml of DAPI (Sigma) solution at a final concentration of 1 μ g/ml (DAPI stock solution of 1 mg/ml was prepared by re-suspending in water and diluted in PBS)
- Spin down the suspension and remove the solution leaving the last few (~10) microliters
- Coat the slide cover with poly-lysine (Sigma) solution to fix cells on the slides and obtain a clear monolayer of cells (few drops of the lysine are added to the slides and air dried before addition of cells)
- Add ~5 μ l of cell suspension to the slides

Cells were observed in fluorescent microscope (Nikon ELLIPSE TE 2000-U) at 60X and HCI image programme was used to capture images.

2.2.1.6 Western Blot

Protein expression by yeast cells was checked using Western Blot. The proteins were extracted using the TCA protocol.

TCA (Trichloro acetic acid) protein extraction from yeast cells

- Harvest 5×10^7 cells
- Spin down for 5 minutes at 3000rpm
- Discard supernatant and re-suspend in 1 ml 20%TCA (20mg TCA in 100 ml H₂O)
- Spin down for 2 minutes at 13000 rpm, remove the supernatant and re-suspend in 200 μ l of 20 % TCA
- Add 1 eppendorf lid of glass beads and ribolyse 3 x 20 seconds at 6.5
- Collect the supernatant: puncture bottom with a needle, place a 2 ml screw cap tube in a 15 ml tube and put the punctured tube on top of the screw cap tube, spin for 5 minutes at 4000 rpm

- Remove bottom tube with the supernatant and spin for 5 minutes at maximum speed
- Remove all supernatant and re-suspend pellet in 200 µl of 1x sample buffer/250 mM Tris pH 8.5 [for 5 ml, add 1.25 ml of 4x sample buffer (250mM Tris pH 6.8, 8 % SDS, 20 % glycerol, 20 % β-mercaptaethanol and 0.4 % bromophenol blue) to 833 µl Tris 1.5M and H₂O to 5 ml].
- Boil samples for 5 minutes
- Load 15-50 µl on a gel or store at -20°C until used

SDS PAGE Western Blotting (BioRAD)

The proteins were run on a SDS-PAGE gel (Sodium Dodecyl Sulfate polyacrylamide gel electrophoresis) and detected using Western Blot using the following protocol:

- Assemble gel apparatus according to kit instructions
- Make resolving gel (100 µl 10 % SDS, 2.5 ml 1.5M Tris pH8.8, 3.34 ml 30% acrylamide, 4 ml H₂O, 50 µl 10% APS and 10 µl TEMED)
- Pipette the gel solution into the assembly and overlay with isopropanol to exclude air and ensure a flat surface.
- Allow to set for about 15 minutes, pour off isopropanol and rinse with tap water
- Make stacking gel (50 µl 10 % SDS, 1.25ml 0.5M Tris pH6.8, 650 µl 30 % acrylamide, 3.05 ml H₂O, 50 µl 10% APS and 10 µl TEMED) and quickly pour into the gel plates and insert comb. Allow to set for at least 5 minutes
- Remove combs and place in electrophoresis tank
- Fill the tank with electrophoresis running buffer 1x [Running buffer 10x: for 1l, mix 147,15 g glycine (1.96M), 50 ml SDS 20 % (1 %), 500 ml 1M Tris pH8.3 (500mM) and H₂O to 1l] and remove air bubbles from bottom of plates before running.
- Run at 200V for 45 minutes (depending on the size of protein)
- Remove gel assembly from tank and discard running buffer. Take the gel plates out of assembly unit, pull apart the glass plates and trim off the stacking gel.
- Make the western sandwich by placing sponge, two layers of filter paper, gel, nitrocellulose membrane (AmershamTM), two layers of filter paper and sponge. Keep all components wet with transfer buffer, remove all air bubbles and make sure that the membrane is placed on the upper face of the gel.

- Fill with transfer buffer [for 1l, mix 200 ml methanol (20 %), 3.02 g Tris-base (25mM), 14.4 g glycine(196mM), 1.85 ml SDS 20% (0.037 %) and H₂O to 1l] and transfer at 60V for 2 hours.
- Take apart the sandwich and check protein transfer by spraying Ponceau (0.1 % in 5 % acetic acid) solution on the membrane. Leave for about 2 minutes and rinse the Ponceau solution out with tap water.
- Block the membrane in 5 % milk solution (in PBS 1x-tween 0.1 %, 1 ml of tween in 1L of PBS 1x) and incubate for 1 hour shaking at room temperature. Wash three times in PBS-tween, 10 minutes per wash.
- Add primary antibody (1/2000 diluted HA-probe F-7 mouse monoclonal, Santa Cruz Biotechnology) diluted in 5 % milk in PBS/Tween and incubate overnight shaking at 4°C
- Wash 3 times in PBS-tween, 10 minutes per wash.
- Add secondary antibody (1/3000 diluted rabbit anti mouse, DAKO) diluted in 5 % milk in PBS/Tween and incubate 1 hour shaking at room temperature
- Wash 3 times in PBS-tween, 10 minutes per wash
- Spread 1 ml of developing solution (ECL system+,Amersham™) to the membrane
- Drain the blot and place in developing cassette and expose the film (Amersham™ Hyper film ECL) under dark room conditions
- Wait 2 to 3 minutes and develop the film on X-ray Film processor (MI-5, JENCONS-PLS).

2.2.1.7 HPLC measurement of free intracellular GemC-TP and dNTPs levels (Kumar *et al.*, 2010)

HPLC was used to quantify intracellular GemC-TP and dNTPs levels using positively charged resin SAX (strong anion exchange) column. The principle of the method is based on the binding strength between the negatively charged phosphorylated nucleosides and GemC which are retained by the columns. Nucleosides are eluted by gradient elution, which releases the nucleosides according to their binding strength. Different retention time characterises each nucleoside and a peak is released at specific time. The peaks are then converted into pmol by calibration with standards of known nucleoside content.

A. Collecting *S. pombe* cells

- Inoculate 10 ml of media with one colony (primary culture)
- Inoculate secondary culture to reach 5×10^6 cells/ml (inoculate 400 ml)
- Collect 20×10^8 cells on a filter (Millipore 0.8 μ m), fit the filter on a filter carrier and connect to a vacuum.
- Cautiously put the filter in a 15ml Falcon tube after filtration, freeze the tube in liquid nitrogen and store at -80°C until use.

B. Isolate dNTPs and NTPs by Freon-trioctylamine extraction

Nucleotides were extracted by TCA which extracts and precipitates nucleotides. To prevent interference with chromatography columns, the acid was then extracted from the solution by Freon-trioctylamine.

Note: All solutions are filter sterilized and kept on ice.

- Prepare per sample: 1.5 ml eppendorf tube with 800 μ l ice cold Freon-trioctylamine mixture [10/2.8: 10 ml Freon (Sigma-aldrich) and 2.8ml trioctylamine (Sigma-aldrich)], 1.5 ml eppendorf tube with 700 μ l ice cold Freon-trioctylamine mixture and empty 1.5 ml eppendorf tube (to collect samples)
- Add 700 μ l 12% TCA to extract nucleotides and 15mM MgCl_2 to stabilise nucleotides to Falcon tube containing the filter and vortex for 30 seconds
- Incubate on rotator in cold room for 7 minutes
- Vortex for 2 minutes and incubate on rotator for 6 minutes
- Vortex for 30 seconds and remove the filter
- Centrifuge 2 minutes at 4000xg in cold room
- Pipette the supernatant into the tube with 800 μ l Freon mixture
- Vortex making sure the two phases are well mixed
- Centrifuge for 1 minute maximum speed
- Repeat the above steps with the tube with 700 μ l Freon mixture
- Collect the upper phase and keep at -20°C until use

3. Separate dNTPs from NTPs (Boronate column)

To prevent interference of NTPs in the measurement (NTP levels are significantly higher than dNTPs and can interfere with dNTP measurement if not separated), dNTPs were separated from NTPs by a boronate column. dNTPs bind with less strength (with

2-OH groups) than NTPs, which have 3-OH groups. dNTPs are eluted by the ambic (ammonium bicarbonate) buffer whereas NTPs remain bound to the column.

Preparation of boronate column:

Mix 1.3 g of boronate mix (BIORAD) in 50 ml of H₂O and keep the mixture overnight in cold room before use

- Fill the plastic tubes (funnel tubes) with 1.2 ml of the solution and leave to drain until no water is left
- Wash the boronate grains with 2 x 6 ml sodium boronate buffer and keep in cold room until use (NOTE: the columns are stored in sodium boronate buffer)

To separate NTPs from dNTPs:

- Equilibrate columns with 2 x 6 ml of ambic buffer (50mM ammonium carbonate pH8.9 + 15mM MgCl₂)
- Mix 475µl of sample (the remaining solution is kept for NTP measurement) with 25µl of 1M ammonium carbonate and adjust to pH 9 (for NTPs to bind) with HCl 6M using PH measurement strips
- Load the sample on the equilibrated columns and discard flow through
- Elute dNTPs with 2.5 ml of ambic buffer into a 15 ml Falcon tube on ice and keep at -20°C until use
- Regenerate columns with 2 x 6 ml of 0.1M sodium boronate pH8.9 (to wash out NTPs) and store in cold room (the columns can be kept up to a year).

4. Run HPLC

KH₂PO₄ buffer (running buffer)

For 1l solution

Mix KH₂PO₄ with 950 ml (0.436M KH₂PO₄ for NTPs and 0.36M for dNTPs)

Adjust to pH 3.35 with phosphoric acid 85-90% and filter sterilize

Under the hood add 25 ml acetonitril to prevent from potential bacterial contamination and filter-sterilised water to 1l

Samples

Samples were prepared in ambic buffer and adjusted to ~pH4 with ~6.8µl of HCl 6M (pH measured with strips). 100pmol (in 200µl) of NTPs and dNTPs standards were loaded on HPLC columns. GemC-TP (total of 200pmol in 200µl) was loaded. NTP samples were diluted 10x in ambic and dNTP samples were loaded without dilution.

HPLC programme

Nucleosides were separated with a HPLC column (28 cm SAX) on DIONEX PDA-100 photodiode Array detector (Dionex RF 2000 Fluorescence detector) using CHROMELEON programme. The column was stored in methanol and rinsed with sterile water before use (Note: this step is necessary to prevent salt precipitation from the running buffer). Samples were run with a flow of 1 ml/minute and the “gradient” programme (1 ml 0.36M KH_2PO_4 buffer for 1 min, followed by 35 minutes of 0.36M KH_2PO_4 buffer, 5 minutes gradient 0.36M→0.436M KH_2PO_4 buffer and 20 minutes of 0.436M KH_2PO_4 buffer).

5. Calculation of dNTP levels

To determine concentrations of dTNPs and GemC-TP, we converted HPLC peaks into pmol/ 10^8 cells. To correct for variations that might occur during cell collection, dNTP peak heights were normalized to NTPs levels. Nucleotide levels were chosen for normalisation as they normally don't vary in cells. Because CTP and TTP showed variations after GemC treatment, we normalised to ATP and GTP levels. The normalisation value was termed “k” and was determined by dividing treated samples by non treated samples. Average of ATPk and GTPk were then used to determine K value that was used for normalisation of height levels (by dividing peak heights by K value). To determine pmol of dTNPs/ 10^8 cells, we used a formula that takes in account the volume changes during the preparation of samples. The formula is explained as follow:

- ❖ As we run 200 μl out of 2500 μl (eluted dNTPs from boronate columns) we divided the normalised height values by 200 and multiplied by 2500
- ❖ For the boronate column, we used 475 μl out of 700 μl (Freon extraction) so we divided the above result by 475 and multiplied by 700
- ❖ The above value is calculated for the total amount of collected cells (20×10^8 cells), however we want to calculate levels/ 10^8 cells, we hence divided the result by 20
- ❖ We then calibrated to the standards values. The standards heights correspond to 100 pmol, we multiplied the calculated value by 100 and divided by standards heights.
- ❖ Formula= $\frac{(((700 * (2500 * (\text{sample height} / 200))) / 475) / 20) * 100}{\text{standard height}}$

2.2.2 Molecular biology

Plasmids were purified using the plasmid purification MACHEREY-NAGEL (05/2009 rev.06) Midi prep kit. DNA for cloning was recovered from agarose gels using MACHEREY-NAGEL gel extraction kit (NucleoSpin Extract II, March 2009/Rev.08) and transformation into *E. coli* was carried out using BIO-RAD MicroPulser™ (protocol from catalogue number 165-2100).

2.2.2.1 PCR, restriction digest, agarose gel electrophoresis, DNA measurement and ligation

General PCR conditions to amplify genes: PCR reaction: 5µl of Buffer 10x, 2µl of MgSO₄ 25mM or MgCl₂ 25mM, 5µl of dNTPs 2mM each, 1.5µl of each primer 10µM, 100ng of DNA, 1µl of polymerase (polymerases are given in relevant result section), and H₂O to 50µl.

PCR conditions: 2 minutes at 95°C, 30 cycles of 30 seconds at 95°C, 30 seconds at appropriate annealing temperature and extension (time depending on the PCR product) at 72°C each, and final extension 5 minutes at 72°C.

General digestion to check sizes: add 0.5 µl (10U) of the appropriate enzyme to a mix containing 1x buffer, DNA and H₂O to 20 µl and incubate for 1 hour at 37°C. Load 5µl of the digested mixture on a 0.7% agarose gel containing ethidium bromide.

General digestion for cloning: add 1 µl of the appropriate enzyme (20U) to a mix containing 1x buffer, 5 µg of plasmid and H₂O in 100µl and incubate overnight at 37°C. Load on agarose gel (0.7% to 2% depending on DNA size) containing 1/10000 diluted SYBR DNA gel stain. DNA was recovered from the gel and ligated before transformation into *E. coli*. To dephosphorylate blunt end plasmids and decrease self-ligation, cut plasmids were treated with CIP phosphatase (NEB), 1 µl (20U) was added to the digested mixture and incubated 1 hour at 37°C.

Agarose gel preparation: melt required amount of agarose gel (% depends on the size of the digested product) in TAE buffer 1x, for gel purification purposes or TBE buffer 1x to check sizes. Leave to cool before adding ethidium bromide (Fluka, stock solution 1 %), for visualisation only, or SYBR® DNA gel stain (Invitrogen) for visualisation and

purification. The SYBR[®] DNA was diluted 10,000 times and ethidium bromide diluted ~1/25000 times. Pour the gel in the casting tray and leave to cool.

DNA quantification: DNA was quantified using Invitrogen Qubit Fluorometer: Dilute samples, mix 100 µl of the diluted sample with 100 µl of PICOGREEN (Invitrogen) diluted 200x and measure (see manual for machine setting).

Ligation: A 1:3 (plasmid/insert) molar ratio was generally used for ligation, in a total of 20 µl, mix 100 ng of the plasmid with the appropriate amount of insert, 1 µl of ligase (Promega), 1x ligase buffer and H₂O. Incubate the mixture for an hour at room temperature and overnight at 4°C before transformation into *E. coli*.

Annealing oligonucleotides (protocol from

http://www.genosys.co.uk/oligos/tech_info/annealing.html):

Re-suspend oligonucleotides at the same molar concentration (100 pmol/µl) using annealing buffer (10mM Tris, pH 7.5-8.0, 1mM EDTA, 50mM NaCl). Mix equal volumes of both primers and heat at 95°C for 4 minutes. Remove and the heat block to allow slow cooling to room temperature.

2.2.2.2 Small scale plasmid purification (boiling lysis miniprep)

For small scale plasmid purification, the boiling lysis protocol was used to check clones.

- Inoculate overnight cultures in 2 ml of LB containing the appropriate antibiotic
- Spin 1.5 ml of the culture at 13,000x g for 15 seconds at room temperature
- Re-suspend in 350 µl of boiling buffer (buffer preparation: for 50ml, mix 250µl of 2M Tris pH 7.5, 5ml of EDTA 0.5M, 1.25 ml Triton X-100, 4g of sucrose and fill to 50ml with H₂O)
- Add 25 µl of lysozyme 10 mg/ml (solution in TE) to lyse cell walls
- Vortex and leave 5 minutes at room temperature, boil 2 minutes
- Spin at maximum speed for 15 minutes at room temperature to remove cell wall debris
- Pick out the pellet with a tooth pick and add 1 µl of RNase 50 µg/ml to the suspension to digest RNA.
- Incubate 30 minutes at 37°C

- Add 1 volume of phenol chloroform to extract proteins, vortex and centrifuge at maximum speed for 5 minutes at room temperature
- Collect the upper phase and add, 75 μ l of 3M NaAc (unpH-ed) and 250 μ l of isopropanol to precipitate the DNA
- Vortex and leave 5 minutes at room temperature
- Spin at maximum speed for 15 minutes at room temperature
- Wash the pellet with 1 ml of 70% ethanol (spin at maximum speed for 2 minutes)
- Air dry the pellet for at least 1 hour at room temperature and re-suspend in 50 μ l of TE

2.2.2.3 Site directed mutagenesis (Agilent Technologies QuickChange Site-directed Mutagenesis kit Revision B.01)

The aim of this method is to mutate one or more targeted base using primers containing the desired mutation. Briefly, the base switch is carried out using a plasmid with the gene of interest, two complementary (forward and reverse) synthetic oligonucleotides containing the mutation and a high fidelity polymerase (*pfuTurbo*).

The mutation is introduced by the primers and then extended by polymerase which extends the primers in a temperature cycler. Methylated non mutated parental plasmid is then digested by DpnI. Mutated plasmid, which contains nicks that are introduced after synthesis, is transformed into *E. coli* competent cells which repair the nicks. The strategy is outlined in Agilent Technologies QuickChange Site-directed Mutagenesis kit Revision B.01.

- Add DNA (20 ng of plasmid) to a mix containing 5 μ l of 10x reaction buffer, 200nM of each primer, 0.1mM of total dNTPs, 1 μ l of *Pfu Turbo* DNA polymerase, 2.5 U/ μ l (Stratagene) and ddH₂O to 50 μ l.
- Put the mix into a PCR cycler (95°C for 30 seconds followed by a 12 cycles each of 95°C for 30 seconds, 55°C for 1 minute and 68°C for 6 minutes).
- Cool the reaction on ice for 2 minutes before treatment with DpnI. 1 μ l of DpnI (10U/ μ l) was added to the reaction and incubated at 37°C for an hour.
- Transform *E.coli* cells with 1 μ l of the digested product (BIO-RAD MicroPulser *E. coli* transformation)

3 Setting up a system to study nucleoside analogue in *S. pombe*

As mentioned in the introduction, toxicity of NAs depends on two major proteins: the transporter, for the import of the drug into cells, and the kinase, which phosphorylates the (pro) drug into their mono phosphorylated form. The two proteins are naturally present in mammalian cells as part of the deoxyribonucleoside salvage pathway but are lacking in fission yeast, which only synthesises deoxynucleosides via the *de novo* pathway. In order to allow efficient uptake and phosphorylation of NAs in *S. pombe*, we have incorporated a transporter and a kinase into the *S. pombe* genome to mimic the mammalian deoxynucleoside salvage pathway. Two widely used anticancer NAs, GemC and AraC, were chosen for this project. While the toxicity of AraC is mainly attributed to incorporation of the triphosphate form (AraC-TP) into DNA, which in turn inhibits DNA synthesis (Galmarini *et al.*, 2001; Sampath *et al.*, 2003; Ewald *et al.*, 2008a), the mechanism by which GemC inhibits DNA synthesis is more complex. The triphosphate form (dFdCTP, GemC-TP) incorporates into DNA and inhibits CTP-synthetase, the diphosphate form (dFdCDP, GemC-DP) inhibits ribonucleotide reductase (RNR), deamination of the monophosphate form (dFdCMP, GemC-MP) results in dFdUMP which inhibits Thymidylate Synthase (TS), one of the key enzymes of nucleotides synthesis (Mini *et al.*, 2006) and detailed in paragraph 1.2.2.2. Because of this complexity I have chosen to use the term GemC for all the forms of the drug and, unless otherwise stated, GemC here refers to effect of the drug in general.

3.1 Kinases

For this project two kinases were chosen: The *Drosophila melanogaster* deoxynucleotide kinase (*dmdNK*), a highly efficient kinase which phosphorylates all nucleosides (Johansson *et al.*, 1999; Vernis *et al.*, 2003), and the human deoxycytidine kinase (*hscCK*), which phosphorylates most anticancer NAs (Chottiner *et al.*, 1991). The *Drosophila* kinase was chosen to allow the phosphorylation of a wider choice of NAs, whereas the human kinase was chosen as it is known to efficiently phosphorylate the deoxycytidine analogues.

3.1.1 Kinase constructs

Integration of the kinases into the yeast genome was subject of a separate project which I carried out as part of my Master's degree, here I only give an overview of the construction process, detailed in my master's dissertation (Gasasira, 2007). DNA coding sequences of the two kinases were separately cloned under the constitutive Alcohol dehydrogenase (Adh) promoter of the pART1 vector (kind gift from Dr N. Rhind, University of Massachussetts Medical School). The genes and the promoter were then integrated into *S. pombe*. The kinases were integrated on chromosome III of the yeast genome replacing the URA4 coding sequence (strategy outlined in *Figure 3-1*).

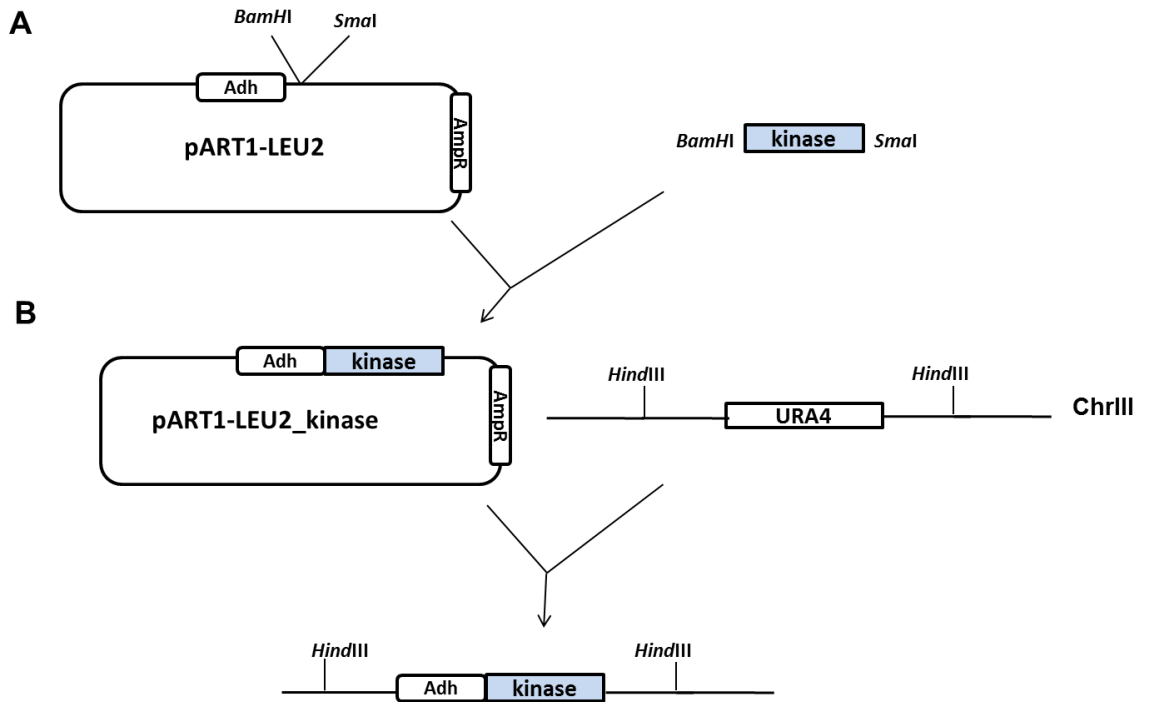
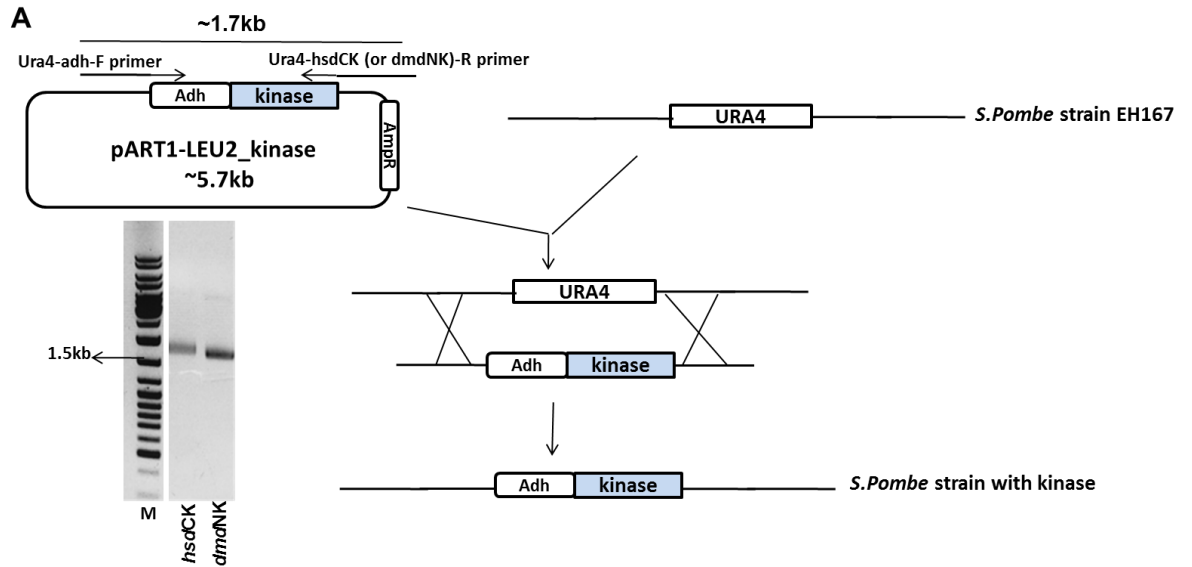


Figure 3-1 Strategy to integrate kinases into *S. pombe*. (A) The kinases coding sequences (either dmNK or hsdCK) were cloned under the Adh promoter of pART1 plasmid using *Bam*HI and *Sma*I restriction sites. They were integrated into the yeast genome using HR-based gene exchange (B).

To sub-clone kinases into pART1, the coding sequence was PCR amplified using DmdNK-FW and DmdNK-REV (for *dmdNK*), and dCK-FW and dCK-REV (for *hsdCK*) primers containing *BamHI* (forward) and *SmaI* (reverse) restriction sites (primers detailed in Gasasira, 2007). *hsdCK* was amplified from the pET-3d plasmid (Chottiner *et al.*, 1991), received from Lenore Urbani, Stanford University School of Medicine and *dmdNK* was received from Vernis (2003). pART1 was shortened by removing the LEU2 sequence cloned under *HindIII*. The kinase sequences were then cloned under *BamHI/SmaI* restriction sites of the plasmid.

To integrate kinases into *S. pombe*, Adh-coupled kinases were PCR amplified using long primers, (Ura4-adh-F, Ura4-hsdCK-R and Ura4-dmdNK-R, detailed in reference Gasasira, 2007), with 100bp of homology to the URA4 coding sequence flanking regions and 20bp identical to Adh (forward primer) and kinases (reverse primer). A band corresponding to the expected size was amplified for each kinase [~1.7kb corresponding to the kinases (~750bp), Adh promoter (~760bp) and long primers (~200bp), *Figure 3-2A*]. The genes were transformed into *S. pombe* (strain EH167, *smt0 leu1-32*, from Edgar Hartsuiker's strain collection), and 5-FOA resistance was used to select for the absence of the URA4 gene, replaced by the kinase. Resistant colonies were PCR checked using check FW and adh reverse primers (Gasasira, 2007). Bands with expected size (200bp) were amplified in positive controls and not in negative controls, confirming the presence of the genes (*Figure 3-2B*). Kinases were then PCR amplified using Ura4seqFW and Ura4seq reverse primers (Gasasira, 2007) and sequenced to confirm that there were no mutations.



B

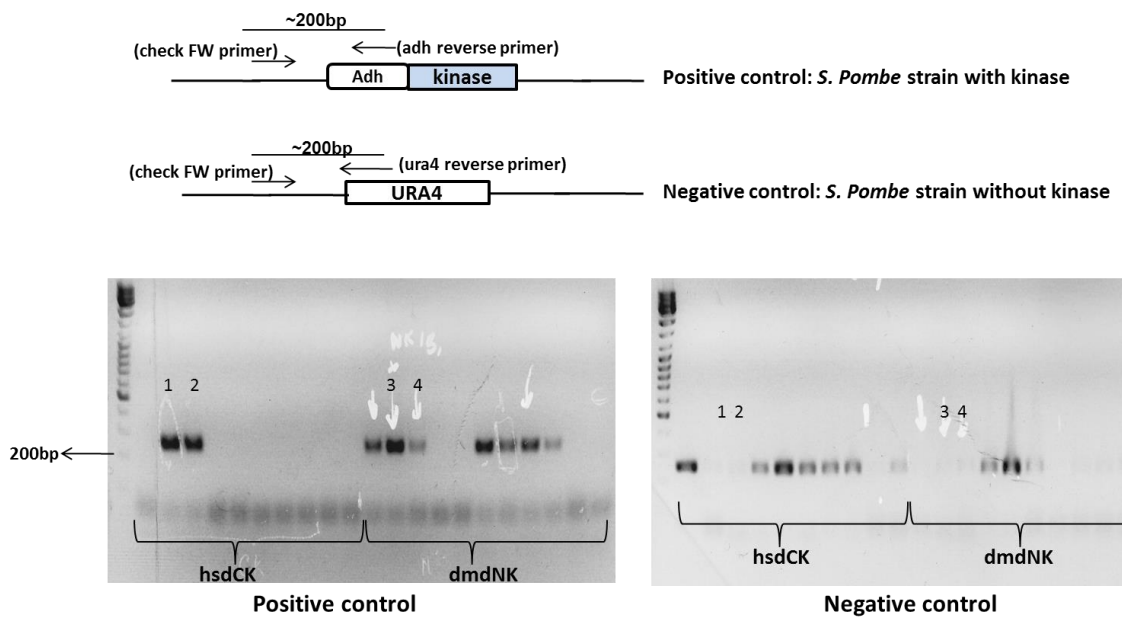


Figure 3-2 Integration of kinases into *S.pombe* genome. (A) Adh coupled kinase coding sequences were PCR amplified using long primers (ura4-adh-F and ura4-hsdCK/dmdNK-R). A band corresponding to the expected size was amplified for each kinase. The kinases were then integrated into *S. pombe* genome, transformants were selected using 5-FOA. (B) Colony PCR on 5-FOA-resistant colonies confirmed the presence of genes at the right locus. Primer sequences are detailed in reference Gasasira master's project, 2007.

3.1.2 Sensitivity of strains with kinases to NAs

As a start of my PhD project, I first tested sensitivity of above described constructs, containing the kinases, to NAs to assess the role of kinases in drug activity.

A. Spot test

To test sensitivity of the strains with kinases to Gemcitabine (GemC) and Cytarabine (AraC) I performed a spot test. Strains with either the *Drosophila* (MG21) or the human (MG22) kinase and wild type (MG19) were treated with different concentrations of GemC and AraC. As shown in *Figure 3-3*, cells containing the kinases were more sensitive to both drugs compared to the wild type, which was resistant to 50 μ M, suggesting a role of the kinases in drug activity. Cells with the human kinase were slightly more sensitive to both drugs than cells containing the *Drosophila* kinase, an effect that might be explained by the specificity of the kinase to deoxycytidine analogues.

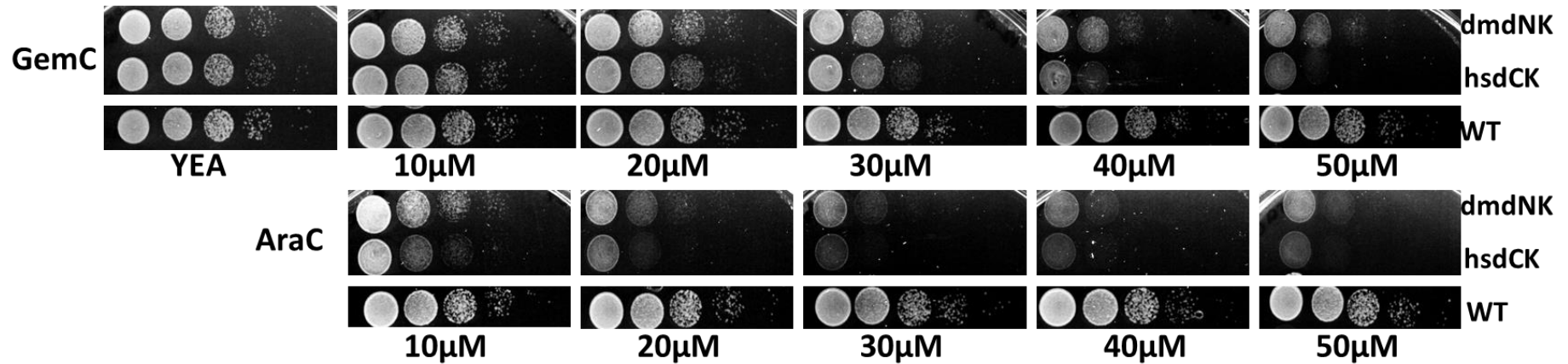


Figure 3-3 Cells with kinases are sensitive to GemC and AraC. Cells with either kinase (MG21, dmdNK and MG22, hsdCK) and WT (MG19) were tested with different concentrations of drugs. Cells were pre cultured in YEL and concentrations ranged from 10^5 to 10 cells. As a control for growth, cells were also plated on media (YEA) without drug. After exposure to the drugs, plates were incubated for two days at 30°C. Cells with kinases showed higher sensitivity to both drugs compared to WT. The sensitivity is higher in cells containing the human kinase and kinase-containing cells showed higher sensitivity to AraC than GemC. The results were reproducible in more than 3 independent experiments.

B. Survival test (acute exposure)

To test the effect of Gemcitabine on a short term exposure in presence of either kinase, cells were treated with the drug and their survival was determined after a short incubation. Strains with either kinase were grown overnight, in YEL at 30°C to reach 2.10^6 cells/ml. 50µM of GemC was added to the cells and incubated at 30°C (shaking). Cells were then collected every hour for 8 hours and GemC washed out with 1 ml of H₂O. 500 cells were plated on YEA (without drug) and incubated at 30°C until formation of colonies. As shown in *Figure 3-4*, the growth of cells with kinases was reduced in presence of the drug. WT cells without kinases showed no difference in growth in presence or absence of Gemcitabine. In presence of the drug, cells with kinases showed a reduced growth (after two hours for *hsdCK* and after four hours for *dmdNK*) compared to untreated cells. This suggests that GemC might lead to an arrest of the cell cycle rather than cell death which would have led to a decrease in colony formation.

The effect of the drug was noticeable in cells with the human kinase after two hours incubation whereas in cells with the *Drosophila* kinase the difference occurred after four hours incubation. This is consistent with the spot test which showed a higher effect of the drug on cells with the human kinase (*Figure 3-3*). This observation that *S. pombe* cells show sensitivity to NA in absence of a specific transporter, suggests that *S. pombe* has an alternative transporter to import deoxynucleosides (dNs) and or that the GemC might diffuse through the *S. pombe* cell wall.

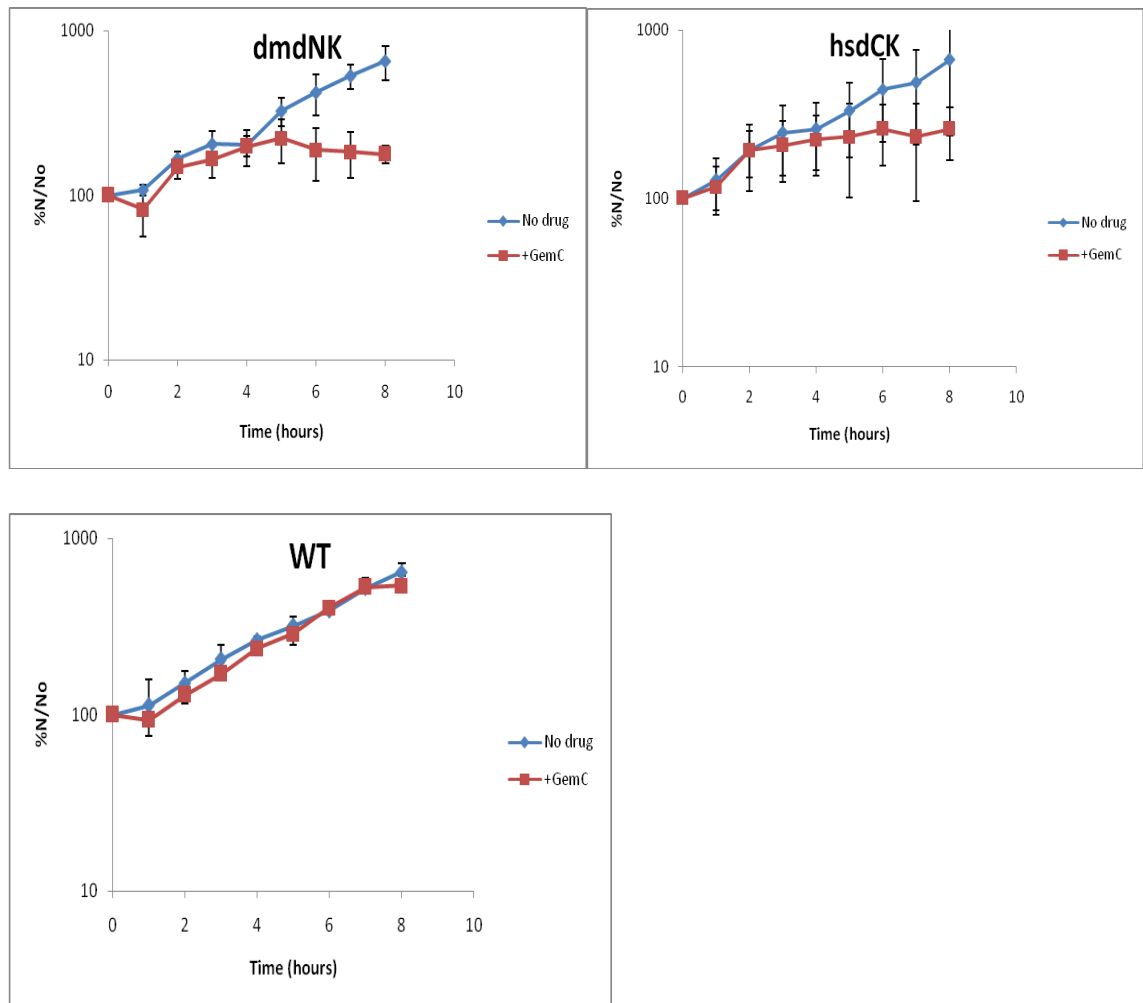


Figure 3-4 Cells with kinases show reduced growth in presence of GemC. Cells were grown in YEL media for overnight to reach $2 \cdot 10^6$ cells/ml. They were then exposed to $50 \mu\text{M}$ GemC and incubated at 30°C . Cells were collected every hour and 500 cells were plated on YEA without drug and incubated at 30°C until formation of colonies. Results show percentages compared to time 0. Error bars, showing standard deviation, were calculated from three independent experiments. Cells with the kinases (MG21, *dmdNK* and MG22, *hsdCK*) showed a reduced growth when treated with the drug (red curves). WT (MG19) was used as a control and showed similar growth with and without treatment.

3.2 Integration of the hENT1 transporter

To increase the uptake of Gemcitabine, we decided to integrate the hENT1 isoform of the human equilibrative nucleoside transporters encoded by the SLC29 gene family. ENTs have a broad selectivity as they transport both purine and pyrimidine nucleosides compared to concentrative nucleoside transporters, CNTs, which have greater affinity for pyrimidine nucleosides (Galmarini *et al.*, 2001). hENT1 and hENT2 are two main isoforms of the hENT transporter family and differ in their sensitivity to the nucleoside analogue nitrobenzylthioinosine. hENT1 is inhibited by nanomolar concentrations whereas hENT2 is inhibited by micromolar range of concentrations (Pastor-Anglada and Baldwin, 2001). Other members, hENT3 and hENT4 complete the ENT family. hENT1 consists of 456 amino acids and its cDNA was first isolated from human placenta (Griffiths *et al.*, 1997; Podgorska *et al.*, 2005). It has been shown to increase nucleoside analogues uptake in human cells (Spratlin *et al.*, 2004) as well as in fission yeast (Sivakumar *et al.*, 2004). In the latter, it has been shown that hENT1 improves incorporation of ³H-thymidine and analogues in *S. pombe* strains expressing herpes virus thymidine kinase.

3.2.1 Testing sensitivity of strains with hENT1 transporter

At first we carried out spot tests to test sensitivity of a strain that contains the human transporter (provided by N.Rhind, Sivakumar *et al.*, 2004) and either kinases to GemC and AraC. The transporter was incorporated into strains with either kinase by crosses and the resulting strains were tested for drug sensitivity. As shown in *Figure 3-5*, there were no differences in sensitivity between cells with and without the transporter to both drugs. *dmdNK/hENT1* cells were slightly more resistant compared to *dmdNK* alone but were more sensitive than the WT without kinase confirming the presence of the kinase. The increased resistance in *dmdNK/hENT1* may be explained by presence of suppressors or mutations that might affect kinase activity. The transporter is reported (Sivakumar *et al.*, 2004) to improve import of NAs into the yeast cells, however, the results above suggested that the transporter is not needed by *S. pombe* cells to take in the drugs, or that the transporter wasn't active. I hence carried out tests to check presence of the hENT1 transporter in the *S. pombe* genome.

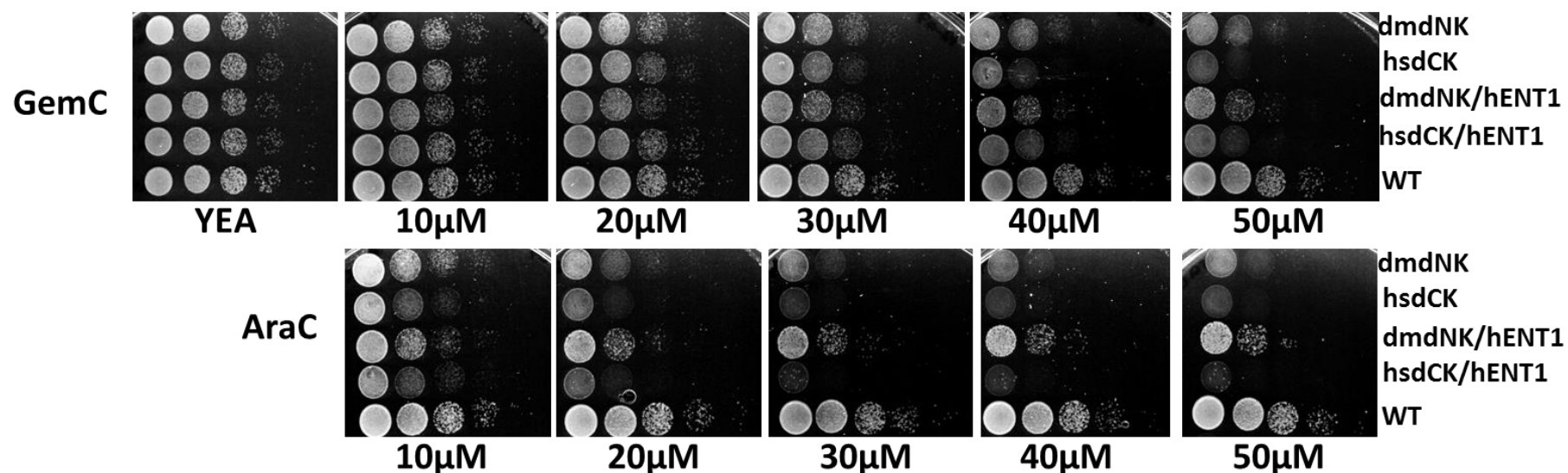


Figure 3-5 Cells with *hENT1* show same sensitivity to *GemC* and *araC* as cells without transporter. Strains with kinases (M21 and M22) and *hENT1* (EH970, *dmdNK/hENT1* and EH966, *hsdCK/hENT1*) were tested with different concentrations of both drugs and incubated for 2 days at 30°C. Cells with and without the transporter showed a similar sensitivity to both drugs compared to WT (MG19). The results were reproducible in more than three independent experiments. *dmdNK/hENT1* cells were slightly more resistant compared to *dmdNK* alone but it was more sensitive than the WT without kinase confirming the presence of the kinase.

3.2.2 Test presence of transporter in *S. pombe* cells

I confirmed the presence of hENT1 in the *S. pombe* genome by PCR which was carried out on genomic DNA isolated from yeast cells with hENT1 (MG042, MG043, MG044, MG104) and without hENT1 (MG020, MG021, MG022, MG028) using primers P011 (ENT1-FW) and P012 (ENT1-REV). PCR conditions were set as described in paragraph 2.2.2.1 using *pfu* polymerase. The annealing temperature was set to 61°C and extension time was 3 minutes.

As expected, a ~1.2kb band was amplified in strains with the transporter whereas no band was observed in strains without the transporter (negative controls) (*Figure 3-6A*). To confirm that the amplified gene corresponds to hENT1, the PCR products were digested with *EcoRI* at ~600bp and a double band of ~600bp was released as shown in *Figure 3-6B*.

Together these results showed that the transporter coding sequence was present in the *S. pombe* genome although strains didn't show an increased sensitivity to GemC or AraC, suggesting that either the protein was not expressed or not functional.

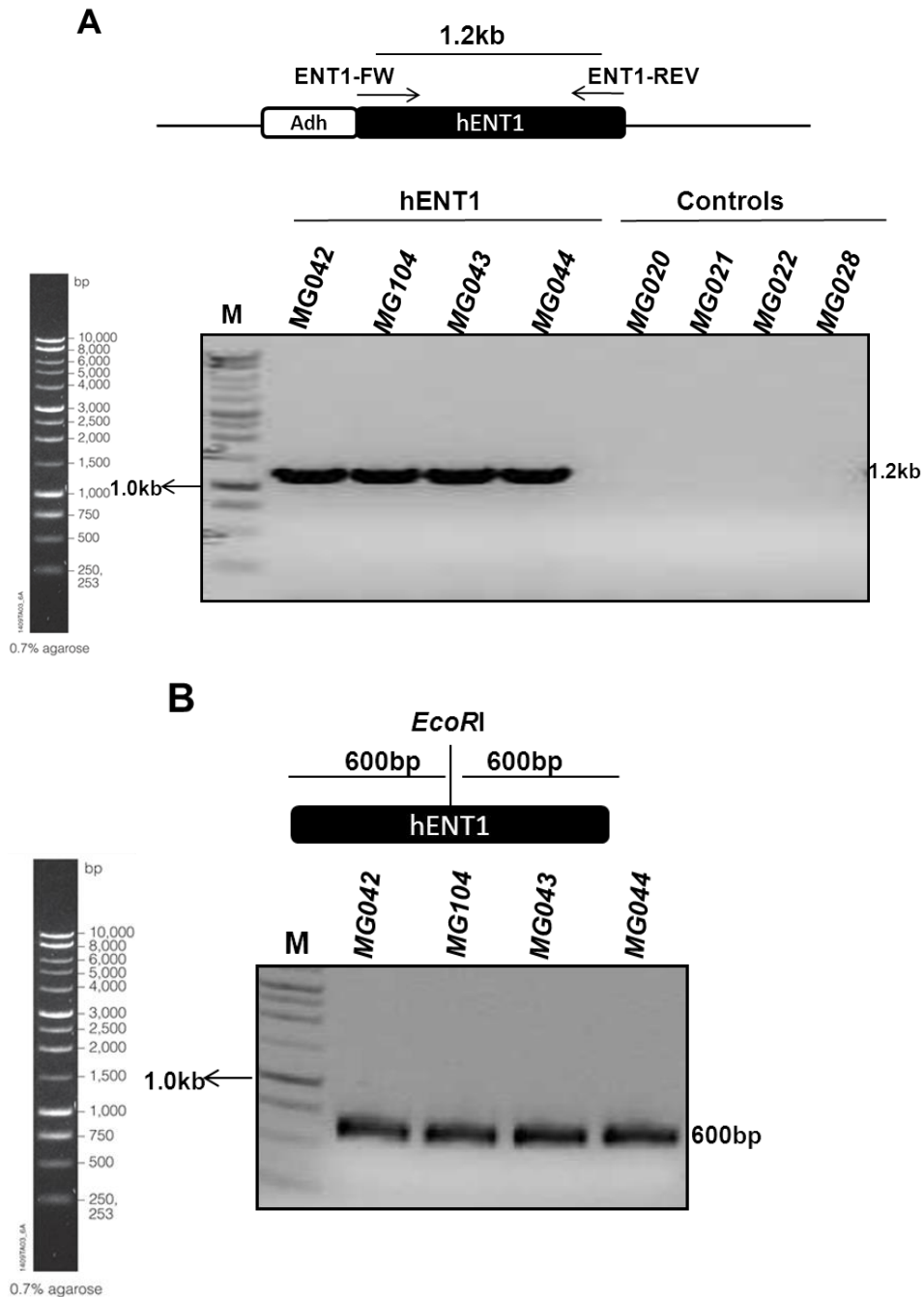


Figure 3-6 Confirmation of presence of hENT1 in *S. pombe* strains by PCR. (A) hENT1 gene was isolated by PCR in strains with the transporter. A band between 1 and 1.5 kb (expected size of ~1.2kb) was amplified in four strains containing hENT1 (in order: MG042, MG104, MG043, MG044) whereas there is no band for the 4 negative controls (in order: MG020, MG021, MG022, MG028). Lane 1 contains a marker (Promega 1kb DNA ladder). **(B)** Digestion of PCR product with *EcoRI* released 2 bands with expected sizes (double ~600bp bands). 1kb DNA ladder was loaded in lane1.

3.2.3 Construct a stable hENT1/kinase strain

In the original MG042 yeast strain (hENT1 from plasmid pFS181, Sivakumar *et al.*, 2004), the hENT1 gene is combined with *leu1* and then integrated in a *leu1-32* strain, making *leu+* as selective marker for hENT1 integration (see *Figure 3-7A*). Strains are then crossed to *leu-* (*leu1-32*) to be able to select for transporter integration, and although rare, a recombination by flanking *leu* fragments may occur and lead to loss of the transporter gene without losing the marker, leaving strains with the *leu1* marker but without the transporter (*Figure 3-7A*).

As the transporter did not increase Gemcitabine or AraC sensitivity, and because the potential instability of the construct could interfere with genome-wide screens for Gemcitabine-sensitive mutants, we decided to construct a stable kinase/hENT1 strain where both genes (the transporter and the kinase) are coupled and separated by a selectable marker. The cloning strategy and integration of the transporter are detailed in *Figure 3-7B*. In short, Adh/hENT1, amplified from *S. pombe* genomic DNA (yeast strain MG044), was cloned into *PacI* and *AscI* restriction sites of the pFA6a-natMX6 plasmid. The transporter was then PCR amplified and the linear PCR fragment was transformed into *S. pombe* using the yeast transformation protocol. Because both hENT1 and kinases are under the Adh promoter, we have reversed the transporter in a such a way that the NAT cassette is located between the two promoters, and any recombination between Adh sequences would lead to a loss of NAT resistance.

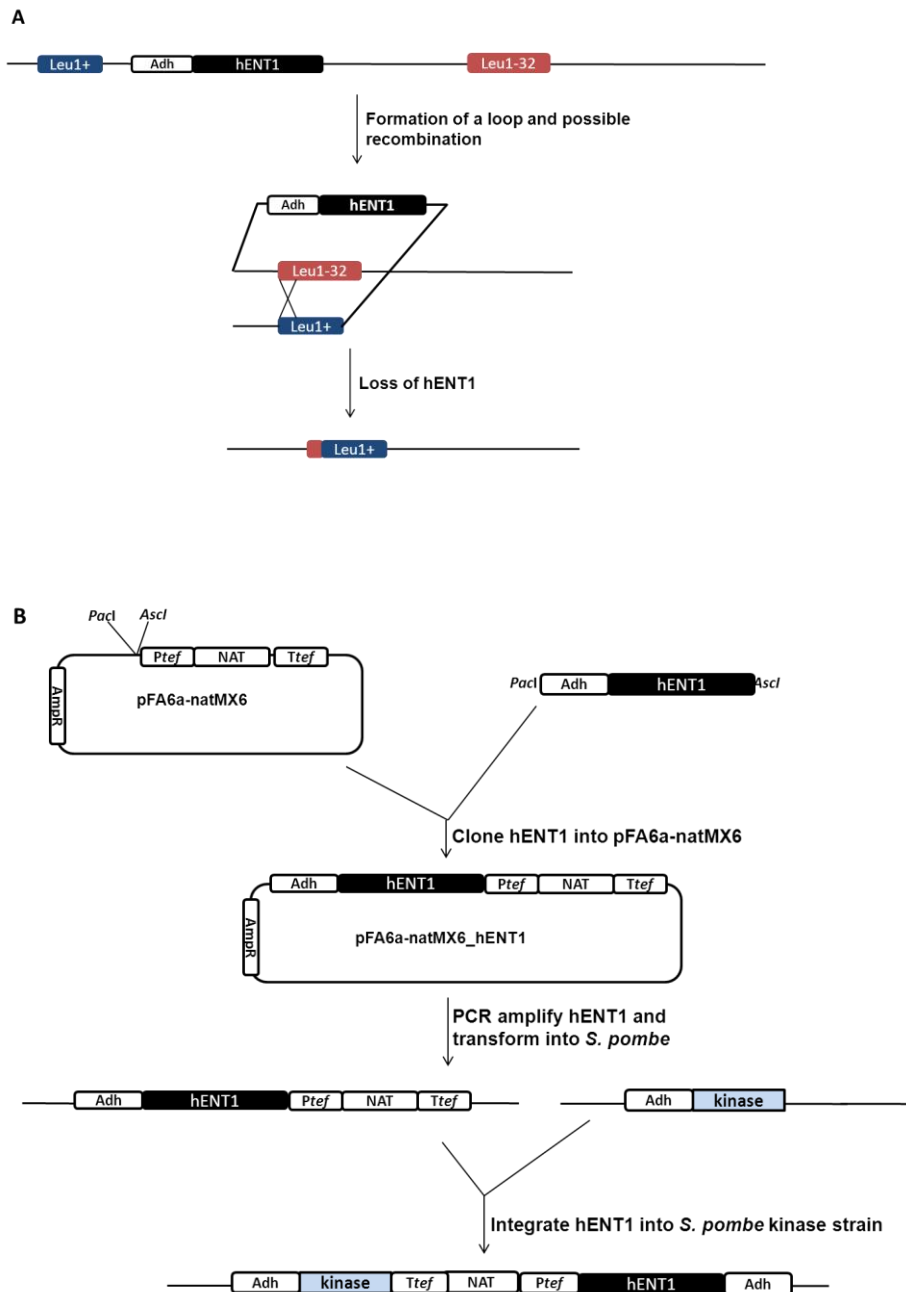


Figure 3-7 Outline of the strategy used to construct a stable kinase/transporter *S. pombe* strain. (A) In the existing hENT1 construct (Sivakumar et al 2004), a loop might form between Leu flanking regions and recombination may lead to a loss of the transporter without losing the marker. **(B)** To construct stable strains, hENT1 coding sequence under the Adh promoter was isolated by PCR from genomic DNA of a strain with the transporter and cloned into *PacI*/*AscI* restriction sites of pFA6a-natMX6. NAT coupled hENT1 was then PCR amplified from the plasmid and integrated downstream the kinases. The NAT marker was integrated between the two genes.

3.2.3.1 Clone hENT1 into pFA6a-natMX6

hENT1 was cloned under *PacI/AscI* restriction sites of pFA6a-natMX6 plasmid. Prior to cloning, the plasmid was checked by digestion with cloning and other restriction enzymes which linearized the plasmid (*Figure 3-8A*). The hENT1 coding sequence under the Adh promoter (Adh/hENT1) was PCR amplified from genomic DNA of the yeast strain MG044 using P015 (FW-adh) and P016 (Rev-ENT1) primers. PCR was carried out following conditions described in Materials and Methods (paragraph 2.2.2.1) using *pfu* polymerase. The annealing temperature was set at 62°C and the extension was set at 3 minutes. As shown in *Figure 3-8B*, a band corresponding to the expected size [~2kb corresponding to Adh promoter (~760bp) and hENT1 (~1.3kb)] was amplified. The PCR product was then cloned into the *PacI/AscI* restriction site of pFA6a-natMX6. 20 clones were checked by digestion with *PacI* and *AscI* and 16 out of 20 clones released the insert (*Figure 3-8C*). Two positive clones (indicated by the arrows) were then sequenced (Eurofins MWG) using Seq005 (FW seq Adh), Seq008 (INT Seq hENT) and Seq009 (Rev Seq hENT) primers. Alignment of the sequences (ebi alignment tool) to the original hENT1 coding sequence

([http://www.ncbi.nlm.nih.gov/nucleotide/118582266?report=genbank&log\\$=nucltop&blast_rank=1&RID=4G96F8P701P](http://www.ncbi.nlm.nih.gov/nucleotide/118582266?report=genbank&log$=nucltop&blast_rank=1&RID=4G96F8P701P)) revealed five DNA mutations, corresponding to four amino acid changes (N81S, M84V, L250S and E428G, *Figure 3-8E*) in each independent clone. A blast analysis (NCBI blast tool) gave no corresponding naturally occurring variant of the transporter, suggesting that the mutations might have been introduced during manipulation of the gene (e.g: PCR). To check the origin of these mutations I sequenced the original pFS18-hENT1 plasmid (Sivakumar *et al.*, 2004), and found that the same mutations were also present in this plasmid.

(<http://www.addgene.org/pgvec1?f=c&plasmidid=12536&cmd=viewseq&seqonly=true>), suggesting that the mutations were not introduced during the handling of the gene but that they are present in the cloning vector and the hENT1 construct.

As these mutations are likely to interfere with hENT1 function, and thus might explain the failure of this gene to increase GemC and AraC sensitivity, we decided to reverse the mutations to match the original WT hENT1 DNA sequence. For the rest of this thesis I will refer to the mutated hENT1 as hENT1⁻.

The reversal of mutations was carried out by site directed mutagenesis as described in Materials and Methods (2.2.2.3) using hENTmut1-4 forward and reverse primers (P021-

P028, *Figure 3-8D*). First I reverse mutated 4 mutations (set of primers hENTmut1-3) and obtained 3 out of 3 positive colonies. Next, I used the reversed mutated plasmid to carry out the last mutagenesis using hENTmut4 set of primers and obtained 4 out of 4 positive colonies. The fully reverse-mutated hENT1 was then sequenced and was 100% identical to the theoretical hENT1. The reverse mutation was carried out on pFA6a-AdhhENT1⁻-natMX6 plasmid, to give pFA6a-AdhhENT1-natMX6 plasmid with fully reverted hENT1, which was then integrated into the *pombe* genome.

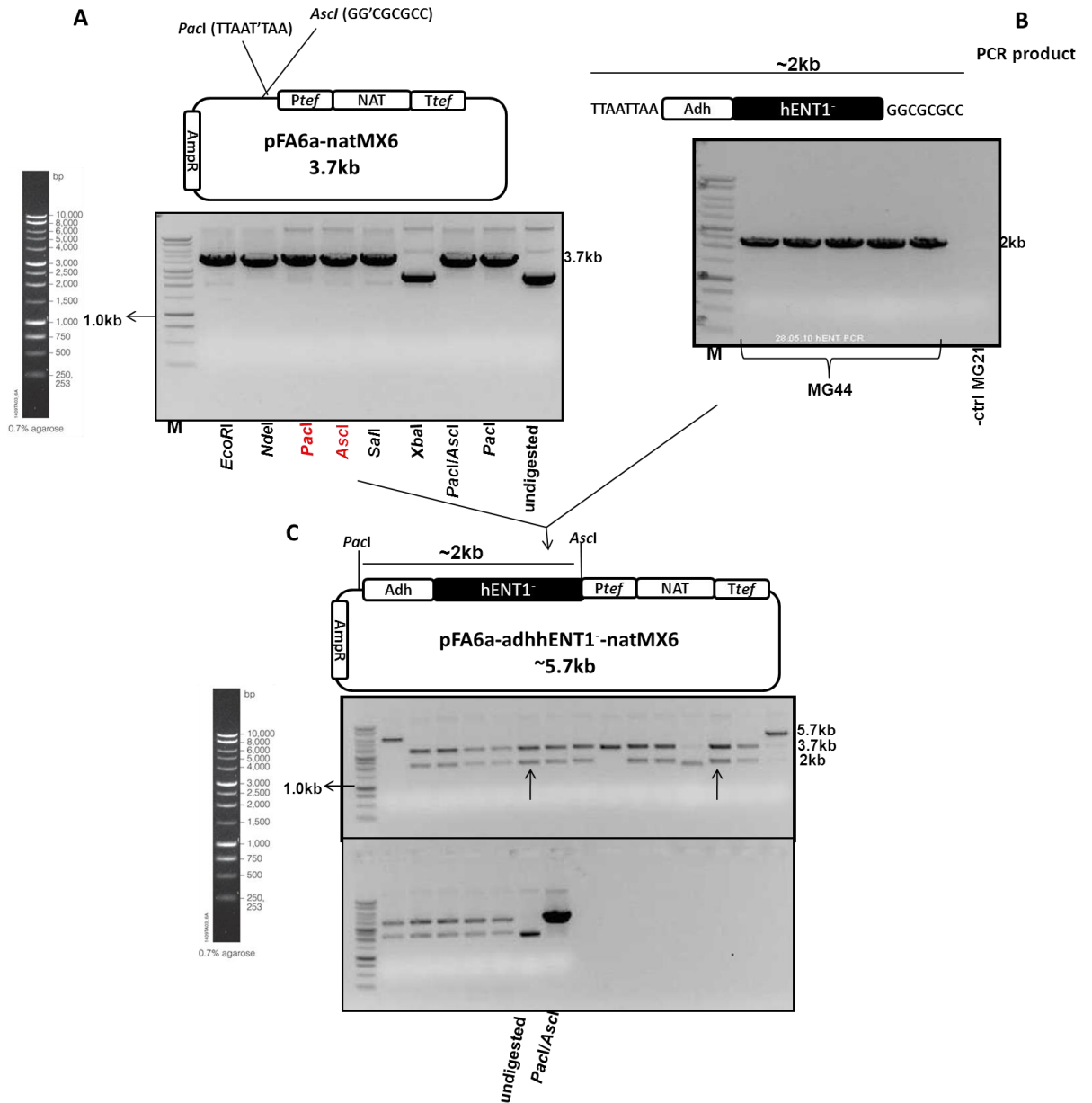


Figure 3-8 Cloning mhENT1 into pFA6a-natMX6 vector. (A) pFA6a-natMX6 plasmid was checked by digestion with a series of enzymes which either linearize the plasmid (*EcoRI*, *NdeI*, *PacI*, *AscI* and *Sall*) or don't cut the plasmid (*XbaI*). Undigested plasmid was loaded as a control and lane 1 was loaded with Promega 1kb ladder. (B) The hENT1 gene coupled to the *Adh* promoter was PCR amplified from genomic DNA from *S. pombe* (MG44). A band corresponding to the expected size (2kb) was detected. *S. pombe* strain without the transporter (MG21) was used as a negative control. Lane 1 was loaded with Promega 1kb DNA ladder. (C) Clones were checked by digestion with *PacI/AscI* which released the insert. Clones 6 and 13 (indicated by arrows) were sequenced.

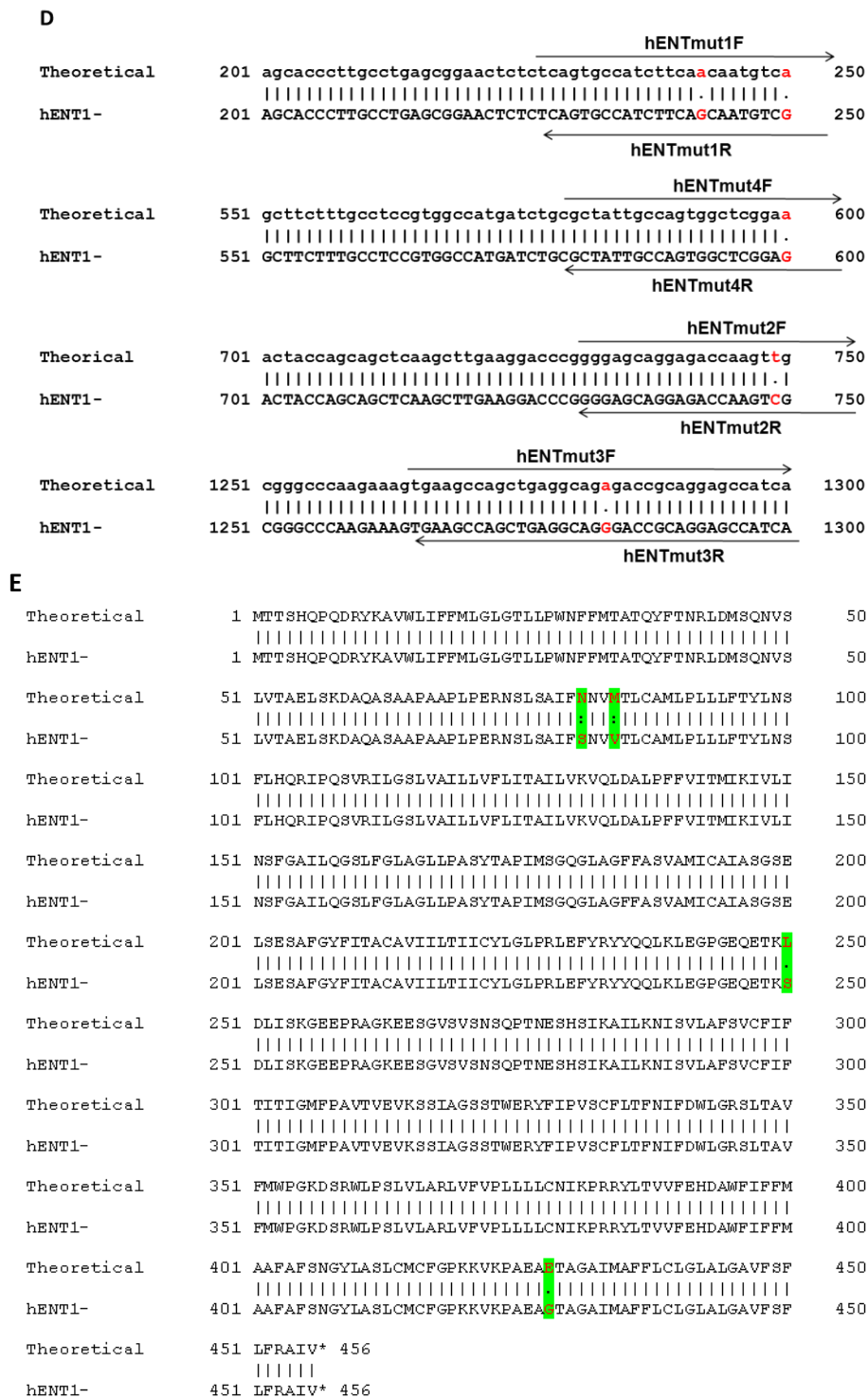


Figure 3-8 (D) Sequence and reverse mutated hENT1. Positive clones from pFA6a-hENT1-natMX6 were sequenced and 5 DNA mutations were found (red) corresponding to 4 amino acids changes (E). To reverse the mutations, a series of primers were used (indicated by arrows). The reversions were introduced using site directed mutagenesis.

3.2.3.2 Integrate hENT1 into *S. pombe*

hENT1 was integrated into *S. pombe* strains that contain either kinase (MG21, *dmdNK* or MG22, *hsdCK*) and a strain without a kinase (MG19, WT). Adh-hENT1 was PCR amplified from pFA6a-Adh-hENT1-natMX6 plasmid using P029 (URA4-FW) and P030 (URA4-Rev) long primers with 100bp homology to the region downstream of the kinases (or *ura4* gene in the absence of the kinase) and transformed into *S. pombe* by classic transformation protocol. PCR conditions were set as described in paragraph 2.2.2.1 using *KOD* polymerase (VWR). The annealing temperature was set to 66°C and extension time was 3 minutes.

A ~3.5kb fragment, total size, corresponding to Adh (~760bp) + hENT1 (~1.3kb) + NATorf (~570bp) + Ptef (~380bp) + Ttef (~235) and long primers (200bp) was amplified (*Figure 3-9A*) and transformed into *S. pombe*. Transformed colonies were selected on nourseothricin (100 µg/ml) using the NAT cassette marker (of the pFA6a-NatMX6 plasmid) and one colony per strain was checked for integration using colony PCR with the primers P041 (5' hENTcheck-fw-NK), P042 (5'hENTcheck-fw-CK), P032 (5'hENTcheck-rev), P033 (3'hENT check-fw), P034 (3'hENTcheck-rev) and P031 (5'hENTcheck-fw) primers (*Figure 3-9B*). Adh-hENT1 was amplified using either P041 (forward for *dmdNK* coupled hENT1) or P042 (forward for *hsdCK* coupled hENT1) and P034 (reverse) primers and sequenced using Seq005 (FW seq FRT), Seq008 (INT Seq hENT) and Seq009 (Rev Seq hENT) primers. DNA sequences showed three DNA mutations in WT/hENT1 construct (G178A, G181A and G757C) and one DNA mutation in *hsdCK*/hENT1 (G181A) and *dmdNK*/hENT1 (G181A) constructs, when compared to the original hENT1 coding sequence. All these mutations created no changes in the protein sequences (see alignments in Appendix I).

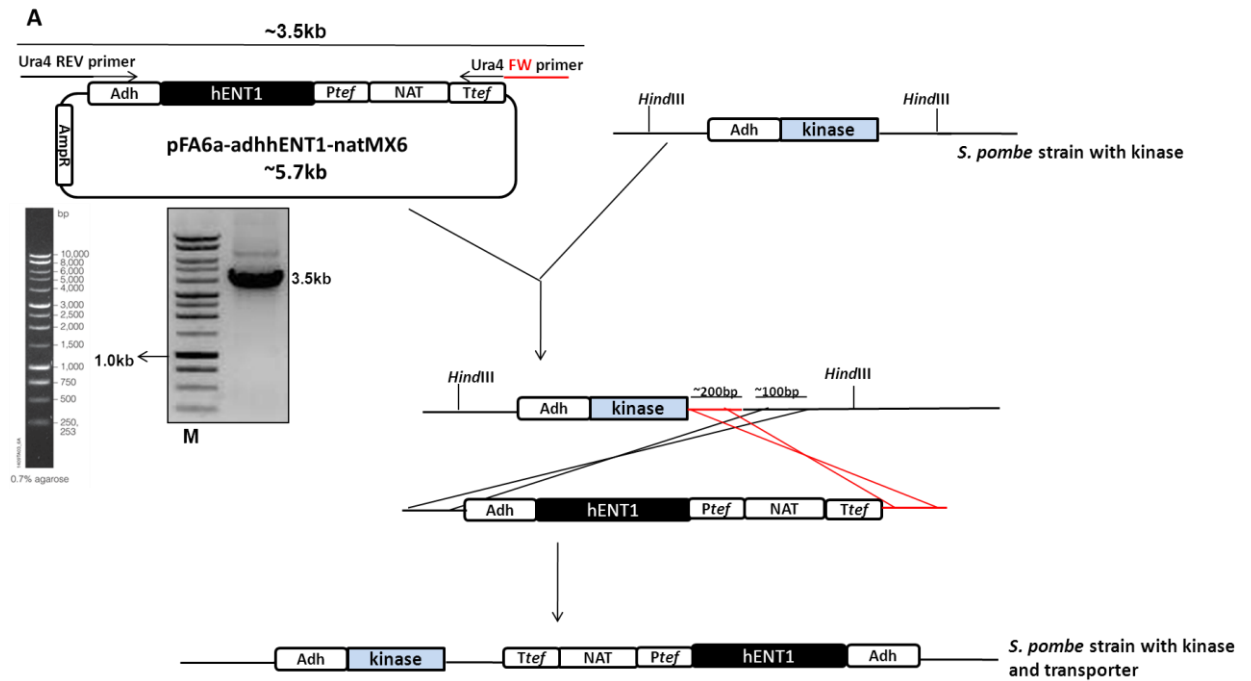


Figure 3-9A Integrate *hENT1* into *S. pombe* genome. The reverse-mutated *hENT1* under the *Adh* promoter and containing a NAT cassette as a marker was integrated into *S. pombe*. The gene was PCR amplified (~3.5kb band on gel) from pFA6a NatMX6. To prevent possible loss of the kinase due to recombination between the two *Adh* promoters, the *hENT1*/NAT was reversed in order to integrate the marker between the two genes. The gene was integrated into strains with either kinase (MG21, *dmdNK* and MG22, *hSDCK*) and WT (MG19). Transformants were selected on media containing Nourseothricin 100 μ g/ml.

B

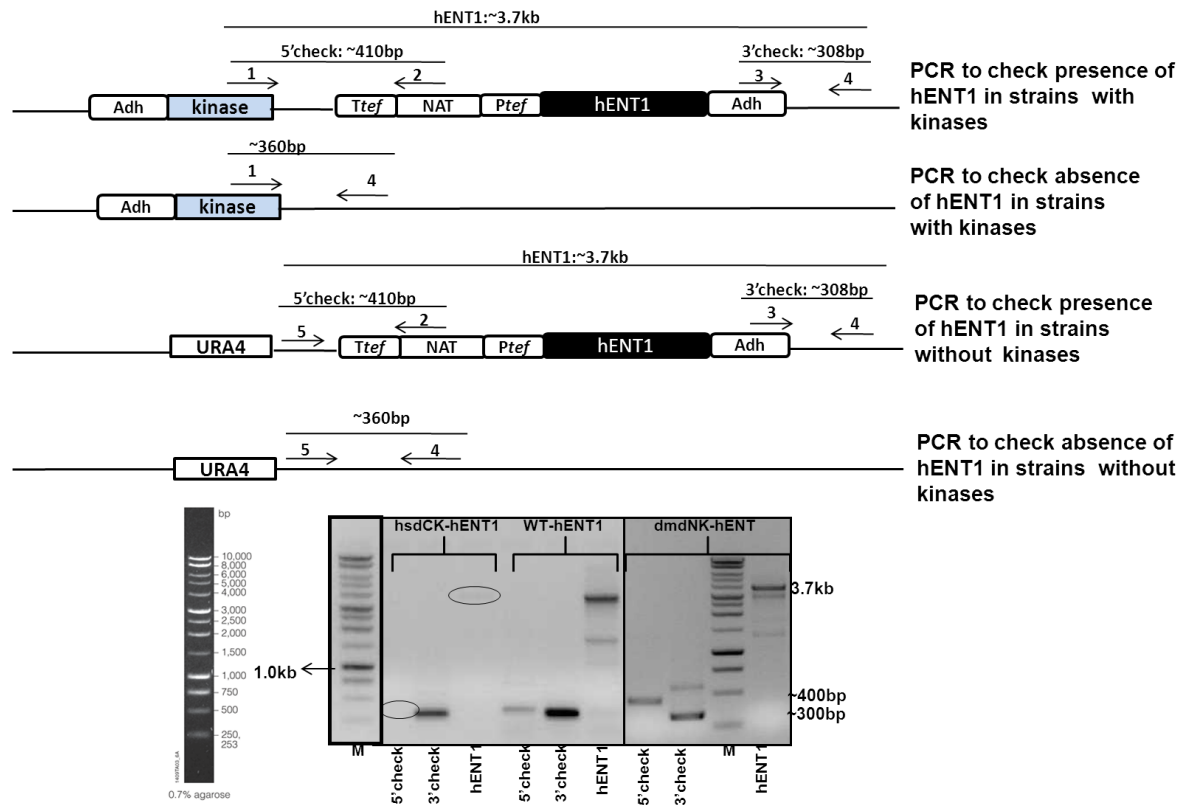


Figure 3-9B. PCR to check integration of hENT1. hENTcheck primers (1: P041 or P042, 2: P032, 3:P033, 4: P034 and 5:P031 (5'hENTcheck-fw) were used to check integration of the transporter at the right locus. PCRs were carried out on genomic DNA from transformed strains and expected bands were amplified (hsdCK-hENT1 5'check and hENT1 in lanes 2 and 4 were faint and barely visible). Additional control was carried out using primers 1 and 4 which isolate either a long fragment (if integration) or a short fragment in case of non integration. The full hENT1 gene was amplified from all three strains and sequenced.

3.2.4 Test sensitivity of reverse mutated hENT1/kinase strains to GemC and AraC

A. Spot tests

Spot tests were carried out to test the sensitivity of the new hENT1 constructs to GemC and AraC. As previously, strains with the transporter and either the *Drosophila* (MG81) or the human (MG70) kinase were tested in comparison to the mutated hENT1⁻ transporter. Strains were grown overnight in YE media. They were then tested on YEA media containing different concentrations of either drug and incubated for two days at 30°C. As shown in *Figure 1-10A*, newly constructed transporter/kinase strains showed high sensitivity to the drugs (no growth at 10µM), whereas strains with mutated hENT1⁻ showed the same sensitivity as strains without the transporter. Additionally, cells with only the transporter (MG71) were as resistant as the WT (MG19), emphasising the role of the kinase in drug activity. Strains with the transporter and kinase also showed slow growth and cell elongation in YEL rich medium (see next paragraph) and consequently further tests were carried out on minimal media. Strains were grown in EMM media and tested on the same media containing different concentrations of the drugs. Due to the slow growth of strains in minimal media, spot tests were incubated for five days at 30°C. As shown in *Figure 3-10B*, cells with the human kinase and the transporter (MG70) are sensitive to concentrations as low as 250nM of AraC and 500nM of GemC, whereas cells with the *Drosophila* kinase and the transporter (MG81) showed sensitivity at 1µM of AraC and 500nM of GemC. The sensitivity to GemC, at this concentration, was however higher in cells with hsdCK. The higher sensitivity of strains containing the human kinase, in comparison to strains with the *Drosophila* kinase, has already been observed (paragraph 3.1.2) and might result from a higher specificity of the kinase for the two NAs, whereas, the high sensitivity of strains with hENT1 clearly suggests a role of the transporter in increasing drug activity.

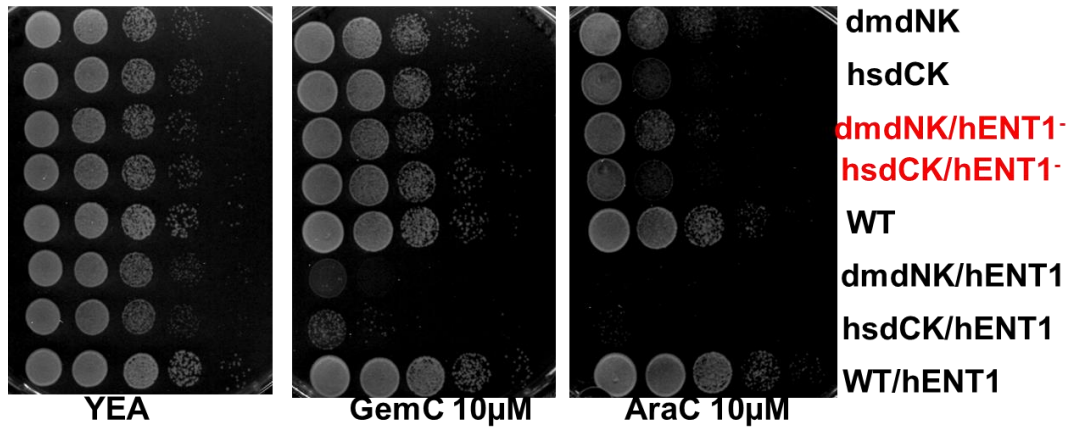


Figure 3-10A. Strains with WT hENT1/ kinase are highly sensitive to GemC and AraC. Sensitivity of the new hENT1/ kinase construct was tested on YEA media with both kinases. Cells were incubated 2 days at 30°C. “New hENT1” (MG70, hsdCK/ hENT1 and MG81, dmdNK/hENT1) strains showed high sensitivity (no growth at 10µM) to both drugs when compared to cells with only the kinases (MG21, dmdNK and MG22, hsdCK) and to mutated hENT1⁻ (MG104, **dmdNK/hENT1⁻** and MG006, **hsdCK/hENT1⁻**). The sensitivity of cells with only the transporter (MG71) was comparable to that of WT cells.

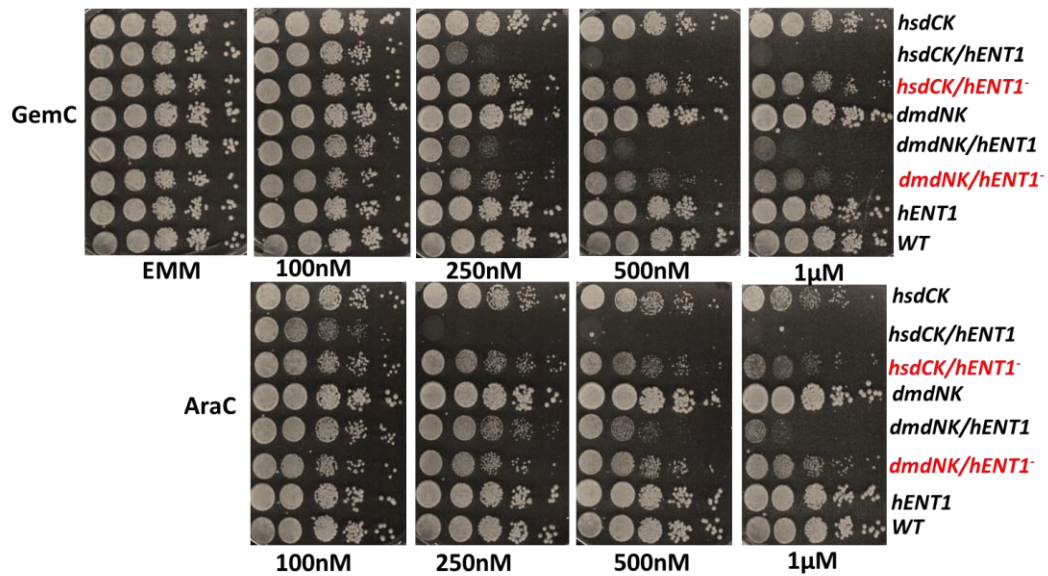


Figure 3-10B. Cells with the new transporter are sensitive to low concentrations of GemC and AraC. Cells were tested on minimal EMM media containing different concentrations of each drug. Cells with the human kinase and the new transporter (*hsdCK/hENT1*, MG70) were sensitive to as low as 250nM of AraC and 500nM of GemC whereas cells with the *Drosophila* kinase and the new transporter (*dmdNK/hENT1*, MG81) showed sensitivity to 500nM of GemC and 1µM of AraC. Strains with only the kinases (*hsdCK*, MG22 and *dmdNK*, MG21), with the mutated transporter (*hsdCK/hENT1*⁻, MG006 and *dmdNK/hENT1*⁻, MG104), with only the transporter (*hENT1*, MG71) and wild type without kinase and transporter (WT, MG19) were tested for comparison. Cells were incubated for 5 days at 30°C. The test was repeated at least three times and results were similar to those shown with the exception of the strain with the *Drosophila* kinase and the mutated transporter (MG104) which showed variations and was more resistant than strain with only the kinase in one experiment however the strain remained more sensitive than the WT without kinase suggesting that the kinase is still present. These variations might indicate presence of suppressors in *dmdNK* cells.

B. Acute exposure

To assess the effect of short exposure of strains with the transporter to GemC, I carried out survival tests. Cells were grown in YEL media for overnight to reach $2 \cdot 10^6$ cells/ml. They were then exposed to 50 μ M of GemC and incubated at 30°C. Cells were collected every hour for eight hours and 500 cells were plated on YEA without drug and incubated at 30°C until formation of colonies (*Figure 3-11*). Cells with the transporter (purple) showed high sensitivity to the drug compared to cells with only the kinase (red) and cells with the human kinase were more sensitive than cells with *Drosophila* kinase. In addition, cells containing the transporter showed a slow growth without treatment (green) when compared to cell without the transporter (blue).

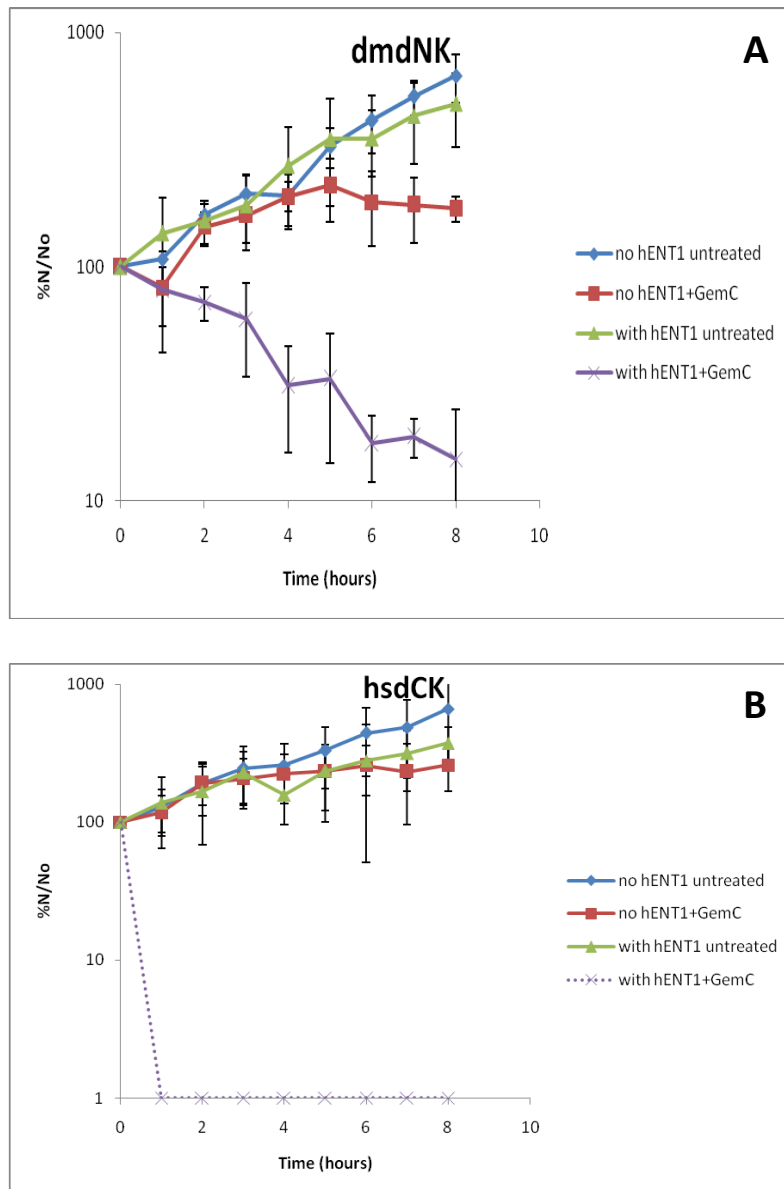


Figure 3-11 Cells with kinases and transporter, *hsdCK*, MG70 (B) and *dmdNK*, MG81 (A) are highly sensitive to GemC. Cells were grown in YEL media overnight to reach 2.10^6 cells/ml. They were then exposed to $50\mu\text{M}$ GemC and incubated at 30°C . Cells were collected every hour and 500 cells were plated on YEA without drug and incubated at 30°C until formation of colonies. Y axis represents % survival of cells relative to survival at time 0. Error bars, showing standard deviation, were calculated from three independent experiments. Cells with the transporter (purple) showed high sensitivity to the drug when compared to cells with only the kinase (red). In addition, cells with the transporter also showed slightly slower growth in media without drug (green curves compared to blue curve, cells with only the kinases). *hsdCK*/*hENT1* cells (B) were highly sensitive and there was no growth after treatment in all the three experiments. To allow plotting on the logarithmic scale, zero values were expressed as “1”.

Both the long and acute exposure tests showed a high sensitivity of cells with the transporter and the kinase to Gemcitabine and AraC (only tested for spot test) compared to cells with only the kinase. The results confirmed that the transporter increases drug sensitivity in *S. pombe*. The absence of sensitivity in cells with only the transporter suggests a crucial role of the kinase in drug activity.

3.3 Further characterisation of the system

3.3.1 YE rich medium affects growth of cells with the transporter and kinase

After overnight incubation at 30°C in liquid media without treatment, I observed that cells with both the kinase and the transporter showed slow growth in YEL media when compared to minimal media (Figure 3-12A). In comparison, cells with only the kinase or the transporter showed a slower growth in minimal media, as expected. This suggested that a combination of both proteins is at the basis of the observed growth abnormality. The slow growth phenotype was emphasised in cells with *hsdCK* when compared to cells with *dmdNK* and, in concordance with other results (paragraphs 3.1.2 and 3.2.4) which showed that *hsdCK* cells were more sensitive to GemC and AraC, this observation might suggest that the specificity of the kinase to cytidine might contribute the observed abnormal growth phenotype.

To further check the abnormal growth, cells were DAPI stained (following the protocol described in Materials and Methods, paragraph 2.2.1.5). Microscopic observation showed that, in rich yeast extract media and not in minimal media, cells were elongated with degraded nuclei (Figure 3-12B).

In addition, HPLC measurement of intracellular dNTPs showed increased levels of dNTP pools in cells grown in rich media (Figure 3-12C, purple) compared to cells grown in minimal media (HPLC data were provided by Dr Andrea Keszthelyi). The increase was observed in both cells with and without the transporter although ratios between dNTPs were higher in cells with the transporter. In EMM media, dNTP levels were equal in absence and presence of the transporter, whereas all four dNTP levels were increased in YEL in presence of the transporter compared to cells without the transporter (purple and red). These results suggested that cells with the transporter could import and phosphorylate dNs from YE media, which would explain the increased

dNTP levels. However, as elevated dNTP levels might result from other mechanisms, such as activation of RNR (involved in dNTPs synthesis) by the checkpoint machinery (reviewed in Labib and De Piccoli, 2011), we cannot exclude the possibility that observed high dNTP levels are due to activated checkpoint in YE media. This suggestion is supported by the observation that cells containing the transporter were elongated in YEL, a mark of cell cycle delay (Nurse *et al.*, 1976).

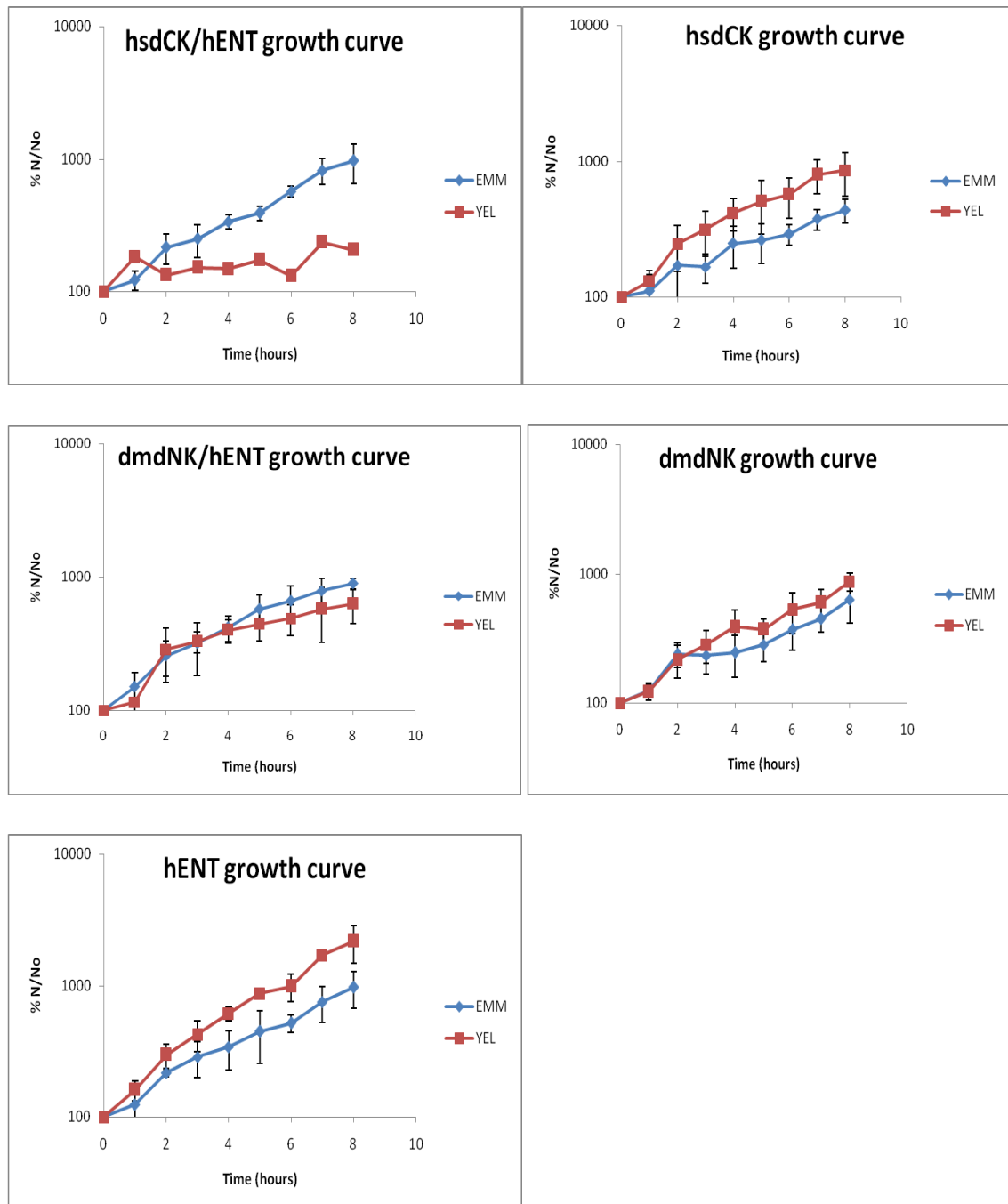


Figure 3-12A. Cells with transporter and kinases show reduced growth in rich YEL media. Cells with either kinase with (MG70, human kinase and MG81, *Drosophila* kinase) and without (MG22, *hsdCK* and MG21, *dmdNK*) transporter and cells with only the transporter (MG71) were grown in both EMM and YEL media at 30°C for eight hours. Cells were counted every hour. Y axis represents % survival relative to time 0 and error bars (standard deviation) were calculated from three independent experiments. *hsdCK*/*hENT*1 cells showed a highly reduced growth in rich media whereas *dmdNK*/*hENT*1 cells growth was slightly slower in rich media. Cells expressing only the transporter or the kinase showed higher growth in rich media than minimum media.

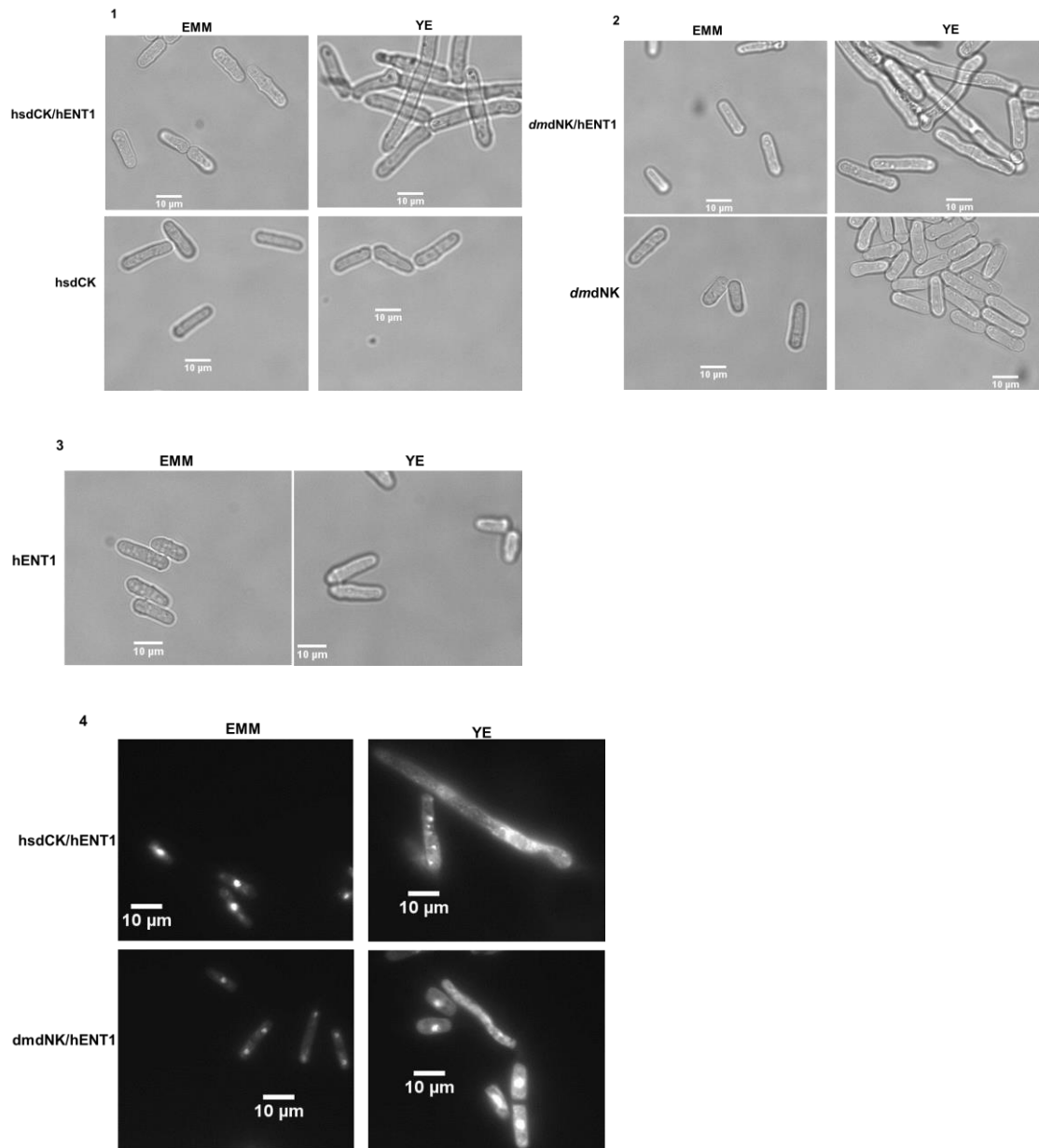


Figure 3-12B. Cells with transporter and kinases are elongated in rich media. Strains with transporter and kinases were incubated overnight at 30°C in EMM and YE. Cells were then collected for DAPI staining and microscope observation. Cells with transporter and both human (**1**, MG70) and *Drosophila* (**2**, MG81) kinases were elongated in rich medium whereas cells with either the kinase (*hsdCK*, MG22 and *dmdNK*, MG21) or the transporter (**3**, MG71) were of normal size in both media. (**4**) DAPI staining showed elongated cells with degraded nuclei in YE.

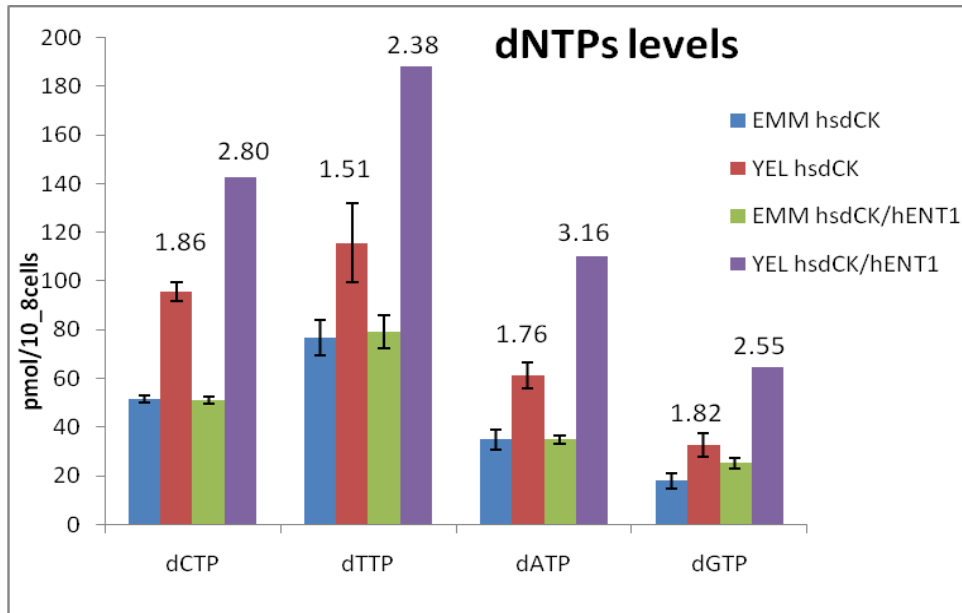


Figure 3-12C. dNTP levels are increased in cells with the transporter in YEL. Intracellular dNTPs pools were measured by HPLC and results showed an increase of all 4 nucleotides in YEL media. The ratio (numbers in the chart) between EMM (blue and green) and YEL (red and purple) are higher in cells with the transporter (MG70) than in cells without the transporter (MG22). Error bars were calculated from three independent experiments which were carried out by Dr Andrea Keszthelyi

3.3.2 Cells with kinase and transporter are more sensitive to gemcitabine in EMM than in YEL

Following the observed growth abnormality and high dNTP levels in YE media, I tested whether the media composition could also affect sensitivity of cells to drugs. In fact, as the high intracellular levels of dNTPs might be a result of nucleoside import through the transporter, one hypothesis might be that a competition between the natural nucleosides and NAs would decrease drug import and/or integration and therefore the sensitivity. To test this hypothesis, cells were grown in rich and minimal media (and minimal media supplied with nucleosides) before treatment with GemC. Experiments in this paragraph and further on were carried out on cells containing the human kinase. Because analysis of both *dmdNK* and *hsdCK* was not realisable within the scope of this project due to time constraints, we have chosen to focus on the *hsdCK* kinase, although both kinases present valuable advantages. The human kinase was mainly chosen for its relevance to human studies and because it has greater affinity for the two deoxycytidine analogues that were used in this project.

Cells with and without hENT1 and containing *hsdCK* kinase were grown in both YEL and EMM media and treated with 50 μ M GemC. Cells were then collected every hour for eight hours and plated on YEA media without drug. Grown colonies were counted after 5 days incubation. At this high concentration, cells without the transporter showed higher sensitivity to the drug in EMM than in YEL. However, in non treated samples, cells also showed slow growth in EMM (*Figure 3-13A*, green/blue curves) as expected. The high sensitivity of cells to GemC in EMM might be explained either by non specific effects (e.g. the lack of nutrients which might increase drug effect), the absence of competition (by dNPs) for the drug import and/or phosphorylation or a combination of both. In cells with both *hsdCK* and hENT1 (*Figure 3-13B*), the sensitivity was higher in YEL than in EMM. This effect might be explained by the fact that cells are already “sick” in YEL media without treatment (elongated cells with slow growth phenotype, *Figure 3-12A* and *B*), which can enhance the drug activity.

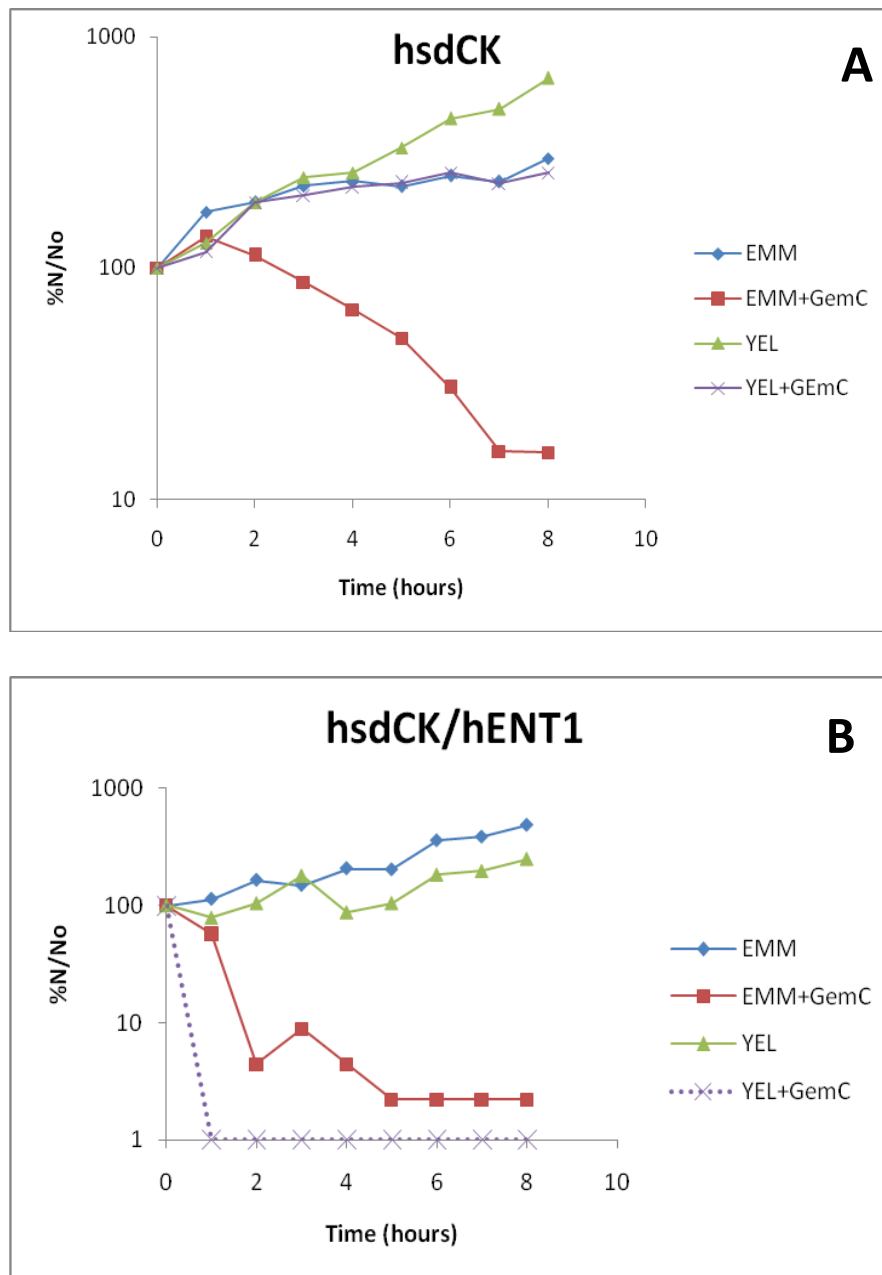


Figure 3-13 *hsdCK* cells are more sensitive to GemC in EMM media than in YEL media.

To compare the sensitivity of *hsdCK* with (MG70) and without transporter (MG22) to GemC in EMM and YEL, cells were grown in both media and treated with 50 μ M of GemC. Cells were then collected every hour and 500 cells were plated on YEA without drug and incubated at 30°C until colonies were formed. Results show % survival relative to time 0 (Y axis) and the X axis represents treatment time in hours. Values are an average of two experiments. (A). shows survival of cells with only the kinase, sensitivity to GemC was increased in EMM (red) compared to YEL (purple). The sensitivity of cells with both the kinase and transporter (MG70) was in contrary higher in YEL than EMM (B). *hsdCK/hENT1* cells were highly sensitive and showed no growth after treatment in YEL. For the clarity of the figure, the zero values were expressed as "1" on the logarithmic scale.

HPLC measurement of intracellular GemC-TP (*Figure 3-14A*) after short term exposure (3hours) showed higher levels of phosphorylated GemC in EMM than in YEL supporting the hypothesis that the drug import and phosphorylation is more effective in minimal media. The levels were higher in presence of the transporter in both media. In EMM media, GemC-TP levels were only slightly elevated (at 5 μ M) in the presence of the transporter when compared to levels in the absence of the transporter, the levels were equal at a lower concentration (0.5 μ M). This observation suggests that in absence of competitive nutrients (for example dNs), non specific *S. pombe* cell membrane transporters act to import the drug, which would explain the high levels in EMM but not in YEL media in the absence of the transporter. The diffusion of NA through the *pombe* cell membrane is also supported by results which showed sensitivity of cells with only the kinase to both GemC and AraC (*Figure 3-3* and *Figure 3-4*).

Additionally, there was a high decrease of dNTP levels after addition of GemC to the media (*Figure 3-14B*) which might be explained by the action of the drug on RNR and other enzymes involved in dNTPs synthesis (Mini *et al.*, 2006). This effect was not observed in cells with only the kinase in YEL, consistent with the low levels of the drug observed in *hsdCK* cells in YEL. This observation suggested that dNTP levels are drug dependent as their levels decreased when drug levels increased. Higher levels of GemC-TP in cells with the transporter compared to cells without transporter in YEL also emphasized the role of the transporter in the import of the drug. These results further support the hypothesis of a possible competition for cellular import between GemC and natural nucleoside (dNs), present in YE media, which might explain the high sensitivity of *hsdCK* cells in EMM as a result of an increased GemC incorporation (due to lack of competition).

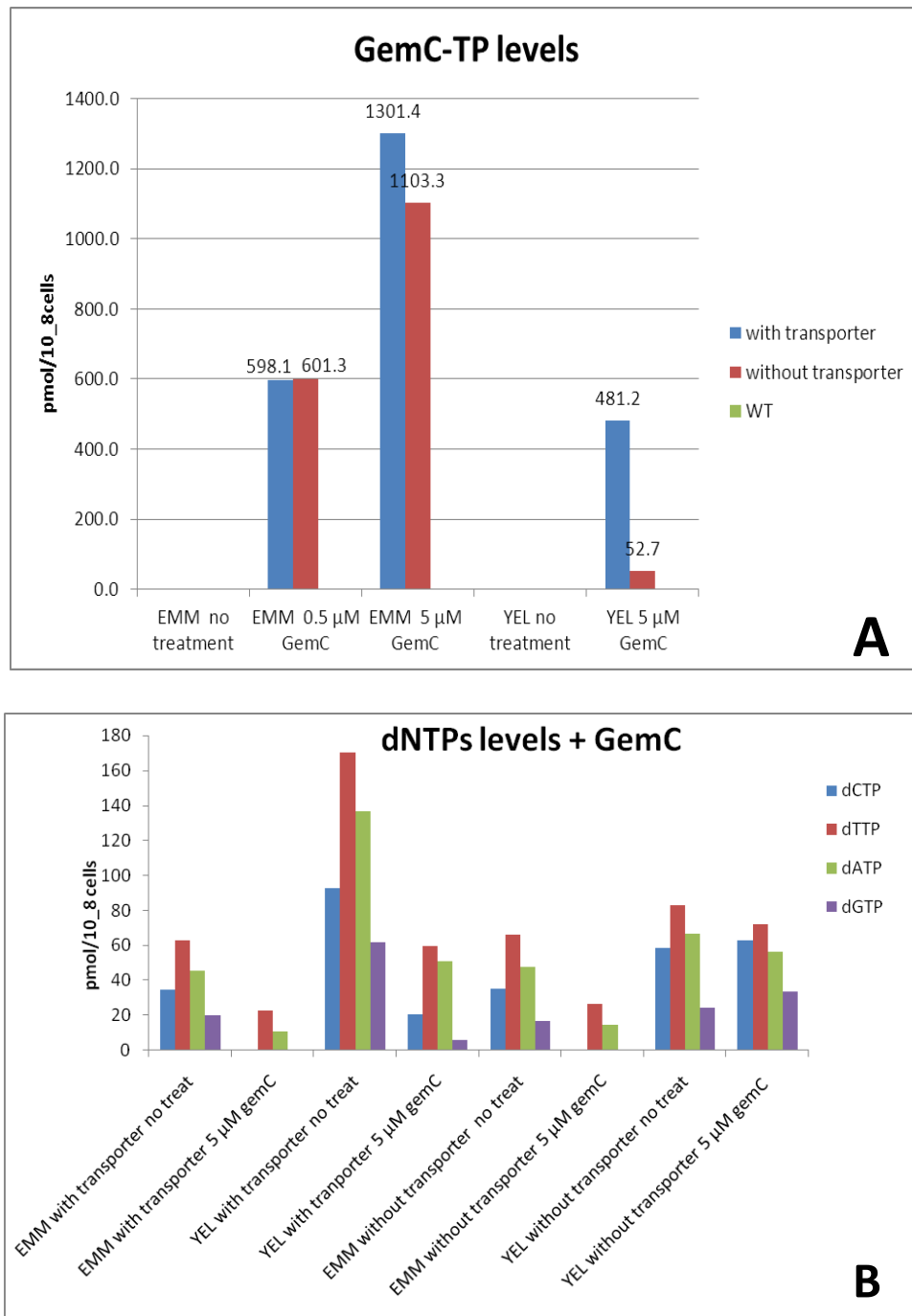


Figure 3-14 Intracellular GemC-TP levels are higher in EMM than in YEL and dNTPs pools decrease in presence of the drug. Cells (strains MG70, with the transporter and MG22 without the transporter) were treated with 0.5 and 5 μM GemC and collected after 3 hours incubation and the levels of GemC-TP and dNTPs measured by HPLC. The results showed high levels of the drug in EMM media in both cells with and without the transporter. In comparison WT without kinase and transporter (MG19) cells were treated with 50 μM of the drug and showed no entry of the drug (A). In YE, GemC levels were higher in cells with the transporter. Levels of dNTPs were decreased in presence of the drug (B) with the exception of cells without transporter in YE where levels remained equal with and without drug. The results are from one experiment that was carried out by Dr Andrea Keszthelyi.

To further investigate the possible competition between GemC and physiological nucleosides, we tested the effect of additional dNs in minimal media. dNs may rescue survival by either competing with the drug for cellular uptake (and phosphorylation) or compensating dNTP pools decreased by the action of GemC on RNR or a combination of both. Cells were grown in EMM, supplied with 5 μ M of each dNs and treated with 1 μ M of GemC. Cells were then collected every hour for eight hours and plated on YEA media (for cells without the transporter) and EMM media (for cells with the transporter). Colonies were counted after four days incubation at 30°C and results showed a rescue to the drug when dNs were added to the medium (*Figure 3-15A*), with higher effect in cells with the transporter (*Figure 3-15A-1*). The results, however, don't allow distinguishing by which mechanisms cells were rescued. HPLC measurement of intracellular GemC-TP levels in presence of additional external dNs showed that GemC-TP levels were decreased by more than half when dNs (5 μ M) were added to the media (*Figure 3-15B-1*) while dNTP levels remained at relatively high levels. These results strongly suggested that a competition for cellular import and phosphorylation between the drug and the nucleosides plays a role in the observed rescue in presence of external dNs. Additional dNs also increased dNTP levels without treatment (*Figure 3-15B-2*), confirming that dNs are imported and phosphorylated. dNTPs were decreased in presence of the drug when compared to levels measured in presence of only nucleosides. Ratio of the four dNTPs was altered in presence of GemC and dNs with higher levels of dATP compared to untreated cells, where dTTP levels were higher. This difference might be explained by the action of the dFdUMP which inhibits thymidilate synthase, an enzyme involved in synthesis of dTTP (Mini *et al.*, 2006). dFdUMP is produced by the action of deoxycytidine monophosphate deaminase on dFdCMP (monophosphate GemC). The increase of dNTP levels after addition of dNs in GemC-treated cells suggests that the observed survival of cells in presence of external dNs might also be a result of a rescue of dNTP pools. The results above, therefore suggest that additional dNs rescue survival to GemC by both competing for drug entry and increasing dNTPs levels affected by the drug.

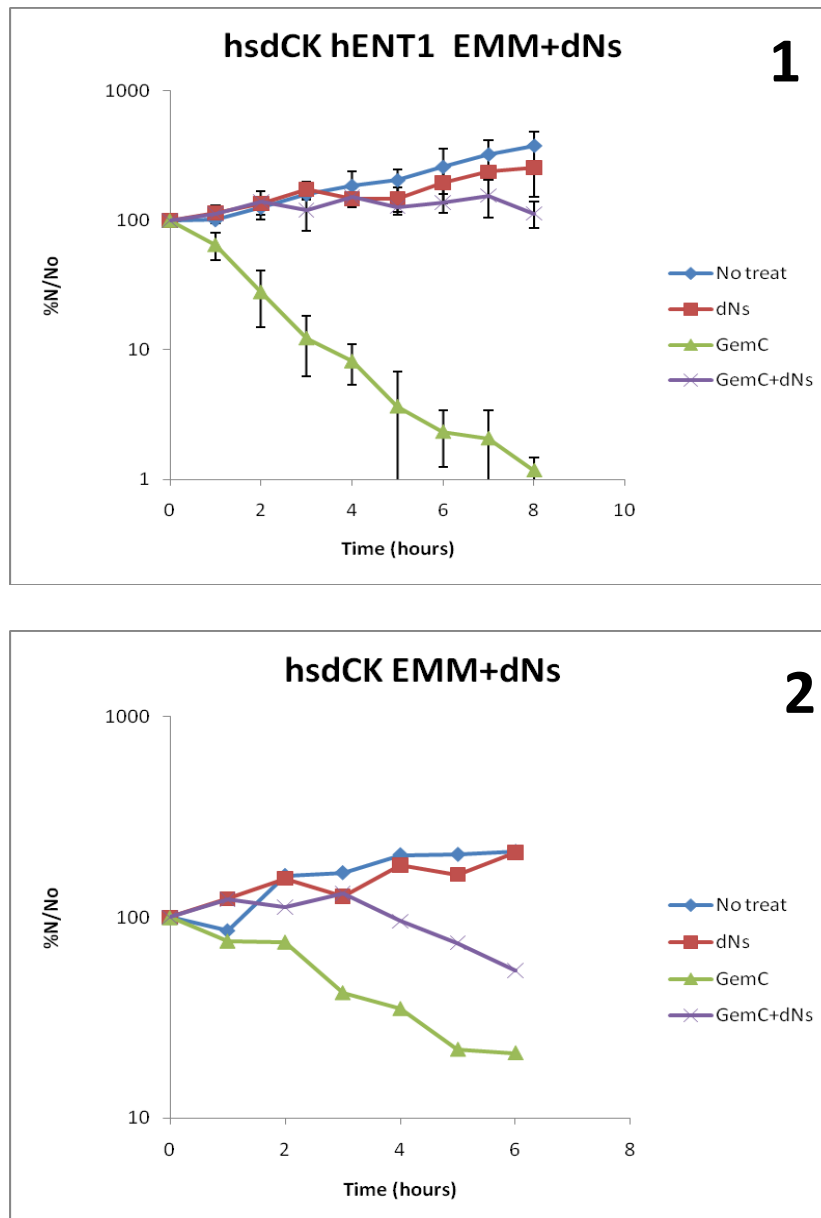


Figure 3-15A. dNs rescued effect of GemC in EMM. 5 μ M of each dN was added to the media before treatment with 1 μ M GemC in cells with transporter (**1**). Cells without transporter (**2**) were treated with 50 μ M of GemC and 50 μ M of dN. Cells were collected every hour and 500 cells were plated on EMM (*hsdCK/hENT1* cells) and YEA (*hsdCK* cells) media and incubated at 30°C until colonies were formed. Results show percentages to time 0. To confirm that dNs were not toxic, cells were also grown in presence of dNs alone and showed normal growth (red). Cells were less sensitive to the drug in media with additional dNs (purple curves). The rescue effect was higher in cells with transporter (**1**) compared to cells without transporter (**2**). Error bars in figure A were calculated from three independent experiments and figure 2 shows two independent experiments. Experiments were carried out on yeast strains MG70, *hsdCK/hENT1* and MG22, *hsdCK*.

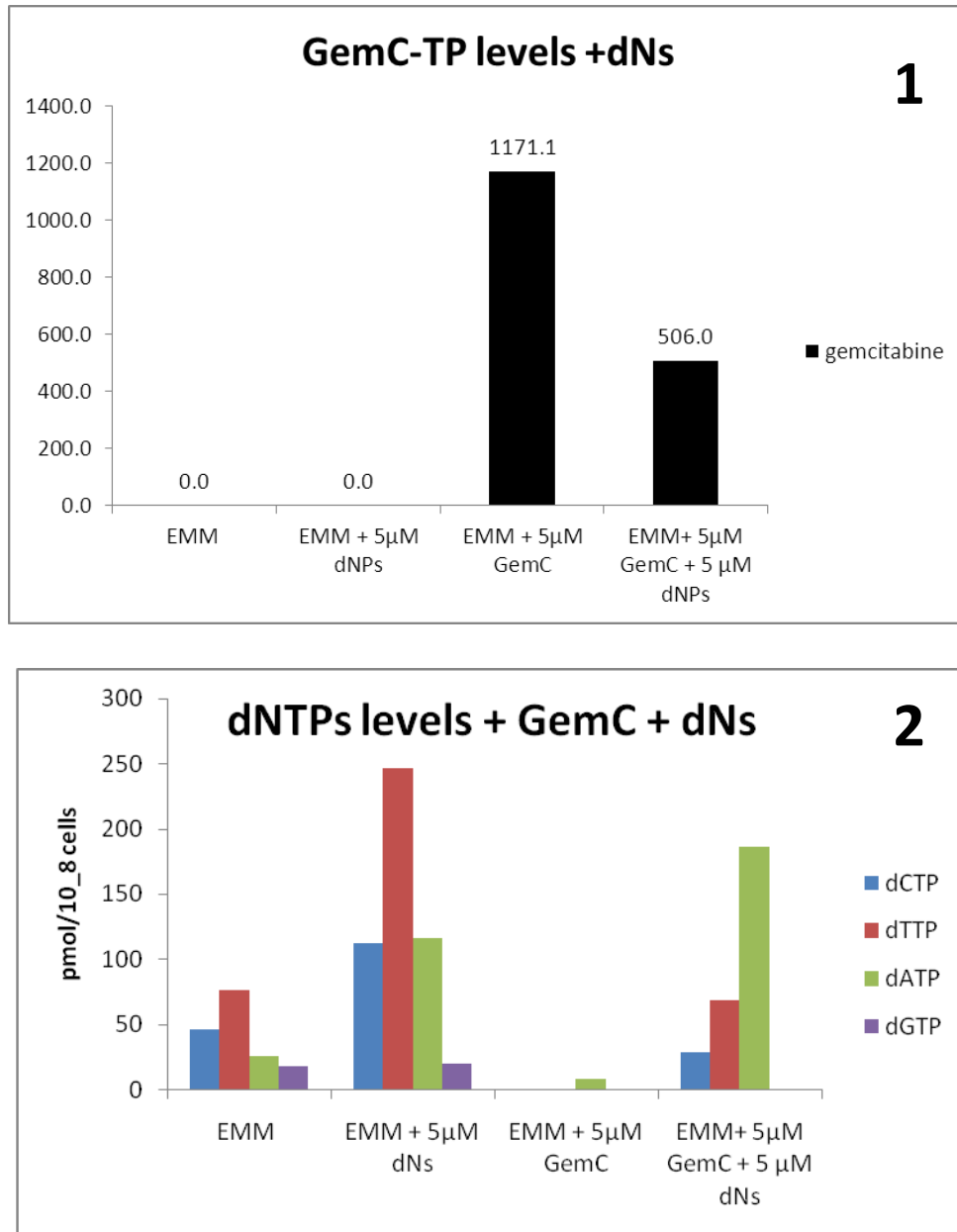


Figure 3-15B. GemC-TP levels are decreased by addition of dNs in EMM (1) and dNTPs levels increase in the presence of dNs (2). Cells (MG70, *hsdCK/hENT1*) were grown in EMM and 5 μ M of GemC and /or dNs were added and incubated for 3 hours. Cells were then collected and intracellular GemC and dNTPs levels were measured by HPLC. GemC levels were 2 fold decreased when dNs were present in the media (1) whereas dNTPs levels were increased when dNs were added (2). dGTP levels were very low and undetectable in +GemC +dNs. The figure shows an average of two experiments.

3.3.3 DNA damage checkpoint is activated by YE media

The elongation of *S. pombe* cells as a mark of cell cycle arrest was first suggested by Nurse (Nurse *et al.*, 1976) who observed cell elongation in division cycle defective mutants. We tested whether cell elongation observed in rich media in presence of the transporter was due to delay in cell cycle (and activation of checkpoint). Because dNTP pools were elevated in cells with the transporter (Figure 3-12C), we hypothesised that the unbalanced nucleotides levels might halt cell cycle progression and induce the checkpoint response. In *S. pombe* the checkpoint is dependent on two kinases which activate subsequent proteins and induce cell cycle delay. The human ATR and ATM homologues, Rad3 and Tel1 respectively, act by phosphorylating checkpoint kinases Chk1 and Cds1 (human Chk2) which in turn activate other proteins required for the mechanism such as Cdc25 which induce cell cycle arrest (Eyfjord and Bodvarsdottir, 2005). We used a *rad3* *S. pombe* mutant to assess the possible role of the machinery in the observed cellular elongation. *rad3* deleted mutants show a complete absence of checkpoint and a temperature sensitive (*rad3ts*) mutant was identified and characterised (Martinho *et al.*, 1998) with permissive temperature at 27°C and restrictive temperature at 35°C. The mutation corresponds to a single amino acid change (A2217V) in the ATP binding site of the kinase. We integrated the human kinase and the transporter into a *rad3ts* mutant (MG314) by crosses and tested the resulting strain (MG363) for elongation in rich media. Cells were pre-grown in minimal media overnight at 30°C, cells were then transferred to EMM and YEL media (10 ml) and incubated overnight at 25°C and 37°C.

As shown in Figure 3-16, at the permissive temperature (25°C) where checkpoint is still active, *rad3ts* cells were elongated in YEL and not in EMM. In addition, at the restrictive 37°C where the checkpoint was inactivated, cell growth was highly affected in YEL and not in EMM (observations during culture, results not shown). I also observed a mix of elongated cells and a lot of cellular debris in *rad3ts* cells in YEL at 37°C suggesting that cells struggle to survive in the absence of checkpoint, although some cells were still elongated. Control WT cells showed no differences at 25 and 37°C suggesting that the observed temperature dependency was specific to *rad3ts* mutants.

The observation that checkpoint defective mutants encounter difficulties to survive in YEL and not in EMM media, suggests that the checkpoint mechanism is involved in response of cells in the rich media. The fact that some cells were still elongated in

rad3ts mutants however implies that the observed elongation is not exclusively *rad3* checkpoint-dependent. The mechanisms underlying the observed cellular elongation were not further investigated as they were not within the scope of this project.

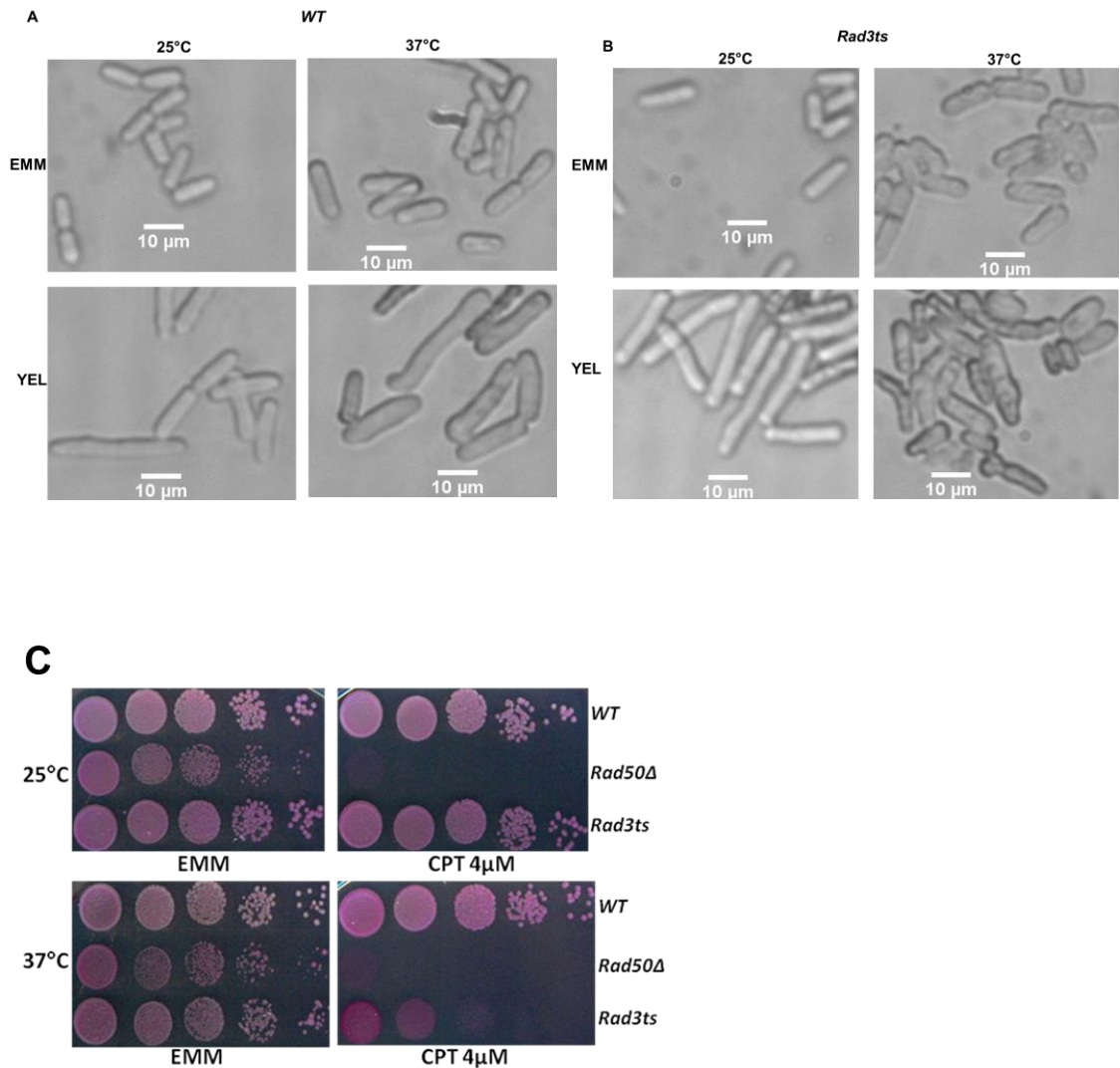


Figure 3-16 *rad3ts* checkpoint defective mutants were affected by YEL. WT (A, MG70) and *rad3ts* (B, MG363) cells containing the human kinase and the transporter were grown overnight on minimal EMM media supplied with uracil and rich YE media at 25°C and 37°C. At the permissive temperature (25°C) *rad3ts* cells were elongated in YE and not in EMM and at the restrictive temperature, 37°C cell survival was affected and cell debris were observed in YE media. At the same restrictive temperature, cells showed normal growth in minimum media. In WT control cells showed the same phenotype for both temperatures (elongation in YEL and normal growth in EMM). (C) Cells were tested on CPT 4 μM to confirm sensitivity of *rad3ts* mutants at the restrictive temperature. A *rad50* deleted mutant (*rad50Δ*, MG119) showed sensitivity at both temperatures whereas wild type (WT, MG70) was resistant at both temperatures. Media contain phloxine 2.5 mg/l and cells were incubated for 5 days at 30°C.

3.4 Discussion

As detailed in this chapter, we have successfully constructed *S. pombe* strains that allow study of the effect of NA treatment in fission yeast by increasing NAs uptake via the hENT1 human transporter and phosphorylation of the NAs into their active form by the human *hsdCK* and the *Drosophila dmdNK* kinases. The study was carried out with two major deoxycytidine NAs, GemC and AraC. However, I anticipate that with either kinases present in the yeast genome, a broader range of NAs can be studied.

A combination of the kinase (either the human *hsdCK* or the *Drosophila dmdNK*) and the human hENT1 transporter highly increased GemC and AraC sensitivity of *S. pombe* cells to concentrations as low as 250nM compared to 40µM in cells with only the kinase (Figure 3-3 and Figure 3-10). *S. pombe* cells that contain only the transporter showed no sensitivity to GemC or AraC, emphasizing the essential role of the kinase in drug activity. The high sensitivity of cells with the transporter was observed in both short and long term exposure. The presence of the transporter however impeded cell growth in rich media (YEL) where we have observed reduced growth compared to growth in EMM (Figure 3-12A). Additional to slow growth, cells with either kinase and the transporter were elongated in rich media and DAPI-stained cells presented elongated cells with degraded nuclei (Figure 3-12B). HPLC measurement of intracellular dNTP levels in cells with human *hsdCK* kinase showed increased dNTP levels in the presence of the transporter in YEL without treatment (Figure 3-12C). Together, the observed cell elongation and elevated dNTP pools raised a question of a possible activation of the checkpoint to protect the genome following import of high levels of dNs from the yeast extract media through the human transporter, as it has been reported that cell elongation is a mark of checkpoint activation in *S. pombe* (Nurse *et al.*, 1976) and that, a ~35 fold increase in dNTP concentrations (in comparison to WT) leads to a delay in cell cycle in *S. cerevisiae* (Chabes and Stillman, 2007). Analysis of a temperature sensitive checkpoint *rad3ts* mutant strongly suggested a role of the checkpoint in response to YEL as checkpoint defective cells struggled to survive in the rich media but had normal growth in EMM (Figure 3-16). However, as some of the *rad3ts* mutant cells were still elongated in rich media, I speculated that the observed elongation phenotype might not be exclusively *rad3* checkpoint-dependent but might also result from other mechanisms or other checkpoint activator such as Tel1. The precise response of the checkpoint machinery and mechanisms responsible for cellular elongation were not further

investigated as it was not within the scope of this project. However, we can ascertain the compound that activates DNA damage checkpoint requires a phosphorylation step, as elongation was only observed when both the transporter and kinase were present. For further analysis cells were grown in EMM media to avoid this effect.

Survival assays showed a higher sensitivity of cells containing *hsdCK* without the transporter to GemC in minimal EMM media compared to GemC-treated cells in rich YEL media (*Figure 3-13*). Cells with both the kinase and transporter showed higher sensitivity to the drug in YEL compared to EMM, possibly due to the presence of growth inhibiting elements in rich media (as we have observed that *hsdCK/hENT1* cells are elongated in YEL without treatment). HPLC measurements of intracellular GemC-TP showed high levels of the drug in EMM compared to YEL in both cells with and without the transporter (*Figure 3-14*), suggesting a competition for transport and/or phosphorylation between the drug and nucleosides present in the yeast extract media. This observation, however doesn't allow to clearly establish a relationship between the high sensitivity and GemC-TP levels. In fact, although intracellular concentrations of GemC-TP have been reported to correlate with DNA synthesis inhibition and drug toxicity (Heinemann *et al.*, 1988), the diphosphate (GemC-DP) and monophosphate (GemC-MP) forms of the drug have also been suggested to contribute to drug toxicity by decreasing dNTP pools which, also inhibits DNA synthesis. GemC-DP inhibits RNR and decreases all four dNTPs (Heinemann *et al.*, 1990), while dFdUMP (resulting from deamination of GemC-MP) is thought to inhibit thymidylate synthase, involved in thymidine synthesis (Mini *et al.*, 2006). Moreover, GemC might also contribute to toxicity by inhibiting RNA synthesis and (Ruiz van Haperen *et al.*, 1993). The sensitivity of cells to GemC might therefore be interpreted as resulting from a combination of all modes of action. HPLC measurement of intracellular levels of dNTPs showed that dNTPs were highly lowered when GemC was added to the media (*Figure 3-14* and *Figure 3-15B*) supporting the suggestion that the drug affects dNTP pools as reported by other studies (Heinemann *et al.*, 1990). In addition, low levels of dNTP pools also correlated with high levels of GemC-TP and supported the "self-potential" phenomenon of the drug, explained by the action of the drug on enzymes involved in dNTPs synthesis which decreases dNTPs levels and favours drug incorporation into the DNA (Mini *et al.*, 2006). Additionally, I have observed that intracellular GemC-TP levels were equally high in EMM media, independent of the presence or absence of the

transporter. The observation that drug levels were high in cells without the transporter suggested that *S. pombe* possesses an alternative pathway (other than the incorporated hENT1 transporter) for drug import. This result was supported by the observation that cells with only the kinases showed sensitivity to high concentrations of GemC and AraC (Figure 3-3).

To verify the hypothesis of competition between natural nucleosides and GemC, we assessed the effect of externally supplied dNs on survival of GemC-treated cells in EMM and observed a rescue of cells when dNs were added to the media. The rescue was observed both in cells with and without the transporter (Figure 3-15A). The rescue of cells by dNs however might also be explained by the fact that the nucleosides re-establish dNTP pools balance, disturbed by the action of the drug on RNR and, supportive to this suggestion HPLC measurements of intracellular dNTPs in cells with added dNs, showed an increase of dNTP pools which were highly decreased after treatment with GemC (Figure 3-15B-2).

Levels of intracellular GemC-TP were also strongly decreased in presence of dNs (Figure 3-15B-1). The exact impact of added dNs on GemC-TP levels is however not clear. Based on the similarities between the NA and natural nucleosides, we can hypothesise that dNs might compete with the drug for import through hENT1 transporter. But it has also been suggested (Goan *et al.*, 1999) that high levels of dNTPs decrease GemC concentrations by down regulating deoxycytidine kinase and hence inhibiting drug phosphorylation, a mechanism that might also contribute to the observed rescue in GemC-treated cells. Together these results strongly support the hypothesis that a competition between GemC and natural nucleosides might be at the basis of the observed higher sensitivity of cells without the transporter in EMM compared to sensitivity in YEL. The results however don't allow us to distinguish clearly at which level the competition occurs (drug uptake or DNA incorporation or both). It is most likely that all these factors contribute to the observed difference in sensitivity.

All together, results presented in this chapter show that the presence of the human hENT1 transporter in combination with either the *Drosophila dmdNK* or the human *hsdCK* kinases highly increases sensitivity of *S. pombe* cells to NAs. Analysis of cells response to deoxycytidine analogues GemC and AraC, suggested that the drug import is

improved by hENT1, although import through the *S. pombe* cellular membrane (by *S. pombe* membrane transporters) was also observed. Kinases play an essential role as cells without the kinases showed similar survival to NAs as WT cells. Results also showed that the GemC acts in competition with natural nucleosides and that GemC affects intracellular dNTP levels. Our results show that we have established a functional system that allows us to study NAs in the fission yeast *S. pombe* by increasing drug uptake and phosphorylating pro drugs into phosphorylated active NAs. The system is a robust tool to study cellular response to NAs.

4 Bioneer (V2) genome wide deletion library screen

To identify genes that might play a role in survival to NA treatment, a genome wide deletion library was screened. The screen takes advantage of the fact that thousands of genes have been separately deleted in the genome, which allows assessing the effect of a given molecule on the survival of a large number of mutants. The *S. pombe* genome-wide deletion mutant library purchased from Bioneer Corporation contains around 3000 haploid deletions of non-essential genes that have been replaced by the KanMX marker gene using homologous recombination (Kim *et al*, 2010). I first identified mutants that are sensitive to a high concentration of GemC, which corresponds to the highest concentration at which WT cells show resistance. Based on these results, a sub library set containing all sensitive mutants was further analysed with different concentrations of the drug, which allowed me to rank mutants according to their sensitivity. Mutants were then classified based on their sensitivity.

4.1 Library screen: analysis

4.1.1 Screen of the library

The first step of the screen was to determine the concentration of the drug that corresponds to the highest concentration at which wild type cells containing the kinase and transporter survive treatment. At this high concentration, we select for all cells that are sensitive to GemC in comparison to WT cells. The concentration was determined by testing WT and *mre11-D65N* mutants on different concentrations of GemC. Under certain background *mre11-D65N* mutants show a slight sensitivity to GemC when compared to WT cells (detailed in next chapter), we hence used this mutant as indicative for sensitivity of cells to the drug. We determined 500nM as the highest concentration at which WT cells survived but *mre11-D65N* cells showed sensitivity (*Figure 4-1A*) and the library was screened using 500nM of GemC. After crosses to integrate the transporter and kinase (detailed in next paragraph) cells were transferred on YEA plates containing G418, cycloheximide and nourseothricin 100µg/ml, 500nM of GemC and Phloxine B 2.5mg/l. Dead cells incorporate Phloxine B and are dark pink, whereas living cells actively export the dye and are coloured in pale pink. The plates were then incubated for 5 days at 30°C. 5 days incubation was chosen in order to allow slow growing mutants to catch up. Mutants were visually scored “sensitive, S” if they were growing on the

control plate and not on the plate with the drug and scored “resistant, R” if they showed equal growth on both plates (*Figure 4-1B*).

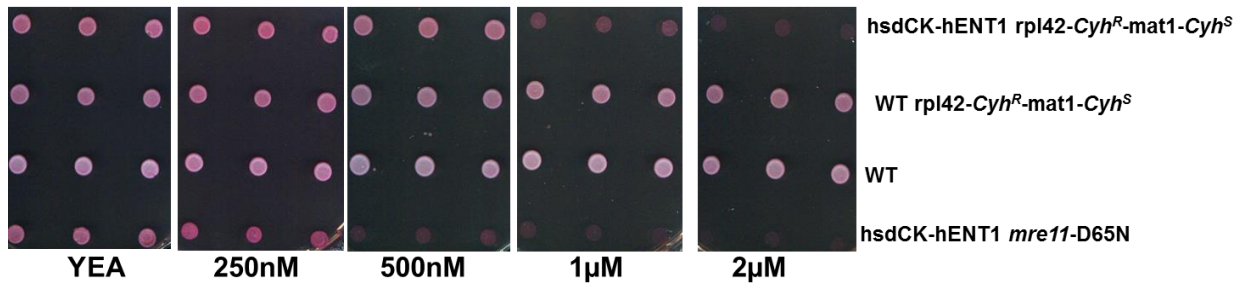


Figure 4-1A Pre-screen of the library. WT strains (*hsdCK-hENT1 rpl42-cyh^R cyh^S*, MG102; WT *rpl42-cyh^S*, MG80 and WT, MG18) and *mre11* nuclease dead (*hsdCK-hENT1 mre11-D65N*, MG182) were tested on YEA containing different concentrations of GemC and incubated for 2 days at 30°C. Plates also contain phloxine 2.5 mg/l. 500nM was chosen for the screen as the highest concentration where the WT showed survival.

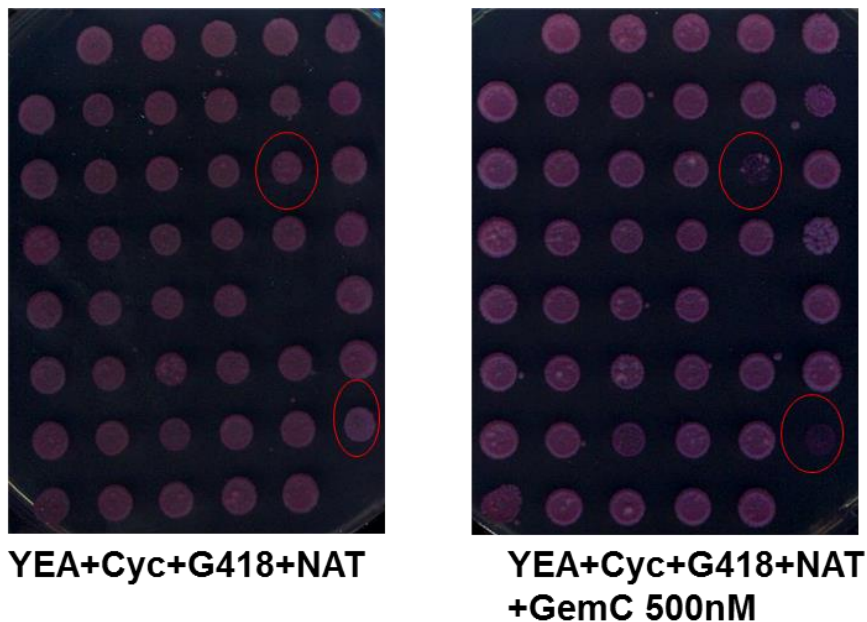


Figure 4-1B. Example of library screen plates. The library was grown in minimal EMM medium supplemented with adenine, leucine and uracil and was then crossed to the strain with *hsdCK/hENT1*. After selection in EMM medium containing selective antibiotics and cycloheximide, the screen was transferred to YE plates containing the same selective antibiotics and cycloheximide, and GemC 500nM. Plates without the drug were used as control. In order to allow slow growing mutants to grow, plates were incubated for 5 days (30°C). Phloxine 2.5 mg/l was used as an indicator for viability. Red circles indicate two examples of mutants that were marked as “sensitive” as they grew on a plate without GemC and not in presence of the drug.

4.1.2 Integration of *hsdCK* kinase and hENT1 transporter into the library

The first step of the screen was to integrate the kinase and the transporter into the library to create *S. pombe* haploid cells containing both genes and the library deletion (strategy outlined in *Figure 4-2*). This was done by crossing the library to a strain containing the human *hsdCK* kinase and hENT1 transporter (*h⁻smt0 mat1M-cyh^S rpl42-cyh^R ura4::adh-hsdCK-NAT-hENT1 ura4aim*, MG102). Integration of genes and mutations into *S. pombe* genome is routinely carried out by crosses and selection of progeny can easily be done on plates for individual strains. High-throughput screens, however present a challenge as we are dealing with thousands of strains at a time and selection of desired mutations can be laborious. We used a strategy named PEM-2 (pombe epistasis marker) presented by Roguev *et al* (2007) which allowed me to select against parental and diploid cells using sensitivity to cycloheximide. Cycloheximide is used as a protein synthesis inhibitor and exerts its toxicity by blocking translation. To select against diploid cells, a cycloheximide sensitive cassette (*cyh^S*) and a cycloheximide resistant (*cyh^R*) mutation (P56Q mutation into the *rpl42* gene) are introduced into the genome. Due to the dominant cycloheximide sensitivity, *cyh^S/cyh^R* cells are sensitive and selected against using the drug, whereas *cyh^R* haploids are resistant. Cycloheximide hence allows selection of haploid non-parental cells in one step. Library mutants containing the KAN resistant cassette were selected using geneticin (G418) and presence of transporter and kinase (NAT resistant cassette) was selected by nourseothricin (NAT). The library (Bioneer library V2) was crossed according to protocol described in Materials and Methods (paragraph 2.2.1.1).

After crosses, I first selected for library mutation to avoid losing slow growth mutants. For the first selection, haploid non-parental cells containing the kanMX marker from the deletion library were selected. Cells were transferred from ELN plates to liquid EMM medium containing G418 (library mutant) and cycloheximide (haploid) 100µg/ml and incubated for 5 days at 30°C. For the second selection, cells were subsequently transferred into liquid EMM medium containing 100µg/ml of G418, cycloheximide and nourseothricin (NAT, for selection of transporter and kinase).

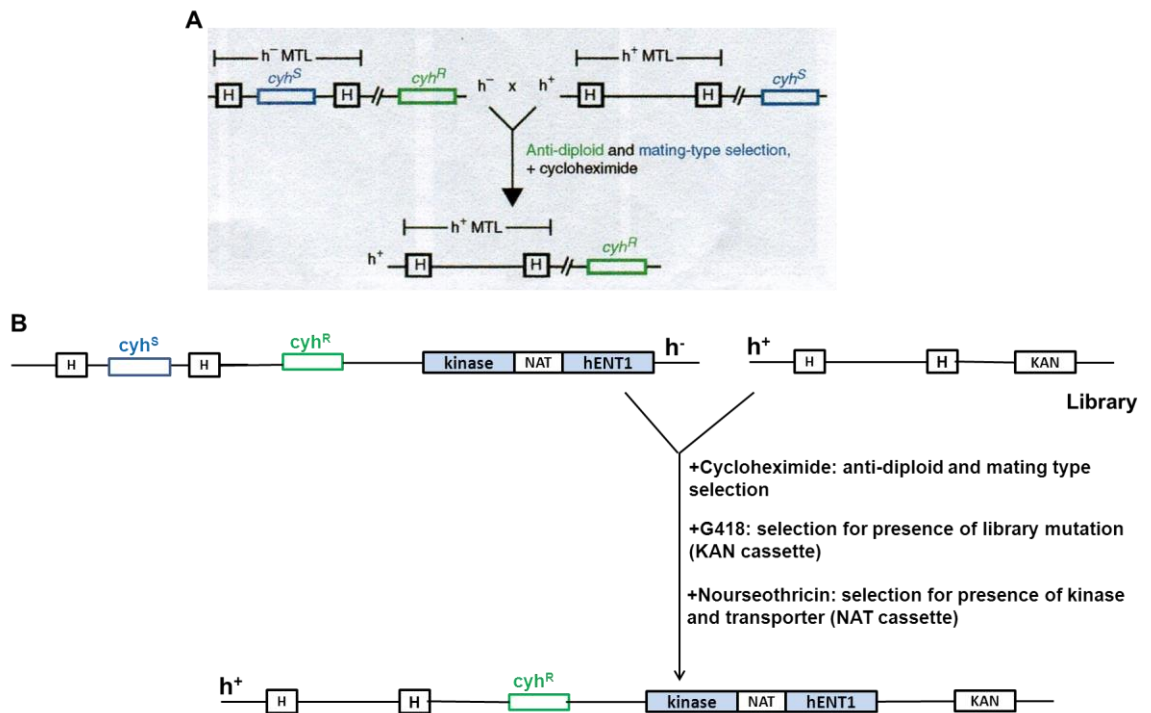


Figure 4-2 Integration of transporter and kinase into the Bioneer deletion library by crosses. (A) PEM-2 strategy as presented by Roguev *et al.* (2007). The Cyh^S (cycloheximide sensitive) cassette is integrated within the h^- mating type locus (h^- MTL) and the Cyh^R (cycloheximide resistant) cassette is introduced by point mutation of the *rpl42* gene. (B) Selection of library mutants using PEM-2 strategy. h^+ Bioneer library was crossed to a h^- Cyh^S/Cyh^R strain containing the transporter and kinase. Selection was carried out using cycloheximide which allowed selection against diploids and parental cells (explained in the text) and G418 and NAT for selection of the library mutant (KAN resistant cassette) and the transporter and kinase (NAT resistance cassette) respectively.

4.1.3 Visual screening

Following three independent screens, mutants were classified and those that were found sensitive in at least one of the three screens were retained for further semi-quantitative analysis. Of a total of 3004 deletion mutants, 456 (15.2%) were sensitive in at least one of the three screens (Table 4-1), 61 (2.0%) of which were sensitive in all three screens (shown in the table, appendix II), 111 (3.7%) were sensitive in 2 out of 3 screens and 284 (9.4%) were sensitive in one out of three screens. 67 (2%) of the strains didn't grow in any of the 3 screens and were not analysed (shown in the table, appendix III).

Several of the sensitive deletion mutants play a known role in genome integrity maintenance. These include replication fork checkpoint genes, *swi3* and *mrc1*, S phase specific cell cycle arrest, *rad26*, and the mitotic kinase, *wee1*, which support the hypothesis of GemC role in inhibiting replication and cell cycle progression. DNA damage checkpoint mutants (*rad3*, *rad17*, *rad9*, *rad1*, *hus1* and *cds1*), homologous recombination mutants (*rhp54*, MRN complex and the DSB binding *rad22*) and excision repair mutants (*apn2*, *rad2* and *ung1*) were also isolated, supporting the role of DNA repair in survival to NA treatment.

Surprisingly, however some of the genes that were identified as sensitive to GemC and AraC in the chapter 5 were not identified through the screen, these include NER and BER genes *rhp14*, *swi10* and *nth1* and the MRN associated gene, *ctp1* whereas other genes such as *rad2* and *ung1* were identified in the screen but were not confirmed by spot tests as both genes were resistant to GemC and AraC treatment. These differences outline limitations of the method, such as possible cross contamination that may occur between wells during the handling of the screen but they may also suggest that the screen is less sensitive in comparison to quantitative methods.

Table 4-1 Library mutants scored as “sensitive” in at least one of three independent screens and analysed under sub library.Names and synonyms correspond to annotation of the pombe genome from <http://www.pombase.org/>.

M-1030H ver2.0 Position	Gene ID	Gene name	Synonyms	Gene description
V2-01-A05	SPAPB18E9.01	trm5		tRNA (guanine) methyltransferase Trm5 (predicted)
V2-01-A06	SPBC365.06	pmt3	ubl2,smt3	SUMO
V2-01-A10	SPAC1D4.11c	lkh1	kic1	dual specificity protein kinase Lkh1
V2-01-C08	SPAC14C4.16	dad3		DASH complex subunit Dad3
V2-01-C09	SPAC17G8.05	med20		mediator complex subunit Med20
V2-01-C10	SPAC212.03			hypothetical protein
V2-01-D02	SPAC1952.02	tma23		ribosome biogenesis protein Tma23 (predicted)
V2-01-D06	SPBC577.02	rpl3801	rpl38-1	60S ribosomal protein L38 (predicted)
V2-01-F01	SPAC16A10.05c	dad1		DASH complex subunit Dad1
V2-01-G02	SPAC23C11.10	usb1		mitochondrial respiratory chain complex III assembly Usb1 (predicted)
V2-01-G07	SPAC13G7.03	upf3		up-frameshift suppressor 3 family protein (predicted)
V2-01-G10	SPAC23C11.08	php3		CCAAT-binding factor complex subunit Php3
V2-01-H01	SPAC1786.04			sequence orphan
V2-01-H07	SPAC13G7.07	arb2		argonaute binding protein 2
V2-01-H09	SPAC19D5.11c	ctf8		DNA replication factor C complex subunit Ctf8 (predicted)
V2-02-B11	SPBC4B4.06	vps25		ESCRT II complex subunit Vps25
V2-02-C04	SPAPB17E12.05	rpl3703	rpl37	60S ribosomal protein L37 (predicted)
V2-02-C07	SPBC16C6.05			mitochondrial translation initiation factor (predicted)

M-1030H ver2.0 Position	Gene ID	Gene name	Synonyms	Gene description
V2-02-C08	SPBC18H10.07			WW domain-binding protein 4 (predicted)
V2-02-C12	SPBCPT2R1.08c	tlh2		RecQ type DNA helicase Tlh1
V2-02-D06	SPBC1539.08	arf6		ADP-ribosylation factor, Arf family Arf6
V2-02-D12	SPBP22H7.08	rps1002	rps10-2,rps10B	40S ribosomal protein S10 (predicted)
V2-02-E02	SPAC6G9.09c	rpl24	rpl24-01,rpl24	60S ribosomal protein L24 (predicted)
V2-02-E06	SPBC1539.10			ribosome biogenesis protein Nop16 (predicted)
V2-02-G09	SPBC2D10.16	mhf1		FANCM-MHF complex subunit Mhf1
V2-02-G10	SPBC337.16	cho1		phosphatidyl-N-methylethanolamine N-methyltransferase (predicted)
V2-03-A08	SPAC6B12.02c	mus7	mms22	DNA repair protein Mus7/Mms22
V2-03-B02	SPCC1223.15c	spc19		DASH complex subunit Spc19
V2-03-B10	SPBC16C6.11	rpl3201	rpl32-1	60S ribosomal protein L32
V2-03-C02	SPCC1259.04	iec3		Ino80 complex subunit Iec3
V2-03-C05	SPAC19D5.01	pyp2		tyrosine phosphatase Pyp2
V2-03-C11	SPBC28F2.11			HMG box protein
V2-03-E03	SPCC74.05	rpl2702	rpl27-2	60S ribosomal protein L27 (predicted)
V2-03-E08	SPAC9E9.08	rad26		ATRIP, ATR checkpoint kinase regulatory subunit Rad26
V2-03-E11	SPBC29A10.10c			tRNA-splicing endonuclease positive effector (predicted)
V2-03-F12	SPBC3D6.10	apn2		AP-endonuclease Apn2
V2-03-G10	SPBC216.05	rad3		ATR checkpoint kinase Rad3
V2-03-G12	SPBC4B4.07c	usp102	mud1	U1 snRNP-associated protein Usp102
V2-03-H09	SPBC16A3.08c			Stm1 homolog (predicted)
V2-03-H10	SPBC21B10.10	rps402	rps4-2	40S ribosomal protein S4 (predicted)

M-1030H ver2.0 Position	Gene ID	Gene name	Synonyms	Gene description
V2-04-A08	SPAC1071.02	mms19		TFIIH regulator Mms19
V2-04-B01	SPBC543.07	pek1	skh1,mkk1	MAP kinase kinase Pek1
V2-04-C06	SPAC328.02			ubiquitin-protein ligase involved in sporulation
V2-04-C08	SPAC10F6.04			RCC domain protein Ats1 (predicted)
V2-04-C09	SPAC11E3.01c	swr1	SPAC2H10.03c	SNF2 family helicase Swr1
V2-04-D05	SPCC895.07	alp14	mtc1	TOG ortholog Alp14
V2-04-D09	SPAC11E3.05			ubiquitin-protein ligase E3, human WDR59 ortholog
V2-04-D11	SPAC144.02	iec1		Ino80 complex subunit Iec1
V2-04-F05	SPCC970.07c	raf2	dos2,cmc2,clr7	Rik1-associated factor Raf2
V2-04-G03	SPCC24B10.09	rps1702	rps17-2,rps17	40S ribosomal protein S17 (predicted)
V2-04-H04	SPCC736.06			mitochondrial aspartate-tRNA ligase (predicted)
V2-04-H10	SPAC13C5.07	mre11	rad32	Rad32 nuclease
V2-05-B03	SPAC17G6.05c			Rhophilin-2 homolog (predicted)
V2-05-B05	SPAC1952.07	rad1		checkpoint clamp complex protein Rad1
V2-05-C02	SPAC17A2.06c	vps8		WD repeat protein Vps8 (predicted)
V2-05-C07	SPAC20G8.08c	fft1		fun thirty related protein Fft1 (predicted)
V2-05-D09	SPAC22G7.08	ppk8		serine/threonine protein kinase Ppk8 (predicted)
V2-05-D11	SPAC24B11.12c			P-type ATPase (predicted)
V2-05-E01	SPAC16C9.06c	upf1		ATP-dependent RNA helicase Upf1
V2-05-E10	SPAC23D3.09	arp42	arp4	SWI/SNF and RSC complex subunit Arp42

M-1030H ver2.0 Position	Gene ID	Gene name	Synonyms	Gene description
V2-05-F01	SPAC1705.02			human 4F5S homolog
V2-05-G08	SPAC22F3.08c	rok1		ATP-dependent RNA helicase Rok1 (predicted)
V2-05-G12	SPAC27D7.14c	tpr1	SPAC637.02c	RNA polymerase II associated Paf1 complex subunit Tpr1
V2-05-H04	SPAC18G6.15	mal3		EB1 family Mal3
V2-06-B03	SPAC3A11.09	sod22		plasma membrane alkali metal cation/H ⁺ antiporter Sod22
V2-06-B04	SPAC3F10.02c	trk1	sptrk	potassium ion transporter Trk1
V2-06-B05	SPAC3H1.06c			membrane transporter (predicted)
V2-06-B07	SPAC56F8.09	rrp8		rRNA methyltransferase Rrp8 (predicted)
V2-06-C04	SPAC3F10.06c			initiator methionine tRNA 2'-O-ribosyl phosphate transferase (predicted)
V2-06-C11	SPAC8C9.12c			mitochondrial iron ion transporter (predicted)
V2-06-D06	SPAC4G9.02	rnh201		ribonuclease H2 complex subunit Rnh201 (predicted)
V2-06-D11	SPAC8E11.02c	rad24		14-3-3 protein Rad24
V2-06-E05	SPAC3H5.07	rpl702	rpl7-2,rpl7,rpl7b	60S ribosomal protein L7
V2-06-E08	SPAC664.02c	arp8		actin-like protein, Ino80 complex subunit Arp8
V2-06-F05	SPAC3H5.12c	rpl501	rpl5-1,rpl5	60S ribosomal protein L5 (predicted)
V2-06-F07	SPAC589.09			sec14 cytosolic factor family (predicted)
V2-06-G08	SPAC688.14	set13		ribosome L32 lysine methyltransferase Set13
V2-06-G09	SPAC806.08c	mod21		gamma tubulin complex subunit Mod21
V2-06-H01	SPAC2H10.01			transcription factor, zf-fungal binuclear cluster type (predicted)
V2-06-H11	SPAC9.10	thi9		thiamine transporter Thi9
V2-07-A12	SPBC2F12.11c	rep2		transcriptional activator, MBF subunit Rep2
V2-07-B12	SPBC2F12.12c			human c19orf29 ortholog

M-1030H ver2.0 Position	Gene ID	Gene name	Synonyms	Gene description
V2-07-C11	SPBC29A3.05	vps71		Swr1 complex subunit Vps71
V2-07-D07	SPBC19C7.02	ubr1	SPBC32F12.14	N-end-recognizing protein Ubr1
V2-07-D11	SPBC29A3.09c			AAA family ATPase Gcn20 (predicted)
V2-07-E03	SPBC13E7.09	vrp1		verprolin
V2-07-F09	SPBC21C3.13	rps1901	rps19-1	40S ribosomal protein S19 (predicted)
V2-07-F12	SPBC31F10.07	lsb5		cortical component Lsb5 (predicted)
V2-07-G01	SPBC106.10	pka1	tpk,git6	cAMP-dependent protein kinase catalytic subunit Pka1
V2-07-G11	SPBC2A9.04c			sir antagonist ortholog (predicted)
V2-07-G12	SPBC31F10.09c	nut2	med10	mediator complex subunit Med10
V2-07-H07	SPBC19F8.08	rps401	rps4-1,rps4,SPBC25H2.17c	40S ribosomal protein S4 (predicted)
V2-08-A01	SPBC31F10.12			RNA-binding protein Tma20 (predicted)
V2-08-A07	SPBC800.04c	rpl4301	rpl43-1,rpl43,rpl37a-1	60S ribosomal protein L37a (predicted)
V2-08-B01	SPBC31F10.16			ChAPs family protein (predicted)
V2-08-B11	SPCC11E10.07c			translation initiation factor eIF2B alpha subunit (predicted)
V2-08-C03	SPBC36.07	iki3		elongator subunit Iki3 (predicted)
V2-08-C06	SPBC685.06	rps001	rps0-1,rpsa-1,rps0	40S ribosomal protein S0A (p40)
V2-08-C08	SPBC9B6.07	nop52		nucleolar protein Nop52 family (predicted)
V2-08-C09	SPBP35G2.10	mit1		SHREC complex subunit Mit1
V2-08-C11	SPCC11E10.08	rik1		silencing protein Rik1
V2-08-D06	SPBC685.07c	rpl2701	rpl27-1	60S ribosomal protein L27
V2-08-D11	SPCC1223.05c	rpl3702	rpl37-2,rpl37	60S ribosomal protein L37 (predicted)
V2-08-E02	SPBC342.05	crb2	rhp9	DNA repair protein Rad9 homolog, Rhp9

M-1030H ver2.0 Position	Gene ID	Gene name	Synonyms	Gene description
V2-08-E03	SPBC365.10	arp5		actin-like protein Arp5
V2-08-E07	SPBC887.10	mcs4		response regulator Mcs4
V2-08-E08	SPBP16F5.03c	tra1		SAGA complex phosphatidylinositol pseudokinase Tra1
V2-08-F08	SPBP16F5.05c			ribosome biogenesis protein Nop8 (predicted)
V2-08-G06	SPBC725.01			aspartate aminotransferase (predicted)
V2-08-H01	SPBC336.01	fbh1	fdh1,fdh	DNA helicase I
V2-08-H07	SPBC902.02c	ctf18	chl12	RFC-like complex subunit Ctf18
V2-09-B03	SPCC4B3.15	mid1	dmf1	medial ring protein Mid1
V2-09-B04	SPCC663.04	rpl39		60S ribosomal protein L39
V2-09-B08	SPCC962.04	rps1201	rps12-1,rps12	40S ribosomal protein S12 (predicted)
V2-09-B09	SPAC1805.04	nup132	Nup133b	nucleoporin Nup132
V2-09-C08	SPBC776.17			rRNA processing protein Rrp7 (predicted)
V2-09-D04	SPCC736.11	ago1	csp9	argonaute
V2-09-D11	SPCC569.05c			spermidine family transporter (predicted)
V2-09-E04	SPCC74.04			amino acid permease (predicted)
V2-09-E06	SPCC24B10.08c	ada2		SAGA complex subunit Ada2
V2-09-F01	SPCC1919.03c	amk2		AMP-activated protein kinase beta subunit Amk2
V2-09-F05	SPAC23C4.11	atp18		F0-ATPase subunit J (predicted)
V2-09-H06	SPCC1739.14	npp106		nucleoporin Npp106
V2-10-A01	SPCC736.08	cbf11		CBF1/Su(H)/LAG-1 family transcription factor Cbf11
V2-10-A07	SPAC694.06c	mrc1		mediator of replication checkpoint 1
V2-10-A12	SPBC3H7.07c	ser2		phosphoserine phosphatase Ser2 (predicted)

M-1030H ver2.0 Position	Gene ID	Gene name	Synonyms	Gene description
V2-10-C04	SPBC1861.07			elongin C (predicted)
V2-10-C09	SPCC24B10.22	pog1	SPCPB16A4.01	mitochondrial DNA polymerase
V2-10-D05	SPBC947.08c	hip4	hpc2	histone promoter control protein Hip4
V2-10-D11	SPBPJ4664.06	gpt1		UDP-glucose-glycoprotein glucosyltransferase Gpt1
V2-10-E04	SPBC1709.14			peptide N-glycanase (predicted)
V2-11-A02	SPAC3H5.08c			WD repeat protein, human WDR44 family
V2-11-A12	SPAC16.01	rho2		Rho family GTPase Rho2
V2-11-B10	SPCC663.14c			TRP-like ion channel (predicted)
V2-11-B11	SPAC10F6.11c	atg17		autophagy associated protein kinase activator Atg17
V2-11-C02	SPAC1687.19c			queuine tRNA-ribosyltransferase (predicted)
V2-11-C04	SPAC30.02c			elongator complex associated protein Kti2 (predicted)
V2-11-D02	SPAC9G1.02	wis4	wak1,wik1	MAP kinase kinase kinase Wis4
V2-11-D09	SPCC1902.01	gaf1	SPCC417.01c	transcription factor Gaf1
V2-11-D12	SPAC1783.05	hrp1	chd1	ATP-dependent DNA helicase Hrp1
V2-11-H01	SPAC4H3.07c			protein phosphatase Fmp31 (predicted)
V2-11-H04	SPBC21H7.04	dbp7		ATP-dependent RNA helicase Dbp7 (predicted)
V2-11-H07	SPBC25D12.05	trm1		N2,N2-dimethylguanosine tRNA methyltransferase
V2-12-A01	SPAC18G6.02c	chp1		chromodomain protein Chp1
V2-12-B01	SPAC1952.09c			acetyl-CoA hydrolase (predicted)
V2-12-B04	SPAC3C7.08c	elf1		AAA family ATPase Elf1
V2-12-B07	SPBC1685.13	fhn1		Fhn1 plasma membrane organization protein
V2-12-C07	SPBC1685.14c			Vid27 family protein

M-1030H ver2.0 Position	Gene ID	Gene name	Synonyms	Gene description
V2-12-D11	SPCC338.16	pof3		F-box protein Pof3
V2-12-F09	SPBC530.06c			translation initiation factor eIF3 alpha subunit (p135) (predicted)
V2-12-F12	SPCP1E11.06	apl4		AP-1 adaptor complex gamma subunit Apl4
V2-12-G10	SPCC1322.03			TRP-like ion channel (predicted)
V2-12-G12	SPCP25A2.02c	rhp26		SNF2 family helicase Rhp26
V2-13-A03	SPBC1683.09c	frp1		ferric-chelate reductase Frp1
V2-13-A05	SPBC691.03c	apl3		AP-2 adaptor complex subunit Alp3 (predicted)
V2-13-C02	SPAC2G11.03c	vps45		vacuolar sorting protein Vps45
V2-13-E05	SPBC31F10.13c	hip1	hir1	hira protein, histone chaperone Hip1
V2-13-H01	SPAC1556.01c	rad50	SPAP4C9.01c	DNA repair protein Rad50
V2-14-A02	SPAC30D11.05	aps3		AP-3 adaptor complex subunit Aps3 (predicted)
V2-14-A09	SPAC4H3.02c	swc3		Swr1 complex subunit Swc3
V2-14-B01	SPCC4B3.12	set9		histone lysine methyltransferase Set9
V2-14-B07	SPAC23H3.13c	gpa2	git8	heterotrimeric G protein alpha-2 subunit Gpa2
V2-14-E03	SPAC11D3.15			5-oxoprolinase (ATP-hydrolyzing) (predicted)
V2-14-G01	SPCC736.07c			unconventional prefoldin involved in translation initiation (predicted)
V2-14-G07	SPAC30D11.10	rad22	rad22A,	DNA recombination protein Rad22
V2-14-G10	SPAPB1E7.04c			chitinase (predicted)
V2-14-H01	SPCPJ732.02c			xylulose kinase (predicted)
V2-15-A03	SPBC24C6.06	gpa1		G-protein alpha subunit
V2-15-B04	SPBC2G2.06c	apl1		AP-2 adaptor complex subunit Apl1 (predicted)
V2-15-B05	SPBC3D6.02	but2		But2 family protein But2

M-1030H ver2.0 Position	Gene ID	Gene name	Synonyms	Gene description
V2-15-B11	SPCC18B5.03	wee1		M phase inhibitor protein kinase Wee1
V2-15-C01	SPBC1734.11	mas5		DNAJ domain protein Mas5 (predicted)
V2-15-C06	SPBC582.10c			ATP-dependent DNA helicase Rhp16b (predicted)
V2-15-C07	SPBP35G2.08c	air1		zinc knuckle TRAMP complex subunit Air1
V2-15-C11	SPCC18B5.11c	cds1		replication checkpoint kinase Cds1
V2-15-E05	SPBC3E7.16c	leu3	SPBC4F6.03c	2-isopropylmalate synthase Leu3
V2-15-E10	SPCC1827.02c			cholinephosphate cytidylyltransferase (predicted)
V2-15-E11	SPCC4F11.03c			sequence orphan
V2-15-F03	SPBC2F12.03c			EST1 family protein (predicted)
V2-16-A02	SPCC188.07	ccq1		telomere maintenance protein Ccq1
V2-16-B03	SPBC21C3.02c	dep1		Sds3-like family protein Dep1
V2-16-C07	SPBC1652.01			ribosomal RNA processing element (RRPE)-binding protein (predicted)
V2-16-D05	SPAC29B12.02c	set2	kmt3	histone lysine methyltransferase Set2
V2-16-D09	SPCC777.03c			nifs homolog, possible cysteine desulfurase
V2-16-E12	SPAC17A2.13c	rad25		14-3-3 protein Rad25
V2-16-G11	SPAC15A10.03c	rhp54	rhp54	Rad54 homolog Rhp54
V2-17-A02	SPAC23C11.04c	pnk1		DNA kinase/phosphatase Pnk1
V2-17-A03	SPAC29A4.20	elp3	kat9	elongator complex, histone acetyltransferase subunit Elp3 (predicted)
V2-17-C03	SPAC2E12.03c			PQ loop protein
V2-17-C04	SPAC3G6.06c	rad2	fen1	FEN-1 endonuclease Rad2
V2-17-C06	SPBC14C8.03	fma2		methionine aminopeptidase Fma2 (predicted)
V2-17-C08	SPBC3B9.09	vps36		ESCRT II complex subunit Vps36

M-1030H ver2.0 Position	Gene ID	Gene name	Synonyms	Gene description
V2-17-D04	SPAC3H1.11	hsr1		transcription factor Hsr1
V2-17-E09	SPBP22H7.04			sequence orphan
V2-17-E12	SPACUNK4.12c	mug138		metallopeptidase (predicted)
V2-17-F01	SPAC1F5.10			ATP-dependent RNA helicase (predicted)
V2-17-F03	SPAC30D11.09	cwf19		complexed with Cdc5 protein Cwf19
V2-17-G07	SPBC32F12.05c	cwf12		complexed with Cdc5 protein Cwf12
V2-17-G10	SPCC306.08c			malate dehydrogenase (predicted)
V2-18-A06	SPAC323.05c			protein methyltransferase Mtq2 (predicted)
V2-18-B01	SPAC637.10c	rpn10	pus1	19S proteasome regulatory subunit Rpn10
V2-18-C07	SPAC664.07c	rad9		checkpoint clamp complex protein Rad9
V2-18-C11	SPAC20G4.07c	sts1	erg4	C-24(28) sterol reductase Sts1
V2-18-D02	SPAC227.18	lys3	SPAC2F7.01	saccharopine dehydrogenase Lys3
V2-18-D05	SPAC11E3.08c	nse6		Smc5-6 complex non-SMC subunit Nse6
V2-18-D06	SPBC1D7.03	mug80		cyclin Clg1 (predicted)
V2-18-D10	SPCC1393.02c	spt2		non-specific DNA binding protein Spt2 (predicted)
V2-18-E07	SPBC28F2.10c	ngg1	ada3, kap1	SAGA complex subunit Ngg1
V2-18-E11	SPCC364.05	vps3		GTPase regulator Vps3 (predicted)
V2-18-F07	SPAC30C2.02	mmd1		deoxyhypusine hydroxylase (predicted)
V2-18-H07	SPAC1399.02			membrane transporter (predicted)
V2-18-H10	SPCC576.11	rpl15		60S ribosomal protein L15 (predicted)
V2-19-A09	SPBC20F10.07			GRAM domain protein
V2-19-A10	SPBC31F10.10c			zf-MYND type zinc finger protein

M-1030H ver2.0 Position	Gene ID	Gene name	Synonyms	Gene description
V2-19-A11	SPBC800.05c	tub1	tub1,alp2,ban5, atb2	tubulin alpha 2
V2-19-B12	SPBP4H10.09	rsv1		transcription factor Rsv1
V2-19-C02	SPAC20G4.04c	hus1		checkpoint clamp complex protein Hus1
V2-19-E05	SPAC630.14c	tup12		transcriptional corepressor Tup12
V2-19-F01	SPAC1B3.16c	vht1		vitamin H transporter Vth1
V2-19-F03	SPAC31G5.09c	spk1		MAP kinase Spk1
V2-19-H01	SPAC1D4.03c	aut12		autophagy associated protein Aut12 (predicted)
V2-19-H11	SPBP35G2.13c	swc2		Swr1 complex complex subunit Swc2
V2-20-A02	SPCC594.02c			conserved fungal protein
V2-20-A04	SPAC23H4.09	cdb4		curved DNA-binding protein Cdb4, peptidase family
V2-20-A05	SPAC31A2.11c	cuf1		nutritional copper sensing transcription factor Cuf1
V2-20-A08	SPAC27D7.03c	mei2		RNA-binding protein involved in meiosis Mei2
V2-20-A10	SPAC1002.06c	bqt2	mug18,rec23	bouquet formation protein Bqt2
V2-20-A12	SPAC1B1.04c			poly(A)-specific ribonuclease complex subunit Pan3 (predicted)
V2-20-B01	SPCC31H12.04c	rpl1202	rpl12-2,rpl12	60S ribosomal protein L12.1/L12A
V2-20-B02	SPCC594.04c			steroid oxidoreductase superfamily protein (predicted)
V2-20-B04	SPAC1F7.12	yak3	yakC,SPAC21E11.01	aldose reductase ARK13 family YakC
V2-20-B07	SPAC1071.11			NADH-dependent flavin oxidoreductase (predicted)
V2-20-B09	SPCC16A11.16c	rpn1302	rpn13,rpn13b	19S proteasome regulatory subunit Rpn13b
V2-20-B10	SPAC1002.07c	ats1		N-acetyltransferase Ats1 (predicted)
V2-20-B12	SPAC1F5.08c	yam8	ehs1	calcium channel regulatory subunit Yam8
V2-20-C01	SPCC364.06	nap1	nap11	nucleosome assembly protein Nap1

M-1030H ver2.0 Position	Gene ID	Gene name	Synonyms	Gene description
V2-20-C03	SPCC757.11c			membrane transporter (predicted)
V2-20-C04	SPAC186.09			pyruvate decarboxylase (predicted)
V2-20-C08	SPAC31A2.15c	dcc1		Ctf18 RFC-like complex subunit Dcc1
V2-20-C09	SPCC1884.02	nic1	SPCC757.01	NiCoT heavy metal ion transporter Nic1
V2-20-C10	SPAC1071.09c			DNAJ domain protein, DNAJC9 family (predicted)
V2-20-C12	SPAC20H4.06c			RNA-binding protein
V2-20-D02	SPCC663.06c			short chain dehydrogenase (predicted)
V2-20-D03	SPCC777.12c			thioredoxin family protein
V2-20-D06	SPBC16D10.07c	sir2		Sir2 family histone deacetylase Sir2
V2-20-D08	SPAC513.07			flavonol reductase/cinnamoyl-CoA reductase family
V2-20-D09	SPCC594.05c	spf1	spp1	Set1C PHD Finger protein Spf1
V2-20-D11	SPAC17A5.07c	ulp2		SUMO deconjugating cysteine peptidase Ulp2 (predicted)
V2-20-E02	SPCC663.10			tRNA (uracil) methyltransferase (predicted)
V2-20-E04	SPAC9E9.15			CIA30 protein (predicted)
V2-20-E05	SPAC6F12.06			Rho GDP dissociation inhibitor Rdi1 (predicted)
V2-20-E06	SPAC26A3.01	sxa1	SPAC2E1P5.06	aspartic protease Sxa1
V2-20-E09	SPCC794.03			amino acid permease (predicted)
V2-20-E10	SPAC1142.07c	vps32	snf7	ESCRT III complex subunit Vps32
V2-20-E11	SPAC17A5.10			conserved fungal protein
V2-20-F05	SPAP27G11.14c			sequence orphan
V2-20-F06	SPBC12C2.04			NAD binding dehydrogenase family protein
V2-20-H01	SPCC576.13	swc5		Swr1 complex subunit Swc5

M-1030H ver2.0 Position	Gene ID	Gene name	Synonyms	Gene description
V2-20-H07	SPAC26H5.10c	tif51		translation elongation factor eIF5A (predicted)
V2-21-B02	SPAC4A8.09c	cwf21		complexed with Cdc5 protein Cwf21
V2-21-D03	SPAC869.06c			HHE domain cation binding protein (predicted)
V2-21-D04	SPBC16C6.03c			ribosome assembly protein (predicted)
V2-21-D09	SPCC1450.08c	wtf16		wtf element Wtf16
V2-21-D11	SPCC737.05			peroxin Pex28/29 (predicted)
V2-21-E07	SPBC685.04c	aps2		AP-2 adaptor complex subunit Aps2 (predicted)
V2-21-E09	SPCC1494.08c			conserved fungal protein
V2-21-F04	SPBC16G5.15c	fkh2		fork head transcription factor Fkh2
V2-21-F08	SPCC1259.08			conserved fungal protein, DUF2457 family
V2-21-G04	SPBC1703.03c			armadillo repeat protein, unknown biological role
V2-21-H01	SPAC2E1P5.03			DNAJ domain protein Erj5 (predicted)
V2-21-H11	SPCC970.05	rpl3601	rpl36-1	60S ribosomal protein L36
V2-22-A08	SPAC31G5.11	pac2		cAMP-independent regulatory protein Pac2
V2-22-A12	SPBC359.04c			cell surface glycoprotein (predicted), DIPSY family
V2-22-D02	SPAC140.04			conserved eukaryotic protein
V2-22-D09	SPAPB1A10.14	pof15		F-box protein (predicted)
V2-22-F07	SPAC26A3.07c	rpl1101	rpl11-1,rpl11	60S ribosomal protein L11 (predicted)
V2-22-F08	SPAC5D6.02c	mug165		sequence orphan
V2-22-F10	SPBC1A4.02c	leu1	SPBC1E8.07c	3-isopropylmalate dehydrogenase Leu1
V2-22-H09	SPBC13E7.06	msd1	mug172	mitotic-spindle disanchored Msd1
V2-22-H10	SPBC23E6.01c		SPBPJ758.01	mRNA processing factor (predicted)

M-1030H ver2.0 Position	Gene ID	Gene name	Synonyms	Gene description
V2-23-A04	SPAC144.11	rps1102	rps11-2,rps11	40S ribosomal protein S11 (predicted)
V2-23-A05	SPBC1734.05c	spf31		DNAJ protein Spf31 (predicted)
V2-23-A07	SPAC1B3.01c			uracil phosphoribosyltransferase (predicted)
V2-23-A09	SPAC11G7.04	ubi1		ribosomal-ubiquitin fusion protein Ubi1 (predicted)
V2-23-A10	SPAC1952.05	gcn5	kat2	SAGA complex histone acetyltransferase catalytic subunit Gcn5
V2-23-A11	SPAC31A2.09c	apm4		AP-2 adaptor complex subunit Apm4 (predicted)
V2-23-B07	SPAC30D11.02c			sequence orphan
V2-23-B10	SPAC1A6.08c	mug125		sequence orphan
V2-23-C03	SPCC622.08c	hta1		histone H2A alpha
V2-23-C09	SPAC13C5.06c	mug121		sequence orphan
V2-23-D11	SPAC4F8.01	did4	SPAC644.03c,vps2	ESCRT III complex subunit Did4
V2-23-E06	SPAC1250.03	ubc14		ubiquitin conjugating enzyme Ubc14 (predicted)
V2-23-E11	SPAC4F8.03	sdo1	SPAC644.01c	SBDS family ribosome maturation protein Sdo1 (predicted)
V2-23-E12	SPAC806.07	ndk1		nucleoside diphosphate kinase Ndk1
V2-23-F04	SPAC1D4.09c	rtf2		replication termination factor Rtf2
V2-23-G03	SPCC825.05c			splicing coactivator SRRM1 (predicted)
V2-23-G10	SPAC2C4.06c			rRNA methyltransferase (predicted)
V2-23-G12	SPAC922.04			sequence orphan
V2-23-H10	SPAC2F7.07c	cph2	rco1	Clr6 histone deacetylase associated PHD protein-2 Cph2
V2-24-A08	SPCC4B3.06c			NADPH-dependent FMN reductase (predicted)
V2-24-A09	SPBC1773.09c	mug184		meiotically upregulated gene Mug184
V2-24-B03	SPBC25B2.10			Usp (universal stress protein) family protein

M-1030H ver2.0 Position	Gene ID	Gene name	Synonyms	Gene description
V2-24-B09	SPBC1921.07c	sgf29	SPBC21D10.13	SAGA complex subunit Sgf29
V2-24-B10	SPAC1610.01		SPAC17A5.17	conserved eukaryotic protein
V2-24-C03	SPBC27B12.08	sip1		Pof6 interacting protein Sip1, predicted AP-1 accessory protein
V2-24-C11	SPAC26A3.04	rpl2002	rpl20,rpl20-2	60S ribosomal protein L20 (predicted)
V2-24-E05	SPCC1393.08			transcription factor, zf-GATA type (predicted)
V2-24-E08	SPAC16E8.12c			ING family homolog Png3 (predicted)
V2-24-E12	SPAC6B12.05c	ies2		Ino80 complex subunit Ies2
V2-24-F09	SPAC10F6.08c	nht1		Ino80 complex HMG box protein Nht1
V2-24-F12	SPAC6F12.03c	fsv1		SNARE Fsv1
V2-24-G01	SPBC12C2.01c		SPBC17F3.03c	sequence orphan
V2-25-A06	SPAC521.05	rps802	rps8-2	40S ribosomal protein S8 (predicted)
V2-25-A12	SPAC977.14c			aldo/keto reductase, unknown biological role
V2-25-B01	SPAP8A3.07c			phospho-2-dehydro-3-deoxyheptonate aldolase (predicted)
V2-25-B02	SPBC146.02			sequence orphan
V2-25-B04	SPBC2G5.03	ctu1		cytosolic thiouridylase subunit Ctu1
V2-25-B05	SPCC18B5.09c			sequence orphan
V2-25-B06	SPAC17C9.08	pnu1	nuc1,end1	mitochondrial endodeoxyribonuclease Pnu1
V2-25-B11	SPAC24B11.09			mitochondrial protein, predicted, human BRP44 ortholog
V2-25-C03	SPBC1A4.04			sequence orphan
V2-25-C04	SPBC530.03c	bag102	bag1-b	BAG family molecular chaperone regulator Bag102 (predicted)
V2-25-C05	SPCC285.10c			SPRY domain protein
V2-25-C07	SPAC30D11.14c			RNA-binding protein (predicted)

M-1030H ver2.0 Position	Gene ID	Gene name	Synonyms	Gene description
V2-25-D04	SPBP8B7.08c			leucine carboxyl methyltransferase Ppm1 (predicted)
V2-25-D05	SPCC338.14			adenosine kinase (predicted)
V2-25-D06	SPCC364.02c	bis1		stress response protein Bis1
V2-25-D07	SPAC25B8.08			conserved fungal protein
V2-25-D10	SPAC1A6.07			sequence orphan
V2-25-D11	SPAC3G9.11c			pyruvate decarboxylase (predicted)
V2-25-E03	SPBC24C6.10c	dip1		WISH/DIP/SPIN90 ortholog Dip1
V2-25-E04	SPCC1183.09c	pmp31	mug75	plasma membrane proteolipid Pmp31
V2-25-E05	SPCC576.12c	mhf2		FANCM-MHF complex subunit Mhf2
V2-25-E07	SPAC8C9.07			rRNA processing protein Fyv7 (predicted)
V2-25-E12	SPBC11B10.10c	pht1		histone H2A variant H2A.Z, Pht1
V2-25-F02	SPBC1718.07c	zfs1	moc4	CCCH tandem zinc finger protein, human Tristetraprolin homolog Zfs1, involved in mRNA catabolism
V2-25-F07	SPAC1F12.07			phosphoserine aminotransferase (predicted)
V2-25-F10	SPAC20H4.03c	tfs1		transcription elongation factor TFIIIS
V2-25-H01	SPBC1347.13c			ribose methyltransferase (predicted)
V2-26-A05	SPBC13A2.04c			PTR family peptide transporter (predicted)
V2-26-B02	SPCC663.11	saf1		splicing associated factor Saf1
V2-26-B06	SPAC16A10.03c			zinc finger protein Pep5/Vps11-like (predicted)
V2-26-B08	SPBC21C3.20c	git1		C2 domain protein Git1
V2-26-B09	SPCC1739.07	cti1		Cut3 interacting protein Cti1, predicted exosome subunit
V2-26-B10	SPAC3A12.13c			translation initiation factor eIF3j (p35)

M-1030H ver2.0 Position	Gene ID	Gene name	Synonyms	Gene description
V2-26-C06	SPAC16E8.01	shd1	sla1	cytoskeletal protein binding protein Sla1 family, Shd1 (predicted)
V2-26-D04	SPCPB16A4.04c	trm8		tRNA (guanine-N7-)-methyltransferase catalytic subunit Trm8 (predicted)
V2-26-D07	SPAC4D7.07c			sequence orphan
V2-26-D11	SPBC21D10.10	bdc1		bromodomain containing protein 1, Bdc1
V2-26-E04	SPAC664.04c	rps1602	rps16-2,rps16	40S ribosomal protein S16 (predicted)
V2-26-E06	SPAC17C9.15c			sequence orphan
V2-26-E10	SPBC1685.02c	rps1202	rps12-2	40S ribosomal protein S12 (predicted)
V2-26-F02	SPCC736.02			sequence orphan
V2-26-F04	SPAC31A2.12			arrestin/PY protein 1 (predicted)
V2-26-G05	SPAC13G7.06	met16		phosphoadenosine phosphosulfate reductase
V2-26-G08	SPCC1442.04c			meiotic recombination protein (predicted)
V2-26-G11	SPCC594.06c			vacuolar SNARE Vam7 (predicted)
V2-26-H05	SPAC13G7.12c			choline kinase (predicted)
V2-27-A05	SPAC3G6.01	hrp3		ATP-dependent DNA helicase Hrp3
V2-27-A11	SPAPJ698.02c	rps002	rpsa-2,rps0-2,rps0	40S ribosomal protein S0B
V2-27-A12	SPAC23A1.16c	rtr1		RNA polymerase II CTD phosphatase Rtr1 (predicted)
V2-27-B01	SPAC23C11.02c	rps23		40S ribosomal protein S23 (predicted)
V2-27-B11	SPCC23B6.05c	ssb3	rpa3	DNA replication factor A subunit Ssb3
V2-27-B12	SPAC30D11.04c	nup124		nucleoporin Nup124
V2-27-C02	SPBC1604.16c			RNA-binding protein, G-patch type (predicted)
V2-27-C09	SPCC11E10.06c	elp4		elongator complex subunit Elp4 (predicted)
V2-27-C12	SPAC31G5.03	rps1101	rps11-1	40S ribosomal protein S11 (predicted)

M-1030H ver2.0 Position	Gene ID	Gene name	Synonyms	Gene description
V2-27-D10	SPBC4F6.10	vps901	vps9a	guanyl-nucleotide exchange factor Vps901 (predicted)
V2-27-D12	SPAC3H5.10	rpl3202	rpl32-2,rpl32	60S ribosomal protein L32 (predicted)
V2-27-E03	SPCC1223.10c	eaf1		RNA polymerase II transcription elongation factor SpEAF
V2-27-E05	SPBC1921.01c	rpl3701	rpl37-1,rpl37	60S ribosomal protein L35a (predicted)
V2-27-E06	SPBC1539.07c			glutathione-dependent formaldehyde dehydrogenase (predicted)
V2-27-E09	SPCC285.14	trs130		TRAPP complex subunit Trs130 (predicted)
V2-27-F07	SPAC9.02c			polyamine N-acetyltransferase (predicted)
V2-27-F08	SPBC29A3.08	pof4		elongin-A, F-box protein Pof4 (predicted)
V2-27-F12	SPAC4F10.19c			zf-HIT protein Hit1 (predicted)
V2-27-G05	SPAC12G12.15	sif3		Sad1 interacting factor 3 (predicted)
V2-27-G06	SPAC12G12.13c	cid14		poly(A) polymerase Cid14
V2-28-A02	SPBC19C7.01	mni1	SPBC32F12.13c	Mago Nashi interacting protein (predicted)
V2-28-A05	SPAC1F7.13c	rpl801	rpl8-1,rpl18,rpk5a,rpl2-1,SPAC21E11.02c	60S ribosomal protein L8 (predicted)
V2-28-A09	SPBC29A10.16c			cytochrome b5 (predicted)
V2-28-A11	SPAC222.04c	ies6		Ino80 complex subunit Ies6
V2-28-B04	SPCC364.03	rpl1702	rpl17-2,rpl17	60S ribosomal protein L17 (predicted)
V2-28-B05	SPAC23C11.15	pst2		Clr6 histone deacetylase complex subunit Pst2
V2-28-B09	SPBC2G2.03c	sbh1		translocon beta subunit Sbh1 (predicted)
V2-28-B12	SPBC365.03c	rpl2101	rpl21,rpl21-1	60S ribosomal protein L21 (predicted)
V2-28-C01	SPBC11C11.01		SPBC17D1.08	U2-associated protein (predicted)
V2-28-D03	SPAPB1A11.03			cytochrome b2 (L-lactate cytochrome-c oxidoreductase) (predicted)

M-1030H ver2.0 Position	Gene ID	Gene name	Synonyms	Gene description
V2-28-E04	SPAC1556.05c	cgr1		ribosome biogenesis CGR1 family (predicted)
V2-28-E06	SPBC25H2.11c	spt7		SAGA complex bromodomain subunit Spt7
V2-28-G07	SPAC17C9.12			VAP family protein (predicted)
V2-28-G11	SPBC19G7.16	iws1		transcription elongation factor complex subunit Iws1 (predicted)
V2-28-H04	SPAC17G8.13c	mst2		histone acetyltransferase Mst2
V2-28-H07	SPAC1556.08c	cbs2	SPAC1F12.01c	protein kinase activator (predicted)
V2-28-H08	SPBC20F10.05	nr11		NRDE-2 family protein (predicted)
V2-28-H11	SPBC1D7.04	mlo3		RNA binding protein Mlo3
V2-29-A06	SPBC19C7.05			cell wall organization protein (predicted)
V2-29-B03	SPBC215.14c	vps20		ESCRT III complex subunit Vps20
V2-29-B05	SPAC23G3.04	ies4		Ino80 complex subunit Ies4
V2-29-C01	SPAC8F11.02c	dph3		diphthamide biosynthesis protein Dph3 (predicted)
V2-29-C03	SPBC23G7.14			sequence orphan
V2-29-C04	SPAC3A11.14c	pk11	klp1,SPAC3H5.03c	kinesin-like protein Pkl1
V2-29-D03	SPBC651.06	mug166	csa1	sequence orphan
V2-29-D08	SPBC4B4.03	rsc1		RSC complex subunit Rsc1
V2-29-E01	SPAC4H3.05	srs2		ATP-dependent DNA helicase, UvrD subfamily
V2-29-E10	SPAC3A12.10	rpl2001	rpl20-1,rpl20,y117b,rpl18a-2	60S ribosomal protein L20a (predicted)
V2-29-F04	SPCC4B3.08	lsg1		Lsk1 complex gamma subunit (predicted)
V2-29-F06	SPCC18.06c	caf1	pop2	CCR4-Not complex CAF1 family ribonuclease subunit Caf1
V2-29-F11	SPCC1753.05	rsm1		RNA export factor Rsm1

M-1030H ver2.0 Position	Gene ID	Gene name	Synonyms	Gene description
V2-29-F12	SPBC1198.03c			Golgin subfamily A member
V2-29-G04	SPCC777.13	vps35		retromer complex subunit Vps35
V2-29-G07	SPAC22F8.12c	shf1		small histone ubiquitination factor Shf1
V2-29-H04	SPAC144.06	apl5		AP-3 adaptor complex subunit Apl5 (predicted)
V2-29-H07	SPAC9E9.11	plr1	plr	pyridoxal reductase Plr1
V2-29-H08	SPCC285.15c	rps2802	rps28-2,rps28	40S ribosomal protein S28, Rps2802
V2-30-A08	SPBC16G5.06			sequence orphan
V2-30-B12	SPAC17A2.10c			sequence orphan
V2-30-C02	SPAC22F3.09c	res2	mcs1,pct1	MBF transcription factor complex subunit Res2
V2-30-C10	SPBC83.02c	rpl4302	rpl43-2,rpl43,rpl37a-2	60S ribosomal protein L37a (predicted)
V2-30-C12	SPAC17A5.08			COPII-coated vesicle component Erp2/3/4 (predicted)
V2-30-D01	SPCC16C4.20c			Ino80 complex subunit (predicted)
V2-30-E04	SPBC18H10.02	lcf1		long-chain-fatty-acid-CoA ligase Lcf1
V2-30-E11	SPBC1734.15	rsc4	brd1	RSC complex subunit Rsc4
V2-30-F10	SPBC119.08	pmk1	spm1	MAP kinase Pmk1
V2-30-G05	SPAC14C4.13	rad17		RFC related checkpoint protein Rad17
V2-30-H10	SPCC594.01		SPCC736.16	DUF1769 family protein
V2-31-B08	SPAC1071.07c	rps1502	rps15-2,rps15	40S ribosomal protein S15 (predicted)
V2-31-C02	SPBC609.05	pob3		FACT complex component Pob3
V2-31-C04	SPBC30D10.04	swi3		replication fork protection complex subunit Swi3
V2-31-D06	SPAC2G11.06	vps4		AAA family ATPase Vps4 (predicted)
V2-31-E04	SPBP8B7.21	ubp3		ubiquitin C-terminal hydrolase Ubp3

M-1030H ver2.0 Position	Gene ID	Gene name	Synonyms	Gene description
V2-31-E10	SPBC6B1.09c	nbs1	slr10	Mre11 complex subunit Nbs1
V2-31-F02	SPAC22A12.04c	rps2201	rps22-1,rps15a-1	40S ribosomal protein S15a (predicted)
V2-31-G10	SPAC31F12.01	zds1	SPAC637.14,mug88	zds family protein phosphatase type A regulator Zds1 (predicted)
V2-31-G12	SPBC8D2.03c	hhf2	ams3,h4.2	histone H4 h4.2
V2-31-H08	SPBC1718.03	ker1		DNA-directed RNA polymerase I complex subunit Ker1
V2-32-A10	SPBC19C2.02	pmt1		DNA methyltransferase homolog
V2-32-C03	SPAC3F10.17			ribosome biogenesis protein Ltv1 (predicted)
V2-32-C06	SPAC6B12.08	mug185		Co-chaperone for ATPase activity (predicted)
V2-32-C12	SPBC713.05			WD repeat protein, human MAPK organizer 1 (MORG1) family (predicted)
V2-32-D04	SPBC660.11	tcg1	mug187	single-stranded telomeric binding protein Tgc1
V2-32-D09	SPCC1183.06	ung1		uracil DNA N-glycosylase Ung1
V2-32-E06	SPBC36.04	cys11	cys1a	cysteine synthase
V2-32-E09	SPCC285.17	spp27	uaf30	RNA polymerase I upstream activation factor complex subunit Spp27
V2-32-E10	SPAC22E12.18			conserved fungal protein
V2-32-F04	SPAC6G10.06			FAD-dependent amino acid oxidase involved in late endosome to Golgi transport (predicted)
V2-32-F05	SPAC1250.04c	atl1		alkyltransferase-like protein Atl1
V2-32-H07	SPCC1906.04	wtf20		wtf element Wtf20
V2-32-H10	SPAC4G9.15			ketoreductase (predicted)
V2-32-H11	SPAC4F10.04	ypa1	rrd1	protein phosphatase type 2A, intrinsic regulator Rrd1 (predicted)
V2-33-B03	SPCC16C4.10			6-phosphogluconolactonase (predicted)
V2-33-B10	SPAC3G9.03	rpl2301	rpl23-1	60S ribosomal protein L23

M-1030H ver2.0 Position	Gene ID	Gene name	Synonyms	Gene description
V2-33-C10	SPCC1682.16	rpt4		19S proteasome regulatory subunit Rpt4 (predicted)
V2-33-C11	SPBC19C2.14	smd3		Sm snRNP core protein Smd3
V2-33-E03	SPBC1778.01c	zuo1	mpp11,SPBC30D10.01	zuotin (predicted)
V2-33-E05	SPBC13G1.12	did2		ESCRT III complex subunit Did2 (predicted)

4.2 Sub library analysis: Optimization of analysis method

The sub library was analysed with different concentrations of GemC and the sensitivity of different mutants was quantified (methods explained in next paragraph). Mutants were then quantitatively ranked according to the value of their sensitivity. To quantify the sensitivity, the library was plated on EMM medium containing different concentrations of GemC (50, 100, 150, 200 and 250nM) and incubated at 30°C for five days. Plates were then scanned every twelve hours and the images were analysed using ImageJ software. The software measures the intensity of the spots (different mutants) which corresponds to cumulative pixel values in a selected region of interest. It then attributes a value which correlates with cell growth on the plate (I will refer to this value as “raw intensity”). The challenge in the analysis of the library was to find a suitable concentration at which small differences in sensitivity can be detected. In fact, at a high concentration, only differences in less sensitive mutants can be detected as highly sensitive mutants are all killed and it is difficult to determine at which levels cells are sensitive. On the contrary, the use of a low concentration would lead to differentiation of only the highly sensitive mutants as the least sensitive mutants would all grow. To determine concentrations to use for further analysis, I compared growth curves distribution at the different concentrations. *Figure 4-3A* shows growth curves distribution of 250 random mutants (untreated and treated with different concentrations of GemC). Growth curves without drug show different growth of mutants as some have a very slow phenotype and others grow well. If we analyse graphs in *Figure 4-3A* by taking raw intensity value of 80000 as an arbitrary cut-off, we see that the number of curves under the cut off increases with the concentration of the drug. At 250nM most (180 out of 250) mutants are under the cut-off whereas at 50nM, only a few mutants (69 out of 250) are under 80000 when compared to untreated mutants (36 out of 250). 50nM, 150nM and 250nM were chosen as concentrations to use to quantify the sublibrary as they covered a wide range of mutants.

Another difficulty lay in finding a suitable method to quantify the sensitivity of mutants. I first compared three methods (detailed in next paragraphs), that allow quantification of the growth, using 4 known mutants (*rad32*, *rad50*, *apn2* and *rad3*) and 150 and 250nM of GemC as examples. All three methods are based on quantification of growth curves, which gives an estimation of growth for each mutant (illustrated in *Figure 4-3B*). The first method measures areas under growth curves (measurement of total growth), the

second method quantifies slopes of growth curves at exponential phase (measurement of growth rate, R value) and the third method measures end points of the curves (measurement of the final growth, K value, or the density at stationary phase). The optimization was carried out on one experiment and mutants were ranked (paragraph 4.3) based on three independent experiments.

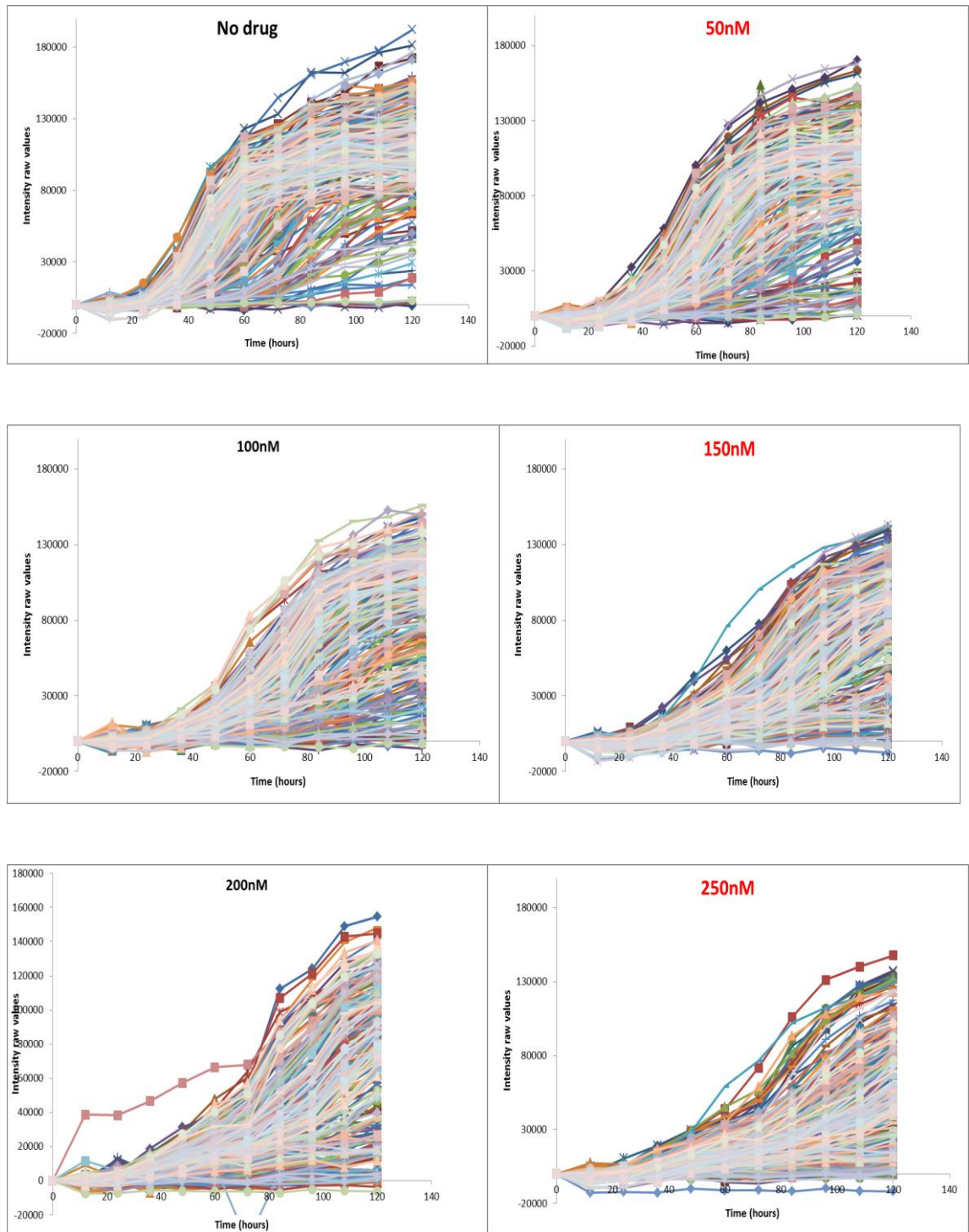


Figure 4-3A. Selection of GemC concentrations for the sub library analysis by analysing distribution of treated mutants. The figure represents 250 random mutants and shows growth curves based on raw intensity values over 5 days incubation. Y axis represents intensity values as measured by ImageJ (arbitrary unit) and X axis represents time (hours). Growth curves without drug show different growth of mutants as some have a very slow phenotype and others grow well. 50nM, 150nM and 250nM were chosen as concentrations that covered a wide range of mutants.

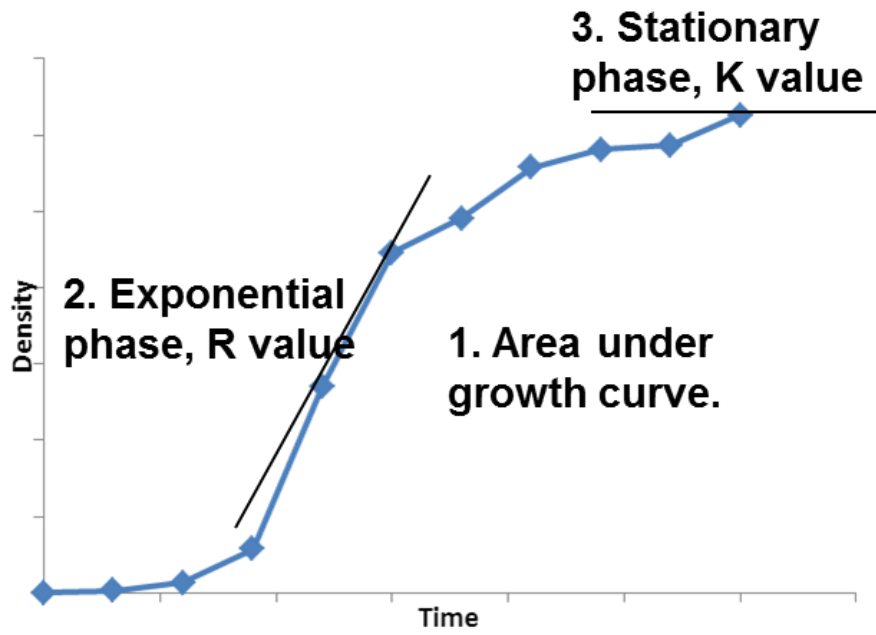


Figure 4-3B. Illustration of the three methods used to quantify mutants' growth. Three methods that quantify the growth curves were compared. See text for explanation

4.2.1 Method 1: ranking by areas under growth curves

The first method tested was the ranking of mutants by the area under the growth curve assuming that the highest difference in area under growth curves between untreated and GemC treated cells ($\Delta G = G_u - G_t$) would represent the most sensitive mutant. *Figure 4-4A*, showing growth curves of selected mutants, suggests a sensitivity of *rad50*, *rad32* and *rad3* mutants as cell growth was clearly reduced (red curves) after treatment with 150nM of GemC in those mutants. Green curves show ΔG values. To quantify the sensitivity, areas underneath curves were calculated using the trapezoid rule to determine area under curve in Microsoft Excel (*Figure 4-4B*). After calculation of the areas, mutants were ranked by the difference between total areas of untreated and GemC-treated cells (the highest total area was given the lowest number in rank). Graphs (*Figure 4-4C-1*) and Table (*Figure 4-4C-2*) show a clear difference in sensitivities of the different mutants to the drug. *rad3* mutant was ranked most sensitive with the highest area under the curve and *apn2* the least sensitive. These calculations however were biased by the fact that some of the mutants showed a slow growth phenotype in absence of the drug (e.g. MRN mutants, *Figure 4-4C-3*). Indeed, because the calculations take in account differences in growth, mutants with slow growth phenotype presented a low value in untreated cells (low G_u) which, in turn affected ΔG values. Ranking of mutants was therefore affected low ΔG values which resulted in low G_u values of some mutants and were not representative of overall differences in growth. This biased effect was more emphasised at high concentrations (250nM) where all mutants were very sensitive to GemC. In MRN mutants (*rad32* and *rad50*), for example, results were highly affected by the slow growth phenotype of these mutants in untreated cells, and ranking by ΔG values suggested that these mutants were less sensitive than *apn2* (*Figure 4-4E-1* and *2*), whereas growth curves (*Figure 4-4D*) and plates (*Figure 4-4E-4*) showed a clear high sensitivity of the MRN mutants compared to *apn2*. Differences in growth, on plates without drug, are shown in *Figure 4-4E-3*. *rad3* and *apn2* mutants (red and blue curves) grow faster when compared to *rad32* and *rad50* mutants (green and purple curves).

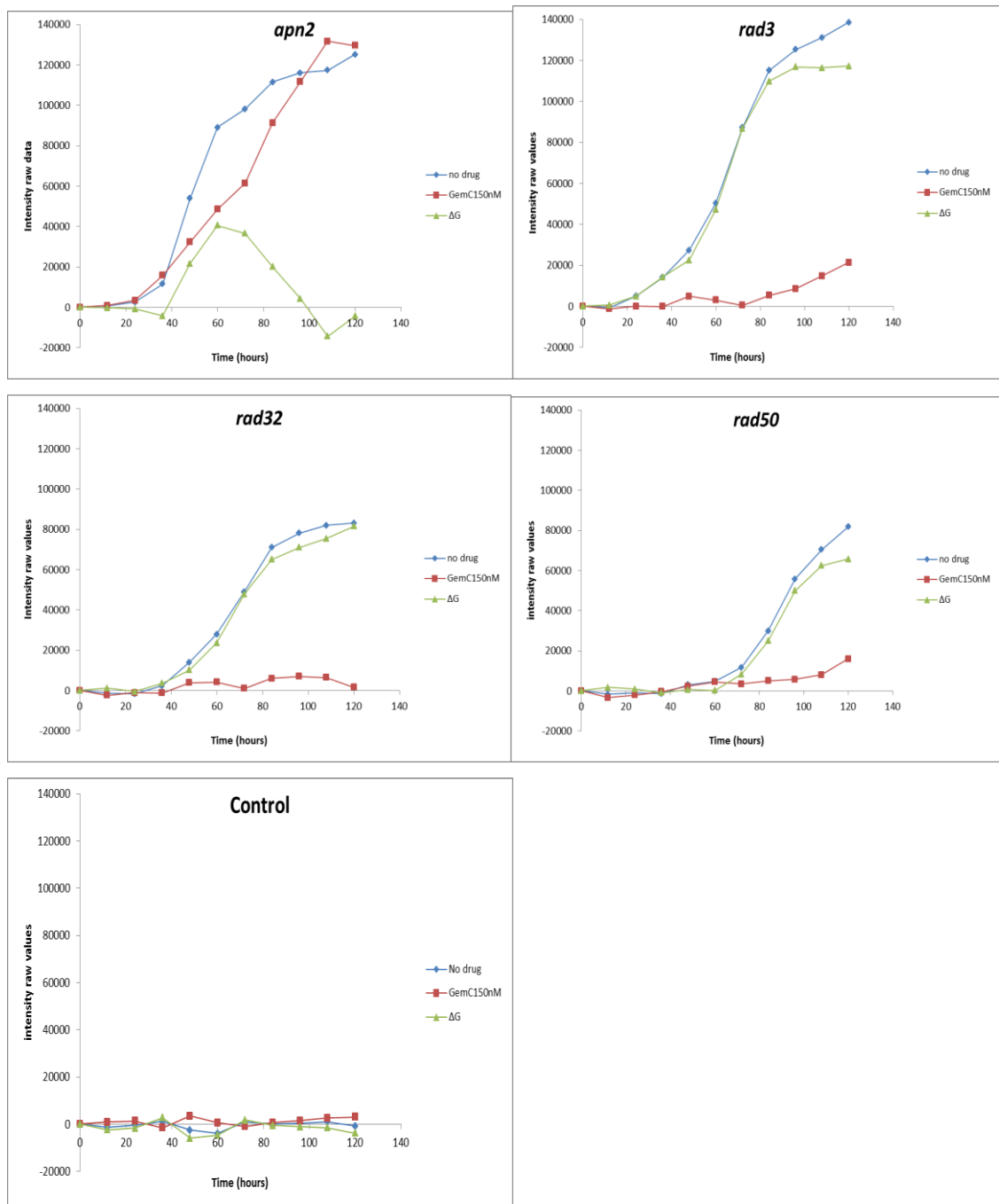


Figure 4-4A. Growth curves of selected library mutants. Y axis represents intensity values as measured by ImageJ (arbitrary unit) and X represents time (hours). At 150nM *rad32*, *rad50* and *rad3* showed high sensitivity to the drug (red curves). *apn2* showed only a mild sensitivity and the control, with an empty well, showed no growth. Plates were incubated at 30°C and scanned every twelve hours for five days. Values at time 0 were subtracted. Green curves represent differences in growth curves (untreated-treated) and blue curves represent growth of untreated cells.

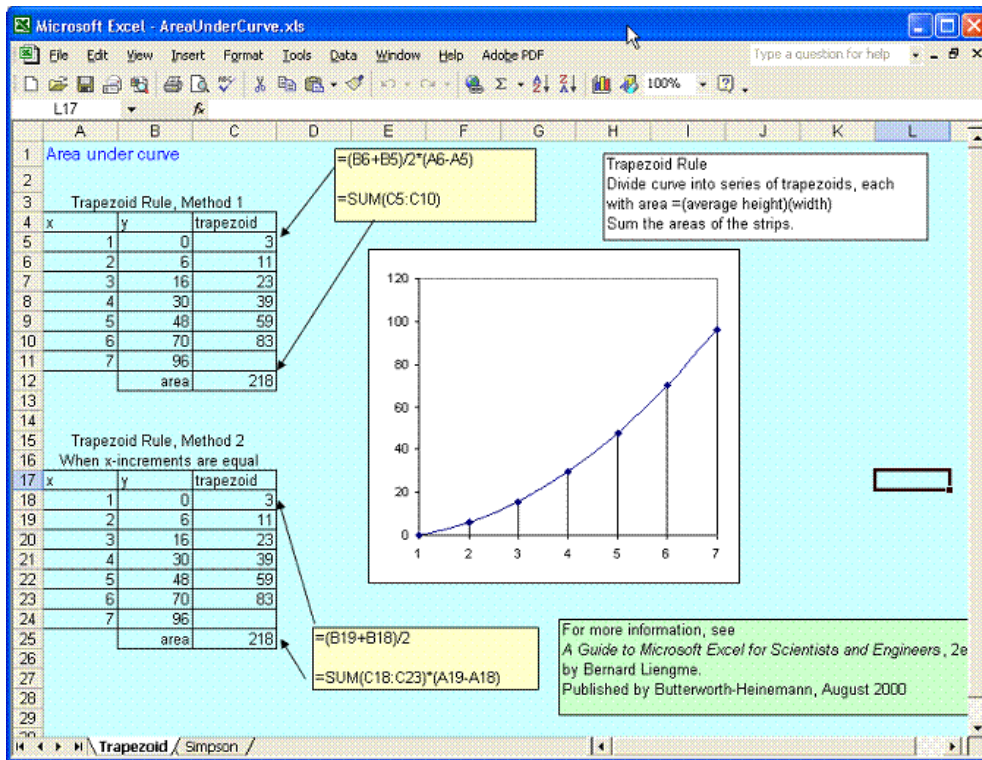


Figure 4-4B. Using Microsoft Excel to apply the trapezoid rule to determine the area under the curve.

(<http://people.stfx.ca/bliengme/ExcelTips/AreaUnderCurve.htm>). Method 2 was used to determine areas.

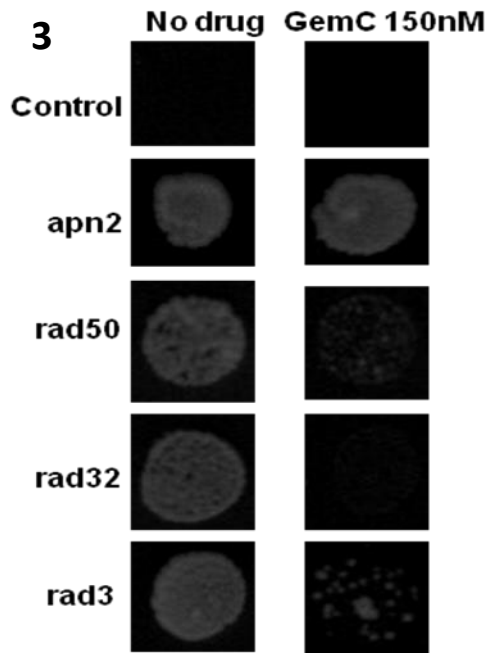
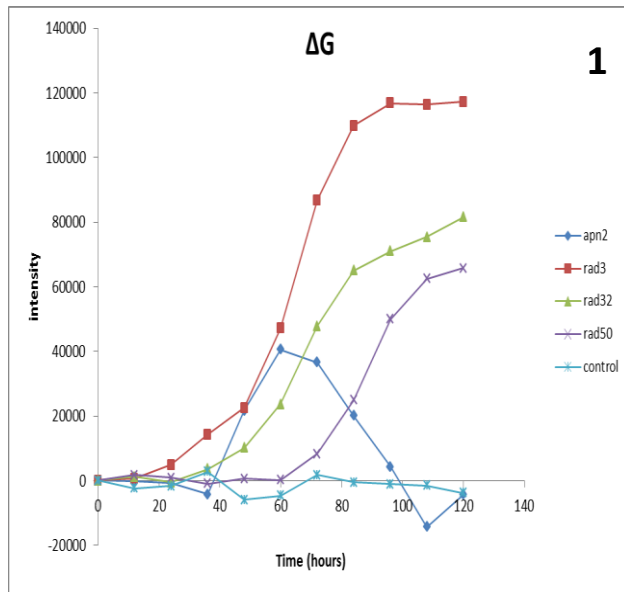


Figure 4-4C Ranking of mutants by the total area under curves at 150nM of GemC.

The ranking table shows a high sensitivity of *rad3* mutant in agreement with the graph (red curve) and the plates. On plate, *rad32* showed less growth in presence of the drug compared to *rad3*, however the growth was also reduced on plate without the drug. Y axis, on the graph, represents intensity values as measured by ImageJ (arbitrary unit) and X represents time (hours). Total areas in table are sums of raw intensity values.

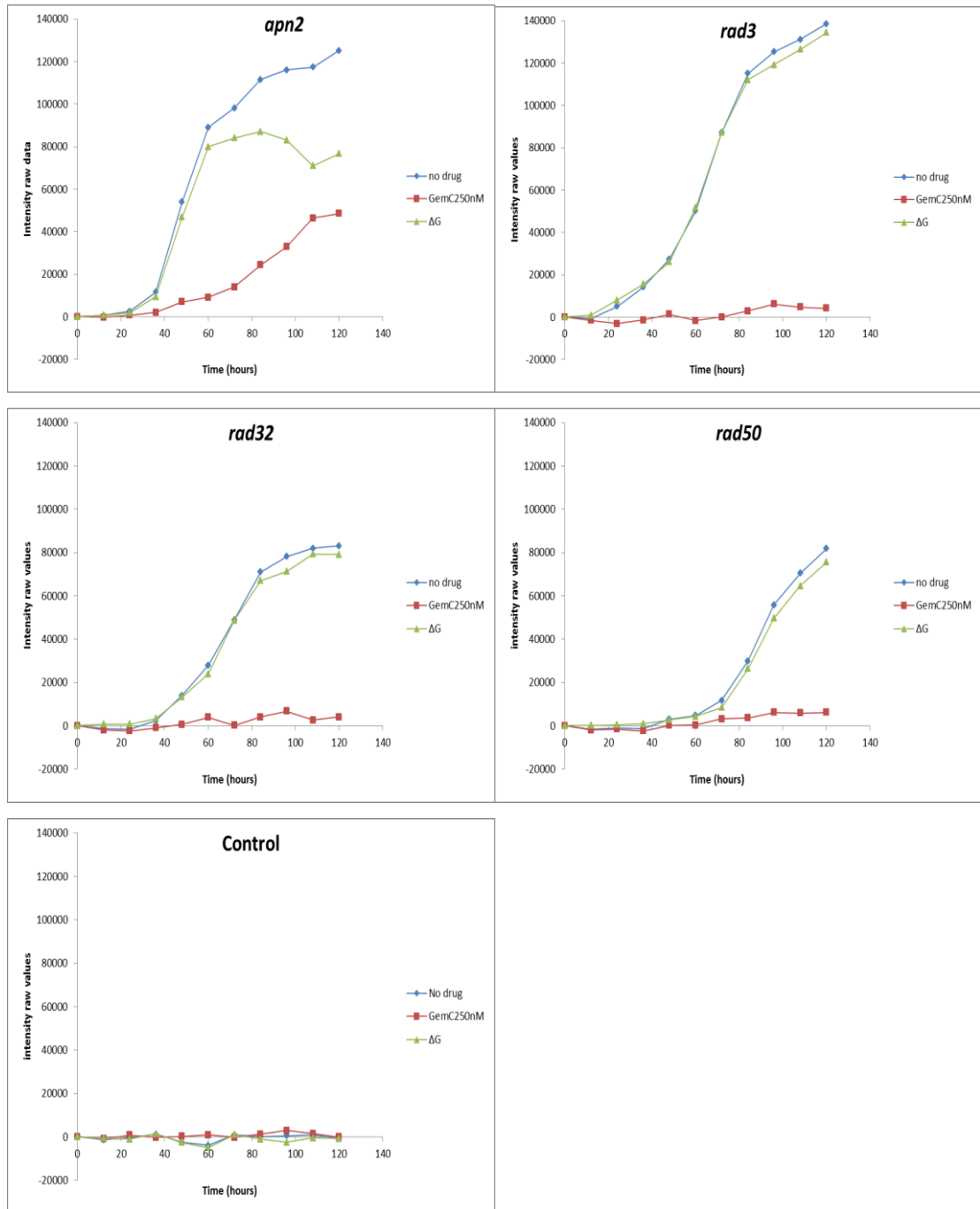
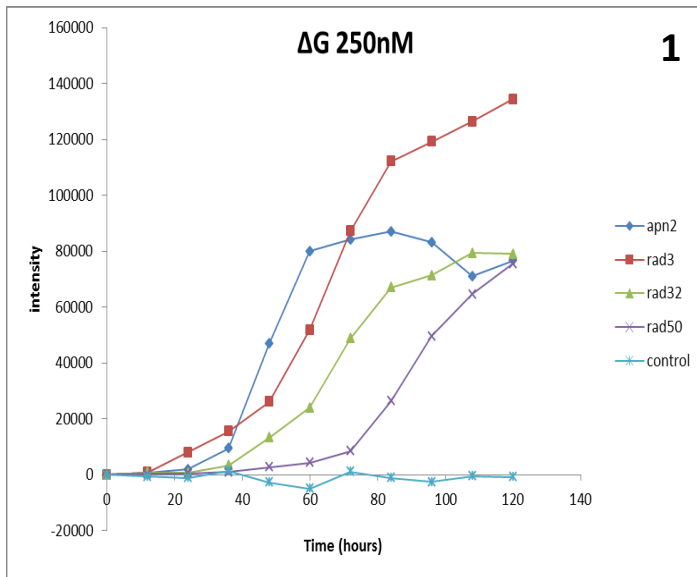


Figure 4-4D. Sensitivity of mutants at 250nM. *rad32* and *rad50* mutants showed high sensitivity to the drug (red curves) when compared to *apn2*. The control (empty well) showed no growth. The growth was determined over 5 day incubation at 30°C. Y axis represents intensity values as measured by ImageJ (arbitrary unit) and X represents time (hours). Values at time 0 were subtracted. Green curves represent differences in growth curves (untreated-treated) and blue curves represent growth of untreated cells.



2

gene	total area	rank
rad3	7373784	1
apn2	6033108	2
rad32	4178802	3
rad50	2348544	4
empty	-135612	control

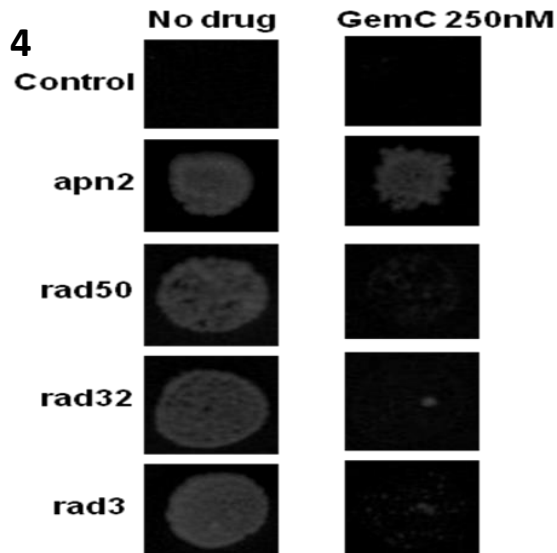
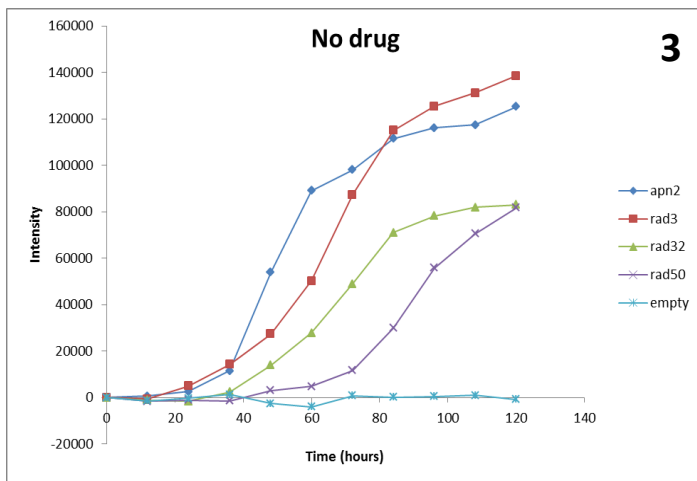
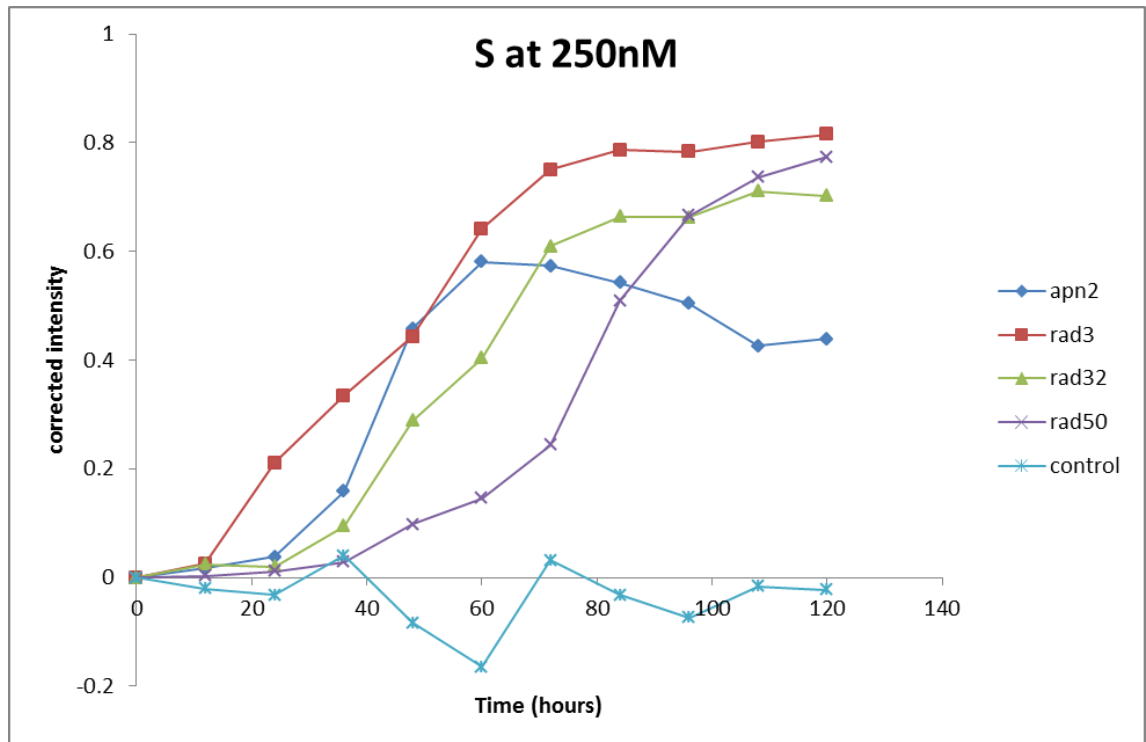


Figure 4-4E. Ranking at 250nM is biased by slow growth phenotype. Y axis on graphs represents intensity values as measured by ImageJ (arbitrary unit) and X represents time (hours). *apn2Δ* mutant was ranked higher than *rad32Δ* and *rad50Δ* mutants whereas on plates the MRN mutants showed a clearly higher sensitivity. The differences in growth in absence of drug are shown in graph “No drug” and show a clear slow growth of the MRN mutants (green and purple curves) compared to *apn2* (blue curve) and *rad3* (red curve).

To minimise the effect of slow growth in untreated cells, I expressed the sensitivity (S) as relative growth defect. S was calculated by the following formula: $S = \Delta G / G_u$ where $\Delta G =$ growth in untreated cells (G_u) – growth in treated cells (G_t). The ranking by corrected values (Figure 4-4F), correlated more to expected observation on plates and, at 250nM *apn2* mutants were ranked lower than MRN mutants. The corrections however slightly altered ranks for the low concentration and suggested that *rad3* is less sensitive than *rad32*. The difference in values, however, is very small (0.007) and is not likely to be significant. The three highly sensitive mutants of the set (*rad3*, *rad32* and *rad50*) remained ranked higher compared to the less sensitive, *apn2* mutant, but a clear distinction of the sensitive mutants was not possible, as values were very close.

Overall, the ranking method by calculation of areas under growth curves allowed a fair classification of mutants which was in accordance with observations on plates and can be used as an approximate ranking of mutants. The measurement of the total areas under growth curves allows to quantify the general sensitivity as it takes in account all the three parameters of a growth curve: (1) a lag phase which might be due to adaptation of the cells to the media or a low number of cells, (2) the growth rate (R value, growth at exponential phase) which is indicative of cell division, and (3) growth at stationary phase (K value) which is indicative of the ability of cells to compete for nutrients present in the media. However, this method only determines the overall growth but it does not differentiate the different parameters that characterise cell sensitivity. The use of the method hence gives an approximate ranking of mutants based on the general sensitivity.



	250nM		150nM	
gene	S($\Delta G/G_u$)	rank	S($\Delta G/G_u$)	rank
empty	2.354	control	3.101	control
rad3	0.984	1	0.925	2
rad32	0.959	2	0.932	1
rad50	0.921	3	0.853	3
apn2	0.758	4	0.153	4

Figure 4-4F. Ranking mutants by relative growth defect, $S = \Delta G/G_u$. Sensitivity of *apn2* mutants were ranked lower than MRN mutants as shown on plates. Values of the highly sensitive mutants are very close. The graph also shows a higher sensitivity of MRN mutants at 250nM (green and purple curves) when compared to *apn2* (bleu curve). S values were calculated using total area values.

4.2.2 Method 2: ranking by growth rate (R value)

The second method I tested was the ranking of mutants by slopes of the growth curves during logarithmic growth as an indicator for growth rates (R values). The steepest slope suggests a higher growth rate. To correct the effect of slow growth phenotype, the sensitivities (S) were expressed as relative values [$S = \Delta R/R_u = (R_{\text{untreated}} - R_{\text{treated}})/R_{\text{untreated}}$]. Slopes were calculated by the general rule “ $(y_2 - y_1)/(x_2 - x_1)$ ” for determination of a slope between two points on a growth curve (Illustrated in *Figure 4-5*). Due to the slow growth phenotype of some mutants (either in untreated cells, such as MRN mutants or possible slow growth phenotype after GemC treatment), growth curves were different for each mutant and the exponential phase occurred at different time point for individual mutants (e.g. the exponential phase for *apn2* occurs around 40 minutes while for *rad32* it occurs around 60 minutes, *Figure 4-5*). We could hence not use single time points to determine R values for all mutants. We determined R values for each time point and used the average of the three highest values as an indication of the growth rate. S values were then determined for each mutant and the highest S value was given the lowest number in ranking and suggested that the mutant was most sensitive. *Figure 4-5B-F* show calculations of R and S values for the 4 tested mutants. R values correlated with growth curves as high R values were determined for untreated cells which showed better growth (blue curves). In addition R values were also in correlation with sensitivity of mutants to the drug as smaller R values were determined for the high concentration (250nM). The *Table 4-2* shows S values and ranking of the 4 mutants for both 150 and 250nM. At the low concentration, S values were comparable for the three highly sensitive mutants (with a difference of 0.01) and suggested that at 150nM, the differences in sensitivities of mutants are only mild. At the higher concentration, sensitivity of mutants was more distinguishable with *rad3* classified as the most sensitive and *apn2* as the least sensitive, as already observed. Values of the most sensitive mutants are however very close and suggest only a subtle difference in sensitivities.

Quantification of growth rate is a precise method and can give a defined ranking of the mutants based on their ability to divide. However, drug concentrations that were used for the analysis are too high and don't allow a precise determination of R as sensitive mutants have flat curves.

Additionally, the analysis required a lot of data in order for the slopes to be precisely calculated. As illustrated in *Figure 4-5F*, showing $S (\Delta R/R_u)$ values for the control (empty well), relative R values were highly different between the drugs (-0.399 for 50nM, -0.020 for 150nM and 0.383 for 250nM) while the curves show no growth for the three concentrations. These differences are probably due to small artificial “bumps” in the curves due to random fluctuations in handling the samples (scanning, image analysis or both). Use of several time points for calculation of R values could correct for this bias and accurately detect the exponential phase for each mutant. With the data set that I have collected, I could only use an average of three time-points as above three points the curves reached the stationary phase. However collection of data at multiple time points (for example every four hours instead of every twelve hours) could allow to accurately determine R values, which in turn allows a precise distinction of growth and a precise ranking of mutants.

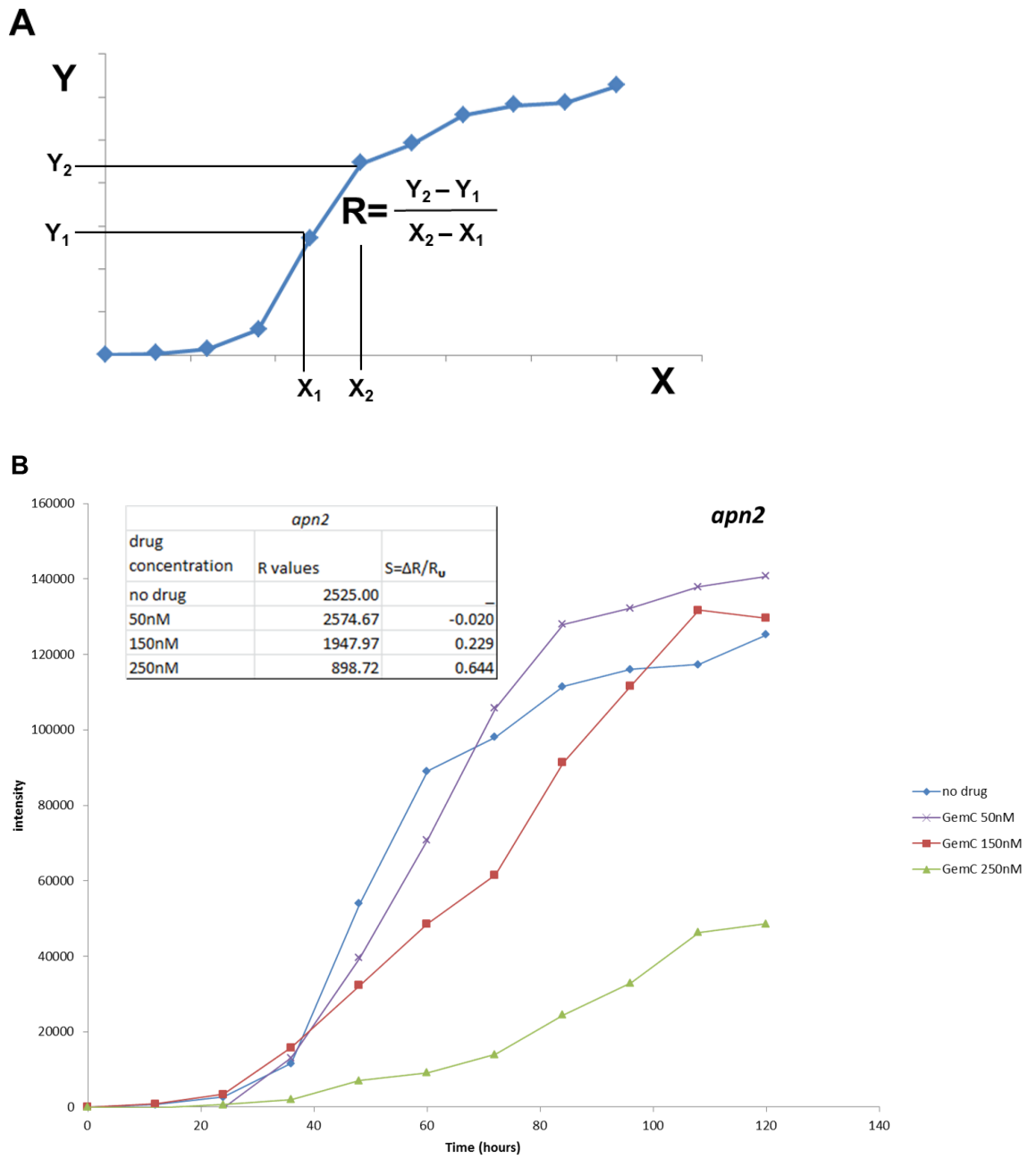


Figure 4-5 Determining R values for the different mutants. (A) Illustration of the general rule for calculation of R values. **(B)** R values for *apn2* correlated with the growth tendency.

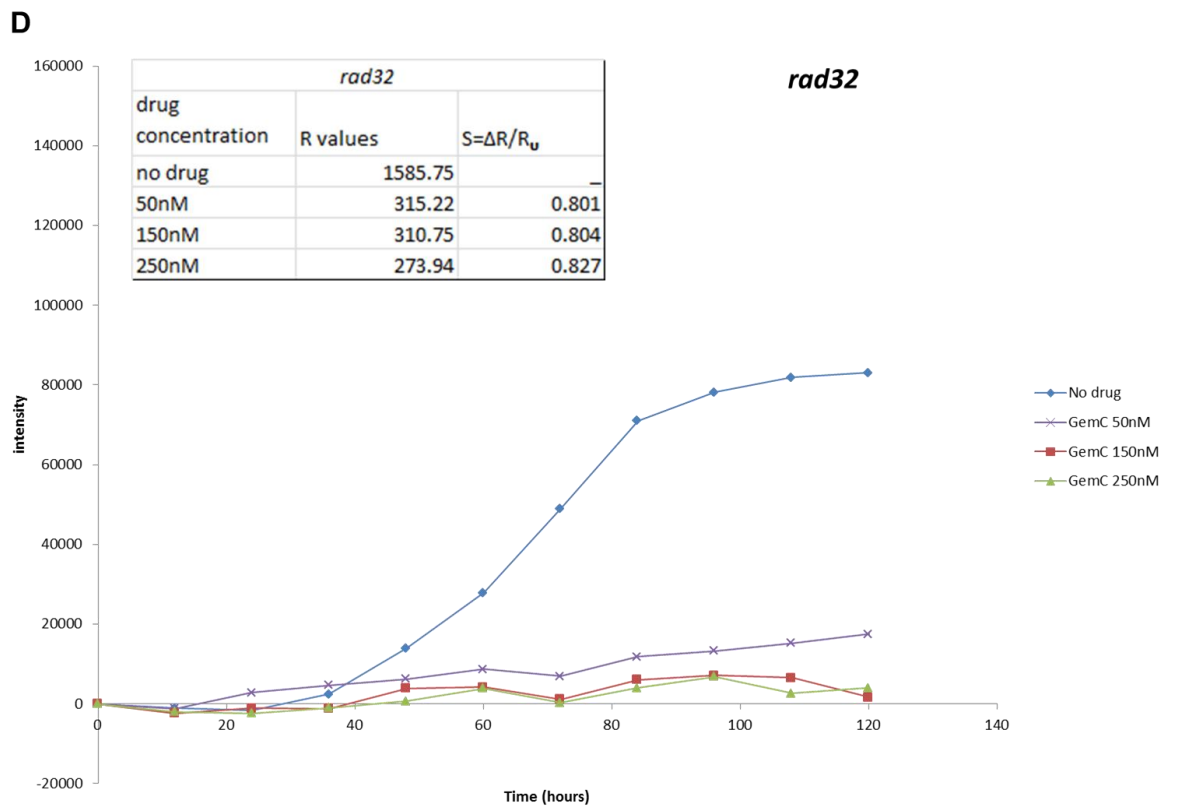
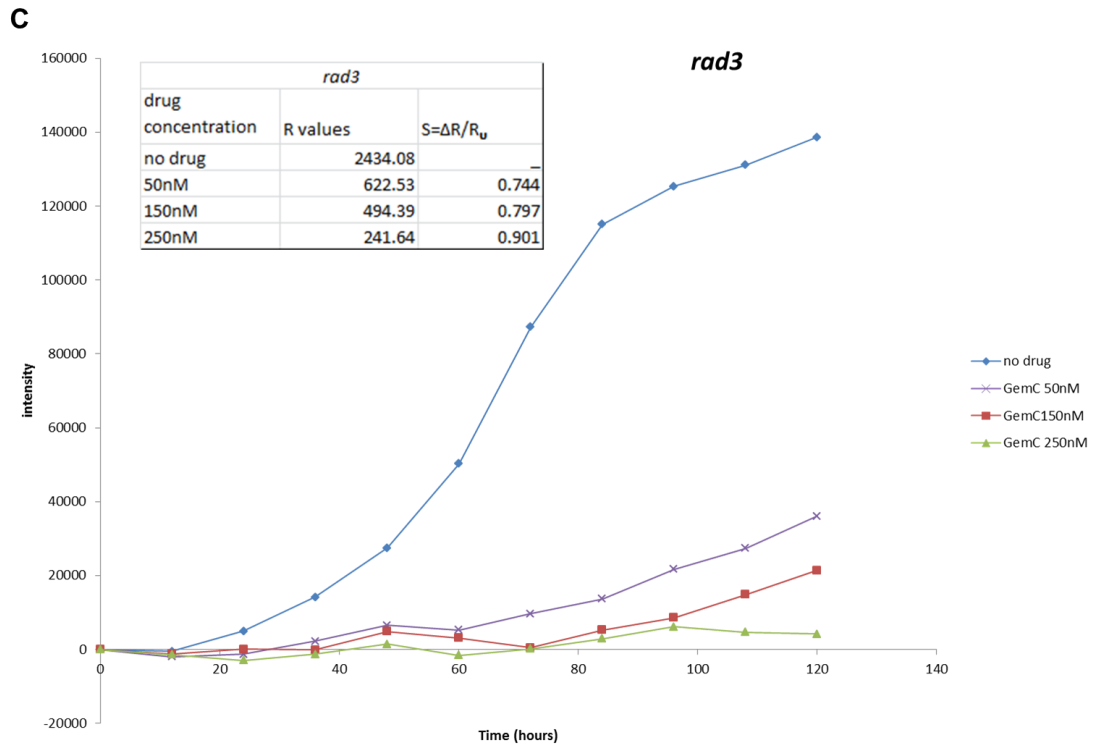


Figure 4-5 (continued). Determining R values for *rad3* (C) and *rad32* (D)

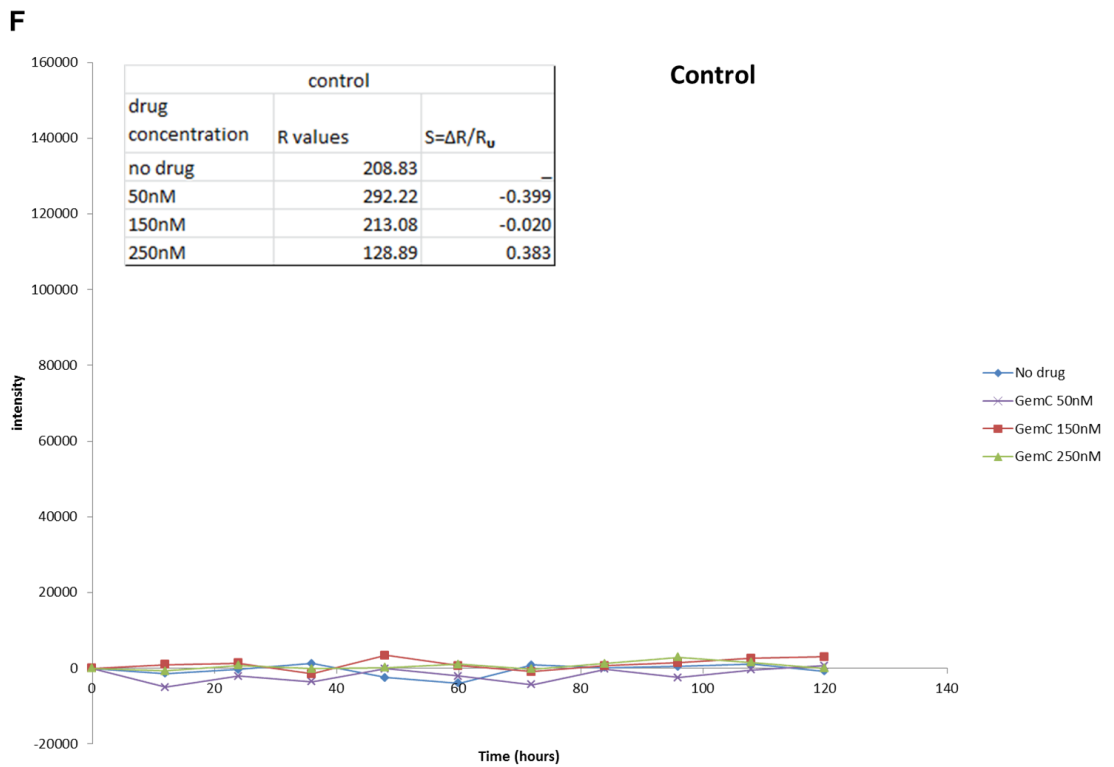
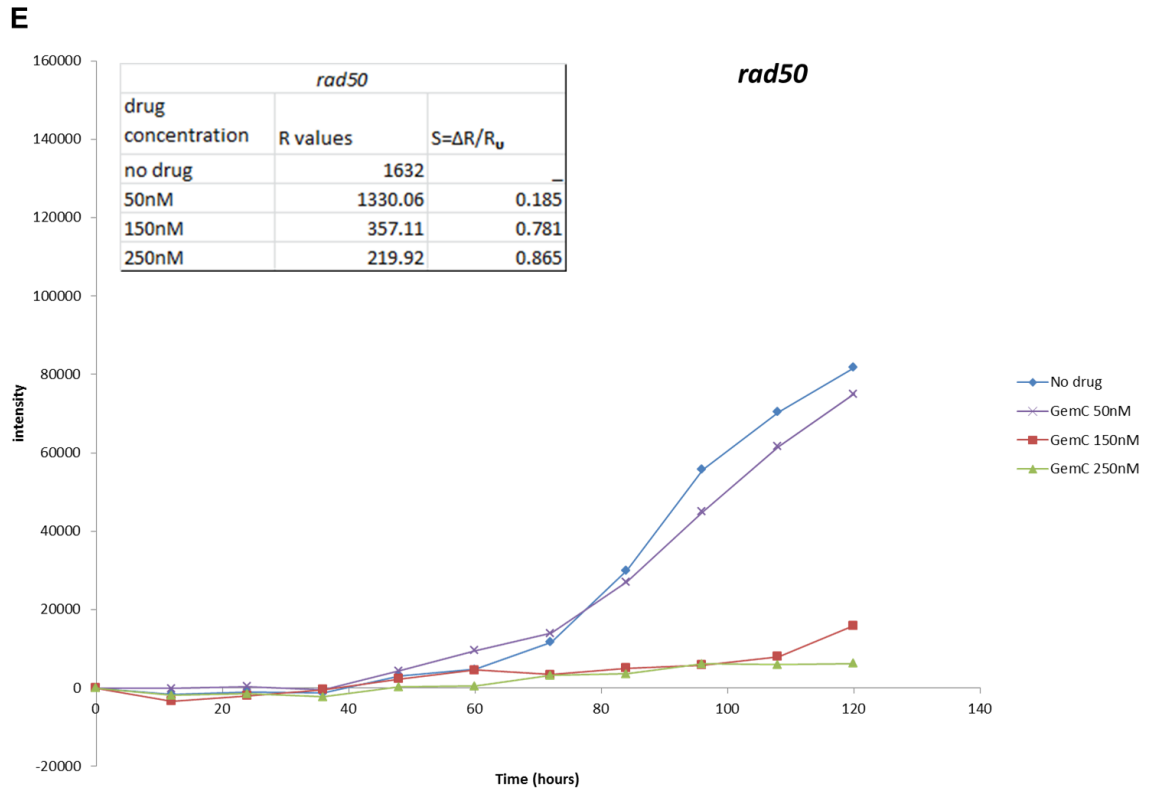


Figure 4-5(continued). Determining R values for *rad50* (E) and control (empty well) (F)

Table 4-2 Ranking mutants by growth rate values. The highly sensitive mutants, *rad3*, *rad32* and *rad50* show a high relative growth rate when compared to the less sensitive *apn2* mutant. At 150nM, relative values are very similar for the highly sensitive mutants. At 250nM, the ranking is altered between *rad32* and *rad50* mutants but the values are very close.

gene	50nM		150nM		250nM	
	S ($\Delta R/R_u$)	rank	S ($\Delta R/R_u$)	rank	S ($\Delta R/R_u$)	rank
<i>rad32</i>	0.801	1	0.804	1	0.827	3
<i>rad3</i>	0.744	2	0.797	2	0.901	1
<i>rad50</i>	0.185	3	0.781	3	0.865	2
<i>apn2</i>	-0.020	4	0.229	4	0.644	4
empty	-0.399	control	-0.02	control	0.383	control

4.2.3 Method 3: ranking mutants by final growth (K value)

The third method I tested was ranking mutants using spot intensity measured after 5 days incubation. We considered that as mutants compete for nutrients in the media, growth at the stationary phase is indicative of growth rate of the different mutants and the final measurements would reflect growth of strains. Measurement of growth after 5 days incubation, hence gives a good indication of the sensitivity as sensitive mutants (no growth) would give low values, while resistant mutants give high values. At 150nM the differences in growth [$\Delta G = G_{\text{untreated}} (G_u) - G_{\text{treated}} (G_t)$] correlated the sensitivity observed on plates: *apn2* was the least sensitive of the tested mutants, whereas *rad3* was the most sensitive (Table 4-3) but at 250nM, *apn2* was classified higher than *rad50* in values. At this high concentration, however, the mutants are highly sensitive and the differences might not be significant. To avert bias linked to slow growth, sensitivity (S) of mutants was determined by dividing ΔG by growth in untreated cells (G_u), ($S = \Delta G / G_u$). At the high concentration, ranks showed a correlation with the observation on plates but the ranking was altered at 150nM with *rad3* classified less sensitive than *rad32*. The differences in values, however were minor (0.02) and can be considered not significant as both mutants remain highly ranked. The measurement of density at the endpoint can reflect either a lower K value (growth at stationary phase), which can indicate differences in utilisation of nutrients resources (after 5 days incubation) or a lower growth rate, which leads to a lower end value. This method can hence be used as a gross classification of the mutants as it does not allow a distinction of the two parameters.

Table 4-3 Ranking mutants by endpoint. Values in table one are measurements of intensity by ImageJ (arbitrary values). At 150nM, mutants were ranked in accordance with previously observed results but the order was altered at 250nM. Values corrected by dividing the difference in growth by the growth in untreated cells ($S=\Delta G/G_u$) gave a ranking that correlated with observations on plates for both drugs (table 2).

150nM			250nM		
gene	ΔG 120h	rank	gene	ΔG 120h	rank
<i>rad3</i>	112975	1	<i>rad3</i>	132880	1
<i>rad32</i>	79068	2	<i>rad32</i>	77688	2
<i>rad50</i>	61760	3	<i>apn2</i>	76860	3
<i>apn2</i>	-3102	4	<i>rad50</i>	71879	4
empty	-3311	control	empty	295	control

S values at 120h					
150nM			250nM		
gene	$S=\Delta G/G_u$	rank	gene	$S=\Delta G/G_u$	rank
<i>rad32</i>	0.673	1	<i>rad3</i>	0.769	1
<i>rad3</i>	0.654	2	<i>rad32</i>	0.662	2
<i>rad50</i>	0.556	3	<i>rad50</i>	0.648	3
<i>apn2</i>	-0.018	4	<i>apn2</i>	0.444	4
empty	-0.102	control	empty	0.009	control

The most precise, ranking by slopes method, could not be used as GemC concentrations were too high and the required data collection was laborious at this stage of my project and could not be achieved. In fact as plates were manually scanned, a twelve hours interval was the minimal interval I could carry out therefore I could not collect sufficient data to accurately determine R values. The two remaining methods allow an approximate ranking and I have chosen to use the ranking by areas under growth curves method as it uses more measurements and takes in account all the growth parameters (lag phase, K and R values) that affect the overall growth. In comparison, the measurement of density at the end point only gives an indication of the growth at the stationary phase. Combined with the three selected concentrations, the ranking by area under growth curves method gives a good ranking of mutants that can be used as a pre-selection for mutants of interest which would be further analysed.

4.3 Sub library analysis: Ranking mutants

As a primary ranking of mutants, I used calculation of areas under growth curves to quantify sensitivity of different sub-library mutants to different concentrations of GemC. S ($\Delta G/G_u$) values were calculated in three independent experiments and the mean values were used for the classification. Mutants were then ranked according to their mean S values. The highest S value was given the lowest number in the ranks and was classified as most sensitive. Table 4-4 summarises mutants ranked according to their sensitivity at 50nM. Raw intensity values for 50nM and ranks for 150nM and 250nM are also given for information. As there was no WT strain in the library, I have used *rec12* Δ as a control for the ranking of mutants as the meiotic protein Rec12 (Cervantes *et al.*, 2000) would not be expected to affect cellular response to GemC. The ranking of *rec12* Δ however is hypothetical and is only used as indicative for WT sensitivity as I did not separately confirm that *rec12* Δ mutants are indeed resistant to GemC. The average (calculated on 15 values) rank for *rec12* was 347 (0.077 ± 0.167) for 50nM, 427 (0.178 ± 0.096) for 150nM and 400 (0.409 ± 0.073) for 250nM. Mutants that are ranked below 347 can hence *a priori* be considered as resistant to GemC.

As shown in Table 4-4, several checkpoint mutants were identified amongst the highly sensitive mutants strongly suggesting a role of the mechanism in response to GemC. Identified checkpoint mutants include: *hus1* (6), *rad26* (7), *rad17* (8), *rad1* (9), *rad3* (22), *mrc1* (25), *cds1* (35), *rad26* (66), *crb2* (*rhp9*, 184), *wee1* (329) and the replication

fork protection gene *swi3* (71). Consistent with the next chapter on analysis of DNA repair specific mutants, DNA repair mutants were also identified amongst the highly sensitive mutants emphasizing the role of the machinery in survival to NAs. These include MRN complex components *rad50* (110), *rad32* (synonym: *mre11*, 39) and *nbs1* (75), DNA repair proteins *mus7* (synonym: *mms22*, 106), *ung1* (72), *rhp54* (172), *srs2* (288) and *pnk1* (318). 20 sequence orphan genes were also isolated in the screen and will be further discussed. The numbers in brackets indicate ranking position out of 456 sensitive mutants at 50nM of GemC.

Table 4-4. List of mutants ranked by sensitivity to 50nM of GemC. Mutants were classified using their S values (details in text). Mean values and standard deviations (stDev) were calculated on three independent screens. Raw intensity values (average of three independent screens) for 50nM and untreated cells are also given. Ranking at 150M and 250nM are given at the end of the table for comparison. Sequence orphan are highlighted in yellow.

Gene ID	Gene name	Synonym	Gene description	total area no drug	50nM			150nM	250nM	
					total area GemC	mean $\Delta G/G$	stDev	rank	rank	rank
SPAC26A3.04	rpl2002	rpl20,rpl20-2	60S ribosomal protein L20 (predicted)	1.46E+06	8.85E+05	4.691	7.241	1	2	456
SPAC16C9.06c	upf1		ATP-dependent RNA helicase Upf1	5.27E+06	4.45E+06	3.282	5.314	2	278	438
SPAC3A11.09	sod22		plasma membrane alkali metal cation/H+ antiporter Sod22	5.36E+06	6.15E+06	2.838	5.037	3	450	449
SPBCPT2R1.08c	tlh2		RecQ type DNA helicase Tlh1	1.33E+06	5.47E+05	1.028	0.839	4	3	442
SPBC2G2.03c	sbh1		translocon beta subunit Sbh1 (predicted)	6.30E+06	3.18E+06	0.920	0.766	5	4	70
SPAC20G4.04c	hus1		checkpoint clamp complex protein Hus1	5.41E+06	9.05E+05	0.864	0.088	6	5	9
SPAC9E9.08	rad26		ATRIP, ATR checkpoint kinase regulatory subunit Rad26	4.55E+06	7.26E+05	0.818	0.178	7	9	7
SPAC14C4.13	rad17		RFC related checkpoint protein Rad17	5.63E+06	1.09E+06	0.799	0.110	8	6	10
SPAC1952.07	rad1		checkpoint clamp complex protein Rad1	9.38E+06	2.00E+06	0.788	0.100	9	11	12
SPAC22F3.09c	res2	mcs1,pct1	MBF transcription factor complex subunit Res2	6.98E+06	1.87E+06	0.735	0.131	10	18	26
SPBC36.04	cys11	cys1a	cysteine synthase	3.23E+06	8.40E+05	0.735	0.313	11	14	19
SPAC6B12.05c	ies2		Ino80 complex subunit Ies2	5.63E+06	1.53E+06	0.725	0.220	12	22	45
SPAC664.02c	arp8		actin-like protein, Ino80 complex subunit Arp8	8.56E+06	2.38E+06	0.720	0.084	13	19	39
SPAC8C9.07			rRNA processing protein Fyv7 (predicted)	1.81E+06	1.22E+06	0.717	0.951	14	13	15
SPAC2G11.06	vps4		AAA family ATPase Vps4 (predicted)	4.63E+06	1.34E+06	0.708	0.099	15	32	22
SPBC29A10.10c			tRNA-splicing endonuclease positive effector (predicted)	7.94E+06	2.89E+06	0.665	0.273	16	28	27
SPBC3H7.07c	ser2		phosphoserine phosphatase Ser2 (predicted)	2.01E+06	7.01E+05	0.662	0.223	17	17	93

Gene ID	Gene name	Synonym	Gene description	total area no drug	50nM				150nM	250nM
					total area GemC	mean $\Delta G/G$	stDev	rank	rank	rank
SPAC4H3.02c	swc3		Swr1 complex subunit Swc3	5.45E+06	2.21E+06	0.641	0.254	18	49	55
SPCC895.07	alp14	mtc1	TOG ortholog Alp14	5.36E+06	1.71E+06	0.632	0.317	19	12	18
SPAC6B12.08	mug185		Co-chaperone for ATPase activity (predicted)	8.95E+06	3.37E+06	0.621	0.130	20	26	29
SPCC576.12c	mhf2		FANCM-MHF complex subunit Mhf2	7.32E+06	2.90E+06	0.619	0.289	21	46	68
SPBC216.05	rad3		ATR checkpoint kinase Rad3	6.73E+06	2.06E+06	0.611	0.291	22	10	11
SPCC736.11	ago1	csp9	argonaute	3.20E+06	1.26E+06	0.605	0.378	23	127	80
SPCC4B3.08	lsg1		Lsk1 complex gamma subunit (predicted)	6.55E+06	3.85E+06	0.588	0.391	24	41	59
SPAC694.06c	mrc1		mediator of replication checkpoint 1	6.00E+06	2.52E+06	0.584	0.094	25	16	16
SPBC20F10.05	nrl1		NRDE-2 family protein (predicted)	7.02E+06	3.32E+06	0.583	0.281	26	80	85
SPAC4F8.03	sdo1	SPAC644.01c	SBDS family ribosome maturation protein Sdo1 (predicted)	3.50E+06	1.46E+06	0.577	0.137	27	102	276
SPBC19C7.05			cell wall organization protein (predicted)	7.37E+06	5.10E+06	0.569	0.476	28	110	202
SPAC30.02c			elongator complex associated protein Kti2 (predicted)	5.45E+06	2.43E+06	0.564	0.149	29	66	75
SPBC1778.01c	zuo1	mpp11,SPBC30 D10.01	zuotin (predicted)	4.49E+06	2.01E+06	0.559	0.143	30	36	21
SPBC365.10	arp5		actin-like protein Arp5	2.34E+06	1.04E+06	0.547	0.211	31	93	341
SPBC21H7.04	dbp7		ATP-dependent RNA helicase Dbp7 (predicted)	1.83E+06	1.09E+06	0.536	0.564	32	310	315
SPAC30D11.10	rad22	rad22A,rad22	DNA recombination protein Rad22	6.62E+06	3.26E+06	0.536	0.416	33	119	97
SPBC19C7.02	ubr1	SPBC32F12.14	N-end-recognizing protein Ubr1	6.88E+06	3.13E+06	0.530	0.349	34	47	35
SPCC18B5.11c	cds1		replication checkpoint kinase Cds1	7.39E+06	3.44E+06	0.528	0.171	35	38	50
SPAC17A5.08			COPII-coated vesicle component Erp2/3/4 (predicted)	9.89E+06	4.70E+06	0.525	0.027	36	96	96
SPBC31F10.13c	hip1	hir1	hira protein, histone chaperone Hip1	2.80E+06	9.94E+05	0.518	0.288	37	63	6
SPBC83.02c	rpl4302	rpl43-2,rpl43,rpl37a-2	60S ribosomal protein L37a (predicted)	7.34E+06	3.54E+06	0.517	0.140	38	151	224
SPAC13C5.07	mre11	rad32	Rad32 nuclease	6.25E+06	3.21E+06	0.513	0.261	39	48	46

Gene ID	Gene name	Synonym	Gene description	total area no drug	50nM			150nM	250nM	
					total area GemC	mean $\Delta G/G$	stDev	rank	rank	
SPCC736.06			mitochondrial aspartate-tRNA ligase (predicted)	4.40E+06	2.60E+06	0.511	0.419	40	15	14
SPCC16C4.10			6-phosphogluconolactonase (predicted)	7.22E+06	3.42E+06	0.510	0.231	41	31	37
SPAC1556.05c	cgr1		ribosome biogenesis CGR1 family (predicted)	5.11E+06	2.54E+06	0.506	0.166	42	79	124
SPCC4B3.15	mid1	dmf1	medial ring protein Mid1	5.11E+06	2.52E+06	0.505	0.023	43	95	136
SPCC18.06c	caf1	pop2	CCR4-Not complex CAF1 family ribonuclease subunit Caf1	6.47E+06	3.45E+06	0.504	0.231	44	160	217
SPAC27D7.14c	tpr1	SPAC637.02c	RNA polymerase II associated Paf1 complex subunit Tpr1	3.72E+06	1.80E+06	0.504	0.328	45	29	64
SPAC1071.02	mms19		TFIIH regulator Mms19	7.71E+06	3.61E+06	0.501	0.175	46	24	44
SPCC663.04	rpl39		60S ribosomal protein L39	3.18E+06	1.65E+06	0.501	0.155	47	368	433
SPAC1952.09c			acetyl-CoA hydrolase (predicted)	1.46E+06	4.15E+05	0.496	0.265	48	1	1
SPAC806.07	ndk1		nucleoside diphosphate kinase Ndk1	8.17E+06	4.29E+06	0.493	0.197	49	56	38
SPCC11E10.06c	elp4		elongator complex subunit Elp4 (predicted)	7.22E+06	3.70E+06	0.485	0.157	50	68	113
SPBC365.03c	rpl2101	rpl21,rpl21-1	60S ribosomal protein L21 (predicted)	4.81E+06	4.04E+06	0.473	0.544	51	434	2
SPCC1739.14	npp106		nucleoporin Npp106	7.60E+06	3.90E+06	0.473	0.141	52	109	101
SPBC27B12.08	sip1		Pof6 interacting protein Sip1, predicted AP-1 accessory protein	7.66E+06	3.94E+06	0.469	0.326	53	159	326
SPBC776.17			rRNA processing protein Rrp7 (predicted)	3.83E+06	1.74E+06	0.468	0.402	54	116	130
SPAC11G7.04	ubi1		ribosomal-ubiquitin fusion protein Ubi1 (predicted)	4.50E+06	3.00E+06	0.466	0.221	55	40	49
SPAC222.04c	ies6		Ino80 complex subunit Ies6	2.88E+06	1.66E+06	0.464	0.144	56	61	82
SPAC8C9.12c			mitochondrial iron ion transporter (predicted)	8.64E+06	4.70E+06	0.460	0.163	57	57	63
SPAC22F8.12c	shf1		small histone ubiquitination factor Shf1	6.55E+06	3.59E+06	0.460	0.072	58	52	83
SPAC11E3.08c	nse6		Smc5-6 complex non-SMC subunit Nse6	1.79E+06	1.05E+06	0.460	0.288	59	30	30
SPAC3H5.08c			WD repeat protein, human WDR44 family	7.39E+06	3.90E+06	0.459	0.233	60	336	309
SPCC11E10.08	rik1		silencing protein Rik1	6.29E+06	3.39E+06	0.457	0.136	61	85	71

Gene ID	Gene name	Synonym	Gene description	total area no drug	50nM				150nM	250nM
					total area GemC	mean ΔG/G	stDev	rank	rank	rank
SPBC19G7.16	iws1		transcription elongation factor complex subunit Iws1 (predicted)	3.55E+06	2.78E+06	0.457	0.455	62	117	5
SPBC337.16	cho1		phosphatidyl-N-methylethanolamine N-methyltransferase (predicted)	3.22E+06	1.67E+06	0.446	0.266	63	42	34
SPBC1A4.04			sequence orphan	3.08E+06	1.74E+06	0.444	0.059	64	60	117
SPBC4B4.03	rsc1		RSC complex subunit Rsc1	6.45E+06	3.42E+06	0.441	0.234	65	50	53
SPAC664.07c	rad9		checkpoint clamp complex protein Rad9	6.11E+06	2.86E+06	0.436	0.365	66	87	69
SPCC23B6.05c	ssb3	rpa3	DNA replication factor A subunit Ssb3	4.91E+06	2.72E+06	0.432	0.226	67	34	47
SPBPJ4664.06	gpt1		UDP-glucose-glycoprotein glucosyltransferase Gpt1	7.48E+06	4.20E+06	0.429	0.248	68	186	199
SPCC594.05c	spf1	spp1	Set1C PHD Finger protein Spf1	6.63E+06	3.78E+06	0.428	0.114	69	53	74
SPBC29A3.05	vps71		Swr1 complex subunit Vps71	8.84E+06	5.07E+06	0.426	0.091	70	73	90
SPBC30D10.04	swi3		replication fork protection complex subunit Swi3	7.09E+06	4.09E+06	0.424	0.141	71	67	56
SPCC1183.06	ung1		uracil DNA N-glycosylase Ung1	1.03E+07	5.98E+06	0.420	0.156	72	161	91
SPAC23G3.04	ies4		Ino80 complex subunit Ies4	9.77E+06	5.66E+06	0.419	0.036	73	58	54
SPAC13G7.12c			choline kinase (predicted)	6.52E+06	3.90E+06	0.419	0.323	74	123	186
SPBC6B1.09c	nbs1	slr10	Mre11 complex subunit Nbs1	9.37E+06	5.47E+06	0.418	0.213	75	171	207
SPAC1556.08c	cbs2	SPAC1F12.01c	protein kinase activator (predicted)	8.57E+06	4.87E+06	0.418	0.074	76	59	109
SPCC11E10.07c			translation initiation factor eIF2B alpha subunit (predicted)	9.76E+06	5.66E+06	0.409	0.182	77	182	225
SPAC1250.03	ubc14		ubiquitin conjugating enzyme Ubc14 (predicted)	8.77E+06	5.14E+06	0.408	0.187	78	104	139
SPCC338.16	pof3		F-box protein Pof3	1.65E+06	1.18E+06	0.399	0.364	79	21	13
SPCC18B5.09c			sequence orphan	7.28E+06	4.35E+06	0.398	0.180	80	82	165
SPCC1827.02c			cholinephosphate cytidyltransferase (predicted)	6.34E+06	3.73E+06	0.394	0.377	81	138	135
SPAC1071.11			NADH-dependent flavin oxidoreductase (predicted)	3.25E+06	2.32E+06	0.392	0.346	82	23	20
SPBC2F12.12c			human c19orf29 ortholog	7.31E+06	4.44E+06	0.392	0.139	83	74	100

Gene ID	Gene name	Synonym	Gene description	total area no drug	50nM			150nM	250nM	
					total area GemC	mean $\Delta G/G$	stDev	rank	rank	
SPBC31F10.09c	nut2	med10	mediator complex subunit Med10	5.57E+06	3.79E+06	0.387	0.245	84	103	115
SPBC800.04c	rpl4301	rpl43-1,rpl43,rpl37a-1	60S ribosomal protein L37a (predicted)	4.85E+06	3.02E+06	0.387	0.243	85	65	66
SPAC328.02			ubiquitin-protein ligase involved in sporulation	1.55E+06	9.79E+05	0.382	0.143	86	7	8
SPAC16A10.05c	dad1		DASH complex subunit Dad1	8.21E+06	5.00E+06	0.380	0.161	87	86	52
SPBC582.10c			ATP-dependent DNA helicase Rhp16b (predicted)	6.64E+06	4.17E+06	0.379	0.083	88	140	183
SPBC685.07c	rpl2701	rpl27-1	60S ribosomal protein L27	3.45E+06	2.24E+06	0.379	0.108	89	132	155
SPAC1805.04	nup132	Nup133b	nucleoporin Nup132	5.85E+06	4.05E+06	0.378	0.185	90	118	111
SPAC31G5.11	pac2		cAMP-independent regulatory protein Pac2	6.93E+06	4.33E+06	0.369	0.131	91	54	60
SPAC1142.07c	vps32	snf7	ESCRT III complex subunit Vps32	4.48E+06	2.75E+06	0.367	0.165	92	164	67
SPCC16C4.20c			Ino80 complex subunit (predicted)	9.10E+06	5.72E+06	0.367	0.069	93	72	61
SPAC3G6.01	hrp3		ATP-dependent DNA helicase Hrp3	4.40E+06	3.60E+06	0.366	0.381	94	44	48
SPAC1952.05	gcn5	kat2	SAGA complex histone acetyltransferase catalytic subunit Gcn5	5.38E+06	3.66E+06	0.364	0.158	95	121	214
SPAC23C11.02c	rps23		40S ribosomal protein S23 (predicted)	3.95E+06	2.54E+06	0.364	0.335	96	201	425
SPAC3A12.10	rpl2001	rpl20-1,rpl20,y117b,rpl18a-2	60S ribosomal protein L20a (predicted)	2.37E+06	1.56E+06	0.359	0.449	97	39	73
SPAC869.06c			HHE domain cation binding protein (predicted)	8.16E+06	5.22E+06	0.358	0.193	98	107	114
SPBC609.05	pob3		FACT complex component Pob3	6.66E+06	4.31E+06	0.356	0.110	99	62	57
SPAC1071.07c	rps1502	rps15-2,rps15	40S ribosomal protein S15 (predicted)	4.05E+06	2.48E+06	0.355	0.301	100	35	36
SPBC2G2.06c	apl1		AP-2 adaptor complex subunit Apl1 (predicted)	6.67E+06	4.44E+06	0.352	0.066	101	252	146
SPBC1861.07			elongin C (predicted)	5.93E+06	4.80E+06	0.351	0.304	102	179	240
SPAC17G8.13c	mst2		histone acetyltransferase Mst2	9.47E+06	5.97E+06	0.349	0.150	103	70	120
SPCC1393.08			transcription factor, zf-GATA type (predicted)	4.11E+06	2.69E+06	0.348	0.138	104	88	72
SPBC1D7.04	mlo3		RNA binding protein Mlo3	5.84E+06	3.85E+06	0.348	0.207	105	150	126

Gene ID	Gene name	Synonym	Gene description	total area no drug	50nM				150nM	250nM
					total area GemC	mean $\Delta G/G$	stDev	rank	rank	rank
SPAC6B12.02c	mus7	mms22	DNA repair protein Mus7/Mms22	4.39E+06	3.15E+06	0.346	0.384	106	71	110
SPBC3D6.02	but2		But2 family protein But2	7.52E+06	5.08E+06	0.344	0.177	107	236	159
SPBC12C2.04			NAD binding dehydrogenase family protein	6.49E+06	4.45E+06	0.342	0.155	108	83	65
SPAC6F12.03c	fsv1		SNARE Fsv1	6.69E+06	4.24E+06	0.341	0.312	109	125	198
SPAC1556.01c	rad50	SPAP4C9.01c	DNA repair protein Rad50	3.43E+06	2.18E+06	0.340	0.278	110	33	24
SPAC13G7.03	upf3		up-frameshift suppressor 3 family protein (predicted)	7.85E+06	5.06E+06	0.340	0.190	111	76	33
SPAC20G4.07c	sts1	erg4	C-24(28) sterol reductase Sts1	7.94E+06	5.04E+06	0.338	0.324	112	69	28
SPBC13G1.12	did2		ESCRT III complex subunit Did2 (predicted)	6.52E+06	4.77E+06	0.337	0.266	113	395	360
SPAC589.09			sec14 cytosolic factor family (predicted)	9.68E+06	6.35E+06	0.336	0.213	114	141	157
SPAPB18E9.01	trm5		tRNA (guanine) methyltransferase Trm5 (predicted)	4.97E+06	3.12E+06	0.335	0.276	115	37	51
SPCC576.13	swc5		Swr1 complex subunit Swc5	6.83E+06	4.65E+06	0.328	0.141	116	75	58
SPCC594.02c			conserved fungal protein	4.77E+06	3.56E+06	0.328	0.247	117	55	25
SPCPJ732.02c			xylulose kinase (predicted)	7.49E+06	5.03E+06	0.326	0.265	118	195	194
SPCC970.07c	raf2	dos2,cmc2,clr7	Rik1-associated factor Raf2	7.52E+06	4.83E+06	0.326	0.252	119	81	121
SPCC1682.16	rpt4		19S proteasome regulatory subunit Rpt4 (predicted)	8.68E+06	5.92E+06	0.323	0.250	120	210	272
SPAPJ698.02c	rps002	rpsa-2,rps0-2,rps0	40S ribosomal protein S0B	3.93E+06	2.69E+06	0.323	0.039	121	268	418
SPCC74.04			amino acid permease (predicted)	6.87E+06	4.79E+06	0.317	0.144	122	408	366
SPAC10F6.11c	atg17		autophagy associated protein kinase activator Atg17	6.56E+06	4.42E+06	0.317	0.121	123	319	252
SPAC17A2.13c	rad25		14-3-3 protein Rad25	5.83E+06	4.29E+06	0.315	0.274	124	143	99
SPAC6G10.06			FAD-dependent amino acid oxidase involved in late endosome to Golgi transport (predicted)	8.73E+06	5.91E+06	0.315	0.126	125	235	205
SPAC19D5.01	pyp2		tyrosine phosphatase Pyp2	7.24E+06	5.22E+06	0.315	0.186	126	149	127

Gene ID	Gene name	Synonym	Gene description	total area no drug	50nM			150nM	250nM	
					total area GemC	mean $\Delta G/G$	stDev	rank	rank	
SPBC13E7.09	vrp1		verprolin	7.86E+06	5.40E+06	0.314	0.054	127	106	86
SPAC23C4.11	atp18		F0-ATPase subunit J (predicted)	3.92E+06	2.70E+06	0.313	0.083	128	43	89
SPAC12G12.13c	cid14		poly(A) polymerase Cid14	2.83E+06	1.90E+06	0.313	0.095	129	51	134
SPCC962.04	rps1201	rps12-1,rps12	40S ribosomal protein S12 (predicted)	7.13E+06	4.93E+06	0.311	0.030	130	313	197
SPAC144.02	iec1		Ino80 complex subunit Iec1	7.38E+06	5.03E+06	0.310	0.115	131	78	84
SPAC1250.04c	atl1		alkyltransferase-like protein Atl1	8.61E+06	5.85E+06	0.310	0.095	132	124	143
SPBC713.05			WD repeat protein, human MAPK organizer 1 (MORG1) family (predicted)	8.75E+06	6.12E+06	0.309	0.151	133	131	79
SPAC17A5.07c	ulp2		SUMO deconjugating cysteine peptidase Ulp2 (predicted)	3.57E+06	2.55E+06	0.309	0.271	134	27	17
SPBC660.11	tcg1	mug187	single-stranded telomeric binding protein Tgc1	8.75E+06	5.99E+06	0.307	0.137	135	98	105
SPAC1B1.04c			poly(A)-specific ribonuclease complex subunit Pan3 (predicted)	8.62E+06	6.29E+06	0.300	0.169	136	238	129
SPAC31A2.15c	dcc1		Ctf18 RFC-like complex subunit Dcc1	5.71E+06	4.03E+06	0.300	0.111	137	139	145
SPBC21C3.13	rps1901	rps19-1	40S ribosomal protein S19 (predicted)	4.22E+06	3.06E+06	0.299	0.333	138	108	150
SPBP8B7.21	ubp3		ubiquitin C-terminal hydrolase Ubp3	7.19E+06	5.24E+06	0.298	0.119	139	115	62
SPAC23C11.08	php3		CCAAT-binding factor complex subunit Php3	7.95E+06	5.45E+06	0.298	0.145	140	99	106
SPBC1685.13	fhn1		Fhn1 plasma membrane organization protein	7.72E+06	5.55E+06	0.295	0.177	141	173	151
SPAC30C2.02	mmd1		deoxyhypusine hydroxylase (predicted)	5.65E+06	3.95E+06	0.294	0.086	142	20	31
SPCC1259.08			conserved fungal protein, DUF2457 family	6.97E+06	4.92E+06	0.294	0.050	143	97	40
SPAC1952.02	tma23		ribosome biogenesis protein Tma23 (predicted)	9.15E+06	6.56E+06	0.292	0.221	144	154	222
SPCC285.17	spp27	uaf30	RNA polymerase I upstream activation factor complex subunit Spp27	9.20E+06	6.50E+06	0.291	0.233	145	203	293
SPBC947.08c	hip4	hpc2	histone promoter control protein Hip4	5.18E+06	3.10E+06	0.288	0.714	146	273	292
SPAC144.06	apl5		AP-3 adaptor complex subunit Apl5 (predicted)	8.68E+06	6.17E+06	0.285	0.094	147	144	132
SPBC691.03c	apl3		AP-2 adaptor complex subunit Alp3 (predicted)	7.28E+06	5.18E+06	0.284	0.241	148	392	318
SPAC3C7.08c	elf1		AAA family ATPase Elf1	5.80E+06	4.68E+06	0.284	0.171	149	166	149

Gene ID	Gene name	Synonym	Gene description	total area no drug	50nM			150nM	250nM	
					total area GemC	mean $\Delta G/G$	stDev	rank	rank	
SPCC569.05c			spermidine family transporter (predicted)	8.72E+06	6.18E+06	0.282	0.103	150	311	349
SPBC31F10.16			ChAPs family protein (predicted)	1.03E+07	7.39E+06	0.281	0.138	151	241	253
SPAC13G7.07	arb2		argonaute binding protein 2	7.49E+06	5.56E+06	0.281	0.298	152	126	200
SPAC24B11.12c			P-type ATPase (predicted)	8.61E+06	6.22E+06	0.281	0.128	153	298	347
SPBC16C6.03c			ribosome assembly protein (predicted)	5.19E+06	4.12E+06	0.278	0.266	154	425	332
SPCC1906.04	wtf20		wtf element Wtf20	1.11E+07	7.85E+06	0.278	0.131	155	148	144
SPCC285.15c	rps2802	rps28-2,rps28	40S ribosomal protein S28, Rps2802	6.31E+06	4.47E+06	0.276	0.113	156	163	147
SPAC17A2.10c			sequence orphan	9.25E+06	6.70E+06	0.276	0.065	157	152	152
SPACUNK4.12c	mug138		metallopeptidase (predicted)	1.03E+07	7.39E+06	0.276	0.142	158	175	154
SPAC23H3.13c	gpa2	git8	heterotrimeric G protein alpha-2 subunit Gpa2	5.47E+06	3.89E+06	0.275	0.095	159	147	302
SPBC685.06	rps001	rps0-1,rpsa-1,rps0	40S ribosomal protein S0A (p40)	6.25E+06	4.44E+06	0.275	0.118	160	142	102
SPBC8D2.03c	hhf2	ams3,h4.2	histone H4 h4.2	9.32E+06	6.33E+06	0.274	0.199	161	196	103
SPCC794.03			amino acid permease (predicted)	8.93E+06	6.54E+06	0.274	0.066	162	254	180
SPBC1198.03c			Golgin subfamily A member	1.03E+07	7.39E+06	0.273	0.194	163	200	216
SPCC825.05c			splicing coactivator SRRM1 (predicted)	6.25E+06	4.65E+06	0.272	0.292	164	357	266
SPAC1071.09c			DNAJ domain protein, DNAJC9 family (predicted)	6.28E+06	4.89E+06	0.271	0.157	165	122	112
SPAC14C4.16	dad3		DASH complex subunit Dad3	1.07E+07	7.82E+06	0.266	0.110	166	130	118
SPAC8F11.02c	dph3		diphthamide biosynthesis protein Dph3 (predicted)	7.17E+06	5.30E+06	0.263	0.067	167	129	119
SPAP8A3.07c			phospho-2-dehydro-3-deoxyheptonate aldolase (predicted)	6.73E+06	5.00E+06	0.261	0.272	168	146	300
SPAC30D11.14c			RNA-binding protein (predicted)	7.03E+06	5.41E+06	0.261	0.348	169	211	228
SPBC28F2.11			HMG box protein	9.09E+06	6.75E+06	0.259	0.175	170	213	296
SPBC2A9.04c			sir antagonist ortholog (predicted)	8.65E+06	6.46E+06	0.257	0.017	171	114	189
SPAC15A10.03c	rhp54	rhp54	Rad54 homolog Rhp54	4.49E+06	3.25E+06	0.257	0.137	172	94	128

Gene ID	Gene name	Synonym	Gene description	total area no drug	50nM				150nM	250nM
					total area GemC	mean $\Delta G/G$	stDev	rank	rank	rank
SPAC17A5.10			conserved fungal protein	8.12E+06	6.09E+06	0.255	0.103	173	176	123
SPBC106.10	pka1	tpk.git6	cAMP-dependent protein kinase catalytic subunit Pka1	9.50E+06	7.08E+06	0.252	0.092	174	198	219
SPAC3G9.03	rpl2301	rpl23-1	60S ribosomal protein L23	8.07E+06	6.07E+06	0.250	0.149	175	385	363
SPCC16A11.16c	rpn1302	rpn13,rpn13b	19S proteasome regulatory subunit Rpn13b	7.41E+06	5.61E+06	0.250	0.110	176	128	116
SPBC119.08	pmk1	spm1	MAP kinase Pmk1	9.87E+06	7.39E+06	0.250	0.104	177	318	364
SPBC1683.09c	frp1		ferric-chelate reductase Frp1	6.93E+06	5.36E+06	0.249	0.212	178	216	301
SPCC594.06c			vacuolar SNARE Vam7 (predicted)	6.10E+06	5.22E+06	0.249	0.260	179	100	187
SPAC9E9.11	plr1	plr	pyridoxal reductase Plr1	9.44E+06	7.10E+06	0.247	0.121	180	231	288
SPAC20G8.08c	fft1		fun thirty related protein Fft1 (predicted)	8.29E+06	6.25E+06	0.245	0.037	181	233	185
SPBC19C2.14	smd3		Sm snRNP core protein Smd3	8.36E+06	6.25E+06	0.245	0.111	182	378	220
SPAC9.10	thi9		thiamine transporter Thi9	9.29E+06	7.04E+06	0.244	0.071	183	208	201
SPBC342.05	crb2	rhp9	DNA repair protein Rad9 homolog, Rhp9	8.10E+06	6.08E+06	0.242	0.089	184	168	138
SPBC215.14c	vps20		ESCRT III complex subunit Vps20	8.50E+06	6.44E+06	0.242	0.042	185	223	239
SPCC4F11.03c			sequence orphan	7.21E+06	5.63E+06	0.241	0.382	186	224	278
SPCC4B3.12	set9		histone lysine methyltransferase Set9	7.92E+06	6.17E+06	0.241	0.154	187	315	307
SPCC31H12.04c	rpl1202	rpl12-2,rpl12	60S ribosomal protein L12.1/L12A	5.42E+06	4.31E+06	0.241	0.248	188	421	395
SPBP35G2.08c	air1		zinc knuckle TRAMP complex subunit Air1	5.56E+06	4.22E+06	0.240	0.088	189	379	407
SPAC1F5.08c	yam8	ehs1	calcium channel regulatory subunit Yam8	7.97E+06	5.98E+06	0.240	0.165	190	187	95
SPAC31F12.01	zds1	SPAC637.14,mu g88	zds family protein phosphatase type A regulator Zds1 (predicted)	9.24E+06	7.01E+06	0.240	0.129	191	247	254
SPAC2E12.03c			PQ loop protein	7.27E+06	5.48E+06	0.240	0.210	192	282	308
SPBC1921.07c	sgf29	SPBC21D10.13	SAGA complex subunit Sgf29	6.21E+06	4.73E+06	0.239	0.076	193	167	255
SPBP35G2.13c	swc2		Swr1 complex complex subunit Swc2	7.15E+06	5.47E+06	0.238	0.058	194	84	92
SPBC11C11.01		SPBC17D1.08	U2-associated protein (predicted)	9.50E+06	7.31E+06	0.237	0.094	195	192	297
SPBC21C3.20c	git1		C2 domain protein Git1	5.42E+06	4.03E+06	0.236	0.183	196	45	76

Gene ID	Gene name	Synonym	Gene description	total area no drug	50nM				150nM	250nM
					total area GemC	mean $\Delta G/G$	stDev	rank	rank	rank
SPAC4G9.15			ketoreductase (predicted)	3.93E+06	3.28E+06	0.236	0.237	197	323	427
SPAC3H5.10	rpl3202	rpl32-2,rpl32	60S ribosomal protein L32 (predicted)	6.63E+06	5.04E+06	0.236	0.248	198	212	265
SPAC4G9.02	rnh201		ribonuclease H2 complex subunit Rnh201 (predicted)	9.03E+06	6.77E+06	0.235	0.169	199	113	77
SPAC22A12.04c	rps2201	rps22-1,rps15a-1	40S ribosomal protein S15a (predicted)	5.98E+06	4.34E+06	0.235	0.135	200	300	323
SPAC29A4.20	elp3	kat9	elongator complex, histone acetyltransferase subunit Elp3 (predicted)	8.30E+06	6.34E+06	0.235	0.063	201	341	367
SPAPB1E7.04c			chitinase (predicted)	5.85E+06	4.67E+06	0.233	0.250	202	303	131
SPBC16G5.06			sequence orphan	8.26E+06	6.16E+06	0.232	0.244	203	184	167
SPBC359.04c			cell surface glycoprotein (predicted), DIPSY family	8.12E+06	6.26E+06	0.228	0.014	204	255	247
SPAC4F10.04	ypa1	rrd1	protein phosphatase type 2A, intrinsic regulator Rrd1 (predicted)	8.51E+06	6.48E+06	0.227	0.138	205	262	277
SPAC1687.19c			queuine tRNA-ribosyltransferase (predicted)	8.51E+06	6.56E+06	0.227	0.049	206	308	289
SPBC1685.14c			Vid27 family protein	8.98E+06	6.98E+06	0.224	0.013	207	277	256
SPCC622.08c	hta1		histone H2A alpha	9.55E+06	7.26E+06	0.224	0.273	208	334	384
SPCC594.01		SPCC736.16	DUF1769 family protein	7.27E+06	5.42E+06	0.223	0.117	209	232	153
SPBC365.06	pmt3	ubl2,smt3	SUMO	9.72E+06	7.51E+06	0.223	0.092	210	92	94
SPAC17C9.12			VAP family protein (predicted)	8.36E+06	6.52E+06	0.222	0.190	211	145	269
SPBC651.06	mug166	csa1	sequence orphan	9.27E+06	7.23E+06	0.222	0.071	212	245	322
SPAP27G11.14c			sequence orphan	8.20E+06	6.38E+06	0.221	0.149	213	64	43
SPCC1884.02	nic1	SPCC757.01	NiCoT heavy metal ion transporter Nic1	8.11E+06	6.17E+06	0.220	0.108	214	285	321
SPCC1753.05	rsm1		RNA export factor Rsm1	7.20E+06	5.85E+06	0.219	0.078	215	242	305
SPBC31F10.07	lsb5		cortical component Lsb5 (predicted)	1.02E+07	7.97E+06	0.219	0.086	216	185	275
SPAC3F10.17			ribosome biogenesis protein Ltv1 (predicted)	1.00E+07	7.81E+06	0.217	0.104	217	248	270
SPBC1734.05c	spf31		DNAJ protein Spf31 (predicted)	6.17E+06	5.04E+06	0.216	0.140	218	271	137
SPAC18G6.15	mal3		EB1 family Mal3	1.05E+07	8.22E+06	0.215	0.097	219	296	166

Gene ID	Gene name	Synonym	Gene description	total area no drug	50nM				150nM	250nM
					total area GemC	mean $\Delta G/G$	stDev	rank	rank	rank
SPCP25A2.02c	rhp26		SNF2 family helicase Rhp26	4.95E+06	3.14E+06	0.215	0.402	220	158	171
SPAC30D11.04c	nup124		nucleoporin Nup124	6.53E+06	5.11E+06	0.214	0.148	221	91	133
SPBC725.01			aspartate aminotransferase (predicted)	6.33E+06	5.14E+06	0.214	0.132	222	312	299
SPCC663.14c			TRP-like ion channel (predicted)	7.13E+06	5.73E+06	0.213	0.270	223	251	409
SPCC576.11	rpl15		60S ribosomal protein L15 (predicted)	9.12E+06	7.14E+06	0.212	0.097	224	181	178
SPAC227.18	lys3	SPAC2F7.01	saccharopine dehydrogenase Lys3	9.07E+06	7.01E+06	0.212	0.177	225	387	279
SPAPB1A11.03			cytochrome b2 (L-lactate cytochrome-c oxidoreductase) (predicted)	1.11E+07	8.68E+06	0.211	0.076	226	157	268
SPCC1393.02c	spt2		non-specific DNA binding protein Spt2 (predicted)	1.00E+07	7.90E+06	0.210	0.199	227	180	172
SPAC11E3.05			ubiquitin-protein ligase E3, human WDR59 ortholog	2.78E+06	3.30E+06	0.209	0.670	228	307	396
SPAC13C5.06c	mug121		sequence orphan	8.14E+06	6.54E+06	0.207	0.214	229	329	378
SPCC737.05			peroxin Pex28/29 (predicted)	8.71E+06	6.88E+06	0.205	0.136	230	289	212
SPCC1223.15c	spc19		DASH complex subunit Spc19	8.56E+06	6.82E+06	0.205	0.015	231	227	125
SPAC13G7.06	met16		phosphoadenosine phosphosulfate reductase	6.90E+06	5.51E+06	0.204	0.120	232	169	204
SPAC1B3.16c	vht1		vitamin H transporter Vth1	7.74E+06	6.16E+06	0.201	0.059	233	133	81
SPCC188.07	ccq1		telomere maintenance protein Ccq1	8.12E+06	6.63E+06	0.200	0.159	234	266	371
SPBC1718.03	ker1		DNA-directed RNA polymerase I complex subunit Ker1	6.13E+06	4.81E+06	0.199	0.202	235	383	382
SPBC1718.07c	zfs1	moc4	CCCH tandem zinc finger protein, human Tristetraprolin homolog Zfs1, involved in mRNA catabolism	7.72E+06	6.18E+06	0.199	0.071	236	274	324
SPAC27D7.03c	mei2		RNA-binding protein involved in meiosis Mei2	7.98E+06	6.35E+06	0.198	0.122	237	189	176
SPAPB1A10.14	pof15		F-box protein (predicted)	8.01E+06	6.29E+06	0.197	0.226	238	292	249
SPBC9B6.07	nop52		nucleolar protein Nop52 family (predicted)	4.44E+06	4.19E+06	0.197	0.403	239	324	295

Gene ID	Gene name	Synonym	Gene description	total area no drug	50nM				150nM	250nM
					total area GemC	mean $\Delta G/G$	stDev	rank	rank	rank
SPBC19F8.08	rps401	rps4-1,rps4,SPBC25H2.17c	40S ribosomal protein S4 (predicted)	7.20E+06	5.92E+06	0.195	0.151	240	253	374
SPAC30D11.05	aps3		AP-3 adaptor complex subunit Aps3 (predicted)	6.03E+06	4.86E+06	0.194	0.153	241	165	88
SPBC1539.10			ribosome biogenesis protein Nop16 (predicted)	7.27E+06	5.94E+06	0.193	0.084	242	340	397
SPBC25D12.05	trm1		N2,N2-dimethylguanosine tRNA methyltransferase	7.54E+06	6.05E+06	0.193	0.143	243	259	281
SPBC3E7.16c	leu3	SPBC4F6.03c	2-isopropylmalate synthase Leu3	5.23E+06	4.33E+06	0.193	0.206	244	228	190
SPAC18G6.02c	chp1		chromodomain protein Chp1	4.78E+06	3.79E+06	0.193	0.148	245	193	182
SPCC1259.04	iec3		Ino80 complex subunit Iec3	6.82E+06	4.84E+06	0.191	0.581	246	136	179
SPAC2G11.03c	vps45		vacuolar sorting protein Vps45	7.14E+06	5.67E+06	0.190	0.234	247	338	439
SPAC144.11	rps1102	rps11-2,rps11	40S ribosomal protein S11 (predicted)	4.08E+06	3.93E+06	0.189	0.554	248	390	339
SPBP8B7.08c			leucine carboxyl methyltransferase Ppm1 (predicted)	6.48E+06	5.89E+06	0.188	0.409	249	287	369
SPAC26A3.01	sxa1	SPAC2E1P5.06	aspartic protease Sxa1	8.59E+06	6.98E+06	0.187	0.090	250	297	290
SPAC56F8.09	rrp8		rRNA methyltransferase Rrp8 (predicted)	8.30E+06	6.76E+06	0.186	0.152	251	240	336
SPBC336.01	fbh1	fdh1,fdh	DNA helicase I	6.04E+06	5.28E+06	0.185	0.142	252	209	280
SPBC1734.15	rsc4	brd1	RSC complex subunit Rsc4	9.47E+06	7.48E+06	0.182	0.257	253	257	181
SPAC17G6.05c			Rhophilin-2 homolog (predicted)	7.25E+06	5.80E+06	0.182	0.182	254	226	229
SPAC1D4.09c	rtf2		replication termination factor Rtf2	8.02E+06	6.53E+06	0.181	0.230	255	316	354
SPAC1705.02			human 4F5S homolog	8.38E+06	6.88E+06	0.180	0.027	256	207	170
SPBC902.02c	ctf18	chl12	RFC-like complex subunit Ctf18	6.92E+06	5.67E+06	0.180	0.060	257	270	262
SPCC1322.03			TRP-like ion channel (predicted)	6.59E+06	5.15E+06	0.179	0.382	258	363	355
SPCC970.05	rpl3601	rpl36-1	60S ribosomal protein L36	7.46E+06	6.16E+06	0.179	0.058	259	174	164
SPBP22H7.08	rps1002	rps10-2,rps10B	40S ribosomal protein S10 (predicted)	2.84E+06	1.75E+06	0.179	0.407	260	8	41
SPAC3A11.14c	pk11	k1p1,SPAC3H5.03c	kinesin-like protein Pk11	8.73E+06	7.16E+06	0.178	0.035	261	155	213

Gene ID	Gene name	Synonym	Gene description	total area no drug	50nM			150nM	250nM	
					total area GemC	mean $\Delta G/G$	stDev	rank	rank	
SPBC146.02			sequence orphan	7.54E+06	6.13E+06	0.177	0.324	262	220	345
SPBC19C2.02	pmt1		DNA methyltransferase homolog	9.24E+06	7.53E+06	0.177	0.088	263	269	193
SPAC2H10.01			transcription factor, zf-fungal binuclear cluster type (predicted)	9.00E+06	7.41E+06	0.176	0.022	264	244	259
SPCC1450.08c	wtf16		wtf element Wtf16	6.55E+06	5.77E+06	0.175	0.319	265	342	242
SPCC1183.09c	pmp31	mug75	plasma membrane proteolipid Pmp31	6.44E+06	5.28E+06	0.175	0.325	266	229	191
SPAC688.14	set13		ribosome L32 lysine methyltransferase Set13	9.15E+06	7.54E+06	0.174	0.105	267	230	203
SPBC18H10.02	lcf1		long-chain-fatty-acid-CoA ligase Lcf1	1.09E+07	8.93E+06	0.173	0.112	268	225	163
SPCC24B10.09	rps1702	rps17-2,rps17	40S ribosomal protein S17 (predicted)	8.30E+06	6.88E+06	0.172	0.048	269	299	362
SPAC1F7.12	yak3	yakC,SPAC21E11.01	aldose reductase ARK13 family YakC	9.10E+06	7.53E+06	0.170	0.094	270	258	184
SPAC22G7.08	ppk8		serine/threonine protein kinase Ppk8 (predicted)	9.04E+06	7.53E+06	0.170	0.088	271	178	206
SPAC16.01	rho2		Rho family GTPase Rho2	6.61E+06	5.78E+06	0.169	0.104	272	431	413
SPCP1E11.06	apl4		AP-1 adaptor complex gamma subunit Apl4	7.51E+06	6.39E+06	0.167	0.174	273	366	415
SPBC23G7.14			sequence orphan	9.26E+06	7.69E+06	0.167	0.054	274	205	245
SPBC577.02	rpl3801	rpl38-1	60S ribosomal protein L38 (predicted)	8.47E+06	7.09E+06	0.165	0.057	275	332	408
SPBC13E7.06	msd1	mug172	mitotic-spindle disanchored Msd1	8.92E+06	7.51E+06	0.164	0.180	276	295	286
SPAC1002.06c	bqt2	mug18,rec23	bouquet formation protein Bqt2	7.71E+06	6.43E+06	0.163	0.118	277	326	218
SPAC6F12.06			Rho GDP dissociation inhibitor Rdi1 (predicted)	6.87E+06	5.85E+06	0.163	0.226	278	352	241
SPAC9G1.02	wis4	wak1,wik1	MAP kinase kinase kinase Wis4	7.12E+06	5.89E+06	0.163	0.071	279	335	287
SPAC806.08c	mod21		gamma tubulin complex subunit Mod21	9.39E+06	7.91E+06	0.162	0.077	280	221	227
SPAC1786.04			sequence orphan	1.02E+07	8.60E+06	0.161	0.078	281	288	312
SPAC1A6.08c	mug125		sequence orphan	6.46E+06	5.38E+06	0.160	0.305	282	276	188
SPAC11E3.01c	swr1	SPAC2H10.03c	SNF2 family helicase Swr1	8.69E+06	7.32E+06	0.156	0.075	283	249	267
SPBC21D10.10	bdcl		bromodomain containing protein 1, Bdc1	7.30E+06	6.06E+06	0.155	0.219	284	153	314
SPAC140.04			conserved eukaryotic protein	7.31E+06	6.01E+06	0.155	0.348	285	353	237

Gene ID	Gene name	Synonym	Gene description	total area no drug	50nM				150nM	250nM
					total area GemC	mean $\Delta G/G$	stDev	rank	rank	rank
SPAC20H4.06c			RNA-binding protein	9.24E+06	7.87E+06	0.154	0.072	286	349	311
SPAC922.04			sequence orphan	5.58E+06	5.45E+06	0.154	0.591	287	197	244
SPAC4H3.05	srs2		ATP-dependent DNA helicase, UvrD subfamily	7.13E+06	6.08E+06	0.150	0.127	288	120	78
SPBP35G2.10	mit1		SHREC complex subunit Mit1	6.89E+06	5.91E+06	0.150	0.057	289	280	333
SPAC1B3.01c			uracil phosphoribosyltransferase (predicted)	8.85E+06	7.55E+06	0.149	0.039	290	328	173
SPBC1539.08	arf6		ADP-ribosylation factor, Arf family Arf6	9.30E+06	7.87E+06	0.146	0.145	291	265	243
SPAC1F5.10			ATP-dependent RNA helicase (predicted)	3.30E+06	2.71E+06	0.146	0.277	292	77	32
SPBP4H10.09	rsv1		transcription factor Rsv1	6.80E+06	5.57E+06	0.146	0.328	293	327	273
SPBC29A3.09c			AAA family ATPase Gcn20 (predicted)	9.00E+06	7.57E+06	0.140	0.159	294	284	264
SPAC4A8.09c	cwf21		complexed with Cdc5 protein Cwf21	7.23E+06	6.21E+06	0.139	0.099	295	361	140
SPCC736.08	cbf11		CBF1/Su(H)/LAG-1 family transcription factor Cbf11	7.29E+06	6.28E+06	0.139	0.029	296	359	325
SPBC32F12.05c	cwf12		complexed with Cdc5 protein Cwf12	7.80E+06	6.56E+06	0.139	0.208	297	135	104
SPBC31F10.12			RNA-binding protein Tma20 (predicted)	7.87E+06	6.68E+06	0.138	0.230	298	237	361
SPAC16A10.03c			zinc finger protein Pep5/Vps11-like (predicted)	5.39E+06	4.39E+06	0.138	0.264	299	204	282
SPAC19D5.11c	ctf8		DNA replication factor C complex subunit Ctf8 (predicted)	7.87E+06	6.90E+06	0.138	0.151	300	156	142
SPBC16D10.07c	sir2		Sir2 family histone deacetylase Sir2	7.64E+06	6.54E+06	0.135	0.231	301	177	108
SPBC21C3.02c	dep1		Sds3-like family protein Dep1	8.95E+06	7.74E+06	0.135	0.037	302	418	392
SPAC2E1P5.03			DNAJ domain protein Erj5 (predicted)	7.44E+06	6.39E+06	0.133	0.139	303	188	158
SPAC22E12.18			conserved fungal protein	6.92E+06	6.03E+06	0.130	0.010	304	391	330
SPAC3F10.02c	trk1	sptrk	potassium ion transporter Trk1	8.75E+06	7.52E+06	0.128	0.193	305	374	394
SPBC4B4.07c	usp102	mud1	U1 snRNP-associated protein Usp102	9.90E+06	8.59E+06	0.128	0.080	306	281	232
SPAC10F6.04			RCC domain protein Ats1 (predicted)	7.92E+06	6.72E+06	0.125	0.400	307	294	331
SPBC2G5.03	ctu1		cytosolic thiouridylase subunit Ctu1	6.33E+06	5.58E+06	0.125	0.295	308	206	271
SPAC22F3.08c	rok1		ATP-dependent RNA helicase Rok1 (predicted)	5.84E+06	5.11E+06	0.122	0.056	309	260	215

Gene ID	Gene name	Synonym	Gene description	total area no drug	50nM				150nM	250nM
					total area GemC	mean $\Delta G/G$	stDev	rank	rank	rank
SPAC637.10c	rpn10	pus1	19S proteasome regulatory subunit Rpn10	9.10E+06	7.90E+06	0.122	0.163	310	304	174
SPAC1D4.11c	lkh1	kic1	dual specificity protein kinase Lkh1	7.59E+06	6.57E+06	0.120	0.283	311	137	156
SPAC10F6.08c	nht1		Ino80 complex HMG box protein Nht1	5.69E+06	4.82E+06	0.119	0.437	312	134	196
SPAC5D6.02c	mug165		sequence orphan	7.87E+06	6.83E+06	0.118	0.191	313	406	230
SPAC8E11.02c	rad24		14-3-3 protein Rad24	6.67E+06	5.87E+06	0.118	0.302	314	89	23
SPBC1773.09c	mug184		meiotically upregulated gene Mug184	7.18E+06	6.37E+06	0.118	0.182	315	283	401
SPCC364.02c	bis1		stress response protein Bis1	7.53E+06	6.58E+06	0.118	0.214	316	261	298
SPAPB17E12.05	rpl3703	rpl37	60S ribosomal protein L37 (predicted)	5.12E+06	4.42E+06	0.116	0.415	317	290	294
SPAC23C11.04c	pnk1		DNA kinase/phosphatase Pnk1	5.76E+06	4.60E+06	0.115	0.374	318	330	250
SPBC16A3.08c			Stm1 homolog (predicted)	7.99E+06	7.08E+06	0.114	0.031	319	279	357
SPAC3F10.06c			initiator methionine tRNA 2'-O-ribosyl phosphate transferase (predicted)	8.32E+06	7.42E+06	0.113	0.089	320	217	234
SPBC14C8.03	fma2		methionine aminopeptidase Fma2 (predicted)	7.01E+06	6.17E+06	0.112	0.212	321	403	365
SPCC364.05	vps3		GTPase regulator Vps3 (predicted)	6.69E+06	5.97E+06	0.112	0.219	322	372	258
SPBC16G5.15c	fkh2		fork head transcription factor Fkh2	7.10E+06	6.29E+06	0.111	0.208	323	389	431
SPAC3H1.06c			membrane transporter (predicted)	7.47E+06	6.58E+06	0.111	0.075	324	190	221
SPAC212.03			hypothetical protein	1.02E+07	9.05E+06	0.108	0.116	325	351	352
SPCC663.10			tRNA (uracil) methyltransferase (predicted)	8.43E+06	7.48E+06	0.108	0.115	326	376	261
SPAC4F8.01	did4	SPAC644.03c,v ps2	ESCRT III complex subunit Did4	7.01E+06	6.31E+06	0.108	0.229	327	407	434
SPAC26H5.10c	tif51		translation elongation factor eIF5A (predicted)	7.63E+06	6.88E+06	0.107	0.176	328	263	177
SPCC18B5.03	wee1		M phase inhibitor protein kinase Wee1	7.94E+06	7.01E+06	0.106	0.200	329	398	316
SPAC30D11.02c			sequence orphan	7.64E+06	6.75E+06	0.105	0.252	330	439	338
SPAC521.05	rps802	rps8-2	40S ribosomal protein S8 (predicted)	5.42E+06	4.85E+06	0.105	0.085	331	414	437
SPCC663.06c			short chain dehydrogenase (predicted)	8.01E+06	7.21E+06	0.105	0.065	332	305	223
SPAC3H5.07	rpl702	rpl7-2,rpl7,rpl7b	60S ribosomal protein L7	6.96E+06	6.21E+06	0.105	0.036	333	320	329

Gene ID	Gene name	Synonym	Gene description	total area no drug	50nM				150nM	250nM
					total area GemC	mean $\Delta G/G$	stDev	rank	rank	rank
SPBC1652.01			ribosomal RNA processing element (RRPE)-binding protein (predicted)	6.84E+06	5.65E+06	0.103	0.189	334	404	385
SPBC2D10.16	mhf1		FANCM-MHF complex subunit Mhf1	8.79E+06	7.89E+06	0.101	0.161	335	371	390
SPAC1783.05	hrp1	chd1	ATP-dependent DNA helicase Hrp1	5.40E+06	5.03E+06	0.098	0.166	336	386	260
SPAC6G9.09c	rpl24	rpl24-01,rpl24	60S ribosomal protein L24 (predicted)	8.98E+06	7.96E+06	0.098	0.115	337	405	430
SPBC2F12.11c	rep2		transcriptional activator, MBF subunit Rep2	7.31E+06	6.67E+06	0.098	0.160	338	194	235
SPAC977.14c			aldo/keto reductase, unknown biological role	6.74E+06	6.09E+06	0.096	0.087	339	337	373
SPAC17C9.15c			sequence orphan	6.10E+06	5.51E+06	0.096	0.326	340	162	192
SPAC186.09			pyruvate decarboxylase (predicted)	7.33E+06	6.77E+06	0.091	0.149	341	422	283
SPAC513.07			flavonol reductase/cinnamoyl-CoA reductase family	7.64E+06	6.94E+06	0.087	0.182	342	183	141
SPAC2C4.06c			rRNA methyltransferase (predicted)	9.39E+06	8.64E+06	0.083	0.423	343	355	350
SPBC685.04c	aps2		AP-2 adaptor complex subunit Aps2 (predicted)	7.29E+06	6.89E+06	0.080	0.264	344	364	340
SPAC29B12.02c	set2	kmt3	histone lysine methyltransferase Set2	7.94E+06	7.39E+06	0.080	0.200	345	344	320
SPBC1604.16c			RNA-binding protein, G-patch type (predicted)	7.46E+06	6.82E+06	0.078	0.242	346	218	274
SPBC1703.03c			armadillo repeat protein, unknown biological role	4.87E+06	4.87E+06	0.077	0.239	347	286	410
SPAC3G6.06c	rad2	fen1	FEN-1 endonuclease Rad2	6.18E+06	5.75E+06	0.077	0.086	348	410	403
SPCC1494.08c			conserved fungal protein	7.61E+06	7.18E+06	0.076	0.121	349	402	337
SPBC11B10.10c	pht1		histone H2A variant H2A.Z, Pht1	5.42E+06	4.90E+06	0.076	0.322	350	275	122
SPCC777.13	vps35		retromer complex subunit Vps35	1.38E+06	1.59E+06	0.076	0.342	351	234	411
SPAC9E9.15			CIA30 protein (predicted)	7.91E+06	7.27E+06	0.076	0.080	352	339	175
SPBC16C6.05			mitochondrial translation initiation factor (predicted)	8.69E+06	7.95E+06	0.075	0.121	353	388	388
SPCC777.03c			nifs homolog, possible cysteine desulfurase	8.51E+06	7.89E+06	0.075	0.254	354	415	380
SPAC23C11.10	usb1		mitochondrial respiratory chain complex III assembly Usb1 (predicted)	9.56E+06	8.55E+06	0.072	0.333	355	317	248
SPAC31A2.09c	apm4		AP-2 adaptor complex subunit Apm4 (predicted)	7.64E+06	6.96E+06	0.071	0.074	356	400	335

Gene ID	Gene name	Synonym	Gene description	total area no drug	50nM			150nM	250nM	
					total area GemC	mean $\Delta G/G$	stDev	rank	rank	
SPBC1A4.02c	leu1	SPBC1E8.07c	3-isopropylmalate dehydrogenase Leu1	8.48E+06	7.87E+06	0.071	0.101	357	438	348
SPAC31G5.09c	spk1		MAP kinase Spk1	8.32E+06	7.75E+06	0.071	0.176	358	256	236
SPCC306.08c			malate dehydrogenase (predicted)	7.78E+06	7.18E+06	0.071	0.300	359	250	161
SPCC777.12c			thioredoxin family protein	8.73E+06	8.22E+06	0.064	0.118	360	343	208
SPAC17G8.05	med20		mediator complex subunit Med20	9.18E+06	8.61E+06	0.063	0.041	361	354	393
SPCC364.06	nap1	nap11	nucleosome assembly protein Nap1	6.69E+06	5.98E+06	0.058	0.272	362	426	238
SPCC285.10c			SPRY domain protein	6.64E+06	6.19E+06	0.055	0.342	363	325	372
SPCC736.02			sequence orphan	5.20E+06	4.87E+06	0.055	0.117	364	373	421
SPBC3D6.10	apn2		AP-endonuclease Apn2	8.58E+06	8.00E+06	0.054	0.153	365	382	209
SPAC1610.01		SPAC17A5.17	conserved eukaryotic protein	6.77E+06	6.40E+06	0.051	0.095	366	393	356
SPAC23C11.15	pst2		Clr6 histone deacetylase complex subunit Pst2	4.19E+06	4.62E+06	0.051	0.625	367	90	233
SPAC9.02c			polyamine N-acetyltransferase (predicted)	7.63E+06	7.30E+06	0.051	0.080	368	101	148
SPBC36.07	iki3		elongator subunit Iki3 (predicted)	7.80E+06	7.44E+06	0.049	0.095	369	358	353
SPBC530.03c	bag102	bag1-b	BAG family molecular chaperone regulator Bag102 (predicted)	7.73E+06	7.40E+06	0.048	0.494	370	331	327
SPBC1685.02c	rps1202	rps12-2	40S ribosomal protein S12 (predicted)	7.17E+06	6.84E+06	0.047	0.385	371	309	310
SPBC21B10.10	rps402	rps4-2	40S ribosomal protein S4 (predicted)	8.29E+06	7.93E+06	0.044	0.094	372	399	420
SPBC29A10.16c			cytochrome b5 (predicted)	7.53E+06	7.26E+06	0.040	0.341	373	272	306
SPAC1D4.03c	aut12		autophagy associated protein Aut12 (predicted)	7.17E+06	6.93E+06	0.034	0.083	374	381	351
SPBC19C7.01	mni1	SPBC32F12.13c	Mago Nashi interacting protein (predicted)	5.59E+06	6.25E+06	0.032	0.457	375	170	284
SPAC17A2.06c	vps8		WD repeat protein Vps8 (predicted)	6.01E+06	5.60E+06	0.030	0.336	376	367	375
SPBC530.06c			translation initiation factor eIF3 alpha subunit (p135) (predicted)	7.83E+06	7.58E+06	0.030	0.185	377	411	386
SPBC887.10	mcs4		response regulator Mcs4	3.96E+06	3.18E+06	0.026	0.365	378	105	263
SPCC1223.05c	rpl3702	rpl37-2,rpl37	60S ribosomal protein L37 (predicted)	3.23E+06	2.64E+06	0.025	0.256	379	448	423
SPAC1002.07c	ats1		N-acetyltransferase Ats1 (predicted)	6.77E+06	6.40E+06	0.022	0.327	380	333	162

Gene ID	Gene name	Synonym	Gene description	total area no drug	50nM				150nM	250nM
					total area GemC	mean $\Delta G/G$	stDev	rank	rank	rank
SPAC3G9.11c			pyruvate decarboxylase (predicted)	6.56E+06	6.46E+06	0.020	0.202	381	293	359
SPBC24C6.10c	dip1		WISH/DIP/SPIN90 ortholog Dip1	6.69E+06	6.47E+06	0.019	0.275	382	264	432
SPBC3B9.09	vps36		ESCRT II complex subunit Vps36	7.27E+06	7.01E+06	0.018	0.203	383	430	440
SPAC23H4.09	cdb4		curved DNA-binding protein Cdb4, peptidase family	8.00E+06	7.86E+06	0.015	0.047	384	243	168
SPBC1347.13c			ribose methyltransferase (predicted)	5.31E+06	5.22E+06	0.015	0.067	385	112	169
SPCC1442.04c			meiotic recombination protein (predicted)	8.01E+06	7.93E+06	0.015	0.166	386	321	343
SPCC338.14			adenosine kinase (predicted)	7.63E+06	7.45E+06	0.014	0.151	387	348	398
SPAC630.14c	tup12		transcriptional corepressor Tup12	4.23E+06	4.12E+06	0.014	0.269	388	214	87
SPBC25B2.10			Usp (universal stress protein) family protein	7.26E+06	7.19E+06	0.013	0.042	389	412	412
SPBC1734.11	mas5		DNAJ domain protein Mas5 (predicted)	1.76E+06	1.64E+06	0.011	0.258	390	347	402
SPBC13A2.04c			PTR family peptide transporter (predicted)	7.98E+06	7.79E+06	0.009	0.243	391	345	414
SPBC12C2.01c		SPBC17F3.03c	sequence orphan	4.27E+06	4.57E+06	0.005	0.315	392	191	231
SPBC800.05c	tub1	tub1,alp2,ban5,atb2	tubulin alpha 2	6.00E+06	5.75E+06	0.004	0.316	393	377	211
SPBC2F12.03c			EST1 family protein (predicted)	6.63E+06	6.68E+06	0.003	0.167	394	375	251
SPBC23E6.01c		SPBPJ758.01	mRNA processing factor (predicted)	8.41E+06	8.29E+06	0.003	0.090	395	429	346
SPAC1A6.07			sequence orphan	7.36E+06	7.32E+06	0.002	0.058	396	350	303
SPCPB16A4.04c	trm8		tRNA (guanine-N7-)-methyltransferase catalytic subunit Trm8 (predicted)	5.51E+06	5.27E+06	-0.001	0.205	397	322	195
SPBC4B4.06	vps25		ESCRT II complex subunit Vps25	6.66E+06	6.67E+06	-0.001	0.077	398	302	319
SPAC31A2.12			arrestin/PY protein 1 (predicted)	7.11E+06	6.85E+06	-0.001	0.289	399	246	313
SPAC16E8.12c			ING family homolog Png3 (predicted)	5.99E+06	6.01E+06	-0.007	0.180	400	384	291
SPCC1223.10c	eaf1		RNA polymerase II transcription elongation factor SpEAF	7.66E+06	8.07E+06	-0.008	0.483	401	306	317
SPAC17C9.08	pnu1	nuc1,end1	mitochondrial endodeoxyribonuclease Pnu1	6.87E+06	6.80E+06	-0.012	0.314	402	346	370
SPAC23D3.09	arp42	arp4	SWI/SNF and RSC complex subunit Arp42	5.46E+06	5.34E+06	-0.012	0.279	403	301	160

Gene ID	Gene name	Synonym	Gene description	total area no drug	50nM				150nM	250nM
					total area GemC	mean $\Delta G/G$	stDev	rank	rank	rank
SPBC1709.14			peptide N-glycanase (predicted)	7.13E+06	7.48E+06	-0.023	0.347	404	435	416
SPAC4H3.07c			protein phosphatase Fmp31 (predicted)	4.27E+06	3.99E+06	-0.025	0.537	405	172	107
SPCC736.07c			unconventional prefoldin involved in translation initiation (predicted)	7.29E+06	7.45E+06	-0.027	0.065	406	397	391
SPCC4B3.06c			NADPH-dependent FMN reductase (predicted)	5.58E+06	6.59E+06	-0.031	0.551	407	215	257
SPAC323.05c			protein methyltransferase Mtq2 (predicted)	8.89E+06	8.65E+06	-0.033	0.311	408	401	344
SPAC11D3.15			5-oxoprolinase (ATP-hydrolyzing) (predicted)	5.88E+06	6.10E+06	-0.035	0.036	409	436	428
SPAC1F12.07			phosphoserine aminotransferase (predicted)	3.23E+06	3.17E+06	-0.036	0.207	410	202	376
SPAC24B11.09			mitochondrial protein, predicted, human BRP44 ortholog	4.00E+06	4.26E+06	-0.040	0.291	411	199	334
SPBC1D7.03	mug80		cyclin Clg1 (predicted)	7.04E+06	7.03E+06	-0.041	0.199	412	428	383
SPAC4D7.07c			sequence orphan	7.36E+06	7.92E+06	-0.046	0.276	413	356	358
SPAC25B8.08			conserved fungal protein	7.18E+06	7.51E+06	-0.047	0.029	414	396	399
SPCC74.05	rpl2702	rpl27-2	60S ribosomal protein L27 (predicted)	8.42E+06	8.72E+06	-0.048	0.099	415	441	443
SPAC31G5.03	rps1101	rps11-1	40S ribosomal protein S11 (predicted)	2.76E+06	2.63E+06	-0.054	0.560	416	239	246
SPCC285.14	trs130		TRAPP complex subunit Trs130 (predicted)	6.52E+06	7.38E+06	-0.055	0.237	417	432	436
SPBP22H7.04			sequence orphan	8.53E+06	8.85E+06	-0.059	0.277	418	420	405
SPBP16F5.03c	tra1		SAGA complex phosphatidylinositol pseudokinase Tra1	7.38E+06	7.66E+06	-0.065	0.208	419	447	444
SPBC31F10.10c			zf-MYND type zinc finger protein	5.98E+06	6.26E+06	-0.070	0.395	420	409	226
SPAC30D11.09	cwf19		complexed with Cdc5 protein Cwf19	6.62E+06	7.02E+06	-0.082	0.258	421	424	381
SPBP16F5.05c			ribosome biogenesis protein Nop8 (predicted)	7.85E+06	8.42E+06	-0.082	0.367	422	437	435
SPBC543.07	pek1	skh1,mkk1	MAP kinase kinase Pek1	7.64E+06	7.97E+06	-0.083	0.281	423	419	419
SPBC18H10.07			WW domain-binding protein 4 (predicted)	7.18E+06	7.69E+06	-0.085	0.158	424	440	422
SPAC12G12.15	sif3		Sad1 interacting factor 3 (predicted)	7.37E+06	8.43E+06	-0.094	0.235	425	365	389
SPCC24B10.08c	ada2		SAGA complex subunit Ada2	6.00E+06	6.94E+06	-0.095	0.847	426	25	42
SPBC1921.01c	rpl3701	rpl37-1,rpl37	60S ribosomal protein L35a (predicted)	5.40E+06	5.99E+06	-0.121	0.305	427	380	406

Gene ID	Gene name	Synonym	Gene description	total area no drug	50nM				150nM	250nM
					total area GemC	mean $\Delta G/G$	stDev	rank	rank	rank
SPAC2F7.07c	cph2	rco1	Clr6 histone deacetylase associated PHD protein-2 Cph2	5.95E+06	5.96E+06	-0.124	0.476	428	267	4
SPCC757.11c			membrane transporter (predicted)	5.34E+06	3.83E+06	-0.125	0.895	429	442	304
SPCC594.04c			steroid oxidoreductase superfamily protein (predicted)	4.79E+06	4.19E+06	-0.126	0.486	430	219	445
SPAC3H1.11	hsr1		transcription factor Hsr1	7.09E+06	6.42E+06	-0.128	0.623	431	423	342
SPBC16C6.11	rpl3201	rpl32-1	60S ribosomal protein L32	3.18E+06	3.53E+06	-0.130	0.139	432	413	441
SPCC1919.03c	amk2		AMP-activated protein kinase beta subunit Amk2	1.61E+06	9.85E+05	-0.133	0.793	433	111	447
SPAC31A2.11c	cuf1		nutritional copper sensing transcription factor Cuf1	5.80E+06	6.06E+06	-0.144	0.476	434	314	285
SPAC3H5.12c	rpl501	rpl5-1,rpl5	60S ribosomal protein L5 (predicted)	3.74E+06	4.09E+06	-0.151	0.211	435	370	400
SPBC4F6.10	vps901	vps9a	guanyl-nucleotide exchange factor Vps901 (predicted)	5.59E+06	6.02E+06	-0.154	0.557	436	291	210
SPBC24C6.06	gpa1		G-protein alpha subunit	5.54E+06	5.68E+06	-0.161	0.273	437	445	446
SPAC20H4.03c	tfs1		transcription elongation factor TFHS	4.83E+06	5.08E+06	-0.168	0.348	438	394	404
SPAC23A1.16c	rtr1		RNA polymerase II CTD phosphatase Rtr1 (predicted)	5.02E+06	5.87E+06	-0.169	0.477	439	360	426
SPCC364.03	rpl1702	rpl17-2,rpl17	60S ribosomal protein L17 (predicted)	6.11E+06	7.24E+06	-0.183	0.452	440	449	448
SPBC28F2.10c	ngg1	ada3, kap1	SAGA complex subunit Ngg1	4.88E+06	5.53E+06	-0.194	0.250	441	222	98
SPAC664.04c	rps1602	rps16-2,rps16	40S ribosomal protein S16 (predicted)	6.04E+06	6.32E+06	-0.197	0.368	442	369	424
SPBC1539.07c			glutathione-dependent formaldehyde dehydrogenase (predicted)	8.43E+06	1.02E+07	-0.203	0.320	443	443	429
SPCC24B10.22	pog1	SPCPB16A4.01	mitochondrial DNA polymerase	6.55E+06	7.16E+06	-0.203	0.500	444	427	368
SPBC20F10.07			GRAM domain protein	5.74E+06	6.73E+06	-0.203	0.381	445	444	328
SPAC3A12.13c			translation initiation factor eIF3j (p35)	2.54E+06	3.10E+06	-0.226	0.186	446	451	451
SPAC16E8.01	shd1	sla1	cytoskeletal protein binding protein Sla1 family, Shd1 (predicted)	5.54E+06	6.52E+06	-0.228	0.423	447	416	377

Gene ID	Gene name	Synonym	Gene description	total area no drug	50nM				150nM	250nM
					total area GemC	mean $\Delta G/G$	stDev	rank	rank	rank
SPCC1902.01	gaf1	SPCC417.01c	transcription factor Gaf1	4.13E+06	4.72E+06	-0.248	0.365	448	452	450
SPBC29A3.08	pof4		elongin-A, F-box protein Pof4 (predicted)	6.98E+06	8.74E+06	-0.252	0.133	449	417	417
SPCC663.11	saf1		splicing associated factor Saf1	5.46E+06	6.74E+06	-0.335	0.477	450	362	387
SPAC1399.02			membrane transporter (predicted)	5.37E+06	6.69E+06	-0.377	0.602	451	433	379
SPCC1739.07	cti1		Cut3 interacting protein Cti1, predicted exosome subunit	4.61E+06	5.46E+06	-0.459	0.900	452	446	452
SPAC26A3.07c	rpl1101	rpl11-1,rpl11	60S ribosomal protein L11 (predicted)	2.13E+06	2.57E+06	-0.634	0.799	453	453	454
SPAC4F10.19c			zf-HIT protein Hit1 (predicted)	2.94E+06	4.55E+06	-0.913	0.473	454	454	453
SPBC25H2.11c	spt7		SAGA complex bromodomain subunit Spt7	7.16E+04	1.09E+05	-1.238	0.517	455	455	3
SPAC1F7.13c	rpl801	rpl8-1,rpl18,rpk5a,rpl2-1,SPAC21E11.02c	60S ribosomal protein L8 (predicted)	1.05E+06	2.07E+06	-1.990	2.311	456	456	455

4.4 Gene Ontology (GO) analysis

GO annotation is provided by the Gene Ontology Consortium (<http://geneontology.org>) and aims to “unify” terms used in gene descriptions by classifying genes in defined categories (Ashburner *et al.*, 2000).

GO analysis of the library was carried out with the Cytoscape 2.8 platform using the BINGO 2.44 plugin. Cytoscape is a bioinformatics tool used to visualise biological networks (Smoot *et al.*, 2011), whereas BINGO (Biological Networks Gene Ontology) is a tool used to determine over-representation of GO categories in a set of genes. BINGO first classifies genes into categories (biological processes for example) and using statistical analysis the programme determines which GOs are under or over represented in a set of genes. I used BINGO analysis to determine which GOs are over-represented in the sub library (456 sensitive mutants) using the Bioneer library (V2) as a reference. For example, if we want to know representation of DNA repair genes in the sub library, BINGO calculates total of DNA repair genes that are present in the Bioneer library and then determines how many of those are present in the sub library. Over-represented GOs are then ranked according to a corrected p-value which represents the probability that a GO was wrongly identified as being over-represented. A small corrected p-value indicates high certainty. For BINGO analysis I selected over-represented GOs using the hypergeometric statistical test with Benjamin and Hochberg False Discovery Correction (Benjamini and Hochberg, 1995) at significance levels of 0.05. Presented GOs analysis was carried out on the first 114 (25%) highly sensitive mutants of the sub library (analysis of the whole sub library is given in appendix IV). *Figure 4-6* shows a screenshot of the cytoscape visualisation output, showing significant enrichment of DNA-related processes. *Table 4-5* shows over-represented biological processes ranked according to their corrected p-values. The role of DNA repair mechanisms in response to GemC treatment was supported by over-representation of genes involved in the processes. The checkpoint machinery was also over-represented.

Table 4-5 List of over-represented biological processes GOs in the highly sensitive mutants of the sub library. GOs were determined at significance level of 0.05 and ranked by corrected P-value. Values range from 8.96E-12 (lowest corrected p-value for intra-S DNA damage checkpoint) to 4.37E-02 (highest corrected p-value for regulation of gene expression). DNA repair was over-represented, through the DNA repair (5.92E-04), DSBR via homologous recombination (3.47E-03), recombination repair (8.50E-03) and DSBR (1.28E-02) ontologies. DNA damage checkpoint processes were also over-represented.

GO-ID	p-value	corr p-value	selected	total	Description
31573	1.24E-14	8.96E-12	11	13	intra-S DNA damage checkpoint
77	8.06E-10	2.91E-07	11	26	DNA damage checkpoint
42770	1.32E-09	3.16E-07	11	27	DNA damage response, signal transduction
31570	3.27E-09	5.90E-07	11	29	DNA integrity checkpoint
8156	9.05E-09	1.31E-06	9	19	negative regulation of DNA replication
75	1.68E-08	2.02E-06	13	49	cell cycle checkpoint
6974	3.75E-08	3.86E-06	20	128	response to DNA damage stimulus
51053	4.42E-08	3.99E-06	9	22	negative regulation of DNA metabolic process
6275	7.03E-08	5.63E-06	9	23	regulation of DNA replication
76	1.48E-07	8.88E-06	7	13	DNA replication checkpoint
32297	1.48E-07	8.88E-06	7	13	negative regulation of DNA-dependent DNA replication initiation
30174	1.48E-07	8.88E-06	7	13	regulation of DNA-dependent DNA replication initiation
90304	2.50E-07	1.39E-05	40	472	nucleic acid metabolic process
90329	5.19E-07	2.68E-05	7	15	regulation of DNA-dependent DNA replication
45934	1.10E-06	4.85E-05	16	103	negative regulation of nucleobase, nucleoside, nucleotide and nucleic acid metabolic process
51172	1.10E-06	4.85E-05	16	103	negative regulation of nitrogen compound metabolic process
51276	1.14E-06	4.85E-05	24	216	chromosome organization
10558	1.44E-06	5.77E-05	16	105	negative regulation of macromolecule biosynthetic process
6259	1.63E-06	6.18E-05	20	160	DNA metabolic process

GO-ID	p-value	corr p-value	selected	total	Description
6139	1.99E-06	7.19E-05	42	549	nucleobase, nucleoside, nucleotide and nucleic acid metabolic process
31327	3.09E-06	1.03E-04	16	111	negative regulation of cellular biosynthetic process
51052	3.16E-06	1.03E-04	9	34	regulation of DNA metabolic process
9890	3.49E-06	1.09E-04	16	112	negative regulation of biosynthetic process
10556	4.64E-06	1.36E-04	29	318	regulation of macromolecule biosynthetic process
60255	4.71E-06	1.36E-04	31	354	regulation of macromolecule metabolic process
31326	7.69E-06	2.13E-04	29	326	regulation of cellular biosynthetic process
10605	8.79E-06	2.34E-04	16	120	negative regulation of macromolecule metabolic process
9889	9.25E-06	2.34E-04	29	329	regulation of biosynthetic process
34641	9.43E-06	2.34E-04	47	687	cellular nitrogen compound metabolic process
6807	1.21E-05	2.83E-04	47	693	nitrogen compound metabolic process
31324	1.22E-05	2.83E-04	16	123	negative regulation of cellular metabolic process
44260	1.56E-05	3.52E-04	63	1068	cellular macromolecule metabolic process
19219	1.90E-05	4.15E-04	27	305	regulation of nucleobase, nucleoside, nucleotide and nucleic acid metabolic process
48523	1.96E-05	4.15E-04	19	172	negative regulation of cellular process
51171	2.42E-05	4.98E-04	27	309	regulation of nitrogen compound metabolic process
9892	2.49E-05	4.98E-04	16	130	negative regulation of metabolic process
43170	2.98E-05	5.80E-04	63	1087	macromolecule metabolic process
6281	3.12E-05	5.92E-04	13	91	DNA repair
80090	4.58E-05	8.47E-04	31	395	regulation of primary metabolic process
48519	4.75E-05	8.56E-04	19	183	negative regulation of biological process
9987	4.91E-05	8.64E-04	105	2317	cellular process
16568	6.18E-05	1.06E-03	15	125	chromatin modification
34645	6.82E-05	1.14E-03	31	403	cellular macromolecule biosynthetic process
9059	7.16E-05	1.17E-03	31	404	macromolecule biosynthetic process
31323	8.68E-05	1.39E-03	31	408	regulation of cellular metabolic process

GO-ID	p-value	corr p-value	selected	total	Description
51726	1.17E-04	1.83E-03	15	132	regulation of cell cycle
19222	1.32E-04	2.03E-03	31	417	regulation of metabolic process
6310	1.94E-04	2.91E-03	9	55	DNA recombination
10467	2.25E-04	3.31E-03	32	449	gene expression
724	2.41E-04	3.47E-03	5	16	double-strand break repair via homologous recombination
6325	2.48E-04	3.50E-03	15	141	chromatin organization
6338	2.93E-04	4.06E-03	12	98	chromatin remodeling
6260	3.37E-04	4.58E-03	8	47	DNA replication
7531	3.65E-04	4.70E-03	4	10	mating type determination
7530	3.65E-04	4.70E-03	4	10	sex determination
45165	3.65E-04	4.70E-03	4	10	cell fate commitment
6656	5.25E-04	6.34E-03	3	5	phosphatidylcholine biosynthetic process
46470	5.25E-04	6.34E-03	3	5	phosphatidylcholine metabolic process
60249	5.36E-04	6.34E-03	6	28	anatomical structure homeostasis
32200	5.36E-04	6.34E-03	6	28	telomere organization
723	5.36E-04	6.34E-03	6	28	telomere maintenance
44238	6.51E-04	7.57E-03	72	1422	primary metabolic process
9058	6.98E-04	7.99E-03	39	627	biosynthetic process
725	7.54E-04	8.50E-03	5	20	recombinational repair
44249	8.22E-04	9.12E-03	38	610	cellular biosynthetic process
65007	9.63E-04	1.05E-02	45	772	biological regulation
6302	1.20E-03	1.28E-02	5	22	double-strand break repair
6368	1.20E-03	1.28E-02	5	22	RNA elongation from RNA polymerase II promoter
734	1.47E-03	1.51E-02	2	2	gene conversion at mating-type locus, DNA repair synthesis
6657	1.47E-03	1.51E-02	2	2	CDP-choline pathway
31056	1.49E-03	1.52E-02	5	23	regulation of histone modification

GO-ID	p-value	corr p-value	selected	total	Description
6355	1.59E-03	1.59E-02	18	221	regulation of transcription, DNA-dependent
51252	2.38E-03	2.35E-02	18	229	regulation of RNA metabolic process
16070	2.44E-03	2.38E-02	23	326	RNA metabolic process
6312	2.70E-03	2.53E-02	3	8	mitotic recombination
42439	2.70E-03	2.53E-02	3	8	ethanolamine and derivative metabolic process
42138	2.70E-03	2.53E-02	3	8	meiotic DNA double-strand break formation
6354	3.17E-03	2.89E-02	5	27	RNA elongation
45449	3.17E-03	2.89E-02	18	235	regulation of transcription
44237	3.84E-03	3.46E-02	72	1497	cellular metabolic process
7533	3.94E-03	3.50E-02	3	9	mating type switching
7534	4.30E-03	3.73E-02	2	3	gene conversion at mating-type locus
48478	4.30E-03	3.73E-02	2	3	replication fork protection
6412	4.34E-03	3.73E-02	13	150	translation
50789	4.45E-03	3.77E-02	38	666	regulation of biological process
16043	4.69E-03	3.93E-02	34	578	cellular component organization
33044	5.10E-03	4.18E-02	5	30	regulation of chromosome organization
30466	5.15E-03	4.18E-02	4	19	chromatin silencing at silent mating-type cassette
7093	5.15E-03	4.18E-02	4	19	mitotic cell cycle checkpoint
8152	5.35E-03	4.28E-02	73	1539	metabolic process
50794	5.48E-03	4.34E-02	37	651	regulation of cellular process
40029	5.58E-03	4.37E-02	7	57	regulation of gene expression, epigenetic

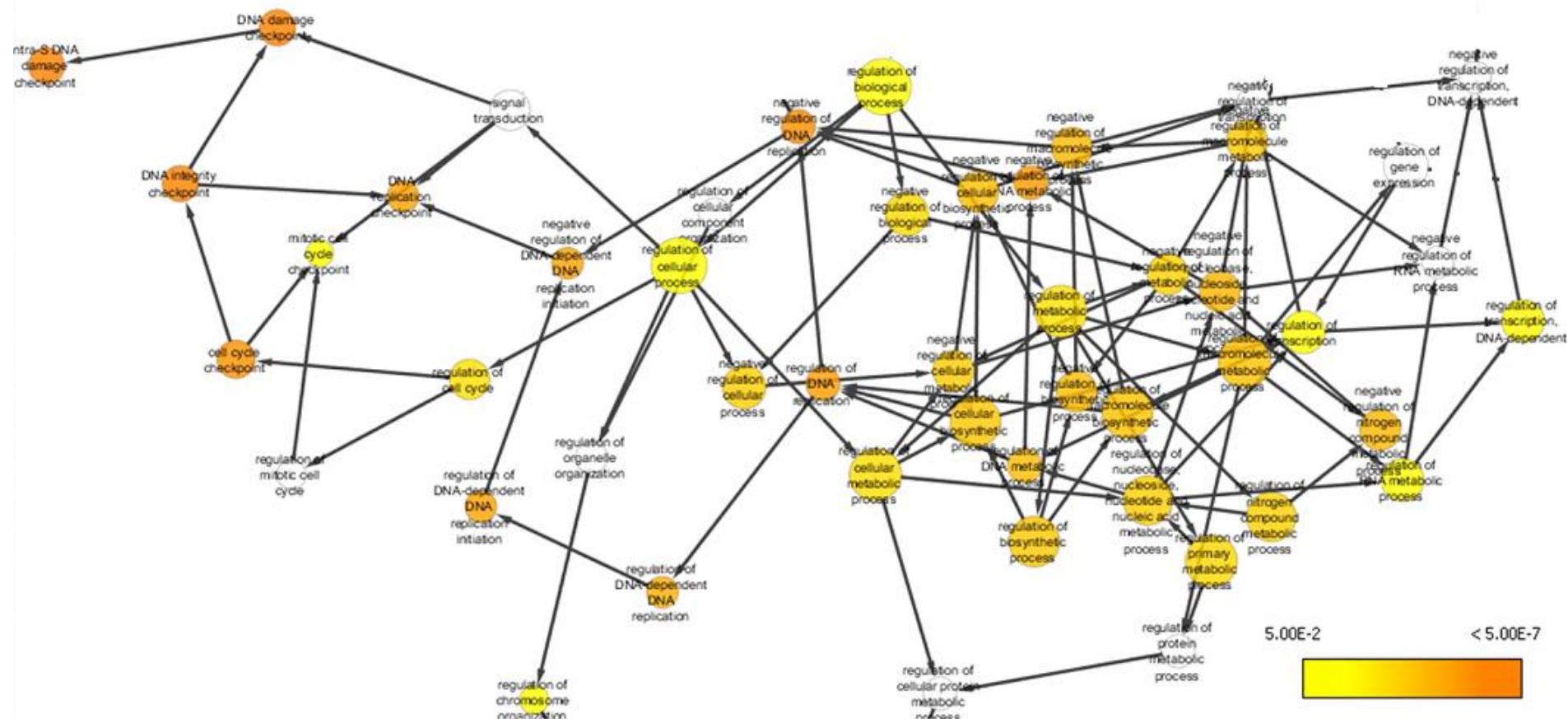


Figure 4-6 A screenshot of a biological network as generated by Cytoscape. The Image shows a section of Cytoscape output of over-represented biological processes in the first 114 most sensitive mutants of the sub library. Over-represented processes are coloured and the legend for colours is given in the right corner.

4.5 Discussion

High throughput screening is widely used in *S. pombe* to identify novel genes that may play a role in the response to drugs. We have used a *S. pombe* genome wide deletion library (Bioneer V2) to identify genes that respond to GemC treatment. The library was crossed to a strain containing the human *hsdCK* kinase and hENT1 transporter and screened with 500nM of GemC. 15% of genes (456 genes out of 3004 genes from the library) were visually identified as sensitive to the drug in at least one out of three independent screens and were further analysed as “sub library”. Three concentrations (50, 150 and 250nM) of the drug were used to quantify sensitivities of the different mutants and sensitivity was determined by calculation of area under growth curves. The mutants were classified according to their sensitivity [$S = \Delta G/G = (G_u - G_t)/G_u$] at 50nM. Optimization of methods tested to rank the sub library is detailed in paragraph 4.2.

Expectedly and supportive to results in chapter 5, DNA repair mechanisms were over-represented in the set of sensitive mutants (Table 4-5, GO analysis) emphasizing the role of repair mechanisms in response to GemC. Other over-represented processes included DNA damage checkpoint processes which, were also strongly expected.

4.5.1 Specific mutants from the library screen

Several identified genes play a known role in DNA repair further supporting the role of the mechanism in response to GemC treatment (The role of DNA repair in response to GemC and AraC is largely covered in chapter 5). Amongst isolated DNA repair genes that were also identified in other *S. pombe* genome wide screens to DNA damaging agents (Deshpande *et al.*, 2009), *mre11^{rad32}*, *pnk1*, *rhp54* and *mms22* (also known as *mus7*) were identified as sensitive to CPT, MMS, 4-NQO, inducing base adducts and top1 cleavable complexes (Miao *et al.*, 2006), and HU, while *srs2* was identified as sensitive to CPT and 4-NQO (Deshpande *et al.*, 2009). In addition we have identified *mms19*; *rad50* and *nbs1* as highly sensitive to GemC. The role of MRN (*mre11*, *rad50*, *nbs1*) complex in DNA repair is extensively discussed in chapter 5. *mms22* has shown a role in repair of DSBs and *mms22*Δ mutants are hypersensitive to DNA damaging agents CPT, MMS and HU (Dovey and Russell, 2007). In addition, genetic interactions between *mms22* and HR genes suggested that *mms22* acts as a substitute in the absence

of the HR repair (Dovey and Russell, 2007). Amongst HR genes which interacted with *mms22*, *rad22* and *rph54* were also identified as sensitive to GemC in this screen. Pnk1 is the *S. pombe* homologue of the human PNKP gene and possesses a 5' DNA kinase and 3' DNA phosphatase activities. Pnk1 is thought to be required for repair of DNA strand breaks by generating 5' phosphate and 3' hydroxyl ends required by DNA ligase (Meijer *et al.*, 2002). The role of PNK1 in DNA strand breaks repair is supported by the observation that *pnk1Δ* mutants are hypersensitive to DNA damaging agents CPT and γ -radiation (Meijer *et al.*, 2002). High sensitivity of *pnk1Δ* mutants to GemC might indicate that similarly to CPT and γ -radiation, GemC induces DNA breaks that require Pnk1 to generate compatible ends. Srs2 is a helicase which has shown a role in survival of cells to UV in *S. pombe* (Wang *et al.*, 2001). The precise role of the helicase in the cells survival is however not clearly established. *S. cerevisiae* Srs2 has shown multiple roles in genome maintenance, including replication fork checkpoint, DSB repair by HR and NHEJ and PRR (Marini and Krejci, 2010). The sensitivity of *srs2Δ* mutants to GemC suggests a role of the helicase in response to the drug but further analysis are required to establish the role of the helicase in response to the NA. Surprisingly, with the exception of *mms19* (Kou *et al.*, 2008), we did not isolate genes which play a role in nucleotide excision repair. Indeed due to the fact that GemC is a nucleoside analogue, we were expecting NER genes to be actively involved in survival to the drug. Several NER mutants however were individually confirmed by spot test as sensitive to GemC and AraC (discussed in chapter 5). *mms19 Δ* mutants were not previously isolated in other screens which, indicates that the response of *mms19* might be GemC-related. BER repair was poorly represented with only *ung1* glycosylase identified as sensitive to GemC (classified at position 72 out of 456 to the sensitivity at 50nM). *apn2* and *rad2* nucleases were also isolated in the large screen but they were ranked low in the sub library (*apn2*: 365 at 50nM, 382 at 150nM and 209 at 250nM; *rad2*: 348 at 50nM, 410 at 150nM and 403 at 250nM) suggesting that the mutants are not highly sensitive to GemC. Sensitivity of *apn2* however was confirmed by spot tests as *apn2Δ* mutants were highly sensitive to GemC and AraC. On the other hand *ung1Δ* mutants were resistant to both drugs (chapter 5). None of the MMR and PRR genes were isolated in the screen indicating that the mutants are not sensitive to GemC.

In addition to DNA repair genes, we have also isolated several genes which play a role in the DNA damage checkpoint. The role of the DNA damage checkpoint was also strongly expected, as other studies have shown a role of the machinery in sensitivity to GemC in a human cell line (Ewald *et al.*, 2008b). Isolated DNA damage checkpoint mutants include the *rad9-hus1-rad1* complex, *rad17*, *rad26*, *rad3*, *mrc1*, *cds1*, *crb2* and the replication checkpoint *swi3*. However, it is worth noting that the DNA damage checkpoint effector *chk1* was not isolated in the screen, probably due to the fact that *chk1Δ* mutant is not present in the deletion library. All the isolated checkpoint mutants were also identified in other screens (Deshpande *et al.*, 2009; Pan *et al.*, 2012) and confirm the role of the checkpoint in response to DNA damaging agents. Comparability between our screen and other screens to DNA damaging agents indicates the accuracy of the screen. However the fact that genes that were not identified in the screen were found sensitive by quantitative assays (spot test) suggest that the screen is less sensitive than these assays or that mutants in the library are not correct.

In the quest to understanding the complex response of cells to GemC treatment, we have isolated several genes of the chromatin remodelling Ino80 complex (*iec1*, *iec3*, *ies2*, *ies4*, *ies6*, *nht1* and *arp8*) which peaked our curiosity as it suggested that the mechanism might respond to the drug. Analysis of *S. cerevisiae* has shown that deletion in Ino80 complex genes *ino80*, *arp8* and *arp5* results in hypersensitivity of cells to DNA damaging agents HU and MMS (van Attikum *et al.*, 2004). Additionally the study showed that the complex is recruited at DSB site by the H2A histone. Consistently another study has shown that histone H2AX is phosphorylated in response to GemC in mammalian cells (Ewald *et al.*, 2007) and we have also isolated histone H2A variant, H2A-alpha, *hta1Δ* mutant in our screen (208 at 50nM). Together, these data suggest a role of the Ino80 complex and histone H2A in response to GemC and further analysis of the Ino80 complex might help to elucidate the nature of GemC-DNA induced damage. Indeed as the complex has been suggested to localise at DSBs (van Attikum *et al.*, 2004), response of the complex to GemC might indicate that the drug induces similar breaks. In addition, Ino80 is a chromatin remodelling protein complex (van Attikum *et al.*, 2004) and sensitivity of the mutants to GemC and AraC (e.g: analysis of *arp8* growth curves, *Figure 4-7A*) might indicate that chromatin remodelling is involved in

response to the NAs. Considering that NAs treatment may impede replication and that DNA repair mechanisms have been shown to play a role in responding to the drugs, the high sensitivity of a mutant deficient in chromatin remodelling might be of a particular interest in the quest to understanding the complex cellular response to NA induced lesion.

Following the interest of NA in interfering with DNA replication, we have isolated replication genes *ssb3* (*rpa3*) and *ctf8*. These genes were also identified as sensitive to CPT, MMS, 4-NQO and HU, DNA damaging agents which inhibit replication (Deshpande *et al.*, 2009). This concordance in results is in line with the idea that GemC indeed acts by interfering with DNA replication. In addition we have isolated DNA replication checkpoint gene *swi3* (also identified for sensitivity to CPT and HU, Deshpande *et al.*, 2009) which further supports impediment of replication by GemC. *swi3* also showed sensitivity to AraC (Figure 4-7B), supporting the hypothesis that the AraC interferes with DNA the replication. *swi3* (human homologous Tipin) forms a complex with *swi1* (human homologous Timeless) which protects replication forks in fission yeast (Noguchi *et al.*, 2004). Maintenance of replication forks by *swi3* is replication-checkpoint dependent (shown by analysis of *cds1Δ* and *chk1Δ* mutants) to protect stalled forks but it is checkpoint independent in response to collapsed forks (Rapp *et al.*, 2010). Further analysis of the gene in combination with the checkpoint mutants might be indicative to the action of NAs on replication fork (stalled or collapsed fork), which presents an interest for understanding the nature of NA-induced damage. Indeed if checkpoint defective (for example *cds1Δ/swi3Δ* double mutants) are more resistant to NAs than *swi3Δ* single mutants, it would indicate that NA leads to stalled replication as the response of *swi3* would require presence of checkpoint. On the contrary if *cds1Δ/swi3Δ* double mutants show a similar sensitivity as *swi3Δ* single mutants, results would indicate that NAs lead to collapsed replication fork as *cds1* is not required for *swi3* response. The *swi3* gene is hence a particularly interesting gene that could help to elucidate the nature of NA-induced DNA damage.

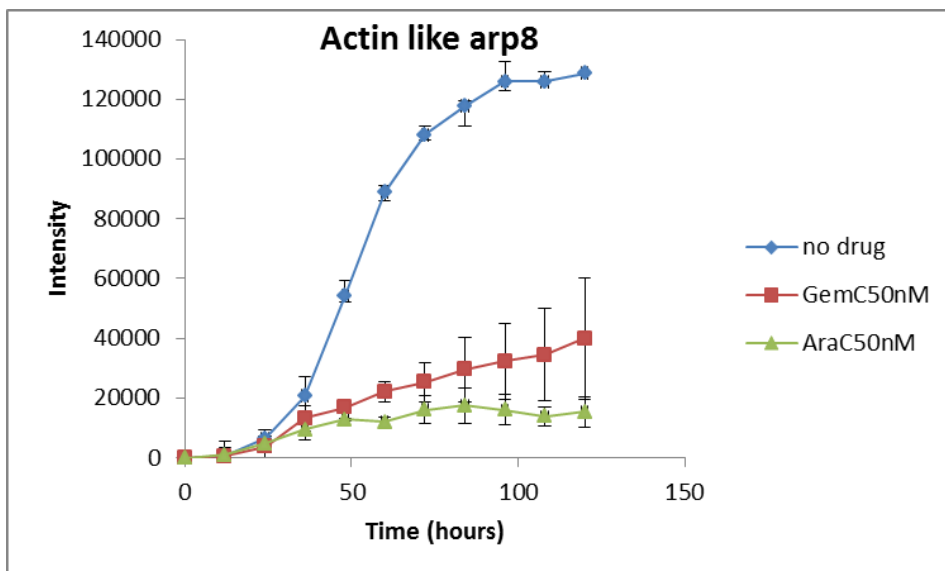


Figure 4-7A. *Actin like protein arp8 is sensitive to GemC and AraC.* Growth curves of the mutant exposed to 50nM of GemC and AraC showed high sensitivity of the mutant to both drugs. Standard errors were calculated from three experiments.

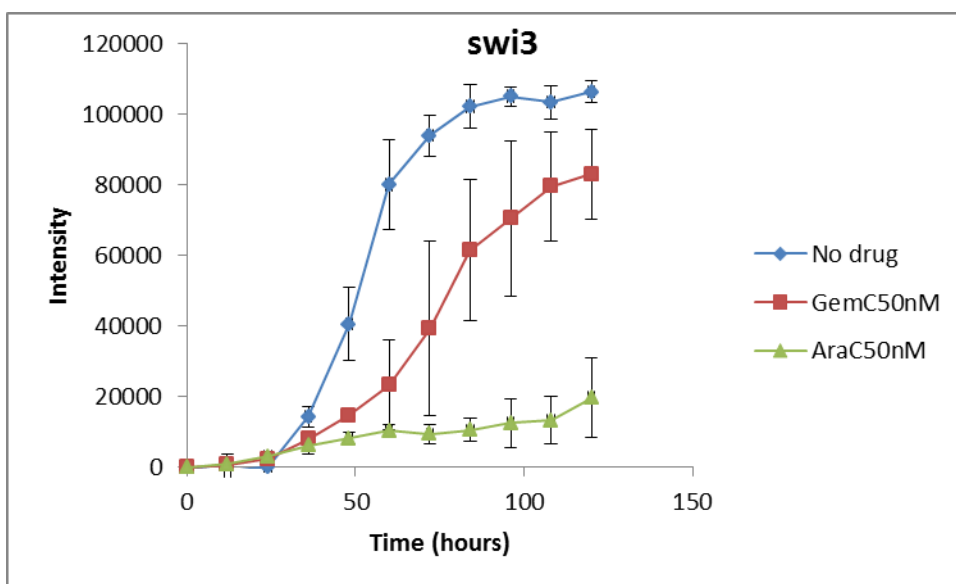


Figure 4-7B. *swi3 is sensitive to GemC and AraC.* Growth curves of the mutant exposed to 50nM of GemC and AraC showed high sensitivity of the mutant to both drugs. Standard errors were calculated from three experiments.

4.5.2 Analysis of sequence orphan genes

We have isolated 20 sequence orphan genes that were sensitive to GemC and are only found in *S. pombe* (data from *S. pombe* database, PomBase, <http://www.pombase.org/>). Four of those genes (SPBC651.06, SPAC13C5.06c, SPAC1A6.08c and SPAC5D6.02c) were described as meiotic up regulated genes, mug166, mug121, mug125 and mug165 respectively but are not characterised yet. Three of the genes were found to be sensitive to other DNA damaging agents and further supported similarities between GemC and other DNA damaging agents. These are: SPCC736.02, SPCC4F11.03c and SPBC16G5.06, sensitive to CPT (PomBase) and SPAC4D7.07c, sensitive to Thiabendazole, TBZ, toxic for microtubules and is used to check spindle checkpoint (Pan, Lei *et al.*, 2012) (PomBase). Table 4-6 below summarizes analysis of sequence orphan genes. It would be interesting to characterise the highly sensitive of these sequences, for example SPBC1A4.04 (64), SPCC18B5.09c (80) and SPAC17A2.10c (157) and assess their potential function and role in sensitivity to GemC and other NAs.

Table 4-6 List of sequence orphan genes that were sensitive to GemC.

Gene ID	Gene name	rank 50nM	Gene description	Description PomBase
SPBC1A4.04		64	sequence orphan	unknown
SPCC18B5.09c		80	sequence orphan	unknown
SPAC17A2.10c		157	sequence orphan	unknown
SPCC4F11.03c		186	sequence orphan	sensitive to DNA damaging agents
SPBC16G5.06		203	sequence orphan	sensitive to DNA damaging agents
SPBC651.06	mug166	212	sequence orphan	meiotic upregulated gene
SPAP27G11.14c		213	sequence orphan	unknown
SPAC13C5.06c	mug121	229	sequence orphan	meiotic upregulated gene
SPBC146.02		262	sequence orphan	unknown
SPBC23G7.14		274	sequence orphan	unknown
SPAC1786.04		281	sequence orphan	unknown
SPAC1A6.08c	mug125	282	sequence orphan	meiotic upregulated gene
SPAC922.04		287	sequence orphan	unknown
SPAC5D6.02c	mug165	313	sequence orphan	meiotic upregulated gene
SPAC30D11.02c		330	sequence orphan	unknown
SPAC17C9.15c		340	sequence orphan	unknown
SPCC736.02		364	sequence orphan	sensitive to DNA damaging agents
SPBC12C2.01c		392	sequence orphan	unknown
SPAC4D7.07c		413	sequence orphan	sensitive to Thiabendazole (TBZ)
SPBP22H7.04		418	sequence orphan	unknown

4.5.3 Conclusion

In summary, analysis of the genome wide deletion library strongly indicated a role of DNA damage checkpoint and DNA repair mechanisms in response to GemC. Most of identified genes were also found in other screens in response to DNA damaging agents which endorsed accuracy of the screen and suggested similarities between GemC and other DNA damaging agents, notably CPT and HU which also inhibit DNA synthesis. In addition, the analysis showed the wide response of cells to GemC treatment and identified new genes which might present a particular interest for further understanding the action of the drug. These include the Ino80 complex which might allow identify if chromatin remodelling is involved in response to GemC and *swi3* gene, which in combination with checkpoint mutants, might allow differentiate whether GemC incorporation leads to stalled or collapsed replication fork. Further characterisation of the highly sensitive sequence orphan genes SPBC1A4.04, SPCC18B5.09c and SPAC17A2.10c might also help to identify new genes and their function in response to NAs.

5 Repair of NA-induced DNA damage

Multiple cellular mechanisms might act in response to NA induced damage. In this PhD project, I aimed to identify and characterise DNA repair mechanisms that might interfere with sensitivity of cells to GemC and AraC using *S. pombe* DNA repair defective mutants. Studies have shown a coordinated response of repair mechanisms to NA (Ewald *et al.*, 2008b, Wang *et al.*, 2008), however, little is known about these responses. Distinct DNA repair mechanisms may act to repair GemC and AraC induced DNA damage depending on the nature of the damage (DSBs, SSBs, mismatches or incorporated nucleoside analogues). Although it is clear now that GemC and AraC kill proliferating cells by inhibiting DNA synthesis, the exact nature of drug-induced DNA damage is not fully understood. As both NAs lead to replication fork stalling (Galmarini *et al.*, 2001; Jordheim *et al.*, 2005), it is thought that when replication forks run into the drugs, they might induce DSBs as it has been shown that stalled replication forks can lead to formation of DSBs if the fork collapses (Branzei and Foiani, 2005). There is however no direct evidence that GemC or AraC causes DSBs. Organisms have evolved mechanisms to protect the genome when DSBs occur and, along with the replication checkpoint, homologous recombination (HR) repair is believed to be an important pathway which deals with DNA damage following replication arrest (Lambert *et al.*, 2007). The observation that histone H2AX, which is involved in DSB repair by homologous recombination (Xie *et al.*, 2005), is phosphorylated following treatment with GemC in mammalian cells (Ewald *et al.*, 2007) might indicate that HR responds to GemC induced DNA damage. The involvement of HR in response to GemC is also supported by observation that GemC increases radio sensitivity of mammalian cell lines probably by competing for HR repair (Wachters *et al.*, 2003). HR is carried out by members of the evolutionary conserved Rad52 epitasia group including the *S. pombe rad52* homologue *rad22*, *rad51* and the MRN complex. Although not a core HR complex, the involvement of MRN in the first steps of HR has been confirmed in several studies (Symington, 2002, Hartsuiker *et al.*, 2009a). The complex has shown a role in resistance to other DNA damaging agents which interfere with replication such as CPT by removing the top1 covalent complex from the DNA (Hartsuiker *et al.*, 2009b and

detailed in paragraph 1.2.1.3). We have hence hypothesised that similarly MRN might respond to NA treatment by removing the NAs from the DNA and allowing subsequent repair, and investigated the possible role of the MRN complex in response to GemC and AraC.

5.1 MRN-CtIP^{Ctp1} complex mutants are highly sensitive to GemC and AraC

The MRN (Mre11, Rad50 and NBS1) complex and its associated protein CtIP (*S.pombe* Ctp1) are extensively discussed in paragraph 1.1.3.3.2. To assess a possible role of the MRN-CtIP complex in survival to NA treatment, we used spot tests to determine the sensitivity of MRN deleted mutants (*rad50*Δ and *nbs1*Δ), *mre11* nuclease dead (*mre11-D65N*) and *ctp1*Δ in *hsdCK* and *dmdNK* with and without the hENT1 transporter to both GemC and AraC. *mre11-D65N* is a point mutation which abolishes the nuclease activity and has been used to determine the role of the nuclease in response to anti-cancer drugs such as camptothecin (Hartsuiker *et al.*, 2009b). First we tested sensitivity of *rad50*Δ and *mre11-D65N* mutants to GemC in absence of the transporter, and results showed that both mutants were more sensitive to the drug than the WT (*Figure 5-1*). The sensitivity was higher in *rad50*Δ mutants when compared to the sensitivity of the nuclease dead mutant. Both mutants showed a higher sensitivity in presence of the *Drosophila* kinase when compared to sensitivity in *hsdCK* cells.

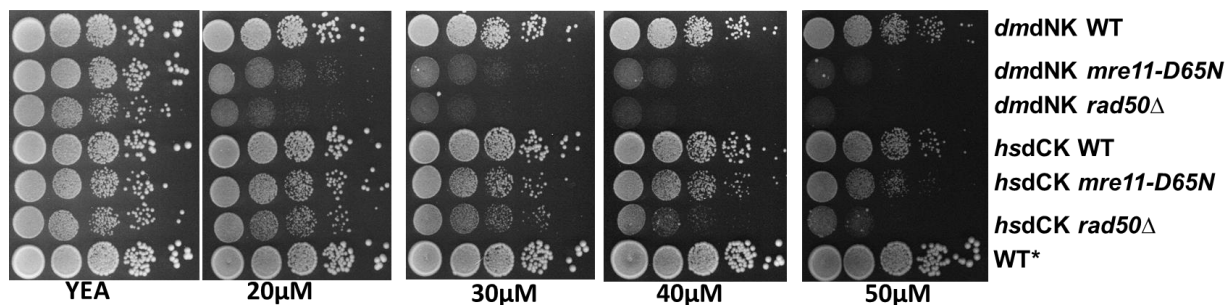


Figure 5-1 *rad50Δ* and *mre11-D65N* mutants without transporter were more sensitive to *GemC* than the *WT*. Cells with *hsdCK*, *rad50Δ* (MG178) and *mre11-D65N* (MG177) and cells with *dmdNK*, *rad50Δ* (MG176) and *mre11-D65N* (MG175) were tested. Cells were tested on YEA with *GemC* and incubated for 4 days at 30°C. Cells were diluted over a range of 10^5 to 10 cells per spot. WT* without transporter and kinase was tested as a control. *rad50Δ* showed high sensitivity to the drug, *mre11-D65N* is more sensitive than WT. The experiment was repeated two times giving similar results.

To confirm the observed sensitivity, we tested the mutants in presence of the transporter. Due to the observation that YE media affected growth of cells with hENT1 (described in paragraph 3.3.1), all mutants containing the transporter were tested in EMM media. In addition, because nucleoside/nucleotide metabolism might be affected by deletion of *ura4* gene (as the kinases and transporter were integrated into *ura4* locus) and interfere with the NAs, I have used *ura4-aim* strain to integrate *ura4* gene. In *ura4-aim*, the *ura4* coding sequence is integrated at a non-coding region 15kb upstream of *ade6* (Grimm *et al.*, 1994). All mutants containing the transporter are consequently in *ura4+* background (*ura4-aim* or URA4 as a marker for gene deletion).

As shown in *Figure 5-2*, MRN deleted mutants containing the human, *hsdCK* (A) or the *Drosophila*, *dmdNK* (B) kinases and the transporter showed a high sensitivity to GemC and AraC. Compared to WT cells, *mre11-D65N* mutant showed less sensitivity than *rad50Δ*, *nbs1Δ* and *ctp1Δ* mutants. Sensitivity to CPT confirmed that the mutants were MRN defective. In comparison to observed high sensitivity of *mre11-D65N* containing only the kinase, *mre11-D65N* cells with the kinase and the transporter only showed a mild sensitivity in comparison to WT cells.

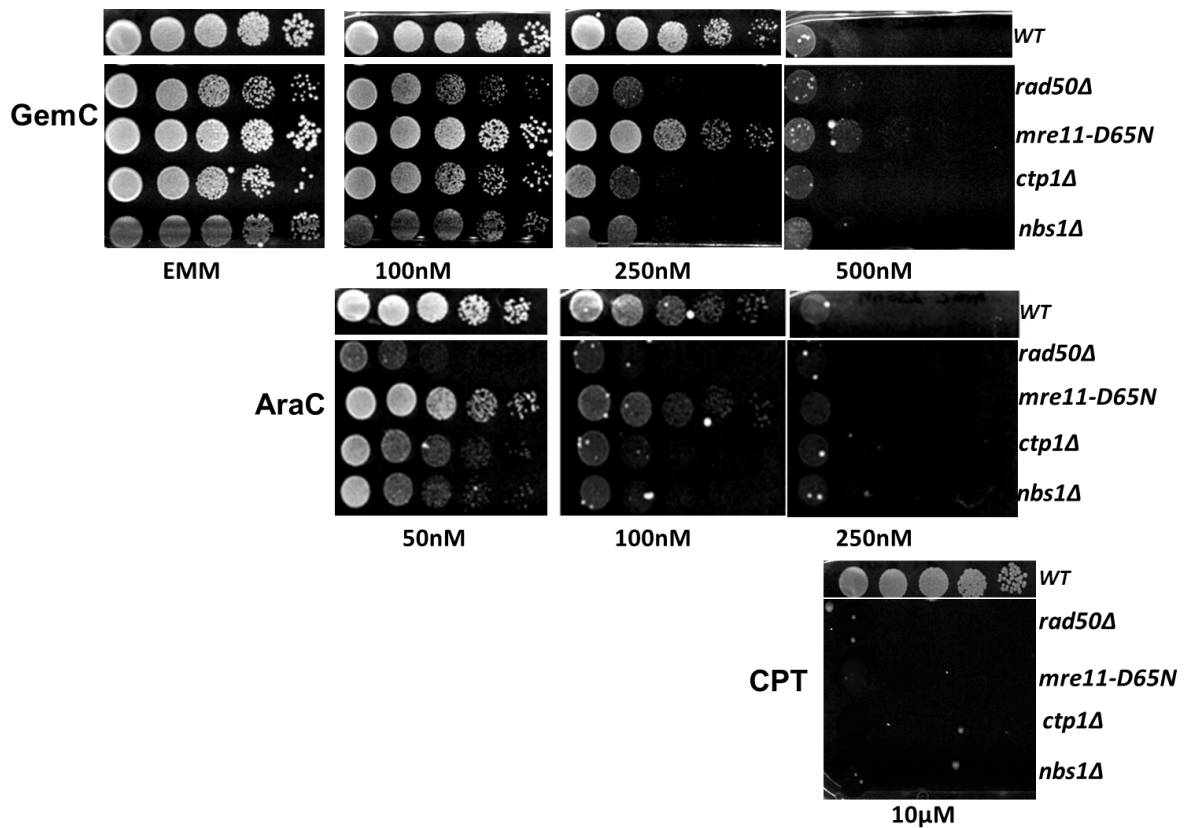


Figure 5-2A. MRN mutants with *hsdCK/hENT1* were sensitive to *GemC* and *AraC*. *rad50Δ* (MG119), *mre11-D65N* (MG297), *nbs1Δ* (MG295) and *ctp1Δ* (MG131) were tested. Cells were diluted over a range of 10^5 to 10 cells per spot, spotted on minimal (EMM) media with different concentrations of either drug and incubated for 5 days at 30°C. WT (MG85) was used as a control. Strains were also spotted on camptothecin (CPT) as positive control for MRN mutants. *ctp1Δ* and MRN null mutants (*rad50Δ*, *nbs1Δ*) showed high sensitivity compared to the WT, *mre11* nuclease dead mutants were slightly more sensitive than the WT but less sensitive than other MRN mutants. *rad50Δ* and *ctp1Δ* mutants were tested 4 times and were sensitive in all 4; *mre11-D65N* was tested 2 times and showed the same results and *nbs1Δ* was sensitive 2 times out of 3 tests. WT cells were spotted on same plates as the mutants.

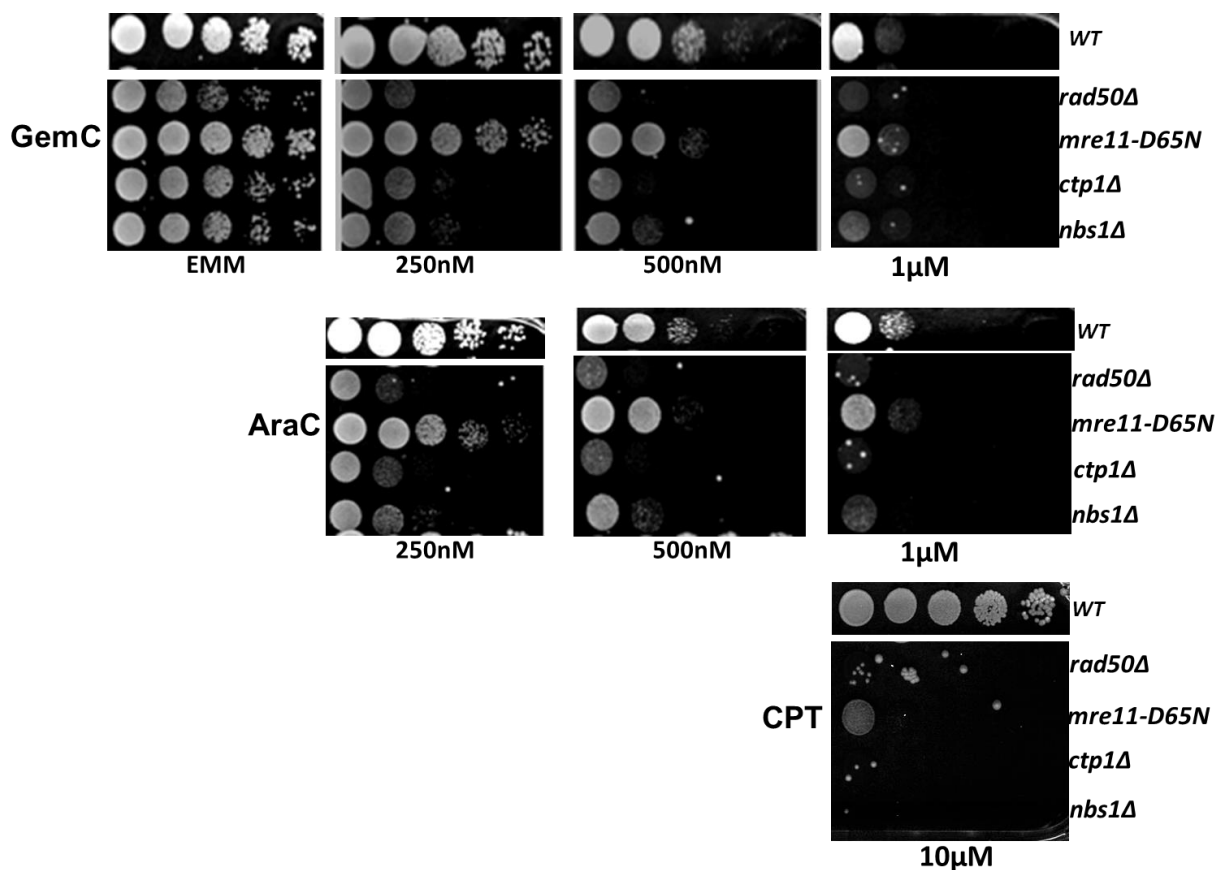


Figure 5-2B. MRN mutants with *dmdNK/hENT1* were sensitive to GemC and AraC. *rad50Δ* (MG117), *mre11-D65N* (MG121), *nbs1Δ* (MG293) and *ctp1Δ* (MG164) were tested. Cells were diluted to over a range of 10^5 to 10 cells per spot, plated on minimum (EMM) media with different concentrations of either drug and incubated for 5 days at 30°C. WT (MG83) was plated as a control. Strains were also plated on camptothecin (CPT) as positive control for MRN mutants. *ctp1Δ* and MRN null mutants (*rad50Δ*, *nbs1Δ*) showed high sensitivity compared to the WT, *mre11-D65N* was slightly more sensitive than the WT but showed less sensitivity when compared to *rad50Δ*, *nbs1Δ* and *ctp1Δ* mutants. *rad50Δ*, *ctp1Δ* and *nbs1Δ* were sensitive in all 3 tests whereas *mre11-D65N* mutants were sensitive twice out of three tests. WT cells were plated same plates as the mutants.

Additionally, it has previously been reported that GemC enhances formation of top1 mediated cleavage complexes and that resistance to the drug was increased in human cells deficient in top1 (Pourquier *et al.*, 2002). To exclude the possibility that the sensitivity of MRN mutants to GemC is caused by GemC-induced Top1 covalent complex formation, I tested if deletion of Top1 rescues GemC sensitivity in MRN defective cells.

As shown in *Figure 5-3*, *top1* Δ mutants are slightly more resistant to GemC when compared to WT (visible at 500nM), suggesting that, indeed, the enzyme might contribute to the drug sensitivity as its absence rescues cells. On the other hand, *top1* Δ *rad50* Δ displayed a same sensitivity to GemC as the *rad50* Δ single mutants. *top1* Δ and *top1* Δ *rad50* Δ mutants were highly resistant to CPT when compared to *rad50* Δ mutants suggesting that *top1* deletion rescues *rad50* deletion in response to CPT and, confirming that the cells are indeed *top1* defective. These results suggest that the observed sensitivity of *rad50* Δ mutants to GemC is not dependent on *top1*.

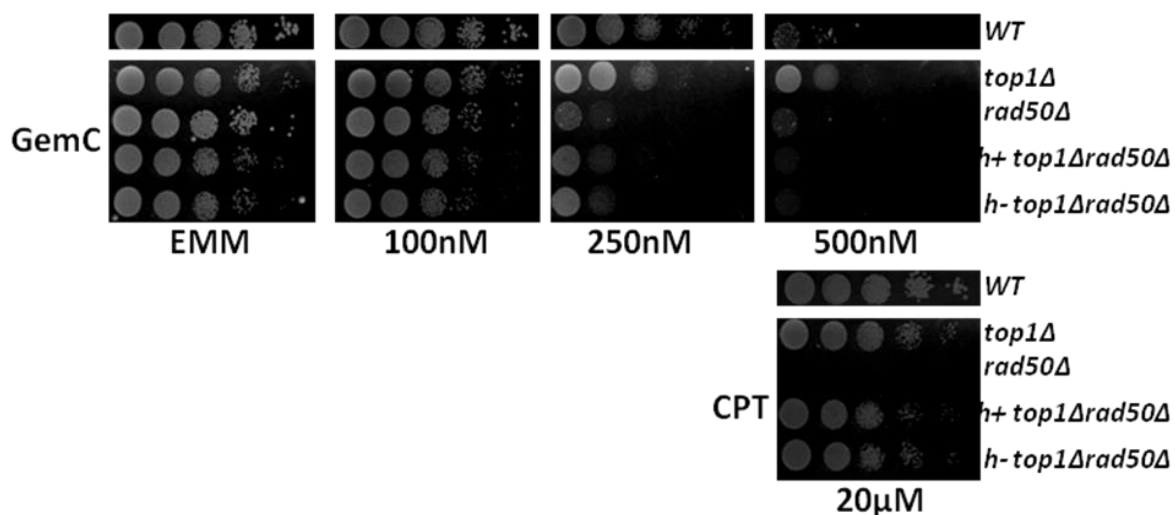


Figure 5-3 *top1* deletion does not increase resistance of *rad50Δ* mutant to *GemC* in cells with *hsdCK/hENT1*. *top1Δ* (MG281) and *rad50 top1* double mutants (*h+top1Δrad50Δ*, MG349 and *h-top1Δrad50Δ*, MG350) were tested on EMM containing different concentrations of *GemC*. WT (MG85) and *rad50Δ* (MG119) were tested as controls. Cells were also plated on high concentration of CPT to confirm mutations. *top1* deleted cells were slightly more resistant than the WT whereas the double mutants showed the same sensitivity as *rad50* deleted mutants. *top1Δ* and *top1Δrad50Δ* showed the same survival to CPT as the WT. Experiments were carried out once and WT strains were spotted on the same plates.

5.2 NER and BER mutants are sensitive to GemC and AraC treatment but MMR and PRR mutants are resistant to the drugs

Apart from HR, other repair pathways might act in response to NA induced lesions. A study by Moufarij *et al* (2003) showed that GemC suppresses repair of Cisplatin induced lesions which accumulate in GemC treated mammalian cells. Because Cisplatin induces DNA adducts that are generally repaired by NER (Basu and Krishnamurthy, 2010) the study by Moufarij *et al* might indicate that GemC-induced damage compete with Cisplatin induced adducts for NER repair. Apart from this study, there is no direct evidence in the literature linking NER to the repair of GemC-induced damage. Deletion of NER genes, CSB, XPB, XPF and ERCC1 have been shown to increase sensitivity to CNDAC (2'-C-cyano-2'-deoxy-1- β -D-arabino-pentofuranosylcytosine), a NA which acts by inducing single strand breaks (Wang *et al.*, 2008). It is not fully clear however what triggers NER response in CNDAC treated cells, the presence of modified nucleoside or the resulting single strand break. Although CNDAC and GemC and AraC-induced damage are of a different nature, it is possible that NER deals similarly with GemC and AraC-induced damage. In addition, it has been shown that AraC (Gmeiner *et al.*, 1998) and GemC (Konerding *et al.*, 2002) induce distortion of the DNA helixes, which might trigger NER response as it is now established that NER detects damage that disrupt the DNA-structure (reviewed by Fleck, 2004 and Fuss and Tainer, 2011). Moreover it has been suggested that GemC might induce mismatches (Robinson *et al.*, 2003) probably by disturbing dNTP pools as it has been shown that imbalanced dNTP pools lead to mismatch incorporation in *S. cerevisiae* (Kumar *et al.*, 2011). GemC can hence trigger MMR. Additionally, because NAs are incorporated during replication, NA treatment might also induce post replication repair which might occur in the second round of replication and act by bypassing incorporated NA. We assessed sensitivity of NER, BER, MMR and PRR mutants to treatment with GemC and AraC. As study of all mutants in both *hsdCK* and *dmdNK* backgrounds added a degree of complexity to the analyse, we have chosen to focus on the human kinase, firstly because of its specificity for the two deoxycytidine analogues studied in this project and secondly, because of its relevance to studies in humans.

5.2.1 *rhp14*, *rhp41/rhp42* and *swi10* defective mutants are highly sensitive to GemC and AraC but *rad13Δ* mutants are resistant to both drugs

NER is the main repair pathway for removing bulky lesions (notably caused by UV) from DNA and therefore constitutes an important protector of genome integrity. Two major pathways, which differ by the recognition of the damage, act in NER: Global Genome NER (GG-NER) and Transcription Coupled NER (TC-NER). We have tested the sensitivity of XPA^{*rhp14*} and XPC^{*rhp41/rhp42*} (in *S.pombe*, the activity of XPC is accomplished by two homologues *rhp41* and *rhp42*, Marti *et al.*, 2003) which are involved in recognition and verification of damage, and XPG^{*rad13*} and ERCC1^{*swi10*} which carry out incision at the damaged region. Previous studies showed that *rhp14Δ* (Hohl *et al.*, 2001), *rhp41Δ rhp42Δ* and *swi10Δ* (Marti *et al.*, 2003) and *rad13Δ* (McCready *et al.*, 1989) mutants showed increased sensitivity to UV when compared to WT cells, confirming that the genes are involved in NER repair. Results (Figure 5-4) showed that *rhp14Δ*, *rhp41Δ rhp42Δ* and *swi10Δ* mutants were highly sensitive to GemC and AraC when compared to WT cells. Sensitivity was higher in *rhp14Δ* compared to *rhp41Δ rhp42Δ* and *swi10Δ* mutants, and the sensitivity of *rhp14Δ* was more elevated on AraC compared to GemC. On the other hand, *rad13Δ* showed a similar survival to both drugs as WT cells. High sensitivity of all mutants to UV confirmed that the mutants were defective for NER.

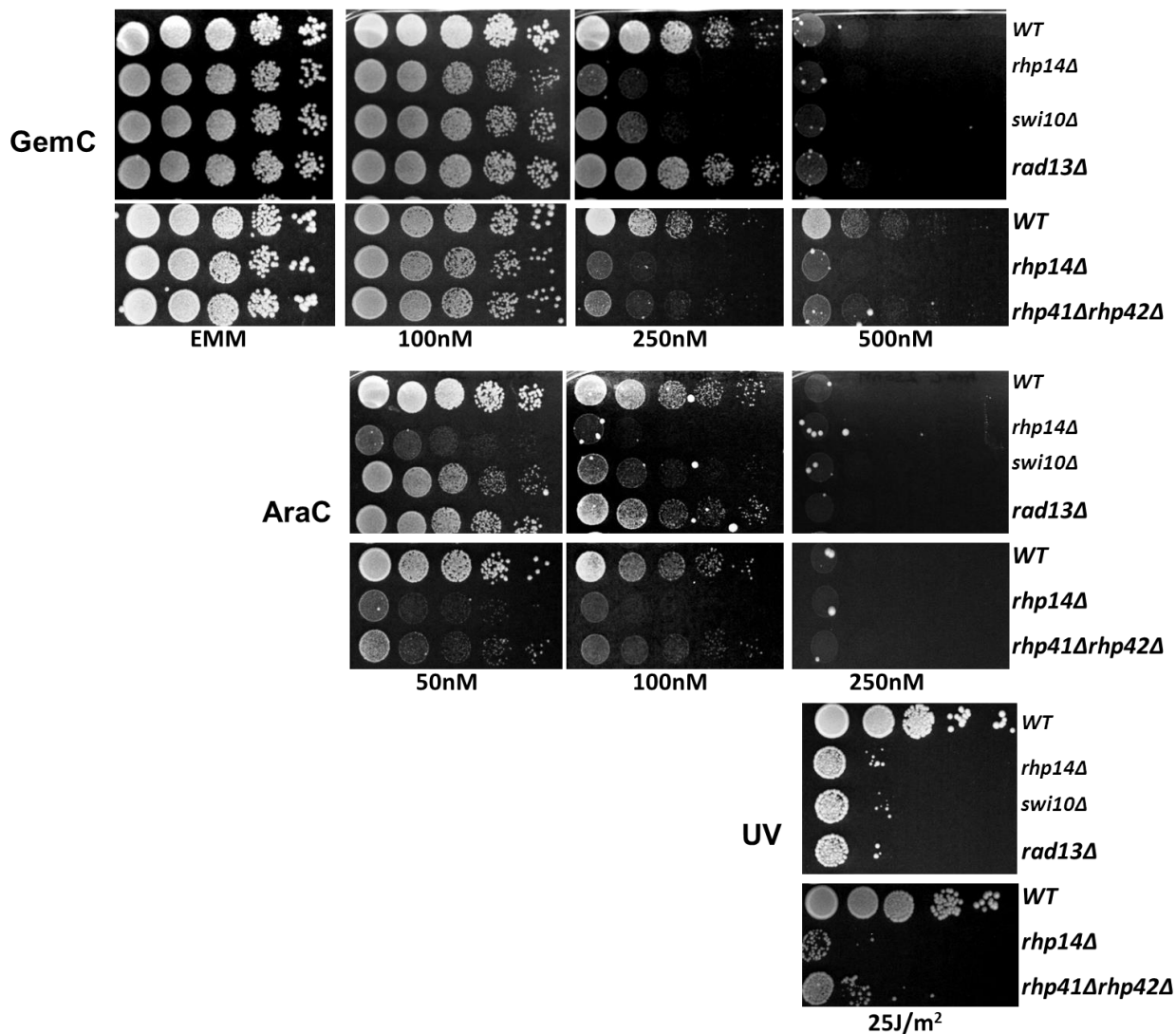


Figure 5-4 NER mutants with *hsdCK/hENT1* are sensitive to GemC and AraC. *rhp14Δ* (MG276), *rhp41Δrhp42Δ* (MG359), *swi10Δ* (MG107) and *rad13Δ* (MG111) were tested. Cells were spotted on minimum (EMM) media with different concentrations of both drugs and incubated for 5 days at 30°C. WT (MG85) was spotted as a control. Strains were tested with UV light as positive control for NER defective mutants. All the mutants, with the exception of *rad13Δ* mutants, showed high sensitivity to both drugs when compared to WT. *rhp14* mutants showed higher sensitivity than the two other mutants with a more noticeable sensitivity to AraC. *rad13Δ* mutant showed a same survival as WT cells. *swi10Δ* and *rhp14Δ* were sensitive in 7 out of 8 tests, *rad13Δ* was resistant in all 8 tests and *rhp41Δ rhp42Δ* was tested three times and sensitive in the 3 tests.

5.2.2 *nth1* and *apn2* mutants are highly sensitive to GemC and AraC

BER repairs base damage that results mainly from endogenous metabolic processes such as oxidation and deamination of bases (for example deamination of cytosine to uracil). To assess the potential role of the BER pathway, we investigated the role of *nth1* (involved in removal of oxidised pyrimidines) and *ung1* (removal of uracil) glycosylases as well as *rad2* (FEN-1 homologue) and *apn2* (AP endonuclease) nucleases in survival to GemC and AraC treatment. Apn2 processes the AP site to remove the abasic sugar-phosphate while Rad2 removes a flap before synthesis in the long patch BER repair pathway (see introduction, paragraph 1.1.3.3.1). The roles of *S. pombe nth1*, *apn2* and *rad2* in BER repair were confirmed by the high sensitivity of *nth1* Δ (Osman *et al.*, 2003; Sugimoto *et al.*, 2005), *apn2* Δ (Alseth *et al.*, 2004; Sugimoto *et al.*, 2005; Nilsen *et al.*, 2012) and *rad2* Δ (Kunz and Fleck 2001; Osman *et al.*, 2003) mutants to MMS, a DNA damaging agent that induces base damage. *S. pombe ung1* is not fully characterised but shows high homology to human UNG which suggests its role in removing uracil residues (Fleck, 2004; Kanamitsu and Ikeda, 2010). As both GemC and AraC are modified on the sugar moiety, and the base is unmodified, it might be expected that BER mutants would not be sensitive to GemC and AraC treatment. Surprisingly, as shown in *Figure 5-5*, *nth1* Δ and *apn2* Δ are highly sensitive to both GemC and AraC when compared to WT cells. Sensitivity of *apn2* Δ is higher to AraC than to GemC, whereas both *apn2* Δ and *nth1* Δ showed a similar sensitivity to GemC. In contrast, *ung1* Δ and *rad2* Δ mutants were slightly more resistant to both drugs when compared to the WT, the resistance was higher in *ung1* Δ mutants. *ung1* Δ and *rad2* Δ cells were however highly sensitive in comparison to WT without transporter and kinase, which confirmed that the transporter and kinase are present in the mutants, although they might not be fully functional due to presence of possible suppressors which might impede the function of either the transporter or the kinase (see discussion).

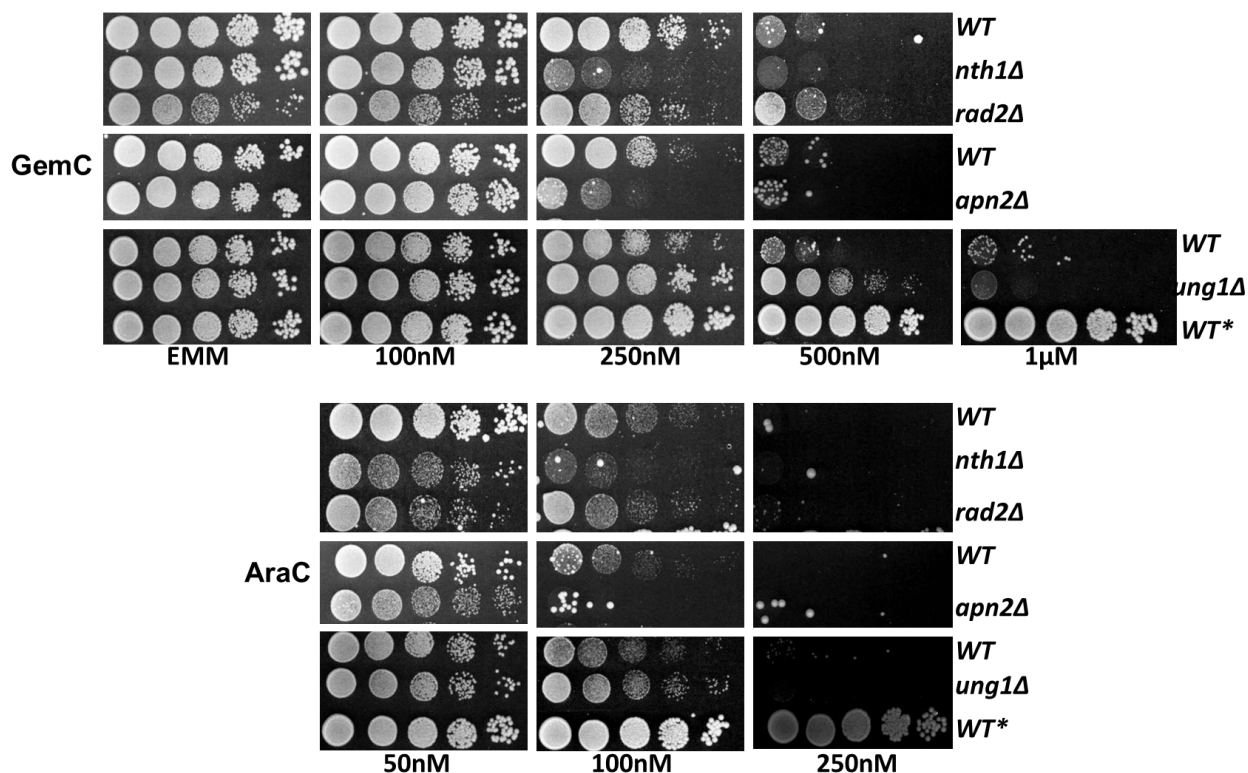


Figure 5-5 Sensitivity of BER mutants with *hsdCK/hENT1* to GemC and AraC. *nth1Δ* (MG274), *rad2Δ* (MG300), *apn2Δ* (MG319) and *ung1Δ* (MG309) were tested. Cells were spotted on minimum (EMM) media with different concentrations of both drugs and incubated for 5 days at 30°C. WT (MG85) and WT* without transporter and kinase (MG19) were used as a control. *nth1Δ* and *apn2Δ* mutants showed sensitivity to both drugs, whereas *rad2Δ* and *ung1Δ* mutants were not affected by the drugs. In contrary, *ung1Δ* mutants showed a resistant effect to both drugs when compared to the WT and *rad2Δ* was slightly more resistant to GemC than the WT but showed a similar growth to WT on AraC. Both *ung1Δ* and *rad2Δ* mutants are more sensitive than the WT* without transporter and kinase which confirms the presence of the transporter and kinase. *nth1Δ* was sensitive in 3 out of 3 tests, other mutants were tested 2 times.

5.2.3 Mismatch repair (MMR) defective mutants are more resistant to GemC and AraC compared to WT cells

MMR uses excision repair to remove mismatched bases and insertion/deletion loops (IDLs), resulting from errors by replication polymerases. We hypothesised that GemC might induce mismatches as it has been shown that GemC induces dNTP pools reduction through inhibition of RNR (Heinemann *et al.*, 1990) and that unbalanced dNTP levels can lead to mutations in the DNA in *S. cerevisiae* (Kumar *et al.*, 2011). In addition, analysis of human HCT1116 cells showed that GemC increases sensitivity of MMR-deficient cells to irradiation when compared to radio sensitivity in MMR-proficient cells (Robinson *et al.*, 2003). High sensitivity of HCT116 cells to irradiation in MMR-deficient GemC treated-cells was attributed to high levels of GemC- induced mutations into the DNA which, further sensitise cells irradiation treatment (Robinson *et al.*, 2003). These results indirectly suggest that MMR might deal with GemC induced DNA damage. The potential role of MMR in response to GemC and AraC was examined by testing MMR deleted mutants for sensitivity to both drugs. We analysed *msh2*, *msh6*, *mlh1*, *pms1* deleted mutants and, although not MMR specific, *exo1* was also analysed in this section. *S. pombe* Msh homologues Msh2 (also known as Swi8) and Msh6 recognise single mismatches and initiate the repair. The role of Msh2 and Msh6 in mismatch repair in *S. pombe* was shown by the increase of mutation rate in *msh2* Δ and *msh6* Δ mutants when compared to MMR proficient cells (Fleck, 2004). Mlh1 and Pms1 are *S. pombe* homologues of Mlh which act by coordinating interaction between the recognition heterodimers and other proteins. The role of the two proteins in mismatch repair was also revealed by increased mutation rate in *mlh1* Δ and *pms1* Δ mutants (Fleck, 2004). Exo1 removes the mismatch from the DNA and makes the nick available for subsequent repair. The role of *S. pombe* Exo1 in MMR was shown by its interaction with mismatch recognition protein Msh2 (Tishkoff *et al.*, 1997).

As shown in *Figure 5-6*, with the exception of *msh6* Δ which showed a similar survival to AraC as WT, all MMR mutants were more resistant to both drugs when compared to WT cells. The effect is less strong in *exo1* Δ mutants, which were only slightly more resistant than WT. *msh2* Δ mutants showed the highest resistance. The high sensitivity of the mutants compared to a wild type strain without the transporter and kinase suggested

that the transporter and kinase were present. A possible explanation to this resistance might be presence of suppressors (either in the kinase or the transporter) which would decrease drug sensitivity. Indeed it has been shown that MMR deficient mutants have an increased mutation rate which (Fleck, 2004), could suggest that mutations might have been induced in the transporter and/or kinase and affect their function. To exclude the possibility of presence of suppressors, backcrosses of the mutants to a WT strain with functional transporter and kinase should be carried out. Test of the progeny from the backcross for sensitivity to GemC and AraC would allow determine if suppressors are present. Indeed, if some MMR proficient strains resulting from the backcross show resistance to either drug in comparison to WT, it would indicate that suppressors have been introduced in either the kinase or the transporter (or both). Due to time constraints, I could not run this test and therefore cannot confirm that the observed resistance is due to MMR deficiency. However these preliminary results might suggest a role of the MMR in increasing GemC and AraC toxicity.

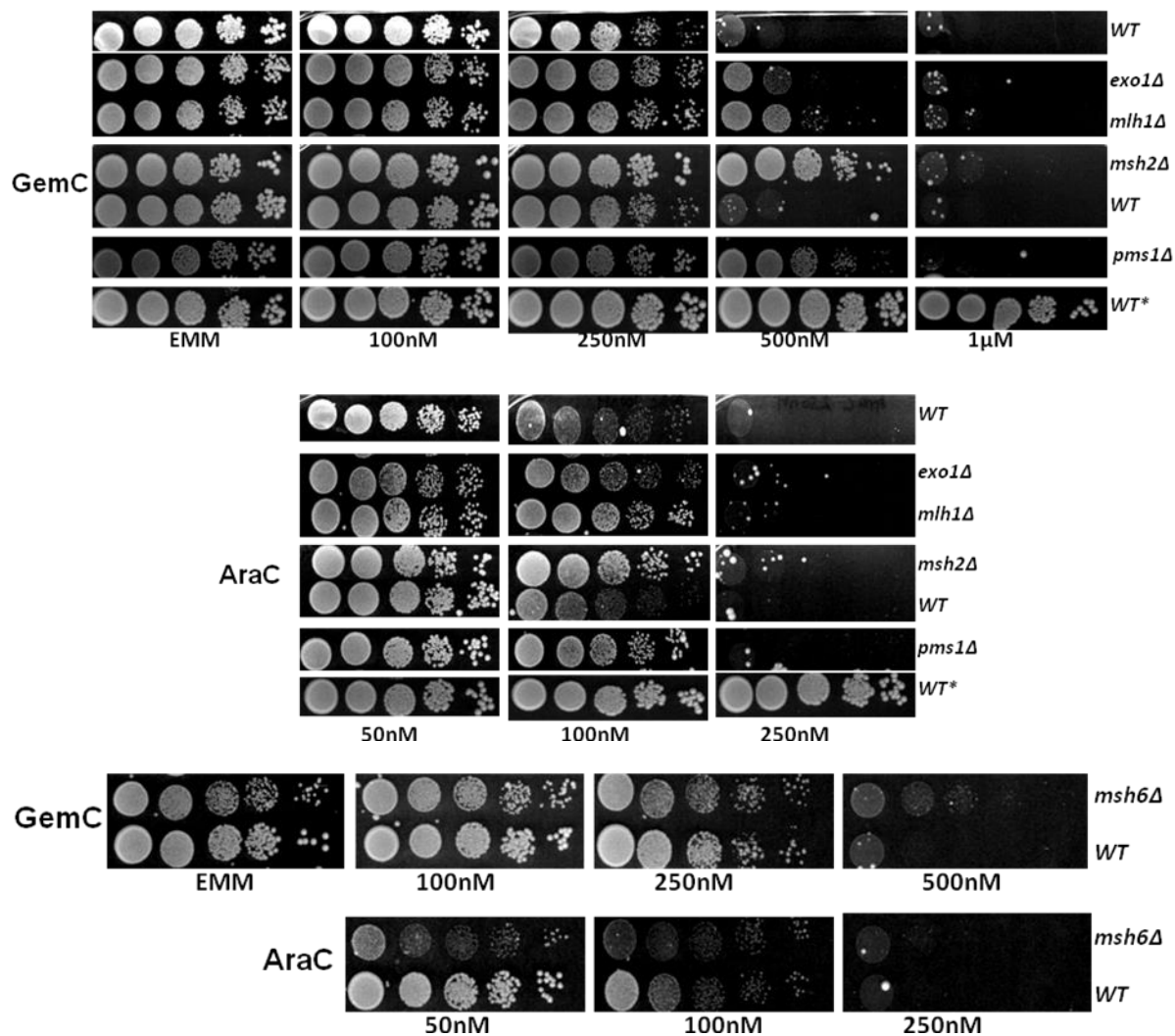


Figure 5-6 MMR mutants with *hsdCK/hENT1* are resistant to *GemC* and not to *AraC*. *exo1Δ*, (MG273), *mlh1Δ* (MG270), *msh2Δ* (MG303), *pms1Δ* (MG328) and *msh6Δ* (AK119) were tested. Cells were spotted on minimum (EMM) media with different concentrations of either drug and incubated for 5 days at 30°C. WT (MG85) and WT without transporter and kinase (WT*, MG19) were plated as controls. All mutants showed resistance to both drugs when compared to WT. Cells were more sensitive than the wild type without transporter and kinase (WT*) which confirmed the presence of the transporter and kinase in the mutants. *mlh1Δ* and *exo1Δ* results were reproducible in three tests, other mutants were tested two times and gave similar results.

5.2.4 Post replication repair (PRR) mutants are not sensitive to GemC and AraC

Because GemC and AraC are incorporated during DNA replication, we evaluated the possible role of PRR in response to the two drugs. One of the PRR mechanisms is translesion synthesis (TLS) which allows cells to bypass replication blockage by switching from high fidelity replication polymerases to error prone TLS polymerases (detailed in introduction, paragraph 1.1.3.4). We assessed the role of TLS polymerase zeta ($\text{pol}\zeta$) which extends the DNA opposite the site of the lesion. $\text{Pol}\zeta$ is formed of two subunits: the catalytic Rev3 subunit and the accessory Rev7 subunit. Disruption of the *rev3* in mice leads to lethality during development, illustrating the importance of the gene (Gan *et al.*, 2008). We have tested sensitivity of *rev3* Δ mutants to GemC and AraC and, as show in *Figure 5-7*, *rev3* Δ mutants showed a same survival as WT to both drugs.

Another protein involved in PRR is Rhp18 (*S. pombe* homologue of the *S. cerevisiae* Rad18), which carries out monoubiquitination of PCNA and allows choice of appropriate PRR pathway. Indeed, in *S. cerevisiae*, PCNA monoubiquitination by the Rad18/Rad6 complex leads to error prone TLS, while further polyubiquitination by Rad5 favours the error free template switch (Lee and Myung, 2008 and detailed in paragraph 1.1.3.4). *S. cerevisiae rad18* (Broomfield *et al.*, 2001) and *S. pombe rhp18* (Verkade *et al.*, 2001) defective mutants were sensitive to DNA damaging elements such as UV, suggesting the role of the gene in DNA repair. We tested *rhp18* Δ mutants for sensitivity to GemC and AraC and, as shown in *Figure 5-7*, *rhp18* Δ mutants are slightly more resistant than the WT to both drugs suggesting that the gene might improve drug activity. A potential explanation to this resistance might be that the presence of TLS favors NA DNA-incorporation which, in the long term, becomes lethal to the cells while in the absence of the tolerance pathway DNA repair mechanisms might deal with the drug induced damage.

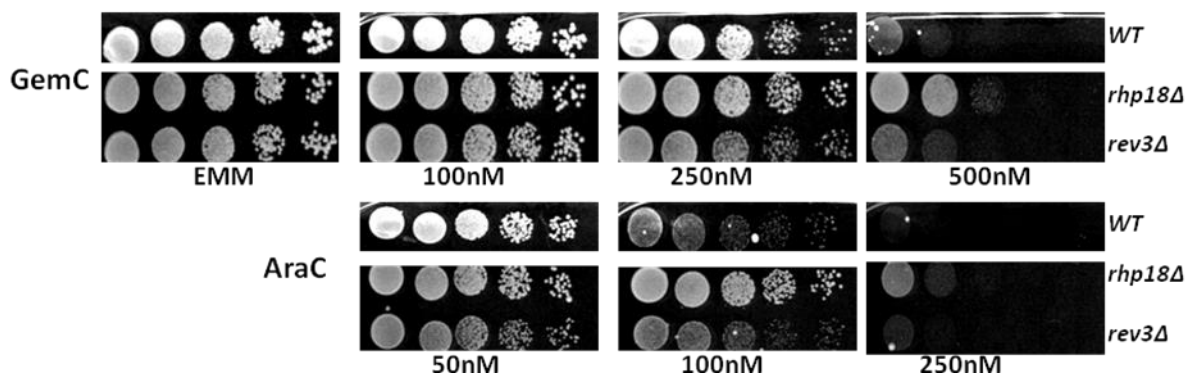


Figure 5-7 PRR mutants with *hsdCK/hENT1* are resistant to *GemC* and *AraC*. *rhp18Δ* (MG115) and *rev3Δ* (MG269) were tested. Cells were spotted on minimum (EMM) media with different concentrations of both drugs and incubated for 5 days at 30°C. WT (MG85) was plated as control. *rev3Δ* mutants were equally as sensitive as the WT to both drugs whereas *rhp18Δ* showed a slight resistance when compared to WT. The results were reproducible in three experiments.

5.3 Sensitivity of double mutants to GemC

Possible genetic interactions between some of the genes that were analysed in the previous paragraphs were assessed by analysis of double mutants. As analysis of interactions of each single gene was unrealizable within the scope of the project, I analysed interactions between some of the highly sensitive mutants of interest. Analysis of double mutants can result in three different outcomes: epistasis, synergy and rescue. Two genes are referred to as epistatic when the double mutants have the same sensitivity as the most sensitive of the single mutants suggesting that the genes act in a same pathway. When the double mutants are more sensitive than the most sensitive of the single mutants, the genes are qualified as “synergistic”, which implies that the genes have functions in different pathways. Genes qualified as “redundant”, meaning that the genes possess a functional overlap in response to the drug, can also result in a higher sensitivity of double mutants. A rescue or genetic suppression response is observed in double mutants when the deletion of a second gene suppresses the phenotype of a first gene and the double mutant becomes less sensitive than the single mutants. The genetic suppression can also result in an intermediate state where the result of double mutants is between the single mutants responses, meaning that the most sensitive phenotype has been suppressed. This observation indicates that the presence of the suppressor gene is toxic in the absence of the suppressed gene. For example if gene B contributes to the toxicity of the drug in presence of gene A, deletion of A makes cells sensitive to the drug while deletion of both A and B, makes cells resistant to the drug. In this case gene B suppresses the phenotype of gene A.

5.3.1 The MRN complex genetically interacts with *nth1* and acts in parallel with *apn2* and *rhp14* in response to GemC

To assess genetic interactions between the MRN complex and other proteins in response to GemC treatment, *rad50* deleted and *mre11* nuclease dead mutants were analysed in combination with other mutants. *mre11-D65N* mutants were combined with *nth1* Δ and *apn2* Δ mutants and tested for sensitivity to the drug. The nuclease dead mutants were also combined with *rhp14* Δ mutants to evaluate a link between the nuclease and the

NER protein. The same double mutants were created in an MRN deficient (*rad50* deleted mutants) background. *rhp14Δ mre11-D65N* and *apn2Δ mre11-D65N* double mutants showed a slight higher sensitivity when compared to either single mutant, while *nth1Δ mre11-D65N* mutants showed a sensitivity which was lower than *nth1Δ* mutants but comparable to *mre11-D65N* nuclease dead mutants (Figure 5-8A), suggesting that *mre11-D65N* rescues *nth1Δ* sensitivity. The higher sensitivity of *mre11-D65N rhp14Δ* and *apn2Δ* double mutants compared to single mutants suggests that the two genes act in different pathways in response to GemC treatment. The observed rescue of *nth1Δ mre11-D65N* in comparison to *nth1Δ* single mutants implies that inactivation of Mre11 nuclease suppresses the *nth1* phenotype which might indicate that Mre11 acts upstream Nth1 in response to GemC treatment.

In comparison to *mre11-D65N* double mutants, *rad50Δ apn2Δ* and *rad50Δ rhp14Δ* double mutants were significantly more sensitive than *apn2Δ* and *rhp14Δ* single mutants and slightly more sensitive than *rad50Δ* single mutants (visible at 100 and 150nM) indicating that the proteins act in different pathways in response to GemC. On the other hand, *nth1Δ rad50Δ* double mutants showed a reduced sensitivity when compared to either single mutant (Figure 5-8B) suggesting a rescue of the single mutants. A control test on CPT confirmed the presence of the *rad50* and *mre11-D65N* mutations.

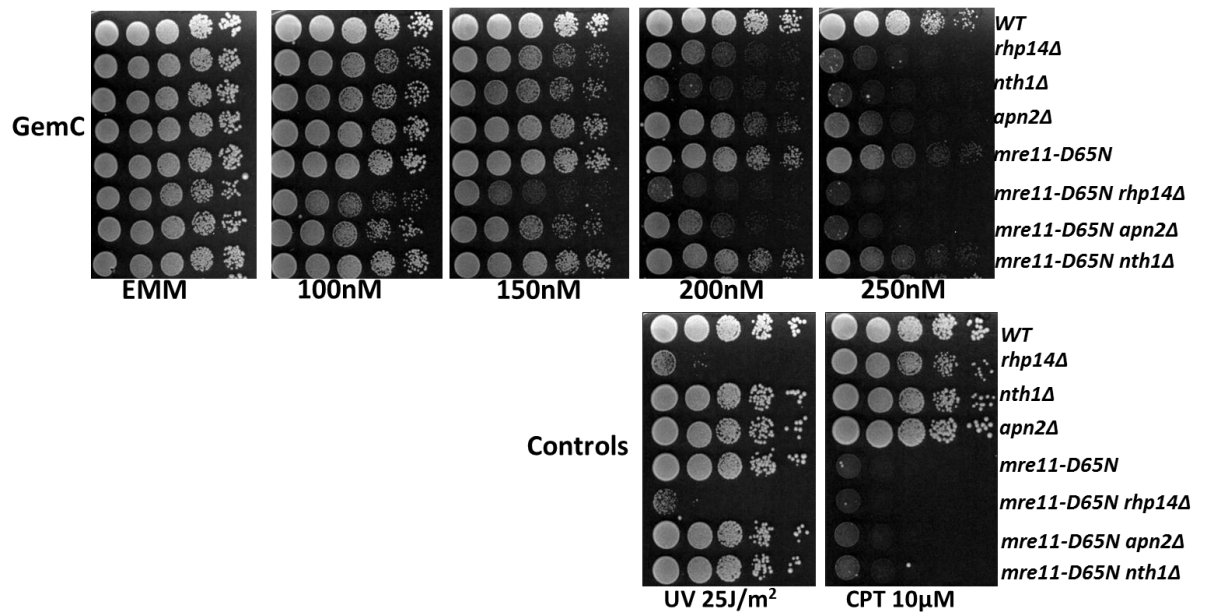


Figure 5-8A. Different sensitivity of *mre11-D65N* double mutants with *hsdCK/hENT1* to *GemC*. *mre11-D65N rhp14Δ* (AK91), *mre11-D65N apn2Δ* (AK69) and *mre11-D65N nth1Δ* (MG355) were tested. Cells were spotted on minimum (EMM) media with different concentrations of *GemC* and incubated for 5 days at 30°C. WT (MG85) and single mutants *rhp14Δ* (MG276), *nth1Δ* (MG274), *apn2Δ* (MG319) and *mre11-D65N* (MG297) were plated as controls. Sensitivity to UV (*rhp14*) and CPT (*mre11-D65N*) was used to confirm mutations. *mre11-D65N rhp14Δ* and *mre11-D65N apn2Δ* mutants showed higher sensitivity to *GemC* (visible at 150nM for *rhp14* double mutants and 200nM for *apn2* double mutants) than the single mutants. *mre11-D65N nth1Δ* double mutants showed a same sensitivity as *mre11-D65N* nuclease dead mutant (visible at 250nM) but was more resistant than *nth1Δ*. The results were reproducible in two experiments.

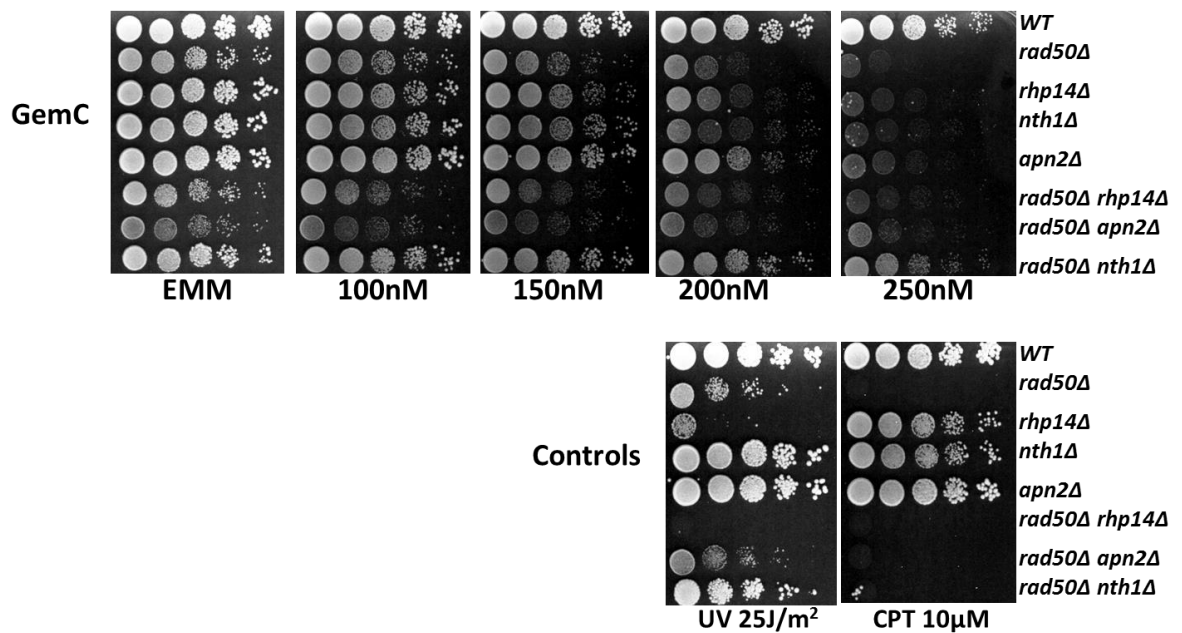


Figure 5-8B. Different sensitivity of *rad50* double mutants with *hsdCK/hENT1* to *GemC*. *rad50Δ rhp14Δ* (AK93), *rad50Δ apn2Δ* (AK104) and *rad50Δ nth1Δ* (MG357) were tested. Cells were spotted on minimum (EMM) media with different concentrations of *GemC* and incubated for 5 days at 30°C. WT (MG85) and single mutants *rhp14Δ* (MG276), *nth1Δ* (MG274), *apn2Δ* (MG319) and *rad50Δ* (MG119) were plated as controls. Sensitivity to UV (*rhp14*) and CPT (*rad50Δ*) was used to confirm mutations. *rad50Δ rhp14Δ* and *rad50Δ apn2Δ* mutants were more sensitive to *GemC* than *rhp14Δ* and *apn2Δ* single mutants but were only slightly more sensitive than *rad50Δ* single mutants (visible at 100nM and 150nM). *nth1* double mutants were more resistant than any of the single mutant. The results were reproducible in two experiments.

5.3.2 NER epistasis analyses

Epistasis analysis between NER genes was carried out to assess possible redundancy within the pathway in response to GemC. *rad13*, *rhp14* and *swi10* were analysed in double deletion combinations (Figure 5-9). *rhp14* Δ *rad13* Δ double mutants showed a same sensitivity as *rhp14* Δ mutants confirming that *rad13* Δ mutants are not sensitive to GemC. On the other hand, *rad13* Δ *swi10* Δ double mutants showed a same survival as *rad13* Δ and WT cells suggesting that *rad13* might rescue *swi10* phenotype. This result is however preliminary as the experiment was only carried out once and needs to be confirmed.

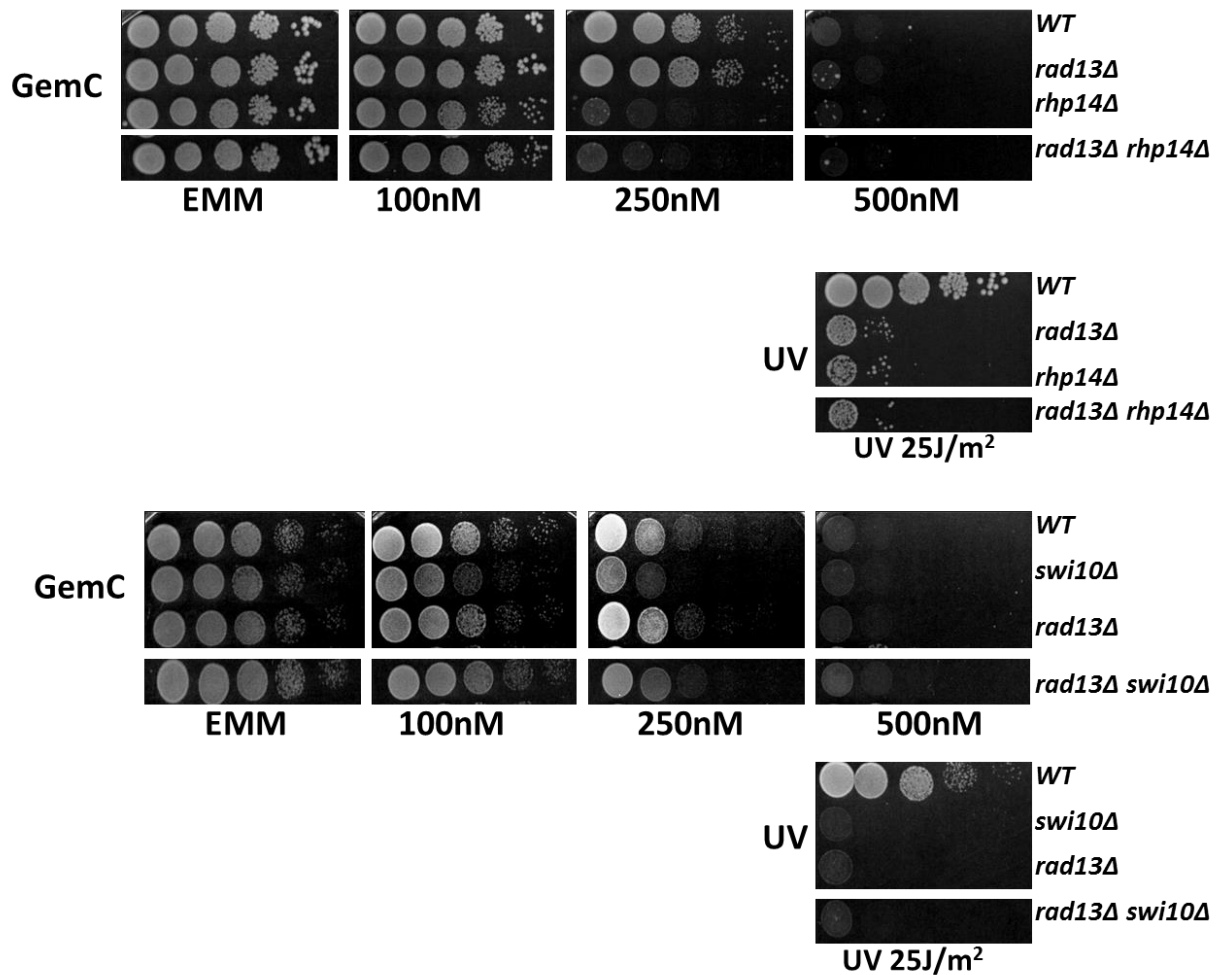


Figure 5-9 Sensitivity of NER double mutants with *hsdCK/hENT1* to GemC. *rad13Δ rhp14Δ* (MG312) and *rad13Δ swi10Δ* (MG362) were tested on minimum (EMM) media with different concentrations of the drug and incubated at 30°C for 5 days for *rhp14* double mutants and 2 days for *rad13* double mutants. WT (MG85) and single mutants *rhp14Δ* (MG276), *rad13Δ* (MG111) and *swi10Δ* (MG107) were plated as controls. Sensitivity to UV was used to confirm mutations. *rad3Δ rhp14Δ* showed the same sensitivity as *rhp14* single mutant and *rad13Δ swi10Δ* double mutants showed a same survival as *rad13Δ* single mutants and were less sensitive than *swi10Δ*. *rad13Δ rhp14Δ* mutants were tested two times and gave similar results. *rad13Δ swi10Δ* mutants were tested once.

5.4 Discussion

It is difficult to predict DNA damage repair mechanisms that could respond to and contribute to resistance of cells to GemC and AraC treatment as the exact nature of drug-induced damage (direct or indirect damage) has not yet been clearly established. DNA repair mechanisms form a complex network where proteins and protein complexes constantly interact with each other. For the clarity of the analysis I have attributed genes to different pathways, but some genes may act in more than one defined pathway while some other genes have roles in other cellular processes, for example the role of the MRN complex in the DNA damage checkpoint.

MRN mutants are sensitive to AraC and GemC

Because the MRN complex has shown a role in resistance to CPT (Hartsuiker *et al.*, 2009b), we first tested the possibility that the complex might similarly contribute to cellular resistance to GemC and AraC. The high sensitivity of MRN- Ctp1^{CtIP} mutants (*rad50Δ*, *nbs1Δ*, *ctp1Δ*) compared to WT cells (*Figure 5-1* and *Figure 5-2*) clearly suggested a role of the complex in responding to GemC and AraC induced DNA damage. The complex may play a role either as a sensor for NA induced damage or it might act to repair the damage or both. To assess whether the MRN complex plays a role in removal of the incorporated drug, we tested sensitivity of mutants defective in Mre11 nuclease activity. The sensitivity of *mre11* nuclease dead mutant (*mre11-D65N*) suggested a possible role of the nuclease in response to GemC-induced DNA damage. The high sensitivity of *mre11-D65N* mutant however was only observed in cells without the transporter (*Figure 5-1*) as *mre11-D65N* with transporter were only slightly affected when compared to WT cells (*Figure 5-2*). A possible explanation for this difference in sensitivities might be that in presence of the transporter, cells accumulate different forms of the drug which in turn activate different pathways. These differences might be explained by different mechanisms of action of GemC which would be dependent on the quantity of the drug. GemC acts either by decreasing nucleotides pools through inhibition of RNR by dFdCDP (the diphosphate form of the drug) or being incorporated

into DNA (dFdCTP, the triphosphate form of the drug). Accumulation of dFdCDP in cells might lead to dNTPs depletion and stalled replication fork while dFdCTP would incorporate the DNA. One possibility might be that in presence of low amount of GemC, dFdCTP is predominant in cells and hence Mre11 responds to DNA incorporated GemC, while in presence of high GemC levels, dFdCDP also accumulates in cells and leads to formation of lesion that are repaired independently of Mre11. Another possibility might be that, the high levels of GemC in cells with the transporter might lead to accumulation of suppressor mutations, which would affect the activity of the Mre11 nuclease. The possible role of Mre11 in removal of NA is further discussed in chapter 7.

Additionally, it has been suggested that GemC enhances formation of top1 mediated DNA complexes (Pourquier *et al.*, 2002) which could also explain the role of MRN complex in response to the drug. Indeed as the complex plays a role in removal of the DNA-top1 complex, it is possible that MRN would play a role in GemC-top1 induced complexes but not to other GemC induced damage. We tested sensitivity of *top1* Δ and *top1* Δ *rad50* Δ mutants to GemC and results (Figure 5-3) suggest that top1 is not the main cellular target for GemC as the removal of the enzyme only slightly affects drug sensitivity. In addition, because deletion of *top1* did not increase resistance of *rad50* Δ mutants to the drug, the results also suggest that the role of MRN in GemC-treated cells is not dependent on the DNA-top1 complex.

NER deleted mutants are sensitive to AraC and GemC

High sensitivity of NER DNA damage signalling *rhp14* Δ ^{XPA} and *rhp41* Δ *rhp42* Δ ^{XPC} mutants to GemC and AraC (Figure 5-4) strongly suggests a role of NER in repair of GemC and AraC induced DNA damage. The ability of NER proteins to sense distortion of the DNA backbone might explain the potential role of the repair mechanism in recognising DNA damage induced by GemC and AraC, as it has been suggested that both drugs induce distortion of the DNA helices (Gmeiner *et al.*, 1998; Konerding *et al.*, 2002). In addition, we have noticed that *rhp14* Δ mutants are more sensitive to AraC

compared to GemC. This difference in sensitivity might be explained by the fact that AraC is mainly incorporated into the DNA (detection by NER) while GemC is incorporated into DNA but also inhibits RNR causing depletion of dNTP pools and interfering with replication. It is possible that GemC induces different DNA damage which are not detected by the excision repair (e.g DSBs) but are repaired by other pathways. Assuming that NER is the main repair pathway for DNA-incorporated NAs, the removal of NER would then have greater effect on AraC-treated cells than GemC-treated cells, which are repaired by other pathways.

Additionally, the observed high sensitivity of *rhp14*Δ mutants in comparison to *rhp41*Δ *rhp42*Δ might indicate that *rhp14* plays a more important role than *rhp41/42* in recognition of GemC and AraC induced DNA damage. Because *rhp41/42*^{XPC} is only involved in GG-NER while *rhp14*^{XPA} is recruited by both GG-NER and TC-NER proteins (see introduction paragraph 1.1.3.3.1 for details), it is possible that in absence of *rhp41/42*^{XPC}, TC-NER detects drug-induced damage while in absence of *rhp14*^{XPA}, both TCR and GG-NER are abolished, making cells more sensitive to the NAs. A sensitivity test of the TC-NER specific gene CSB (*S. pombe rhp26*) to GemC and AraC might help to confirm that the subpathway is also involved in repair of the two NAs-induced damage.

swi10^{ERCC1} deleted mutants showed a high sensitivity to both drugs compared to WT whereas *rad13*^{XPG} deleted mutant showed a same survival as WT cells (*Figure 5-4*). The observation that *swi10*, which incises the DNA at 5' end, is more sensitive than *rad13* which proceeds to 3' incision, is consistent with localisation of the drugs at the 3' end after chain termination (Ewald *et al.*, 2008a) and implies that only the 5' incision is required for removal of the drugs from the DNA.

BER deleted mutants are sensitive to AraC and GemC

Surprisingly, BER defective mutants showed a high sensitivity to both NAs and implied that the pathway is involved in repairing GemC and AraC induced DNA damage. It is worth noting that all *S. pombe* strains that were used in this project possess a deletion of

the *apn1* gene (Dr Hartsuiker, personal communication). In *S. pombe*, two genes, *apn1* and *apn2*, are thought to encode proteins which exert the APE1 activity (Fleck, 2004). However, while *apn2*Δ mutants are highly sensitive to MMS (Alseth *et al.*, 2004) suggesting a role of the gene in BER, *apn1*Δ mutants showed similar survival to MMS as WT cells (Osman *et al.*, 2003) suggesting that the gene does not play a major role in BER (or that *apn1*'s role is redundant) in *S. pombe*. However, as WT cells (used as control) also possess the *apn1* deletion, the observed sensitivity to GemC and AraC is likely independent of *apn1*Δ. High sensitivity was observed in *nth1*Δ and *apn2*Δ mutants while *rad2*Δ was slightly more resistant than WT (Figure 5-5). The observation that deletion of *apn2* and *nth1*, which process the abasic site, increases sensitivity of cells to both GemC and AraC might indicate that DNA processing activity might be required after removal of the NA from the DNA.

In addition, because it has been shown that deamination of dFdC (GemC) by deoxycytidine deaminase results in formation dFdU (difluorodeoxyuridine) which might be incorporated into DNA and contribute to the toxicity of GemC (Veltkamp *et al.*, 2008), we tested the sensitivity of uracil specific glycosylase, *ung1*Δ mutants to both AraC and GemC. Deletion of *ung1* would be expected to increase drug sensitivity in GemC treated cells as dFdU wouldn't be removed from the DNA. On the contrary we have observed that *ung1*Δ mutants are more resistant to both GemC and AraC than the WT cells (Figure 5-5), suggesting that the glycosylase exacerbates NA toxicity. The fact that the resistance was observed in both GemC and AraC treated cells suggest that the *ung1* response is not dFdU related but that the glycosylase responds to NAs in general.

It is not clear the resistance of *ung1* and *rad2* deleted mutants when compared to the WT. A possible explanation to the observed resistance in comparison to WT might be presence of suppressors in the transporter and/or the kinase which would decrease drug activity. In fact, it has been suggested that deletion of *ung1* (Ikeda *et al.*, 2009) and *rad2* (Kunz and Fleck, 2001) in *S. pombe* increases spontaneous mutations when compared to WT, which could explain that mutations might occur in the transporter and/or the kinase and impede with function of the two proteins. The high sensitivity of the mutants compared to a wild type strain without the transporter and kinase however confirmed

that the transporter and kinase were present, although their full functionality is not proven. As mentioned in paragraph 5.2.3 in regards to MMR deficient mutants which showed a similar resistance phenotype, a backcross test would allow assessing whether suppressors are indeed present in the transporter and/or kinase. The resistance of *rad2Δ* and *ung1Δ* mutants is hence to be confirmed by a backcross test. It is however unclear how the two genes might contribute to drug toxicity. A possible hypothesis might be that in an attempt to remove the drugs, the proteins remain fixed to the DNA and create a DNA-protein complex which is harmful for the cell as it may induce subsequent damage such as DSBs, but may also block access of other repair mechanisms to the site of lesion. Deletion of the genes would hence be beneficial for the cell as drug-induced damage would be exposed to other repair pathways. Analysis of *rad2Δ* double mutants in combination with nucleases which remove proteins from the DNA such as *tdp1* (Pouliot *et al.*, 1999; Caldecott, 2003) and *mre11* (Hartsuiker *et al.*, 2009) could help to assess whether Rad2 is fixed to the DNA, as deletion of *rad2* would in principle rescue the nuclease sensitivity. In contrast to above suggestion *rad2Δ mre11-D65N* double mutants were highly sensitive to GemC in comparison to either single mutant (Dr Keszthelyi, personal communication) suggesting that the nucleases rather act in different pathways.

Another possible explanation to the resistance observed in *rad2Δ* mutants, might be that the nuclease induces DNA nicks or other repair intermediates which are specific to GemC and AraC and are lethal to the cell. In fact, Rad27 (*S. cerevisiae* Rad2 homologue) and FEN-1 (human Rad2 homologue) have been shown to play role in maturation of Okazaki fragments by removing the primer flap (Zheng and Shen, 2011) and, because GemC is also incorporated into Okazaki fragments (Konerding *et al.*, 2002) we can hypothesise that *rad2* removes the drug from the DNA during the Okazaki maturation process, and that the nuclease creates nicks that need to be repaired. Because Rad2 exerts a 5' → 3' exonuclease activity (Fleck, 2004) which is opposite the location of the NA (at 3' end), it is possible that NA incorporation results in short Okazaki fragments, with GemC at the 3' end. These fragments could be removed by the *rad2*

nuclease leading to formation of DNA nicks. Deletion of the nuclease would therefore be beneficial for cell survival.

Preliminary results suggest that MMR and PRR mutants are hyperresistant to AraC and GemC when compared to WT cells

Results presented in *Figure 5-6* don't allow to draw a clear conclusion on the possible role of MMR mutants in response (or not) to GemC and AraC. These preliminary results, that need to be confirmed by backcrosses, suggest that MMR augment GemC and AraC toxicity as the removal of the pathway increases drug resistance. A possible explanation might be a phenomenon referred to as the "methylation tolerance" [(Friedberg, 2006), p157] which was observed with MMR in response to O⁶-methylguanine (O⁶-methyl-G). When O⁶-methyl-G is incorporated into the DNA during replication, a C or T is paired to the methylated base. O⁶-methyl-G-C (or T) structures are then recognised by the MMR mechanism as a threat for the cell. However, instead of removing the modified guanine, MMR proteins remove the intact C or T, creating a nick into the DNA. In this regards, deletion of MMR genes is beneficial to the cell because if MMR is present, it continues to excise the DNA opposite O⁶-methyl-G which increases strand breaks, potentially dangerous for the cell while in MMR deficiency, cells are tolerant to O⁶-methyl-G. We can imagine a similar scenario for GemC and AraC, if the MMR recognises the NAs but removes the nucleotides opposite the drugs instead of removing the drugs.

In addition to the mentioned DNA repair pathways, GemC and AraC induced damage might also be by passed by the cell during replication. We tested the role of PRR in response to GemC and AraC by deleting two PRR genes, *rhp18* and *rev3*. Deletion of *rhp18* increased resistance of cells to both drugs when compared to WT cells (*Figure 5-7*) suggesting that *rhp18* improves drug sensitivity as its absence desensitised cells to the drugs. However, here also we can not exclude the possibility that the observed resistance is due to potential suppressors in the transporter and/or the kinase as backcross tests were not carried out. If proven, these results suggest that ubiquitination of PCNA (by *rhp18*) and activation of PRR is harmful for the cells after treatment with

NAs. However, *rev3Δ* mutants showed a similar survival as WT (Figure 5-7) and suggested that the polymerase is not important for cell survival. As several polymerases act in PRR, including REV1 (*S. pombe rev1*), polη and polι (*S. pombe eso1*) (Waters *et al.*, 2009), the fact that *rev3Δ* mutants are not sensitive to the drugs might either indicate that other polymerases act to bypass incorporated NA or that the PRR is not activated in response to NA treatment. Sensitivity test of *eso1Δ* mutants to GemC and AraC, for example, might help to assess whether other PRR polymerases are involved in cellular survival to NAs.

Epistasis analyse show that the MRN complex act in parallel with BER and NER in response to GemC

We have observed a high sensitivity of *mre11-D65N rhp14Δ* and *mre11-D65N apn2Δ* double mutants compared to *mre11-D65N* and *rhp14Δ* and *apn2Δ* single mutants respectively (Figure 5-8A). These results suggested that *rhp14* (NER damage signalling gene) and *apn2* (BER abasic site processing nuclease) act in different pathways to the *mre11* nuclease in response to GemC treatment. The synergistic response between *apn2* and *mre11* nucleases can be rationalized by their nuclease activities which might act in a redundant way to remove the NA from the DNA. The link between *rhp14* and *mre11* is less clear but the synergistic nature of the response confirms that *mre11* and NER act in different pathways in response to GemC. Similarly to *mre11-D65N rhp14Δ* and *mre11-D65N apn2Δ* double mutants, *rad50Δ rhp14Δ* and *rad50Δ apn2Δ* were more sensitive to GemC than *rad50Δ* and *rhp14Δ* and *apn2Δ* single mutants respectively (Figure 5-8B). This synergistic response between *apn2Δ* and *rad50Δ* and *rhp14Δ* and *rad50Δ* further supports the hypothesis that *rhp14* and *apn2* act in different pathways as the MRN complex in response to GemC.

Inactivation of the MRN complex (*rad50Δ*) and Mre11 nuclease activity (*mre11-D65N*) clearly increased survival of *nth1Δ* (*nth1* is BER bifunctional glycosylase which removes the damaged based and processes the abasic site) mutants as *mre11-D65N nth1Δ* and *rad50Δ nth1Δ* double mutants were more resistant than *nth1Δ* single mutants

(Figure 5-8A and B). These results imply that deletion of the MRN complex or inactivation of the Mre11 nuclease activity suppress the *nth1* phenotype and that MRN and Mre11 nuclease genetically interact with *nth1* in response to GemC. However, on contrary to the *mre11-D65N-nth1Δ* which showed similar survival as *mre11-D65N* single mutants, *rad50Δ nth1Δ* double mutants were more resistant than *rad50Δ* single mutants. *rad50Δ nth1Δ* cells were sensitive to CPT, confirming that cells are *rad50* deficient and, because *rad50Δ nth1Δ* were more sensitive to GemC than WT cells with *hsdCK/hENT1*, I excluded the possibility that suppressors in transporter and/or kinase might have affected their function and decreased drug effect.

The rescue of *nth1Δ* by both *rad50Δ* and *mre11-D65N* mutants is not understood. The fact that viability of *mre11-D65N nth1Δ* double mutant was restored to *mre11-D65N* single mutant level might indicate that Mre11 acts upstream of Nth1 in response to GemC. A possible hypothesis might be that Mre11 nuclease responds to GemC-induced damage and creates an intermediate state which requires *nth1* for the repair. Removal of Mre11 would hence mean that N1 is not needed for repair of GemC-induced damage, which in turn would explain that *nth1Δ* mutants become less sensitive in the absence of the Mre11 nuclease activity. On the other hand, the observation that sensitivity of *nth1Δ rad50Δ* double mutants was restored to almost WT survival might indicate that the MRN complex response to GemC also requires presence of *nth1*. Indeed it has been shown that *S. pombe nth1* genetically interacts with the homologous recombination gene *mms1* (Vejrup-Hansen *et al.*, 2011). In the study, Vejrups *et al* suggested a model in which repair of MMS induced damage by BER creates SSBs which are further converted into DSB during replication. Replication induced DSBs are then repaired by HR which requires the *mms1* gene. Hence the deletion of *mms1* in *nth1 WT* background leads to accumulation of DSBs created by *nth1*, while if *mms1* and *nth1* are both deleted, *nth1*-dependent DSBs are also abolished and the role of *mms1* in MMS induced damage becomes minor. If we hypothesise a similar scenario in response to GemC, it is possible that *nth1* induces DSBs which, are further processed by the MRN complex. Deletion of *nth1* would hence indicate that there are no *nth1* induced DSBs and the role of MRN complex becomes less important which would explain that MRN defective

mutants become less sensitive in absence of *nth1*. To confirm that the observed rescue is BER-dependent, we should test sensitivity of another *S. pombe* glycosylase, such as *mag1*, in combination with *rad50Δ* and *mre11-D65N* mutants to GemC.

Analysis of NER double mutants confirmed that *rad13* is not required for survival of cells to GemC as *rhp14Δ rad13Δ* was as sensitive as *rhp14Δ* (Figure 5-9). Surprisingly, *rad13Δ* rescued *swi10Δ* as the *rad13Δ swi10Δ* double mutant showed a similar survival as *rad13Δ* and WT. This surprising observation needs to be confirmed as tests were carried out only once. One possible explanation to the rescue observed in *swi10Δ rad13Δ* double mutants might be that in the absence of Swi10, Rad13 tries to remove GemC, however as Rad13 incises at 3' end, it is possible that the nuclease runs into the incorporated NA (located at the 3' end) and remains fixed to the DNA, creating a DNA bound protein complex which is harmful for the cell. If both proteins are removed, NA-induced damage becomes available for other repair pathways, which would explain that cells become resistant to the drug. An alternative explanation might be the existence of another nuclease which substitutes for *rad13* but triggers *swi10* response. Indeed, because *rad13Δ* rescues *swi10Δ*, results suggest that *rad13* acts upstream *swi10*, however, the observation that *rad13Δ* mutants showed a similar survival as WT might indicate that *rad13*'s role is redundant. Analysis of *swi10Δ* in combination with other nuclease mutants (e.g: *mre11-D65N*) could help to assess whether the nucleases act in a same pathway.

All together, results presented in this chapter indicate that several repair pathways play a role in the response to GemC and AraC induced DNA damage. Sensitivity of MRN-defective *rad50Δ* and *mre11-D65N* mutants suggests a role of the MRN complex in response to drug induced damage, and high sensitivity of NER (*rhp14Δ*, *rhp41Δrhp42Δ* and *swi10Δ*) and BER (*nth1Δ* and *apn2Δ*) mutants clearly suggest a role of these two pathways. Due to the observation that all mutants which are known to induce high mutation rates (MMR mutants, *ung1* and *rad2*) showed a rescue phenotype when compared to WT, it is possible that this observed phenotype is due to potential suppressors that affect function of the transporter and/or the kinase or other genes and

that the results don't present a significant biological effect of NAs. These results however need to be confirmed by backcross tests.

Table 5-2 to Table 5-4 show a summary of the different sensitivities and *Figure 5-10* gives a simplified overview of the possible involvement of DNA repair in response to GemC and AraC as identified by analysis of sensitive mutants in this chapter. Further genetic interaction analyses however are required to identify possible interaction between the different actors.

Table 5-1 Representation of phenotype growth of different mutants.


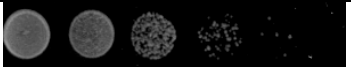




Growth	Viability symbol
	+++++
	++++
	+++
	++
	+
	-
More resistant than WT	+++++++
Not tested	N/A

Table 5-2 Summary sensitivity of MRN mutants. MRN mutants were tested in both *dmdNK* and *hsdCK* with and without transporter background. See table 5-1 for interpretation of symbols.

Strain	Viability	
	GemC 50 μ M	AraC
<i>dmdNK</i> WT	+++++	N/A
<i>mre11-D65N dmdNK</i>	+	
<i>rad50Δ dmdNK</i>	-	
<i>hsdCK</i> WT	+++++	
<i>mre11-D65N hsdCK</i>	+++	
<i>rad50Δ hsdCK</i>	+	
	GemC 500nM	
<i>dmdNK</i> WT hENT1	+++++	+++++
<i>mre11-D65N dmdNK</i> hENT1	+++	++++
<i>rad50Δ dmdNK</i> hENT1	+	+
<i>nbs1Δ dmdNK</i> hENT1	+	+
<i>ctp1Δ dmdNK</i> hENT1	+	+
	GemC 250nM	AraC 100nM
<i>hsdCK</i> WT hENT1	+++++	+++++
<i>mre11-D65N hsdCK</i> hENT1	+++++	+++++
<i>rad50Δ hsdCK</i> hENT1	++	+
<i>nbs1Δ hsdCK</i> hENT1	++	+
<i>ctp1Δ hsdCK</i> hENT1	++	+

Table 5-3 Summary sensitivity of different repair mutants. All mutants were tested in hsdCK/hENT1 background. See table 5-1 for interpretation of symbols.

Strain	Pathway	Viability	
		GemC 250nM	AraC 100nM
WT		+++++	+++++
<i>rhp14Δ</i>	NER	+	+
<i>swi10Δ</i>	NER	++	++
<i>rhp41Δrhp42Δ</i>	NER	++ (small colonies)	++ (small colonies)
<i>rad13Δ</i>	NER	+++++	+++++
<i>nth1Δ</i>	BER	++	++
<i>apn2Δ</i>	BER	++	-
<i>rad2Δ</i>	BER	+++++++	+++++
<i>ung1Δ</i>	BER	+++++++	+++++
<i>exo1Δ</i>	MMR	+++++++	+++++++
<i>mlh1Δ</i>	MMR	+++++++	+++++++
<i>msh2Δ</i>	MMR	+++++++	+++++++
<i>pms1Δ</i>	MMR	+++++++	+++++++
<i>msh6Δ</i>	MMR	+++++++	+++++
<i>rev3Δ</i>	PRR	+++++	+++++
<i>rhp18Δ</i>	PRR	+++++++	+++++++

Table 5-4 Summary sensitivity of different double mutants. All mutants were tested in hsdCK/hENT1 background. See table 5-1 for interpretation of symbols.

Strain	Viability GemC 200nM
WT	+++++
<i>rhp14Δ</i>	+++
<i>apn2Δ</i>	++++
<i>nth1Δ</i>	++
<i>rad50Δ</i>	+++
<i>mre11-D65N</i>	+++++
<i>mre11-D65N rhp14Δ</i>	+
<i>mre11-D65N apn2Δ</i>	++
<i>mre11-D65N nth1Δ</i>	+++++
<i>rad50Δ rhp14Δ</i>	+ (and small colonies)
<i>rad50Δ apn2Δ</i>	+ (and small colonies)
<i>rad50Δ nth1Δ</i>	+++++
	Viability GemC 250nM
WT	+++++
<i>rhp14Δ</i>	+
<i>rad13Δ</i>	+++++
<i>rad13 rhp14Δ</i>	+
	Viability GemC 250nM (*Two days incubation)
WT	+++
<i>swi10Δ</i>	++
<i>rad13Δ</i>	+++
<i>rad13 swi10Δ</i>	+++

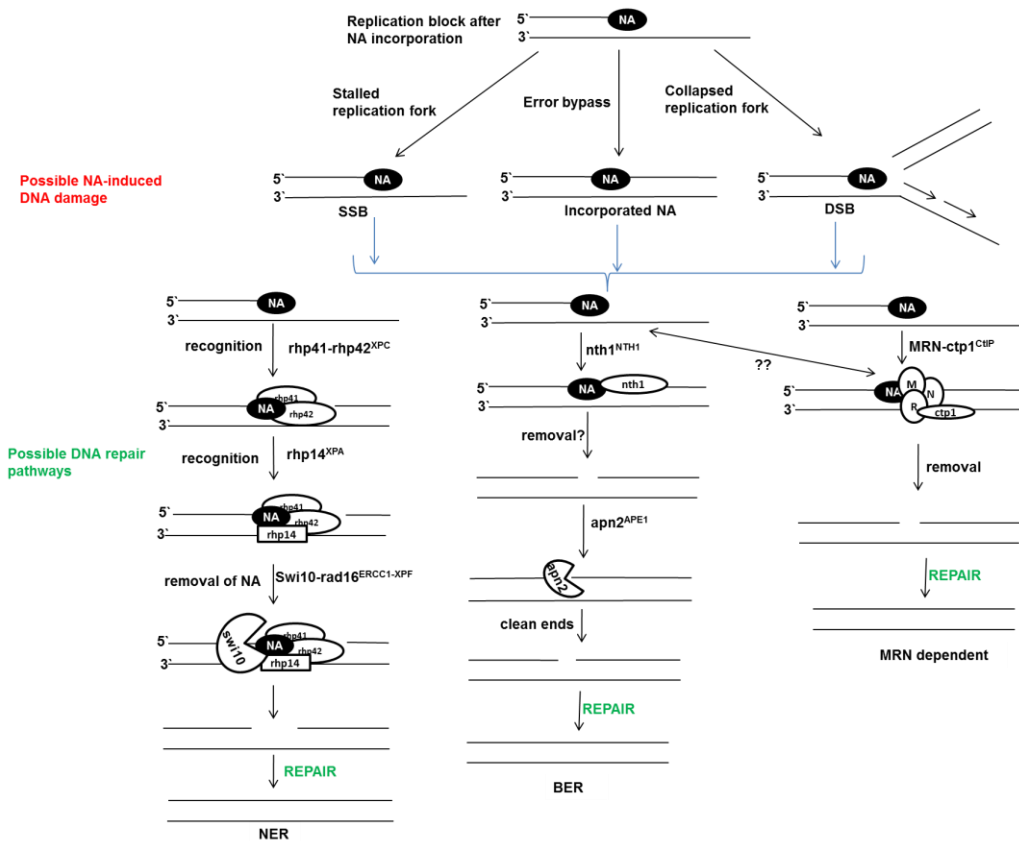


Figure 5-10 Possible repair mechanisms that may respond to GemC and AraC (NA) induced DNA damage as suggested by analysis of DNA repair mutants. Different types of DNA changes might be induced following incorporation of NA during replication. These include: (1) single stranded DNA which results from stalled replication fork, (2) incorporated NA which might results from bypass of the NA by replication and (3) DSB which might arise if a replication fork encounters the NA and collapses. In addition, NA might also be incorporated during DNA repair (Iwasaki *et al.*, 1997) and constitute a target for the repair mechanisms. Several DNA repair scenarios are possible depending on the type of the alteration and, as I did not distinguish specific types of change into DNA, I use the original substrate (DNA-incorporated NA) to illustrate that identified repair genes are not related to any specific damage. In NER, the damage is recognised by *rhp41* and *rhp42* (homologues of XPC) and confirmed by *rhp14* (XPA). The complex then recruits *swi10-rad16* (ERCC1-XPF), which incises the DNA and makes the lesion available for repair. In BER, the damage is recognised by *nth1* (NTH1) which might remove the NA and creates an intermediate that requires processing by *apn2* (APN1), which cleans DNA ends and makes the lesion available for repair. In MRN-dependent repair, MRN-ctp1^{CTIP} complex recognises the damage and *mre11* nuclease removes the NA from the DNA making the lesion available for repair. A possible link between MRN and *nth1* was also suggested by the results.

6 The FLP nick system: a tool to study DNA bound protein complexes

DNA bound protein complexes, such as topoisomerase cleavable complexes, are intermediate physiological complexes that act in several cellular mechanisms, including DNA replication. These complexes have been used in cancer therapy with drugs that act by increasing the half-life of the complexes (detailed in paragraph 1.2.1). However, cells have shown resistance to these drugs by removing the proteins from the DNA, which allows subsequent repair (see paragraph 1.2.1.3). In order to further study removal of DNA bound proteins, I attempted to set up a system in *S. pombe* to allow study of these complexes at specific sites in the genome.

A system known as “FLP-nick system” has been successfully established in *S. cerevisiae* (Nielsen *et al.*, 2009), and takes advantage of a step arrest FLP mutant (FLP-H305L) which cleaves and remains bound to the DNA leading to formation of a covalently linked DNA-protein complex (Parsons *et al.*, 1988). The FLP protein, from the *S. cerevisiae* 2 μ plasmid, is a member of the site-specific recombinase family, which similarly to topoisomerases, cleave the DNA via a tyrosyl residue (Andrews *et al.*, 1985; Parsons *et al.*, 1988; Pommier, 2009). The FLP cleaves the DNA at a specific FLP recognition target (FRT), which is composed of 48bp of three repeats of 13bp sequences (GAAGTTCCTATAC) and a spacer region. The first two sequences are inverted and separated by 8bp (Andrews *et al.*, 1985). The enzyme cuts at the beginning of the spacer region and is covalently bound to the 3' end of the cleaved strand, leaving an 8bp overhang at the 5' end (Andrews *et al.*, 1985; Parsons *et al.*, 1988). The FRT target can be integrated at any site of interest into the yeast genome allowing study of specific regions. This ability to introduce the target at a chosen site into the genome constitutes the strength of the system as it would allow us to specifically study the response to DNA bound proteins at specific sites. Moreover, because FRT can be inserted in both forward (effect on leading strand) and reverse (effect on lagging strand) directions, it would allow study of strand specificity of the response during replication.

6.1 Strategy to construct “FLP nick” strains

To construct “FLP-nick” strains, human hemagglutinin (HA) tagged FLP-H305L coding sequence under the uracil regulatable promoter (*urg1*) was integrated into the *S. pombe* genome using a recombinase mediated cassette exchange (RMCE) method using a CRE-LOX system (Watson *et al.*, 2008). RMCE uses the ability of cre recombinase to create a nick into the DNA and allow genetic exchange. CRE recombinase cuts into the lox site which induces the recombination and gene exchange between a CRE-LOX plasmid and the *S. pombe* base strain (*Figure 6-1A*). In RMCE presented by Watson *et al* (2008), sequences to be exchanged are flanked by loxP and loxM3 recognition sites which differ by mutations in the spacer region and are unable to recombine with each other.

To study the effect of DNA bound protein complexes on replication, the FRT was inserted in both forward (effect on leading strand) and reverse (effect on lagging strand) directions close to a well characterised origin of replication sequence (*Figure 6-1B*). The target was synthesised as oligonucleotides and cloned into pFA6a-natMX6, to couple FRT to the Nourseothricin (NAT) resistant cassette. NAT coupled FRT was integrated into the *S. pombe* genome using classic HR based exchange and the NAT resistant cassette was used as a marker for integration.

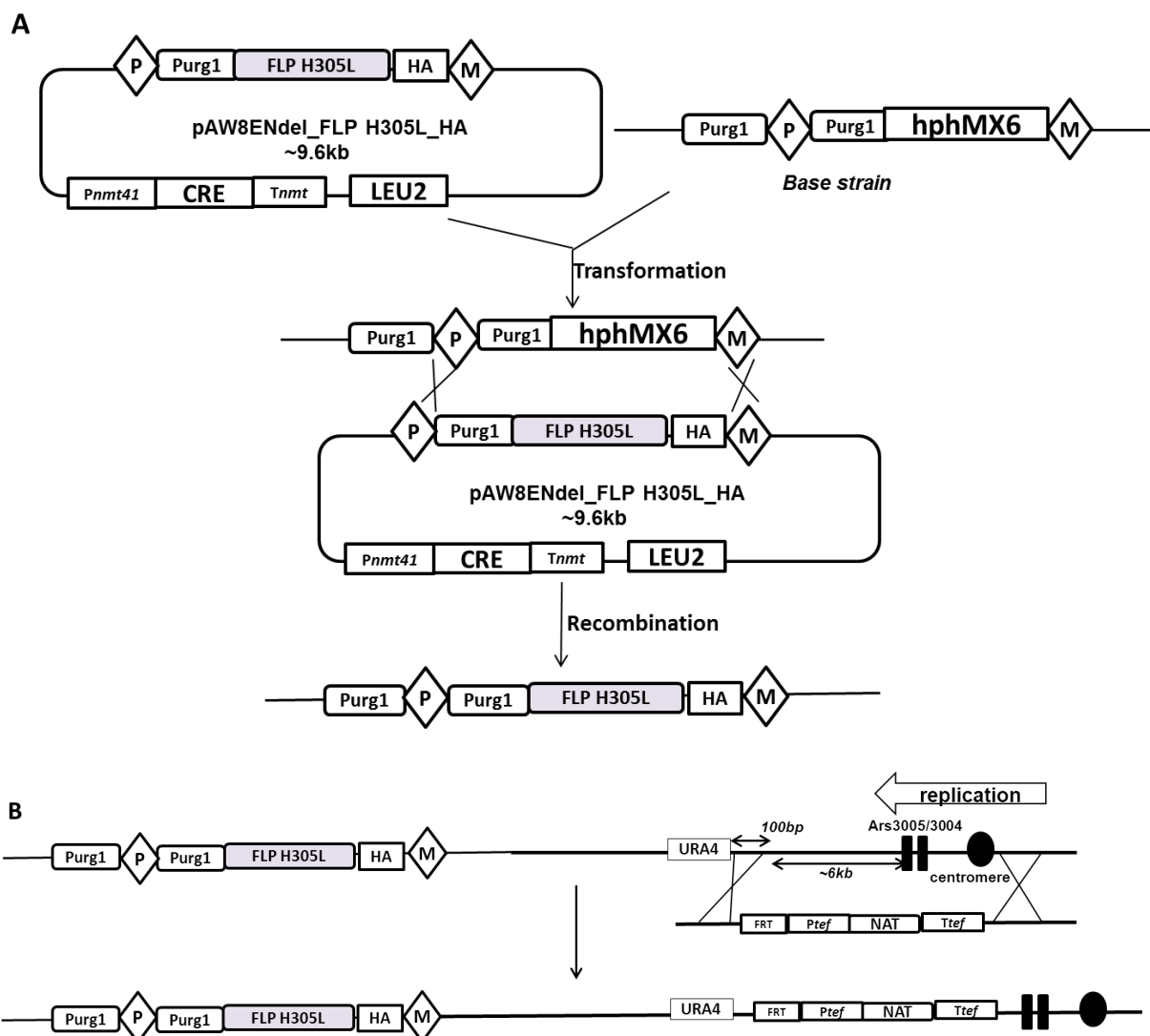


Figure 6-1 General strategy used to construct “FLP-nick” strains. **(A)** pAW8ENdel plasmid, containing HA tagged FLP-H305L, was transformed into a “cre-lox” *S. pombe* base strain. Gene exchange between the plasmid and the base strain is triggered by the cre recombinase which creates a nick into the lox sites, and leads to integration of the FLP into *S. pombe* genome. Hygromycin-sensitive cells which have lost the hph resistance cassette (and contain the FLP) were selected for further steps. **(B)** FRT coupled to the NAT resistant cassette was then integrated in “FLP strains” using classing HR based exchange. P=loxP and M=loxM3

6.1.1 Integrate FLP-H305L_HA into *S. pombe*

6.1.1.1 Cloning HA tagged FLP-H305L into pAW8ENdeI cre-lox plasmids

The FLP-H305L coding sequence was PCR amplified from the pFV17D FLP H305L plasmid (Nielsen *et al.*, 2009) and cloned under *NdeI* and *SacI* restriction sites of the pAW8ENdeI cre-lox plasmids (Watson *et al.*, 2011 and personal communication). The green fluorescent protein (GFP) tag in pAW8ENdeI cre-lox plasmids was then replaced by an HA tag to create HA-tagged FLP-H305L. The general strategy to construct pAW8ENdeI_FLP-H305L_HA plasmids is outlined in *Figure 6-2*.

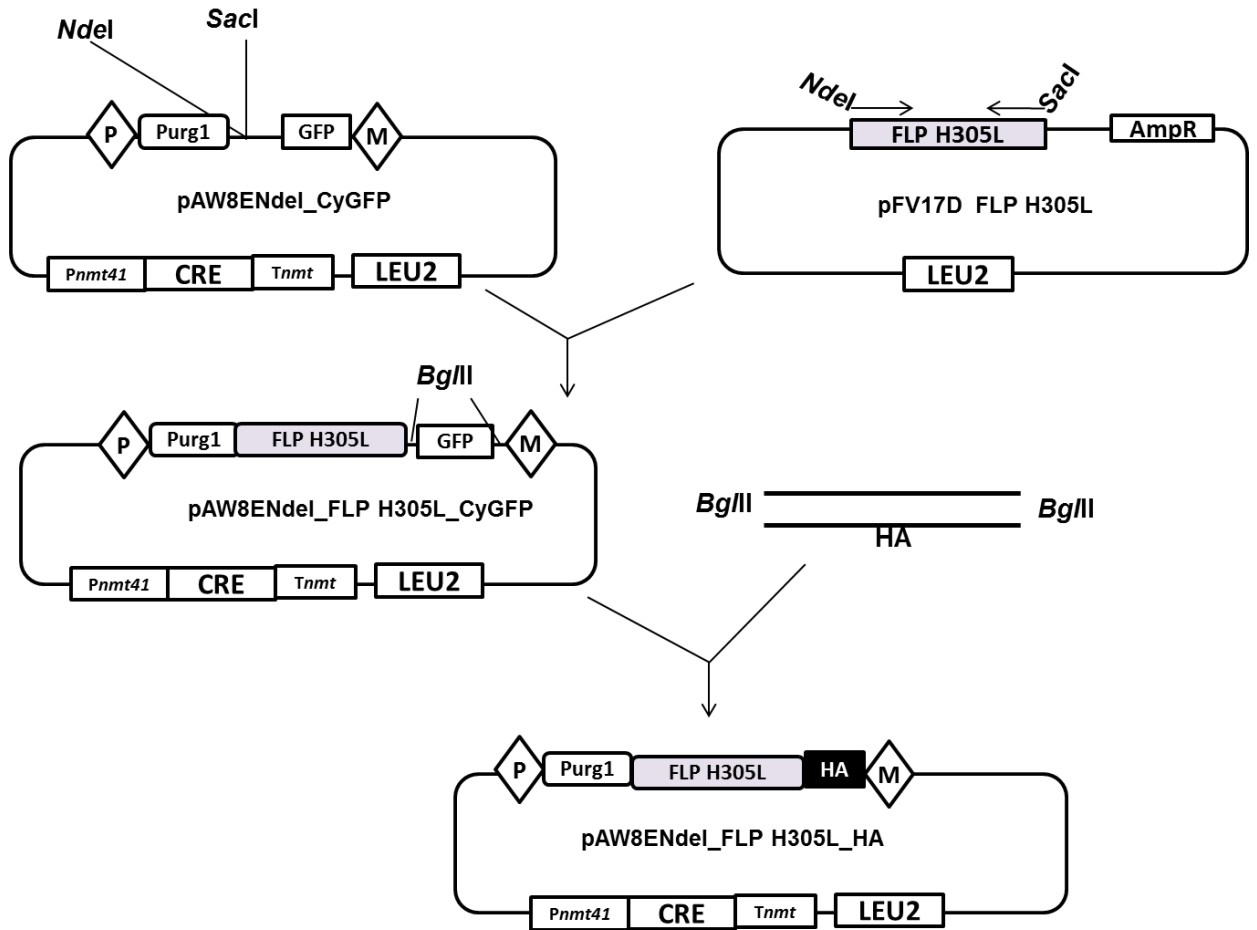


Figure 6-2 Construction of *pAW8NdeI_FLP H305L_HA* plasmids. The *FLP H305L* gene was PCR amplified from the *pFV17D* plasmid and cloned into *NdeI* and *SacI* restriction sites of *pAW8NdeI* plasmids. *HA*, synthesised as oligonucleotides, was then cloned into *BglII* restriction site, replacing the *GFP* tag by the *HA* tag.

A. Preparing FLP H305L

pFV17D FLP H305L was checked by digestion with *EcoRI* which released two fragments as expected (*Figure 6-3A*). The FLP H305L ORF was cloned using the *NdeI* restriction site however, as the ORF contains an internal *NdeI* site, the first step was to remove this *NdeI* site. This was done by site directed mutagenesis to mutate the first A of the recognition site at position 1089 (C**A**TATG) into a T conserving the alanine amino acid (GCA→GCT, 5'3' open reading frame 1). Mutagenesis was carried out according to the site directed mutagenesis protocol from Agilent Technologies (see Materials and Methods, paragraph 2.2.2.3). P001 (Flp-NdeI_quik_F) and P002 (Flp-NdeI_quik_R) primers were used to carry out the mutagenesis. DNA isolated from transformed colonies was sequenced using seq001 (Nde-FW) primer (Sequencing was carried out by Eurofins MWG). Alignment using EMBOSS alignment tool, confirmed the mutation and showed that no other mutations were introduced. One alignment is given in *Figure 6-3 (B)*.

B. Amplification of FLP H305L and cloning into pAW8ENdeI cre-lox plasmids

The *NdeI* mutated FLP-H305L gene was PCR amplified and cloned into the cre-lox expressive pAW8E vectors, pAW8ENdeI_0SS_CyEGFP, pAW8ENdeI_1SS_CyEGFP and pAW8ENdeI_2SS_CyEGFP. The three plasmids differ by the presence of one (1SS) or two (2SS) start stop (atgtaa) codons, integrated between the promoter and the FLP gene. Because the FLP protein induces nicks into the genome that might constitute a threat to the cells when not efficiently suppressed, start-stop codons were introduced to reduce gene expression and protein levels (by decreasing the activity of the promoter). pAW8ENdeI plasmids were checked by digestion with *BglIII* (NEB) which released the CyEGFP tag (~700bp) (Figure 6-4A-1). FLP H305L was PCR amplified using P005 (FLP-NdeI-F) and P006 (FLP-SacI-R) primers. PCR conditions are described in paragraph 2.2.2.1 and *pfu* polymerase (Agilent) was used. The annealing temperature was 65°C and extension time was 75 seconds at 72°C. A band corresponding to the FLP size (1.2kb) was amplified (Figure 6-4A-2) and cloned into *NdeI*/*SacI* restriction sites of pAW8ENdeI plasmids. For cloning, both the plasmids and the insert were digested by *NdeI* and *SacI* (digestion conditions in Materials and Methods). 5µl of the digested products were run on an agarose gel (0.7% agarose containing ethidium bromide) to check sizes and Figure 6-4A-3 shows a linearised pAW8ENdeI_0SS plasmid (~9.0kb) in lane 2 and the FLP-H305L (~1.2kb) in lane 3. Digested products were then run on a 0.7% agarose gel containing SYBR DNA gel stain and the bands were extracted from the agarose as described in Materials and Methods. In first instance, FLP-H305L was cloned into pAW8ENdeI_0SS-cgfp plasmid. This plasmid differs from the used pAW8ENdeI_0SS_CyEGFP, in that it contains a long *urg1* promoter in comparison to the short *urg1* promoter present in pAW8ENdeI_CyEGFP plasmids (Watson, personal communication). We later decided to use pAW8ENdeI_CyEGFP plasmids and hence transferred FLP-H305L from pAW8ENdeI_0SS-cgfp to pAW8ENdeI_CyEGFP plasmids. To construct pAW8ENdeI_0SS_FLP H305L_cgfp, purified plasmid and insert were ligated (see Materials and Methods). To check insertion, the plasmid was digested by *NdeI* and *SacI* which released the insert. The positive clone (Figure 6-4A-4) was sequenced using Seq 002 (FW seq FLP) and Seq003 (Rev seq FLP) primers and it was confirmed that no mutation was present in the FLP gene. Insertion of FLP-H305L into

pAW8ENdeI_CyEGFP plasmids was carried out by cutting out FLP-H305L from pAW8ENdeI_0SS_FLP H305L_cgfp using *NdeI/SacI* and cloning into *NdeI/SacI* digested pAW8ENdeI_CyEGFP plasmids (Figure 6-4B-1). After transformation into *E.coli*, colonies were tested for the presence of the FLP by digestion with cloning restriction enzymes, *NdeI* and *SacI* (Figure 6-4B-2). These clones were unlikely to contain mutations as there were no PCR processes involved, therefore they were not sequenced before *S. pombe* transformation. Sequences after transformation in *S. pombe* confirmed that there were no mutations into the FLP genes.

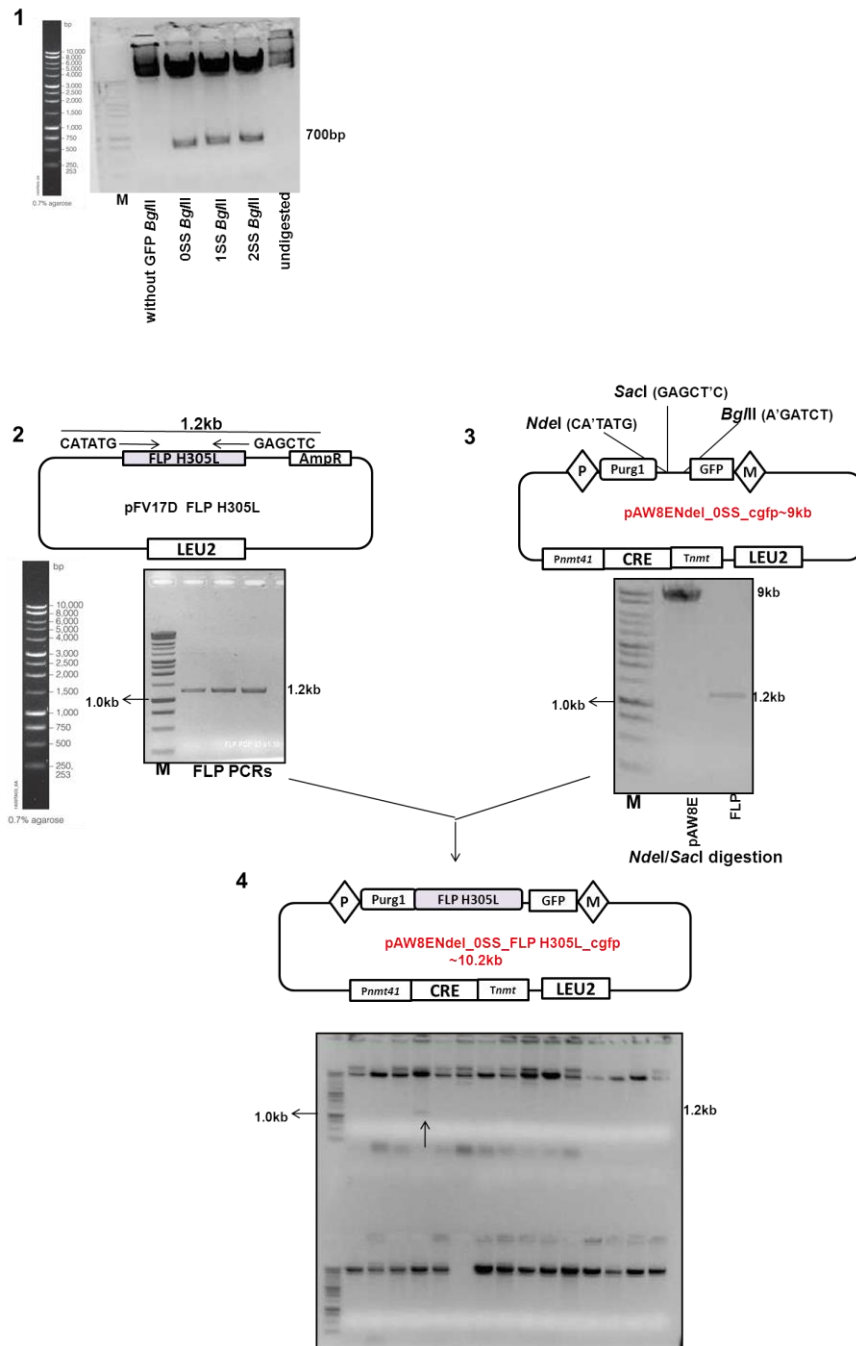


Figure 6-4A. Cloning of H305L gene into cre lox pAW8ENdel_OSS_cgfp plasmid. (1) pAW8ENdel cre-lox plasmids were checked by digestion with *Bgl*II which releases the CyEGFP tag (~700bp). Undigested plasmid (lane5) and pAW8E without CyGFP digested by *Bgl*II (lane2) were run as controls. (2) FLP H305L gene was PCR amplified and (3) both the FLP PCR product and plasmid were digested with cloning restriction enzymes *Nde*I and *Sac*I. (4) Clones were checked by digestion with the cloning enzymes which released the insert (~1.2kb band). In a total of 37 checked colonies, 1 colony contained the insert and was sequenced to confirm presence of FLP H305L without additional mutation.

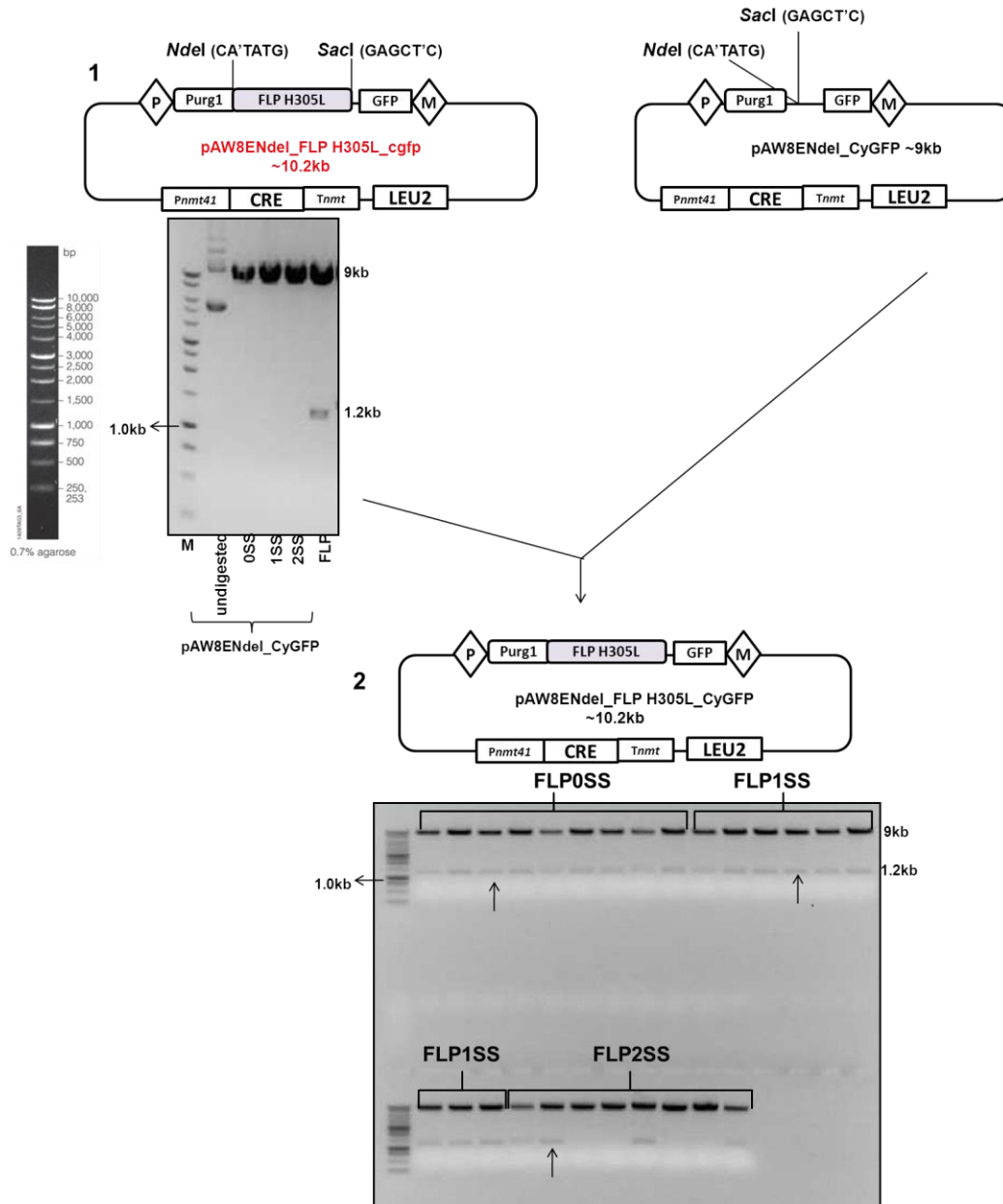


Figure 6-4B. Cloning of H305L gene into cre lox pAW8ENdel_CyGFP plasmids. (1) pAW8ENdel cre-lox plasmids were checked by digestion with *NdeI/SacI* which linearised the plasmid. FLP-H305L was released from pAW8ENdel_OSS_FLP H305L_cgfp by digestion with *NdeI* and *SacI* (lane6). Undigested plasmid pAW8ENdel_CyGFP (OSS) was run in lane2 for control. (2) After ligation and E.coli transformation, clones were digested with cloning enzymes to check for the presence FLP H305L gene. 9 out of 9 tested colonies contained the insert in FLP0SS and FLP1SS plasmids and 4 out of 8 tested colonies contained the insert in FLP2SS plasmid. Positive colonies (indicated by arrows) were used for further steps.

C. Replacing CyEGFP tag by HA tag in pAW8ENdeI _FLP H305L_CyEGFP cre-lox plasmids

In the study carried out on *S. cerevisiae* (Nielsen *et al.*, 2009), the HA tag was used as a tag for the FLP protein. We decided to use the same tag and replace the CyEGFP tag by the HA tag. HA was synthesised as oligonucleotides P019 (HA-F_ *Bgl*III *Nde*I mutated) and P020 (HA-R_ *Bgl*III *Nde*I mutated) and annealed using the protocol described in Materials and Methods (Figure 6-5A). Annealed HA showed a defined band at ~100bp whereas a control (unannealed FW HA oligonucleotide) showed a smear (Figure 6-5A). The pAW8ENdeI _FLP H305L_CyEGFP plasmids and annealed oligos were then digested with restriction enzyme *Bgl*III, extracted from an agarose gel (2% for HA and 0.7% for the plasmids) and ligated. Due to the small size of the insert, *Bam*HI was used to confirm HA insertion. *Bam*HI has a single restriction site in the plasmid and a site in the HA tag, in case of insertion a ~1.5kb fragment was released whereas the enzyme linearized the plasmids in absence of the insert (Figure 6-5C). Two positive clones per plasmid were sequenced using Seq004 (HA-FW) primer and this confirmed that there are no mutations in the tag.

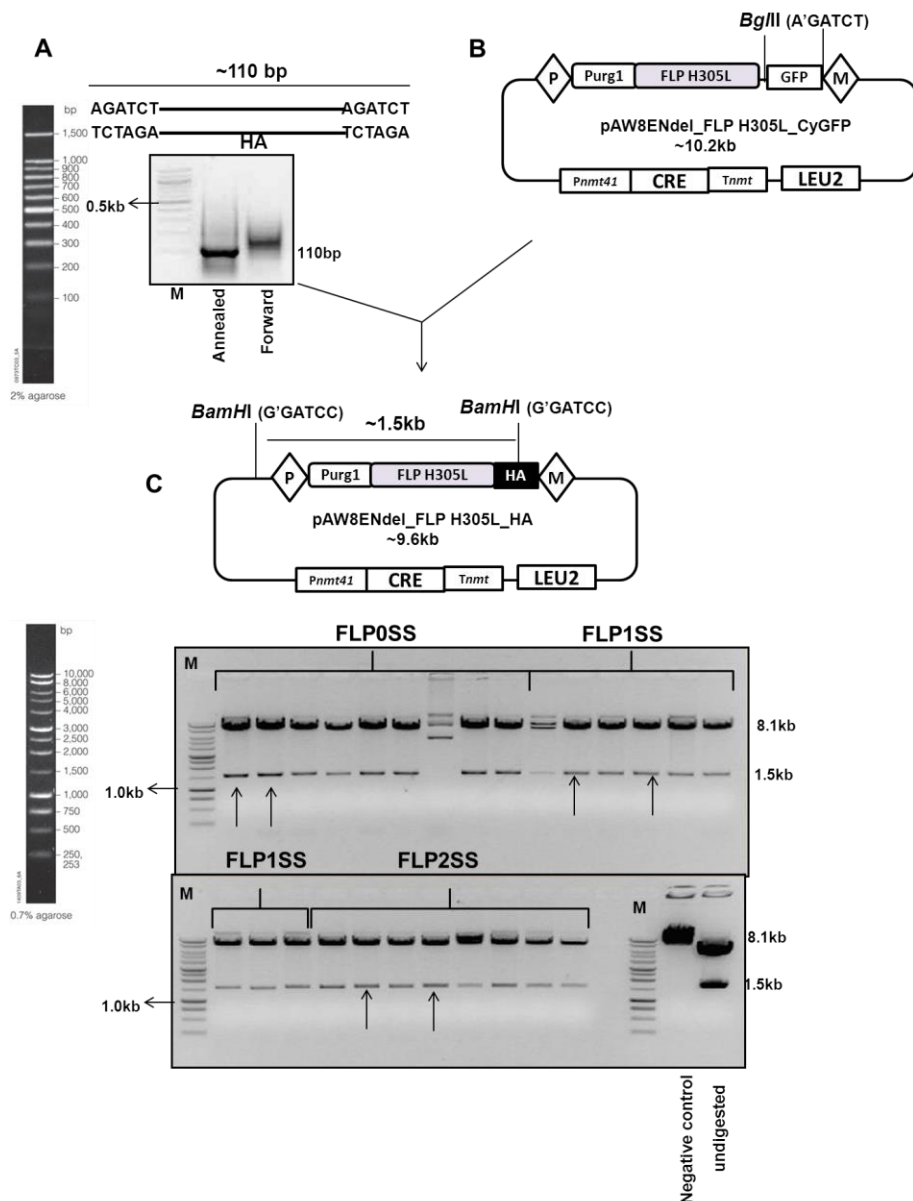


Figure 6-5 Replacing CyEGFP tag by HA tag in pAW8ENdel_FLP H305L_CyEGFP plasmids.

HA tag oligonucleotides were annealed and cloned at the *Bgl*II restriction sites of pAW8E vectors replacing the CyEGFP tag. (A) Annealed oligos were loaded in lane two and the single forward oligo loaded in lane three as a control. Lane 1 contains Promega 100bp Marker, on the left. A clear band was observed in annealed oligos, while the control showed a smear. (B) The plasmid was digested with *Bgl*II to release the tag (gel on figure 6-4). (C) Clones were checked for integration of the insert by digestion with *Bam*HI which in case of integration released a 1.5kb fragment and a linear plasmid in absence of the insert. The plasmid without the insert (negative control) and undigested plasmids were run as controls. 8 out of 9 tested colonies contained the HA tag in FLP0SS and FLP1SS plasmids, while 8 out of 8 had the tag in FLP2SS plasmid. Two positive clones (indicated by the arrows) were sequenced and confirmed the presence of the tag in each plasmid (OSS, 1SS and 2SS).

6.1.1.2 Transform FLP H305L_HA into *S. pombe*

To integrate FLP H305L_HA, the pAW8ENdeI_FLP H305L_HA plasmids were transformed into *S. pombe* strain MG52 (obtained from Dr Watson) using the transformation protocol described in Materials and Methods. To select for colonies containing the FLP gene, we followed the protocol described in Watson *et al* (2008) for RMCE exchange (Figure 6-6A). After transformation, cells were plated on YNBA minimal media supplemented with adenine 0.1g/l, which allows selection of transformants containing the plasmids (LEU marker). Adenine was added to the media as base strains are *ade6-704*. Cells were grown at 30°C for five days and single colonies were re-streaked on the same minimal media containing adenine. Cells were then grown overnight (30°C, shaking) in minimal media supplied with adenine (0.1g/l) and leucine (0.1g/l) for the exchange by recombination which is triggered by the Cre recombinase.

As Cre recombinase is expressed under the *nmt* promoter (Watson *et al.*, 2008), it is important to use media without thiamine in order to keep the promoter active and allow recombination. In addition, to avoid undesired expression of the FLP protein (which might be harmful to the cell) under the *urg1* promoter, we used media without uracil. 500 cells were plated on minimal media with adenine and leucine to allow them to lose the plasmid, and after 3 days incubation at 30°C, 40 colonies were streaked on the same media and incubated two days at 30°C. In the final step, cells were replica plated on minimal media with adenine to check for loss of the plasmid (*leu-* cells), YEA media with hygromycin 100µg/ml for the presence of FLP (loss of hygromycin cassette), YEA (to check viability of the cells with the FLP on rich media) and minimal media+adenine+leucine. Cells that were sensitive to hygromycin and didn't grow on minimal media (with adenine) were selected for further steps. Integration of the genes was checked by PCR using the protocol in Materials and Methods. PCR products (Figure 6-6B) confirmed the presence of the gene in the right locus. The full FLP genes were then PCR amplified using the same PCR conditions and sequenced using seq002 (FW seq FLP) and seq003 (Rev seq FLP) primers. The sequences confirmed that no mutation was present in the genes.

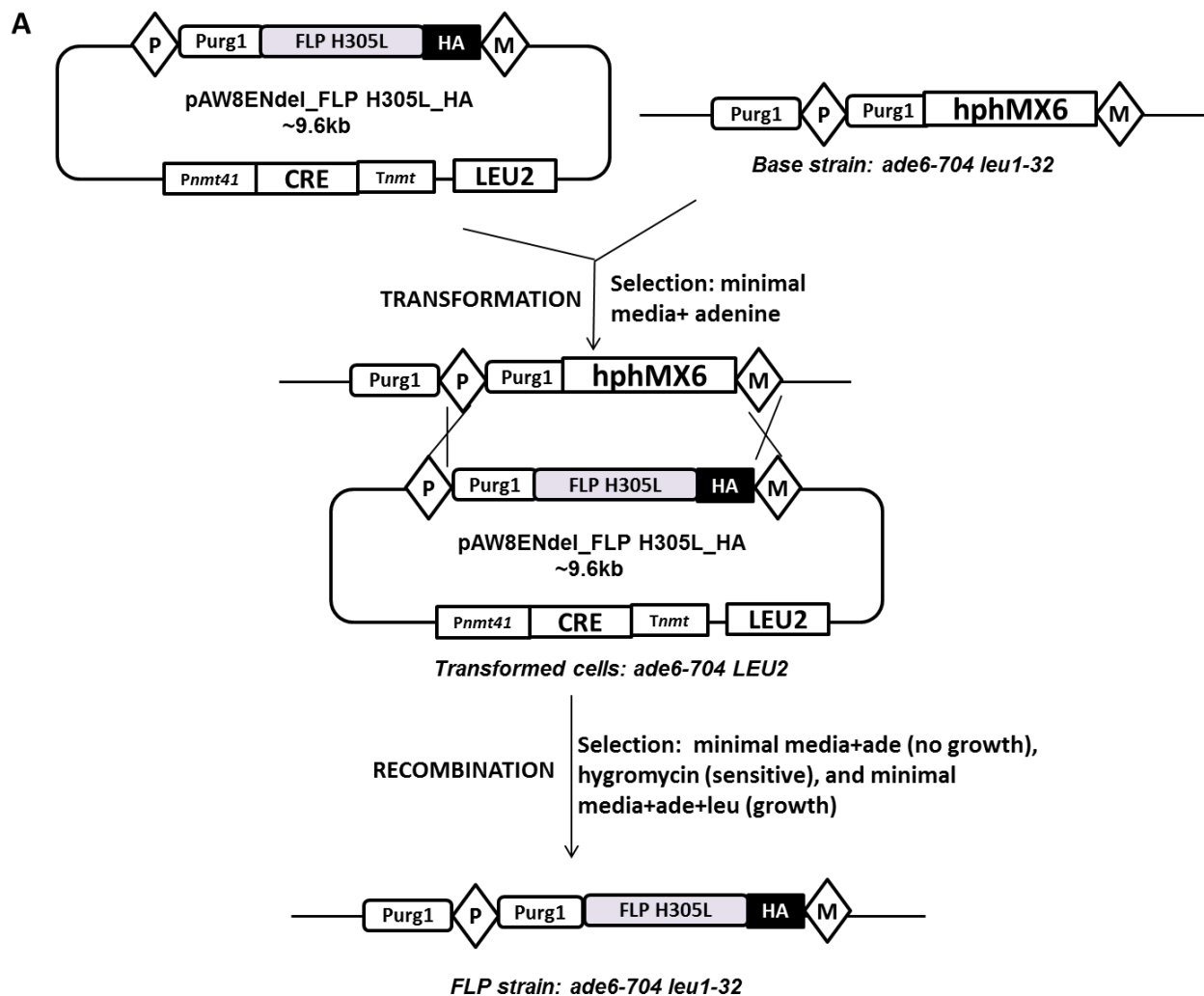


Figure 6-6A. Integration of FLP H305L_HA into *S. pombe*. pAW8E_FLP H305L_HA plasmids were transformed into *S. pombe* base strain MG52. Transformants containing the plasmids (LEU2 marker) were selected on minimal media with adenine. After recombination between the lox sequences, triggered by the cre recombinase, recombinants were grown in minimal media supplemented with adenine and leucine to select for cells that have lost the plasmids. Cells were then replica plated on hygromycin (check for the loss of *hph* cassette and presence of FLP), minimum media + adenine (check for the loss of the plasmid) and minimal media + adenine+ leucine. In total, 56 out of 120 colonies contained the FLP, 144 out of 160 colonies contained the FLP1SS and 119 out of 160 colonies contained the FLP2SS. Genomic DNA was isolated from one colony of each strain (one colony for FLP, one colony for FLP1SS and one colony for FLP2SS)

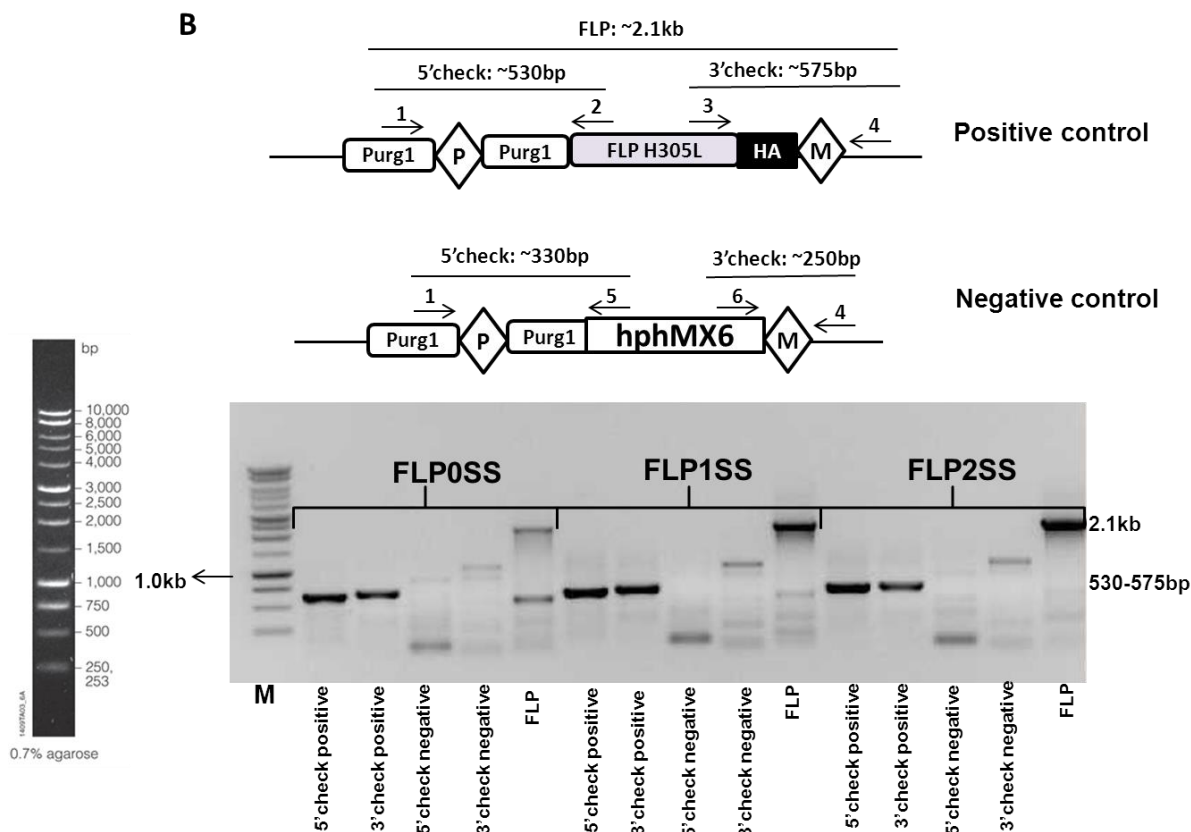
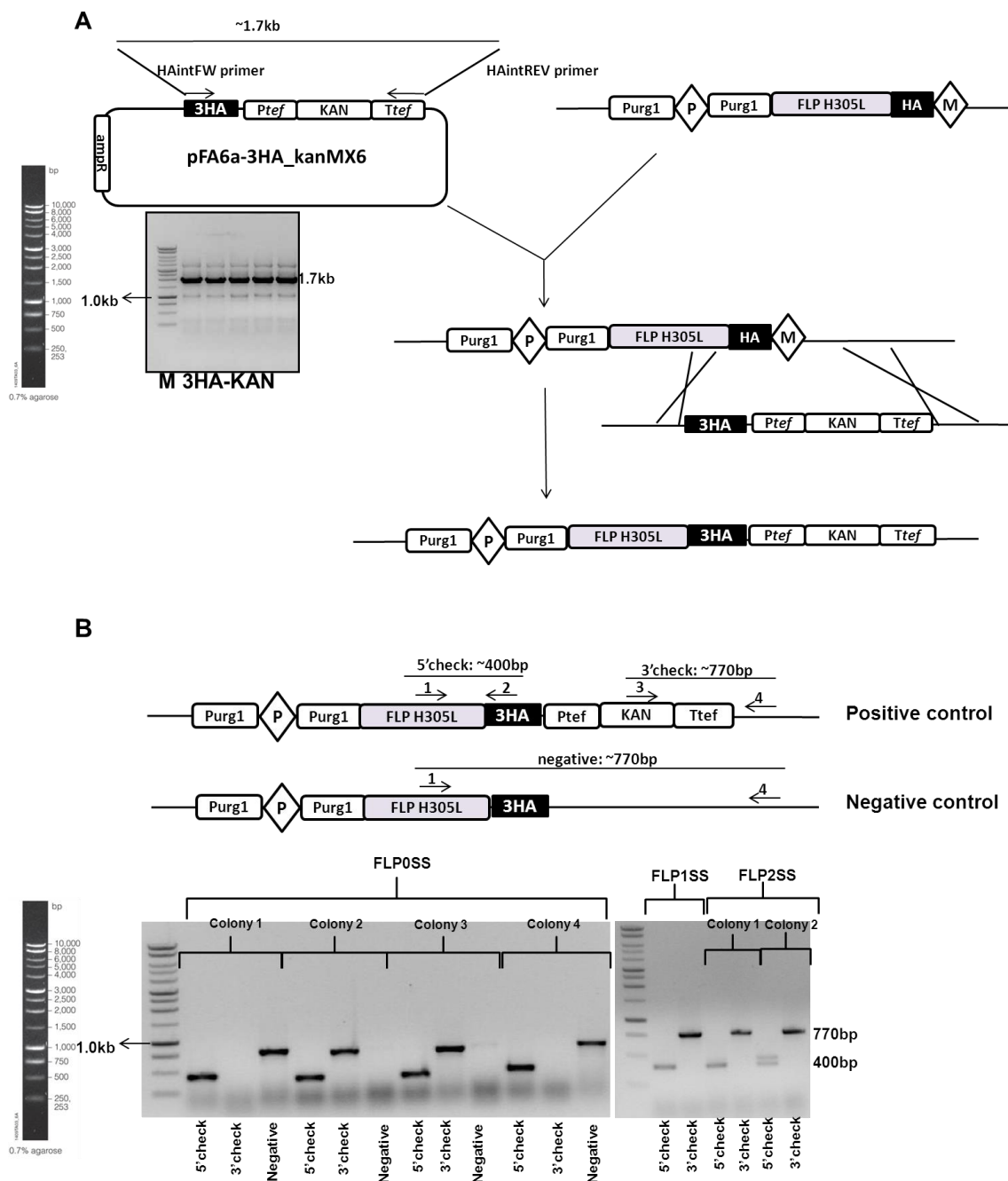


Figure 6-6B. PCR checking integration of FLP H305L_HA into *S. pombe*. Positive colonies containing FLP H305L were checked by PCR on genomic DNA using the following primers: 1: P043 (5'FLP check-fw-urg1), 2: P036 (5'FLP check-rev), 3: P037 (3'FLP check-fw), 4: P038 (3'FLP check-rev), 5:P049 (5'hphcheck-rev), 6: P050 (3'hphcheck-fw). Bands with expected sizes, 530bp for 5'check, 575bp for 3'check and ~2.1kb for isolation of the whole FLP gene, were isolated. Negative controls, using oligos to confirm the absence of the FLP, showed weak bands that do not correspond to the expected sizes (330bp for 5'check and 250bp for 3'check). These products might be due to unspecific priming of the oligos. Whole FLP sequence was isolated using primers 1 and 4, sequenced and confirmed that there was no mutation in the three sequences (FLP, FLP1SS and FLP2SS).

6.1.1.3 Integration of 3HA-KAN into “FLP strains”

FLP gene expression was induced by addition of uracil which activates the *urg1* promoter (Watt *et al.*, 2008), but Western Blot using mouse anti HA antibody failed to detect the protein. Analysis of the sequences showed a mistake in the design of primers which placed a stop codon between the FLP gene and the HA, explaining why the protein could not be detected. The tag was subsequently inserted into the “FLP” *S. pombe* strains by transformation, removing the stop codon. The 3HA tag was PCR amplified from the pFA6a-3HA-kanMX6 (Bahler *et al.*, 1998) plasmid using P044 (HAintFW) and P045 (HA intREV) long primers with 100bp homology to the FLP and downstream region. PCR was carried out following PCR conditions as described in paragraph 2.2.2.1 using *phusion* polymerase (Fisher). The annealing temperature was 66°C and extension time was 3 minutes. A band was amplified that corresponds to the expected size (1.7kb) (Figure 6-7A).

The PCR product was cleaned using the MACHEREY-NAGEL PCR clean kit (Materials and Methods). The tag was then inserted by recombination using transformation. Positive colonies were selected on media with G418 (KAN cassette) and colony PCR was used to check integration at the correct locus (Figure 6-7B).



6.1.1.4 Expressing FLP proteins

Expression of the FLP protein was confirmed by Western Blot using mouse anti HA antibody (Santa Cruz Biotechnology) and rabbit anti mouse secondary antibody (DAKO). The experiment was carried out following the protocol described in Materials and Methods. Cells were grown in 100 ml of YNB media supplemented with adenine and leucine (0.1g/l) to reach $5 \cdot 10^6$ cells/ml. FLP expression was triggered by the addition of uracil 0.25 mg/ml (Watt *et al.*, 2008) which induces the *urg1* promoter. 10 ml ($5 \cdot 10^7$ cells) of samples were collected after 5, 30, 60, 120 and 240 minutes for protein extraction. Protein was purified using the TCA protein extraction protocol as described in Materials and Methods (paragraph 2.2.1.6). As shown in *Figure 6-8*, a band corresponding to the size of FLP (50kDa) was detected in the “FLP” without STARTSTOP codon strain in the presence of uracil after 30 minutes induction. There was no detection of the protein in the absence of uracil at time 0. In FLP strains with STARTSTOP codons, there was no detection of the protein at all times points despite a long exposure of the membrane (the membrane was exposed for 30 minutes). This suggests that the presence of start-stop codons decreases protein expression below detectable levels as PCR check (*Figure 6-7*) confirmed that the FLP genes and the HA tag were present in the strains. As the prime aim was to express the protein, we did not further investigate the effect of the start-stop codons on the FLP expression.

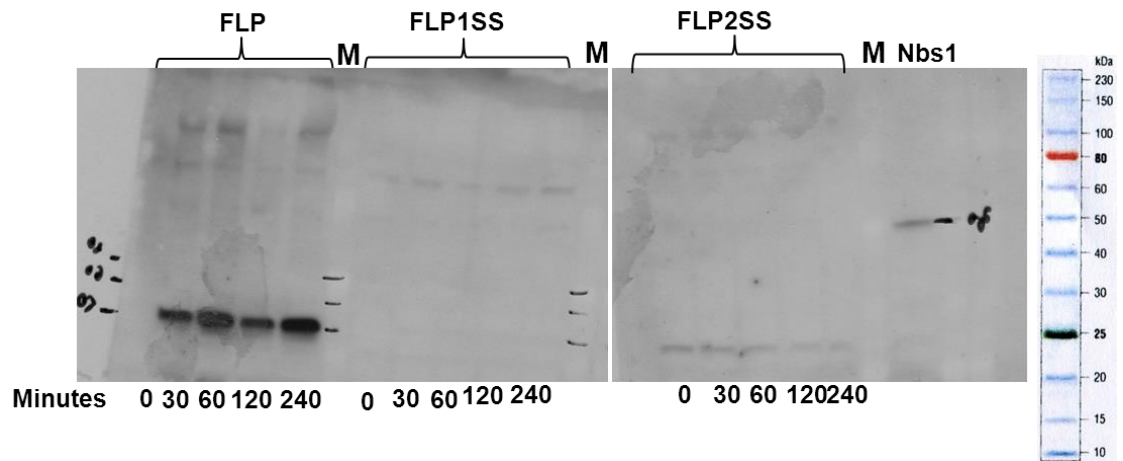


Figure 6-8 Detection of FLP expression by western blot. After 30 minutes incubation with uracil, a band corresponding to the size of the FLP protein (50kDa) was detected in the FLP strain but there was no detection in strains with low expression (1SS and 2SS) of the protein. Protein expression was detected using mouse anti HA tag primary antibody and rabbit anti mouse secondary antibody. Yeast strains MG86 (FLP), MG90 (FLP1SS) and MG91 (FLP2SS) were used in the experiment. Nbs1 (80kDa) was used as a positive control for the Western blot and Fisher protein ladder was used a size marker (coloured marker on the right).

6.1.2 Integrate FRT sequence into *S. pombe*

To study the effect of DNA-bound FLP on cell survival, the FLP recognition target (FRT, 5'-GAAGTTCCTATACTTTCTAGAGAATAGGAACTTCCGAATAGGAACTTC-3') was integrated close to an autonomously replicating sequence (ars3004/ars3005) located upstream of the *ura4* fragment (Lambert *et al.*, 2005). The target was first cloned into the *SalI* restriction site of the pFA6a-NatMX6 vector to use NAT as marker for the integration. NAT-coupled FRT was then inserted into a non-transcribed region on chromosome III between the 1.8 *HindIII* fragment which contains the URA4 ORF and ars3004/ars3005. NAT-FRT was integrated at about 100bp after the *HindIII* site (strategy outlined in Figure 6-9).

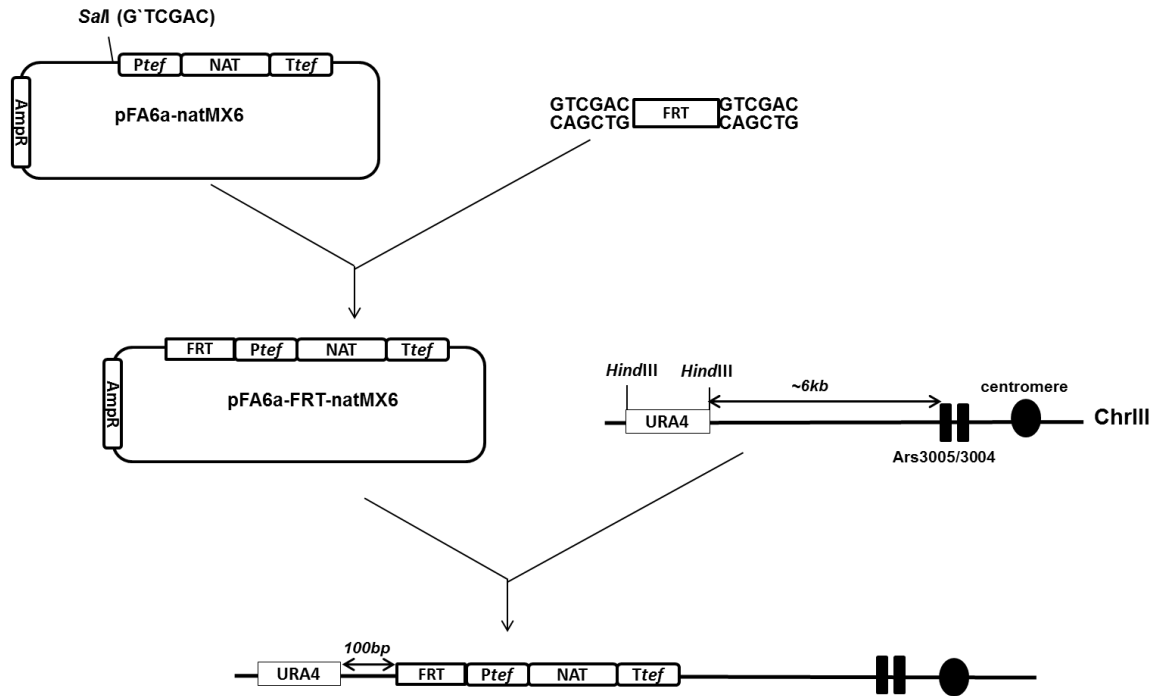


Figure 6-9 General strategy used to integrate FRT target into *S. pombe*. FRT oligonucleotides were cloned under the *SalI* restriction site of pFA6a-natMX6 vector. NAT coupled FRT (to select for integration) was then integrated into the yeast genome upstream of the 1.8 *HindIII* fragment which contains *URA4* ORF and close to an autonomously replicating sequence (*ars*).

6.1.2.1 Cloning the FRT sequence into pFA6a-natMX6

FRT was synthesised as complementary oligonucleotides, P013 (FRT-SalI-F) and P014 (FRT-SalI-R), and annealed using protocols described in Materials and Methods. Both the plasmid and annealed FRT were digested with *SalI* and the plasmid was dephosphorylated for an hour at 37°C by CIP phosphatase (NEB) before ligation. As shown in *Figure 6-10*, bands with expected sizes were detected on a gel: ~70bp for the FRT (fragment corresponding to FRT site, 48bp + restriction site 12bp + 5bp on each side to of the oligos) and ~4kb for the plasmid. Due to the small size of the insert, presence of FRT into pFA6a-NatMX6 after ligation was checked by digestion with *XbaI* which cuts into the FRT sequence but not in the plasmid, linearizing the plasmid with the insert (*Figure 6-10*). 5 positive clones (indicated by arrows) were sequenced using seq005 (FW seq FRT) primer and confirmed the presence of the target in forward and reverse directions.

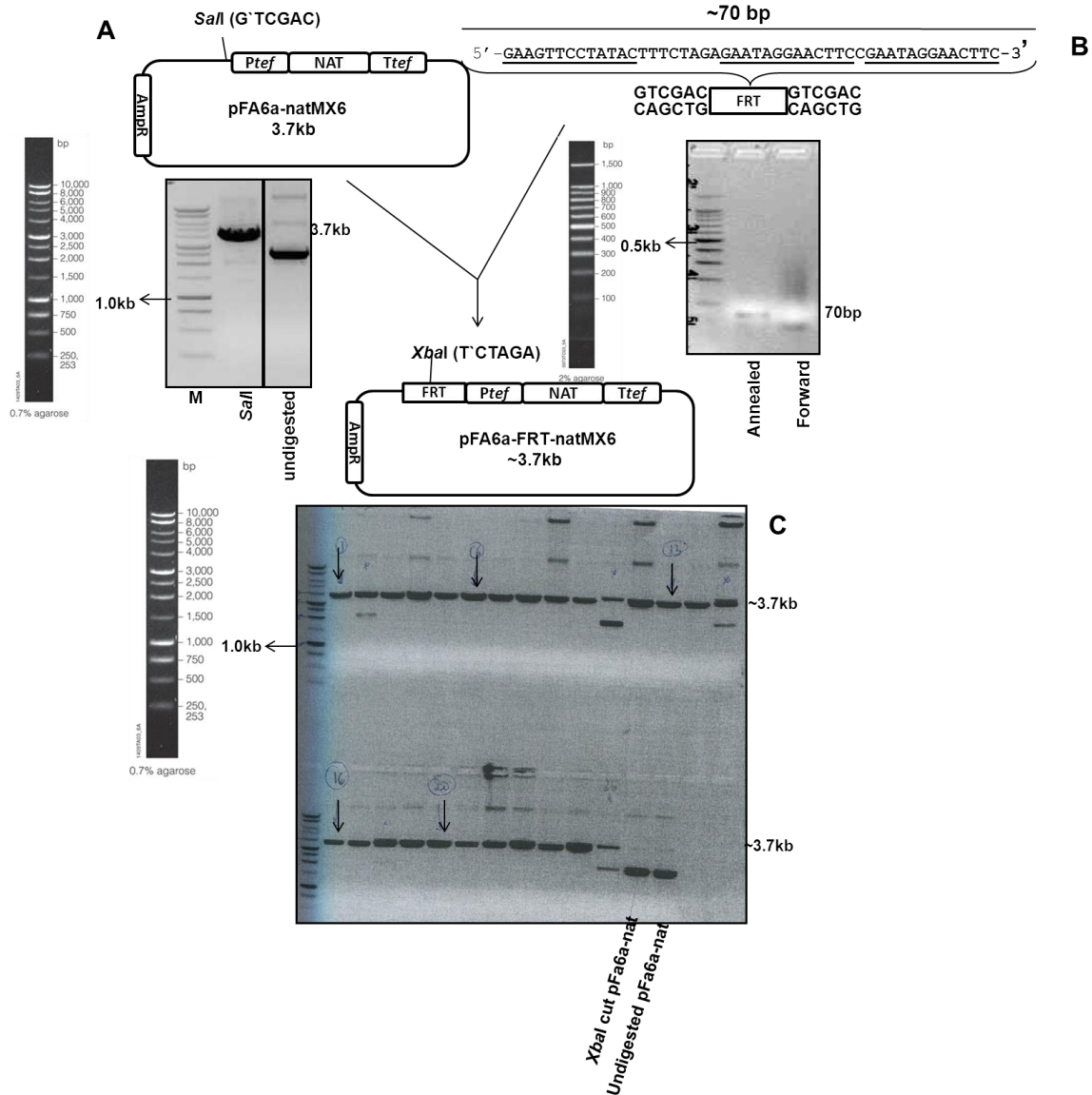


Figure 6-10 Cloning of the FRT sequence into pFA6a-natMX6. FRT oligonucleotides were annealed and cloned into the *SalI* restriction site of pFA6a-natMX6. **(A)** The plasmid was linearized by digestion with *SalI* (lane 2), undigested plasmid is loaded in lane 3 as a control. Lane 1 contains 1kb DNA marker (Promega). **(B)** Annealed FRT oligos were loaded on a 2% gel (lane 2) and unannealed FRT-*SalI*-FW loaded in lane 3 as a control. Lane 1 was loaded with 100bp DNA marker (Promega). A ~70bp defined fragment corresponding to the FRT site was detected in lane 2. **(C)** Presence of FRT in pFA6a-NatMX6 was checked by digestion with *XbaI* which cuts into the FRT sequence but not the plasmid. pFA6a-nat undigested and digested by *XbaI* were loaded as controls and confirmed that the enzyme does not cut into the plasmid. 18 clones out of 26 digested clones contained the insert and clones indicated by arrows were sequenced and the FRT was confirmed. Underlined sequences into the FRT indicate regions of recognition of FLP.

6.1.2.2 Transform FRT sequence into *S. pombe*

FRT was transformed into *S. pombe* cells using the classic transformation protocol (see Materials and Methods) and inserted into the *S. pombe* genome by recombination. NAT-coupled FRT (in forward and reverse direction) was amplified from pFA6a-FRT-natMX6 vector using P059 (FRTintURA4FW) and P053 (FRTintURA4REV) long primers with 100bp homology to the region upstream of the *ura4* coding sequence and 20bp homology to either pFA6aNAT plasmid sequence before FRT (FW) or the NAT cassette (REV). PCR was carried out following conditions as described in paragraph 2.2.2.1 using *phusion* polymerase (Fisher). The annealing temperature was 66°C and the extension time was 3 minutes.

As shown in *Figure 6-11A*, a band with the expected size [~1.5kb fragment corresponding to the NAT cassette with the *tef* promoter and terminator (~1.2kb), FRT target (~70bp) and long primers (~200bp)] was amplified. The target was then integrated into *S. pombe* chromosome III between the *URA4* gene and an origin of replication sequence (*ars3005/ars3005*). FRT was first integrated into MG52 (*h-urg1::loxP-hph-loxM3 ade6-704 leu1-32*) which was later crossed to “FLP” strains. NAT-resistant colonies were PCR checked for integration by colony PCR, using P040 (3'URA4 check-FW), P056 (FRTcheck5'REV), P057 (FRTcheck3'FW) and P058 (FRTcheck3'REV). *Figure 6-11B* shows bands with expected sizes at both 5' (~1.1kb) and 3' (~400bp) sites. Genomic DNA was extracted from positive colonies and FRT was PCR amplified using P040 and P056 primers. FRT was then sequenced using seq006 (FRT int seq) and it was confirmed that there were no mutations in the FRT.

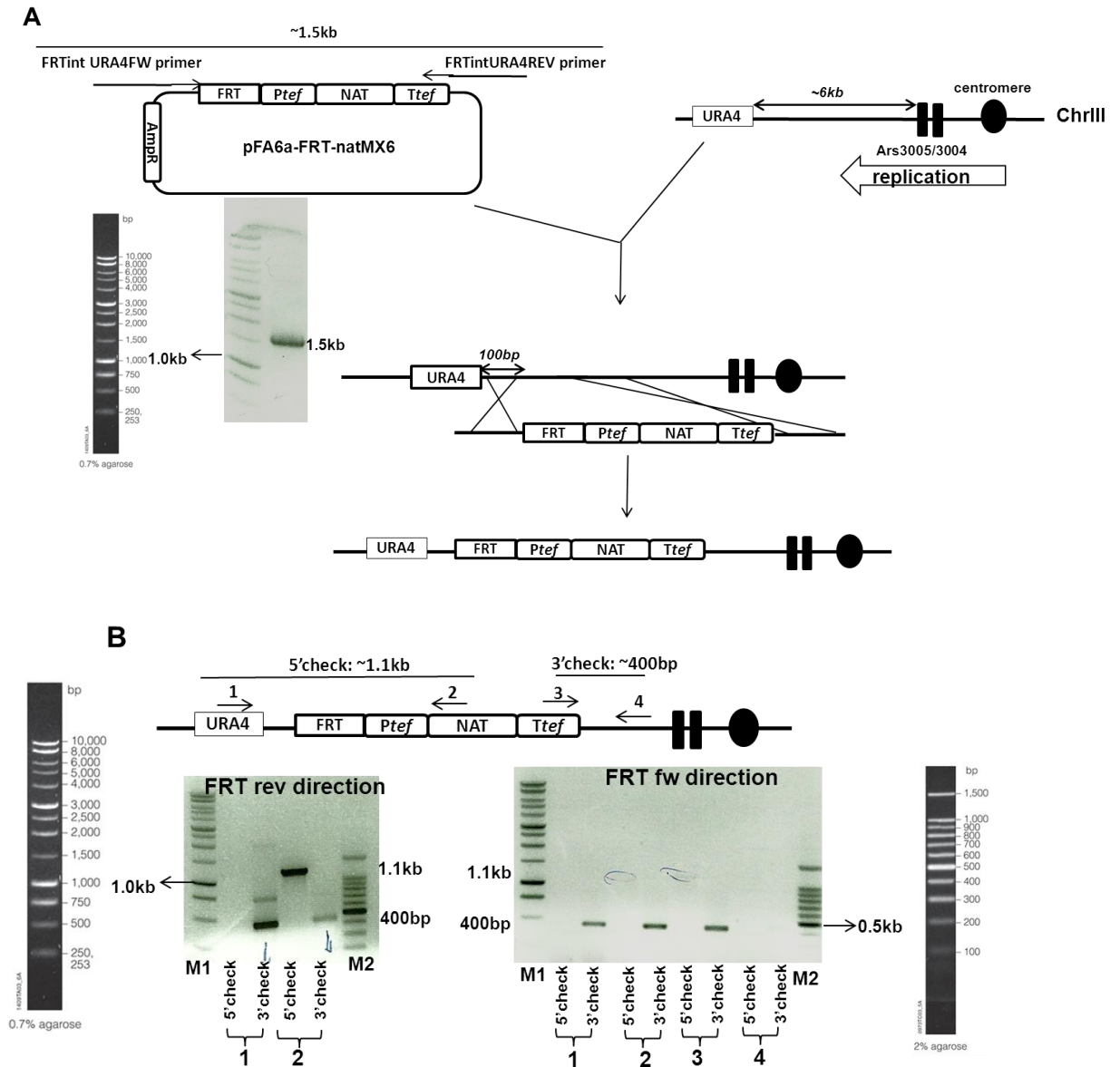


Figure 6-11 Integrate FRT sequence into the *S. pombe* genome. (A) The target coupled to NAT was PCR amplified from pAF6a-FRT-natMX6 using long primers (P053 and P059) with homology to the region upstream of the URA4 gene. A band with expected size (~1.5kb) was amplified. The target was transformed into *S. pombe* strain (MG52) and inserted on chromosome III, between the URA4 gene and an origin of replication sequence, using HR dependent integration. (B) Transformants (resistant to NAT) were PCR checked for integration. 1: P040, 2: P056, 3: P057 and 4: P058 primers were used and fragments corresponding to the expected sizes were amplified in two colonies (colonies 2 and 3) tested for the presence of forward FRT and in one colony (colony 2) of reverse FRT. Genomic DNA was isolated from positive colonies and fragments amplified with primers 1 and 2 were sent for sequencing. The dot in the figure indicates the position of the centromere on the chromosome. M1=1kb DNA ladder and M2=100bp DNA ladder.

6.2 Analysis of “FLP nick” strains

Integration of the “FLP nick” constructs into *S. pombe* was carried out by crossing mutants strains of interest with constructs containing the FLP gene and the FRT target using kanamycin (3HA-kan) and NAT resistant cassettes as selection for the presence of FLP and FRT respectively. To test the viability of strains with the “FLP-nick” system, we first combined the system with MRN defective mutants to assess the role of the complex in survival of cells to potential nicks induced by the FLP-nick. As MRN has been shown to be involved in removal of DNA bound proteins (topoisomerases), we hypothesised that “FLP-nick” cells wouldn’t survive in the absence of MRN and Nielsen *et al.* (2009) have shown that MRX defective mutants don’t survive in the presence of the FLP-nick system. “FLP-nick” cells were crossed with *mre11-D65N* and *rad50Δ* mutants (MRN defective mutants) and tested for survival to uracil (induction FLP expression). To test viability of cells after a long term exposure to uracil, I carried out spot tests on EMM minimal media containing different concentrations of uracil. Results in *Figure 6-12* showed no differences between the MRN mutants and the WT after 5 days incubation at 30°C. Cells containing only the FLP (or FLP1SS) and cells with only the target in both directions also showed similar survival when compared to cells with both the FLP and the target. Sensitivity of MRN mutants to CPT confirmed that cells were MRN defective. Observation after three days incubation showed similar results (not shown).

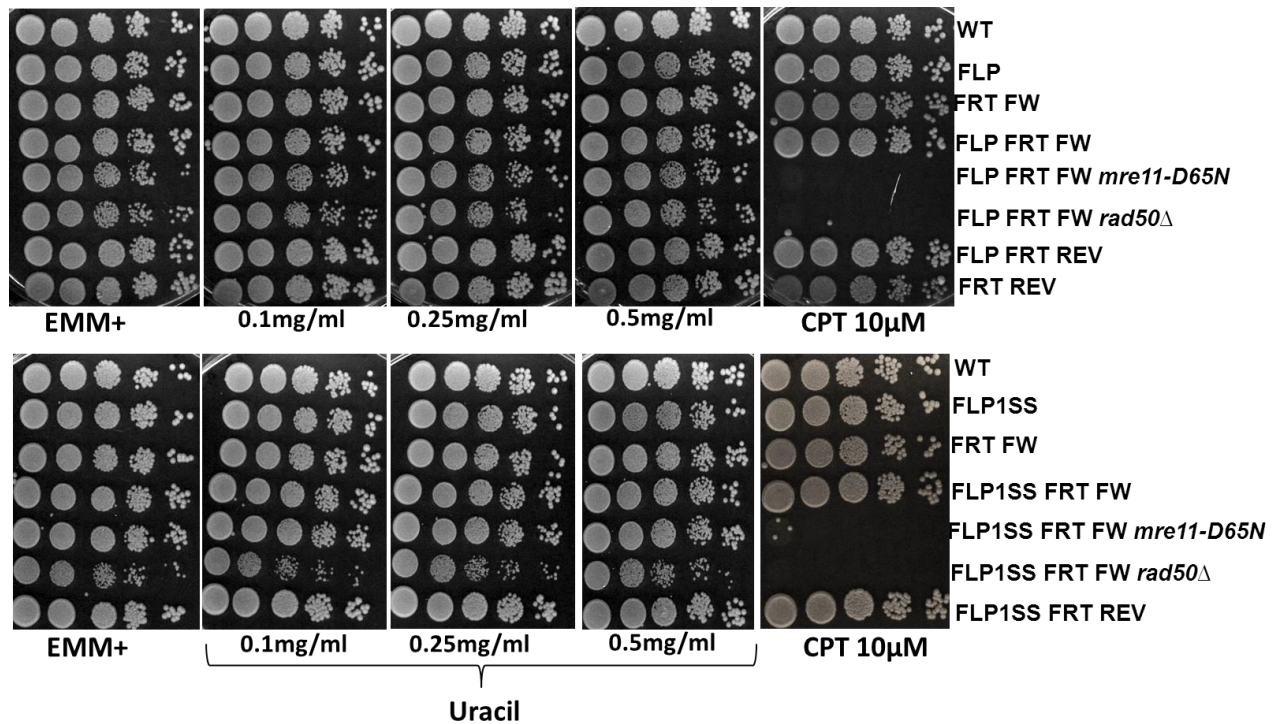


Figure 6-12 FLP-nick MRN defective strains are resistant to FLP induction with uracil during continuous exposure. Tests were carried out on minimal EMM media supplied with adenine and leucine. Different concentrations of uracil were added to trigger FLP expression and plates were incubated for five days at 30°C. Tested strains were: WT (MG19), FLP (MG86), FRT FW (MG132), FLP FRT FW (MG148), FLP FRT FW *mre11-D65N* (MG165), FLP FRT FW *rad50Δ* (MG278), FLP FRT REV (MG133), FRT REV (MG130), FLP 1SS (M90), FLP 1SS FRT FW (MG151), FLP 1SS FRT FW *mre11-D65N* (MG166), FLP1SS FRT FW *rad50Δ* (MG279), FLP1SS FRT REV (MG135). All strains showed similar survival to uracil. Cells were also tested with CPT to confirm that strains are MRN defective. The experiment was carried out once.

Acute exposure survival assay to uracil was carried out to assess whether cells are affected after a short term induction of the system and if they recover from the induced nicks. To carry out tests, cells were grown to exponential phase (cell density of 2.10^6 cells/ml) and 25mg/l of uracil were added to the cells to induce FLP expression (Watt *et al.*, 2008). Samples were collected every 30 minutes for the first hour and every hour for the remaining three hours. Uracil was then washed out and cells were plated on minimal media without uracil and incubated for 5 days at 30°C. Results in *Figure 6-13* show a slight reduction of cell growth in *mre11-D65N* and *rad50Δ* mutants between 0 and 60 minutes after addition of uracil to the media. This effect was more noticeable in *rad50Δ* mutants. WT cells showed a better growth in the presence of uracil, probably due to the presence of uracil as an additional nutrient for the cells when compared to media without uracil. After 2 hours incubation with uracil, *mre11-D65N* and *rad50Δ* mutants recovered growth and reached the same levels as cells without uracil. The test was carried out in cells containing the FLP without start-stop codon and FRT in forward direction. These results further suggest that in *S. pombe* MRN defective mutants, the FLP-nick system affects cell growth immediately after induction of the system, but that cells regain a normal growth after a long term exposure, probably due to repair of FLP induced nicks which allows cells to survive. To assess whether the target was still present in the cells, I sequenced the FRT from 19 colonies [5 colonies FLP/FRTrev WT (MG133), 5 colonies FLP/FRTrev *mre11-D65N* (MG159) 4 colonies FLP1SS/FRTrev WT (MG135) and 5 colonies FLP1SS/FRTrev *mre11-D65N* (MG160)] that grew on survival plates after 4 hours incubation with uracil. Results (not shown) showed that there were no mutations present in the FRT site in all colonies, confirming that the recognition site is present into the *S. pombe* genome of survival colonies. The FLP protein from the same survival colonies was not sequenced due to time constraints.

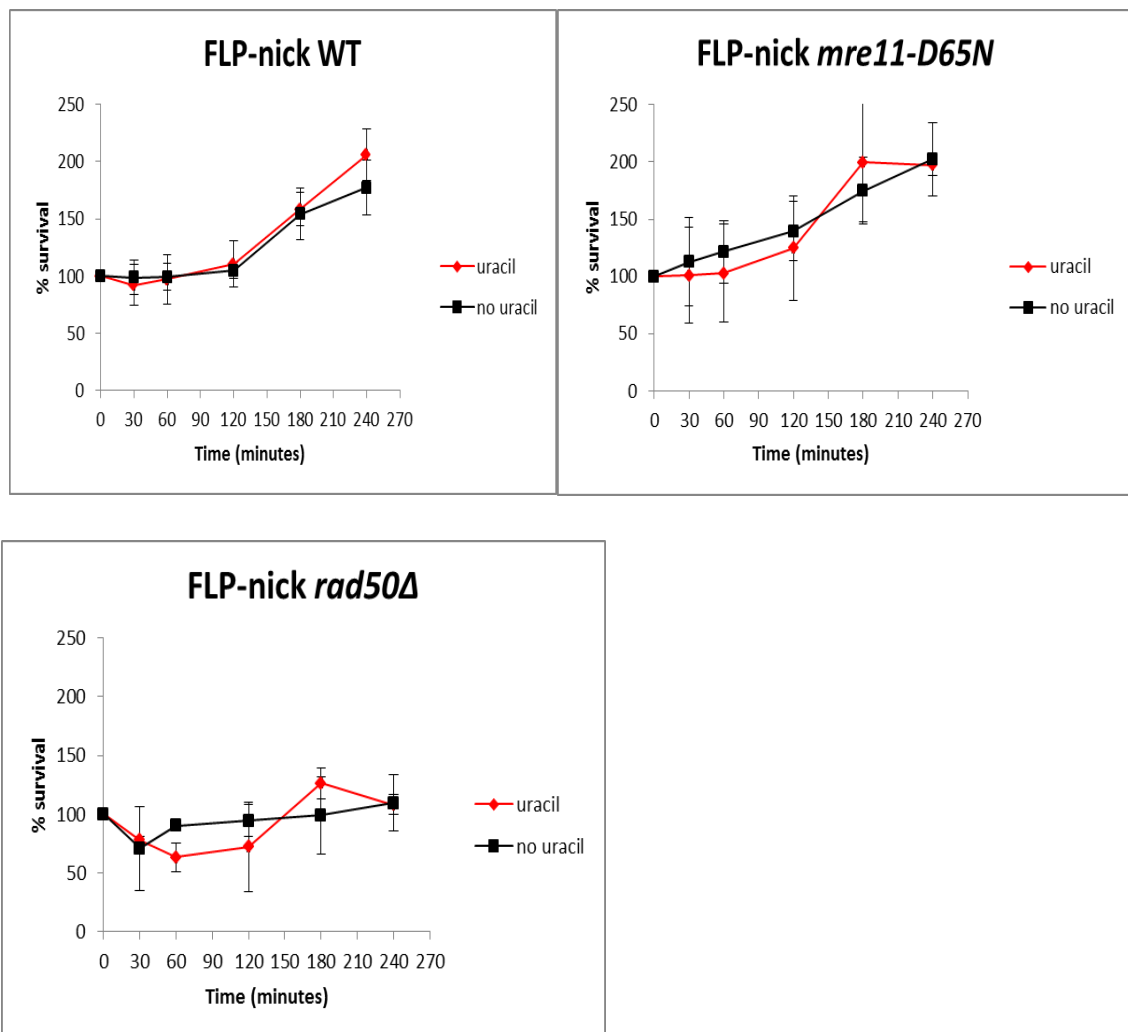


Figure 6-13 FLP-nick MRN defective strains show a reduced growth after 30 minutes incubation with uracil. Tests were carried out in minimalEMM media supplied with adenine and leucine. FLP-nick FW (MG148), FLP -nick *mre11-D65N* (MG165) and FLP-nick *rad50Δ* (MG278) were tested. Cells were grown to reach a density of 2.10^6 cells/ml before addition of uracil 25mg/l. Cells were then collected after 30, 60, 120, 180 and 240 minutes, uracil was washed out and 200 cells were plated on EMM+leu+ade and incubated for 5 days at 30°C. % survival is calculated to time 0 before addition of uracil (Y axis). X axis shows time in minutes. Error bars show standard deviation calculated on three experiments. After 30 minutes incubation with uracil, FLP-nick MRN defective mutants showed a slightly reduced growth but recovered after 120 minutes.

6.3 Discussion

DNA-bound proteins complexes are used in cancer therapy which kills proliferating cancer cells by trapping proteins to the DNA inducing breaks and leading to cell death (e.g. CPT and etoposide). Study of the repair of DNA bound protein, therefore, is an important step in understanding mechanisms underlying resistance of cancer cells to these drugs.

Because cells defective in MRN complex are sensitive to drugs that block proteins to the DNA (e.g. CPT) and *S. cerevisiae* MRX defective mutants have shown a reduced growth in the presence of the FLP-nick system (Nielsen *et al.*, 2009), I tested the FLP-nick system by introducing FLP H305L and FRT into MRN mutants. The system was introduced in *mre11-D65N* and *rad50Δ* mutants and spot test results (*Figure 6-12*) showed a similar survival of cells regardless of the presence or absence of the system in both WT and MRN defective mutants. These results suggested that either the FLP-nick system is not induced in the cells or that the MRN complex has no effect on the induced nick after a long term exposure. The differences in MRN response in comparison to observation in *S.cerevisiae*, which showed sensitivity of MRN defective mutants to the FLP-nick system (Nielsen *et al.*, 2009), would suggest that the two yeasts respond differently to FLP induced DNA damage. Short term exposure showed a slight decrease in cell number in MRN mutants during the first hour of exposure but the number increased again after 120 minutes (*Figure 6-13*) reaching the WT levels and, suggesting that MRN mutants recover from FLP-nick induced damage. The first approach to understanding the differences in result is to confirm that the FLP-nick is induced in cells. This would be achieved by Chromatin Immunoprecipitation (ChIP) assay for example (discussed later). If ChIP results confirm that a nick is indeed induced in FLP-nick cells, our results would suggest that the absence of the MRN complex leads to a temporary arrest of the cell cycle rather than cell death which would be less noticeable on long term exposure. In fact as the FLP only induces a single nick (presence of the FRT on specific site) in comparison to CPT which induces genome-wide nicks, we can imagine that when the nick is induced, cell cycle is arrested and the nick is repaired allowing cell survival. One hypothesis might be that following repair of FLP induced

breaks, FRT cleavage site is lost as it was shown that the FLP –nick system induces DSBs in *S. cerevisiae* (Nielsen *et al.*, 2009) and that repair of DSBs might lead to loss of nucleotides during processing of DNA ends (Pardo *et al.*, 2009). It is hence possible that following repair of FLP-induced DSBs, the cleavage site is lost and the FLP cannot induce further nicks into the DNA, leading to cell survival. To assess this hypothesis, I have sequenced the FRT site from colonies after 4 hours incubation with uracil and results (not shown) showed that the target was intact, suggesting that the FRT site is still present in the cells after 4 hours incubation with uracil. Another possibility might be that after prolonged exposure to uracil (spot test), the FLP induction leads to a suppression of the target (or the FLP) and that the grown colonies have acquired mutations into the FLP or the FRT. This would imply that the target is not recognised by the FLP and hence there are no DNA bound proteins and no FLP induced nicks in the cells. To confirm this hypothesis, we could sequence the FLP and FRT from survival colonies after a long term exposure to uracil. Another explanation might be the existence of other proteins such as Tdp1, which is also involved in removal of CPT-top1 complexes (Pouliot *et al.*, 1999; Caldecott, 2003), to remove the FLP from the DNA and allow subsequent repair and cell survival. This suggestion however is in contrast with results observed in *S. cerevisiae*, as FLP-nick MRX defective mutants showed a reduced growth in comparison to FLP-nick WT strain, while there were no differences in growth between the FLP-nick WT and FLP-nick TDP1 defective mutants (Nielsen *et al.*, 2009), suggesting that TDP1 does not have a role in survival of cells to FLP induced nicks.

Due to time constraints, I could not carry out full characterisation of the system however I can suggest recommendations to further assess the functionality of the FLP-nick system in the *pombe* genome:

- In vivo confirmation that FLP H305L binds to the FRT target and that it cleaves the DNA at the FRT site. This would be achieved by Chromatin Immunoprecipitation (ChIP) assay which is a commonly used method for analysis of DNA-protein interactions. ChIP takes advantage of the fact that the protein binding site sequence is known and allows assessing if a protein binds to its DNA site (reviewed by Das *et al.*, 2004). Because the binding of FLP H305L

requires the cleavage step (Parsons *et al.*, 1988; Nielsen *et al.*, 2009), the ChIP assay also allows confirmation that FLP H305L creates a nick at the FRT site.

- Confirm the absence of suppressors in the FLP H305L protein and FRT site which would impede the binding property and explain absence of response after a long term exposure. This would be done by sequencing the FLP gene and FRT site from survival colonies after a long term exposure to uracil.
- Confirm acute exposure survival tests to uracil by extending incubation time to at least 8 hours. In fact graphs in *Figure 6-13* suggest that following uracil induction, MRN mutants` growth is decreased in the first hour but cells recover to reach a peak at 180 minutes. After 180 minutes, cells seem to decrease again. By extending the analysis time we can assess whether the pattern (decrease/increase after 3 hours incubation) is repeated or if it is an experimental artefact. Because 3 hours are within the *S. pombe* doubling time in EMM media (Forsburg and Rhind, 2006), if the pattern (lower peaks at 120 and 300 minutes) is confirmed, results might indicate that the MRN response to FLP-nick system is cell cycle dependent. Analysis of FLP-nick system in *S. cerevisiae* suggested that the system induces S phase specific double strand breaks which require homologous recombination as the HR protein Rad52 was recruited to the FRT site (Nielsen *et al.*, 2009). Because *S. pombe* MRN complex has shown a role in initiation of HR (Hartsuiker *et al.*, 2009), we can hypothesise that similarly to *cerevisiae*, FLP-nick system induces S phase specific DSBs in *S. pombe* which would require the MRN complex. The breaks would be however short lived as cells seem to recover. Analysis of synchronised *S. pombe* cells, for example *cdc25* which blocks cells in G2 phase (Forsburg, and Rhind, 2006), in combination with MRN and FLP nick system could allow to determine at which phase MRN mutants are most vulnerable after induction of FLP-nick system. We can for example carry out similar acute exposure survival assay with *cdc25* mutants in combination with MRN mutants and the FLP-nick system. Results would show MRN defective mutants response after release of synchronised cells, which in turn gives an indication of which phase the MRN mutants are most sensitive.

In summary, results presented in this chapter describe the setting up of the FLP-nick system in *S. pombe*. Establishing the system would be a very useful tool to study and understand the removal of DNA bound proteins in the fission yeast. I have integrated both the FLP H305L step arrest mutant and the FRT, FLP recognition target, into the *S. pombe* genome and combined the system with MRN mutants for characterisation of the system. Preliminary results don't allow me to conclude that the system is functional; the results however constitute a basis for further analyses.

7 General discussion

We have successfully set up a system which allows us to study the effect of nucleoside analogues treatment in *S. pombe* by increasing NA uptake and carrying out phosphorylation of NA into their active form. To achieve this, we have integrated the human hENT1 transporter (Griffiths *et al.*, 1997) and either the human *hsdCK* kinase (Chottiner *et al.*, 1991; Van Rompay *et al.*, 2003) or the *Drosophila dmdNK* kinase (Petersen *et al.*, 1998; Johansson *et al.*, 1999; Vernis *et al.*, 2003) into the *S. pombe* genome. Although in this project we have mainly worked with the human kinase, the *Drosophila* kinase also offers valuable advantages (study of a wide range of NAs as the kinase phosphorylates all nucleosides). Our results suggest that similarly to *hsdCK*, *dmdNK* also increases drug toxicity of GemC and AraC (Figure 3-10 and Figure 3-11), two NAs used in this project, suggesting that *dmdNK* efficiently phosphorylates NAs in *S. pombe*. We have observed that the hENT1 transporter is not as essential as the kinase for NA toxicity in *S. pombe* as cells expressing only the transporter showed a similar survival as wild type cells to both NAs while cells containing only the kinase showed a higher sensitivity to GemC and AraC compared to wild type cells. The results suggest that the kinase is indispensable for NAs activity and that the NAs might be imported through the yeast cell membrane. Higher sensitivity of cells with both hENT1 and kinase in comparison to sensitivity of cells with only the kinase, however, suggest that hENT1 considerably enhances NAs activity in *S. pombe*. To our surprise, we have observed that growth of cells with the transporter and kinase was affected in rich media without treatment and that observed cell elongation might be checkpoint dependent as *rad3ts* mutants struggled to survive in YEL media (Figure 3-12B and Figure 3-16). The role of the DNA checkpoint in response to YEL media could however be more studied by, for example, combining the hENT1/kinase system with mutants defective in key DNA checkpoint effectors *cds1* and *chk1*. As a result of this abnormal growth in YEL, cells containing the transporter and kinase were further analysed in EMM media. Characterisation of the hENT1/kinase system is widely discussed in chapter 3.

7.1 GemC might induce the arrest of DNA replication forks

The main challenge in assessing molecular mechanisms underlying resistance to GemC is that the exact nature of the induced DNA damage has not yet been characterised. Indeed, although it is clear now that GemC kills proliferating cancer cells by interfering with DNA replication (Iwasaki *et al.*, 1997; Galmarini *et al.*, 2001; Shi *et al.*, 2001; Garcia-Diaz *et al.*, 2010), the resulting effect on DNA is not defined. When the replication fork encounters an obstacle, it may either lead to a “stalled replication fork”, where the replication proteins remain assembled and protect DNA ends or to a “collapsed replication fork”, where the replisome has dissociated (Lambert and Carr, 2005). One of the first outcomes of a stalled replication fork is formation of single stranded DNA (ssDNA) which results from the action of helicases that continue to unwind the DNA ahead of the replication obstacle (Branzei and Foiani, 2007). The first cellular response to this ssDNA is to activate the checkpoint in order to stabilise the fork and prevent it from collapsing (Lambert and Carr, 2005; Branzei and Foiani, 2007; Sabatinos, 2010). Several checkpoint proteins have been identified that play a role in protecting cells from stalled replication forks (reviewed by Lambert and Carr, 2005). In our screen, we have identified some of these genes that are known to respond to stalled replication fork, indicating that indeed GemC leads to arrested replication fork. Identified genes in our screen include *ssb3* (*rpa3*) which coat the ssDNA and activates subsequent checkpoints (Lambert *et al.*, 2007; Sabatinos, 2010), the clamp like *rad9-rad1-hus1* complex and its loader *rad17* which coordinate the DNA damage checkpoint (Lambert and Carr, 2005), *mrc1* which stabilises the replication fork (Lambert *et al.*, 2007) and *swi3* which forms a complex with *swi1* to protect the replication forks (Noguchi *et al.*, 2004). We have also identified several genes of the Ino80 protein complex which plays a role in chromatin remodelling (van Attikum *et al.*, 2004). As it has been shown in *S. cerevisiae* that the Ino80 complex is required for recovery of stalled replication forks (Shimada *et al.*, 2008), our results further support a presence of stalled replication forks in GemC-treated cells. Moreover, due to similarities between our screen and other *S. pombe* genome wide screens against CPT and HU, two drugs which are known to lead to replication arrest (Deshpande *et al.*, 2009; Pan *et al.*, 2012), it is highly likely that GemC also induces similar fork arrest. Supportive to these

observations, FACS analysis of GemC-treated cells confirmed that GemC leads to arrested replication (Dr Keszthelyi, personal communication).

Collapsed replication forks occur when the stalled fork cannot be stabilised and proteins of the replisome disassemble (Lambert and Carr, 2005). It is thought that in fission yeast, stalled replication fork rapidly collapses and that homologous recombination proteins are required to maintain the collapsed DNA replication forks (Lambert *et al.*, 2007; Sabatinos, 2010). Amongst HR proteins which respond to collapsed fork, Rad22 and the MRN complex (Lambert *et al.*, 2007) were also identified in our screen, suggesting that HR might be required to stabilise potentially GemC induced collapsed replication fork. Surprisingly, we did not isolate the core HR gene *rad51* (or *rhp51*) in our screen. This might be due to contamination in the library and the role of *rhp51* in response to GemC would need to be attested. Supportive to the possible role of HR recombination in response to GemC, we have confirmed by spot tests that MRN-ctp1 defective mutants (*Rad50Δ*, *nbs1Δ*, *ctp1Δ*) are highly sensitive to both GemC and AraC when compared to WT cells (*Figure 5-1* and *Figure 5-2*). Indeed several studies have shown that the MRN complex acts in HR (reviewed in Williams *et al.*, 2010) and the observation that MRN mutants are sensitive to both GemC and AraC indicates that HR might be required in response to NA-induced DNA damage. The role of the MRN complex in response to GemC was also observed in human cell lines as *mre11Δ* and *rad50Δ* mutants showed increased sensitivity to GemC (Ewald *et al.*, 2008b).

7.2 Mre11 removes GemC from the DNA to allow repair

One of the hypotheses of this project was to assess whether the NAs are removed from the DNA in order to allow subsequent repair. To verify this hypothesis, we have tested the sensitivity of *mre11* nuclease dead mutant to GemC. Indeed it has been shown in *S. pombe* that the Mre11 nuclease initiates HR by removing Spo11^{Rec12} from the DNA (Hartsuiker *et al.*, 2009a) and plays a role in survival of cells to DNA damaging agents such as CPT by removing trapped topoisomerase from DNA and allowing subsequent repair (Hartsuiker *et al.*, 2009b). In respect to this removal activity, we have investigated

if a similar removal activity might be involved in resistance to NAs. Our results suggest that indeed Mre11 plays a role in response to GemC as an *mre11* nuclease dead mutant (*mre11-D65N*), lacking exo- and endonuclease activity, showed sensitivity to the NA when compared to WT cells (Figure 5-1). Moreover, measurements of incorporated GemC (indicative of removal of the drug) by Mass Spectrophotometry (Figure 7-1, data from Dr Keszthelyi) showed that incorporated GemC was slightly higher in *mre11-D65N* mutants compared to WT cells, further supporting the role of Mre11 nuclease in removal of GemC. Levels of incorporated GemC-TP were higher in MRN null mutants and emphasised the role of the complex in removal of incorporated GemC. The observation that incorporated GemC levels are considerably high in MRN null mutants when compared to levels in *mre11-D65N* mutants indicates that other MRN-dependent nucleases might act to remove the NA. Based on the high sensitivity of *mre11-D65N* mutants to GemC in comparison to WT cells and on higher levels of incorporated GemC in the nuclease dead mutants compared to levels in WT, we can conclude that Mre11 nuclease responds to GemC treatment by removing the drug from the DNA. The 3'→5' exonuclease activity of the Mre11 nuclease is in accordance with the localisation of the NA at 3' end of the DNA (Ewald *et al.*, 2008) and may explain the removal activity of the nuclease.

Drug sensitivity of *mre11* nuclease dead mutants however was variable depending on the presence or absence of the transporter. In the presence of the transporter (tested in EMM media), cells showed only a slight sensitivity to both GemC and AraC when compared to WT, while cells without the transporter (tested on YEA media) showed a clearly higher sensitivity to GemC (AraC not tested). To explain this confusing observation, we hypothesised that the response of Mre11 to GemC depends on cellular concentration of GemC as we have observed that levels of intracellular GemC-TP are 9 times more elevated in cells containing the transporter and kinase when compared to cells with only the kinase (in YE media, Figure 3-14). In EMM media however, GemC-TP levels were equally high regardless of the presence or absence of the transporter (Figure 3-14). Spot tests analysis of *mre11-D65N* mutants on EMM media confirmed that *mre11-D65N* cells with only the kinase are more sensitive to GemC than cells with both the kinase and the transporter when compared to WT cells (Dr Keszthelyi, personal

communication). Because GemC-TP levels are equal in the cells, we can hypothesise that Mre11 response to GemC is dependent on other GemC metabolites which might vary in absence or presence of the transporter. In fact, in addition to GemC-DP it has been shown that GemC also forms dFdU (difluorodeoxyuridine), resulting from deamination of dFdC by deoxycytidine deaminase and dephosphorylation of dFdUMP (Heinemann *et al.*, 1988; Mini *et al.*, 2006; Veltkamp *et al.*, 2008). It is possible that in presence of the transporter, all the forms (or one specific intermediate) of GemC accumulate in the cells and induce various DNA damages, while in absence of the transporter GemC-TP is the predominant product that kills the cells. Mre11 would hence respond to remove GemC-TP from the DNA. But in presence of other forms of the drug, Mre11 activity might not be required and GemC would trigger other DNA repair mechanisms (discussed in the next paragraph).

In summary, our results suggest that Mre11 nuclease plays a role in removal of the GemC from the DNA, but the role of the nuclease is minor for survival in presence of high levels of the drugs. As analysis of *S. pombe* Mre11 has shown that the nuclease is required homologous recombination (Tavassoli *et al.*, 1995; Wilson *et al.*, 1999, Hartsuiker *et al.*, 2009a), these results further support the hypothesis of a possible involvement of HR in response to GemC treatment.

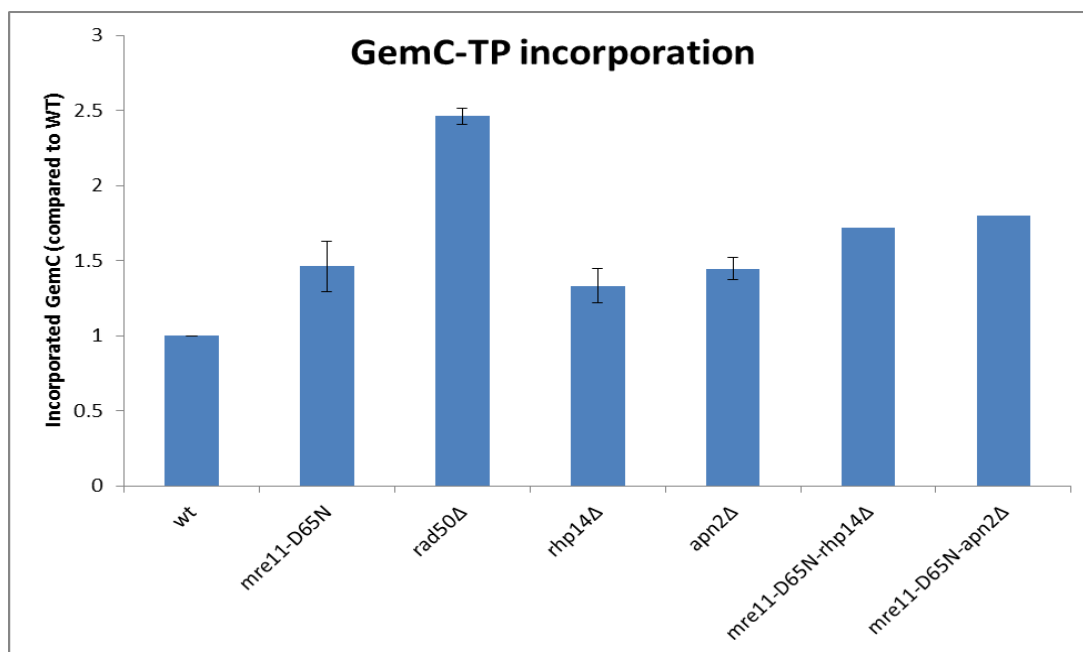


Figure 7-1 Incorporated GemC levels are higher in *mre11-D65N* mutants than WT

Cells, strains MG85 (wt), MG297 (*mre11-D65N*), MG119 (*rad50Δ*), MG276 (*rhp14Δ*), MG319 (*apn2Δ*), AK091 (*mre11-D65N; rhp14Δ*) and AK069 (*mre11-D65N; apn2Δ*) were treated with 50μM GemC and 0.05μM of heavy deoxycytidine (heavy dC, $^{15}\text{N}_3$ dC). $0.5-1 \times 10^9$ cells were collected after 3 hours incubation and lysed to isolate DNA. DNA was hydrolysed and integrated GemC was measured by Mass Spectrophotometry (results provided by Dr Andrea Keszthelyi). The results were normalised to heavy dC levels and calculated in comparison to WT (1). Results showed that levels of incorporated GemC are higher in *mre11-D65N* mutants. Similar high levels were also observed in *rhp14* and *apn2* defective mutants. *Rad50* deleted mutants showed the highest levels. Cells are in *hscCK/hENT1* background.

7.3 NER and BER excision repair genes play a role in sensitivity to GemC and AraC

Surprisingly and in contrast to what we had predicted by the nature of the used drug (nucleoside analogue), the genome-wide library screen isolated only one gene (*mms19*) which plays a role in NER. Spot test analysis of specific mutants, however, suggested a role of NER in response to NAs. NER damage signalling *rhp14^{XPA}* and *rhp41/42^{XPC}* deleted mutants were highly sensitive to GemC and AraC (Figure 5-4), suggesting a role of the pathway in sensing NA-induced damage. Distortion of the DNA at the site of integration of AraC (Gmeiner *et al.*, 1998) and GemC (Konerding *et al.*, 2002) may explain the role of NER, involved in sensing UV induced bulky DNA adducts (Fleck, 2004), in detecting NA induced damage. In addition to damage signalling proteins, *swi10^{ERCC1}* nuclease deleted cells also showed a high sensitivity to both drugs. This sensitivity was not observed in *rad13^{XPG}* defective cells, which suggested the 3' end incision is not required in the response of NER to the drugs. Differences in the nucleases end specificity (5' incision for *swi10* and 3' incision for *rad13*) are in accordance with the 3' localisation of the NA after chain termination (Ewald *et al.*, 2008a). High levels of incorporated GemC, measured in *rhp14Δ* (Figure 7-1), *rhp41/42Δ* and *swi10Δ* but not in *rad13Δ* (Dr Andrea Keszthelyi, personal communication) mutants when compared to WT cells suggested that the NER plays a role in removal of the drug. Moreover, analysis of sensitivity of *rhp14Δ rad13Δ* double mutants to GemC confirmed that *rad13* does not act in response to NA treatment, as the double mutants showed a same sensitivity as *rhp14* deleted mutants (Figure 5-9). *rad13Δ swi10Δ* mutants however suggested that *rad13* might possess a redundant role in response to GemC, and that another nuclease might trigger *swi10* response as *rad13* deletion rescued *swi10Δ* (illustrated in Figure 7-2) Considering the nature of the tested drugs (nucleoside analogues) it was not surprising that the nucleotide excision repair pathway responds to AraC and GemC treatment.

BER repair was poorly represented with only *ung1* isolated as sensitive to GemC in the library screen. Surprisingly, however BER deleted mutants showed sensitivity to both GemC and AraC in spot tests analysis. As BER repairs damage that affects base, we did

not expect that the pathway would respond to GemC and AraC as the two NAs have changes in the sugar moiety. Deletion of *apn2* which processes the abasic site after removal of the damaged base (Marti and Fleck, 2004) conferred high sensitivity to both GemC and AraC suggesting that the nuclease plays a role in response to both NAs. Mass spectrophotometry measurements (results provided by Dr Keszthelyi) of incorporated GemC in *apn2Δ* mutants (Figure 7-1) showed that GemC levels were higher in the mutants when compared to levels in WT cells, indicating that the nuclease plays a role in removal of the drug from the DNA. It is not clear how the BER activity of *apn2* may contribute to GemC and AraC removal as the nuclease “cleans” the DNA after the damaged base has been removed. An additional role of the nuclease in removal of nucleosides analogues from DNA 3' end has been observed in vitro (Chou *et al.*, 2000) that might explain the role of *apn2* in removal of the two NAs from the DNA. However the proposed 3'→5' exonuclease activity has a preference for L- configuration NA while GemC and AraC are in D-configuration (Chou *et al.*, 2000). There is however a possibility that *S. pombe apn2* exerts this 3'→5' exonuclease activity to remove GemC and AraC from the DNA.

nth1 defective mutants also showed a high sensitivity to both nucleoside analogues suggesting that the glycosylase responds to the drugs. It is not clear how the glycosylase responds to the NA: either by its glycosylase activity required for the removal of the damaged base or its lyase activity which processes the DNA after removal of the abasic sugar (Krokan *et al.*, 2000; Alseth *et al.*, 2004). A possible hypothesis might be that the lyase activity of *nth1* cuts into the modified sugar and generates DNA nicks that are further processed by other repair pathways. Indeed, it has been suggested that *nth1* generates DSBs in response to MMS which are then processed by homologous recombination. This suggestion was drawn after observation that *nth1* requires the HR gene *mms1* in response to MMS in *S. pombe* (Vejrup-Hansen *et al.*, 2011). Deletion of *mms1* rescued *nth1Δ* suggesting that repair of MMS-induced damage by *nth1* requires the presence of *mms1*. The possible interaction between BER and HR was also suggested by Memisoglu *et al.* (2000) after observation of genetic interactions between BER glycosylase *mag1* and the HR gene *rad51*. Consistently, we have also observed

that deletion of *rad50* rescued *nth1Δ* as *nth1Δ rad50Δ* double mutants were less sensitive to GemC when compared to *nth1Δ* single mutant (Figure 5-8B). In addition, *nth1Δ mre11-D65N* double mutant was less sensitive than *nth1Δ* single mutant (Figure 5-8A) indicating that *mre11* nuclease activity rescues *nth1Δ*. The sensitivity of *nth1Δ mre11-D65N* was similar to the sensitivity of *mre11-D65N* suggesting that *mre11* nuclease acts upstream of *nth1*. Given our observations and suggestions by other studies (Memisoglu *et al.*, 2000; Vejrup-Hansen *et al.*, 2011), there is a possibility that Nth1 responds to GemC by inducing breaks which in turn trigger HR repair. The exact mechanism by which the Nth1 would remove the nucleoside analogues however is not understood. Our results suggest that Mre11 nuclease responds to GemC and creates an intermediate state which triggers *nth1* activity. Nth1 then induces DSBs which require the MRN complex (illustrated in Figure 7-2).

On the contrary to *nth1*, we predicted that the uracil glycosylase *ung1* mutant would be sensitive to GemC. First because it was shown that one of the GemC cellular metabolite is dFdU (difluorodeoxyuridine) which might be incorporated into the DNA (Mini *et al.*, 2006) and would be removed by the uracil specific glycosylase and second, because *ung1* was isolated in the screen of the genome wide deletion library (chapter 4). Surprisingly *ung1Δ* mutants showed resistance in comparison to WT cells, suggesting that the gene increases drug toxicity. The resistance to drugs was also observed in *rad2Δ* mutants. Because both *rad2* (Kunz and Fleck, 2001) and *ung1* (Ikeda *et al.*, 2009) have been linked to increased mutagenesis it is possible that the observed resistance in the two mutants is due to suppressors in the kinase and/or the transporter or other genes, which would impede their activities and decrease drug toxicity. The resistance of *rad2Δ* and *ung1Δ* mutants is hence subject to confirmation. Rad2 possesses multiple functions including Okazaki fragment maturation, NHEJ and UV-damage excision repair in *S. pombe* (Marti and Fleck, 2004; Fleck, 2004). Because NAs are incorporated during DNA replication, a possible hypothesis to the role of *rad2* in enhancing GemC and AraC toxicity might be that during the Okazaki fragments maturation, Rad2 removes the Okazaki fragment containing NA, and generates nicks that are lethal to the cells. 5'→3' exonuclease activity of Rad2 (Fleck, 2004) is consistent with this hypothesis. Analysis

of other nucleases involved in removal of DNA flaps during maturation of the Okazaki fragments could help to identify if they also contribute to resistance of cells to GemC and AraC treatment. A suitable candidate nuclease is the Dna2 nuclease which has been identified to play a role in maturation of Okazaki fragments during DNA replication and possesses a 5' resection activity (Kang *et al.*, 2000, Zhu *et al.*, 2008).

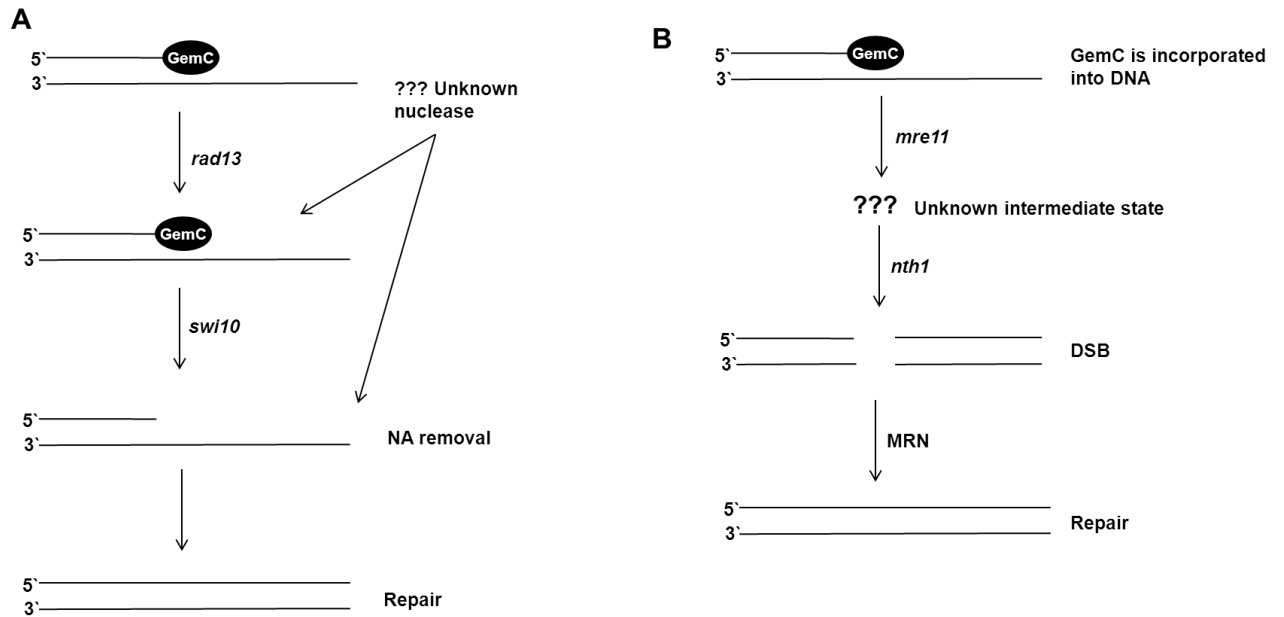


Figure 7-2 Schematic representation of possible repair of GemC-induced damage by NER and BER. (A) *swi10* response to GemC is triggered by *rad13* and another nuclease, which might also have a *swi10* – independent role in response to GemC. *swi10* (or the other nuclease) remove the NA from the DNA and makes the lesion available for repair. **(B)** *mre11* responds to GemC and induces an unknown state which recruits *nth1*. *nth1* creates DSBs which require the MRN complex for repair.

7.4 MMR and PRR defective mutants are resistant to treatment with GemC and AraC

MMR defective mutants (*msh2*, *msh6* and *mlh1*) showed resistance to both NAs when compared to WT cells, suggesting that the pathway increases drug toxicity. However as MMR defective mutants exhibit a strong mutator phenotype (Fleck, 2004), there is a possibility that suppressors have been introduced into the transporter and/or kinase or other genes and affected their function. Resistance of MMR defective cells is hence to be confirmed. If a biological effect is proven, results would suggest that MMR genes enhance GemC and AraC toxicity. A possible explanation to this resistance phenomenon may be a “futile cycle” which would remove base opposite NA and create nicks into the DNA as observed in resistance of MMR deficient mutants in response to O⁶-methylguanine (O⁶-methyl-G) [(Friedberg, 2006), p157 and illustrated in Figure 7-3].

Post replication repair polymerase *rev3Δ* mutant showed a similar survival as WT suggesting that the translesion polymerase is not required for survival of cells the NAs. PCNA ubiquitinating *rhp18Δ* mutants, on the other hand, showed a slight resistance when compared to WT cells and suggested that the gene enhances drugs` toxicity. These results imply that PCNA ubiquitination by Rhp18, which in turn activates PRR in response to NA treatment, is harmful for the cell.

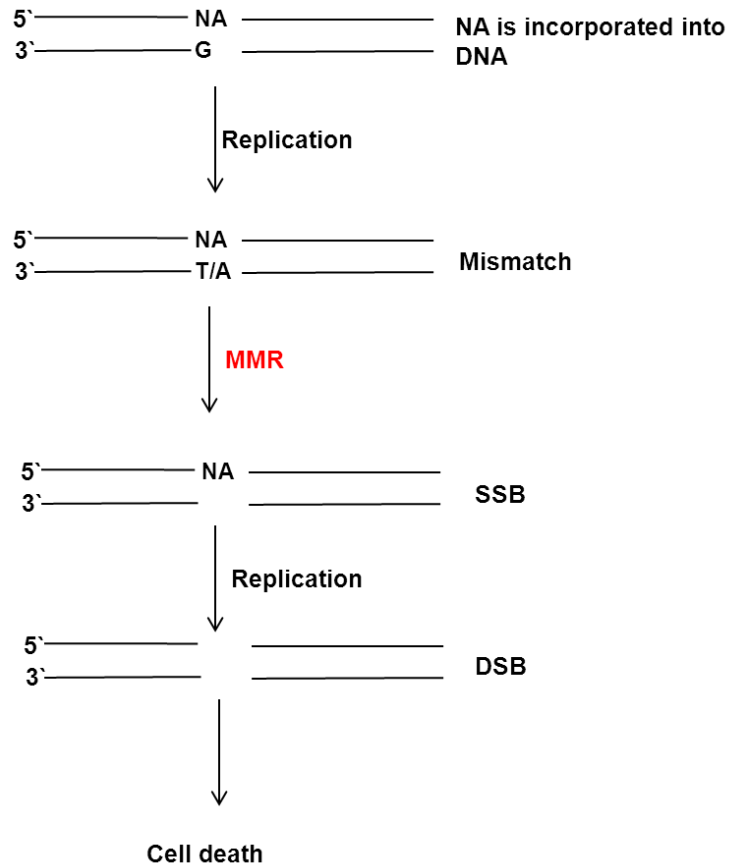


Figure 7-3 Schematic representation of possible enhancement of drug toxicity by MMR. After NA incorporation into DNA, cells replicate and mismatches are incorporated. MMR removes the physiological nucleoside and creates a SSB, which if unrepaired, is converted into a DSB by replication. DSB then leads to cell death. If MMR is absent, the NA might be repaired by other repair pathways or tolerated by the cell, which leads to cell survival. NA symbolises GemC or AraC which are deoxycytidine analogues and are paired to G.

7.5 Conclusion

In conclusion, in this project:

- We have set up and characterised an efficient system which allows study of the biological effect of nucleoside analogues in *S. pombe* by increasing their uptake and facilitating phosphorylation.
- We have identified novel genes that play a role in resistance to GemC treatment by screening a genome wide deletion library.
- We have characterised the response of known DNA repair genes to two NAs, GemC and AraC, and identified several sensitive mutants which play a role in resistance of cells to both drugs. These include MRN-Ctp1 complex, *rhp14*, *rhp41/42*, *swi10*, *nth1* and *apn2*.
- We have set up a system in *S. pombe* that allows study of DNA-bound proteins at specific sites. Further characterisation tests are required to confirm that the system is functional.

References

- Abraham, R.T. & Tibbetts, R.S. 2005. Cell biology: Guiding ATM to broken DNA. *Science (New York, N.Y.)*, vol. 308, no. 5721, pp. 510-511.
- Achanta, G., Pelicano, H., Feng, L., Plunkett, W. & Huang, P. 2001. Interaction of p53 and DNA-PK in Response to Nucleoside Analogues: Potential Role as a Sensor Complex for DNA Damage. *Cancer Research*, vol. 61, no. 24, pp. 8723-8729.
- Aguilera, A. & Gomez-Gonzales, B. 2008. Genome instability: a mechanistic view of its causes and consequences. *Nature Genetics*, vol. 9, pp. 204-217.
- Aldred, P.M.R. & Borts, R.H. 2007. Humanizing mismatch repair in yeast: towards effective identification of hereditary non-polyposis colorectal cancer alleles. *Biochemical Society Transactions*, vol. 35, no. 6, pp. 1525-1528.
- Alleva, J.L. & Doetsch, P.W. 1998. Characterization of *Schizosaccharomyces pombe* Rad2 protein, a FEN-1 homolog. *Nucleic Acids Research*, vol. 26, no. 16, pp. 3645-3650.
- Alseth, I., Korvald, H., Osman, F., Seeberg, E. & Bjørås, M. 2004. A general role of the DNA glycosylase Nth1 in the abasic sites cleavage step of base excision repair in *Schizosaccharomyces pombe*. *Nucleic Acids Research*, vol. 32, no. 17, pp. 5119-5125.
- Andersen, P.L., Xu, F. & Xiao, W. 2008. Eukaryotic DNA damage tolerance and translesion synthesis through covalent modifications of PCNA. *Cell Research*, vol. 18, pp. 162-173.
- Andrews, B.J., Proteau, G.A., Beatty, L.G. & Sadowski, P.D. 1985. The FLP recombinase of the 2 μ circle DNA of yeast: Interaction with its target sequences. *Cell*, vol. 40, no. 4, pp. 795-803.
- Arnér, E.S.J. & Eriksson, S. 1995. Mammalian deoxyribonucleoside kinases. *Pharmacology & Therapeutics*, vol. 67, no. 2, pp. 155-186.
- Ashburner M, Ball CA, Blake JA, Botstein D, Butler H, Cherry JM, Davis AP, Dolinski K, Dwight SS, Eppig JT, Harris MA, Hill DP, Issel-Tarver L, Kasarskis A, Lewis S, Matese JC, Richardson JE, Ringwald M, Rubin GM, Sherlock G. 2000. Gene Ontology: tool for the unification of biology. *Nature Genetics*, vol. 25, no. 1, pp. 25.
- Aslett, M. & Wood, V. 2006. Gene Ontology annotation status of the fission yeast genome: preliminary coverage approaches 100%. *Yeast*, vol. 23, pp. 913-919.
- Bahler, J., Wu, J., Longtine, M.S., Shah, N.G., Mckenzie III, A., Steveer, A.B., Wach, A., Philippsen, P. & Pringle, J.R. 1998. Heterologous modules for Efficient and Versatile PCR-based Gene Targeting in *Schizosaccharomyces pombe*. *Yeast*, vol. 14, no. 943, pp. 951.

- Bahmed, K., Nitiss, K.C. & Nitiss, J.L. 2010. Yeast Tdp1 regulates the fidelity of nonhomologous end joining. *Proceedings of the National Academy of Sciences of the USA.*, vol. 107, no. 9, pp. 4057-4062.
- Bahmed, K., Seth, A., Nitiss, K.C. & Nitiss, J.L. 2011. End-processing during non-homologous end-joining: a role for exonuclease 1. *Nucleic Acids Research*, vol. 39, no. 3, pp. 970-978.
- Baker, N.M., Rajan, R. & Mondragón, A. 2009. Structural studies of type I topoisomerases. *Nucleic Acids Research*, vol. 37, no. 3, pp. 693-701.
- Baldwin EL, O.N. 2005. Etoposide, topoisomerase II and cancer. *Current Medical Chemistry-Anticancer Agents*. vol. 5, no. 4, pp. 363-372.
- Baldwin, S.A., Beal, P.R., Yao, S.Y., King, A.E., Cass, C.E. & Young, J.D. 2004. The equilibrative nucleoside transporter family, SLC29. *European Journal of Physiology*, vol. 447, pp. 735-743.
- Basu, A. & Krishnamurthy, S. 2010. Cellular Responses to Cisplatin-Induced DNA Damage. *Journal of Nucleic Acids*, vol. 2010, Article ID 201367, 16 pages, 2010.doi:10.4061/2010/201367
- Benjamini, Y. & Hochberg, Y. 1995. Controlling the false discovery rate. *Journal of the Royal Statistical Society*, vol. 57, no. 1, pp. 289-300.
- Bergman, A.M., Giaccone, G., van Moorsel, C.J.A., Mauritz, R., Noordhuis, P., Pinedo, H.M. & Peters, G.J. 2000. Cross-resistance in the 2'2'-difluorodeoxyctidine (gemcitabine)-resistant human ovarian cancer cell line AG6000 to standard and investigational drugs. *European Journal of Cancer*, vol. 36, pp. 1974-1983.
- Boiteux, S. & Guillet, M. 2004. Abasic sites in DNA: repair and biological consequences in *Saccharomyces cerevisiae*. *DNA Repair*, vol. 3, no. 1, pp. 1-12.
- Boone, C., Bussey, H. & Andrews, B. 2007. Exploring genetic interactions and networks with yeast. *Nature Reviews Genetics*, vol. 8, pp. 437.
- Borde, V. 2007. The multiple roles of the Mre11 complex for meiotic recombination. *Chromosome Research*, vol. 15, no. 5, pp. 551-563.
- Branzei, D. & Foiani, M. 2007. Interplay of replication checkpoints and repair proteins at stalled replication forks. *DNA Repair*, vol. 6, no. 7, pp. 994-1003.
- Branzei, D. & Foiani, M. 2005. The DNA damage response during DNA replication. *Current Opinion in Cell Biology*, vol. 17, no. 6, pp. 568-575.
- Broomfield, S., Hryciw, T. & Xiao, W. 2001. DNA postreplication repair and mutagenesis in *Saccharomyces cerevisiae*. *Mutation Research/DNA Repair*, vol. 486, no. 3, pp. 167-184.

- Bugreev, D.V., Rossi, M.J. & Mazin, A.V. 2011. Cooperation of RAD51 and RAD54 in regression of a model replication fork. *Nucleic Acids Research*, vol. 39, no. 6, pp. 2153-2164.
- Burden, D.A. & Osheroff, N. 1998. Mechanism of action of eukaryotic topoisomerase II and drugs targeted to the enzyme. *Biochimica et Biophysica Acta (BBA) - Gene Structure and Expression*, vol. 1400, no. 1-3, pp. 139-154.
- Cachedenier, I.S., Muñoz, P., Flores, J.M., Klatt, P. & Blasco, M.A. 2007. Deficient mismatch repair improves organismal fitness and survival of mice with dysfunctional telomeres. *Genes and Development*, vol. 21, pp. 2234-2247.
- Caldecott, K.W. 2003. DNA Single-Strand Break Repair and Spinocerebellar Ataxia. *Cell*, vol. 112, no. 1, pp. 7-10.
- Carr, A.M. 1995. DNA structure checkpoints in fission yeast. *Seminars in Cell Biology*, vol. 6, no. 2, pp. 65-72.
- Caspari, T. & Carr, A.M. 1999. DNA structure checkpoint pathways in *Schizosaccharomyces pombe*. *Biochimie*, vol. 81, pp. 173-181.
- Caspari, T., Dahlen, M., Kanter-Smoler, G. & et al. 2000. Characterization of *Schizosaccharomyces pombe* Hus1: a PCNA-Related Protein That Associates with Rad1 and Rad9. *Molecular and Cellular Biology*, vol. 20, no. 4, pp. 1254-1262.
- Cerqueira, Nuno M. F. S. A, Fernandes, P.A. & Ramos, M.J. 2007. Understanding Ribonucleotide Reductase Inactivation by Gemcitabine. *Chemistry- A European Journal*. vol. 13, pp. 8507-8515.
- Cervantes, M.D., Farah, J.A. & Smith, G.R. 2000. Meiotic DNA Breaks Associated with Recombination in *S. pombe*. *Molecular Cell*, vol. 5, pp. 883-888.
- Chabes, A. & Stillman, B. 2007. Constitutively high dNTP concentration inhibits cell cycle progression and the DNA damage checkpoint in yeast *Saccharomyces cerevisiae*. *Proceedings of the National Academy of Sciences of the USA*. vol. 104, no. 4, pp. 1183-1188.
- Chahwan, C., Nakamura, T.M., Sivakumar, S., Russell, P. & Rhind, N. 2003. The Fission Yeast Rad32 (Mre11)-Rad50-Nbs1 Complex Is required for the S-Phase DNA Damage Checkpoint. *Molecular and Cellular Biology*, vol. 23, no. 18, pp. 6564-6573.
- Champoux, J.J. 2001. DNA topoisomerases: structure, function, and mechanism. *Annual Review of Biochemistry*, vol. 70, pp. 369-413.
- Chang, D.J. & Cimprich, K.A. 2009. DNA Damage Tolerance: When It's OK to Make Mistakes. *Nature Chemical Biology*, vol. 5, no. 2, pp. 82-90.

- Chen, Y. & Chou, K. 2011. DNA lesion bypass polymerases and 4'-thio- β -D-arabinofuranosylcytosine (T-araC). *International Journal of Biochemistry and Molecular Biology*, vol. 2, no. 4, pp. 340-346.
- Chimply, K. & Mathews, C.K. 2001. Mouse ribonucleotide reductase control: influence of substrate binding upon interactions with allosteric effectors. *Journal Biological Chemistry*, vol. 276, no. 10, pp. 7093-7100.
- Chottiner, E.G., Shewach, D.S., Datta, N.S., Ashcraft, E., Gribbin, D., Ginsburg, D., Fox, H. & Mitchell, B.S. 1991. Cloning and expression of human deoxycytidine kinase cDNA. *Proceedings of the National Academy of Sciences of the USA*, vol. 88, pp. 1531-1535.
- Chou, K., Kukhanova, M. & Cheng, Y. 2000. A novel action of human apurinic/aprimidinic endonuclease: excision of L-configuration deoxyribonucleoside analogs from the 3' termini of DNA. *The Journal of Biological Chemistry*, vol. 275, no. 40, pp. 31009-31015.
- Clerici, M., Mantiero, D., Lucchini, G. & Longhese, M.P. 2005. The *Saccharomyces cerevisiae* Sae2 Protein Promotes Resection and Bridging of Double Strand Break Ends. *The Journal of Biological Chemistry*, vol. 280, no. 46, pp. 38631-38638.
- Das, P.M., Ramachandran, K., vanWert, J. & Singal, R. 2004. Chromatin immunoprecipitation assay. *BioTechniques*, vol. 37, pp. 961-969.
- de Laat, W.L., Jaspers, N.G. & Hoeijmakers, J.H. 1999. Molecular mechanism of nucleotide excision repair. *Genes Development*, vol. 13, pp. 768-785.
- Deb ethune, L., Kohlhagen, G., Grandas, A. & Pommier, Y. 2002. Processing of nucleopeptides mimicking the topoisomerase I-DNA covalent complex by tyrosyl-DNA phosphodiesterase. *Nucleic Acids Research*, vol. 30, no. 5, pp. 1198-1204.
- DeMott, M.S., Shen, B., Park, M.S., Bambara, R.A. & Zigman, S. 1996. Human RAD2 Homolog 1 5'- to 3'-Exo/Endonuclease Can Efficiently Excise a Displaced DNA Fragment Containing a 5'-Terminal Abasic Lesion by Endonuclease Activity. *The journal of Biological Chemistry*, vol. 271, no. 47, pp. 30068-30076.
- Deshpande, G.P., Hayles, J., Hoe, K., Kim, D., Park, H. & Hartsuiker, E. 2009. Screening a genome-wide *S. pombe* deletion library identifies novel genes and pathways involved in genome stability maintenance. *DNA Repair*, vol. 8, no. 5, pp. 672-679.
- Deweese, J.E. & Osheroff, N. 2009. The DNA cleavage reaction of topoisomerase II: wolf in sheep's clothing. *Nucleic Acids Research*, vol. 37, no. 3, pp. 738-748.
- Dong-Uk, K. et al. 2010. Analysis of a genome-wide set of gene deletions in the fission yeast *Schizosaccharomyces pombe*. *Nature Biotechnology*, vol. 28, no. 6, pp. 617-623.

- Dovey, C.L. & Russell, P. 2007. Mms22 Preserves Genomic Integrity during DNA Replication in *Schizosaccharomyces pombe*. *Genetics*, vol. 177, pp. 47-61.
- Elder, R.T., Zhu, X., Priet, S., Chen, M., Yu, M., Navarro, J., Sire, J. & Zhao, Y. 2003. A fission yeast homologue of the human uracil-DNA-glycosylase and their roles in causing DNA damage after overexpression. *Biochemical and Biophysical Research Communications*, vol. 306, no. 3, pp. 693-700.
- Elledge, S.J., Zhou, Z. & Allen, J.B. 1992. Ribonucleotide reductase: regulation, regulation, regulation. *Trends In Biochemical Sciences*, vol. 17, pp. 119-123.
- Eriksson, S., Munch-Petersen, B., Johansson, K. & Eklund, H. 2002. Structure and function of cellular deoxyribonucleoside kinases. *Cellular and Molecular Life Sciences*, vol. 59, pp. 1327-1346.
- Ewald, B., Sampath, D. & Plunkett, W. 2008 (a). Nucleoside analogs: molecular mechanisms signaling cell death. *Oncogene*, vol. 27, no. 50, pp. 6522-6537.
- Ewald, B., Sampath, D. & Plunkett, W. 2007. H2AX phosphorylation marks gemcitabine-induced stalled replication forks and their collapse upon S-phase checkpoint abrogation. *Molecular Cancer Therapeutics*, vol. 6, no. 4, pp. 1239-1248.
- Ewald, B., Sampath, D. & Plunkett, W. 2008 (b). ATM and the Mre11-Rad50-Nbs1 Complex Respond to Nucleoside Analogue-Induced Stalled Replication Forks and Contribute to Drug Resistance. *Cancer Research*, vol. 68, pp. 7947-7955.
- Eyford, J.E. & Bodvarsdottir, S.K. 2005. Genomic instability and cancer: Networks involved in response to DNA damage. *Mutation Research/Fundamental and Molecular Mechanisms of Mutagenesis*, vol. 592, pp. 18-28.
- Fagbemi, A.F., Orelli, B. & Schärer, O.D. 2011. Regulation of endonuclease activity in human nucleotide excision repair. *DNA Repair*, vol. 10, no. 7, pp. 722-729.
- Falbo, K.B. & Shen, X. 2006. Chromatin Remodeling in DNA Replication. *Journal of Cellular Biochemistry*, vol. 97, pp. 684-689.
- Feng, L., Achanta, G., Pelicano, H., Zhang, W., Plunkett, W. & Huang, P. 2000. Role of p53 in cellular response to anticancer nucleoside analog-induced DNA damage. *International Journal of Molecular Medicine*, vol. 5, no. 6, pp. 597-604.
- Flanagan, S.A., Robinson, B.W., Krokosky, C.M. & Shewach, D.S. 2007. Mismatched nucleotides as the lesions responsible for radiosensitization with gemcitabine: a new paradigm for antimetabolite radiosensitizers. *Molecular Cancer Therapeutics*, vol. 6, no. 6, pp. 1858-1868.
- Fleck, O. 2004. DNA repair pathways. *The Molecular Biology of Schizosaccharomyces pombe: Genetics, Genomics and Beyond*, ed. E. Richard, Springer, pp. 101-115.

- Forsburg, S.L. 2001. The art and design of genetic screens: yeast. *Nature Reviews Genetics*, vol. 2, pp. 659-668.
- Forsburg, S.L. & Rhind, N. 2006. Basic methods for fission yeast. *Yeast*, vol. 23, pp. 173-183.
- Friedberg, E.C. & Friedberg, E.C. 2006. *DNA Repair and Mutagenesis*, 2nd edn, ASM Press, Washington, D.C.
- Fuss, J.O. & Tainer, J.A. 2011. XPB and XPD helicases in TFIIH orchestrate DNA duplex opening and damage verification to coordinate repair with transcription and cell cycle via CAK kinase. *DNA Repair*, vol. 10, no. 7, pp. 697-713.
- Gai, D., Chang, Y.P. & Chen, X.S. 2010. Origin DNA melting and unwinding in DNA replication. *Current Opinion in Structural Biology*, vol. 20, no. 6, pp. 756-762.
- Galmarini, C.M., Mackey, J.R. & Dumontet, C. 2001. Nucleoside analogues: mechanisms of drug resistance and reversal strategies. *Leukemia : Official Journal of the Leukemia Society of America*, vol. 15, no. 6, pp. 875-890.
- Galmarini, C.M., Mackey, J.R. & Dumontet, C. 2002. Nucleoside analogues and nucleobases in cancer treatment. *The Lancet Oncology*, vol. 3, no. 7, pp. 415-424.
- Gan, G.N., Wittschieben, J.P., Wittschieben, Ø. & Wood, R.D. 2008. DNA polymerase zeta (pol ζ) in higher eukaryotes. *Cell Research*, vol. 18, pp. 174-183.
- Gandhi, V., Legha, J., Chen, F., Hertel, L.W. & Plunkett, W. 1996. Excision of 2',2'-Difluorodeoxycytidine (Gemcitabine) Monophosphate Residues from DNA. *Cancer Research*, vol. 56, pp. 4453-4459.
- Garcia-Diaz, M., Murray, M.S., Kunkel, T.A. & Chou, K. 2010. Interaction between DNA Polymerase lambda and anticancer Nucleoside Analogs. *The journal of Biological Chemistry*, vol. 285, no. 22, pp. 16874-16879.
- Gasasira U, M.F. 2007. Improvement of nucleoside analogue uptake in *Schizosaccharomyces pombe*. Master's edn, University of Sussex.
- George-Lucian, M. & Alan, D.D. 2009. How the Fanconi Anemia Pathway Guards the Genome. *Annual Review of Genetics*, vol. 43, pp. 223-249.
- Gmeiner, W.H., Skradis, A., Pon, R.T. & Liu, J. 1998. Cytarabine-induced destabilization of a model Okazaki fragment. *Nucleic Acids Research*, vol. 26, no. 10, pp. 2359-2365.
- Goan, Y., Zhou, B., Hu, E., Mi, S. & Yen, Y. 1999. Overexpression of Ribonucleotide Reductase as a Mechanism of Resistance to 2,2-Difluorodeoxycytidine in the Human KB Cancer Cell Line. *Cancer Research*, vol. 59, pp. 4204-4207.

- Griffiths, M., Beaumont, N., Yao, S.Y., Sundaram, M., Boumah, C.E., Davies, A., Kwong, F.Y., Coe, I., Cass, C.E., Young, J.D. & Baldwin, S.A. 1997. Cloning of a human nucleoside transporter implicated in the cellular uptake of adenosine and chemotherapeutic drugs. *Nature Medicine*, vol. 3, no. 1, pp. 89-93.
- Grimm, C., Bahler, J. & Kohli, J. 1994. M26 Recombinational Hotspot and Physical Conversion Tract Analysis in the *adeb* Gene of *Schizosaccharomyces pombe*. *Genetics*, vol. 135, pp. 41-51.
- Haggard, H.W. 1938. The Conception of Cancer Before and After Johannes Müller. *Bulletin of the New York Academy of Medicine*, vol. 14, no. 4, pp. 183-197.
- Hanahan, D. & Weinberg, R.A. 2000. The Hallmarks of Cancer. *Cell*, vol. 100, pp. 57-70.
- Hanahan, D. & Weinberg, R. 2011. Hallmarks of Cancer: The Next Generation. *Cell*, vol. 144, no. 5, pp. 646-674.
- Harper, W.J. & Elledge, S.J. 2007. The DNA Damage Response: Ten Years After. *Molecular Cell*, vol. 28, pp. 739-745.
- Hartsuiker, E., Mizuno, K., Molnar, M., Kohli, J., Ohta, K. & Carr, A.M. 2009(a). Ctp1^{Ct1P} and Rad32^{Mre11} nuclease activity are required for Rec12^{Spo11} removal, but Rec12^{Spo11} removal is dispensable for other MRN-dependent meiotic functions. *Molecular and Cellular Biology*, vol. 29, no. 7, pp. 1671-1681.
- Hartsuiker, E., Neale, M.J. & Carr, A.M. 2009(b). Distinct Requirements for the Rad32^{Mre11} Nuclease and Ctp1^{Ct1P} in the Removal of Covalently Bound Topoisomerase I and II from DNA. *Molecular Cell*, vol. 33, no. 1, pp. 117-123.
- Heinemann, V., Hertel, L.W., Grindey, G.B. & Plunkett, W. 1988. Comparison of the Cellular Pharmacokinetics and Toxicity of 2',2'-Difluorodeoxycytidine and 1- β -D-Arabinofuranosylcytosin. *Cancer Research*, vol. 48, pp. 4024-4031.
- Heinemann, V., Xu, Y.Z., Chubb, S., Sen, A., Hertel, L.W., Grindey, G.B. & Plunkett, W. 1990. Inhibition of ribonucleotide reduction in CCRF-CEM cells by 2',2'-difluorodeoxycytidine. *Molecular Pharmacology*, vol. 38, no. 4, pp. 567-572.
- Hentges, P., Van Driessche, B., Tafforeau, L., Vandenhoute, J. & Carr, A.M. 2005. Three novel antibiotics marker cassettes for gene disruption and marker switching in *Schizosaccharomyces pombe*. *Yeast*, vol. 22, pp. 1013-1019.
- Hirano, Y. & Sugimoto, K. 2006. ATR Homolog Mec1 Controls Association of DNA Polymerase α -Rev1 Complex with Regions near a Double-Strand Break. *Current Biology*, vol. 16, pp. 586-590.
- Hodson, J.A., Bailis, J.M. & Forsburg, S.L. 2003. Efficient labeling of fission yeast *Schizosaccharomyces pombe* with thymidine and BUdR. *Nucleic Acids Research*, vol. 31, no. 21, pp. e134.

- Hoeijmakers, J. 2001. Genome maintenance mechanisms for preventing cancer. *Nature*, vol. 411, no. 6835, pp. 366-374.
- Hohl, M., Christensen, O., Kunz, C., Naegeli, H. & Fleck, O. 2001. Binding and Repair of Mismatched DNA Mediated by Rhp14, the Fission Yeast Homologue of Human XPA. *The Journal of Biological Chemistry*, vol. 276, no. 3, pp. 30766-30772.
- Houtgraaf, J.H., Versmissen, J. & van der Giessen, W.J. 2006. A concise review of DNA damage checkpoints and repair in mammalian cells. *Cardiovascular Revascularization Medicine*, vol. 7, no. 3, pp. 165-172.
- Hsiang, Y., Lihou, M. & Liu, L. 1989. Arrest of replication forks by drug-stabilized topoisomerase I-DNA cleavable complexes as a mechanism of cell killing by camptothecin. *Cancer Research*, vol. 49, no. 18, pp. 5077-5082.
- Huang, J. & Dynan, W.S. 2002. Reconstitution of the mammalian DNA double-strand break end-joining reaction reveals a requirement for an Mre11/Rad50/NBS1-containing fraction. *Nucleic Acids Research*, vol. 30, no. 3, pp. 667-674.
- Huang, M. & Graves, L. 2003. De novo synthesis of pyrimidine nucleotides: emerging interfaces with signal transduction pathways. *Cellular and Molecular Life Sciences*, vol. 60, no. 2, pp. 321-336.
- Huang, P., Chubb, S., Hertel, L.W., Grindey, G.B. & Plunkett, W. 1991. Action of 2'2'-difluorodeoxycytidine on DNA Synthesis. *Cancer Research*, vol. 51, pp. 6110-6117.
- Huffman, J.L., Sundheim, O. & Tainer, J.A. 2005. DNA base damage recognition and removal: New twists and grooves. *Mutation Research/Fundamental and Molecular Mechanisms of Mutagenesis*, vol. 577, no. 1-2, pp. 55-76.
- Hurley, L.H. 2002. DNA and its associated processes as targets for cancer therapy. *Nature Reviews Cancer*, vol. 2, pp. 188-200.
- Ikeda, M., Ikeda, R. & Ikeda, S. 2009. Spontaneous mutation in uracil DNA glycosylase-deficient cells of a fission yeast *Schizosaccharomyces pombe*. *Current Topics in Biochemical Research*, vol. 11, no. 1, pp. 55-60.
- Ip, S.C.Y., Rass, U., Blanco, M.G., Flynn, H.R., Skehel, J.M. & West, S.C. 2008. Identification of Holliday junction resolvases from humans and yeast. *Nature*, vol. 456, no. 7220, pp. 357-361.
- Iwasaki, H., Huang, P., Keating, M.J. & Plunkett, W. 1997. Differential Incorporation of Ara-C, Gemcitabine, and Fludarabine into Replicating and Repairing DNA in Proliferating Human Leukemia Cells. *Blood*, vol. 90, no. 1, pp. 270-278.

- Jansen, J.G., Tsaalbi-Shtylik, A., Hendriks, G., Verspuy, J., Gali, H., Haracska, L. & de Wind, N. 2009. Mammalian polymerase ζ is essential for post-replication repair of UV-induced DNA lesions. *DNA Repair*, vol. 8, no. 12, pp. 1444-1451.
- Jiri, B. & Jiri, L. 2007. DNA damage checkpoints: from initiation to recovery or adaptation. *Current Opinion in Cell Biology*, vol. 19, pp. 238-245.
- Johansson, M., van Rompay, A.R., Degrève, B., Balzarini, J. & Karlsson, A. 1999. Cloning and characterization of the multisubstrate deoxyribonucleoside kinase of *Drosophila melanogaster*. *The Journal of Biological Chemistry*, vol. 274, no. 34, pp. 23814-23819.
- Johnson, R.E., Washington, M.T., Haracska, L., Prakash, S. & Prakash, L. 2000. Eukaryotic polymerases iota and zeta act sequentially to bypass DNA lesions", *Nature*, vol. 406, no. 6799, pp. 1015-1019.
- Johnson, R.E., Prakash, L. & Prakash, S. 2012. Pol31 and Pol32 subunits of yeast DNA polymerase δ are also essential subunits of DNA polymerase ζ . *Proceedings of the National Academy of Sciences of the USA*, vol. 109, no. 31, pp. 12455-12460.
- Jordheim, L.P. & Dumontet, C. 2007. Review of recent studies on resistance to cytotoxic deoxynucleoside analogues. *Biochimica et Biophysica Acta*, vol. 1776, pp. 138-159.
- Jordheim, L.P., Galmarini, C.M. & Dumontet, C. 2005. Metabolism, mechanism of action and resistance to cytotoxic nucleoside analogues. *Bulletin du Cancer*, vol. 92, no. 3, pp. 239-248.
- Jung, K.-. & Marx, A. 2005. Nucleotide analogues as probes for DNA polymerases. *Cellular and Molecular Life Sciences*, vol. 62, pp. 2080-2091.
- Kanamitsu, K. & Ikeda, S. 2010. Early Steps in the DNA Base Excision Repair Pathway of a Fission Yeast *Schizosaccharomyces pombe*. *Journal of Nucleic Acids*, vol. doi:10.4061/2010/450926.
- Kang, H., Choi, E., Bae, S., Lee, K., Gim, B., Kim, H., Park, C., MacNeill, S.A. & Seo, Y. 2000. Genetic Analyses of *Schizosaccharomyces pombe* Dna2 Reveal That Dna2 Plays an Essential Role in Okazaki Fragment Metabolism. *Genetics*, vol. 155, pp. 1055-1067.
- Karow, J.K., Constantinou, A., Li, J., West, S.C. & Hickson, I.D. 2000. The Bloom's syndrome gene product promotes branch migration of Holliday junctions. *Proceedings of the National Academy of Sciences of the USA*, vol. 97, no. 12, pp. 6504-6508.
- Karran, P. 2000. DNA double strand break repair in mammalian cells. *Current Opinion in Genetics & Development*, vol. 10, no. 2, pp. 144-150.
- Kaye, S.B. 1998. New antimetabolites in cancer chemotherapy and their clinical impact. *British Journal of Cancer*, vol. 78 supplement 3, pp. 1-7.

- Kelley, M.R., Kow, Y.W. & Wilson III, D.M. 2003. Disparity between DNA Base Excision Repair in Yeast and Mammals: Translational Implications. *Cancer Research*, vol. 63, pp. 549-554.
- Khanna, K.K. & Jackson, S.P. 2001. DNA double-strand breaks: signalling, repair and cancer connection. *Nature Genetics*, vol. 27, pp. 247-254.
- Khanna, K.K., Lavin, M.F., Jackson, S.P. & Mulhern, T.D. 2001. ATM, a central controller of cellular responses to DNA damage. *Cell Death and Differentiation*, vol. 8, pp. 1052-1065.
- Kim DU, Hayles J, Kim D, Wood V, Park HO, Won M, Yoo HS, Duhig T, Nam M, Palmer G, Han S, Jeffery L, Baek ST, Lee H, Shim YS, Lee M, Kim L, Heo KS, Noh EJ, Lee AR, Jang YJ, Chung KS, Choi SJ, Park JY, Park Y, Kim HM, Park SK, Park HJ, Kang EJ, Kim HB, Kang HS, Park HM, Kim K, Song K, Song KB, Nurse P, Hoe KL. 2010. Analysis of a genome-wide set of gene deletions in the fission yeast *Schizosaccharomyces pombe*. *Nature Biotechnology*, vol. 28, no. 6, pp. 617.
- Kleijer, W.J., Laugel, V., Berneburg, M., Nardo, T., Fawcett, H., Gratchev, A., Jaspers, N.G., Sarasin, A., Stefanini, M. & Lehmann, A.R. 2008. *DNA Repair*, vol. 7, pp. 744-750
- Knobel, P.A. & Marti, T.M. 2011. Translesion DNA synthesis in the context of cancer research. *Cancer Cell International*, vol. 11, pp. 39.
- Knudson Jr, A.G. 1971. Mutation and Cancer: Statistical Study of Retinoblastoma. *Proceedings of the National Academy of Sciences of the USA*, vol. 68, no. 4, pp. 820-823.
- Kobayashi, T., Rein, T. & DePamphilis, M.L. 1998. Identification of primary initiation sites for DNA replication in the Hamster Dihydrofolate Reductase Gene Initiation Zone. *Molecular Cellular Biology*, vol. 18, no. 6, pp. 3266.
- Konerding, D., James, T.L., Trump, E., Soto, A.M., Marky, L.A. & Gmeiner, W.H. 2002. NMR Structure of a Gemcitabine-Substituted Model Okazaki Fragment. *Biochemistry*, vol. 41, pp. 839-846.
- Kornberg, A. & Baker, T.A. 1992, *DNA replication*, 2nd edn, W.H. Freeman, New York.
- Kou, H., Zhou, Y., Gorospe, R.M.C. & Wang, Z. 2008. Mms19 protein functions in nucleotide excision repair by sustaining an adequate cellular concentration of the TFIIH component Rad3. *Proceedings of the National Academy of Sciences of the USA*, vol. 105, no. 41, pp. 15714-15719.
- Krogh, B. & Symington, L. 2004. Recombination proteins in yeast. *Annual Review of Genetics*, vol. 38, pp. 233-271.
- Krokan, H.E., Nilsen, H., Skorpen, F., Otterlei, M. & Slupphaug, G. 2000. Base excision repair of DNA in mammalian cells. *FEBS letters*, vol. 476, no. 1-2, pp. 73-77.

- Kumar, D., Abdulovic, A.L., Viberg, J.r., Nilsson, A.K., Kunkel, T.A. & Chabes, A. 2011. Mechanisms of mutagenesis in vivo due to imbalanced dNTP pools. *Nucleic Acids Research*, vol. 39, no. 4, pp. 1360-1371.
- Kumar, D., Viberg, J., Nilsson, A.K. & Chabes, A. 2010. Highly mutagenic and severely imbalanced dNTP pools can escape detection by the S-phasecheckpoint. *Nucleic Acids Research*, vol. 38, no. 12, pp. 3975-3983.
- Kunz, B.A., Kohalmi, S.E., Kunkel, T.A., Mathews, C.K., McIntosh, E.M. & Reidy, J.A. 1994. Deoxyribonucleoside triphosphate levels: A critical factor in the maintenance of genetic stability. *Mutation Research/Reviews in Genetic Toxicology*, vol. 318, no. 1, pp. 1-64.
- Kunz, C. & Fleck, O. 2001, "Role of the DNA Repair Nucleases Rad13, Rad2 and Uve1 of *Schizosaccharomyces pombe* in Mismatch Correction. *Journal of Molecular Biology*, vol. 313, pp. 241-253.
- Labib, K. & De Piccoli, G. 2011. Surviving chromosome replication: the many roles of the S-phase checkpoint pathway. *Philosophical Transactions of the Royal Society*, vol. 366, pp. 3554-3561.
- Lamarque, B.J., Orazio, N.I. & Weitzman, M.D. 2010. The MRN complex in double-strand break repair and telomere maintenance. *FEBS letters*, vol. 584, no. 17, pp. 3682-3695.
- Lambert, S. & Carr, A.M. 2005. Checkpoint responses to replication fork barriers. *Biochimie*, vol. 87, no. 7, pp. 591-602.
- Lambert, S., Froget, B. & Carr, A.M. 2007. Arrested replication fork processing: Interplay between checkpoints and recombination. *DNA Repair*, vol. 6, no. 7, pp. 1042-1061.
- Lambert, S., Watson, A., Sheedy, D.M., Martin, B. & Carr, A.M. 2005. Gross Chromosomal Rearrangements and Elevated Recombination at an Inducible Site-Specific Replication Fork Barrier. *Cell*, vol. 121, pp. 689-702.
- Langerak, P., Mejia-Ramirez, E., Limbo, O. & Russell, P. 2011. Release of Ku and MRN from DNA Ends by Mre11 Nuclease Activity and Ctp1 Is Required for Homologous Recombination Repair of Double-Strand Breaks. *PLoS Genetics*, vol. 7, no. 9, pp. e1002271
- Lavin, M.F., Kozlov, S., Gueven, N., Peng, C., Birrell, G., Chen, P. & Scott, S. 2005. ATM and cellular responses to DNA damage. ed. E.A. Nigg, Springer, Netherlands, pp. 457-476.
- Lawrence, C.W. & Maher, V.M. 2001. Eukaryotic mutagenesis and translesion replication dependent on polymerase ζ and rev1 protein. *Biochemical Society Transactions*, vol. 29, no. 2, pp. 187-191.
- Lee, K. & Myung, K. 2008. PCNA Modifications for Regulation of Post-Replication Repair Pathways. *Molecules and Cells*, vol. 26, no. 1, pp. 5-11.

- Lehmann, A.R. 1996. Molecular biology of DNA repair in the fission yeast *Schizosaccharomyces pombe*. *Mutation Research/DNA Repair*, vol. 363, no. 3, pp. 147-161.
- Li, C. & Jin, J. 2010. DNA replication licensing control and rereplication prevention. *Protein Cell*, vol. 1, no. 3, pp. 227-236.
- Li, Y. & Araki, H. 2013. Loading and activation of DNA replicative helicases: the key step of initiation of DNA replication. *Genes to Cells*, pp. 1-12.
- Li, T.K. & Liu, L.F. 2001. Tumor cell death induced by topoisomerase-targeting drugs. *Annual Review of Pharmacology and Toxicology*, vol. 41, pp. 53-77.
- Li, X. & Heyer, W. 2008. Homologous recombination in DNA repair and DNA damage tolerance. *Cell Research*, vol. 18, no. 1, pp. 99-113.
- Liao, S., Toczylowski, T. & Yan, H. 2008. Identification of the *Xenopus* DNA2 protein as a major nuclease for the 5'-3' strand-specific processing of DNA ends. *Nucleic Acids Research*, vol. 36, no. 19, pp. 6091-6100.
- Limbo, O., Porter-Goff, M., Rhind, N. & Russell, P. 2011. Mre11 nuclease activity and Ctp1 regulate Chk1 activation by Rad3^{ATR} and Tel1^{ATM} checkpoint kinases at double-strand breaks. *Molecular and Cellular Biology*, vol. 31, no. 3, pp. 573-583.
- Limbo, O., Chahwan, C., Yamada, Y., de Bruin, R.A.M., Wittenberg, C. & Russell, P. 2007. Ctp1 Is a Cell-Cycle-Regulated Protein that Functions with Mre11 Complex to Control Double-Strand Break Repair by Homologous Recombination. *Molecular Cell*, vol. 28, no. 1, pp. 134-146.
- Lindsay, H. D., Griffiths, D.J.F., Edwards, R. J., Christensen, P.U., Murray, J.M., Osman, F., Walworth, N. & Carr, A.M. 1998. S-phase-specific activation of Cds1 kinase defines a subpathway of the checkpoint response in *Schizosaccharomyces pombe*. *Genes & Development*, vol. 12, no. 3, pp. 382-395
- Liu, C., Pouliot, J.J. & Nash, H.A. 2002. Repair of topoisomerase I covalent complexes in the absence of the tyrosyl-DNA phosphodiesterase Tdp1. *Proceedings of the National Academy of Sciences of the USA*, vol. 99, no. 23, pp. 14970-14975.
- Liu, L.F., Desai, S.D., Li, T.K., Mao, Y., Sun, M. & Sim, S.P. 2000. Mechanism of action of camptothecin. *Annals of the New York Academy of Sciences*, vol. 922, pp. 1-10.
- Liu, L. 1989. DNA topoisomerase poisons as antitumor drugs. *Annual Review of Biochemistry* Vol. 58, pp. 351-375
- Llorente, B. & Symington, L.S. 2004. The Mre11 nuclease is not required for 5' to 3' resection at multiple HO-induced double strand breaks. *Molecular and Cellular Biology*, vol. 24, no. 21, pp. 9682-9694.

- Loeb, K.R. & Loeb, L.A. 2000. Significance of multiple mutations in cancer. *Carcinogenesis*, vol. 21, no. 3, pp. 379-385.
- Lombaerts, M., Tijsterman, M., Brandsma, J.A., Verhage, R.A. & Brouwer, J. 1999. Removal of cyclobutane pyrimidine dimers by the UV damage repair and nucleotide excision repair pathways of *Schizosaccharomyces pombe* at nucleotide resolution. *Nucleic Acids Research*, vol. 27, no. 14, pp. 2868-2874.
- Major, P.P., Egan, E.M., Beardsley, G.P., Minden, M.D. & Kufe, D.W. 1981. Lethality of human myeloblasts correlates with the incorporation of arabinofuranosylcytosine into DNA. *Proceedings of the National Academy of Sciences of the USA*, vol. 78, no. 5, pp. 3235-3239.
- Malik, M., Nitiss, K.C., Enriquez-Rios, V. & Nitiss, J.L. 2006. Roles of nonhomologous end-joining pathways in surviving topoisomerase II-mediated DNA damage. *Molecular Cancer Therapeutics*, vol. 5, no. 6, pp. 1405-1414.
- Manolis, K.G., Nimmo, E.R., Hartsuiker, E., Carr, A.M., Jeggo, P.A. & Allshire, R.C. 2001. Novel functional requirements for non-homologous DNA end joining in *Schizosaccharomyces pombe*. *EMBO Journal*, vol. 20, no. 1-2, pp. 210-221.
- Marce, S., Molina-Arcas, M., Villamor, N., Casado, F.J., Pastor-Anglada, M. & Colomer, D. 2006. Expression of human equilibrative nucleoside transporter 1 (hENT1) and its correlation with gemcitabine uptake and cytotoxicity in mantle cell lymphoma. *Haematologica*, vol. 91, pp. 895-902.
- Marini, V. & Krejci, L. 2010. Srs2: the "Odd-Job Man" in DNA repair. *DNA repair*, vol. 9, pp.268-275.
- Marti, T.M. & Fleck, O. 2004. DNA repair nucleases. *Cellular and Molecular Life Sciences*, vol. 61, pp. 336-354.
- Marti, T.M., Kunz, C. & Fleck, O. 2003. Repair of damaged and mismatched DNA by the XPC homologues Rhp41 and Rhp42 of fission yeast. *Genetics*, vol. 164, pp. 457-467.
- Marti, T.M., Kunz, C. & Fleck, O. 2002. DNA Mismatch Repair and Mutation Avoidance Pathways. *Journal of Cellular Physiology*, vol. 191, pp. 28-41.
- Martin, S.A., Hewish, M., Lord, C.J. & Ashworth, A. 2010. Genomic instability and the selection of treatments for cancer. *Journal of Pathology*, vol. 220, pp. 281-289.
- Martinho, R.G., Lindsay, H.D., Flaggs, G., DeMaggio, A.J., Hoekstra, M.F., Carr, A.M. & Bentley, N.J. 1998. Analysis of Rad3 and Chk1 protein kinases defines different checkpoint responses. *The EMBO Journal*, vol. 17, no. 24, pp. 7239-7249.
- Masai, H., You, Z. & Arai, K. 2005. Control of DNA Replication: Regulation and Activation of Eukaryotic Replicative Helicase, MCM. *IUBMB Life*, vol. 57, no. 4/5, pp. 323-335.

- Mathews, C.K. 2006. DNA precursor metabolism and genomic stability. *The FASEB Journal*, vol. 20, pp. 1300-1314.
- Maynard, S., Schurman, S.H., Harboe, C., de Souza-Pinto, N.C. & Vilhelm, B.A. 2009. Base excision repair of oxidative DNA damage and association with cancer and aging. *Carcinogenesis*, vol. 30, no. 1, pp. 2-10.
- McCready, S.J., Burkill, H., Evans, S. & Cox, B.S. 1989. The *Saccharomyces cerevisiae* RAD2 gene complements a *Schizosaccharomyces pombe* repair mutation. *Current Genetics*, vol. 15, no. 1, pp. 27-30.
- McCready, S.J., Osman, F. & Yasui, A. 2000. Repair of UV damage in the fission yeast *Schizosaccharomyces pombe*. *Fundamental and Molecular Mechanism of Mutagenesis*, vol. 451, pp. 197-210.
- McKinnon, P.J. & Caldecott, K.W. 2007. DNA Strand Break Repair and Human Genetic Disease. *Annual Review of Genomics & Human Genetics*, vol. 8, pp. 37-55.
- McVey, M. & Lee, S.E. 2008. MMEJ repair of double-strand breaks (director's cut): deleted sequences and alternative endings. *Trends in Genetics*, vol. 24, no. 11, pp. 529-538.
- Meijer, M., Karimi-Bucheri, F., Huang, T.Y., Weinfeld, M. & Young, D. 2002. Pnk1, a DNA kinase/phosphatase required for normal response to DNA damage by gamma radiation or camptothecin in *Schizosaccharomyces pombe*. *The Journal of Biological Chemistry*, vol. 277, no. 6, pp. 4050-4055.
- Memisoglu, A. & Samson, L. 2000. Base excision repair in yeast and mammals. *Mutation Research/Fundamental and Molecular Mechanisms of Mutagenesis*, vol. 451, no. 1-2, pp. 39-51.
- Memisoglu, A. & Samson, L. 2000. Contribution of Base Excision Repair, Nucleotide Excision Repair and DNA Recombination to Alkylation Resistance of the Fission Yeast *Schizosaccharomyces pombe*. *Journal of Bacteriology*, vol. 182, no. 8, pp. 2104-2112.
- Mendez, J. & Stillman, B. 2003. Perpetuating the double helix: molecular machines at eukaryotic DNA replication origins. *BioEssays*, vol. 25, pp. 1158-1167.
- Mesner, L. D., Li, X., Dijkwel, P.A. & Hamlin, J.L. 2003. The Dihydrofolate Reductase Origin of Replication Does Not Contain Any Nonredundant Genetic Elements Required for Origin Activity. *Molecular and Cellular Biology*, vol. 23, no. 3, pp. 804-814.
- Miao, Z., Rao, V.A., Agama, K., Antony, S., Kohn, K.W. & Pommier, Y. 2006. 4-Nitroquinoline-1-Oxide Induces the Formation of Cellular Topoisomerase I-DNA Cleavage Complexes. *Cancer Research*, vol. 66, no. 3, pp. 6540-6545.

- Mini, E., Nobili, S., Caciagli, B., Landini, I. & Mazzei, T. 2006. Cellular pharmacology of gemcitabine. *Annals of Oncology*, vol. 17, no. 5, pp. v7-v12.
- Moraes, M.C.S., Neto, J.B.C. & Menck, C.F.M. 2012. DNA repair mechanisms protect our genome from carcinogenesis. *Frontiers in Bioscience*, vol. 17, pp. 1362-1388.
- Moses, R.E. 2001. DNA damage processing defects and disease. *Annual Review of Genomics and Human Genetics*, vol. 2, pp. 41-68.
- Moufarij, M., Phillips, D.R. & Cullinane, C. 2003. Gemcitabine Potentiates Cisplatin Cytotoxicity and Inhibits Repair of Cisplatin-DNA Damage in Ovarian Cancer Cell Lines. *Molecular Pharmacology*, vol. 63, no. 4, pp. 862-869.
- Murai, J., Huang, S.N., Das, B.B., Dexheimer, T.S., Takeda, S. & Pommier, Y. 2012. Tyrosyl-DNA Phosphodiesterase 1 (TDP1) Repairs DNA Damage Induced by Topoisomerases I and II and Base Alkylation in Vertebrate Cells. *The Journal of Biological Chemistry*, vol. 287, no. 16, pp. 12848-12857.
- Muraki, K., Nyhan, K., Han, L. & Murnane, J.P. 2012. Mechanisms of telomere loss and their consequences for chromosome instability. *Frontiers in Oncology*, vol. 2, pp. 135.
- Murga, M. & Fernández-Capetillo, O. 2007. Genomic instability: on the birth and death of cancer. *Clinical and Translational Oncology*, vol. 9, pp. 216-220.
- Naegeli, H. & Sugawara, K. 2011. The xeroderma pigmentosum pathway: Decision tree analysis of DNA quality. *DNA Repair*, vol. 10, no. 7, pp. 673-683.
- Nakamura, T.M., Du, L., Redon, C. & Russell, P. 2004. Histone H2A Phosphorylation Controls Crb2 Recruitment at DNA Breaks, Maintains Checkpoint Arrest, and Influences DNA Repair in Fission Yeast. *Molecular and Cellular Biology*, vol. 24, no. 14, pp. 6215-6230.
- Nakayama, H. 2002. RecQ family helicases: roles as tumor suppressor proteins. *Oncogene*, vol. 21, pp. 9008-9021.
- Nasheuer, H.P., Pospiech, H. & Syvaoja, J. 2006. Progress towards the Anatomy of the Eukaryotic DNA Replication Fork. *Genome Dynamics and Stability*, vol. 1, pp. 27-68.
- Negrini, S., Gorgoulis, V.G. & Halazonetis, T.D. 2010. Genomic instability - an evolving hallmark of cancer. *Molecular Cell Biology*, vol. 11, pp. 220-228.
- Newlon, C.S. 1996. DNA Replication in Yeast. *DNA Replication in Eukaryotic Cells* Cold Spring Harbor Laboratory Press, United States of America, pp. 873-914.
- Nicolette, M.L., Lee, K., Guo, Z., Rani, M., Chow, J.M., Lee, S.E. & Paull, T.T. 2010. Mre11–Rad50–Xrs2 and Sae2 promote 5' strand resection of DNA double-strand breaks. *Nature Structural and Molecular Biology*, vol. 17, no. 12, pp. 1478-1485.

- Nielsen, I., Bentsen, I.B., Lisby, M., Hansen, S., Mundbjerg, K., Andersen, A.H. & Bjergbaek, L. 2009. A Flp-nick system to study repair of a single protein-bound nick *in vivo* - a model system for repair of TopI-DNA cleavage intermediates. *Nature Methods*, vol. 6, pp. 753-757.
- Nilsen, L., Forstrøm, R.J., Bjørås, M., Magnar & Ingrun Alseth 2012. AP endonuclease independent repair of abasic sites in *Schizosaccharomyces pombe*. *Nucleic Acids Research*, vol. 40, no. 5, pp. 2000-2009.
- Nimonkar, A.V., Genschel, J., Kinoshita, E., Polaczek, P., Campbell, J.L., Wyman, C., Modrich, P. & Kowalczykowski, S.C. 2011. BLM–DNA2–RPA–MRN and EXO1–BLM–RPA–MRN constitute two DNA end resection machineries for human DNA break repair. *Genes and Development*, vol. 25, pp. 350-362.
- Nitiss, J.L. 2009. Targeting DNA topoisomerase II in cancer therapy. *Nature Review of Cancer*, vol. 9, no. 5, pp. 338-350.
- Noguchi, E., Noguchi, C., McDonald, H.W., Yates, J.R. & Russell, P. 2004. Swi1 and Swi3 Are Components of a Replication Fork Protection Complex in Fission Yeast. *Molecular and Cellular Biology*, vol. 24, no. 19, pp. 8342-8355.
- Noll, D.M., McGregor Mason, T. & Miller, P.S. 2006. Formation and Repair of Interstrand Cross-Links in DNA. *Chemical Reviews*, vol. 106, no. 2, pp. 277-301.
- Nowak, M.A., Komarova, L.N., Sengupta, A., Jallepalli, P.V., Shih, L., Vogelstein, B. & Lengauer, C. 2002. The role of chromosomal instability in tumor initiation. *Proceedings of the National Academy of Sciences of the USA*, vol. 99, no. 25, pp. 16226-16231.
- Nurse, P., Thuriaux, P. & Nasmyth, K. 1976. Genetic control of the cell division cycle in the fission yeast *Schizosaccharomyces pombe*. *Molecular and General Genetics*, vol. 146, pp. 167-178.
- Oguri, T., Achiwa, H., Muramatsu, H., Ozasa, H., Sato, S., Shimizu, S., Yamazaki, H., Eimoto, T. & Ueda, R. 2007. The absence of human equilibrative nucleoside transporter 1 expression predicts non response to gemcitabine-containing chemotherapy in non-small cell lung cancer. *Cancer Letters*, vol. 256, pp. 112-119.
- Osman, F., Bjørås, M., Alseth, I., Morland, I., McCready, S., Seeberg, E. & Tsaneva, I. 2003. A new *Schizosaccharomyces pombe* base excision repair mutant, *nth1*, reveals overlapping pathways for repair of DNA base damage. *Molecular Microbiology*, vol. 48, no. 2, pp. 465-480.
- Pan, X., Lei, B., Zhou, N., Feng, B., Yao, W., Zhao, X., Yu, Y. & Lu, H. 2012. Identification of novel genes involved in DNA damage response by screening a genome-wide *Schizosaccharomyces pombe* deletion library. *BioMed Central Genomics*, vol. 13, no. 662.

- Pancaldi, V., Saraç, O., Rallis, C., McLean, J., Přeavorovský, M., Gould, K., Beyer, A. & Bähler, J. 2012. Predicting the Fission Yeast Protein Interaction Network. *Genes Genomes Genetics*, vol. 2, pp. 453.
- Papamichael, D. 2000. The use of thymidilate synthase inhibitors in the treatment of advanced colorectal cancer: current status. *Stem Cells*, vol. 18, pp. 166-175.
- Paques, F. & Haber, J.E. 1999. Multiple Pathways of Recombination Induced by Double-Strand Breaks in *Saccharomyces cerevisiae*. *Microbiology and Molecular Biology Reviews*, vol. 63, no. 2, pp. 349-404.
- Pardo, B., Gómez-González, B. & Aguilera, A. 2009. DNA repair in mammalian cells: DNA double-strand break repair: how to fix a broken relationship. *Cellular and Molecular Life Sciences*, vol. 66, no. 6, pp. 1039-1056.
- Parrilla-Castellar, E.R., Arlander, S.J.H. & Karnitz, L. 2004. Dial 9-1-1 for DNA damage: the Rad9-Hus1-Rad1 (9-1-1) clamp complex. *DNA Repair*, vol. 3, pp. 1009-1014.
- Parsons, R.L., Prasad, P.V., Harshey, R.M. & Jayaram, M. 1988. Step-Arrest Mutants of FLP Recombinase: Implications for the Catalytic Mechanism of DNA Recombination. *Molecular and Cellular Biology*, vol. 8, no. 8, pp. 3303-3310.
- Pastor-Anglada, M., Molina-Arcas, M., Casado, F.J., Bellosillo, B., Colomer, D. & Gil, J. 2004. Nucleoside transporters in chronic lymphocytic leukaemia. *Leukemia*, vol. 18, pp. 385-393.
- Pastor-Anglada, M. & Baldwin, S.A. 2001. Recent Advances in the Molecular Biology and Physiology of Nucleoside and Nucleobase Transporters. *Drug Development Research*, vol. 52, pp. 431-437.
- Pastor-Anglada, M., Cano-Soldado, P., Molina-Arcas, M., Lostao, M.P., Larráyoiz, I., Martínez-Picado, J. & Casado, F.J. 2005. Cell entry and export of nucleoside analogues. *Virus Research*, vol. 107, no. 2, pp. 151-164.
- Peltomaki, P. 2003. Role of DNA mismatch defects in the pathogenesis of human cancer. *Journal of Clinical Oncology*, vol. 21, no. 6, pp. 1174-1179.
- Peng, G., Dai, H., Zhang, W., Hsieh, H., Pan, M., Park, Y., Tsai, R.Y., Bedrosian, I., Lee, J., Ira, G. & Lin, S. 2012. Human Nuclease/Helicase DNA2 Alleviates Replication Stress by Promoting DNA End Resection. *Cancer Research*, vol. 72, no. 11, pp. 2802-2813.
- Petersen, B.M., Piskur, J. & Søndergaard, L. 1998. Four Deoxynucleoside Kinase Activities from *Drosophila melanogaster* Are Contained within a Single Monomeric Enzyme, a New Multifunctional Deoxynucleoside Kinase. *The Journal of Biological Chemistry*, vol. 273, no. 7, pp. 3926-3931.

- Petrini, J.H.J. & Stracker, T.H. 2003. The cellular responses to DNA double-strand breaks: defining the sensors and mediators. *Trends in Cell Biology*, vol. 13, no. 9, pp. 458-462.
- Pfeiffer, P., Goedecke, W. & Obe, G. 2000. Mechanisms of DNA double-strand repair and their potential to induce chromosomal aberrations. *Mutagenesis*, vol. 15, no. 4, pp. 289-302.
- Podgorska, M., Kocbuch, K. & Pawelczyk, T. 2005. Recent advances in studies on biochemical and structural properties of equilibrative and concentrative nucleoside transporters. *Acta Biochimica Polonica*, vol. 52, no. 4, pp. 749-758.
- Pommier, Y. 2009. DNA topoisomerase I inhibitors: chemistry, biology, and interfacial inhibition. *Chemical Reviews*, vol. 109, no. 7, pp. 2894-2902.
- Pommier, Y. 2004. Camptothecins and topoisomerase I: a foot in the door. Targeting the genome beyond topoisomerase I with camptothecins and novel anticancer drugs: importance of DNA replication, repair and cell cycle checkpoints. *Current Medicinal Chemistry-Anti-Cancer Agents*, vol. 4, no. 5, pp. 429-434.
- Pommier, Y., Pourquier, P., Fan, Y. & Strumberg, D. 1998. Mechanism of action of eukaryotic DNA topoisomerase I and drugs targeted to the enzyme. *Biochimica et Biophysica Acta - Gene Structure and Expression*, vol. 1400, no. 1-3, pp. 83-105.
- Pouliot, J.J., Robertson, C.A. & Nash, H.A. 2001. Pathways for repair of topoisomerase I covalent complexes in *Saccharomyces cerevisiae*. *Genes Cells*, vol. 6, no. 8, pp. 677-687.
- Pouliot, J.J., Yao, K.C., Robertson, C.A. & Nash, H.A. 1999. Yeast gene for a Tyr-DNA phosphodiesterase that repairs topoisomerase I complexes. *Science*, vol. 286, no. 5439, pp. 552-555.
- Pourquier, P., Gioffre, C., Kohlhagen, G., Urasaki, Y., Goldwasser, F., Hertel, L.W., Yu, S., Pon, R.T., Gmeiner, W.H. & Pommier, Y. 2002. Gemcitabine (2',2'-difluoro-2'-deoxycytidine), an antimetabolite that poisons topoisomerase I. *Clinical Cancer Research*, vol. 8, no. 8, pp. 2499-2504.
- Pourquier, P., Takebayashi, Y., Urasaki, Y., Gioffre, C., Kohlhagen, G. & Pommier, Y. 2000. Induction of topoisomerase I cleavage complexes by 1-beta-D-arabinofuranosylcytosine (ara-C) *in vitro* and in ara-C-treated cells. *Proceedings of the National Academy of Sciences of the USA*, vol. 97, no. 4, pp. 1885-1890.
- Rampazzo, C., Miazzi, C., Franzolin, E., Pontarin, G., Ferraro, P., Frangini, M., Reichard, P. & Bianchi, V. 2010. Regulation by degradation, a cellular defence against deoxyribonucleotide pool imbalances. *Mutation Research/Genetic Toxicology and Environmental Mutagenesis*, vol. 703, no. 1, pp. 2-10.

- Rapp, J.B., Noguchi, C., Das, M.M., Wong, L.K., Ansbach, A.B., Holmes, A.M., Arcangioli, B. & Noguchi, E. 2010. Checkpoint-Dependent and -Independent Roles of Swi3 in Replication Fork Recovery and Sister Chromatid Cohesion in Fission Yeast. *PLoS ONE*, vol. 5, no. 10, pp. e13379.
- Reichrath, J. 2006. DNA repair mechanisms: underestimated key players for cancer prevention and therapy. *Journal of Molecular Histology*, vol. 37, pp. 179-181.
- Reinhardt, H.C. & Yaffe, M.B. 2009. Kinases that Control the Cell Cycle in Response to DNA Damage: Chk1, Chk2, and MK2. *Current Opinion in Cell Biology*, vol. 21, no. 2, pp. 245-255.
- Reis, C.C., Batista, S. & Ferreira, M.G. 2012. The fission yeast MRN complex tethers dysfunctional telomeres for NHEJ repair. *The EMBO Journal*, vol. 31, no. 24, pp. 4576-4586.
- Robinson, B.W., Im, M.M., Ljungman, M., Praz, F. & Shewach, Donna S. 2003. Enhanced Radiosensitization with Gemcitabine in Mismatch Repair-Deficient HCT116 Cells. *Cancer Research*, vol. 63, no. 20, pp. 6935-6941.
- Rodel, C., Jupitz, T. & Schmidt, H. 1997. Complementation of the DNA repair-deficient *swi10* mutant of fission yeast by the human *ERCC1* gene. *Nucleic Acids Research*, vol. 25, no. 4, pp. 2823-2827.
- Rogojina, A.T., Li, Z., Nitiss, K.C. & Nitiss, J.L. 2007. Using yeast tools to dissect the action of anticancer drugs: mechanisms of enzyme inhibition and cell killing by agents targeting DNA topoisomerases. *Yeast as Tool in Cancer Research*, ed. J.L.e.a. Nitiss, Springer, The Netherlands, pp. 409-427.
- Roguev, A., Wiren, M., Weissman, J.s. & Krogan, N.J. 2007. High-throughput genetic interaction mapping in the fission yeast *Schizosaccharomyces pombe*. *Nature Methods*, vol. 4, no. 10, pp. 861-866.
- Rudolf, F.B. 1994. The biochemistry and physiology of nucleotides^{1,2,3}. *Journal of Nutrition*, vol. 124, pp. 124S-127S.
- Rudolph, C., Kunz, C., Parisi, S., Lehmann, E., Hartsuiker, E., Fartmann, B., Kramer, W., Kohli, J. & Fleck, O. 1999. The *msh2* Gene of *Schizosaccharomyces pombe* Is Involved in Mismatch Repair, Mating-Type Switching, and Meiotic Chromosome Organization. *Molecular and Cellular Biology*, vol. 19, no. 1, pp. 241-250.
- Rudolph, C., Fleck, O. & Kohli, J. 1998. *Schizosaccharomyces pombe* *exo1* is involved in the same mismatch repair pathway as *msh2* and *pms1*. *Current Genetics*, vol. 34, pp. 343-350.
- Ruiz van Haperen, V.W.T., Veerman, G., Vermorken, J.B. & Peters, G.J. 1993. 2',2'-Difluoro-deoxycytidine (gemcitabine) incorporation into RNA and DNA of tumour cell lines. *Biochemical Pharmacology*, vol. 46, no. 4, pp. 762-766.

- Sabatinos, S.A. 2010. Recovering a stalled replication fork. *Nature Education*, vol. 3, no. 9, pp. 31.
- Sampath, D., Rao, V. & Plunkett, W. 2003. Mechanisms of apoptosis induction by nucleoside analogs. *Oncogene*, vol. 22, no. 56, pp. 9063-9074.
- Sancar, A., Lindsey-Boltz, L.A., Uensal-Kacmaz, K. & Situart, L. 2004. Molecular mechanisms of mammalian DNA repair and the DNA damage checkpoints. *Annual Review of Biochemistry*, vol. 73, pp. 39-85.
- Sartori, A.A., Lukas, C., Coates, J., Mistrik, M., Shuang, F., Bartek, J., Baer, R., Lukas, J. & Jackson, S.P. 2007. Human CtIP promotes DNA end resection. *Nature*, vol. 450, no. 7169, pp. 509-514.
- Schar, P., Baur, M., Schneider, C. & Kohli, J. 1997. Mismatch Repair in *Schizosaccharomyces pombe* requires the MutI Homologous Gene Pms1: Molecular Cloning and Functional Analysis. *Genetics*, vol. 146, pp. 1275-1286.
- Schar, P. 2001. Spontaneous DNA Damage Genome Instability and Cancer- When DNA Replication Escapes Control. *Cell*, vol. 104, pp. 329-332.
- Scharer, O.D. 2003. Chemistry and Biology of DNA Repair. *Angewandte Chemie International Edition*, vol. 42, pp. 2946-2974.
- Schofield, M. & Hsieh, P. 2003. DNA mismatch repair: Molecular mechanisms and biological function. *Annual Review of Microbiology*, vol. 57, pp. 579-608.
- Scalfani, R.A. & Holzen, T.M. 2007. Cell cycle regulation of DNA replication. *Annual Review of Genetics*, vol. 41, pp. 237-280.
- Seifert, M. & Reichrath, J. 2006. The role of the human mismatch repair gene hMSH2 in DNA repair, cell cycle control and apoptosis: implication for pathogenesis, progression and therapy of cancer. *Journal of Molecular Histology*, vol. 37, pp. 301-307.
- Shen, X., Ranallo, R., Choi, E. & Wu, C. 2003. Involvement of Actin-Related Proteins in ATP-Dependent Chromatin Remodeling. *Molecular Cell*, vol. 12, pp. 147-155.
- Shi, Z., Azuma, A., Sampath, D., Li, Y., Huang, P. & Plunkett, W. 2001. S-Phase Arrest by Nucleoside Analogues and Abrogation of Survival without Cell Cycle Progression by 7-Hydroxystaurosporine. *Cancer Research*, vol. 61, no. 3, pp. 1065-1072.
- Shimada, K., Oma, Y., Schleker, T., Kugou, K., Ohta, K., Harata, M. & Gasser, S.M. 2008. Ino80 Chromatin Remodeling Complex Promotes Recovery of Stalled Replication Forks. *Current Biology*, vol. 18, no. 8, pp. 566-575.

Sijbers, A.M., de Laat, W.L., Ariza, R.R., Biggerstaff, M., Wei, Y.F., Moggs, J.G., Carter, K.C., Shell, B.K., Evans, E., de Jong, M.C., Rademakers, S., de Rooij, J., Jaspers, N.G., Hoeijmakers, J.H. & Wood, R.D. 1996. Xeroderma Pigmentosum Group F Caused by a Defect in a Structure-Specific DNA Repair Endonuclease. *Cell*, vol. 86, pp. 811-822.

Sivakumar, S., Porter-Goff, M., Patel, P.K., Benoit, K. & Rhind, N. 2004. In vivo labeling of fission yeast DNA with thymidine and thymidine analogs. *Methods*, vol. 33, no. 3, pp. 213-219.

Smoot, M.E., Ono, K., Ruscheinski, J., Wang, P. & Ideker, T. 2011. Cytoscape 2.8: new features for data integration and network visualization. *Bioinformatics*, vol. 27, no. 3, pp. 431-432.

Spratlin, J., Sangha, R., Glubrecht, D., Dabbagh, L., Young, J.D., Dumontet, C., Cass, C., Lai, R. & Mackey, J.R. 2004. The Absence of Human Equilibrative Nucleoside Transporter 1 Is Associated with Reduced Survival in Patients With Gemcitabine-Treated Pancreas Adenocarcinoma. *Clinical Cancer Research*, vol. 10, pp. 6956-6961.

Stojic, L., Brun, R. & Jiricny, J. 2004. Mismatch repair and DNA damage signalling. *DNA Repair*, vol. 3, no. 8-9, pp. 1091-1101.

Stracker, T.H., Usui, T. & Petrini, J.H.J. 2009. Taking the time to make important decisions: The checkpoint effector kinases Chk1 and Chk2 and the DNA damage response. *DNA Repair*, vol. 8, pp. 1047-1054.

Stryer, L. (ed) 1988, *Biochemistry*, third edn, Edition Freeman.

Sugimoto, T., Igawa, E., Tanihigashi, H., Matsubara, M., Ide, H. & Ikeda, S. 2005. Roles of base excision repair enzymes Nth1p and Apn2p from *Schizosaccharomyces pombe* in processing alkylation and oxidative DNA damage. *DNA Repair*, vol. 4, no. 11, pp. 1270-1280.

Svendsen, J.M. & Harper, J.W. 2010. GEN1/Yen1 and the SLX4 complex: solutions to the problem of Holliday junction resolution. *GENES & DEVELOPMENT*, vol. 24, pp. 521-536.

Symington, L.S. 2002. Role of RAD52 epistasis group genes in homologous recombination and double-strand break repair. *Microbiology and Molecular Biology Reviews*, vol. 66, no. 4, pp. 630-670

Szankasi, P. & Smith, G.R. 1995. A Role for Exonuclease I from *S. pombe* in Mutation Avoidance and Mismatch Correction. *Science*, vol. 267, pp. 1166-1169.

Takeda, S., Nakamura, K., Taniguchi, Y. & Paull, T.T. 2007. Ctp1/CtIP and the MRN Complex Collaborate in the Initial Steps of Homologous Recombination. *Molecular Cell*, vol. 28, no. 3, pp. 351-352.

Tanaka, H., Arakawa, H., Yamaguchi, T., Shiraishi, K., Fukuda, S., Matsui, K., Takei, Y. & Nakamura, Y. 2000. A ribonucleotide reductase gene involved in a p53-dependent cell-cycle checkpoint for DNA damage. *Nature*, vol. 404, no. 6773, pp. 42-49.

- Tavassoli, M., Shayeghi, M., Nasim, A. & Watts, F.Z. 1995. Cloning and characterisation of the *Schizosaccharomyces pombe* rad32 gene: a gene required for repair of double strand breaks and recombination. *Nucleic Acids Research*, vol. 23, no. 3, pp. 383-388.
- Tishkoff, D.X., Boerger, A.L., Bertrand, P., Filosi, N., Gaida, G.M., Kane, M.F. & Kolodner, R.D. 1997. Identification and characterization of *Saccharomyces cerevisiae* EXO1, a gene encoding an exonuclease that interacts with MSH2. *Proceedings of the National Academy of Sciences of the USA*, vol. 94, no. 14, pp. 7487-7492.
- Ueno, M., Nakazaki, T., Akamatsu, Y., Watanabe, K., Tomita, K., Lindsay, H.D., Sinagawa, H. & Iwasaki, H. 2003. Molecular characterisation of the *Schizosaccharomyces pombe* nbs1+ gene involved in DNA repair and telomere maintenance. *Molecular and Cellular Biology*, vol. 23, no. 18, pp. 6553-6563.
- van Attikum, H., Fritsch, O., Hohn, B. & Gasser, S.M. 2004. Recruitment of the INO80 Complex by H2A Phosphorylation Links ATP-Dependent Chromatin Remodeling with DNA Double-Strand Break Repair. *Cell*, vol. 119, pp. 777-788.
- van Brabant, A.J., Stan, R. & Ellis, N.A. 2000. DNA helicases, genomic instability and human genetic disease. *Annual Review of Genomics and Human Genetics*, vol. 1, pp. 409-459.
- Van Rompay, A.R., Johansson, M. & Karlsson, A. 2003. Substrate specificity and phosphorylation of antiviral and anticancer nucleoside analogues by human deoxyribonucleoside kinases and ribonucleoside kinases. *Pharmacology & Therapeutics*, vol. 100, no. 2, pp. 119-139.
- Vejrup-Hansen, R., Mizuno, K., Miyabe, I., Fleck, O., Holmberg, C., Murray, J.M., Carr, A.M. & Nielsen, O. 2011. *Schizosaccharomyces pombe* Mms1 channels repair of perturbed replication into Rhp51 independent homologous recombination. *DNA Repair*, vol. 10, no. 3, pp. 283-295.
- Veltkamp, S.A., pluim, D., van Eijndhoven, M.A.J., Bolijn, M.J., Ong, F.H.G., Govindarajan, R., Unadkat, J.D., Beijnen, J.H. & Schellens, J.H.M. 2008. New insights into the pharmacology and cytotoxicity of gemcitabine and 2',2'-difluorodeoxyuridine. *Molecular Cancer Therapeutics*, vol. 8, pp. 2415-2425.
- Verkade, H.M., Teli, T., Laursen, L.V., Murray, J.M. & O'Connell, M.J. 2001. A homologue of the Rad18 postreplication repair gene is required for DNA damage responses throughout the fission yeast cell cycle. *Molecular Genetics and Genomics*, vol. 265, no. 6, pp. 993-1003.
- Vernis, L., Piskur, J. & Diffley, J.F. 2003. Reconstitution of an efficient thymidine salvage pathway in *Saccharomyces cerevisiae*. *Nucleic Acids Research*, vol. 31, no. 19, pp. e120.
- Wachters, F.M., van Putten, J.W.G., Maring, J.G., Zdzienicka, M.Z., Groen, H.J.M. & Kampinga, H.H. 2003. Selective targeting of homologous DNA recombination repair by gemcitabine. *International Journal of Radiation Oncology, Biology, Physics*, vol. 57, no. 2, pp. 553-562.

- Waga, S. & Stillman, B. 1998. The DNA replication fork in eukaryotic cells. *Annual Review of Biochemistry*, vol. 67, pp. 721-751.
- Walworth, N.C. & Bernards, R. 1996. rad-Dependent Response of the chk1-Encoded Protein Kinase at the DNA Damage Checkpoint. *Science*, vol. 271, pp. 353-356
- Wang, J.C. 1998. Moving one DNA double helix through another by a type II DNA topoisomerase: the story of a simple molecular machine. *Quarterly Reviews of Biophysics*, vol. 31, no. 2, pp. 107-144.
- Wang, S., Goodwin, A., Hickson, I.D. & Norbury, C.J. 2001. Involvement of *Schizosaccharomyces pombe* Srs2 in cellular responses to DNA damage. *Nucleic Acids Research*, vol. 29, no. 14, pp. 2963-2972.
- Wang, J., Lohman, G.J.S. & Stubbe, J. 2009. Mechanism of Inactivation of Human Ribonucleotide Reductase with p53R2 by Gemcitabine 5'-Diphosphate. *Biochemistry*, vol. 48, pp. 11612-11621.
- Wang, Y., Liu, X., Matsuda, A. & Plunkett, W. 2008. Repair of 2'-C-Cyano-2'-Deoxy-1-beta-d-arabino-Pentofuranosylcytosine-Induced DNA Single-Strand Breaks by Transcription-Coupled Nucleotide Excision repair. *Cancer Research*, vol. 68, no. 10, pp. 3881-3889.
- Waters, L.S., Minesinger, B.K., Wiltrot, M.E., D'Souza, S., Woodruff, R.V. & Walker, G.C. 2009. Eukaryotic Translesion Polymerases and Their Roles and Regulation in DNA Damage Tolerance. *Microbiology and Molecular Biology Reviews*, vol. 73, no. 1, pp. 134-154.
- Watson, A.T., Garcia, V., Bone, N., Carr, A.M. & Armstrong, J. 2008. Gene tagging and gene replacement using recombinase-mediated cassette exchange in *Schizosaccharomyces pombe*. *Gene*, vol. 407, pp. 63-74.
- Watson, A.T., Werler, P. & Carr, A.M. 2011. Regulation of gene expression at the fission yeast *Schizosaccharomyces pombe* *urg1* locus. *Gene*, vol. 484, no. 1-2, pp. 75-85.
- Watt, S., Mata, J., Lopez-Maury, L., Marguerat, S., Burns, G. & Bahler, J. 2008. *urg1*: A Uracil-Regulatable Promoter System for fission Yeast with Short Induction and Repression Times. *PLoS ONE*, vol. 3, no. 1, pp. e1428 (1)-e1428 (8).
- Wei, K., Clark, A.B., Wong, E., Kane, M.F., Mazur, D.J., Parris, T., Kolas, N.K., Russell, R., Hou, H.J., Kneitz, B., Yang, G., Kunkel, T.A., Kolodner, R.D., Cohen, P.E. & Edelman, W. 2003. Inactivation of Exonuclease 1 in mice results in DNA mismatch repair defects, increased cancer susceptibility, and male and female sterility. *Genes and Development*, vol. 17, pp. 603-614.
- Williams, G.J., Lees-Miller, S.P. & Tainer, J.A. 2010. Mre11-Rad50-Nbs1 conformations and the control of sensing, signaling, and effector responses at DNA double-strand breaks. *DNA Repair*, vol. 9, no. 12, pp. 1299-1306.

- Wilson, S., Warr, N., Taylor, D.L. & Watts, F.Z. 1999. The role of *Schizosaccharomyces pombe* Rad32, the Mre11 homologue, and other DNA damage response proteins in non-homologous end joining and telomere length maintenance. *Nucleic Acids Research*, vol. 27, no. 13, pp. 2655-2661.
- Wood, V. et al. 2002. The genome sequence of *Schizosaccharomyces pombe*. *Nature*, vol. 415, no. 6874, pp. 871-880.
- Wyman, C. & Kanaar, R. 2006. DNA Double-Strand Break Repair: All's Well that Ends Well. *Annual Review of Genetics*, pp. 363-383.
- Xie, A., Puget, N., Shim, I., Odate, S., Jarzyna, I., Bassing, C.H., Alt, F.W. & Scully, R. 2005. Control of Sister Chromatid Recombination by Histone H2AX. *Molecular Cell*, vol. 16, no. 6, pp. 1017-1025.
- Yanagida, M. 2002. The model unicellular eukaryote, *Schizosaccharomyces pombe*. *Genome Biology*, vol. 3, no. 3, pp. 2003.1-2003.4.
- You, Z. & Bailis, J.M. 2010. DNA damage and decisions: CtIP coordinates DNA repair and cell cycle checkpoints. *Trends in Cell Biology*, vol. 20, no. 7, pp. 402-409.
- Young, J.A., Schreckhise, R.W., Steiner, W.W. & Smith, G.R. 2002. Meiotic Recombination Remote from Prominent DNA Break Sites in *S. pombe*. *Molecular Cell*, vol. 9, pp. 253-263.
- Yukiko, O., Tuneko, O. & Hisao, M. 1997. Identification of a predominant replication origin in fission yeast. *Nucleic Acids Research*, vol. 25, no. 3, pp. 530-536.
- Zahn-Zabal, M., Lehmann, E. & Kohli, J. 1995. Hot Spots of recombination in Fission Yeast: Inactivation of the M26 Hot Spot by Deletion of the *ade6* Promoter and the Novel Hotspot *ura4-aim*. *Genetics*, vol. 140, pp. 469-478.
- Zheng, L. & Shen, B. 2011. Okazaki fragment maturation: nucleases take centre stage. *Journal of Molecular Cell Biology*, vol. 3, pp. 23-30.
- Zhu, Z., Chung, W., Shim, E.Y., Lee, S.E. & Ira, G. 2008. Sgs1 helicase and two nucleases Dna2 and Exo1 resect DNA double strand break ends. *Cell*, vol. 134, no. 6, pp. 981-994.
- Zhu, C., Johansson, M. & Karlsson, A. 2000. Incorporation of Nucleoside Analogs into Nuclear or Mitochondrial DNA Is Determined by the Intracellular Phosphorylation Site. *The Journal of Biological Chemistry*, vol. 275, no. 35, pp. 26727-26731.
- Zhu, W., Abbas, T. & Dutta, A. 2005. DNA Replication and Genomic Instability. *Genome Instability in Cancer Development*, ed. E.A. Nigg, Springer, The Netherlands, pp. 249-279.

Zhu, X. & Sadowski, P.D. 1995. Cleavage-dependent Ligation by the FLP Recombinase Characterization of mutant FLP protein with an alteration in a catalytic amino acid. *The Journal of Biological Chemistry*, vol. 270, no. 39, pp. 23044-23054.

Zou, Y., Liu, Y., Wu, X. & Shell, S.M. 2006. Functions of Human Replication Protein A (RPA): From DNA Replication to DNA Damage and Stress Responses. *Journal of Cellular Physiology*, vol. 208, pp. 267-273.

Websites

<http://globocan.iarc.fr/factsheets/populations/factsheet.asp?uno=900>

<http://www.cancerresearchuk.org/cancer-info/cancerstats/mortality/uk-cancer-mortality-statistics>

http://www.genosys.co.uk/oligos/tech_info/annealing.html

[http://www.ncbi.nlm.nih.gov/nucleotide/118582266?report=genbank&log\\$=nucltop&blast_rank=1&RID=4G](http://www.ncbi.nlm.nih.gov/nucleotide/118582266?report=genbank&log$=nucltop&blast_rank=1&RID=4G)

<http://www.addgene.org/pgvec1?f=c&plasmidid=12536&cmd=viewseq&seqonly=true>

<http://www-bcf.usc.edu/~forsburg/main4.html>

<http://www.pombase.org/>

<http://geneontology.org>

<http://people.stfx.ca/bliengme/ExcelTips/AreaUnderCurve.htm>

Appendices

I. Alignment of back mutated hENT1 after integration into *S.*

pombe

```

hsdCK/hENT1      TCACACAATTGCCCGGAACAGGAAGGAGAAAAACAGCCCCCAGTGCCAGACCCAGACACAG 60
dmdNK/hENT1      TCACACAATTGCCCGGAACAGGAAGGAGAAAAACAGCCCCCAGTGCCAGACCCAGACACAG 60
Theoretical      TCACACAATTGCCCGGAACAGGAAGGAGAAAAACAGCCCCCAGTGCCAGACCCAGACACAG 60
WT/hENT1         TCACACAATTGCCCGGAACAGGAAGGAGAAAAACAGCCCCCAGTGCCAGACCCAGACACAG 60
*****

hsdCK/hENT1      GAAGAAGGCCATGATGGCTCCTGCGGTCTCTGCCTCAGCTGGCTTCAC TTCTTGGGCC 120
dmdNK/hENT1      GAAGAAGGCCATGATGGCTCCTGCGGTCTCTGCCTCAGCTGGCTTCAC TTCTTGGGCC 120
Theoretical      GAAGAAGGCCATGATGGCTCCTGCGGTCTCTGCCTCAGCTGGCTTCAC TTCTTGGGCC 120
WT/hENT1         GAAGAAGGCCATGATGGCTCCTGCGGTCTCTGCCTCAGCTGGCTTCAC TTCTTGGGCC 120
*****

hsdCK/hENT1      GAAGCACATGCAGAGGCTGGCGAGGTAGCCGTTGGAGAAGGCAAAGGCAGCCATGAA 180
dmdNK/hENT1      GAAGCACATGCAGAGGCTGGCGAGGTAGCCGTTGGAGAAGGCAAAGGCAGCCATGAA 180
Theoretical      GAAGCACATGCAGAGGCTGGCGAGGTAGCCGTTGGAGAAGGCAAAGGCAGCCATGAA 180
WT/hENT1         GAAGCACATGCAGAGGCTGGCGAGGTAGCCGTTGGAGAAGGCAAAGGCAGCCATGAA 180
*****

hsdCK/hENT1      ATGAACCAGGCATCGTGCTCGAAGACCACAGTCAGGTAGCGGCGGGGCTTAATGTTGCA 240
dmdNK/hENT1      ATGAACCAGGCATCGTGCTCGAAGACCACAGTCAGGTAGCGGCGGGGCTTAATGTTGCA 240
Theoretical      ATGAACCAGGCATCGTGCTCGAAGACCACAGTCAGGTAGCGGCGGGGCTTAATGTTGCA 240
WT/hENT1         ATGAACCAGGCATCGTGCTCGAAGACCACAGTCAGGTAGCGGCGGGGCTTAATGTTGCA 240
*****

hsdCK/hENT1      CAGCAGCAGCAGTGGCACAACACCAGCCGGGCCAGCACCAGGCTTGGCAGCCAGCGGCT 300
dmdNK/hENT1      CAGCAGCAGCAGTGGCACAACACCAGCCGGGCCAGCACCAGGCTTGGCAGCCAGCGGCT 300
Theoretical      CAGCAGCAGCAGTGGCACAACACCAGCCGGGCCAGCACCAGGCTTGGCAGCCAGCGGCT 300
WT/hENT1         CAGCAGCAGCAGTGGCACAACACCAGCCGGGCCAGCACCAGGCTTGGCAGCCAGCGGCT 300
*****

hsdCK/hENT1      GTCCTTCCCAGGCCACATGAATACAGCTGTGAGGCTCCGGCCCAACCAGTCAAAGATATT 360
dmdNK/hENT1      GTCCTTCCCAGGCCACATGAATACAGCTGTGAGGCTCCGGCCCAACCAGTCAAAGATATT 360
Theoretical      GTCCTTCCCAGGCCACATGAATACAGCTGTGAGGCTCCGGCCCAACCAGTCAAAGATATT 360
WT/hENT1         GTCCTTCCCAGGCCACATGAATACAGCTGTGAGGCTCCGGCCCAACCAGTCAAAGATATT 360
*****

hsdCK/hENT1      GAAAGTCAAGAAACAGGACACAGGAATGAAGTAACGTTCCAGGTGCTGCTGCCTGCGAT 420
dmdNK/hENT1      GAAAGTCAAGAAACAGGACACAGGAATGAAGTAACGTTCCAGGTGCTGCTGCCTGCGAT 420
Theoretical      GAAAGTCAAGAAACAGGACACAGGAATGAAGTAACGTTCCAGGTGCTGCTGCCTGCGAT 420
WT/hENT1         GAAAGTCAAGAAACAGGACACAGGAATGAAGTAACGTTCCAGGTGCTGCTGCCTGCGAT 420
*****

```

hsdCK/hENT1	GCTGGACTTGACCTCAACAGTCACGGCTGGAAACATCCCAATGGTGATAGTGAAGATGAA	480
dmdNK/hENT1	GCTGGACTTGACCTCAACAGTCACGGCTGGAAACATCCCAATGGTGATAGTGAAGATGAA	480
Theoretical	GCTGGACTTGACCTCAACAGTCACGGCTGGAAACATCCCAATGGTGATAGTGAAGATGAA	480
WT/hENT1	GCTGGACTTGACCTCAACAGTCACGGCTGGAAACATCCCAATGGTGATAGTGAAGATGAA	480

hsdCK/hENT1	GCAGACAGAGAAAGCCAGGACTGAGATATTTTTCAGGATGGCTTTGATAGAGTGGCTTTC	540
dmdNK/hENT1	GCAGACAGAGAAAGCCAGGACTGAGATATTTTTCAGGATGGCTTTGATAGAGTGGCTTTC	540
Theoretical	GCAGACAGAGAAAGCCAGGACTGAGATATTTTTCAGGATGGCTTTGATAGAGTGGCTTTC	540
WT/hENT1	GCAGACAGAGAAAGCCAGGACTGAGATATTTTTCAGGATGGCTTTGATAGAGTGGCTTTC	540

hsdCK/hENT1	ATTGGTGGGCTGAGAGTTGGAGACTGAAACTCCAGATTCCTCTTTGCCTGCTCTTGGCTC	600
dmdNK/hENT1	ATTGGTGGGCTGAGAGTTGGAGACTGAAACTCCAGATTCCTCTTTGCCTGCTCTTGGCTC	600
Theoretical	ATTGGTGGGCTGAGAGTTGGAGACTGAAACTCCAGATTCCTCTTTGCCTGCTCTTGGCTC	600
WT/hENT1	ATTGGTGGGCTGAGAGTTGGAGACTGAAACTCCAGATTCCTCTTTGCCTGCTCTTGGCTC	600

hsdCK/hENT1	CTCTCCTTTGCTAATGAGGTCCAACCTTGGTCTCCTGCTCCCCGGGTCCTTCAAGCTTGAG	660
dmdNK/hENT1	CTCTCCTTTGCTAATGAGGTCCAACCTTGGTCTCCTGCTCCCCGGGTCCTTCAAGCTTGAG	660
Theoretical	CTCTCCTTTGCTAATGAGGTCCAACCTTGGTCTCCTGCTCCCCGGGTCCTTCAAGCTTGAG	660
WT/hENT1	CTCTCCTTTGCTAATGAGGTCCAACCTTGGTCTCCTGCTCCCCGGGTCCTTCAAGCTTGAG	660

hsdCK/hENT1	CTGCTGGTAGTAGCGGTAGAATTCCAGCGGGGCAGGCCAGGTAACAGATGATGGTCAA	720
dmdNK/hENT1	CTGCTGGTAGTAGCGGTAGAATTCCAGCGGGGCAGGCCAGGTAACAGATGATGGTCAA	720
Theoretical	CTGCTGGTAGTAGCGGTAGAATTCCAGCGGGGCAGGCCAGGTAACAGATGATGGTCAA	720
WT/hENT1	CTGCTGGTAGTAGCGGTAGAATTCCAGCGGGGCAGGCCAGGTAACAGATGATGGTCAA	720

hsdCK/hENT1	AATGATAACAGCACAGGCTGTGATAAAGTAGCCGAA	780
dmdNK/hENT1	AATGATAACAGCACAGGCTGTGATAAAGTAGCCGAA	780
Theoretical	AATGATAACAGCACAGGCTGTGATAAAGTAGCCGAA	780
WT/hENT1	AATGATAACAGCACAGGCTGTGATAAAGTAGCCGAA	780

hsdCK/hENT1	ACTGGCAATAGCGCAGATCATGGCCACGGAGGCAAAGAAGCCTGCTAGGCCCTGGCCACT	840
dmdNK/hENT1	ACTGGCAATAGCGCAGATCATGGCCACGGAGGCAAAGAAGCCTGCTAGGCCCTGGCCACT	840
Theoretical	ACTGGCAATAGCGCAGATCATGGCCACGGAGGCAAAGAAGCCTGCTAGGCCCTGGCCACT	840
WT/hENT1	ACTGGCAATAGCGCAGATCATGGCCACGGAGGCAAAGAAGCCTGCTAGGCCCTGGCCACT	840

hsdCK/hENT1	CATGATGGGGCCGTGTAGCTGGCAGGCAGAAGGCCAGCCAGACCAAACAGGCTGCCCTG	900
dmdNK/hENT1	CATGATGGGGCCGTGTAGCTGGCAGGCAGAAGGCCAGCCAGACCAAACAGGCTGCCCTG	900
Theoretical	CATGATGGGGCCGTGTAGCTGGCAGGCAGAAGGCCAGCCAGACCAAACAGGCTGCCCTG	900
WT/hENT1	CATGATGGGGCCGTGTAGCTGGCAGGCAGAAGGCCAGCCAGACCAAACAGGCTGCCCTG	900

hsdCK/hENT1	CAGGATGGCACCAAATGAATTAATGAGCACGATCTTGATCATGGTGATGACAAAGAAGGG	960
dmdNK/hENT1	CAGGATGGCACCAAATGAATTAATGAGCACGATCTTGATCATGGTGATGACAAAGAAGGG	960
Theoretical	CAGGATGGCACCAAATGAATTAATGAGCACGATCTTGATCATGGTGATGACAAAGAAGGG	960
WT/hENT1	CAGGATGGCACCAAATGAATTAATGAGCACGATCTTGATCATGGTGATGACAAAGAAGGG	960

```

hsdCK/hENT1 CAGAGCATCCAGCTGCACCTTACCAGGATGGCAGTGATCAGAAACACCAGCAGGATGGC 1020
dmdNK/hENT1 CAGAGCATCCAGCTGCACCTTACCAGGATGGCAGTGATCAGAAACACCAGCAGGATGGC 1020
Theoretical CAGAGCATCCAGCTGCACCTTACCAGGATGGCAGTGATCAGAAACACCAGCAGGATGGC 1020
WT/hENT1 CAGAGCATCCAGCTGCACCTTACCAGGATGGCAGTGATCAGAAACACCAGCAGGATGGC 1020
*****

hsdCK/hENT1 CACCAGGCTGCCCAGGATCCGTACGGACTGGGGGATCCTCTGATGCAGGAAGGAGTTGAG 1080
dmdNK/hENT1 CACCAGGCTGCCCAGGATCCGTACGGACTGGGGGATCCTCTGATGCAGGAAGGAGTTGAG 1080
Theoretical CACCAGGCTGCCCAGGATCCGTACGGACTGGGGGATCCTCTGATGCAGGAAGGAGTTGAG 1080
WT/hENT1 CACCAGGCTGCCCAGGATCCGTACGGACTGGGGGATCCTCTGATGCAGGAAGGAGTTGAG 1080
*****

hsdCK/hENT1 GTAGGTGAATAACAGCAGGGGCAGCATGGCACATAGGGTCATGACATTGTTGAAGATGGC 1140
dmdNK/hENT1 GTAGGTGAATAACAGCAGGGGCAGCATGGCACATAGGGTCATGACATTGTTGAAGATGGC 1140
Theoretical GTAGGTGAATAACAGCAGGGGCAGCATGGCACATAGGGTCATGACATTGTTGAAGATGGC 1140
WT/hENT1 GTAGGTGAATAACAGCAGGGGCAGCATGGCACATAGGGTCATGACATTGTTGAAGATGGC 1140
*****

hsdCK/hENT1 ACTGAGAGAGTTCCGCTCAGGCAAGGGTGCTGCAGGGGCGGCTGACGCCTGGGCGTCCTT 1200
dmdNK/hENT1 ACTGAGAGAGTTCCGCTCAGGCAAGGGTGCTGCAGGGGCGGCTGACGCCTGGGCGTCCTT 1200
Theoretical ACTGAGAGAGTTCCGCTCAGGCAAGGGTGCTGCAGGGGCGGCTGACGCCTGGGCGTCCTT 1200
WT/hENT1 ACTGAGAGAGTTCCGCTCAGGCAAGGGTGCTGCAGGGGCGGCTGACGCCTGGGCGTCCTT 1200
*****

hsdCK/hENT1 GCTCAGTTCAGCAGTGACCAAGGACACATTTCTGGGACATGTCCAGGCGGTTTGTGAAATA 1260
dmdNK/hENT1 GCTCAGTTCAGCAGTGACCAAGGACACATTTCTGGGACATGTCCAGGCGGTTTGTGAAATA 1260
Theoretical GCTCAGTTCAGCAGTGACCAAGGACACATTTCTGGGACATGTCCAGGCGGTTTGTGAAATA 1260
WT/hENT1 GCTCAGTTCAGCAGTGACCAAGGACACATTTCTGGGACATGTCCAGGCGGTTTGTGAAATA 1260
*****

hsdCK/hENT CTGAGTGGCCGTCATGAAAAAATTCACGGGAGCAGCGTTCCAGACCCAGCATGAAGAA 1320
dmdNK/hENT CTGAGTGGCCGTCATGAAAAAATTCACGGGAGCAGCGTTCCAGACCCAGCATGAAGAA 1320
Theoretical CTGAGTGGCCGTCATGAAAAAATTCACGGGAGCAGCGTTCCAGACCCAGCATGAAGAA 1320
WT/hENT CTGAGTGGCCGTCATGAAAAAATTCACGGGAGCAGCGTTCCAGACCCAGCATGAAGAA 1320
*****

hsdCK/hENT1 GATAAGCCAGACAGCTTTGTATCTGTCTGAGGCTGGTGACTGGTTGTTCAT 1371
dmdNK/hENT1 GATAAGCCAGACAGCTTTGTATCTGTCTGAGGCTGGTGACTGGTTGTTCAT 1371
Theoretical GATAAGCCAGACAGCTTTGTATCTGTCTGAGGCTGGTGACTGGTTGTTCAT 1371
WT/hENT1 GATAAGCCAGACAGCTTTGTATCTGTCTGAGGCTGGTGACTGGTTGTTCAT 1371
*****

```

Alignment of DNA sequences to check the back mutated hENT1. 3 mutations were found in WT hENT1 and one mutation in both hsdCK and dmdNK (highlights). Theoretical hENT1 was downloaded from

[http://www.ncbi.nlm.nih.gov/nucleotide/118582266?report=genbank&log\\$=nucltop&blast_rank=1](http://www.ncbi.nlm.nih.gov/nucleotide/118582266?report=genbank&log$=nucltop&blast_rank=1)

Back mutated hENT1 protein sequence alignment

```

hsdCK/hENT1      MTTSHQPQDRYKAVWLIFFMLGLGTLTPWNFFMTATQYFTNRLDMSQNVSLVTAELSKDA 60
dmdNK/hENT1      MTTSHQPQDRYKAVWLIFFMLGLGTLTPWNFFMTATQYFTNRLDMSQNVSLVTAELSKDA 60
WT/hENT1         MTTSHQPQDRYKAVWLIFFMLGLGTLTPWNFFMTATQYFTNRLDMSQNVSLVTAELSKDA 60
Theoretical      MTTSHQPQDRYKAVWLIFFMLGLGTLTPWNFFMTATQYFTNRLDMSQNVSLVTAELSKDA 60
                  *****

hsdCK/hENT1      QASAAPAAPLPERNSLSAIFNNVMTLCAMPLLLLFTYLNSFLHQRIPQSVRILGSLVAIL 120
dmdNK/hENT1      QASAAPAAPLPERNSLSAIFNNVMTLCAMPLLLLFTYLNSFLHQRIPQSVRILGSLVAIL 120
WT/hENT1         QASAAPAAPLPERNSLSAIFNNVMTLCAMPLLLLFTYLNSFLHQRIPQSVRILGSLVAIL 120
Theoretical      QASAAPAAPLPERNSLSAIFNNVMTLCAMPLLLLFTYLNSFLHQRIPQSVRILGSLVAIL 120
                  *****

hsdCK/hENT1      LVFLITAILVKVQLDALPFFVITMIKIVLINSFGAILQGSFLFGLAGLLPASYTAPIMSGQ 180
dmdNK/hENT1      LVFLITAILVKVQLDALPFFVITMIKIVLINSFGAILQGSFLFGLAGLLPASYTAPIMSGQ 180
WT/hENT1         LVFLITAILVKVQLDALPFFVITMIKIVLINSFGAILQGSFLFGLAGLLPASYTAPIMSGQ 180
Theoretical      LVFLITAILVKVQLDALPFFVITMIKIVLINSFGAILQGSFLFGLAGLLPASYTAPIMSGQ 180
                  *****

hsdCK/hENT1      GLAGFFASVAMICAIASGSELSESAFGYFITACAVIILTIICYLGLPRLEFYRYQQQLKL 240
dmdNK/hENT1      GLAGFFASVAMICAIASGSELSESAFGYFITACAVIILTIICYLGLPRLEFYRYQQQLKL 240
WT/hENT1         GLAGFFASVAMICAIASGSELSESAFGYFITACAVIILTIICYLGLPRLEFYRYQQQLKL 240
Theoretical      GLAGFFASVAMICAIASGSELSESAFGYFITACAVIILTIICYLGLPRLEFYRYQQQLKL 240
                  *****

hsdCK/hENT1      EGPGEQETKLDLISKGEEPRAGKEESGVSVSNSQPTNESHSHKAILKNISVLAFSVCFIF 300
dmdNK/hENT1      EGPGEQETKLDLISKGEEPRAGKEESGVSVSNSQPTNESHSHKAILKNISVLAFSVCFIF 300
WT/hENT1         EGPGEQETKLDLISKGEEPRAGKEESGVSVSNSQPTNESHSHKAILKNISVLAFSVCFIF 300
Theoretical      EGPGEQETKLDLISKGEEPRAGKEESGVSVSNSQPTNESHSHKAILKNISVLAFSVCFIF 300
                  *****

hsdCK/hENT1      TITIGMFPVAVTEVKSSIAGSSTWERYFIPVSCFLTFNIFDWLGRSLTAVFMWPGKDSRW 360
dmdNK/hENT1      TITIGMFPVAVTEVKSSIAGSSTWERYFIPVSCFLTFNIFDWLGRSLTAVFMWPGKDSRW 360
WT/hENT1         TITIGMFPVAVTEVKSSIAGSSTWERYFIPVSCFLTFNIFDWLGRSLTAVFMWPGKDSRW 360
Theoretical      TITIGMFPVAVTEVKSSIAGSSTWERYFIPVSCFLTFNIFDWLGRSLTAVFMWPGKDSRW 360
                  *****

```

```

hsdCK/hENT1  LPSLVLARLVFVPLLLLCNIKPRRYLTVVFEHDAWFIFMMAAFAFSNGYLASLCMCFGPK 420
dmdNK/hENT1  LPSLVLARLVFVPLLLLCNIKPRRYLTVVFEHDAWFIFMMAAFAFSNGYLASLCMCFGPK 420
WT/hENT1     LPSLVLARLVFVPLLLLCNIKPRRYLTVVFEHDAWFIFMMAAFAFSNGYLASLCMCFGPK 420
Theoretical  LPSLVLARLVFVPLLLLCNIKPRRYLTVVFEHDAWFIFMMAAFAFSNGYLASLCMCFGPK 420
*****

hsdCK/hENT1  KVKPAEAEETAGAIMAFFLCLGLALGAVFSFLFRAIV 456
dmdNK/hENT1  KVKPAEAEETAGAIMAFFLCLGLALGAVFSFLFRAIV 456
WT/hENT1     KVKPAEAEETAGAIMAFFLCLGLALGAVFSFLFRAIV 456
Theoretical  KVKPAEAEETAGAIMAFFLCLGLALGAVFSFLFRAIV 456

```

Alignment of protein sequences to check back mutated hENT1, the three cloned genes are 100% similar to the hENT1 protein.

II. List of library mutants that were sensitive in all three independent screens

Gene ID	Gene name	Gene description
SPAC17G8.05	med20	TATA-box related factor (TRF)
SPAPB17E12.05	rpl3703	60S ribosomal protein L37
SPBP22H7.08	rps1002	40S ribosomal protein S10
SPCC74.05	rpl2702	60S ribosomal protein L27
SPAC11E3.01c	swr1	SNF2 family helicase Swr1
SPAC13C5.07	rad32	Rad32 nuclease
SPAC1952.07	rad1	checkpoint clamp complex protein Rad1
SPAC16C9.06c	upf1	ATP-dependent RNA helicase Upf1
SPAC18G6.15	mal3	EB1 family Mal3
SPAC664.02c		actin-like protein Arp8
SPAC3H5.12c	rpl501	60S ribosomal protein L5
SPBC29A3.05		chromatin remodeling complex subunit
SPBC36.07	iki3	RNA polymerase II elongator subunit Iki3
SPBC342.05	crb2	DNA repair protein RAD9 homolog, Rhp9
SPBP16F5.03c	tra1	phosphatidylinositol kinase
SPAC1805.04	nup132	nucleoporin Nup132
SPBC776.17		rRNA processing protein Rrp7
SPCC24B10.08c		histone acetyltransferase complex subunit Ada2
SPCC1919.03c		AMP-activated protein kinase beta subunit
SPAC23C4.11	atp18	F-0 ATPase subunit J
SPAC694.06c	mrc1	mediator of replication checkpoint 1
SPAC30.02c		RNA polymerase II elongator complex subunit
SPAC9G1.02	wis4	MAP kinase kinase kinase Wis4
SPAC18G6.02c	chp1	chromodomain protein Chp1
SPAC3C7.08c	elf1	AAA family ATPase Elf1
SPAC11D3.15		oxoprolinase

Gene ID	Gene name	Gene description
SPCC736.07c		cell polarity protein
SPBC2G2.06c	apl1	AP-2 adaptor complex subunit Apl1
SPBC2F12.03c		EST1 family protein
SPAC15A10.03c	rhp54	Rad54 homolog Rhp54
SPBC3B9.09	vps36	RBZ zinc finger protein Vps36
SPAC3H1.11	hsr1	transcription factor Hsr1
SPBC32F12.05c	cwf12	complexed with Cdc5 protein Cwf12
SPAC664.07c	rad9	checkpoint clamp complex protein Rad9
SPAC30C2.02	mmd1	deoxyhypusine hydroxylase
SPAC630.14c	tup12	transcriptional corepressor Tup12
SPCC1494.08c		conserved fungal protein
SPBC16G5.15c	fkh2	fork head transcription factor Fkh2
SPAC140.04		conserved fungal protein
SPAC1D4.09c		DUF602 family protein
SPAC1610.01		conserved fungal protein
SPAC10F6.08c		HMG box protein
SPBC24C6.10c		conserved eukaryotic protein
SPBC1718.07c	zfs1	transcription factor Zfs1
SPAC1F12.07		phosphoserine aminotransferase
SPAC20H4.03c	tfs1	transcription elongation factor TFIS
SPCC663.11		ww domain binding protein 11 (wbp11) ortholog
SPAC3A12.13c		translation initiation factor eIF3 complex subunit
SPAC17C9.15c		sequence orphan
SPCC11E10.06c		RNA polymerase II elongator complex subunit Elp4
SPBC25H2.11c		bromodomain protein
SPBC215.14c	vps20	vacuolar sorting protein Vps20
SPBC4B4.03	rsc1	RSC complex subunit Rsc1
SPAC3A12.10	rpl2001	60S ribosomal protein L20a

Gene ID	Gene name	Gene description
SPAC22F3.09c	res2	MBF transcription factor complex subunit Res2
SPAC14C4.13	rad17	RFC related checkpoint protein Rad17
SPCC594.01		DUF1769 family protein
SPBC609.05	pob3	FACT complex component Pob3
SPAC2G11.06	vps4	AAA family ATPase Vps4
SPBC1718.03	ker1	RNA polymerase I transcription factor subunit Ker1
SPBC19C2.14	smd3	Sm snRNP core protein Smd3

III. List of library mutants that did not grow in all three independent screens

Gene ID	Gene name	Gene description
SPAC1782.11	met14	adenylyl-sulfate kinase
SPBC947.14c		sequence orphan
SPBC15D4.02		transcription factor
SPBC16C6.02c	vps1302	chorein homolog
SPBC26H8.12		cytochrome c heme lyase
SPBC32F12.06	pch1	cyclin Pch1
SPAC8C9.03	cgs1	cAMP-dependent protein kinase regulatory subunit Cgs1
SPBC16H5.03c	fub2	SUMO E1-like activator enzyme Fub2
SPBPB7E8.02		conserved protein (fungal bacterial protazoan)
SPAC11D3.18c		nicotinic acid plasma membrane transporter
SPCC825.01		ribosome biogenesis ATPase, Arb family
SPAC11G7.02	pub1	ubiquitin-protein ligase E3
SPAC1D4.13	byr1	MAP kinase kinase Byr1
SPAC18B11.07c	rhp6	Rad6 homolog Rhp6
SPAC25G10.03	zip1	transcription factor Zip1
SPAC31G5.19		ATPase with bromodomain protein
SPBC29A3.18	cyt1	cytochrome c1
SPCC970.10c	brl2	ubiquitin-protein ligase E3
SPBC18H10.06c	swd2	COMPASS complex subunit Swd2
SPAC19A8.05c	sst4	sorting receptor for ubiquitinated membrane proteins
SPAC8C9.06c		mitochondrial translation regulator
SPCC11E10.04		ATPase expression protein homolog
SPAC9E9.03	leu2	3-isopropylmalate dehydratase Leu2
SPBC146.13c	myo1	myosin type I
SPCC663.01c	ekc1	protein phosphatase regulatory subunit Ekc1
SPBC1711.13	his2	histidinol dehydrogenase His2

Gene ID	Gene name	Gene description
SPAC17A2.09c	csx1	RNA-binding protein Csx1
SPCC285.09c	cgs2	cAMP-specific phosphodiesterase Cgs2
SPBC947.02	apl2	AP-1 adaptor complex subunit Apl2
SPAC23E2.03c	ste7	meiotic suppressor protein Ste7
SPAPYUG7.02c	sin1	stress activated MAP kinase interacting protein Sin1
SPBC56F2.11	met6	homoserine O-acetyltransferase
SPBC21.05c	ral2	Ras guanyl-nucleotide exchange factor Ral2
SPBP4H10.11c	lcf2	long-chain-fatty-acid-CoA ligase
SPAC343.16	lys2	homoaconitate hydratase Lys2
SPBC651.05c	dot2	EAP30 family protein Dot2
SPCC31H12.08c	ccr4	CCR4-Not complex subunit Ccr4
SPBC29A3.02c	his7	phosphoribosyl-AMP cyclohydrolase/phosphoribosyl-ATP pyrophosphohydrolase His7
SPBC211.06	gfh1	gamma tubulin complex subunit Gfh1
SPBC30D10.16	pha2	phrenate dehydratase
SPAC1D4.06c	csk1	cyclin-dependent kinase activating kinase Csk1
SPCC1442.01	ste6	guanyl-nucleotide exchange factor Ste6
SPAC3C7.03c	rhp55	RecA family ATPase Rhp55
SPBC2D10.11c		nucleosome assembly protein Nap2
SPBC3B8.03		saccharopine dehydrogenase
SPAC17H9.09c	ras1	GTPase Ras1
SPAP7G5.04c	lys1	aminoadipate-semialdehyde dehydrogenase
SPBC16H5.06	rip1	ubiquinol-cytochrome-c reductase complex subunit 5
SPBC428.05c	arg12	argininosuccinate synthase
SPCC613.10	qcr2	ubiquinol-cytochrome-c reductase complex core protein Qcr2
SPBC106.17c	cys2	homoserine O-acetyltransferase
SPCC1739.06c		uroporphyrin methyltransferase
SPAC29A4.18	prw1	Clr6 histone deacetylase complex subunit Prw1
SPAC10F6.12c	mam4	protein-S isoprenylcysteine O-methyltransferase Mam4

Gene ID	Gene name	Gene description
SPAC25G10.05c	his1	ATP phosphoribosyltransferase
SPCC162.05	coq3	hexaprenyldihydroxybenzoate methyltransferase
SPCC1795.06	map2	P-factor
SPCC1322.10		conserved fungal protein
SPAC26F1.05	mug106	sequence orphan
SPAC14C4.14	atp1	F1-ATPase alpha subunit
SPBC725.09c	hob3	BAR adaptor protein Hob3
SPBPJ4664.01	dps1	decaprenyl diphosphate synthase subunit Dps1
SPAC17C9.02c	lys7	alpha-aminoadipate reductase phosphopantetheinyl transferase Lys7
SPAC589.12		cell wall organization membrane protein
SPAC15E1.03	rpl42	60S ribosomal protein L36/L42
ED666		Positive Strain
ED668		Positive Strain

IV. Over-represented biological processes in the sub library (456 sensitive mutants) at significance level of 0.05%

GO-ID	p-value	corr p-value	selected	total	Description
51276	1.89E-15	1.54E-12	79	218	chromosome organization
10467	2.33E-15	1.54E-12	129	451	gene expression
44260	6.74E-12	2.98E-09	230	1072	cellular macromolecule metabolic process
43170	1.46E-11	4.65E-09	232	1091	macromolecule metabolic process
90304	1.75E-11	4.65E-09	124	475	nucleic acid metabolic process
6325	3.57E-10	7.90E-08	51	141	chromatin organization
16070	3.62E-09	6.87E-07	89	328	RNA metabolic process
16568	5.08E-09	8.43E-07	45	125	chromatin modification
6338	8.09E-09	1.19E-06	38	98	chromatin remodeling
6139	2.11E-08	2.56E-06	129	552	nucleobase, nucleoside, nucleotide and nucleic acid metabolic process
42770	2.12E-08	2.56E-06	17	27	DNA damage response, signal transduction
6412	4.07E-08	4.50E-06	49	150	translation
31573	5.87E-08	5.99E-06	11	13	intra-S DNA damage checkpoint
34645	6.85E-08	6.49E-06	100	404	cellular macromolecule biosynthetic process
9059	7.86E-08	6.95E-06	100	405	macromolecule biosynthetic process
77	8.99E-08	7.45E-06	16	26	DNA damage checkpoint
45934	1.83E-07	1.35E-05	37	104	negative regulation of nucleobase, nucleoside, nucleotide and nucleic acid metabolic process
51172	1.83E-07	1.35E-05	37	104	negative regulation of nitrogen compound metabolic process
10556	2.87E-07	2.00E-05	82	320	regulation of macromolecule biosynthetic process
10558	3.21E-07	2.11E-05	37	106	negative regulation of macromolecule biosynthetic process
22613	3.34E-07	2.11E-05	40	119	ribonucleoprotein complex biogenesis
42254	3.63E-07	2.19E-05	39	115	ribosome biogenesis
60255	5.60E-07	3.23E-05	88	356	regulation of macromolecule metabolic process

GO-ID	p-value	corr p-value	selected	total	Description
6396	7.17E-07	3.88E-05	46	149	RNA processing
31570	7.31E-07	3.88E-05	16	29	DNA integrity checkpoint
31326	9.00E-07	4.59E-05	82	328	regulation of cellular biosynthetic process
9889	1.36E-06	6.67E-05	82	331	regulation of biosynthetic process
31327	1.53E-06	7.27E-05	37	112	negative regulation of cellular biosynthetic process
9890	1.96E-06	8.97E-05	37	113	negative regulation of biosynthetic process
75	3.08E-06	1.36E-04	21	49	cell cycle checkpoint
10605	4.47E-06	1.91E-04	38	121	negative regulation of macromolecule metabolic process
6996	4.64E-06	1.93E-04	102	449	organelle organization
48523	5.09E-06	2.05E-04	49	173	negative regulation of cellular process
34641	5.38E-06	2.07E-04	144	690	cellular nitrogen compound metabolic process
6807	5.45E-06	2.07E-04	145	696	nitrogen compound metabolic process
44238	7.44E-06	2.72E-04	262	1426	primary metabolic process
48519	7.62E-06	2.72E-04	51	185	negative regulation of biological process
9987	7.79E-06	2.72E-04	391	2323	cellular process
31323	8.12E-06	2.76E-04	94	410	regulation of cellular metabolic process
31324	8.59E-06	2.85E-04	38	124	negative regulation of cellular metabolic process
19222	1.19E-05	3.86E-04	95	419	regulation of metabolic process
51171	1.23E-05	3.90E-04	75	311	regulation of nitrogen compound metabolic process
6355	1.26E-05	3.90E-04	58	223	regulation of transcription, DNA-dependent
9892	1.40E-05	4.23E-04	39	131	negative regulation of metabolic process
19219	1.45E-05	4.28E-04	74	307	regulation of nucleobase, nucleoside, nucleotide and nucleic acid metabolic process
51252	1.93E-05	5.58E-04	59	231	regulation of RNA metabolic process
45449	2.19E-05	6.18E-04	60	237	regulation of transcription
10468	2.91E-05	8.03E-04	72	302	regulation of gene expression
45892	3.51E-05	9.49E-04	27	81	negative regulation of transcription, DNA-dependent

GO-ID	p-value	corr p-value	selected	total	Description
80090	3.90E-05	1.03E-03	89	397	regulation of primary metabolic process
6259	4.26E-05	1.11E-03	44	161	DNA metabolic process
16481	4.49E-05	1.12E-03	27	82	negative regulation of transcription
51253	4.49E-05	1.12E-03	27	82	negative regulation of RNA metabolic process
7059	9.12E-05	2.20E-03	27	85	chromosome segregation
10629	9.12E-05	2.20E-03	27	85	negative regulation of gene expression
6974	1.15E-04	2.73E-03	36	128	response to DNA damage stimulus
34470	1.27E-04	2.92E-03	28	91	ncRNA processing
22403	1.28E-04	2.92E-03	46	178	cell cycle phase
34660	1.38E-04	3.01E-03	29	96	ncRNA metabolic process
51053	1.41E-04	3.01E-03	11	22	negative regulation of DNA metabolic process
32200	1.43E-04	3.01E-03	13	29	telomere organization
723	1.43E-04	3.01E-03	13	29	telomere maintenance
60249	1.43E-04	3.01E-03	13	29	anatomical structure homeostasis
34728	1.63E-04	3.38E-03	14	33	nucleosome organization
8156	1.66E-04	3.38E-03	10	19	negative regulation of DNA replication
51052	2.39E-04	4.81E-03	14	34	regulation of DNA metabolic process
278	3.06E-04	6.06E-03	19	55	mitotic cell cycle
6357	3.26E-04	6.37E-03	27	91	regulation of transcription from RNA polymerase II promoter
44249	3.37E-04	6.48E-03	122	611	cellular biosynthetic process
43486	3.63E-04	6.78E-03	7	11	histone exchange
43044	3.63E-04	6.78E-03	7	11	ATP-dependent chromatin remodeling
65007	4.22E-04	7.79E-03	149	776	biological regulation
16043	4.67E-04	8.49E-03	116	580	cellular component organization
7049	4.86E-04	8.67E-03	51	214	cell cycle
9058	4.90E-04	8.67E-03	124	628	biosynthetic process
51726	5.01E-04	8.75E-03	35	132	regulation of cell cycle

GO-ID	p-value	corr p-value	selected	total	Description
44237	5.57E-04	9.61E-03	263	1501	cellular metabolic process
40029	6.58E-04	1.12E-02	19	58	regulation of gene expression, epigenetic
45814	7.19E-04	1.19E-02	18	54	negative regulation of gene expression, epigenetic
6342	7.19E-04	1.19E-02	18	54	chromatin silencing
6368	7.49E-04	1.21E-02	10	22	RNA elongation from RNA polymerase II promoter
9893	7.59E-04	1.21E-02	25	86	positive regulation of metabolic process
31325	7.59E-04	1.21E-02	25	86	positive regulation of cellular metabolic process
8152	9.15E-04	1.43E-02	268	1543	metabolic process
6333	9.15E-04	1.43E-02	12	30	chromatin assembly or disassembly
22402	9.72E-04	1.50E-02	48	204	cell cycle process
48522	1.05E-03	1.60E-02	35	137	positive regulation of cellular process
6366	1.06E-03	1.60E-02	34	132	transcription from RNA polymerase II promoter
6275	1.15E-03	1.71E-02	10	23	regulation of DNA replication
16458	1.17E-03	1.72E-02	18	56	gene silencing ubiquitin-dependent protein catabolic process via the multivesicular body sorting pathway
43162	1.20E-03	1.75E-02	8	16	pathway
8104	1.32E-03	1.91E-02	56	250	protein localization
48518	1.37E-03	1.95E-02	36	144	positive regulation of biological process
76	1.42E-03	1.95E-02	7	13	DNA replication checkpoint
32297	1.42E-03	1.95E-02	7	13	negative regulation of DNA-dependent DNA replication initiation
30174	1.42E-03	1.95E-02	7	13	regulation of DNA-dependent DNA replication initiation
43328	1.42E-03	1.95E-02	7	13	protein targeting to vacuole involved in ubiquitin-dependent protein catabolic process via the multivesicular body sorting pathway
33036	1.51E-03	2.01E-02	63	290	macromolecule localization
30466	1.52E-03	2.01E-02	9	20	chromatin silencing at silent mating-type cassette
32774	1.53E-03	2.01E-02	37	150	RNA biosynthetic process

GO-ID	p-value	corr p-value	selected	total	Description
16072	1.53E-03	2.01E-02	15	44	rRNA metabolic process
23033	1.62E-03	2.10E-02	34	135	signaling pathway
31056	1.70E-03	2.19E-02	10	24	regulation of histone modification
122	1.78E-03	2.27E-02	11	28	negative regulation of transcription from RNA polymerase II promoter
50794	1.86E-03	2.36E-02	125	654	regulation of cellular process
23034	1.90E-03	2.38E-02	32	126	intracellular signaling pathway
6399	2.06E-03	2.55E-02	17	54	tRNA metabolic process
51569	2.42E-03	2.97E-02	4	5	regulation of histone H3-K4 methylation
6323	2.48E-03	2.99E-02	11	29	DNA packaging
71103	2.48E-03	2.99E-02	11	29	DNA conformation change
6310	2.56E-03	3.06E-02	17	55	DNA recombination
6351	2.60E-03	3.08E-02	36	149	transcription, DNA-dependent
279	2.77E-03	3.24E-02	38	160	M phase
6364	2.78E-03	3.24E-02	14	42	rRNA processing
44267	2.88E-03	3.33E-02	122	643	cellular protein metabolic process
32509	3.07E-03	3.43E-02	8	18	endosome transport via multivesicular body sorting pathway
32511	3.07E-03	3.43E-02	8	18	late endosome to vacuole transport via multivesicular body sorting pathway
70925	3.07E-03	3.43E-02	8	18	organelle assembly
65008	3.08E-03	3.43E-02	44	193	regulation of biological quality
50789	3.21E-03	3.52E-02	126	669	regulation of biological process
6260	3.21E-03	3.52E-02	15	47	DNA replication
51325	3.37E-03	3.67E-02	9	22	interphase
51572	3.60E-03	3.86E-02	3	3	negative regulation of histone H3-K4 methylation
31061	3.60E-03	3.86E-02	3	3	negative regulation of histone methylation
19538	3.63E-03	3.86E-02	124	659	protein metabolic process
6397	4.03E-03	4.22E-02	15	48	mRNA processing
90329	4.03E-03	4.22E-02	7	15	regulation of DNA-dependent DNA replication

GO-ID	p-value	corr p-value	selected	total	Description
33044	4.54E-03	4.67E-02	11	31	regulation of chromosome organization
30702	4.54E-03	4.67E-02	11	31	chromatin silencing at centromere
10604	4.70E-03	4.77E-02	22	82	positive regulation of macromolecule metabolic process
6354	4.74E-03	4.77E-02	10	27	RNA elongation
65004	4.74E-03	4.77E-02	10	27	protein-DNA complex assembly

